VOL. 676 NO. 1 JULY 29, 1994

13th Int. Symp. on HPLC of Proteins, Peptides and Polynucleotides, San Francisco, CA, November 30–December 3, 1993

JOURNAL OF CHROMATOGRAPHY A

INCLUDING ELECTROPHORESIS AND OTHER SEPARATION METHODS

SYMPOSIUM VOLUMES

ELSEVIER

JOURNAL OF CHROMATOGRAPHY A

INCLUDING ELECTROPHORESIS AND OTHER SEPARATION METHODS

Scope. The *Journal of Chromatography A* publishes papers on all aspects of **chromatography, electrophoresis** and related methods. Contributions consist mainly of research papers dealing with chromatographic theory, instrumental developments and their applications. In the *Symposium volumes*, which are under separate editorship, proceedings of symposia on chromatography, electrophoresis and related methods are published. *Journal of Chromatography B: Biomedical Applications* —This journal, which is under separate editorship, deals with the following aspects: developments in and applications of chromatographic and electrophoretic techniques related to clinical diagnosis or alterations during medical treatment; screening and profiling of body fluids or tissues related to the analysis of active substances and to metabolic disorders; drug level monitoring and pharmacokinetic studies; clinical toxicology; forensic medicine; veterinary medicine; occupational medicine; results from basic medical research with direct consequences in clinical practice.

Submission of Papers. The preferred medium of submission is on disk with accompanying manuscript (see *Electronic manuscripts* in the Instructions to Authors, which can be obtained from the publisher, Elsevier Science B.V., P.O. Box 330, 1000 AH Amsterdam, Netherlands). Manuscripts (in English; *four* copies are required) should be submitted to: Editorial Office of *Journal of Chromatography A*, P.O. Box 681, 1000 AR Amsterdam, Netherlands, Telefax (+31-20) 5862 304, or to: The Editor of *Journal of Chromatography B: Biomedical Applications*, P.O. Box 681, 1000 AR Amsterdam, Netherlands. Review articles are invited or proposed in writing to the Editors who welcome suggestions for subjects. An outline of the proposed review should first be forwarded to the Editors for preliminary discussion prior to preparation. Submission of an article is understood to imply that the article is original and unpublished and is not being considered for publication elsewhere. For copyright regulations, see below.

Publication information. *Journal of Chromatography A* (ISSN 0021-9673): for 1994 Vols. 652–682 are scheduled for publication. *Journal of Chromatography B: Biomedical Applications* (ISSN 0378-4347): for 1994 Vols. 652–662 are scheduled for publication. Subscription prices for *Journal of Chromatography A*, *Journal of Chromatography B: Biomedical Applications* or a combined subscription are available upon request from the publisher. Subscriptions are accepted on a prepaid basis only and are entered on a calendar year basis. Issues are sent by surface mail except to the following countries where air delivery via SAL is ensured: Argentina, Australia, Brazil, Canada, China, Hong Kong, India, Israel, Japan, Malaysia, Mexico, New Zealand, Pakistan, Singapore, South Africa, South Korea, Taiwan, Thailand, USA. For all other countries airmail rates are available upon request. Claims for missing issues must be made within six months of our publication (mailing) date. Please address all your requests regarding orders and subscription queries to: Elsevier Science B.V., Journal Department, P.O. Box 211, 1000 AE Amsterdam, Netherlands. Tel.: (+31-20) 5803 642; Fax: (+31-20) 5803 598. Customers in the USA and Canada wishing information on this and other Elsevier journals, please contact Journal Information Center, Elsevier Science Inc., 655 Avenue of the Americas, New York, NY 10010, USA, Tel. (+1-212) 633 3750, Telefax (+1-212) 633 3764.

Abstracts/Contents Lists published in Analytical Abstracts, Biochemical Abstracts, Biological Abstracts, Chemical Abstracts, Chemical Titles, Chromatography Abstracts, Current Awareness in Biological Sciences (CABS), Current Contents/Life Sciences, Current Contents/Physical, Chemical & Earth Sciences, Deep-Sea Research/Part B: Oceanographic Literature Review, Excerpta Medica, Index Medicus, Mass Spectrometry Bulletin, PASCAL-CNRS, Referativnyi Zhurnal, Research Alert and Science Citation Index.

US Mailing Notice. *Journal of Chromatography A* (ISSN 0021-9673) is published weekly (total 52 issues) by Elsevier Science B.V., (Sara Burgerhartstraat 25, P.O. Box 211, 1000 AE Amsterdam, Netherlands). Annual subscription price in the USA US$ 4994.00 (US$ price valid in North, Central and South America only) including air speed delivery. Second class postage paid at Jamaica, NY 11431. **USA POSTMASTERS**: Send address changes to *Journal of Chromatography A*, Publications Expediting, Inc., 200 Meacham Avenue, Elmont, NY 11003. Airfreight and mailing in the USA by Publications Expediting.

See inside back cover for Publication Schedule, Information for Authors and information on Advertisements.

0021-9673/94/$07.00

Printed in the Netherlands

For Contents see p. VII.

Chiral HPLC Column

Application Guide for Chiral HPLC Column Selection

SECOND EDITION!

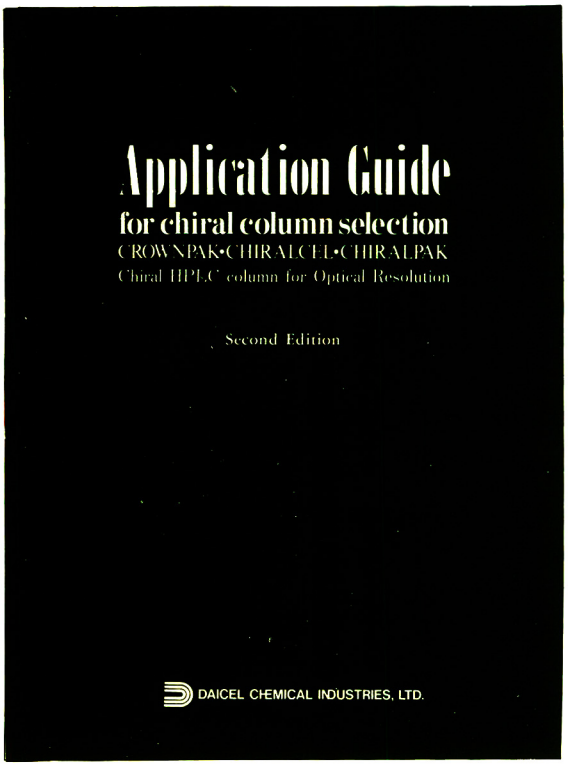

GREEN BOOK

The 112-page green book contains chromatographic resolutions of over 350 chiral separations, cross-indexed by chemical compound class, structure, and the type of chiral column respectively. This book also lists chromatographic data together with analytical conditions and structural information. A quick reference guide for column selection from a wide range of DAICEL chiral HPLC columns is included.

To request this book, please let us know by fax or mail.

DAICEL CHEMICAL INDUSTRIES, LTD.

AMERICA

CHIRAL TECHNOLOGIES, INC.

730 Springdale Drive, P.O. Box 564, Exton, PA 19341
Phone: +1-215-594-2100
Facsimile: +1-215-594-2325

EUROPE

DAICEL (EUROPA) GmbH

Oststr. 22
D-40211 Düsseldorf, Germany
Phone: +49-211-369848
Facsimile: +49-211-364429

ASIA/OCEANIA

DAICEL CHEMICAL INDUSTRIES, LTD.
CHIRAL CHEMICALS NDD
8-1, Kasumigaseki 3-chome,
Chiyoda-ku, Tokyo 100, JAPAN
Phone: + 81-3-3507-3151
Facsimile: + 81-3-3507-3193

Chromatography of Mycotoxins

Techniques and Applications

edited by **V. Betina**

Journal of Chromatography Library Volume 54

This work comprises two parts, Part A: Techniques and Part B: Applications. In Part A the most important principles of sample preparation, extraction, clean-up, and of established and prospective chromatographic techniques are discussed in relation to mycotoxins. In Part B the most important data, scattered in the literature, on thin-layer, liquid, and gas chromatography of mycotoxins have been compiled. Mycotoxins are mostly arranged according to families, such as aflatoxins, trichothecenes, lactones etc. Chromatography of individual important mycotoxins and multi-mycotoxin chromatographic analyses are also included. Applications are presented in three chapters devoted to thin-layer, liquid, and gas chromatography of mycotoxins.

1993 xiv + 440 pages
Price: US $ 180.00 / Dfl. 315.00
ISBN 0-444-81521-X

ELSEVIER SCIENCE B.V.

ORDER INFORMATION

For USA and Canada
ELSEVIER SCIENCE INC.
P.O. Box 945
Madison Square Station
New York, NY 10160-0757
Fax: (212) 633 3880

In all other countries
ELSEVIER SCIENCE B.V.
P.O. Box 330
1000 AH Amsterdam
The Netherlands
Fax: (+31-20) 5862 845

US$ prices are valid only for the USA & Canada and are subject to exchange rate fluctuations; in all other countries the Dutch guilder price (Dfl.) is definitive. Customers in the European Union should add the appropriate VAT rate applicable in their country to the price(s). Books are sent postfree if prepaid.

JOURNAL OF CHROMATOGRAPHY A

VOL. 676 (1994)

JOURNAL OF CHROMATOGRAPHY A

INCLUDING ELECTROPHORESIS AND OTHER SEPARATION METHODS

SYMPOSIUM VOLUMES

ELSEVIER

Amsterdam — Lausanne — New York — Oxford — Shannon — Tokyo

J. Chromatogr. A, Vol. 676 (1994)

Cable car, ca. 1875
California Street & Central (now Presidio Avenue)

0021-9673/94/$07.00

Printed in the Netherlands

SYMPOSIUM ISSUE

13TH INTERNATIONAL SYMPOSIUM ON HIGH-PERFORMANCE LIQUID CHROMATOGRAPHY OF PROTEINS, PEPTIDES AND POLYNUCLEOTIDES

San Francisco, CA (USA), November 30–December 3, 1993

Guest Editors

JOSEPH J. DeSTEPHANO
(West Chester, PA, USA)

MILTON T.W. HEARN
(Clayton, Australia)

JAN-CHRISTER JANSON
(Uppsala, Sweden)

MICHAEL KUNITANI
(Emeryville, CA, USA)

BENGT ÖSTERLUND
(Uppsala, Sweden)

FRED E. REGNIER
(West Lafayette, IN, USA)

KLAUS K. UNGER
(Mainz, Germany)

TIMOTHY WEHR
(Hercules, CA, USA)

VOL. 676, NO. 1 JOURNAL OF CHROMATOGRAPHY A JULY 29, 1994

CONTENTS

13TH INTERNATIONAL SYMPOSIUM ON HIGH-PERFORMANCE LIQUID CHROMATOGRAPHY OF PROTEINS, PEPTIDES AND POLYNUCLEOTIDES, SAN FRANCISCO, CA, NOVEMBER 30–DECEMBER 3, 1993

ELSEVIER

Journal of Chromatography A, 676 (1994) 1

JOURNAL OF CHROMATOGRAPHY A

Foreword

The 13th International Symposium on High-Performance Liquid Chromatography of Proteins, Peptides, and Polynucleotides was held at the Embarcadero Hyatt Regency hotel in San Francisco, U.S.A. from 30 November through 3 December, 1993. Delegates from Europe, Asia, America, Africa, and Australia enjoyed the beauty of the city, luxury of the hotel, and quality of the conference facilities while participating in lectures and discussions on the latest developments in separation and detection technology as it applies to the isolation and characterization of proteins, peptides, and polynucleotides. Presentations of advances in biological mass spectrometry, capillary electrophoresis of glycoproteins and polysaccharides, antisense DNA, large scale separations of proteins, and new methods in microanalysis and structure elucidation were enthusiastically received by the attendees.

The format of the meeting followed that of previous symposia in this series. Topics discussed in oral, poster, and discussion sessions related to new separation technology and fundamental principles of separation systems, micro- and macro-scale preparative separations, new high resolution methods for the purification and analysis of biological macromolecules, interaction of macromolecules with surfaces, analytical immunology and the application of new separation and detection technology to biotechnology, protein chemistry, and molecular biology. Vigorous discussions of papers indicated a high level of attendee participation and provided both insight and excitement. As in the past, the attendees were a mixture of old-time biochemical separation people, new-comers, protein chemists, and biotechnologists drawn almost equally from academia and industry. Approximately twenty student travel grants were awarded to insure student participation in the symposium.

An evening social program, sponsored by E. Merck, Pharmacia, and PerSeptive Biosystems, consisting of cocktail parties, buffer dinners, and a dinner cruise around San Francisco provided a relaxing counter-balance to the intense pace of the scientific sessions of the day. Old friendships made at previous symposia were renewed, new friends were found, and discussions of science continued long into the night.

The meeting was co-sponsored by the Forum for Separation Science of Indiana, the permanent committee of this symposium series, and the California Society for Separation Science (CASS). We are all indebted to Paddy Batchelder for expertly handling correspondence with the attendees, negotiating with vendors for the myriad of services necessary for the symposium, and coordinating the various aspects of both the social and scientific program. Special thanks go to Tim Wehr, Michael Kunitani, Robert Stevenson, and Bill Hancock for selecting the meeting site and organizing the social program. Thanks should also go to Klaus Unger, Joe DeStephano, Jan-Christer Janson, Tim Wehr, and Michael Kunitani for their assistance in organizing the scientific program. Finally, I would like to thank all the attendees who came to San Francisco, contributed so enthusiastically to the symposium, and shared their own unique insights with the rest of us.

Lafayette, IN (USA) (Fred E. Regnier)

SSDI 0021-9673(94)00592-W

ELSEVIER

Journal of Chromatography A, 676 (1994) 3–15

JOURNAL OF CHROMATOGRAPHY A

Reversed-phase liquid chromatography as a useful probe of hydrophobic interactions involved in protein folding and protein stability

Robert S. Hodges*[,a], Bing-Yan Zhu[b], Nian E. Zhou[b], Colin T. Mant[a]

[a]*Department of Biochemistry and the Medical Research Council Group in Protein Structure and Function, University of Alberta, Edmonton, Alberta T6G 2H7, Canada*

[b]*Protein Engineering Network of Centres of Excellence, University of Alberta, Edmonton, Alberta T6G 2H7, Canada*

Abstract

We have evaluated the potential of reversed-phase liquid chromatography (RPLC) as a probe of hydrophobic interactions involved in protein folding and stability. Our approach was to apply RPLC to a *de novo* designed model protein system, namely a two-stranded α-helical coiled coil. It was shown that the reversed-phase retention behaviour of various synthetic analogues of monomeric α-helices and dimeric coiled-coil structures correlated well with their stability in solution, as monitored by circular dichroism during guanidine hydrochloride and temperature denaturation studies. In addition, an explanation is offered as to why amphipathic coiled coils, an important structural motif in many biological systems, are more stable at low pH compared to physiological pH values. The results of this study suggest that not only may RPLC prove to be a useful and rapid complementary technique for understanding protein interactions, but also the *de novo* designed coiled-coil model described here is an excellent model system for such studies.

1. Introduction

One of the most difficult and important challenges currently facing biochemists is understanding protein folding and stability; specifically, how does the amino acid sequence of a protein determine its three-dimensional structure and the pathway of folding, as well as its resultant stability? The goal of predicting polypeptide and protein conformation from primary structure information, including the interactions responsible for stabilizing this conformation, is being pursued by many researchers, using a variety of methodologies.

A very promising approach to such studies is the utilization of reversed-phase liquid chromatography (RPLC) as a physicochemical model of biological systems. Hydrophobic interactions are the major driving force for protein folding and stability; the hydrophobic interactions between peptides or proteins and the non-polar stationary phase upon which this chromatographic mode depends [1] may well reflect similar interactions between the non-polar residues that stabilize the folded or three-dimensional structure of the native protein molecule.

Several previous studies have attempted to equate conformational stability of proteins with

* Corresponding author.

0021-9673/94/$07.00
SSDI 0021-9673(94)00169-A

their reversed-phase retention behaviour. However, these studies have tended to focus on such concerns as protein conformational changes due to denaturation during RPLC [2–8], thermodynamics of protein unfolding during RPLC [3,6,9,10] or simple observations of protein conformational changes under RPLC conditions [11], *i.e.*, generally little attempt is made to correlate protein primary structure with protein folding or stability of the folded protein molecule. Even studies where such correlation between peptide [10] or protein [7] retention behaviour with protein folding is attempted, tend to offer limited insight into the contribution of individual interior amino acid side-chains to protein stability.

In the authors' view, the best approach to gauging the effectiveness of RPLC as a probe to further our understanding of the hydrophobic forces responsible for protein folding and stability is to focus on work conducted with defined model peptide and protein systems, the results of which can then be extrapolated to peptides and proteins as a whole. A promising candidate for such a model system is represented by *de novo* designed model two-stranded α-helical coiled-coils. Hodges and co-workers [12–26] have carried out extensive studies on the stability and properties of such synthetic coiled coils, and the credentials of this biologically important motif for the purposes of the present study appeared excellent. For example, such a model system fits well with the proposed mechanism of protein folding which involves the collision of secondary structural elements, resulting in the progressive association of these elements which leads to the native conformation [27]. In addition, about 50% of all α-helices in soluble globular proteins are amphipathic [28,29], *i.e.*, with opposing polar and non-polar faces; such structures are also found in many fibrous proteins, *e.g.*, myosin [30,31] and tropomyosin [32] as well as smaller molecules such as polypeptide hormones [33,34], polypeptide venoms [35,36] and polypeptide antibiotics [37,38], reflecting their wide distribution in secondary structural motifs. Indeed, by their very nature, amphipathic α-helices play an important role in the hydrophobic interactions involved in protein folding and stability. The coiled-coil structure itself is also a widespread protein quaternary structure, with more than 200 proteins thought, at present, to contain the coiled-coil motif [39] and many more are expected to be discovered.

From a practical point of view, the model amphipathic α-helical peptides described by Hodges and co-workers [12–26] are large enough to form a stable three-dimensional structure capable of tolerating sequence changes, yet small enough for easy chemical synthesis of analogues. Further, the hydrophobic domain of these model amphipathic peptides will bind preferentially to a reversed-phase packing, *i.e.*, only this part of the peptide sequence would be expected to have a major effect on peptide retention behaviour during RPLC. Thus, it is reasonable to expect that even subtle variations in hydrophobicity of the preferred binding domain will be of a magnitude able to be expressed as a variation in RPLC retention time. Relative retention behaviour of various model peptide analogues could then be extrapolated to the way in which such amphipathic structures interact with each other within native protein molecules. Although other researchers have utilized synthetic amphipathic peptides in conjunction with RPLC for protein stability studies [40,41], the model peptides employed (consisting of only lysine and leucine residues) lacked the biological relevance of those reported in the present study.

It is interesting to note that, as long as 18 years ago, Horváth *et al.* [42] postulated that the hydrophobic stationary phase of reversed-phase packings may be a useful probe for investigation of amphipathic helices induced or stabilized in hydrophobic environments. We believe we are now in a position to test more fully and further develop this hypothesis with our peptide/protein model. Thus, the present study describes our initial evaluation of RPLC as a probe of biological systems by attempting to correlate the stability of model single and double-stranded amphipathic α-helical peptides with their chromatographic retention patterns.

2. Experimental

2.1. Materials

HPLC-grade water and acetonitrile were obtained from J.T. Baker (Phillipsburg, NJ, USA). ACS-grade orthophosphoric acid and triethylamine (TEA, redistilled before use) was obtained from Anachemia (Toronto, Canada). Trifluoroacetic acid (TFA) was obtained from Aldrich (Milwaukee, WI, USA). Trifluoroethanol (TFE) was obtained from Sigma (St. Louis, MO, USA). Guanidine hydrochloride (Gdn · HCl) was obtained from Schwarz/Mann Biotech, Cleveland, OH, USA.

2.2. Instrumentation

Peptide synthesis was carried out on an Applied Biosystems peptide synthesizer Model 430A (Foster City, CA, USA). Crude peptides were purified by an Applied Biosystems 400 solvent-delivery system connected to a 783A programmable absorbance detector.

The analytical HPLC system consisted of an HP1090 liquid chromatograph (Hewlett-Packard, Avondale, PA, USA), coupled to an HP1040A detection system, HP9000 series 300 computer, HP9133 disc drive, HP2225A Thinkjet printer and HP7460A plotter.

Amino acid analyses of purified peptides were carried out on a Beckman Model 6300 amino acid analyzer (Beckman Instruments, Fullerton, CA, USA).

The correct primary ion molecular masses of peptides were confirmed by time-of-flight mass spectroscopy on a BIOION-20 Nordic (Uppsala, Sweden).

Circular dichroism spectra were recorded on a JASCO J-500C Spectropolarimeter (Easton, MD, USA) attached to a JASCO DP-500N data processor and a Lauda (Model RMS) water bath (Brinkman Instruments, Rexdale, Canada) used to control the temperature of the cell. The instrument was routinely calibrated with an aqueous solution of recrystallized *d*-camphorsulphonic acid at 290 nm. Constant nitrogen flushing was employed.

2.3. Columns

Analytical HPLC runs were performed on a Zorbax 300-SB C_8 reversed-phase column (250 × 4.6 mm I.D., 5-μm particle size, 300-Å pore size) from Rockland Technologies, Wilmington, DE, USA.

Crude peptides were purified on a semi-preparative SynChropak RP-P C_{18} reversed-phase column (250 × 10 mm I.D., 6.5 μm, 300 Å) from SynChrom, Lafayette, IN, USA.

2.4. Peptide synthesis

Peptides were synthesized on co-poly(styrene–1% divinylbenzene) benzhydrylamine hydrochloride resin (0.92 mmol/g resin). All amino acids were protected at the α-amino position with the *tert.*-butyloxycarbonyl (Boc) group and the following side-chain protecting groups were used: 4-methylbenzyl (Cys), benzyl (Glu) and 2-chlorobenzyloxycarbonyl (Lys). All amino acids were single coupled as preformed symmetrical anhydrides (with the exception of Gln, which was coupled as the hydroxybenzotriazole active ester) in dichloromethane. Boc groups were removed at each cycle with an 80-s reaction with TFA–dichloromethane (33:67, v/v), followed by a second reaction with TFA–dichloromethane (50:50, v/v) for 18 min. Neutralizations were carried out using 10% (v/v) diisopropylethylamine in dimethylformamide. N-Terminal residues were acetylated using acetic anhydride–dichloromethane (25:75, v/v) for 10 min. The peptides were cleaved from the resin by treatment with anhydrous hydrogen fluoride (20 ml/g resin) containing 10% (v/v) anisole and 2% (v/v) 1,2-ethanedithiol for 1 h at −4°C. The resins were then washed with diethyl ether (3 × 25 ml) and the peptides extracted with neat acetic acid (3 × 25 ml). The resulting peptide solutions were then lyophilized prior to purification.

3. Results and discussion

3.1. Synthetic model protein

The model amphipathic peptide analogues described in this study were based on a repeating pattern of hydrophobic residues, first identified by Hodges *et al.* [43], throughout the entire length of the 284-residue polypeptide chain of the two-stranded α-helical coiled-coil protein, rabbit skeletal α-tropomyosin. These workers proposed that tropomyosin and other two-stranded α-helical coiled-coil proteins were stabilized by hydrophobic residues at positions 2 and 5 of a repeating heptad sequence, X–N–X–X–N–X–X–X–N–X–X–N–X–X–X–N . . . . . ., where N is a non-polar residue. This pattern of hydrophobes is often referred to as a 3–4 or 4–3 repeat.

The synthetic peptide analogues employed for the present study (Fig. 1, top) are, thus, polyheptapeptides of 35 residues based on the repeating sequence:

$$[\overset{a}{N}-\overset{b}{X}-\overset{c}{X}-\overset{d}{N}-\overset{e}{X}-\overset{f}{X}-\overset{g}{X}]_n$$

where the hydrophobic residues are denoted N. The high α-helix-forming potential of this sequence has been well documented [12–26,43]. Fig. 1 (bottom) illustrates a cross-section of two molecules of synthetic analogue "L", represented as helical wheels. The amphipathicity of this sequence is very apparent, with the leucine residues at positions a and d forming the hydro-

```
   1 2       6   8         12 13   15 16     19 20   22        26 27   29
   g a b c d e f g a         d e     g a       d e     g a       d e     g a       d        Denotion  Figure(s)
Ac-K-C-E-A-L-E-G-K-L-E-A-L-E-G-K-L-E-A-L-E-G-K-L-E-A-L-E-G-K-L-E-A-L-E-G-NH2              L         6,7
Ac-----------------------V-------------V-------------V-------------------NH2              LVd       2-5
Ac-----------------------I-------------I-------------I-------------------NH2              LId       2-5
Ac-------------------------------I-----I---------------------------------NH2              I         7
Ac-------------------------------V-----V---------------------------------NH2              V         7
Ac-------------------------------F-----F---------------------------------NH2              F         6,7
Ac-------------------------------Y-----Y---------------------------------NH2              Y         7
Ac-Q---------K-Q-----------K---Q-A-------K---Q---------K---Q-------------NH2              EKQ       8-10
Ac-E---------K-E-----------K---E-A-------K---E---------K---E-------------NH2              EKE       8-10
```

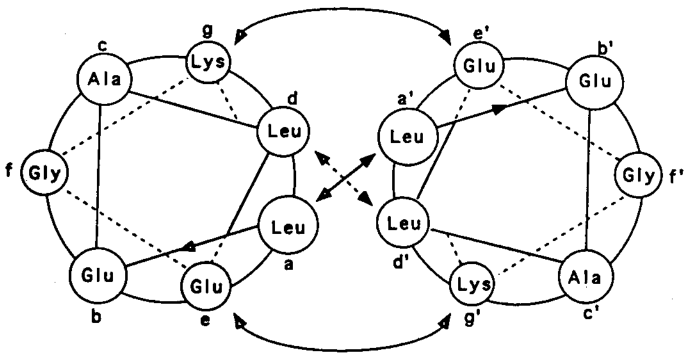

Fig. 1. Amino acid sequences of synthetic model peptides used in this study. Top: primary sequences of peptide analogues, where the N-terminal amino acid of each chain is acetylated (Ac–) and the C-terminal carboxyl group is amidated (–NH_2). Peptide L may be considered the "native" peptide structure, where all of the a and d positions (save residue 2) responsible for stabilizing the coiled coil, are occupied by leucine. The only residues shown for the other analogues are those where a substitution has been made in the "native" sequence. The residue number and heptad position of substituted residues are also shown. Bottom: helical wheel representation of a cross-section, looking from the N-terminal end, of two helices in a coiled coil containing the "native" heptapeptide sequence Leu–Glu–Ala–Leu–Glu–Gly–Lys. The α-helices descend into the page on proceeding from residues a to g. The chains are in-register and parallel. The non-polar residues in positions a and a′ and d and d′ interact and are responsible for the formation and stabilization of the coiled coil. Possible interchain ionic interactions could occur between g and e′ and between g′ and e.

phobic face. A coiled coil is formed by the two molecules wrapping around each other at their hydrophobic faces. Based upon the high resolution X-ray structure by O'Shea *et al.* [44] in 1991, these hydrophobes are 83% buried in the coiled coil.

From Fig. 1 (bottom), the coiled coil is stabilized by hydrophobic interactions between the individual α-helices with residue a interacting with a′ and residue d with d′. This coiled coil also exhibits interchain ionic interactions between lysine and glutamic acid residues at positions g and e′ (i to i′ + 5 or, for example, K1 in chain 1 with E6 in chain 2). There are also intrachain repulsive interactions along the α-helix, *e.g.*, glutamic acid at e with glutamic acid at b; these are $i \rightarrow i + 4$ interactions or glutamic acid at b with glutamic acid at e; these are $i \rightarrow i + 3$ interactions.

The 35-residue lengths of the analogues was based on the work of Lau *et al.* [14], who demonstrated that, with leucine occupying all the hydrophobic a and d positions in the repeating heptad, two-stranded α-helical coiled coils were formed in benign medium at pH 7.0. The presence of a disulphide bridge at position 2–2′ (hydrophobic position a in the first heptad) in the peptide sequence confers further stability to the two-stranded coiled coil [18].

3.2. Retention behaviour of amphipathic α-helices in RPLC

On binding to a reversed-phase column, the high hydrophobicity of the stationary phase disrupts the interchain hydrophobic interactions of a coiled coil such as that shown in Fig. 1 (bottom), whilst stabilizing the secondary (α-helical) structure. In fact, Zhou *et al.* [17] showed that such amphipathic peptides remain α-helical when bound to the reversed-phase column and, due to the preferred binding domain created by the non-polar face of the α-helix, are much more retentive than peptides of the same composition but lacking the preferred binding domain. Similar results were reported by Steiner *et al.* [45], who examined the reversed-phase retention behaviour of a six-helix bundle template-assembled synthetic protein (TASP) molecule and its amphipathic building blocks.

3.3. Correlation of single-stranded amphipathic α-helical peptides with their stability in solution

Fig. 2 shows the sequences of peptide analogues LVd and LId (Fig. 1, top) represented as helical nets, with the hydrophobic faces of the peptides (made up of hydrophobic residues in positions a and d of the heptad repeat) lying between the dotted lines. The only difference between the two analogues lies in the substitution of valine at residue numbers 12, 19 and 26 (all at position d of the heptad sequence) in

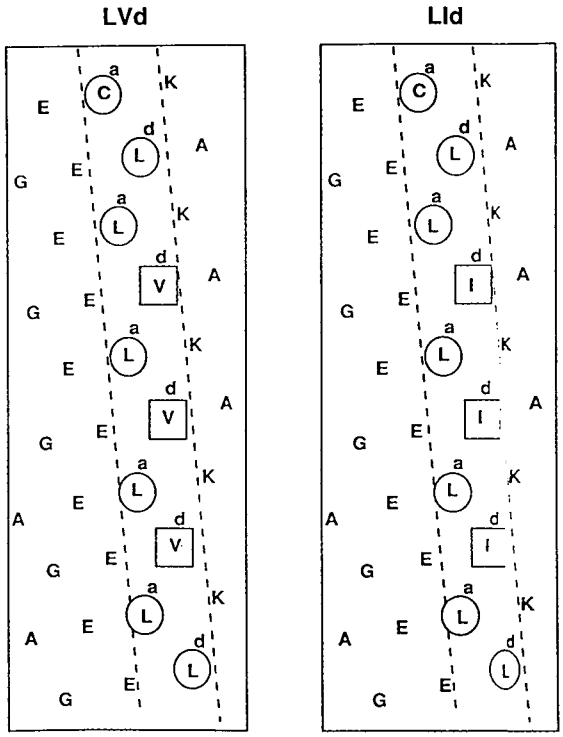

Fig. 2. Sequences of amphipathic α-helical peptides LVd and LId represented as α-helical nets. The radius of the α-helix is taken as 2.5 Å with 3.6 residues per turn, a residue translation of 1.5 Å, and thus a pitch of 5.4 Å. The area between the dotted lines represents the hydrophobic domain of the amphipathic α-helix containing hydrophobic (circled or boxed) residues only. These two peptides differ only in the boxed residues within this domain, containing either valine (LVd) or isoleucine (LId) at the positions shown.

peptide LVd (Fig. 2, left) by isoleucine in peptide LId (Fig. 2, right). The hydrophobicity of isoleucine, as expressed by hydrophobicity coefficients obtained from RPLC peptide retention data [46], is greater than that of valine at pH 2 and pH 7. Thus, it would be expected that peptide LId would have a more hydrophobic face along the helix than peptide LVd, and be more retentive on binding to a reversed-phase column.

Fig. 3 shows the reversed-phase elution profiles of the two peptides, under reducing conditions (to ensure no disulphide bridge formation), at pH 2 and pH 7. As expected, in both cases the isoleucine-substituted analogue, LId, was retained longer on the column than the valine-substituted analogue, LVd. The peptides are eluted earlier at pH 7 compared to pH 2 due to the increased overall hydrophilicity of the peptides as the glutamic acid residues are deprotonated (become negatively charged) at the higher pH value. Temperature denaturation of the individual α-helical analogues in 50% TFE (a helix-inducing solvent) was now carried out (this denaturation monitored by circular dichroism) and the results compared to their reversed-phase retention times. Apart from its helix-inducing properties, the presence of 50% TFE also serves to disrupt coiled-coil structure and maintain the peptides as monomeric α-helical strands. From the thermal denaturation profiles shown in Fig. 4, peptide LId is clearly more stable in solution than peptide LVd, with $t_{1/2}$ values (the temperature at which the α-helicity of the peptides is reduced by 50%) of 42.2°C (LId) and 36.7°C (LVd). Hence, the temperature denaturation behaviour of the two amphipathic α-helical analogues (Fig. 4) correlates very well with their comparative retention behaviour during RPLC (Fig. 3); or, to put it another way, the hydrophobicity of the non-polar faces of the peptides, as expressed by their retentiveness during RPLC, correlates well with their helical stability.

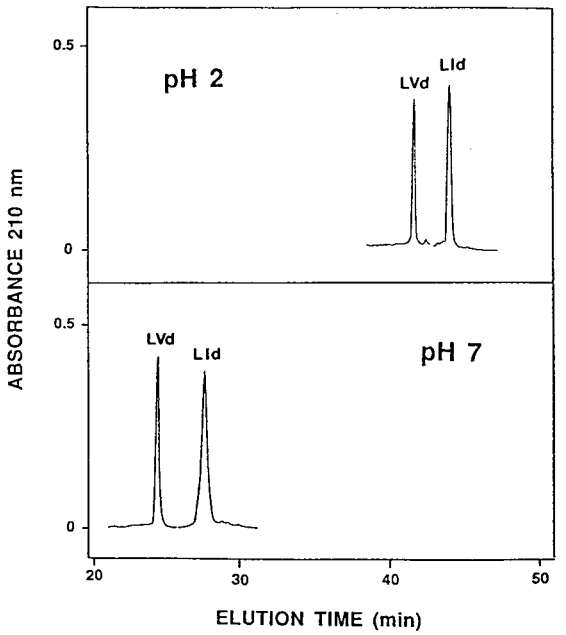

Fig. 3. Reversed-phase chromatography of single-stranded amphipathic α-helical peptides at pH 2 (top panel) and pH 7 (lower panel). The sequences of peptides LVd and LId are shown in Figs. 1 and 2.

3.4. Correlation of stability of two-stranded amphipathic α-helical coiled coils with retention behaviour during RPLC

Since hydrophobicity is a general parameter of protein folding and stability, it might be supposed that the relative hydrophobicity of an amphipathic helix as expressed by its strength of adsorption to a hydrophobic stationary phase may reflect the strength of interchain interactions in the native protein, *i.e.*, the more hydrophobic or amphipathic the helix, the greater the stability of interchain hydrophobic interactions. Since, from Fig. 3, the hydrophobicity of the non-polar face of LId was shown to be of a greater magnitude than that of LVd, the stability of the LId–LId coiled coil would be expected to be more stable than the LVd–LVd coiled-coil structure. Fig. 5 shows the Gdn·HCl denaturation profiles of the two oxidized coiled coils at pH 7. Clearly, as expected, the stability of the isoleucine-substituted coiled coil is more stable than the valine-substituted analogue, with $[\text{Gdn·HCl}]_{1/2}$ (Gdn–HCl concentration required for 50% loss of helicity) values of 4.8 and 1.5 *M*, respectively.

The concept of probing the stability of such

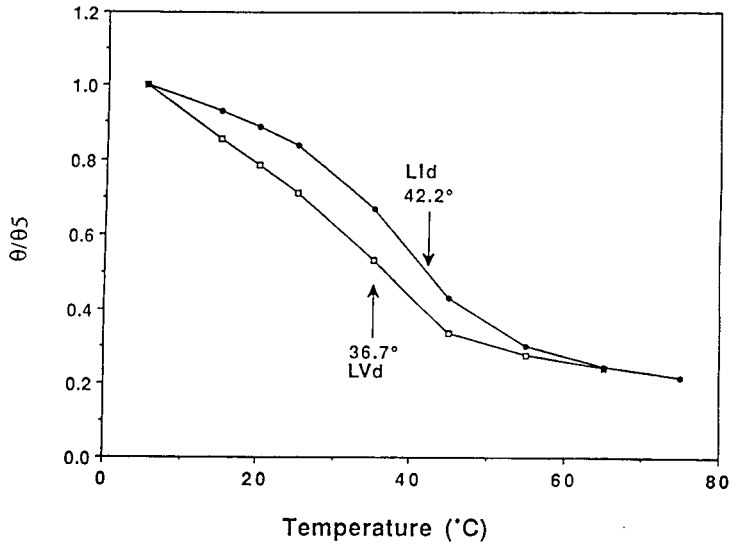

Fig. 4. Thermal melting profiles of single-stranded amphipathic α-helical peptides in 0.1 *M* KCl + 50 m*M* potassium phosphate buffer–trifluoroethanol (1:1, v/v) at pH 7. The sequences of peptides LVd (□) and LId (●) are shown in Figs. 1 and 2. θ/θ_5 represents the ratio of the ellipticity at 220 nm at the indicated temperature to the ellipticity at 5°C.

model coiled coils by RPLC was now taken a step further by examining the retention behaviour of a series of synthetic peptide analogues, where two residues at a time were substituted in the hydrophobic face of the amphipathic helix. Thus, two leucines at residue numbers 16 and 19 (positions a and d, respectively, of the central heptad) were replaced by hydrophobic amino acids isoleucine (peptide I), valine (V), phenylalanine (F) or tyrosine (Y). The leucine-

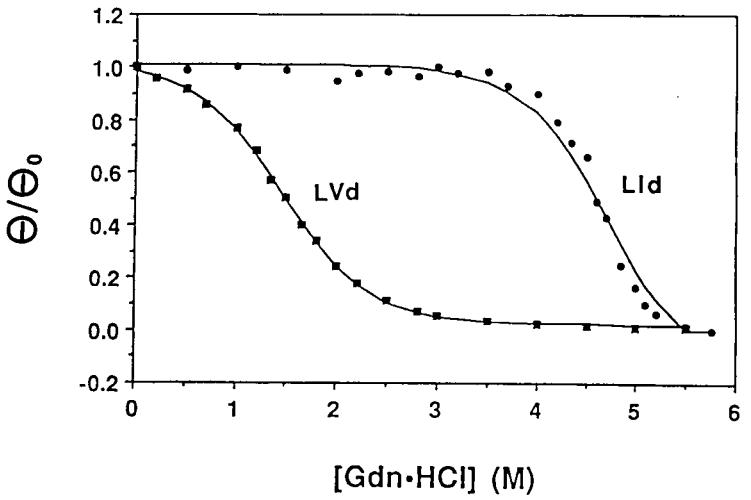

Fig. 5. Guanidine hydrochloride (Gdn · HCl) denaturation profiles of two-stranded α-helical coiled coils of amphipathic peptides LVd (■) and LId (●) in 0.1 *M* KCl, 50 m*M* potassium phosphate buffer at pH 7 and 20°C. θ/θ_0 represents the ratio of molar ellipticity at 220 nm at the indicated molarity of Gdn · HCl to the ellipticity in the absence of Gdn · HCl. The oxidized peptide pairs of LVd and LId (sequences shown in Figs. 1 and 2) are linked by a disulphide bridge at position 2 and 2′ of the sequence.

substituted ("native") analogue was denoted L (Fig. 1).

Fig. 6 compares the reversed-phase elution profiles of the leucine (top) and phenylalanine (bottom) analogues under reducing conditions (L_r, F_r) or under oxidized conditions (L_o, F_o). Under reducing conditions, the two analogues L_r and F_r bind as monomeric α-helices. Under oxidized conditions, it may be expected that the disulphide-bridged dimers (L_o, F_o) would be eluted later than their respective single-stranded α-helices (assuming denaturation of the coiled-coil structure by the hydrophobic stationary phase), since the overall hydrophobicity has been doubled. However, from Fig. 6, it can be seen that the disulphide-bridged dimers are, in fact, being eluted prior to their monomeric forms. This observation can be accounted for if there is little denaturation of the coiled-coil structure, the stability of which is considerably enhanced by the presence of the disulphide bridge at position 2 of the peptide sequence. Thus, there is incomplete exposure of the hydrophobic residues on the interacting hydrophobic faces of the amphipathic helices to the reversed-phase matrix, *i.e.*, the hydrophobes are buried in the coiled coil making the dimers less hydrophobic than the respective reduced monomers. The more stable the coiled coil, the more hydrophobic surface area of each α-helix is buried and, hence, the greater the difference in retention time between the single-stranded α-helix and the disulphide-bridged coiled coil. Thus, in the case of the Phe analogue coiled coil (F_o), it is less stable than the Leu analogue coiled coil (L_o), reflecting the preferred hydrophobic interactions of leucine compared to phenylalanine; thus, the *difference* in retention time between the single-stranded amphipathic α-helix and its respective two-stranded oxidized coiled coil is less for F compared to L, since the coiled-coil structure of the former (F_o) is unfolded to a greater extent than the latter (L_o) by the hydrophobic stationary phase and, hence, exposes more of its hydrophobic surface area to the reversed-phase matrix.

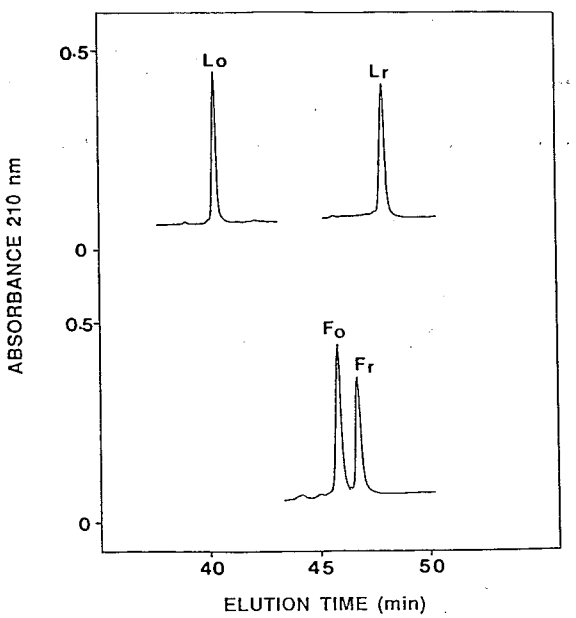

Fig. 6. Comparison of reversed-phase chromatography of single-stranded amphipathic α-helical peptides and double-stranded α-helical coiled-coil peptides at pH 7. The sequences of peptides L and F are shown in Fig. 1. The subscripts "o" and "r" denote oxidized (double-stranded, *i.e.*, linked by a disulphide bridge) and reduced (*i.e.*, single-stranded) forms of the peptides.

Similar observations of the relative RPLC retention times of the oxidized two-stranded dimers *versus* those of the respective monomeric α-helices were now made for the I, V and Y analogues (Fig. 1). Fig. 7 shows a plot of the free energy of unfolding (ΔG) for each coiled-coil protein (derived from Gdn · HCl denaturation data) *versus* the difference in reversed-phase retention time between reduced monomeric α-helix and the oxidized coiled coil for peptides L, F, I, V, Y. The ΔG term represents the stability of the coiled-coil protein and the excellent correlation of the ΔG values for each coiled-coil analogue with the difference in retention times of respective dimeric and monomeric analogues is quite clear. It should be noted that the unfolding of these model coiled coils is a reversible process [26]; furthermore, through thermodynamic characterization of the structural stability of the coiled-coil region of the basic region leucine zipper (bZIP) transcription factor GCN4, it has been indicated that the unfolding of this structural motif is a two-state process [47].

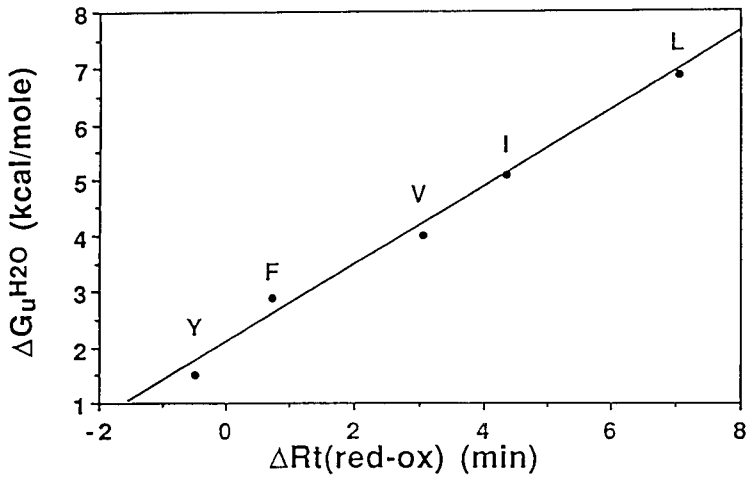

Fig. 7. Free energy of unfolding of model proteins *versus* the difference in reversed-phase retention time between the reduced monomeric amphipathic α-helical peptides and the oxidized dimeric α-helical coiled coils [ΔRt (redox)]. $\Delta G_u^{H_2O}$ is the free energy of unfolding in the absence of guanidine hydrochloride and is estimated by extrapolating the free energy of unfolding at each individual concentration of guanidine hydrochloride (ΔGu) to zero concentration assuming that they are linearly related [51]. The sequences of peptide analogues denoted Y, F, V, I and L are shown in Fig. 1.

3.5. Role of RPLC in explaining the effect of pH on protein stability

For more than 25 years, there has been no explanation as to why two-stranded α-helical coiled-coils are more stable at low pH (*e.g.*, pH 2) compared to pH 7 [14,16,19,48,49]. To investigate this problem with our model system, two peptide analogues, denoted EKQ and EKE (Figs. 1 and 8), were synthesized and their reversed-phase retention behaviour compared with their stability in solution at low and neutral pH.

Fig. 8 (left) shows a cross-section of the peptide analogues presented as helical wheels. The hydrophobic (leucine) residues on the non-polar face of each amphipathic α-helix in positions a and d are identical, *i.e.*, the hydrophobic surfaces of each α-helix are identical. The only difference between the two helices is the glutamic acid (peptide EKE) or glutamine (EKQ) residue at position g on the helix (denoted by arrow). The lysine and glutamic acid residues at positions e and b, respectively, serve to stabilize the individual α-helices by intra-chain attractions. It has been demonstrated previously [50] that ion pairs may form between glutamic acid and lysine residues in i, i + 3 or i + 4 positions along the α-helix, with the i + 4 interactions being dominant. From Fig. 8 (right) which presents the analogues as helical nets, it can be seen that the glutamic acid (EKE) and glutamine (EKQ) residues at position g on the helix (Fig, 8, left) are closely adjacent to the hydrophobic face of the helix (between the dotted lines). The arrows denote the intrachain attractions along the hydrophilic face of each helix.

The retention behaviour of the two peptide analogues during RPLC was now investigated at pH 2 and pH 7, the results of which are shown in Fig. 9. At pH 2, peptide EKE is eluted later than peptide EKQ; in contrast, at pH 7, the elution order is reversed with peptide EKE now being eluted considerably earlier than peptide EKQ. In addition, change in pH had little effect on the retention time of peptide EKQ. These results can be summarized as follows: in order of decreasing retention time, *i.e.*, decreasing hydrophobicity of the peptide hydrophobic face interacting with the reversed-phase matrix,

$$\text{EKE,pH2} > \text{EKQ,pH2} = \text{EKQ,pH7} > \text{EKE,pH7}$$

It is interesting to note that, if only the hydro-

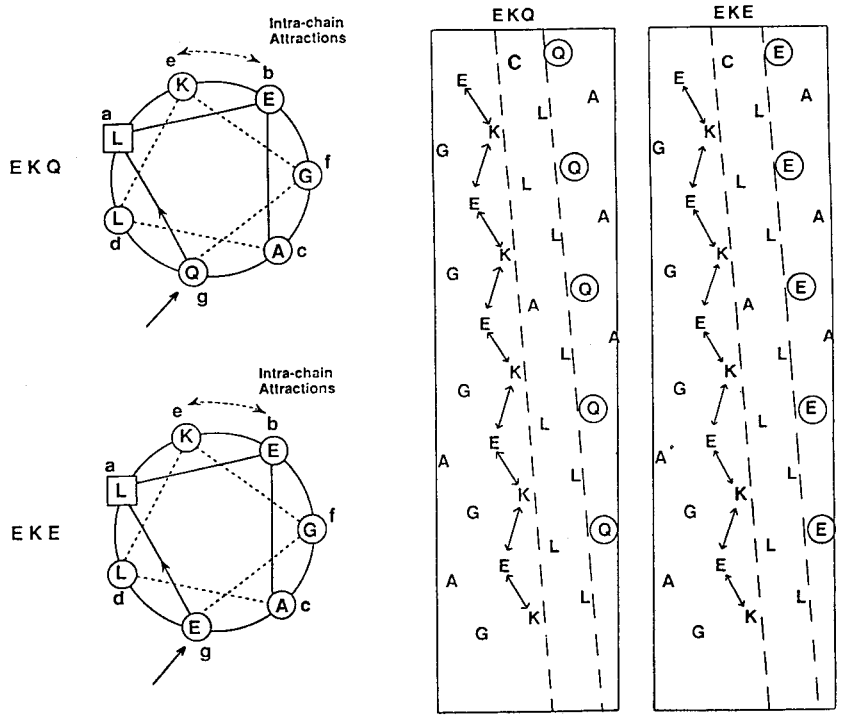

Fig. 8. Left: cross-sections of amphipathic α-helical peptides EKQ and EKE represented as helical wheels, looking from the N-terminal end. The dotted lines represent potential intrachain electrostatic interactions between positively charged lysine at position e and a negatively charged glutamic acid at position b. Right: sequences of amphipathic α-helical peptides EKQ and EKE represented as α-helical nets (see Fig. 2 for details). The arrows represented potential intrachain electrostatic interactions between lysine and glutamic acid as noted above. The substituted (glutamine and glutamic acid) residues at position g (see helical wheel presentation) are circled. The linear sequences of peptides EKQ and EKE are shown in Fig. 1.

phobic areas between the dotted lines on the helical nets (Fig. 8, right) were interacting with the hydrophobic stationary phase, then a substitution of glutamine for glutamic acid at position g on the helix (Fig. 8, left) should have no effect on retention behaviour of the peptide analogue at low pH, *i.e.*, the retention times of EKE and EKQ should be the same at pH 2, where glutamic acid, as well as glutamine, is electroneutral. Clearly, since the two peptides are well separated at pH 2 (Fig. 9), the residue at position g on the helix is contributing to the retention process, indicating that the surface area of the helices interacting with the hydrophobic stationary phase is larger than at first surmised. In fact, O'Shea *et al.* [44], during studies on the X-ray structure of the GCN4 leucine zipper coiled coil, noted that the methylene groups of the residue side-chains at positions e and g also contact the hydrophobic side-chains at positions a and d, protecting the hydrophobic interface from solvent. Thus, the hydrophobic interface is actually formed by side-chains of four residues at positions a, d, e and g of the heptad repeat. The retention behaviour during RPLC of the two peptides can thus be rationalized by considering the effect of pH on glutamic acid. At low pH, a protonated glutamic acid residue is more hydrophobic than glutamine [46], which agrees with the longer retention time of peptide EKE compared to peptide EKQ at pH 2 (Fig. 9). However, at pH 7, an ionized glutamic acid residue is considerably more hydrophilic than a glutamine residue [46], which now agrees with peptide EKE being eluted prior to peptide EKQ at pH 7 (Fig. 9). It should be noted that protona-

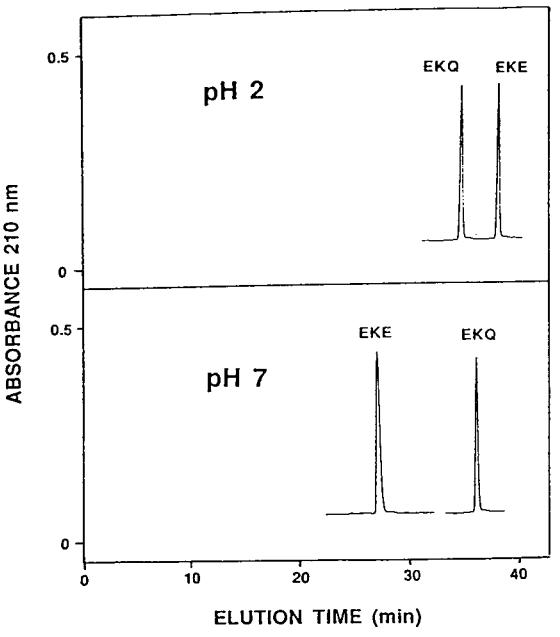

Fig. 9. Effect of pH on reversed-phase chromatographic profiles of single-stranded amphipathic α-helical peptides. The sequences of peptides EKQ and EKE are shown in Figs. 1 and 8.

tion or deprotonation of the glutamic acid residue at position b on the helix (Fig. 8, left), and which is considerably distant from the preferred binding domain, has little or no effect on the retention behaviour of the peptide analogues, as evidenced by the almost identical retention behaviour of peptide EKQ at both pH 2 (neutral, protonated Glu residues) and pH 7 (ionized Glu residues).

The stability of the single-stranded α-helices was now investigated at low and high pH, by temperature denaturation studies of the α-helices in 50% TFE. Loss of helical content with increasing temperature was again monitored by circular dichroism. The results, shown in Fig. 10, can be summarized as follows: in order of decreasing stability,

$$\text{EKE,pH3} > \text{EKQ,pH3} = \text{EKQ,pH7} > \text{EKE,pH7}$$

Clearly, these results correlate very well with the retention behaviour of the peptides illustrated in Fig. 9, *i.e.*, increasing hydrophobicity of the peptides, as expressed by increasing retention time, corresponds with increasing peptide stabili-

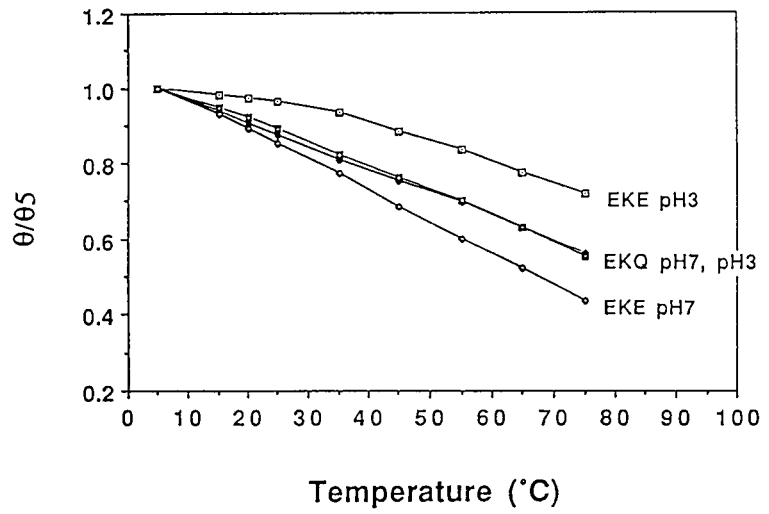

Fig. 10. Thermal melting profiles of single-stranded amphipathic α-helical peptides in 0.1 *M* KCl + 50 m*M* potassium phosphate buffer–trifluoroethanol (1:1, v/v) at pH 3 and pH 7. The sequences of peptides EKQ and EKE are shown in Figs. 1 and 8. θ/θ_5 represents the ratio of the ellipticity at 220 nm at the indicated temperature to the ellipticity at 5°C.

ty in solution. Thus, the protonation of the glutamic acid residue adjacent to the hydrophobic face of peptide EKE (Fig. 8, right) at pH 2 is stabilizing the helix, *i.e.*, the amphipathicity of the helix is being increased. Again, it should be noted that the glutamic acid residue in position b on the helix (Fig. 8, left) which is involved in an ion pair (at pH 7) with lysine at position e, and which is not adjacent to the hydrophobic face of the helix (Fig. 8, right), has no effect on peptide stability with a change in pH, as shown by the essentially identical temperature stability profiles of peptide EKQ at both pH 3 and pH 7 (Fig. 10).

Considering the importance of interchain ionic interactions (e–g′ and e′–g) to stabilizing a parallel and in-register structure of a two-stranded α-helical coiled coil [44], it may be expected that a reduction in pH to pH 2, thereby protonating glutamic acid residues taking part in interchain ion pairs, would have a destabilizing effect on coiled-coil stability. However, from the present study, it is clear that the loss of these ionic interactions between the two helices is more than compensated for by the increase in hydrophobicity of the hydrophobic interface between the chains as glutamic acid in this interface is protonated.

4. Conclusions

In summary, this study represents our initial survey on the potential of RPLC for use as a probe of hydrophobic interactions involved in protein folding and protein stability. By applying RPLC to a *de novo* designed model protein system, namely a two-stranded amphipathic α-helical coiled coil, it was shown that the reversed-phase retention behaviour of various synthetic analogues of monomeric α-helices and dimeric coiled-coil structures correlated well with their stability in solution. In addition, light has now been shed on the long-standing question of why coiled coils, an important structural motif in many biological systems, are more stable at low pH compared to physiological pH values. While not suggesting that RPLC of amphipathic α-helices and the corresponding dimeric coiled-coil structures is an infallible reflection of all hydrophobic interactions stabilizing native proteins, this technique nonetheless shows great promise as a useful (and extremely rapid) complementary technique for understanding peptide/protein interactions.

5. Acknowledgements

This work was supported by the Medical Research Council of Canada Group in Protein Structure and Function, and the Protein Engineering Network of Centres of Excellence program supported by the Government of Canada.

References

[1] C.T. Mant and R.S. Hodges (Editors), *High-Performance Liquid Chromatography of Peptides and Proteins: Separation, Analysis and Conformation*, CRC Press, Boca Raton, FL, 1991.
[2] S.A. Cohen, K.P. Benedek, S. Dong, Y. Tapuhi and B.L. Karger, *Anal. Chem.*, 56 (1984) 217.
[3] K. Benedek, S. Dong and B.L. Karger, *J. Chromatogr.*, 317 (1984) 227.
[4] S.A. Cohen, K. Benedek, Y. Tapuhi, J.C. Ford and B.L. Karger, *Anal. Biochem.*, 144 (1985) 275.
[5] R.H. Ingraham, S.Y.M. Lau, A.K. Taneja and R.S. Hodges, *J. Chromatogr.*, 327 (1985) 77.
[6] S.-L. Wu, K. Benedek and B.L. Karger, *J. Chromatogr.*, 359 (1986) 3.
[7] E. Watson and W.-C. Kenney, *J. Chromatogr.*, 606 (1992) 165.
[8] R. Rosenfeld and K. Benedek, *J. Chromatogr.*, 632 (1993) 29.
[9] K. Benedek, *J. Chromatogr.*, 646 (1993) 91.
[10] A.W. Purcell, M.I. Aguilar and M.T.W. Hearn, *J. Chromatogr.*, 593 (1992) 103.
[11] A.J. Sadler, R. Micanovic, G.E. Katzenstein, R.V. Lewis and C.R. Middaugh, *J. Chromatogr.*, 317 (1984) 93.
[12] R.S. Hodges, A.K. Saund, P.C.S. Chong, S.A. St.-Pierre and R.E. Reid, *J. Biol. Chem.*, 256 (1981) 1214.
[13] J.A. Talbot and R.S. Hodges, *Acc. Chem. Res.*, 15 (1982) 224.
[14] S.Y.M. Lau, A.K. Taneja and R.S. Hodges, *J. Biol. Chem.*, 259 (1984) 13253.
[15] S.Y.M. Lau, A.K. Taneja and R.S. Hodges, *J. Chromatogr.*, 317 (1984) 129.

[16] R.S. Hodges, P.D. Semchuk, A.K. Taneja, C.M. Kay, J.M.R. Parker and C.T. Mant, *Pept. Res.*, 1 (1988) 19.
[17] N.E. Zhou, C.T. Mant and R.S. Hodges, *Pept. Res.*, 3 (1990) 8.
[18] R.S. Hodges, N.E. Zhou, C.M. Kay and P.D. Semchuk, *Pept. Res.*, 3 (1990) 123.
[19] N.E. Zhou, B.-Y. Zhu, C.M. Kay and R.S. Hodges, *Biopolymers*, 32 (1992) 419.
[20] N.E. Zhou, C.M. Kay and R.S. Hodges, *J. Biol. Chem.*, 267 (1992) 2664.
[21] R.S. Hodges, *Curr. Biol.*, 2 (1992) 122.
[22] N.E. Zhou, C.M. Kay and R.S. Hodges, *Biochemistry*, 31 (1992) 5739.
[23] B.-Y. Zhu, N.E. Zhou, P.D. Semchuk, C.M. Kay and R.S. Hodges, *Int. J. Pept. Protein Res.*, 40 (1992) 171.
[24] N.E. Zhou, C.M. Kay and R.S. Hodges, *Biochemistry*, 32 (1993) 3178.
[25] B.-Y. Zhu, N.E. Zhou, C.M. Kay and R.S. Hodges, *Protein Sci.*, 2 (1993) 383.
[26] O.D. Monera, N.E. Zhou, C.M. Kay and R.S. Hodges, *J. Biol. Chem.*, 268 (1993) 19218.
[27] C.T. Mant, N.E. Zhou and R.S. Hodges, in R.M. Epand (Editor), *The Amphipathic Helix*, CRC Press, Boca Raton, FL, 1993, p. 39.
[28] J.L. Cornette, K.B. Cease, H. Margalit, J.L. Spouge, J.A. Berzofsky and C.D. DeLisi, *J. Mol. Biol.*, 195 (1987) 659.
[29] J.P. Segrest, H. DeLoof, J.G. Dohlman, C.G. Brouillette and G.M. Anantharamaiah, *Proteins: Struct. Function Gen.*, 8 (1990) 103.
[30] F.H.C. Crick, *Acta Crystallogr.*, 6 (1953) 689.
[31] C. Cohen and D.A.D. Parry, *Trends Biochem. Sci.*, 11 (1986) 245.
[32] J. Sodek, R.S. Hodges, L.B. Smillie and L. Jurasek, *Proc. Natl. Acad. Sci. U.S.A.*, 69 (1972) 3800.
[33] E.T. Kaiser and F.J. Kezdy, *Proc. Natl. Acad. Sci. U.S.A.*, 80 (1983) 1137.
[34] J. Taylor, D.G. Osterman, R.J. Miller and E.T. Kaiser, *J. Am. Chem. Soc.*, 103 (1984) 6965.
[35] A. Argiolas and T.J. Pisano, *J. Biol. Chem.*, 260 (1985) 1437.
[36] A.W. Bernheimer and B. Rudy, *Biochim. Biophys. Acta*, 864 (1986) 123.
[37] M. Zasloff, B. Martin and H.C. Chen, *Proc. Natl. Acad. Sci. U.S.A.*, 85 (1988) 910.
[38] E. Soravuia, G. Martini and M. Zasloff, *FEBS Lett.*, 228 (1988) 337.
[39] A. Lupas, M. van Dyke and J. Stock, *Science*, 252 (1991) 1162.
[40] R.A. Houghten and J.M. Ostresh, *Biochromatography*, 2 (1987) 80.
[41] J.M. Ostresh, K. Büttner and R.A. Houghten, in C.T. Mant and R.S. Hodges (Editors), *High-Performance Liquid Chromatography of Peptides and Proteins: Separation, Analysis and Conformation*, CRC Press, Boca Raton, FL, 1991, p. 633.
[42] Cs. Horváth, W. Melander and I. Molnár, *J. Chromatogr.*, 125 (1976) 129.
[43] R.S. Hodges, J. Sodek, L.B. Smillie and L Jurasek, *Cold Spring Harbor Symp. Quant. Biol.*, 37 (1972) 299.
[44] E.K. O'Shea, J.D. Klemm, P.S. Kim and T. Alber, *Science*, 254 (1991) 539.
[45] V. Steiner, M. Schär, K.O. Bornsen and M. Mutter, *J. Chromatogr.*, 586 (1991) 43.
[46] D. Guo, C.T. Mant, A.K. Taneja, J.M.R. Parker and R.S. Hodges, *J. Chromatogr.*, 359 (1986) 499.
[47] K.S. Thompson, C.R. Vinson and E. Freire, *Biochemistry*, 32 (1993) 5491.
[48] S. Lowey, *J. Biol. Chem.*, 240 (1965) 2421.
[49] M. Noelken and A. Holtzer, in J. Gergely (Editor), *Biochemistry of Muscle Contraction*, Little, Brown & Co., Boston, MA, 1964, p. 374.
[50] S. Marqusee and R.L. Baldwin, *Proc. Natl. Acad. Sci. U.S.A.*, 84 (1987) 8898.
[51] C.N. Pace, *Methods Enzymol.*, 131 (1986) 266.

ELSEVIER

Journal of Chromatography A, 676 (1994) 17–31

JOURNAL OF CHROMATOGRAPHY A

A comparative study of the retention behaviour and stability of cytochrome *c* in reversed-phase high-performance liquid chromatography

K.L. Richards, M.I. Aguilar *, M.T.W. Hearn

Department of Biochemistry and Centre for Bioprocess Technology, Monash University, Wellington Road, Clayton 3168, Australia

Abstract

The retention behaviour of equine, tuna, canine and bovine cytochrome *c* and the corresponding equine and tuna apocytochrome *c* has been investigated using reversed-phase gradient elution chromatographic procedures. A range of operating temperatures between 5 and 85°C were utilised to monitor the influence of protein unfolding on the corresponding retention parameters. Chromatographic measurements were obtained with both an *n*-octadecyl (C_{18}) and *n*-butyl (C_4) sorbent in order to investigate the role of ligand structure on protein retention. The results demonstrated significant differences in the S and log k_0 values between all cytochrome *c* proteins despite the very high degree of sequence homology. These observations suggest that specific amino acid substitutions are directly involved in the chromatographic contact region of the cytochrome *c* molecules. In addition, the prosthetic haem moiety was also shown to provide a significant structural role in terms of relative protein stability under reversed-phase chromatographic conditions. Overall, the results of the present study further demonstrate the utility of interactive modes of chromatography to provide information on physicochemical aspects of protein–surface interactions.

1. Introduction

The success of reversed-phase high-performance liquid chromatography (RP-HPLC) in the analysis and purification of low-molecular-mass compounds and small peptides is increasingly finding parallels for the analysis of proteins. However, the potential loss of biological activity, the formation of multiple peaks of otherwise pure samples and lower levels of recovery arising from protein denaturation or conformational changes remain the main factors which contribute to the less common use of preparative RP-HPLC compared to ion-exchange and affinity chromatographic methods for protein purification. A number of experimental parameters have been established in order to characterise the interactive behaviour of peptides and proteins in RP-HPLC. Experimentally derived Z or S values, which are empirical terms describing the magnitude of the chromatographic contact region and which are calculated from the slope of isocratic or gradient retention plots, *i.e.* from plots of the logarithmic capacity factor log k, *versus* the reciprocal of the molar concentration $1/[c]$, or the molar fraction, ψ, of the organic modifier have been correlated with various physicochemical parameters of peptides and pro-

* Corresponding author.

0021-9673/94/$07.00
SSDI 0021-9673(94)00092-N

teins [1–6]. In addition, the influence of column temperature, solvent strength and the nature of the *n*-alkyl ligand on peptide retention behaviour has also been studied [8,9]. Investigations have also described the characterisation of protein folding and stability in reversed-phase chromatographic systems [9–19]. In particular, it has been established that the Z/S value of a protein often increases with the degree of denaturation as a result of the formation of (a) larger chromatographic contact region(s) in the unfolded species [7,16]. These studies have therefore established that conformational intermediates with different folded states can give rise to different retention behaviour.

In the present study, the effect of gradient time, operating temperature and type of immobilised *n*-alkyl ligand on the retention behaviour of various closely related cytochrome c species [*i.e.* equine (horse heart), tuna (tuna heart), canine (dog heart) and bovine (cattle heart)] and the corresponding equine and tuna apocytochrome *c* have been examined. In order to validate the relationship between protein conformation and the corresponding retention parameters in RP-HPLC, the retention behaviour of this series of cytochrome *c*-related proteins was monitored under chromatographic conditions chosen to manipulate secondary and tertiary structure.

2. Materials and methods

2.1. Chemicals and reagents

Acetonitrile (HPLC grade) was obtained from Mallinckrodt (Paris, KY, USA) and trifluoroacetic acid (TFA) was purchased from Pierce (Rockford, IL, USA). Water was quartz-distilled and deionised in a Milli-Q system (Millipore, Bedford, MA, USA). Equine (horse heart), tuna (tuna heart), canine (dog heart) and bovine (cattle heart) cytochrome *c* were obtained from Sigma (St. Louis, MO, USA). All other reagents were analytical reagents or the best available grade. All mobile phases were filtered prior to use with a 0.2-μm Millipore Durapore filter.

2.2. Apparatus

All chromatographic measurements of the retention behaviour were performed on a Hewlett-Packard (Waldbronn, Germany) Model HP 1090M liquid chromatograph with a binary-drive solvent-delivery system, equipped with a HP 79847A autosampler and a HP 79846A autoinjector. Temperature was controlled by a HPW90A heated column compartment or for lower temperatures by immersion of the column in a column water jacket coupled to a recirculating cooler (FTS Systems, NY, USA). All measurements were routinely monitored at 215 and 400 nm utilising a HP 79880A diode array detector. Chromatographic analysis and peak integration were carried out by a HP 9153C professional computer with the HP79995A "Chemstation" operating software. Further peak analysis was performed using the "Bandwidth" software developed within this laboratory and compatible with the "Chemstation" software package.

Reversed-phase chromatography was carried out with Bakerbond Widepore *n*-octadecyl silica (C_{18}) and *n*-butyl silica (C_4) stationary phases (J.T. Baker, Phillipsburg, NJ, USA) with nominal particle diameters of 5 μm and an average pore size of 30 nm, packed into 250 × 4.6 mm I.D. stainless-steel cartridges. All pH measurements were performed with an Orion Model SA520 pH meter (Orion, Cambridge, MA, USA).

2.3. Chemical preparation of apocytochrome c

Apocytochrome *c* was prepared by modification of the silver sulphate method [20]. To individual solutions of either equine or tuna cytochrome *c* [1 mg/ml, dissolved in 33% (v/v) acetic acid] was added a 60 molar excess of Ag_2SO_4. The reaction mixture was shielded from light and incubated at 37°C for a period of 48 h. Silver was precipitated by acidification with 1 *M* H_2SO_4 and the supernatant transferred to a fresh reaction vessel. The protein was precipitated from the supernatant by the addition of acetone (3.0 ml) and the solution chilled in ice for

approximately 30 min. The acetone was decanted and the protein pellet was dried under a stream of nitrogen. The protein was redissolved in 0.09% TFA in acetonitrile–water (50:50) and stored at 4°C.

2.4. Chromatographic procedures

Bulk solvents were filtered and degassed by sparging with helium. Linear gradient elution was performed using 0.1% TFA in Milli-Q water and 0.09% TFA in acetonitrile–water (50:50) over gradient times of 30, 45, 60, 90 and 120 min with a flow-rate of 1 ml/min at temperatures of 5, 10, 20, 30, 37, 45, 55, 65, 70, 75, 80 and 85°C. All data points were derived from at least duplicate measurements with retention times between replicates typically varying by less than 1%. The concentrations of protein solutions were 1.0 mg/ml and injection sizes ranged between 2–10 μl. The column dead volume was taken as the retention time of the non-interactive solute, sodium nitrate.

2.5. Computational procedures

The various chromatographic parameters log $\bar{k}$, $\bar{\psi}$, S and log k_0 were calculated using the Pek-n-ese program [3] written in Pascal for IBM-compatible computers. Statistical analysis involved ANOVA linear regression analysis was carried out utilising Sigma Plot (version 5.0) graphics software for IBM-compatible computers.

2.6. Computer analysis of protein structures

The surface distribution of amino acid residues of different cytochrome *c*'s were visualised using a Silicon Graphics Model 4D IRIS workstation using the INSIGHT II operating software from Biosym Technologies (San Diego, CA, USA). The amino acid sequences of each cytochrome *c* molecule were obtained from the PSD-Kyoto protein sequence data base. The atomic coordinates for tuna cytochrome *c* were obtained from the Brookhaven data bank. The tertiary structure of equine, bovine and canine cytochrome *c* were predicted from the X-ray crystallographic structure of tuna cytochrome *c* by substitution of the appropriate amino acid residues in the three-dimensional structure followed by refinement of the structure using molecular dynamics and energy minimisation [21].

3. Results and discussion

3.1. Retention behaviour of cytochrome c on the C_{18} sorbent

Linear solvent strength (LSS) concepts have been widely used in RP-HPLC to derive chromatographic parameters related to the interaction of the solute molecule with the sorbent [1,3–7]. Thus, under regular reversed-phase gradient elution conditions, linear relationships are frequently observed between the logarithm of the median capacity factor, log $\bar{k}$, and the median organic mole fraction, $\bar{\psi}$, with the experimental data readily analysed according to the following empirical expression

$$\log \bar{k} = \log k_0 - S\bar{\psi} \quad (1)$$

The S and log k_0 values can be determined by linear regression analysis of log $\bar{k}$ *versus* $\bar{\psi}$ experimental data according to Eq. 1. Previously, the S and log k_0 values have been related, via the solvophobic theory, to the magnitude of the chromatographic contact area established by the protein solute and the affinity which the solute has for the chromatographic ligands [22]. In the present investigation, gradient elution data were obtained for a series of cytochrome *c* molecules as part of our on-going studies on the mechanism of interaction of proteins in RP-HPLC. In particular, the S and log k_0 values were determined for equine, tuna, canine and bovine cytochrome *c* and the chemically modified proteins, equine apocytochrome *c* and tuna apocytochrome *c*. The amino acid residue differences between these different proteins are listed in Tables 1 and 2. A range of operating temperatures were also utilised to monitor the influence of protein unfolding on the corresponding retention param-

Table 1
Differences in amino acid sequences in four cytochrome *c* species

Species	Sequence position number																		
	4	9	22	28	33	44	46	47	54	58	60	61	62	88	89	92	95	100	103	104
Equine	Glu	Ile	Lys	Thr	His	Pro	Phe	Thr	Asn	Thr	Lys	Glu	Glu	Lys	Thr	Glu	Ile	Lys	Asn	Glu
Tuna	*Ala*	*Thr*	*Asn*	*Val*	*Trp*	*Glu*	*Tyr*	*Ser*	*Ser*	*Val*	*Asn*	*Asn*	*Asp*	Lys	*Gly*	*Gln*	*Val*	*Ser*	*Ser*	–
Canine	Glu	Ile	Lys	Thr	His	Pro	Phe	*Ser*	Asn	Thr	*Gly*	Glu	Glu	*Thr*	*Gly*	*Ala*	Ile	Lys	Asn	Glu
Bovine	Glu	Ile	Lys	Thr	His	Pro	Phe	*Ser*	Asn	Thr	*Gly*	Glu	Glu	Lys	*Gly*	Glu	Ile	Lys	Asn	Glu

Italicised amino acids represent the residues which differ from the amino acid sequence of equine cytochrome *c*.

eters. All cytochrome *c* molecules were chromatographed on the *n*-octadecyl (C_{18}) sorbent at five different gradient times ranging between 30 and 120 min at a flow-rate of 1 ml/min at twelve different temperatures ranging between 5 and 85°C. Fig. 1 shows the chromatographic separation of the four cytochrome *c* molecules with a 120-min gradient time at 25°C. It is clear from this chromatogram that significant selectivity differences exist between these closely related proteins. As discussed below and listed in Table 1, there are only three amino acid differences between the equine and bovine cytochrome *c* and five amino acid differences between the equine and canine cytochrome *c*. The high degree of resolution between these protein molecules indicates that these specific amino acid differences play a significant role in the interactive behaviour of these proteins.

In order to further characterise the retention behaviour of these protein molecules, the retention data obtained for each cytochrome *c* related protein were analysed according to the LSS model to derive values for log $\bar{k}$ and $\bar{\psi}$. The log $\bar{k}$ *versus* $\bar{\psi}$ retention plot for equine holocytochrome *c* over the range of temperatures is shown in Fig. 2. Iterative linear regression analysis of the log $\bar{k}$ *versus* $\bar{\psi}$ experimental data yielded the values of the retention parameters *S* and log k_0 at different temperatures. Fig. 3 shows the change in *S* and log k_0 values of the four cytochrome *c* molecules with increasing temperature for each protein chromatographed on the *n*-octadecyl sorbent. Between the temperatures of 5 and 10°C, with the exception of bovine cytochrome *c*, there was a small but significant decrease in the values of both the *S* and log k_0 values. As the temperature increased between 10 and 80°C, a continuous increase in both the *S* and log k_0 values was observed for all proteins. Except for equine cytochrome *c* which showed a continual increase up to 85°C, between

Table 2
Specific differences in the amino acid composition of four cytochrome *c* species

Species	Compared to species	No. of amino acid residues difference
Equine	Tuna	19
Equine	Bovine	3
Equine	Canine	5
Tuna	Bovine	17
Tuna	Canine	18
Bovine	Canine	2

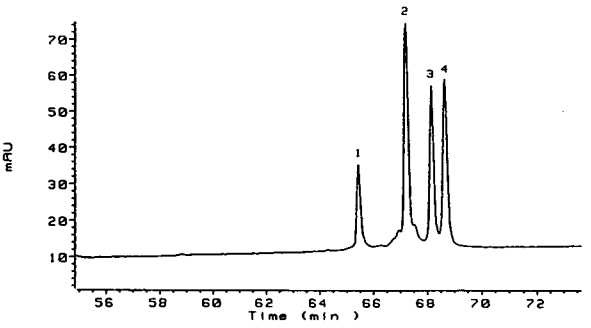

Fig. 1. RP-HPLC chromatogram showing the elution profile of a mixture of (1) bovine, (2) equine, (3) tuna and (4) canine cytochrome *c*. The profile was obtained with a gradient time of 120 min at 25°C. For other chromatographic conditions see the Materials and methods section.

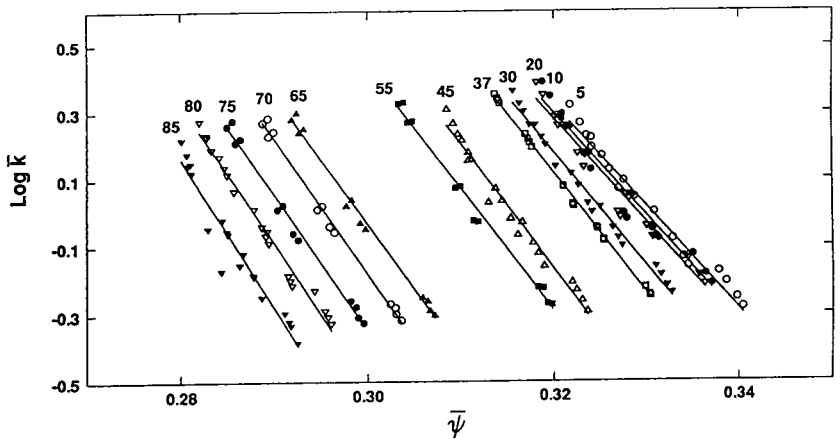

Fig. 2. Plots of log $\bar{k}$ *versus* $\bar{\psi}$ for equine cytochrome *c* chromatographed on a C_{18} sorbent at 12 different temperatures between 5 and 85°C as indicated. For other chromatographic conditions see the Materials and methods section.

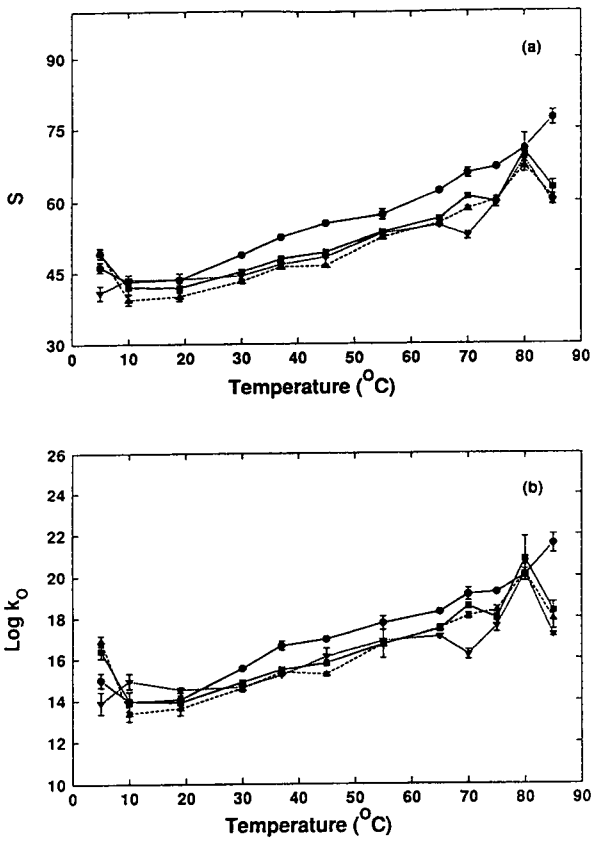

Fig. 3. Dependence of (a) *S* and (b) log k_0 on temperature for each of the holo-cytochrome *c* molecules separated on the C_{18} sorbent. ○ = Equine; □ = tuna; ▲ = canine; ▼ = bovine.

80 and 85°C, both the *S* and log k_0 values for tuna, canine and bovine cytochrome *c* all showed a decrease. If it is recalled that the *S* and log k_0 values represent a measure of the size of the interactive binding region on the surface of the cytochrome *c* protein and its affinity for the stationary phase ligands respectively, then changes in these retention parameters can be related to changes in the structure of the protein which are occurring as a response to increases in the operating temperature. Furthermore, the changes in the *S* value with increasing temperature can be related to the extent of unfolding of the protein structure. The appearance of these retention plots in Fig. 3 can be contrasted with the corresponding data observed for the low-molecular-mass control solutes N-acetyl-L-phenylalanine ethyl ester and penta-L-phenylalanine on the same *n*-octadecyl silica which are shown in Fig. 4. These small solutes have no significant secondary structure and exhibit little change in the magnitude of the *S* value over the entire range of temperatures employed. The corresponding affinity or log k_0 term for these two control solutes demonstrated only a small decrease in value with increased operating temperature, as would also be expected for a conformationally rigid solute. Moreover, as the *S* and log k_0 values obtained for these control

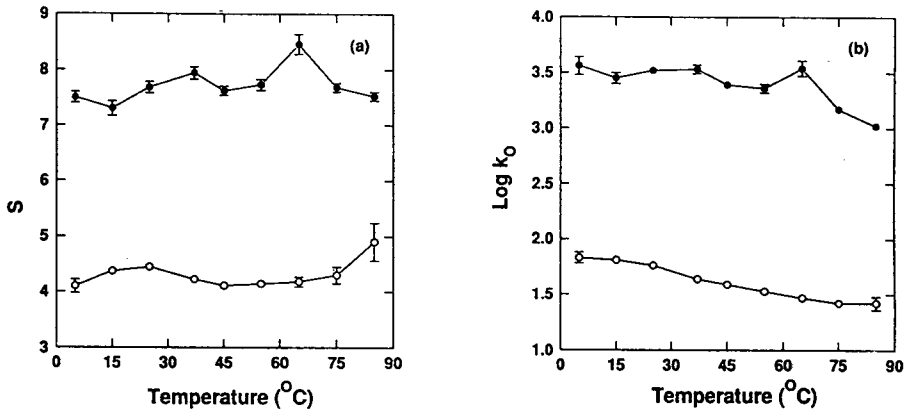

Fig. 4. Dependence of (a) S and (b) log k_0 on temperature for penta-L-phenylalanine (●) and N-acetyl-L-phenylalanine ethyl ester (○) separated on the C_{18} sorbent.

solutes reflected very small changes over the temperatures employed, these results provide evidence that the relative stability and phase characteristics of the sorbent ligands were unchanged with increases in the operating temperature. The changes in the retention data for the cytochrome *c* molecules can thus be related to changes in conformation of these proteins with increases in the operating temperature rather than specific changes in the interactive characteristics of the ligands.

In the low-temperature range 5–10°C, decreases were observed in the experimental S values for three (equine, tuna and canine) cytochrome *c*'s, suggesting a reduction in the contact area of the interactive binding site. The affinity of this interaction was also reduced at 10°C relative to 5°C. At low temperatures, a reduction in the size of the interactive binding region may occur as result of refolding. The experimental data thus suggest that at 5°C the holo-cytochrome *c* molecules may be in a less compact state, compared to that adopted at 10°C. Other studies on the effect of temperature on the three-dimensional structure of equine cytochrome *c* have demonstrated that the cytochrome *c* molecule loses activity at low pH and low temperature arising from the formation of a molten globule state which retains the secondary structural features of the native state, but is characterised by weakened tertiary hydrogen bonding [23–25]. This so-called cold denaturation effect will result in a more expanded tertiary structure with the internalised non-polar amino acid residues still buried and not accessible to the solvent (or other probing ligands). As a consequence of the slightly expanded surface characteristics of this molten globule form, distortion of the geometry of the surface-accessible interacting amino acid side chains will result in a greater contact area (*i.e.* increased S value) and increased free energy change upon binding (*i.e.* higher log k_0) as evident in the increased S and log k_0 values observed at 5°C.

As the temperatures increased over the range 10–80°C, there was a gradual, nearly linear dependence on temperature of the change in the interactive area of cytochrome *c*, as determined by the S values from approximately 14 to 20, which also coincided with an increase in the log k_0 values. The dependence of these parameters on temperature indicates that the protein three-dimensional structure is unfolding, by a process which involves the exposure of previously buried hydrophobic amino acids. Between 80 and 85°C however, while the S and log k_0 values for equine cytochrome *c* continued to increase, these parameters showed a significant decrease for the

tuna, bovine and canine molecules. In addition, between 20 and 85°C, the S and log k_0 values for the equine molecule were consistently higher than the corresponding values for the tuna, bovine and canine molecules. These results demonstrate that the differences in amino acid composition lead to subtle differences in the interactive behaviour of these protein molecules. Whilst there is essentially no difference in the tertiary structures of these proteins in the crystalline state and in bulk solution [26], the differences in retention behaviour suggests that there may be structural differences when placed within the chromatographic environment. What then is the origin of these changes in selectivity, S and log k_0 values at different temperatures observed for these proteins? Table 1 lists the amino acid differences between the different cytochrome c species. For closely related proteins which exhibit significantly different selectivity and band-broadening dependencies on chromatographic variables such as gradient time and temperature, these changes in retention behaviour will have their origin in the amino acid substitutions either by being directly located in the same chromatographic binding region or by causing a change in the tertiary structure, which can affect the shape/composition of the contact region. Of the cytochrome c's examined, the bovine species is the most closely related to the equine species with only three amino acid residue differences. Furthermore, alignment of these amino acid residue replacements at positions 47, 60 and 89 with the equine crystal structure indicates that each amino acid residue difference occupies a solvent exposed position on the surface of the three dimensional structure [27]. These three amino acid residue differences are moreover located in three distinct regions on the surface of the cytochrome c protein. Position 47 ($Thr_{equine} \rightarrow Ser_{bovine}$) is located in the omega (Ω) loop at the bottom of the haem group. Position 60 is located at the N-terminus of the third α-helix where the positively charged lysine residue in the equine protein has been replaced with the non-charged glycine residue in the bovine protein. The remaining amino acid residue difference at position 89 ($Thr_{equine} \rightarrow Gly_{bovine}$) is located on the hydrophilic face of the C-terminal helix. As a consequence of the folding of these proteins, residues 47 and 89 are in close proximity to the haem pocket whilst residue 60 is located on the opposite face of the molecule. Similarly, alignment of the two additional amino acid substitutions which occur between canine and equine cytochrome c at positions 88 ($Lys_{equine} \rightarrow Thr_{canine}$) and 92 ($Glu_{equine} \rightarrow Ala_{canine}$) reveal that these substitutions form a cluster with residue 89, again in close proximity to the haem crevice. Moreover, two of the three amino acid residues in this region in the equine protein are charged (Lys^{88}) or very polar (Glu^{92}), whilst the substituted amino acid residues in the canine protein (Thr^{88} and Ala^{92}) are neutral or non-polar at pH 2. In contrast, there are 19 amino acid residue differences between equine and tuna cytochrome c, 17 of which occupy surface positions within the native crystal structure [27,28] and two occupy internal positions. The change in nett charge accompanying the amino acid substitutions for the tuna species compared to the equine species may account for the differences in the magnitude of the S and log k_0 parameters at each of the temperatures studied. In particular, several amino acid residues which are positively charged in the equine protein are substituted with neutral amino acid residues in the tuna protein, resulting in a relative nett loss of five positive charges for the tuna cytochrome c molecule. Taking into consideration the electrostatic charge differences on the surface of each of the proteins, and the difference in retention behaviour observed when the chromatographic variables were held constant, then clearly these amino acid differences are responsible for the observed differences in selectivity and in the S and log k_0 values. Overall, the experimental data suggest that the amino acid residues flanking the haem crevice are predominant contributors to the S and log k_0 values (*i.e.* the chromatographic contact region) of cytochrome c. Detailed analysis of the hydrophobic surface free energy of each cytochrome c molecule is currently being

investigated with specific reference to the role of the non-polar haem cleft in the protein–ligand interaction.

3.2. The retention behaviour of apocytochrome c on the C_{18} sorbent

In order to establish the role of the haem moiety in the interaction of the holo-protein with the *n*-octadecyl ligands, additional experiments were carried out with the corresponding equine and tuna apocytochrome *c* proteins using the same methods of chromatographic analysis. Injection of both the homogeneous apoproteins at temperatures of 5 and 10°C yielded two distinct, resolvable peak zones. The chromatograms for equine apocytochrome *c* at five different gradient times at 5°C are shown in Fig. 5. As is evident from these data, the appearance of the two peaks was dependent upon operating temperature and column residence time. In general, the degree of peak splitting was greatest at lower temperatures and shorter gradient times. For equine apocytochrome *c* at 5°C, the second peak had almost disappeared when a 120-min gradient time was employed, whilst at 10°C, the second (later eluting) peak was absent when either the 90- and 120-min gradient times were employed. At 20°C, the second peak was not evident for any of the gradient times. Furthermore, the relative proportions of these two peaks changed with increasing gradient times, such that the integrated area of the later-eluting peak (peak 2, Fig. 5) diminished as the area of the early-eluting peak increased (peak 1, Fig. 5). For tuna apocytochrome *c* at 5°C, this peak splitting effect was also observed at all gradient times, whilst the appearance of the second peak was observed at 30, 45 and 60 min at 10°C. A similar phenomenon has been reported in the literature for other homogeneous proteins, where multiple peak formation in the RP-HPLC elution profile has been observed with variations in column residency times and temperature [16–19,29,30]. Furthermore, these investigations have shown that the conformers correspond to both biologically active and denatured structures, with the denatured structure typically eluting later with RP-HPLC systems. The results of the present study with apocytochrome *c* suggest that an additional pathway of conformational change, *i.e. cold* denaturation, can occur as a consequence of reversible conformational changes under gradient elution conditions. Detection of this phenomenon of conformational interconversion is the result of relatively slow kinetic processes which occur within the chromatographic time scale. Assuming that this interconversion can be described by a first-order rate process as outlined in the following scheme

$$\text{Unfolded}_{\text{cold}} \overset{k_1}{\rightleftharpoons} \text{Native} \overset{k_2}{\rightleftharpoons} \text{Denatured}_{\text{hot}}$$

the apparent first-order rate constants for the unfolding process associated with the cold denaturation, k_1, can be determined. This analysis was carried out using the dependence of the natural logarithm of the relative peak area (A) of the second conformer (*i.e.* log $(A_2/[A_1 + A_2])$ on the residency time of the second conformer, as shown in Fig. 6. The rate constants determined from the slopes of these plots are listed in Table 3. On the C_{18} sorbent, the rate 1 constants were greater for equine than for tuna apocytochrome *c*, while the rate of disappearance of the second peak was greater at 10°C than at 5°C.

The dependence of the S and log k_0 values on temperature for the two apocytochrome *c* molecules are shown in Fig. 7. It is generally observed in RP-HPLC that polypeptides elute later in an

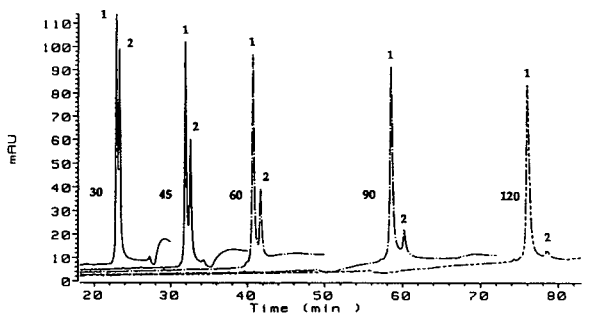

Fig. 5. RP-HPLC chromatogram showing the elution profiles obtained for equine apocytochrome *c* chromatographed on the C_{18} sorbent at 5°C at gradient times of 30, 45, 60, 90 and 120 min, as indicated. The first-eluted conformer is denoted as 1 and the second-eluted conformer is denoted as 2.

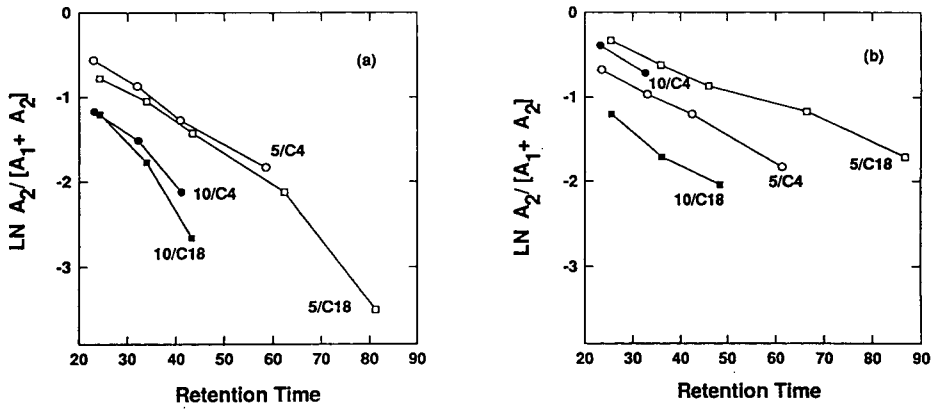

Fig. 6. The rates of structural conversion of the second apocytochrome *c* conformer to the first apocytochrome *c* conformer. Time scales in min. (a) Equine apocytochrome *c*; (b) tuna apocytochrome *c*. 5/C4, 5/C18 corresponds to data derived at 5°C with the C_4 and C_{18} sorbent, respectively; 10/C4, 10/C18 corresponds to data derived at 10°C with the C_4 and C_{18} sorbent, respectively.

unfolded form than in a folded conformation, due to the greater exposure of the inner core hydrophobic amino acid residues [19,30]. In the case of both the equine and tuna apocytochrome *c* two peaks were resolved at 5 and 10°C, with the *S* and log k_0 values of the second peak indicating a larger interactive contact area for this species than for the early-eluting species. However, it is evident that the second peak converts to the first peak at 5°C and to a lesser extent at 10°C, indicating that this type of conformational change was reversible. Between the temperatures of 10 and 85°C, where only one peak was observed, an increase in both these retention parameters was found for the apocytochrome *c* protein molecule. Thus, the temperature-induced increase in both retention pa-

Table 3
First-order rate constants for the cold denaturation of apocytochrome *c*

Temperature (°C)	Column	Rate constant ($mAU\ s^{-1} \times 10^4$)	
		Equine	Tuna
5	C_{18}	8.3	3.3
10	C_{18}	13.3	6.7
5	C_4	6.7	5.0
10	C_4	8.3	6.7

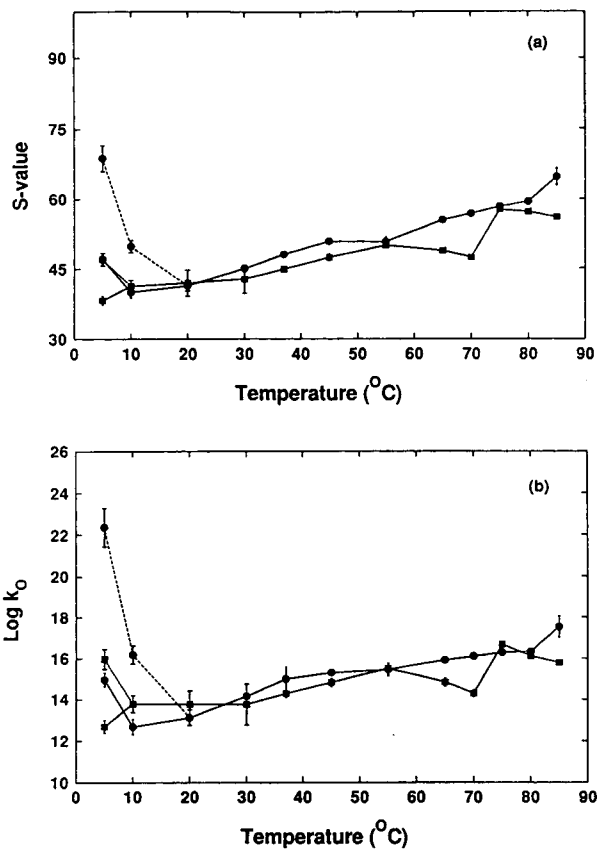

Fig. 7. Dependence of (a) *S* and (b) log k_0 on temperature for equine (○) and tuna (□) apocytochrome *c* separated on the C_{18} sorbent. The data points connected by broken lines represent the *S* and log k_0 values for the second conformer.

rameters is consistent with changes in the protein secondary and tertiary structure. These results suggest that at low temperatures in the presence of both the stationary and mobile phases, apocytochrome *c* adopts a folded conformation, which is subject to denaturation at higher temperatures. Relevant independent studies involving circular dichroism [31–33], Fourier-transform infrared spectroscopy [34] and nuclear magnetic resonance (NMR) spectroscopy [35] measurements of the conformational properties of apocytochrome *c* when associating with lipid micelles or phospholipid vesicles have unequivocally shown that the water–lipid interface induces a highly dynamic folded state in the molecule, involving the stabilisation of secondary structural units. Moreover, these results collectively suggest that the lipid-induced folding of the apoprotein may represent a folded intermediate in the cytochrome *c* folding pathway [35]. These results are vastly different to the bulk solution structure for the apoprotein in the freely solvated monomeric state in physiological buffers, which show an absence of any stabilised secondary structure, with the exception of the N- and C-terminal regions of the polypeptide chain [33]. Thus, these experimental results suggest that apocytochrome *c* can adopt a significant amount of secondary and tertiary structure in the presence of the hydrocarbonaceous adsorbent.

The S and log k_0 values for both the equine holo- and apocytochrome *c* proteins have been replotted for comparison in Fig. 8. It is evident from these plots that the equine holo-protein exhibited higher S and log k_0 values than the apoprotein. A similar relationship between tuna holo- and tuna apocytochrome *c* was also apparent. Furthermore, it is evident from these retention data that although the general unfolding trajectories of these two proteins are similar, they are not identical, with incremental increases in the ΔS and $\Delta\log k_0$ values occurring with temperature. Since the only compositional difference between the apoprotein, when compared to the holo-protein, is the presence/absence of the haem moiety, these results demonstrate that the haem moiety also plays a role in determining the S and log k_0 values associated with the interac-

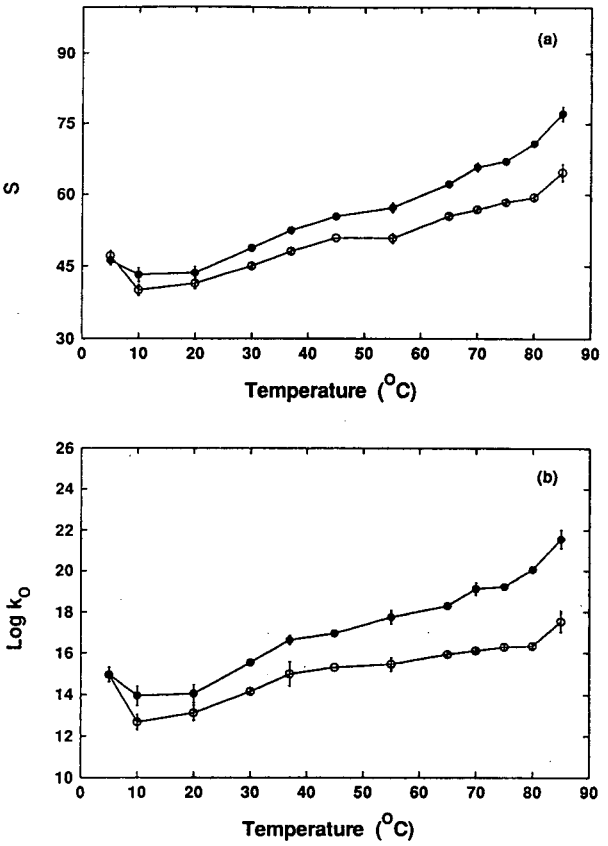

Fig. 8. Dependence of (a) S and (b) log k_0 on temperature for equine holo- (●) and apo- (○) cytochrome *c* separated on the C_{18} sorbent.

tive structure of cytochrome *c*, an effect which becomes more pronounced with increasing temperature. For example, the haem molecule may contribute directly to the binding domain or its removal may cause changes in the three-dimensional structure which then change the properties of the binding domain and in this way change the experimental S and log k_0 values. The haem moiety is located within a hydrophobic crevice in the overall globular structure of the protein, with one hydrophobic exposed edge [28]. It is possible that the protein orients itself with the crevice aligned with the hydrophobic ligands. As the crevice itself is lined with hydrophobic residues, this orientation would facilitate hydrophobic

interaction, especially as the protein unfolds and the hydrophobic contact area is increased.

3.3. Retention behaviour of cytochrome c on the C_4 sorbent

The chemical properties of the *n*-octadecyl and *n*-butyl ligand dictate that both types of *n*-alkyl silica sorbents are likely to interact with the surface topography of the biosolute in a subtly different manner. This view is supported by various literature studies which have demonstrated that different *n*-alkyl chain lengths (in particular, *n*-octadecyl *versus* *n*-butyl) probe different regions on the surface of a biosolute as a consequence of differences in ligand structure [8,11]. In addition, molecular dynamics studies on the mobility of the *n*-alkyl ligands when immobilised onto a silica surface have revealed significant conformational differences in the structure of *n*-octadecyl and *n*-butyl ligands [36], in agreement with results from NMR spectroscopic techniques [37,38]. The different flexibilities of the C_{18} and the C_4 ligands in conjunction with their different chemical properties when presented for interaction with biosolutes were thus anticipated to be revealed as significant changes in chromatographic retention behaviour of the different cytochrome *c*-related proteins.

The four cytochrome *c* molecules were chromatographed at five different gradient times ranging between 30 and 120 min at a flow-rate of 1 ml/min at twelve different temperatures ranging between 5 and 85°C. Fig. 9 shows the change in the *S* and log k_0 values of the cytochrome *c*'s when subjected to increases in temperature. These thermal denaturation curves illustrate that the retention behaviour of the cytochrome *c* molecules in the presence of the C_4 ligands is much more complex than found with the C_{18} ligands. Furthermore, the dependence of *S* and log k_0 on temperature for the control solutes N-acetyl-L-phenylalanine ethyl ester and penta-L-phenylalanine on the C_4 sorbent were similar to that observed with the C_{18} sorbent (data not shown) again demonstrating that the changes in

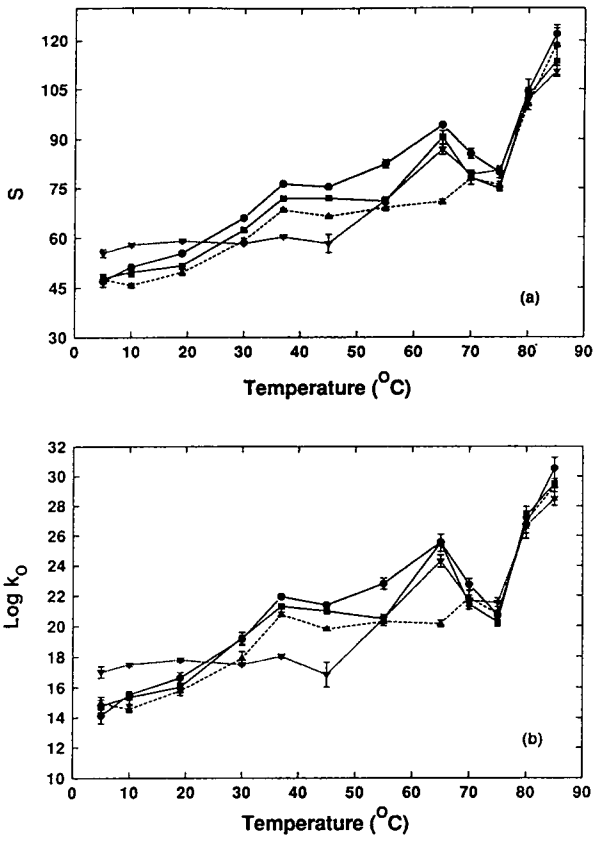

Fig. 9. Dependence of (a) *S* and (b) log k_0 on temperature for each of the holo-cytochrome *c* molecules separated on the C_4 sorbent. ○ = Equine; □ = tuna; ▲ = canine; ▼ = bovine.

S and log k_0 values in Fig. 9 can be related to changes in protein conformation. Initially, between 5 and 37°C there was a steady increase in the magnitude of both the *S* and log k_0 retention parameters. At 5°C, the experimental results suggest that the protein molecules are likely to exist as folded structures, whilst the structures characterised at 37°C are significantly unfolded. Between 37 and 65°C, the *S* and log k_0 values increased further, although the relative changes were less pronounced. Between 65 and 75°C a reproducible decrease in the magnitude of both the retention parameters was observed. In the very high temperature range of 80–85°C both the *S* and log k_0 parameters increased significantly in

value. The overall conformation of the holo-cytochrome *c* molecules may correspond to the fully unfolded form at 85°C. Heat perturbation of the protein structure results in the unfolding of the cytochrome *c* domains, subdomains and specific secondary structures. At some point in the unfolding pathway, the haem moiety will become exposed to the immobilised hydrophobic ligands which will increase the attraction of the protein moiety for the stationary phase. Overall, for the holo-proteins, the experimental results indicate that with the C_4 ligands there are distinct phases during the denaturation of the three-dimensional protein structure which may correspond to the presence of different structural intermediates.

When the retention behaviour of the cytochrome *c* molecules chromatographed on the C_4 sorbent is compared with that observed for the C_{18} (Fig. 3) several important differences are evident. These differences are most noticeable in the low-temperature range 5–10°C and at the higher-temperature range 65–75°C. With the C_{18} sorbent between 5 and 10°C, decreases in the observed retention parameters indicated that the protein was less structured at 5°C, relative to 10°C, whilst on the C_4 column S and log k_0 were observed to increase slightly. Thus, in this low-temperature range the different ligands are affecting the three-dimensional structure of the holo-proteins to different degrees. Between 65 and 75°C, the interactive properties of the proteins with the C_{18} sorbent were characterised by relative increases in the retention parameters, whilst with the C_4 sorbent the structural changes were manifested as a relative decrease in the S and log k_0 values. In addition, comparison of the thermal denaturation curves obtained from the two different *n*-alkyl silicas reveal that the magnitude of the S and log k_0 values obtained with the C_4 sorbent were significantly greater than those obtained with the C_{18} sorbent at each operating temperature employed. These results suggest that the structure of the ligand can significantly affect the way in which the protein is stabilised/destabilised in a hydrophobic environment.

3.4. The retention behaviour of apocytochrome *c* on the C_4 sorbent

The dependence of the S and log k_0 values on temperature obtained from the chromatographic analysis of the two apocytochrome *c* molecules are illustrated in Figs. 10 and 11 together with the data for the corresponding holo-proteins. Inspection of the data in Fig. 10 for equine apocytochrome *c* again reveals more complex retention behaviour than found with the C_{18} sorbent. For both apoproteins in the lower-temperature range 5–10°C, the phenomenon of peak splitting was again observed with the C_4 ligands. For equine apocytochrome *c*, the chromato-

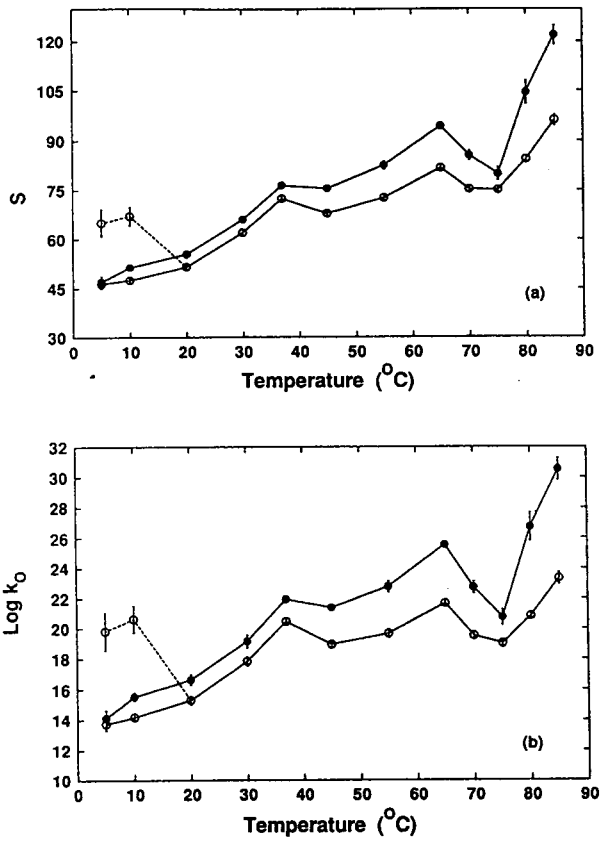

Fig. 10. Dependence of (a) S and (b) log k_0 on temperature for equine holo- (●) and apo- (○) cytochrome *c* separated on the C_4 sorbent. The data points connected by broken lines represent the S and log k_0 values for the second conformer.

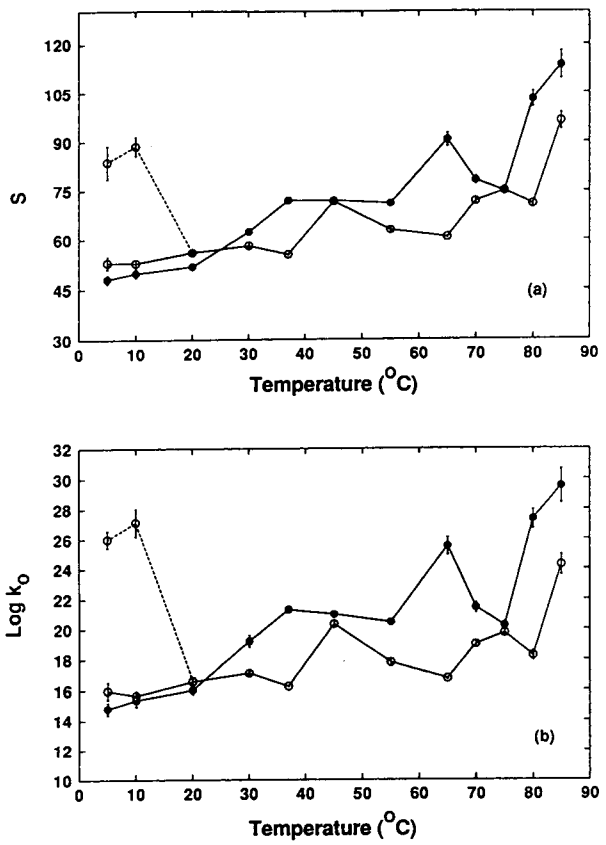

Fig. 11. Dependence of (a) S and (b) log k_0 on temperature for tuna holo- (●) and apo- (○) cytochrome c separated on the C_4 sorbent. The data points connected by broken lines represent the S and log k_0 values for the second conformer.

graphic elution profile was very similar to that shown in Fig. 5 for the C_{18} sorbent. At 5°C the presence of the second peak was detected at each of the five gradient times employed, whilst at 10°C the presence of the second peak was determined at only the 30-, 45- and 60-min gradient times. In addition, the area of the second peak diminished as that of the first peak increased. The apparent first-order rate constants for the structural interconversion for both apoproteins are listed in Table 3. In contrast to the results observed for the C_{18} sorbent, there was very little difference in the apparent rate of unfolding for each apoprotein at either temperature. In addition, at both 5 and 10°C, the second peak was only observed at shorter residency times on the C_4 compared to the C_{18} sorbent, which suggests that the n-octadecyl ligand stabilises this more denatured conformer. If the magnitude of the S and log k_0 values of the second peak are compared with the values obtained for apoprotein at 85°C, they are significantly lower, suggesting that the conformers present at the lower temperatures may not be as unfolded as the structures which exist at high temperatures.

Comparison of the data for the equine holoprotein with the equine apoprotein on the C_4 sorbent reveals a very similar dependence of the S and log k_0 values on temperature. The difference in the magnitude between the retention curves obtained for the holo-protein when compared to the apocytochrome c molecule indicates that the haem moiety is at least partially exposed at all the operating temperatures and contributes increasingly to the interactive segment on the surface of the protein which binds to the ligands as the protein unfolds. The haem is further implicated in a structurally stabilising role, as the phenomenon of peak splitting is not observed for the holo-protein. The high correlation in the retention behaviour evident in these curves suggests the secondary and tertiary structure of both the holo- and the apoprotein are very similar, and as a consequence, in the reversed-phase chromatographic environment they undergo very similar denaturation pathways. In addition, as both equine proteins progressively unfolded as indicated by the retention parameters, it is likely that they are approaching a similar denatured structure at 85°C.

Comparison of the S and log k_0 values obtained for the equine apocytochrome protein molecule chromatographed on C_4 sorbent (Fig. 10), with those obtained from chromatography on the C_{18} sorbent (Fig. 7) reveals that the magnitudes of these parameters were significantly larger at the higher temperatures with the C_4 sorbent than with the C_{18} sorbent. Between 65 and 85°C the S and log k_0 parameters also exhibited large fluctuations when chromatographed on the C_4 sorbent, whilst this was not evident on the n-octadecyl ligands. Furthermore,

the S and log k_0 values for both the first and second peaks remained essentially constant between 5 and 10°C on the C_4 sorbent but decreased over this temperature range on the C_{18} sorbent.

Fig. 11 illustrates the dependence of both S and log k_0 on temperature for tuna apocytochrome *c*. These retention data for tuna apocytochrome *c* protein molecule upon interaction with the C_4 sorbent reveals that S and log k_0 values varied over the entire range of operating temperatures to a much greater degree than was observed for equine apocytochrome *c*. The differences in the shapes of these denaturation curves further implicate a structural role for the prosthetic haem and suggests that the haem moiety has a significant influence on the specific properties of the interactive binding site. Further inspection of Fig. 11 reveals a local maximum in S and log k_0 values at *ca.* 65°C for the holoprotein, which may correspond to the unfolding of significant secondary structural elements, such as α-helices. Due to the lack of the stabilising influence of the haem group in the apoproteins, it is possible that these same structures melt at lower temperatures and are manifested as a local maximum in the S and log k_0 thermal denaturation curves for the apoprotein near 45°C. Between 5 and 10°C, both the equine and tuna apoproteins exhibit the formation of two resolvable peaks. However, the second peak of the equine species was still evident under conditions of longer residency, *i.e.* longer gradient times, and is characterised by larger S and log k_0 values than the corresponding second peak of the tuna species. These results suggest that the equine conformer is more stable in the C_4 chromatographic environment than the tuna conformer, has a higher affinity for the stationary phase ligands and interacts through a larger contact area.

4. Conclusions

In the present study, the retention characteristics of a family of related cytochrome *c* proteins, namely equine, tuna, canine and bovine along with chemically modified cytochrome *c*, *i.e.* equine apocytochrome *c* and tuna apocytochrome *c* have been documented. In particular, the relationship between the experimental S and log k_0 values and the conformational state of these proteins has been investigated. It has been demonstrated that these retention parameters are particularly sensitive to structural changes that occur at or near the interactive binding region on the surface of the protein, as well as in response to manipulation of several chromatographic variables (*i.e.* column residency time, operating temperature, *n*-alkyl ligand structure). Comparisons of the interactive characteristics of the holo-protein *versus* the apoprotein has revealed that the prosthetic haem molecule plays an important role in the structural integrity of the protein in the *n*-alkyl silica chromatographic environment. In particular, the absence of the haem group at low temperatures resulted in the formation of resolvable conformers with otherwise homogeneous preparation of apocytochrome *c*. The results of the present study in terms of the effect of various amino acid substitutions and the putative role of the haem moiety in the interactive behaviour of the cytochrome *c* molecules have laid the foundation for more detailed analysis of the nature of the chromatographic contact region. For example, it can be postulated from these results that the stability of the C-terminal helix significantly determines the interactive binding region on the surface of the molecule. As the C-terminal helix forms part of the hydrophobic crevice, and as the retention behaviour of the holo-protein *versus* the apoprotein demonstrates that the haem moiety may be involved in the contact region, then it can be proposed that the protein is orientated with the haem crevice aligned with the sorbent-phase ligands. Confirmation of this proposal through the application of *in situ* proteolytic techniques will be described in an associated paper [39]. Overall the analysis of the changes in the experimental S and log k_0 retention parameters in response to changes in amino acid sequence and other experimental operating parameters thus provides a powerful tool to elucidate the struc-

tural stability of globular proteins as they interact with hydrophobic surfaces.

5. Acknowledgement

The financial support of the Australian Research Council is gratefully acknowledged.

6. References

[1] M.A. Stadalius, H.S. Gold and L.R. Snyder, *J. Chromatogr.*, 296 (1984) 31.
[2] X. Geng and F.E. Regnier, *J. Chromatogr.*, 296 (1984) 15.
[3] M.I. Aguilar, A.N. Hodder and M.T.W. Hearn, *J. Chromatogr.*, 327 (1985) 115.
[4] M.T.W. Hearn and M.I. Aguilar, *J. Chromatogr.*, 359 (1986) 31.
[5] M.T.W. Hearn and M.I. Aguilar, *J. Chromatogr.*, 392 (1987) 33.
[6] M.T.W. Hearn and M.I. Aguilar, *J. Chromatogr.*, 397 (1987) 47.
[7] M. Kunitani, D. Johnson and L.R. Snyder, *J. Chromatogr.*, 371 (1986) 313.
[8] A.W. Purcell, M.I. Aguilar and M.T.W. Hearn, *J. Chromatogr.*, 593 (1992) 103.
[9] M.I. Aguilar, S. Mougos, J. Boublik, J. Rivier and M.T.W. Hearn, *J. Chromatogr.*, 646 (1993) 53.
[10] P. Oroszlan, S. Wicar, G. Teshima, S.L. Wu, W.S. Hancock and B.L. Karger, *Anal. Chem.*, 64 (1992) 1623.
[11] M. Hanson, K.K. Unger, C.T. Mant and R.S. Hodges, *J. Chromatogr.*, 599 (1992) 65.
[12] K. Benedek, S. Dong and B.L. Karger, *J. Chromatogr.*, 317 (1984) 227.
[13] S.A. Cohen, K. Benedek, Y. Tapuhi, J.C. Ford and B.L. Karger, *Anal. Biochem.*, 144 (1985) 275.
[14] S.A. Cohen, K. Schellenberg, K. Benedek, B.L. Karger, B. Grego and M.T.W. Hearn, *Anal. Biochem.*, 140 (1984) 223.
[15] X.M. Lu, K. Benedek and B.L. Karger, *J. Chromatogr.*, 359 (1986) 19.
[16] S. Lin and B.L. Karger, *J. Chromatogr.*, 536 (1990) 89.
[17] E. Watson and W.C. Kenny, *J. Chromatogr.*, 606 (1992) 165.
[18] R. Rosenfeld and K. Benedek, *J. Chromatogr.*, 632 (1993) 29.
[19] K. Benedek, *J. Chromatogr.*, 646 (1993) 91.
[20] K.G. Paul, *Acta Chem. Scand.*, 4 (1950) 239.
[21] I. Yarovsky, M. Zacchariou, M.I. Aguilar and M.T.W. Hearn, in preparation.
[22] Cs. Horváth, W. Melander and I. Molnár, *J. Chromatogr.*, 125 (1976) 129.
[23] M. Ohgushi and A. Wada, *FEBS Lett.*, 164 (1983) 21.
[24] S. Potekhin and W. Pfeil, *Biophys. Chem.*, 34 (1989) 55.
[25] Y. Kuroda, S. Kidokoro and A. Wada, *J. Mol. Biol.*, 223 (1991) 1139.
[26] G. Williams, G.R, Moore, R. Porteous, M.N. Robinson and R.J.P. Williams, *J. Mol. Biol.*, 183 (1985) 409.
[27] R.E. Dickerson, T. Takano, D. Eisenberg, O.B. Kallai, l. Samson, A. Cooper and E. Margoliash, *J. Biol. Chem.*, 246 (1971) 1511.
[28] G.W. Bushnell, G.V. Louie and G.D. Brayer, *J. Mol. Biol.*, 214 (1990) 585.
[29] M.T.W. Hearn, A.N. Hodder and M.I. Aguilar, *J. Chromatogr.*, 327 (1985) 47.
[30] S.A. Cohen, K. Benedek, S. Dong, Y. Tapuhi and B.L. Karger, *Anal. Chem.*, 56 (1984) 217.
[31] A. Walter, D. Margolis, R. Mohan and R. Blumenthal, *Membr. Biochem.*, 6 (1987) 217.
[32] W. Jordi, Z. Li-Xin, M. Pilon, R. Demel and B. de Kruijff, *J. Biol. Chem.*, 264 (1989) 2292.
[33] H.H. de Jongh and B. de Kruijff, *Biochim. Biophys. Acta*, 1029 (1990) 105.
[34] A. Muga, H.H. Mantsch and W.K. Surewicz, *Biochemistry*, 30 (1991) 2629.
[35] H.H. de Jongh, J.A. Killian and B. de Kruijff, *Biochemistry*, 31 (1992) 1636.
[36] I. Yarovsky, M.I. Aguilar and M.T.W. Hearn, *J. Chromatogr. A*, 660 (1994) 75.
[37] E. Bayer, A. Paulus, B. Peters, G. Laupp, J. Reniers and K. Albert, *J. Chromatogr.*, 364 (1986) 25.
[38] J. Nawrocki and B. Buszewski, *J. Chromatogr.*, 449 (1988) 1.
[39] M.I. Aguilar, D. Clayton and M.T.W. Hearn, in preparation.

ELSEVIER

Journal of Chromatography A, 676 (1994) 33–41

JOURNAL OF CHROMATOGRAPHY A

Effect of protein conformation on experimental bandwidths in reversed-phase high-performance liquid chromatography

K.L. Richards, M.I. Aguilar*, M.T.W. Hearn

Department of Biochemistry and Centre for Bioprocess Technology, Monash University, Wellington Road, Clayton 3168, Australia

Abstract

The dynamic behaviour of a series of closely related cytochrome *c* molecules has been investigated in reversed-phase high-performance liquid chromatography. In particular, the influence of temperature and gradient time on the experimental bandwidths of equine, tuna, canine and bovine cytochrome *c* and equine and tuna apocytochrome *c* has been determined with a C_{18} and a C_4 sorbent. The observed bandbroadening changes are discussed in comparison to the corresponding retention behaviour of the cytochrome *c* molecules reported in the preceding paper [1]. The results demonstrate that bandwidth measurements can be used as an indicator of the conformational status of a protein under a particular set of chromatographic conditions.

1. Introduction

The separation of complex mixtures of polypeptides and proteins by reversed-phase high-performance liquid chromatography has improved considerably in recent years as a consequence of a better understanding of the molecular basis of retention and selectivity, together with significant advances in experimental procedures. However, problems often arise as a result of anomalous bandbroadening of eluted peaks of biopolymers, a phenomenon which can hamper the optimisation of the separation conditions. The source of this bandbroadening behaviour can be attributed to a number of secondary equilibrium processes associated with solute aggregation in the bulk mobile phase or at the stationary phase surface, sol–gel equilibria, multisite interaction with the stationary phase surface, specific ion-interaction equilibria involving ionic additives present in the mobile phase, specific pH-dependent equilibria and specific solute-solvation equilibria. While all these interactions can influence the secondary events which give rise to atypical bandbroadening, the dominant factor with proteins is often the presence of multiple conformers due to conformational interconversion [1–5]. Several investigations have characterised the bandbroadening behaviour of peptide solutes and have found that the presence of defined secondary structure strongly affects the experimental peak width [5–11]. While many investigators have reported the occurrence of bandbroadening phenomena during analytical separations of proteins by RP-HPLC, few workers have, however, systematically characterised the dependence of experimental bandwidths on operating conditions.

The kinetic processes which give rise to bandbroadening behaviour of low-molecular-

* Corresponding author.

0021-9673/94/$07.00
SSDI 0021-9673(94)00312-W

mass, rigid organic molecules in gradient elution are influenced by axial dispersion in the bulk mobile phase, dispersion due to slow mass transfer across the solvent–particle boundary and in the intraparticulate spaces and dispersion due to slow mass transfer of the solute at a heterogeneous stationary phase surface [12]. Thus, for small compounds where the molecular surface area and the respective diffusive properties remain essentially constant throughout the chromatographic analysis, the experimental bandwidth can be directly related by the general plate height theory to several diffusion parameters such as the bulk diffusivity D_M, the intraparticulate boundary diffusivity D_P, the surface diffusivity D_S as well as the column residence time which is controlled by the elution time and the flow-rate [12–15]. However, if the solute undergoes conformational rearrangements which are characterised by a rate constant that is comparable to the chromatographic separation time, additional bandspreading and/or distortion of the experimental peak shape will occur leading to asymmetrical or multiple peak formation [1–5,9–11,16–18]. These changes in bandbroadening behaviour will be associated with changes in the hydrodynamic volume and changes in the chromatographic contact region of the solute. Thus, changes in the shape of a symmetrical peak in response to variation in a specific separation parameter such as temperature or column residency time represent kinetic indicators of the dynamic nature of protein backbone flexibility and the conformational transitions of the solute that occur at the solvent–ligand interface. In a previous paper [1], the retention behaviour of a family of cytochrome *c* molecules was investigated in terms of the influence of temperature on the retention parameters S (related to the chromatographic contact area) and $\log k_0$ (related to the solute affinity for the sorbent). In the present study, bandwidth data associated with the reversed-phase separation of these cytochrome *c* molecules have been examined. The results are discussed in relation to the kinetics of conformational interconversions that occur during the chromatographic migration of these proteins on both a C_{18} and a C_4 sorbent.

2. Materials and methods

The chromatographic apparatus, chemicals and reagents and chromatographic procedures used in the present study are described elsewhere [1]. In order to examine the dependencies of the experimental bandwidth upon temperature and column residence time for the cytochrome *c*-related proteins, the experimental bandwidth was measured at 13.4% of the eluted peak height which corresponds to four standard deviations (i.e. 4σ) [9]. The bandwidths were monitored under a range of experimental gradient elution conditions as previously described [1]. These conditions included gradient times between 30 and 120 min at a flow-rate of 1 ml/min at temperatures between 5 and 85°C. All data points were derived from at least duplicate measurements. The 4σ values were determined using a BANDWIDTH macro-software developed within this laboratory for use with a Hewlett-Packard 79995A Chemstation operating software. As loading conditions for the test proteins were approximately $8 \cdot 10^{-5}$ μM, the possibility of solute aggregation in the mobile phase can be excluded [19], and thus the behaviour of 4σ will directly reflect the solute dynamics at the sorbent interface.

3. Results and discussion

3.1. Bandwidth behaviour of control solutes

In order to evaluate the contribution of secondary and tertiary structures to the overall interactive behaviour exhibited by the protein solute, the bandwidth behaviour of two low-molecular-mass solutes, N-acetyl-L-phenylalanine ethyl ester and penta-L-phenylalanine were investigated. The dependence of the experimental bandwidths on temperature for these two molecules chromatographed on the C_{18} sorbent is shown in Fig. 1. The results demonstrated a small increase in the magnitude of the bandwidth with increasing gradient time. This increase

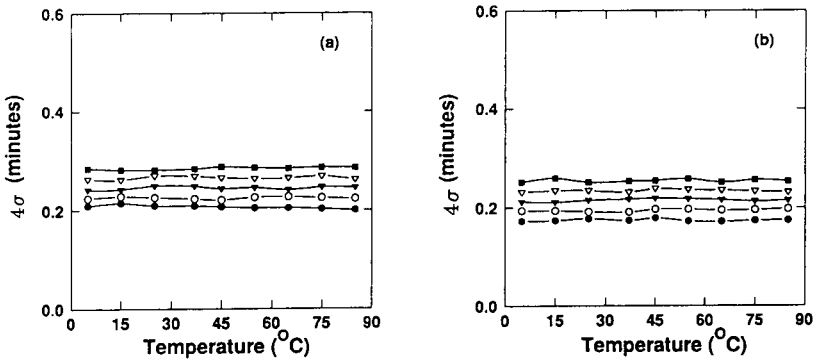

Fig. 1. The dependence of experimental bandwidths, 4σ, on temperature at five different gradient times between 30 and 120 min for (a) penta-L-phenylalanine and (b) N-acetyl-L-phenylalanine ethyl ester chromatographed on the C_{18} sorbent. The gradient times were: ● = 30 min; ○ = 45 min; ▼ = 60 min; ▽ = 90 min; ■ = 120 min.

reflects the axial dispersion of the solute during chromatographic migration which increases proportionately with increased separation time. The results in Fig. 1 also indicate that the bandwidths are essentially independent of operating temperature. These linear dependencies are consistent with either the inability of these solutes to conformationally interconvert or alternatively their ability to interconvert very rapidly with regard to the chromatographic time scale. Almost identical results were obtained for the bandwidth behaviour of these solutes chromatographed on the C_4 sorbent. The mass transport kinetic properties of the control solutes are in accord with many other low-molecular-mass solutes [6,12,13], with the structure and chemical properties of the *n*-alkyl ligands not significantly affecting the peak shape under these well-controlled conditions. Therefore, the bandwidth values shown in Fig. 1 represent the degree of change in 4σ with increasing temperature which would be expected for low-molecular-mass, non-interconverting solutes. As a consequence, significant deviations in the 4σ values associated with the chromatography of the cytochrome *c* molecules from that predicted on the basis of molecular diffusivity arguments for a protein of constant shape, can be attributed to the formation of interconverting species.

3.2. Bandwidth behaviour of cytochrome c on the C_{18} sorbent

Equine cytochrome *c* was chromatographed on the C_{18} sorbent at gradient times between 30 and 120 min and temperatures between 5 and 85°C. The dependence of the experimental bandwidths on gradient time and operating temperature is illustrated in Fig. 2 for both the holo- and the apoprotein. The data for the holo protein (Fig. 2a) reveal that at each temperature, the value of 4σ increased with gradient time, while at each gradient time, 4σ decreased with increasing temperature. However, at certain temperatures, there were large fluctuations in the experimental bandwidths. For example, at 37°C there was a large increase in 4σ at both the 90 and 120 min gradient times. In addition, between 75 and 80°C, a sharp decrease in 4σ was observed. Overall, the results in Fig. 2 are in sharp contrast to the results observed for the control solutes shown in Fig. 1, which exhibited no significant dependency on temperature. Thus, the large changes in the bandwidth behaviour of equine cytochrome *c* over narrow ranges of experimental conditions are indicative of conformational interconversions which occur particularly near 37°C and between 75 and 80°C at the longer gradient times. Furthermore, the 4σ values ob-

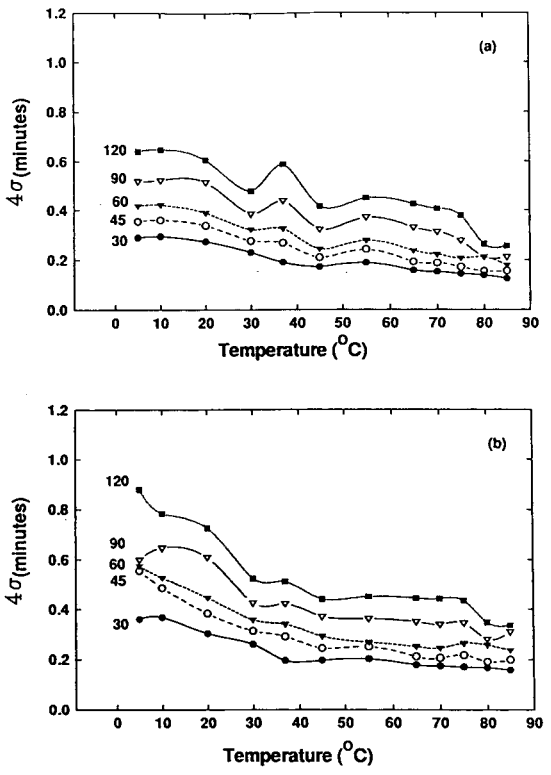

Fig. 2. The dependence of experimental bandwidths, 4σ, on temperature at five different gradient times between 30 and 120 min as indicated for (a) equine cytochrome *c* and (b) equine apocytochrome *c* chromatographed on the C_{18} sorbent.

tained for equine cytochrome *c* were significantly larger at the lower temperatures and longer gradient times than those obtained for the control solutes, as would be expected for larger molecules which occupy a greater hydrodynamic volume and are characterised by a relatively smaller diffusion coefficient. The retention behaviour of the cytochrome *c* molecules reported previously [1] indicated that the S and log k_O values increased over the same temperature range, consistent with the unfolding of the protein molecule at the higher temperatures. Moreover, the extent of interconversion of the unfolded protein to a refolded molecule would decrease at higher temperatures leading to the presence of predominantly only one form of the protein and thus be consistent with the significant decrease in 4σ values. Hence in the low-temperature range, more conformational species will be present, leading to greater perturbation in peak shapes due to these kinetic interconversions. In contrast, at higher temperatures the protein will have less secondary and tertiary structure, ultimately leading to only a single unfolded species migrating in the RP-HPLC system.

The influence of the haem moiety of the cytochrome *c* molecule was studied by chromatographing equine apocytochrome *c* under the same experimental conditions. The dependence of the experimental bandwidths on gradient time and temperature for the apoprotein are shown in Fig. 2b. The elution profile of the apoprotein previously showed [1] the presence of two distinct peaks. The bandwidth data plotted in Fig. 2b represents the experimental bandwidths of the early-eluting peak. As was observed for the holo protein, there was an increase in the value of 4σ with increased gradient time and a decrease in 4σ with increased temperature. Thus, the bandbroadening behaviour of equine apocytochrome *c* was similar to that observed for the holo protein, although the values of 4σ under identical chromatographic conditions for the apoprotein were generally larger. In addition, the variations in 4σ observed at 37°C for the holo protein were not evident for the apoprotein, which suggests that the haem moiety plays a role in the kinetics of structural interconversions which occur during the chromatographic migration. The absence of the haem group would presumably result in a more flexible polypeptide chain with larger hydrodynamic volume which would be manifested as the relatively larger bandwidth values observed at the lower temperatures.

The dependence of experimental bandwidths on gradient time and temperature of tuna cytochrome *c* and tuna apocytochrome *c* are shown in Fig. 3. The results for the holo protein in Fig. 3a demonstrate a similar relationship between 4σ, gradient time and temperature to that observed for equine cytochrome *c*. However, there appears to be a transition in the 4σ values at 37°C which may correspond to a conformational

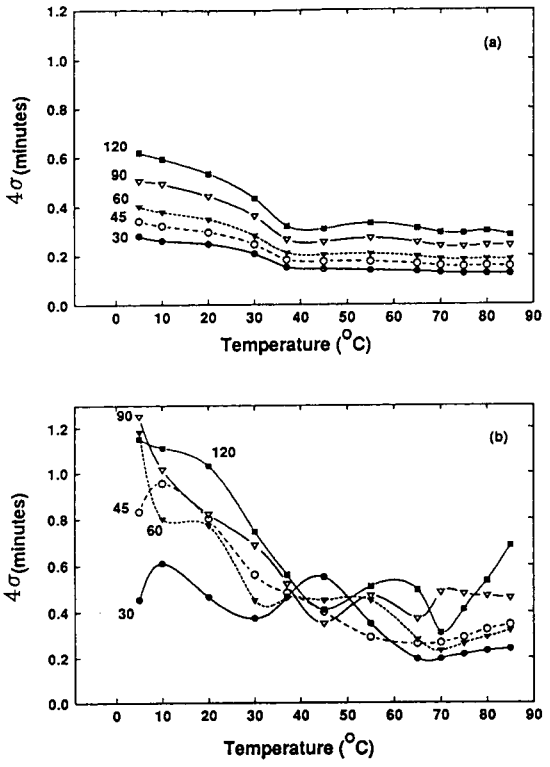

Fig. 3. The dependence of experimental bandwidths, 4σ, on temperature at five different gradient times between 30 and 120 min as indicated for (a) tuna cytochrome *c* and (b) tuna apocytochrome *c* chromatographed on the C_{18} sorbent.

interconversion. Whilst the differences in the amino acid sequence between the equine and the tuna cytochrome *c* molecule do not result in very dramatic changes in the bandwidth behaviour, differences in the relative stability of the two proteins, as manifested in the kinetics of their interaction with the C_{18} sorbent, are evident. The bandbroadening behaviour of the first eluted peak of tuna apocytochrome *c* is shown in Fig. 3b and demonstrates significantly different behaviour to either the equine holo or apocytochrome *c* and the tuna holo cytochrome *c*. While the trend was observed that the value of 4σ decreased with increasing temperature, these values showed considerable divergence at the different gradient times, with a transition evident around 37°C. Thus, the presence of multiple interconverting peaks demonstrates that tuna apocytochrome *c* undergoes conformational interconversion at the lower temperatures. The variance in the bandbroadening behaviour observed may also be a direct result of the cold denaturation phenomenon which takes place at these temperatures. In addition, the differences between tuna holo cytochrome *c* and tuna apocytochrome *c* again demonstrate the crucial role of the prosthetic haem molecule in the kinetics of the conformational and interactive properties of cytochrome *c*, and indicate that in the absence of the haem group, the polypeptide backbone readily interconverts between different conformers.

The dependence of the experimental bandwidths on gradient time and temperature for canine and bovine cytochrome *c* are shown in Fig. 4. Both proteins exhibited similar behaviour

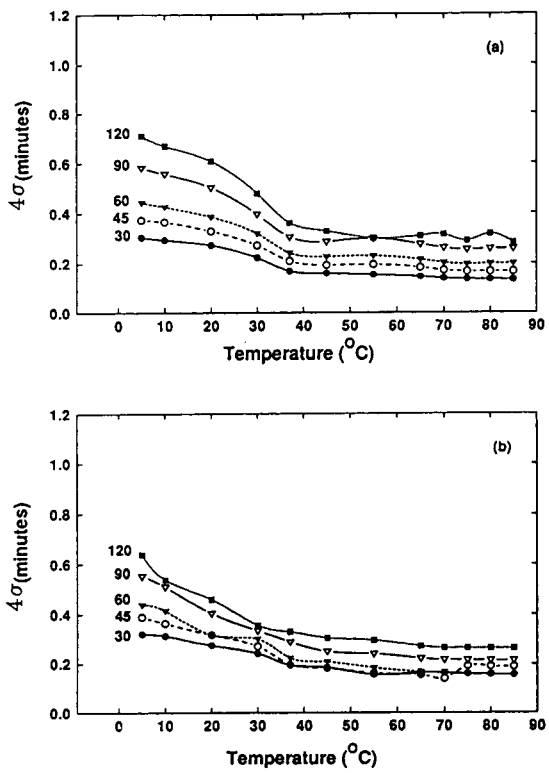

Fig. 4. The dependence of experimental bandwidths, 4σ, on temperature at five different gradient times between 30 and 120 min as indicated for (a) canine cytochrome *c* and (b) bovine cytochrome *c* chromatographed on the C_{18} sorbent.

to that observed for equine and tuna cytochrome *c* with a transition evident around 37°C. Thus between 5 and 37°C the magnitude of 4σ decreased with increasing temperature, while between 37 and 85°C the 4σ value approached a similar magnitude. The small differences in amino acid sequences between the four cytochrome *c* molecules has been shown to significantly influence the resolution of cytochrome *c* molecules [1]. Between 5 and 37°C, it can be seen that the magnitudes of the 4σ values were larger for canine cytochrome *c* while for bovine cytochrome *c* there were smaller differences in the 4σ value between the five gradient times. Whilst there was an overall similarity in the bandwidth dependencies for the four cytochrome *c* molecules, subtle differences were evident in the influence of temperature and column residence time on experimental bandwidth. Since the molecular mass and hence the bulk diffusivity of these four proteins will be similar, these differences in 4σ must reflect differences in the kinetics of the conformational interconversion and ligand interaction and can be directly attributed to the amino acid residue substitutions.

3.3. Bandwidth behaviour of cytochrome c on the C_4 sorbent

In order to investigate the effect of ligand structure on the kinetic behaviour of proteins, all cytochrome *c* molecules were also chromatographed on a C_4 sorbent at temperatures between 5 and 85°C and at gradient times between 30 and 120 min. The dependence of experimental bandwidths on temperature and gradient time are shown in Figs. 5–7. The bandbroadening behaviour for equine cytochrome *c* shown in Fig. 5a illustrates the generally observed trend that 4σ increased with increasing gradient time and decreased with increasing temperature. Again these results are different to those obtained for the non-interconverting control solutes where no dependency on temperature was observed. At lower temperatures, equine cytochrome *c* appears to undergo conformational interconversion, a result which was also apparent from the corresponding retention behaviour [1]. At higher

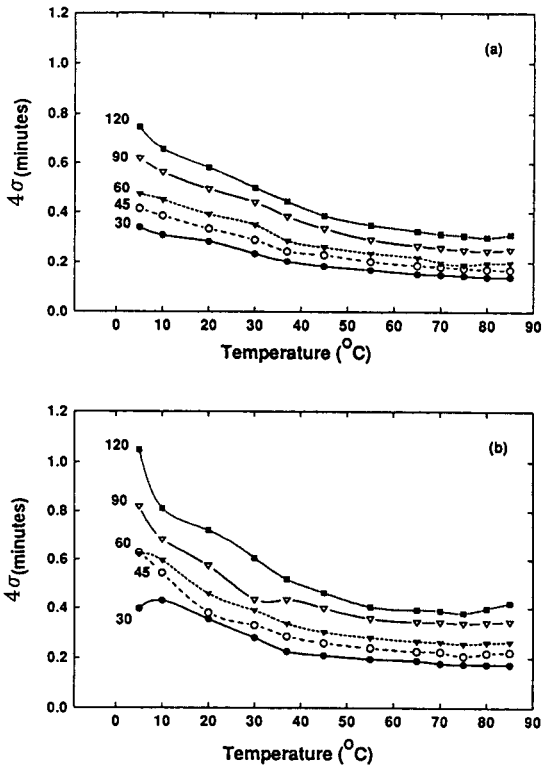

Fig. 5. The dependence of experimental bandwidths, 4σ, on temperature at five different gradient times between 30 and 120 min as indicated for (a) equine cytochrome *c* and (b) equine apocytochrome *c* chromatographed on the C_4 sorbent.

temperatures where 4σ approaches a constant value, it is apparent that the rate of conformational interconversion of the protein molecule is too rapid for this effect to be detected as a bandbroadening change. Comparison of the data shown in Fig. 2a with Fig. 5a reveals some significant differences between the bandwidth behaviour of equine cytochrome *c* on the C_4 and C_{18} sorbents. Firstly, the fluctuations in 4σ at 37°C and 75–80°C observed with the C_{18} sorbent were not apparent with the C_4 sorbent. Secondly, the magnitude of the 4σ values were generally higher with the C_4 sorbent. These differences can be attributed to the differences in the molecular structure of the *n*-alkyl ligands. Hence, the conformational flexibility, the relative hydrophobicity and the extent of ligand solvation are

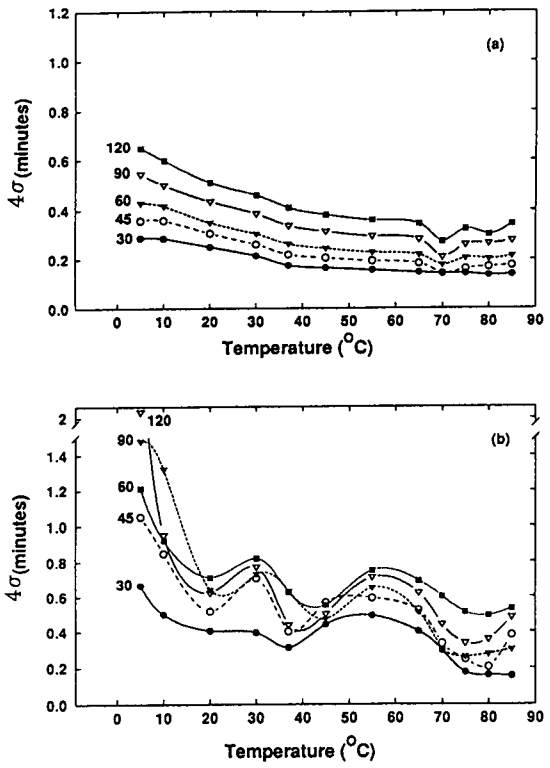

Fig. 6. The dependence of experimental bandwidths, 4σ, on temperature at five different gradient times between 30 and 120 min as indicated for (a) tuna cytochrome *c* and (b) tuna apocytochrome *c* chromatographed on the C_4 sorbent.

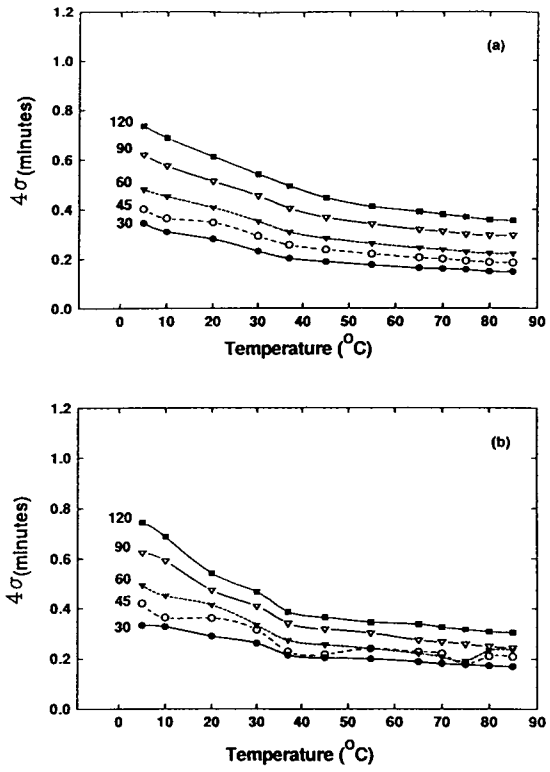

Fig. 7. The dependence of experimental bandwidths, 4σ, on temperature at five different gradient times between 30 and 120 min as indicated for (a) canine cytochrome *c* and (b) bovine cytochrome *c* chromatographed on the C_4 sorbent.

all important factors which influence the adsorption of the protein solute and the potential for the protein solute to undergo conformational interconversion.

The bandbroadening behaviour of equine apocytochrome *c* is illustrated in Fig. 5b. The elution profile of this molecule revealed the presence of two peaks. The data shown in Fig. 5b represent the experimental bandwidths for the first eluted peak. It is evident from this figure that 4σ exhibited a curvilinear dependency on both gradient time and temperature. In addition, a transition in the bandwidth data occurred between 37 and 45°C while at higher temperatures the 4σ value remained constant. Comparison of these data with the bandwidth behaviour of the holo protein in Fig. 5a reveals that much larger 4σ values were observed for the apoprotein with the C_4 sorbent between 5 and 45°C, while similar 4σ values were obtained between 45 and 85°C. Thus, the 4σ values at lower temperatures reflect a significant degree of conformational interconversion on the chromatographic time scale, while at higher temperatures the decrease in 4σ values is indicative of an increasingly rapid rate of interconversion. These results once again demonstrate the influence of the haem group in restricting the conformational flexibility of the cytochrome *c* molecule. Comparison of the bandbroadening behaviour of equine apocytochrome *c* on both the C_4 and the C_{18} sorbent also reveals that significantly larger 4σ values were observed between 5 and 45°C at gradient times of 90 and 120 min with the C_4 sorbent than with the C_{18} sorbent. It was previously shown [1] that the C_{18} sorbent stabilised the structure of

the second peak compared to the C_4 sorbent and the comparative bandwidths observed at the lower temperatures are again consistent with the presence of a greater degree of conformational interconversion on the C_4 sorbent.

The dependence of experimental bandwidths on gradient time and temperature for tuna cytochrome *c* and tuna apocytochrome *c* is illustrated in Fig. 6. As was observed for equine cytochrome *c*, the values of 4σ for tuna cytochrome *c* increased with increasing gradient time and decreased with increasing temperature with a transition around 37°C. However, the magnitude of the 4σ values for tuna cytochrome *c* at the lower temperatures were greater than the corresponding data for equine cytochrome *c*. This result again demonstrates that the amino acid differences influence the protein's dynamic properties when the molecule undergoes conformational interconversion. The influence of the chromatographic ligand can be seen by comparison of Fig. 3a with Fig. 6a. While the magnitude of the 4σ values are similar with each sorbent, the transition in the bandwidth data around 37°C is much more distinct with the C_{18} sorbent than the transition observed with the C_4 sorbent. Thus, the kinetics of conformational interconversion of tuna cytochrome *c* appears to be strongly influenced by the nature of the ligand structure. The bandwidth behaviour of tuna apocytochrome *c* with the C_4 sorbent is shown in Fig. 6b. It can be seen from these data that the changes in the experimental bandwidths were significantly greater than those observed for tuna cytochrome *c* and that there were large fluctuations over the range of temperatures employed. As the phenomenon of peak splitting was also observed for tuna apocytochrome *c* on the C_4 sorbent, the changes in experimental bandwidth can therefore be attributed to conformational interconversion of the protein molecule. Thus, while the bandwidth data shown in Fig. 6b represent the data for the first-eluting peak, it is evident from the bandwidth relationships that several closely related structural conformers may be contributing to the peak corresponding to the early-eluting conformer. The conformational interconversion which tuna apocytochrome *c* undergoes appears to be more extensive as the experimental bandwidths at the lower temperatures are much greater on the C_4 sorbent than on the C_{18} sorbent again demonstrating the stabilising effect of the longer more hydrophobic ligands. These results also further illustrate the influence of the haem group on the structural stability of the cytochrome *c* molecule.

The dependence of experimental bandwidths on gradient time and temperature for canine and bovine cytochrome *c* are shown in Fig. 7a and b, respectively. It can be seen that the bandwidth behaviour of these two molecules is similar to that observed for equine cytochrome *c* with the C_4 sorbent. Thus, 4σ increased with increasing gradient time over the entire temperature range. In addition, between 5 and 45°C, 4σ decreased with increasing temperature, while in the temperature range between 45 and 85°C, 4σ approached a constant value. Comparison with the corresponding data on the C_{18} sorbent in Fig. 4 reveals that the transition in bandwidth values for canine cytochrome *c* which occurred around 37°C is much less distinct with the C_4 sorbent than with the C_{18} sorbent while the data for bovine cytochrome *c* on both sorbents was almost identical. Once again, these results demonstrate that the small differences in amino acid sequence between the four cytochrome *c* molecules gives rise to subtle differences in the interactive behaviour in terms of their relative stability and the nature of the conformational transitions which occur under different experimental conditions.

4. Conclusions

The molecular composition of the interactive contact area of the protein solute which presents itself to the chromatographic surface ultimately determines the affinity of the solute for the stationary phase ligands. Changes which occur in the contact region as a consequence of conformational changes will give rise to changes in the retention behaviour of the solute. If the interconversion of a protein solute generates a family of very closely related conformers in

which the chromatographic contact region has also changed, then the small shifts in retention time between these conformers will result in changes in the experimental bandwidths of the protein. The degree to which these conformers can be resolved will depend on the inherent selectivity of the chromatographic system used. Bandwidth measurements of such interconverting systems are therefore a kinetic indicator of the dynamic properties of the protein under a particular set of chromatographic conditions. In the present study, the analysis of protein bandbroadening behaviour has provided information concerning the effects of protein tertiary structure as well as *n*-alkyl ligand structure on the interactive behaviour of the cytochrome *c* related proteins in RP-HPLC. Examination of the chromatographic bandwidths has provided insight into the relationship between column residence time and temperature and the conformational dynamics which occur during the chromatographic migration of these protein molecules. Overall, the results have demonstrated that the experimental bandwidth is a very sensitive probe of the dynamic status of a protein solute. In particular, the above experiments demonstrate that both extensive and more subtle changes in protein structure influence the experimental bandwidths of a protein as it undergoes conformational interconversions.

Acknowledgement

The financial support of the Australian Research Council is gratefully acknowledged.

References

[1] K.L. Richards, M.I. Aguilar and M.T.W. Hearn, *J. Chromatogr. A*, 676 (1994) 17.
[2] K. Benedek, S. Dong and B.L. Karger, *J. Chromatogr.*, 317 (1984) 227.
[3] S.A. Cohen, K. Benedek, Y. Tapuhi, J.C. Ford and B.L. Karger, *Anal. Biochem.*, 144 (1985) 275.
[4] E. Watson and W.C. Kenny, *J. Chromatogr.*, 606 (1992) 165.
[5] M.T.W. Hearn, A.N. Hodder and M.I. Aguilar, *J. Chromatogr.*, 327 (1985) 47.
[6] M.T.W. Hearn and M.I. Aguilar, *J. Chromatogr.*, 352 (1986) 36.
[7] M.T.W. Hearn and M.I. Aguilar, *J. Chromatogr.*, 359 (1986) 31.
[8] M.T.W. Hearn and M.I. Aguilar, *J. Chromatogr.*, 392 (1987) 33.
[9] A.W. Purcell, M.I. Aguilar and M.T.W. Hearn, *Anal. Chem.*, 65 (1993) 3038.
[10] S.A. Cohen, K. Benedek, S. Dong, Y. Tapuhi and B.L. Karger, *Anal. Chem.*, 56 (1984) 217.
[11] X.M. Lu, K. Benedek and B.L. Karger, *J. Chromatogr.*, 359 (1986) 19.
[12] L.R. Snyder, in Cs. Horváth (Editor), *High Performance Liquid Chromatography —Advances and Perspectives*, Vol. 1, Academic Press, New York, 1980, p. 207.
[13] M.A. Stadalius, H.S. Gold and L.R. Snyder, *J. Chromatogr.*, 327 (1985) 27.
[14] J.C. Giddings, in J.C. Giddings and R.A. Keller (Editors), *Dynamics in Chromatography*, Marcel Dekker, New York, 1965, p. 12.
[15] J.C. Giddings, *J. Chromatogr.*, 3 (1960) 443.
[16] K. Benedek, *J. Chromatogr.*, 646 (1993) 91.
[17] P. Oroszlan, R. Blanco, X.-M. Lu, D. Yarmush and B.L. Karger, *J. Chromatogr.*, 500 (1990) 481.
[18] S.L. Wu, K. Benedek and B.L. Karger, *J. Chromatogr.*, 359 (1986) 3.
[19] M.-F. Jeng, S.W. Englander, G.A. Elove, A.J. Wand and H. Roder, *Biochemistry*, 29 (1990) 10433.

ELSEVIER

Journal of Chromatography A, 676 (1994) 43–49

JOURNAL OF CHROMATOGRAPHY A

Purification of the integral membrane glycoproteins D of Herpes simplex virus types 1 and 2, produced in the recombinant baculovirus expression system, by ion-exchange high-performance liquid chromatography

R.A. Damhof, M. Feijlbrief, S. Welling-Wester, G.W. Welling*

Laboratorium voor Medische Microbiologie, Rijksuniversiteit Groningen, Oostersingel 59, 9713 EZ Groningen, Netherlands

Abstract

Selective elution of Sendai virus integral membrane proteins by ion-exchange high-performance liquid chromatography (HPIEC) using different detergent concentrations was reported before [S. Welling-Wester, M. Feijlbrief, D.G.A.M. Koedijk, M.A. Braaksma, B.R.K. Douma and G.W. Welling, *J. Chromatogr.*, 646 (1993) 37]. In the present study this novel approach was applied to the purification of the integral membrane glycoprotein D of Herpes simplex virus types 1 and 2. The glycoproteins D of types 1 (gD-1) and 2 (gD-2) were cloned into the baculovirus expression system and produced in protein-free cultured insect cells.

Detergent extracts of recombinant baculovirus-infected insect cells containing gD-1 or gD-2 were prepared using pentaethyleneglycol monodecyl ether, for extraction (final concentration 2%, w/v). The same detergent was used as additive in the elution buffers for HPIEC on a Mono Q HR 5/5 column. At low (0.005%) detergent concentration, most of the proteins present in the extract including part of gD were eluted with the sodium chloride gradient whereas a subsequent blank run using the same gradient at higher detergent concentration (0.1%) resulted in selective elution of pure gD.

1. Introduction

One of the structural glycoproteins of Herpes simplex virus, glycoprotein D (gD), which is present in the envelope of the virus particle and as an integral membrane protein in HSV-infected cells, is a confirmed target of the virus-specific immune response [1–5]. Glycoprotein D is a typical transmembrane protein, containing a signal peptide, which is cleaved off and a hydrophobic transmembrane region near the carboxy terminus. Mature gD type 1 (gD-1) contains 369 amino acid residues and mature gD type 2 (gD-2) has 368 residues [6]. Both are glycosylated and have three N-linked glycosylation sites and two to three O-linked sites [6–8]. Multiple polypeptide bands with a molecular mass between 45 000 and 48 000 on sodium dodecyl sulphate–polyacrylamide gel electrophoresis (SDS-PAGE) are found for recombinant gD produced in insect cells. As minor components, bands of lower molecular masses of 33 000, 24 000 and 22 000 may be found [9]. Immunizations with gD proved effective in attenuating the frequency and severity of primary disease in animals and in reducing the likelihood of latency [10]. These properties have led to its being tested as a candidate for a human subunit vaccine [11,12].

* Corresponding author.

0021-9673/94/$07.00
SSDI 0021-9673(94)00109-M

In earlier studies, we used the integral membrane proteins of Sendai virus as a model for the development of methodologies for the purification of membrane proteins using different detergents and different modes of HPLC [13–23]. This resulted in a two step elution protocol with a non-ionic detergent pentaethyleneglycol monodecyl ether ($C_{10}E_5$), at low and high concentration in the eluent for ion-exchange HPLC (HPIEC) [24].

The aim of this study is to investigate whether this method is applicable to the purification of other integral membrane proteins. To this end, the full-length gD polypeptide produced in recombinant baculovirus infected Sf21 insect cells (the cloning strategy will be published elsewhere) in a protein-free insect cell culture medium, will be purified by this procedure.

2. Experimental

2.1. Extraction of recombinant gD from Sf21 cells using non-ionic detergent $C_{10}E_5$ and sample preparation.

Sf21 cells were grown in protein-free insect cell culture medium (Insect X-press; Bio-Whittaker, Walkersville, MD, USA) containing 10 μg/ml gentamicin. Insect cells ($2.5 \cdot 10^8$) were infected at a multiplicity of infection of five plaque-forming units of recombinant baculovirus per cell. After 4 days at 27°C, cells were collected by centrifugation (100 *g*, 10 min, room temperature) and washed three times in ice-cold phosphate buffered saline, pH 7.4 (PBS). For extraction of membrane proteins, the cell pellet was resuspended in 5 ml of ice-cold 20 m*M* Tris–HCl, pH 7.8, 2 m*M* phenylmethylsulfonyl fluoride (PMSF), 1 m*M* tosyllysine chloromethyl ketone (TLCK) and subsequently, 5 ml of the same buffer containing 4% (w/v) $C_{10}E_5$, (Kwant–Hoog Vacolie Recycling and Synthesis, Bedum, Netherlands) was added under limited agitation. The cell suspension was incubated on ice for 1 h. Cell debris was removed by low-speed centrifugation (10 min, 2000 *g*). The supernatant (extract) after ultracentrifugation (70 000 *g*, 1 h, 4°C) contains gD and was stored in aliquots at −80°C.

2.2. HPIEC

Chromatography was performed with a system consisting of an LKB Model 2150 pump (Pharmacia–LKB, Woerden, Netherlands), a Rheodyne (Inacom, Veenendaal, Netherlands) Model 7125 injector and a Waters Model 441 detector (Millipore–Waters, Etten-Leur, Netherlands). Anion-exchange HPLC was performed with a Mono Q HR 5/5 column (50 mm × 5 mm I.D.) (Pharmacia–LKB). The flow-rate was 1 ml/min and absorbance was monitored at 280 nm. The samples of the infected cell extracts were 1:1 diluted with 20 m*M* Tris–HCl, pH 7.8, and centrifuged prior to injection at 14 000 *g* at 4°C for 5 min. After isocratic elution for 12 min, retained proteins were eluted with a linear 12-min gradient from 20 m*M* Tris–HCl, pH 7.8, containing 0.005% $C_{10}E_5$ (buffer A) to 0.5 *M* NaCl in the same buffer (buffer B). Following the gradient and subsequent isocratic elution for 15 min using buffer A, the concentration of detergent was increased to 0.1% $C_{10}E_5$ in 20 m*M* Tris–HCl, pH 7.8 (buffer C). During 30 min of isocratic elution with buffer C, the column was equilibrated. This was followed by a "blank" run, *i.e.* an additional gradient elution without sample injection. During the blank run retained proteins were eluted with a 12-min linear salt-gradient from 0 *M* NaCl in buffer C to 0.5 *M* NaCl in the same buffer (buffer D).

Fractions of 1 ml were collected during gradient elution. For enzyme-linked immunosorbent assay (ELISA), 50 μl of each fraction were used and the remainder was dialyzed (4–6 h, 4°C) against water. Samples of 125 μl of the fractions were lyophilized for SDS-PAGE. The remainder of the fractions were stored at − 80°C. Concentrations of gD in the extract and in the fractions were determined by a combination of ELISA and amino acid analysis.

2.3. SDS-PAGE

Dialyzed and lyophilized samples (125 μl) of some of the HPIEC fractions were analyzed by

SDS-PAGE on 12.5% gels under reducing conditions [25]. After electrophoresis, gels were fixed and silver stained as described [26].

2.4. ELISA

Microtiter plates were coated with serial dilutions (in 50 m*M* $NaHCO_3$ buffer, pH 9.6) of collected fractions for 18 h at 4°C. After washing with PBS containing 1 *M* NaCl and 0.3% Tween-20, plates were incubated with 1:6400 diluted monoclonal antibody (mAb) HD1 for 1 h. The mAb HD1 is specific for gD and directed against gD-1 and gD-2. The mAb HD1 is conformation-dependent [27], and reacts only with conformationally intact gD. After washing, plates were incubated for 1 h at 37°C with peroxidase-labelled sheep anti-mouse IgG (Sanofi Diagnostics Pasteur, Marnes-la-Coquette, France). After colour development with *o*-phenylenediamine dihydrochloride, the absorbance was measured at 492 nm. Glycoprotein D concentrations were calculated at $A_{492} = 1.2$ by using a gD-2 standard in combination with amino acid analysis. The mAb HD1 reacts at an A_{492} of 1.200 with 1.6 μg gD-1 and with 4.0 μg of gD-2.

3. Results and discussion

In a previous study, a two-step purification strategy for a model mixture of integral membrane proteins of Sendai virus was developed. By manipulating the concentration of the non-ionic detergent $C_{10}E_5$ added to eluent buffers during HPIEC, a selective elution of integral membrane proteins could be achieved [24]. This procedure was also successfully applied for the partial purification of a recombinant baculovirus malaria membrane antigen [28]. This prompted us to investigate whether this procedure might be applicable to the purification of other membrane proteins *viz.* the purification of recombinant and full-length gD, produced in baculovirus infected insect cells. Infected Sf21 cells, cultured in protein-free medium, were extracted with 2% $C_{10}E_5$. The extract contained 0.7 mg protein/ml of which 10–15% is gD-1 or gD-2. Samples (110–1000 μl, and containing 77 to 700 μg protein) of a $C_{10}E_5$ detergent extract containing 11.3–104 μg/ml gD-1 were subjected to two consecutive HPIEC-gradient runs with 0.005% $C_{10}E_5$ in the eluent during the first run and 0.1% $C_{10}E_5$ during the second (blank) run. Fractions were collected during the chromatographic steps and analyzed by ELISA to determine the presence of gD-1. In addition, SDS-PAGE was performed on the fractions collected during the salt gradient elution. Table 1 summarizes the purification procedure with the percentage gD-1 present during each purification step. No gD was present in the fractions of the flowthrough, and only trace amounts were found in the first fractions eluted isocratically during equilibration with buffer C.

Glycoprotein D mainly was eluted during the salt gradients, and the SDS-PAGE analyses of these fractions showed that gD that was eluted during the salt gradient in the presence of 0.1% $C_{10}E_5$ (buffer D) was virtually pure (see Fig. 2b). When a 104-μg sample was applied, a relatively large amount of gD-1 was eluted in the first gradient run and the distribution of gD-1 over both gradients resulted in a 85:15 ratio (see Table 2). The elution patterns of the two gra-

Table 1
Purification of glycoprotein D of Herpes simplex virus type 1 from infected Sf21 cells

Purification step	Percentage gD[a] present in purification step
Starting material: extract of infected cells	10–15
HPIEC:	
(1) flow-through isocratic elution with 0.005% $C_{10}E_5$ in buffer	0
(2) salt gradient, 0–0.5 *M* NaCl with 0.005% $C_{10}E_5$ in buffer	20–30
(3) isocratic elution with 0.005% $C_{10}E_5$ in buffer	0
(4) isocratic elution with 0.1% $C_{10}E_5$ in buffer	Trace
(5) salt gradient, 0–0.5 *M* NaCl with 0.1% $C_{10}E_5$ in buffer	> 90

[a] The percentage gD is based on the analysis of the fractions by SDS-PAGE and the gD-specific ELISA.

Table 2
Recovery of gD from an extract of insect cells infected with a recombinant baculovirus by HPIEC using a two-step purification procedure

Extract (μg gD)	Percentage of gD eluted during the first salt gradient detergent: 0.005% $C_{10}E_5$	Percentage of gD eluted during the blank run detergent: 0.1% $C_{10}E_5$	Total yield of gD after first and blank run
gD-1 extract			
1.62	22	78	71[a] (1.15 μg)
11.3	21	79	42 (4.7 μg)
26.0	41	59	51 (13.3 μg)
104	85	15	34 (35 μg)
gD-2 extract			
13.4	44	56	42 (5.6 μg)
30.4	60	40	44(13.5 μg)
60.8	64	36	40 (24.4 μg)

[a] Recovery of gD in percentages.

dient runs obtained after HPIEC of a detergent extract containing 26 μg gD-1 are shown in Fig. 1, together with the concentration of gD-1 in each fraction determined by an ELISA using a gD-specific mAb. Fig. 1a shows the elution pattern in the presence of the 0.005% $C_{10}E_5$, and Fig. 1b shows the elution pattern of the blank run in the presence of 0.1% $C_{10}E_5$. The corresponding SDS gels of the fractions are shown in Fig. 2a and b. In this case 41% of gD-1 was found in the first run and 59% in the blank run. Fig. 2b shows that the fractions of the blank run contain mainly two polypeptide bands of M_r 45 000–48 000. ELISA analysis of the fractions with a gD-specific mAb (Fig. 1b, columns below the chromatogram) confirms the presence of virtually pure, conformationally intact gD-1. Probably due to the presence of not fully glycosylated forms, gD-1 is eluted as a broad peak. When a small amount of the gD-1 (11.3 μg) containing extract was subjected to chromatography, gD-1 was mainly found in fractions that were collected during the second (blank) run, resulting in a 21:79 distribution of gD-1 over both gradients.

The total yield of gD-1, varying from 71 to 34% (Table 2), is relatively low. Part of gD is probably degraded during the purification procedure. This proteolytic degradation in the cell extracts is not unusual for HSV glycoproteins and has been described by others [29].

Extracts (containing gD-2, 121.5 μg/ml) of cells infected with recombinant baculovirus expressing gD-2, were prepared and used for HPIEC. Chromatography was performed using identical conditions as used for the purification of gD-1. Samples of 110, 250 and 500 μl of the gD-2 extract were subjected to the two-step elution protocol and analysis of the fractions by SDS-PAGE and ELISA showed results comparable to those obtained after HPIEC of a gD-1 extract (see Table 2).

To investigate whether gD eluted during the first gradient run is different from that eluted during the blank run, a 26-μg sample of gD-1 extract was used. Fractions 8, 9 and 10 (comparable to fractions 8, 9 and 10 of Fig. 1a) containing gD-1 from the first gradient run were pooled (2.7 ml) and briefly dialyzed against buffer A. A sample of 1.5 ml, containing 1.62 μg gD-1, of the dialyzed fractions was subjected to rechromatography, *i.e.* a complete combination of a first gradient run at low detergent concentration and a second (blank) gradient run at high detergent concentration. Glycoprotein D concentrations determined in every fraction showed that gD-1 which was eluted during the first low detergent gradient in the previous

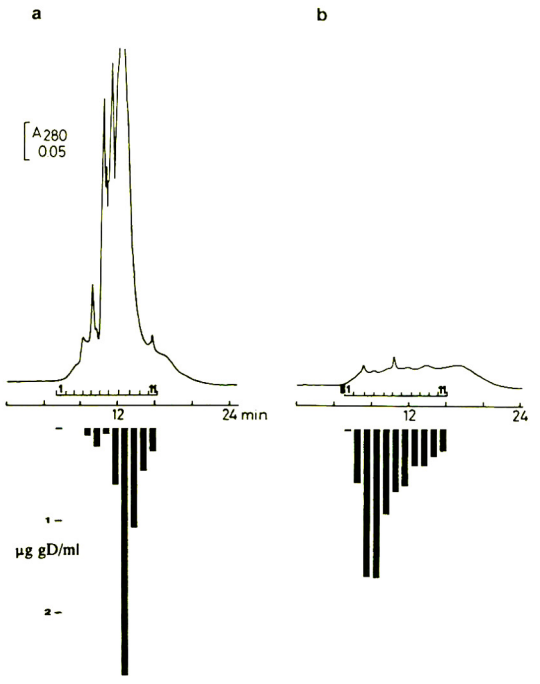

Fig. 1. HPIEC elution profile of a $C_{10}E_5$ extract of insect cells infected with a baculovirus gD recombinant. Chromatography was performed with a Mono Q HR 5/5 column. (a) After isocratic elution retained proteins were eluted with a linear 12-min gradient from 20 m*M* Tris–HCl (pH 7.8) containing 0.005% $C_{10}E_5$ to 0.5 *M* NaCl in the same buffer. This was followed by 15 min isocratic elution with 20 m*M* Tris–HCl (pH 7.8) containing 0.005% $C_{10}E_5$; the column was then equilibrated for 30 min with 20 m*M* Tris–HCl, pH 7.8, containing 0.1% $C_{10}E_5$. (b) The retained proteins were eluted with a linear salt gradient (blank run) in the presence of 0.1% $C_{10}E_5$ in 20 m*M* Tris–HCl buffer, pH 7.8, to 0.5 *M* NaCl in the same buffer. The flow-rate was 1 ml/min and the absorbance was monitored at 280 nm. Fractions were collected as indicated and analyzed by ELISA and by SDS-PAGE. The concentration of gD in the fractions was determined by ELISA with the gD-specific mAb HD1 and are indicated by columns below the elution profile.

chromatography, was re-distributed again over both, low (for 22%) and high (for 78%) detergent runs, indicating that there are no differences between gD-1 molecules eluted in the two runs.

It is not unlikely that besides the mainly electrostatic interaction of proteins with ion-exchange resins other contributions, *i.e.* hydrophobic properties of ion-exchange sorbents [30–33] may play a role in the chromatographic process. Non-ionic detergents may interfere with the interaction of the proteins and the ion-exchange ligands. The samples contain 1% of the detergent and consist at least partly out of micelles with the hydrophobic transmembrane region of gD-1 in the hydrophobic bilayer of the micelle. They are subjected to HPIEC with an eluent containing a relatively low concentration of detergent. The detergent monomers in the eluent will try to establish equilibrium with the detergent micelles that are attached to the column through the electrostatic interaction between gD-1 and the ion-exchange ligands. This will only be partially successful, since the detergent concentration in the eluent is too low and a certain concentration of NaCl will be necessary. In the second run the detergent concentration will be sufficiently high to pull all remaining gD-1 molecules into the eluent at the appropriate salt concentration. This may result in relatively pure membrane protein, because all hydrophilic proteins, which did not need a detergent for solubilization, were already eluted during the first run.

4. Conclusions

A highly purified recombinant gD of HSV types 1 and 2 produced by the baculovirus expression system can be obtained by a two-step purification strategy with HPIEC. At low detergent concentration the hydrophilic proteins in the extract are eluted with a salt gradient and a subsequent blank run with the same gradient at higher detergent concentration results in selective elution of the gD polypeptide which is still structurally and immunologically intact.

5. Acknowledgements

We thank Mr. B. Kwant (Bedum, Netherlands) for the gift of the non-ionic detergent $C_{10}E_5$. The truncated gD-2 was a generous gift of Dr. M. Slaoui, Smith-Kline, Belgium.

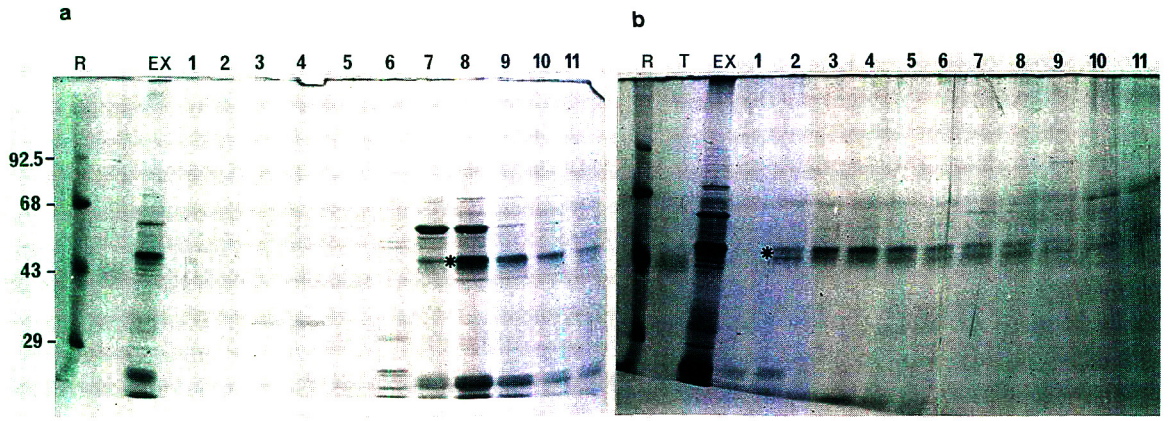

Fig. 2. SDS-PAGE analysis on 12.5% gels under reducing conditions of the fractions collected during chromatography shown in Fig. 1. Lane numbers of the gel correspond to fraction numbers in Fig. 1a and b, respectively. (a) SDS-PAGE analysis of fractions collected during a linear salt gradient in the presence of 0.005% $C_{10}E_5$; (b) SDS-PAGE analysis of the fractions collected during, a blank run, a linear salt gradient in the presence of 0.1% $C_{10}E_5$. Polypeptides were visualized by silver staining. Lanes: T = position of truncated gD-2 (M_r = 37 000–42 000), which was used as control; EX = starting material, extract of the cells infected with the recombinant baculovirus; R = the molecular masses ($\times 10^{-3}$) of reference proteins are given on the left. The asterisk indicates the migration position of glycoprotein D (M_r = 45 000–48 000).

6. References

[1] A.C. Minson, T.C. Hodgman and P. Digard, *J. Gen. Virol.*, 67 (1986) 1001.
[2] E. Heber-Katz, S. Valentine, B. Dietzschold and C. Burns-Purzycki, *J. Exp. Med.*, 167 (1988) 275.
[3] M.A. Tigges, D. Koelle, K. Hartog, R.E. Sekulovich, L. Corey and R.L. Burke, *J. Virol.*, 66 (1992) 1622.
[4] D. Long, T.J. Madara, M. Ponce de Leon, G.H. Cohen, P.C. Montgomery and R.J. Eisenberg, *Infect. Immun.*, 43 (1984) 761.
[5] R.D. Dix and J. Mills, *J. Med. Virol.*, 17 (1985) 9.
[6] L.A. Lasky and D.J. Dowbenko, *DNA*, 3 (1984) 23.
[7] D.L. Sodora, G.H. Cohen and R.J. Eisenberg, *J. Virol.*, 65 (1991) 4424.
[8] F. Serafini-Cessi, F. Dall'Olio, N. Malagolini, L. Pereira and G. Campadelli-Fiume, *J. Gen. Virol.*, 69 (1988) 869.
[9] H. Ghiasi, A.B. Nesburn, R. Kaiwar and S.I. Wechsler, *Arch. Virol.*, 121 (1991) 163.
[10] M.J. Hall and K. Katrak, *Vaccine*, 4 (1986) 138.
[11] E.M. Mishkin, J.R. Fahey, Y. Kino, R.J. Klein, A.S. Abramovitz and S.J. Mento, *Vaccine*, 9 (1991) 147.
[12] S.E. Straus, B. Savarese, M. Tigges, A.C. Freifeld, P.R. Krause, D.M. Margolis, J.L. Meier, D.P. Paar, S.F. Adair, D. Dina, C. Dekker and R.L. Burke, *J. Infect. Dis.*, 167 (1993) 1045.
[13] G.W. Welling, G. Groen and S. Welling-Wester, *J. Chromatogr.*, 266 (1983) 629.
[14] R. van der Zee, S. Welling-Wester and G.W. Welling, *J. Chromatogr.*, 266 (1983) 577.
[15] G.W. Welling, J.R.J. Nijmeijer, R. van der Zee, G. Groen, J.B. Wilterdink and S. Welling-Wester, *J. Chromatogr.*, 297 (1984) 101.
[16] G.W. Welling, G. Groen, K. Slopsema and S. Welling-Wester, *J. Chromatogr.*, 326 (1985) 173.
[17] G.W. Welling, K. Slopsema and S. Welling-Wester, *J. Chromatogr.*, 359 (1986) 307.
[18] G.W. Welling, K. Slopsema and S. Welling-Wester, *J. Chromatogr.*, 397 (1987) 165.
[19] G.W. Welling, B. Kazemier and S. Welling-Wester, *Chromatographia*, 24 (1987) 790.
[20] S. Welling-Wester, B. Kazemier, C. Örvell and G.W. Welling, *J. Chromatogr.*, 443 (1988) 255.
[21] J. van Ede, J.R.J. Nijmeijer, S. Welling-Wester, C. Örvell and G.W. Welling, *J. Chromatogr.*, 476 (1989) 319.
[22] S. Welling-Wester, R.M. Haring, J. Laurens, C. Örvell and G.W. Welling, *J. Chromatogr.*, 476 (1989) 476.
[23] G.W. Welling, Y. Hiemstra, M. Feijlbrief, C. Örvell, J. van Ede and S. Welling-Wester, *J. Chromatogr.*, 599 (1992) 157.
[24] S. Welling-Wester, M. Feijlbrief, D.G.A.M. Koedijk, M.A. Braaksma, B.R.K. Douma and G.W. Welling, *J. Chromatogr.*, 646 (1993) 37.
[25] U.K. Laemmli, *Nature (London)*, 227 (1970) 680.
[26] W. Wray, T. Boulikas, V.P. Wray and R. Hancock, *Anal. Biochem.*, 118 (1981) 197.
[27] L. Pereira, D.V. Dondero, D. Gallo, V. Devlin and J.D. Woodie, *Infect. Immun.*, 35 (1982) 363.
[28] D.L. Narum, G.W. Welling and A.W. Thomas, *J. Chromatogr. A*, 657 (1993) 357.

[29] K.M. Zezulak and P.G. Spear, *J. Virol.*, 50 (1984) 258.
[30] F.E. Regnier and R.M. Chicz, in K.M. Gooding and F.E. Regnier (Editors), *HPLC of Biological Macromolecules* (*Chromatographic Science Series*, Vol. 51), Marcel Dekker, New York, Basel, 1990, pp. 77–93.
[31] K.M. Gooding and M.N. Schmuck, *J. Chromatogr.*, 327 (1985) 139.
[33] M.L. Heinitz, L. Kennedy, W. Kopaciewicz and F.E. Regnier, *J. Chromatogr.*, 443 (1988) 173.
[33] T.W.L. Burke, C.T. Mant, J.A, Black and R.S. Hodges, *J. Chromatogr.*, 476 (1989) 377.

ELSEVIER

Journal of Chromatography A, 676 (1994) 51–63

JOURNAL OF CHROMATOGRAPHY A

High resolution of multiple forms of rabbit reticulocyte hexokinase type I by hydrophobic interaction chromatography

Vilberto Stocchi*, Paola Cardoni, Paola Ceccaroli, Giovanni Piccoli, Luigi Cucchiarini, Roberta De Bellis, Marina Dachà

Istituto di Chimica Biologica "Giorgio Fornaini", Università di Urbino, 61029 Urbino, Italy

Abstract

Hydrophobic interaction chromatography (HIC) has been employed extensively in the separation of proteins by elution using a descending salt gradient, with and without the use of detergents or denaturing agents. In this study, a new hydrophobic interaction chromatographic support, Toyopearl Phenyl 650 S, was investigated in order to examine the distribution of multiple forms of rabbit reticulocyte hexokinase type I. These distinct forms of the enzyme, designated hexokinase Ia, Ia* and Ib, show similar kinetic and physical properties, similar molecular masses (ca. 100 000) and a different intracellular distribution. The results obtained using Toyopearl Phenyl 650 S of 20–50-μm particle diameter show that this HIC support allows very high resolution, comparable to that obtainable with HIC–HPLC columns but with the advantage of charging a higher amount of starting material even with a high protein concentration. These characteristics render Toyopearl Phenyl 650 S suitable for analytical and preparative purposes. Further, in the separation of multiple forms of rabbit reticulocyte hexokinase, the HIC method was shown to be superior to RP-HPLC, making possible the efficient separation of proteins with high molecular mass and their recovery in active forms. The Toyopearl Phenyl 650 S column was also shown to be more efficient than the ion-exchange chromatographic media previously used, allowing a quicker analysis of the multiple forms of rabbit reticulocyte hexokinase under different biological conditions.

1. Introduction

Data published in recent years have clearly shown that the occurrence of multiple forms of enzymes is not unusual but, rather, is a common phenomenon. Hexokinase exists in mammalian tissues as four isoenzymes with distinct properties and tissue distributions [1,2]. It is commonly accepted that red blood cell hexokinase is mainly of type I, and the presence of sub-types has also been described [3]. Multiple forms of red blood cell hexokinase were first reported by Eaton et al. [4], who observed several electrophoretic bands. Many workers have confirmed the existence of two or more distinguishable forms of hexokinase in different mammalian erythrocytes [5–19]. Hexokinase in rabbit reticulocytes is present in three distinct forms, which we designated hexokinase Ia, Ia* and Ib [20]; hexokinase Ia and Ib are present in soluble form, whereas hexokinase Ia* is mainly bound to the mitochondria. In fact, in rabbit erythrocytes

* Corresponding author.

0021-9673/94/$07.00
SSDI 0021-9673(94)00443-D

only the soluble forms Ia and Ib are present whereas hexokinase Ia*, associated with mitochondria, is detectable only in whole blood samples containing reticulocytes [20]. Further, these multiple forms are unstable and glucose, fructose, glycerol and sulphydryl protecting agents are required for the maintenance of their activity during purification procedures. All of these sub-types have high molecular masses (ca. 100 000), differ very little in their isoelectric points and show similar kinetic and physical properties [21].

For these reasons, the chromatographic profile of rabbit reticulocyte hexokinase can be considered of interest in testing the performance of new chromatographic media. Further, the use of the haemolysate allows us to test the efficiency using a real sample with very high protein concentrations. Usually, a mixture of standard pure proteins, such as albumin, cytochrome *c*, lysozyme and myoglobin, is used to test the performance of new chromatographic supports [22]. Although it is possible to gain some information under these "ideal" conditions, the situation can change significantly when a real sample is used, as in the case of haemolysates, tissue homogenates and bacterial lysates. In this paper, we report the rapid and high resolution of rabbit reticulocyte hexokinase sub-types obtained using a new hydrophobic interaction chromatographic support, Toyopearl Phenyl 650 S. This chromatographic matrix permits the efficient elution of proteins according to their different hydrophobicities without the use of detergents or denaturing agents. This allows the separation of proteins under conditions suitable for maintaining biological activity, a characteristic of fundamental importance above all when the proteins under examination are present in very small amounts and in multiple forms. Further, the chemical and physical properties of this support permit the use of flow-rates even higher than those used with HIC–HPLC columns, thus allowing rapid and complete protein separations. Therefore, this support is particularly suitable for the investigation of pattern modifications of enzymes under different biological conditions.

2. Experimental

2.1. Chemicals and reagents

Coenzymes, enzymes, substrates and dithiothreitol were purchased from Sigma (St. Louis, MO, USA). Toyopearl Phenyl 650 S and M and TSKgel Phenyl-5 PW were obtained from Tosohaas Technical Center (Woburn, MA, USA). All other reagents were of analytical-reagent grade.

2.2. Instrumentation

A Kontron Uvikon 860 spectrophotometer was used for optical measurements. The HPLC system consisted of two Model 112 pumps (Beckman, Berkeley, CA, USA), a Model 340 dynamic gradient mixer (Beckman) and a Model 420 gradient controller (Beckman). A Minipuls 2 peristaltic pump (Gilson, Molsheim, France) was used for packing the columns.

2.3. Preparation of Toyopearl Phenyl columns

Toyopearl Phenyl 650 S (20–50-μm particles) and 650 M (40–90-μm particles) had to be separated from fines by decantation, as the presence of fines in suspension can affect the resolution. The required amount of resuspended resin was transferred into a beaker and distilled water was added (four times the resin volume). This solution was mechanically stirred gently and allowed to settle for 60–90 min. The supernatant containing the fines was removed by suction using a water pump. This procedure had to be repeated 2–3 times. For the final decantation, the resin was resuspended in the packing solvent (in our case the equilibrating buffer). Air bubbles were removed by leaving the slurry for 2–3 min in an ultrasonic bath. The settled gel was then resuspended in an equal volume of equilibrating buffer, poured into the appropriate column and packed, using a peristaltic pump, at a flow-rate of 0.5 ml/min.

2.4. Chromatographic conditions

Triply-distilled water was prepared and used for preparing buffers, which were filtered through a 0.22-μm Millipore filter before HPLC analysis. The equilibrating solution used was 5 m*M* sodium potassium phosphate buffer (pH 8.1) containing 3 m*M* 2-mercaptoethanol (2-MSH), 3 m*M* KF, 1 m*M* dithiothreitol (DTT), 5 m*M* glucose and 30% (w/v) ammonium sulphate. Elution was performed using a descending gradient of ammonium sulphate. The profiles of the descending gradients used for separations are given on each chromatogram.

2.5. Hexokinase assay

Hexokinase (EC 2.7.1.1) activity was measured spectrophotometrically at 37°C in a system coupled with glucose-6-phosphate dehydrogenase (EC 1.1.1.49), as described previously [23], except that 6-phosphogluconate dehydrogenase (EC 1.1.1.44) was omitted and the glucose-6-phosphate dehydrogenase concentration was increased to 0.5 IU/ml. One unit of hexokinase activity was defined as the amount of enzyme necessary to catalyse the formation of 1 μmol/min of glucose-6-phosphate at 37°C.

2.6. Protein determination

In the haemolysate, the haemoglobin concentration was determined spectrophotometrically at 540 nm with Drabkin's solution as described by Beutler [24]. Protein concentrations were determined spectrophotometrically at 280 nm in the course of elution of enzymes from the columns.

2.7. "In vivo" preparation of rabbit reticulocytes

Rabbit reticulocytes were obtained by the administration of phenylhydrazine to rabbits followed by the collection of blood samples at day 8 from the beginning of the treatment [19]. Using this procedure, the amount of reticulocytes in the whole blood usually ranged from 40 to 60%. The rabbit reticulocyte lysate used for the experiments came from different rabbits; therefore, the percentage of reticulocytes in the whole blood sample varied. This meant that the chromatographic profile of rabbit reticulocyte hexokinase was not necessarily the same from rabbit to rabbit.

2.8. Preparation of rabbit haemolysate

Whole blood was collected in heparin and immediately centrifuged at 1000 *g* for 10 min at 4°C. After removal of plasma and buffy coat, the red blood cells were washed twice with cold isotonic saline solution. The packed rabbit red blood cells were then lysed by the addition of an equal volume of 0.5% (v/v) Triton X-100 and the solution was left in ice for 30 min. The stroma were then removed by centrifugation at 11 000 *g* for 30 min.

3. Results and discussion

3.1. Separation of multiple forms of rabbit reticulocyte hexokinase by HIC

In mammalian red blood cells, hexokinase type I has been shown to be present in multiple forms [5–19]. Recently, using a new ion-exchange chromatographic support, Toyopearl DEAE 650 S, we had been able to separate three distinct forms of hexokinase from rabbit reticulocytes. It should be pointed out that, among the different anion exchangers commercially available, this chromatographic matrix was the only one which had allowed the complete separation of these three multiple forms [25]. Fig. 1A shows the hexokinase chromatographic profile of a rabbit blood sample with a content of reticulocytes ranging from 40 to 60%. As shown, the different forms of hexokinase can be eluted from Toyopearl DEAE 650 S as three distinct peaks, which we designated Ia, Ia* and Ib. In rabbit reticulocytes the hexokinase designated Ia* is mainly bound to the mitochondria [20]. A similar situation occurs with other tissues such as

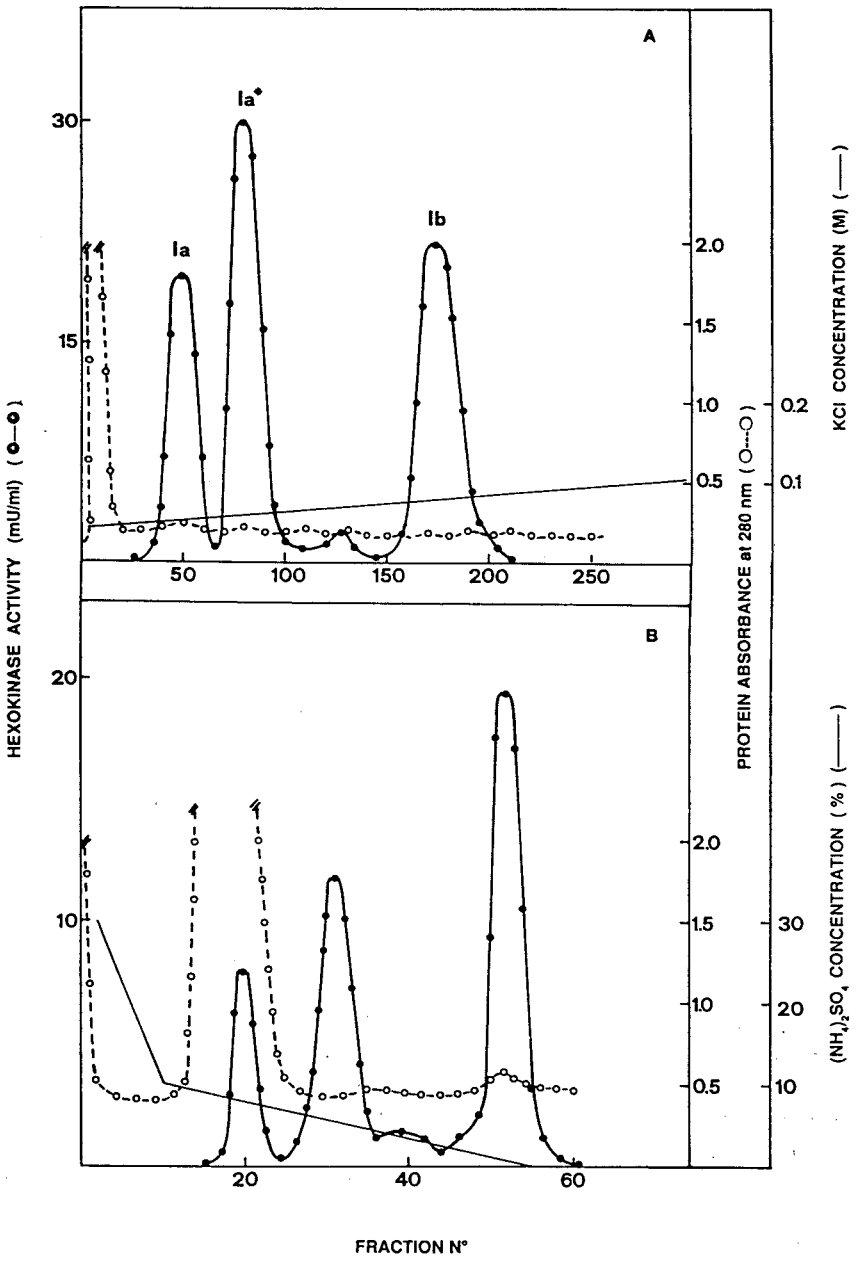

Fig. 1. Separation of multiple forms of hexokinase from rabbit reticulocytes. (A) Toyopearl DEAE 650 S column (15 cm × 1 cm I.D.). A 12-ml sample of haemolysate with a protein concentration of 50 mg/ml was charged on to the column. The column was equilibrated in 5 m*M* sodium potassium phosphate buffer (pH 8.1) containing 3 m*M* KF, 3 m*M* 2-MSH, 1 m*M* DTT and 5 m*M* glucose and operated at 0.3 ml/min at 4°C. The elution of the hexokinase activity was obtained using a 200-ml linear gradient of KCl from 40 to 200 m*M* in the same equilibrating buffer. Fractions of 0.7 ml were collected and assayed for hexokinase activity. (B) Toyopearl Phenyl 650 S column (5 cm × 1.2 cm I.D.). A 500-μl sample of haemolysate with a protein concentration of 190 mg/ml was charged on to the column. The column was equilibrated in the buffer described under Experimental and operated at 0.5 ml/min at room temperature. The hexokinase activity was eluted using a two-step descending gradient of ammonium sulphate from 30 to 10% in 15 min and from 10 to 0% in 90 min. Fractions of 1 ml were collected and assayed for hexokinase activity.

the brain [26–29] and in transformed cell lines, where it has been shown that the increase in hexokinase activity involves mainly the form bound to the mitochondria [30,31]. The binding of the enzyme to these organelles, in the rat brain, is due the presence of nine additional N-terminal hydrophobic amino acids [32]. It is reasonable to assume that a similar situation can occur in rabbit reticulocytes, making the hexokinase Ia* more hydrophobic than hexokinase Ia and Ib, which are present in soluble form. A simple method to distinguish between the bound and soluble forms of the enzyme would be useful in order to study the properties of hexokinase Ia*.

Fig. 1B shows the chromatographic profile obtained using a Toyopearl Phenyl 650 S column. The result is very interesting, not only because this HIC support allows the elution of the more hydrophobic form Ia*, but also because a complete separation of the soluble forms Ia and Ib, which are eluted in the first part of the chromatogram, was possible. However, comparing the two chromatographic profiles shown in Fig. 1, we can observe that, using Toyopearl DEAE 650 S, the haemoglobin is immediately eluted from the column with the equilibrating buffer. With Toyopearl Phenyl 650 S, in contrast, only a small amount of the haemoglobin is removed by washing and most of this protein is eluted concomitantly with hexokinase Ia. In any case, the HIC matrix permits a quick separation of reticulocyte hexokinase sub-types by means of a descending gradient of ammonium sulphate and without the use of detergents or denaturing agents. Further, these experimental conditions allow the recovery of the sub-types of the enzyme in their active form.

3.2. Identification of multiple forms of hexokinase from rabbit reticulocytes using Toyopearl Phenyl 650 S columns

The identification of the three distinct forms of rabbit reticulocyte hexokinase eluted by HIC was performed by charging each peak separated by ion-exchange chromatography on to the Toyopearl Phenyl 650 S columns. The chromatographic profiles of each form (Fig. 2A–C) show that their elution times are in agreement with the complete isozymic pattern obtained by charging a real sample of rabbit reticulocyte lysate on to the column (Fig. 2D). On the basis of these results, hexokinase Ia is the least hydrophobic form, whereas hexokinase Ib shows an intermediate hydrophobicity and, as expected, hexokinase Ia* is the most hydrophobic form. Hexokinase Ia* is mainly bound to the mitochondria, and previous studies have shown that this form of the enzyme sediments in density gradients with these organelles [33]. Only the addition of glucose-6-phosphate or detergents such as saponin or Triton X-100 causes its solubilization.

Kurokawa et al. [34] have reported the separation of mitochondria-bindable hexokinase from rat brain by HIC using a Phenyl-Sepharose column. Under their experimental conditions the enzyme present in soluble form was not adsorbed on the column, but rather was eluted with the equilibrating buffer, while the elution of the mitochondria-bindable hexokinase required the addition of a detergent such as Lubrol PX. In our case, Toyopearl Phenyl 650 S has the advantage of eluting the most hydrophobic form, Ia*, without the use of detergents or denaturing agents. Further, hexokinase Ia and Ib, present in soluble form, were adsorbed to the column and were eluted at the beginning of the gradient in two distinct peaks (Fig. 2D). The good separation of these sub-types was unexpected, as both are present in soluble form and show very similar molecular masses (ca. 100 000), kinetic properties (the K_m value of glucose was 0.04 mM for hexokinase Ia and 0.125 mM for hexokinase Ib; both enzymes have the same K_m value for MgATP, 0.05 mM) and differ very little in their isoelectric points [21].

Further evidence confirming that the identification of multiple forms of hexokinase was correct was also obtained by investigating the chromatographic profile of the enzyme in rabbit erythrocytes. The isozymic profiles obtained using Toyopearl DEAE 650 S (Fig. 3A) and Toyopearl Phenyl 650 S (Fig. 3B) columns only show the presence of the soluble forms Ia and Ib. This is due to the fact that during maturation

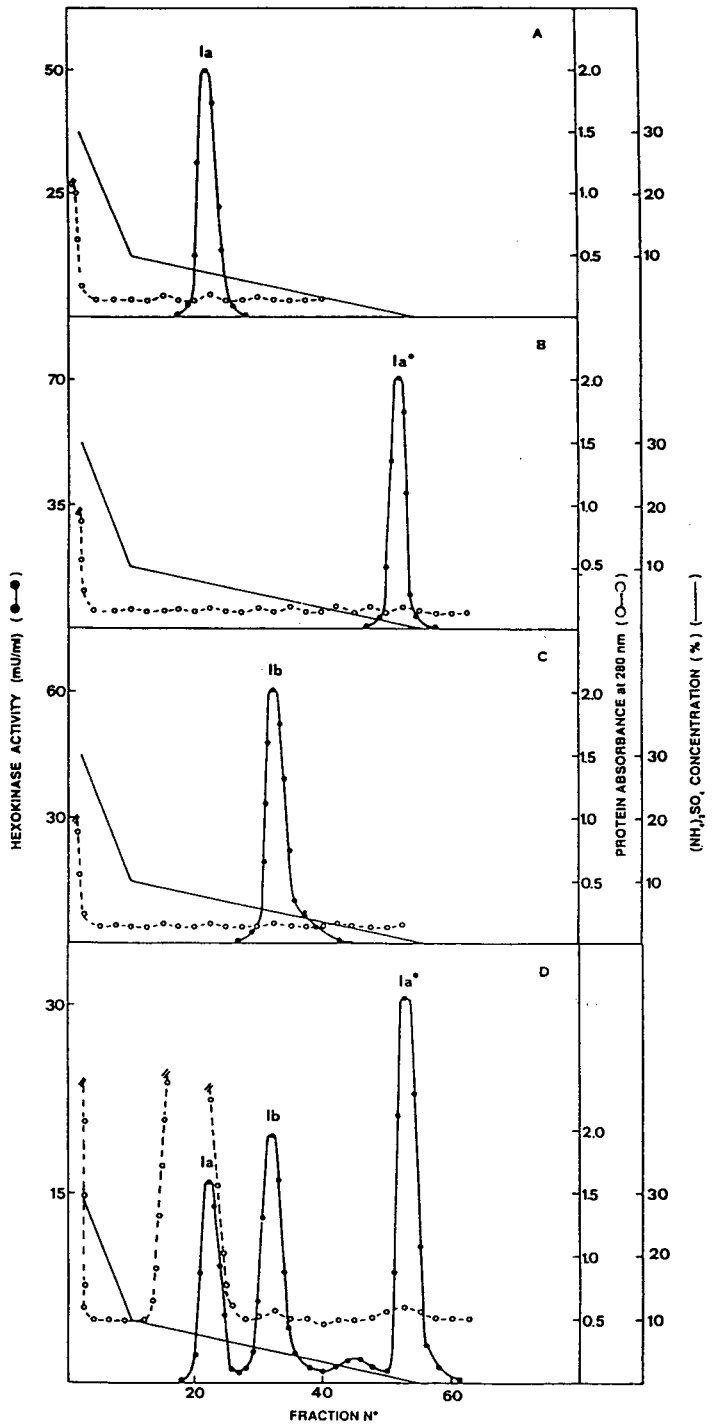

Fig. 2. Identification of multiple forms of hexokinase from rabbit reticulocytes. Hexokinase (A) Ia, (B) Ia* and (C) Ib, eluted from Toyopearl DEAE 650 S, were charged separately on to Toyopearl Phenyl 650 S columns. (D) Complete isozymic profile of rabbit reticulocytes. All chromatographic profiles were obtained using the experimental conditions as in Fig. 1B.

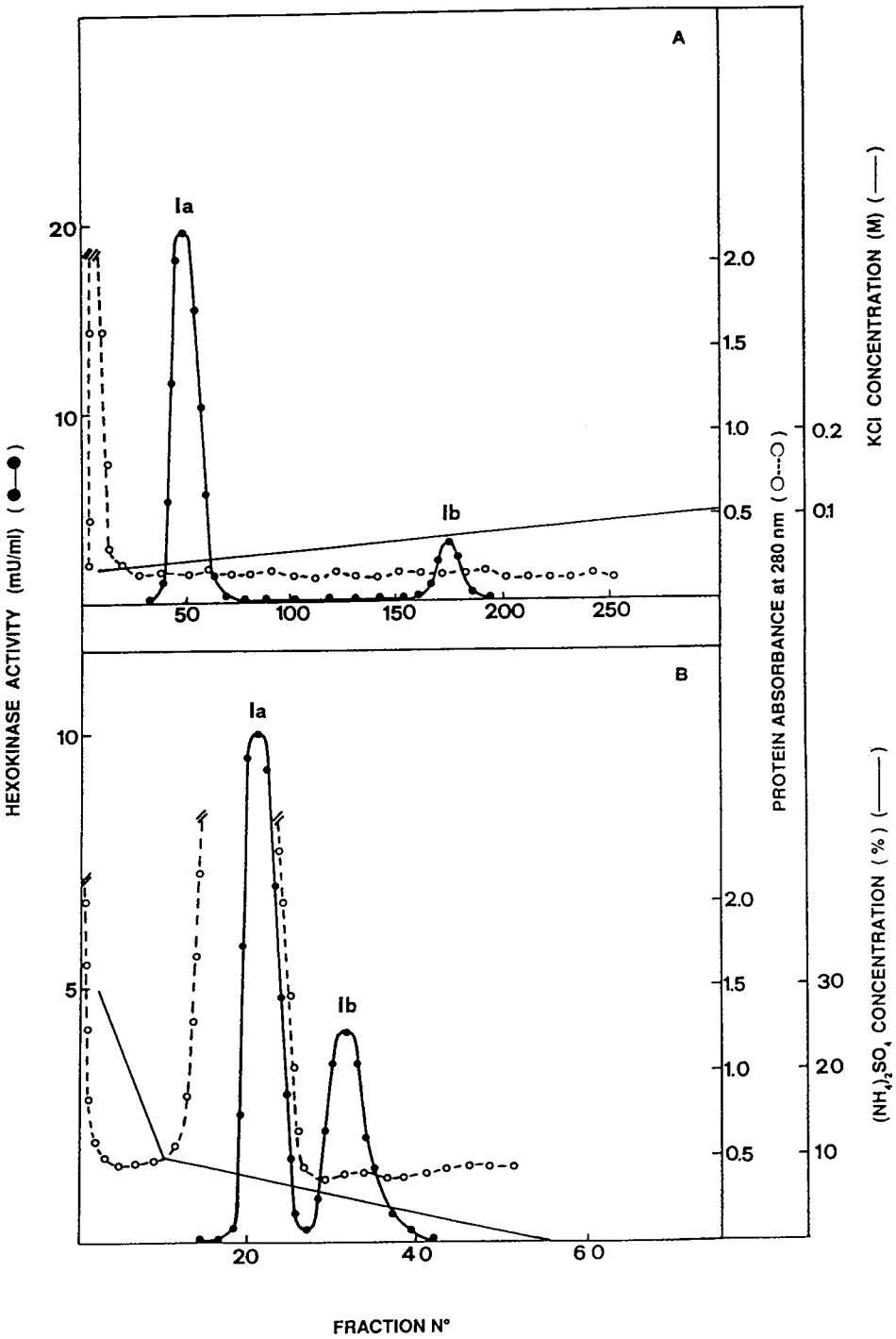

Fig. 3. Separation of multiple forms of hexokinase from rabbit erythrocytes using (A) a Toyopearl DEAE 650 S column and (B) a Toyopearl Phenyl 650 S column. All chromatographic profiles were obtained using the same experimental conditions as in Fig. 1.

of the reticulocytes to erythrocytes there is a significant change in the chromatographic profile of hexokinase. In fact, hexokinase Ia* is completely lost, and only hexokinase Ia and a small amount of hexokinase Ib are present in the erythrocytes. It is of interest that hexokinase Ib, which had previously been shown to undergo a faster decay than hexokinase Ia during the ageing of erythrocytes [18], is also more hydrophobic than hexokinase Ia.

3.3. Influence of flow-rates and salt gradients on resolution

In order to obtain more information on the behaviour of Toyopearl Phenyl 650 S, we investigated the effects of different flow-rates and salt gradients on the resolution of multiple forms of rabbit reticulocyte hexokinase. As regards the effects of flow-rates on the elution of proteins, we performed experiments at 0.5 ml/min (Fig. 4A) and 1.0 ml/min (Fig. 4B). As shown in Fig. 4B, it is possible to maintain a good resolution of multiple forms of hexokinase working at a flow-rate of 1 ml/min as used with HPLC columns. Further, we have shown that this HIC support can be used to separate hexokinase from other tissues even working at a flow-rate of 1.5 ml/min (data not shown). The results obtained show that the rigid methacrylic polymer structure of the Toyopearl HIC resins is mechanically stable, allowing the use of higher flow-rates than with other conventional media.

As another parameter affecting separation in HIC is the salt gradient, we also investigated its influence on the separation of multiple forms of hexokinase. Fig. 5A shows the elution of hexokinase activity using a two-step descending gradient of ammonium sulphate, from 30 to 10% in 8 min and from 10 to 0% in 45 min at a flow-rate of 1.0 ml/min. Fig. 5B shows the chromatographic profile obtained using a different gradient, from 30 to 0% ammonium sulphate in 120 min at a flow-rate of 1.0 ml/min. As shown, the two-step gradient allows a better resolution than a linear gradient with almost the same slope. Probably the use of a two-step gradient, with a drastic decrease in salt concentration in the first step, allows a better separation of soluble forms Ia and Ib. The use of a descending salt gradient of ammonium sulphate allows the elution of enzymes in their active forms. In fact, the solvent conditions in HIC generally stabilize tertiary and quaternary protein structures [35] whereas the use of organic solvents in RP-HPLC promotes the denaturation of proteins [36,37].

3.4. Effects of different particle sizes on resolution

Conventional low-pressure chromatographic procedures usually give a lower resolution than those obtainable using HPLC columns. The efficiency of the Toyopearl Phenyl 650 S column (20–50-μm particles), packed using a peristaltic pump, was assessed by comparing the elution profiles obtained using an HIC–HPLC column. Fig. 6A shows the chromatographic profile of rabbit reticulocyte hexokinase obtained using a TSKgel Phenyl-5 PW HPLC column (10-μm particles). This HIC–HPLC support allows the adsorption of soluble forms Ia and Ib on the column with a very good resolution into sharp peaks. It is interesting that, as shown in Fig. 6B, the low-pressure Toyopearl Phenyl 650 S support allows a resolution comparable to that obtained with HPLC columns, but with the advantage of charging higher amounts of starting material. The amount of sample that can be charged on to the HPLC column is very small because the haemolysate has a high protein concentration (160–200 mg/ml). With rabbit erythrocytes, and also other mammalian red blood cells, the level of hexokinase activity is very low, 0.0003% (w/w) [21]. Therefore, using a TSKgel Phenyl-5 PW HPLC column, only analytical separations can be performed.

Further studies concerning the kinetic, chemical and physical characteristics of each form of hexokinase are limited by the amount of starting material which can be charged on to the column. In fact, using red blood cell haemolysates, the protein concentration ranges from 160 to 200 mg/ml; under these conditions, the amount of starting material that can be injected on to a TSKgel Phenyl-5 PW HPLC column ranges from

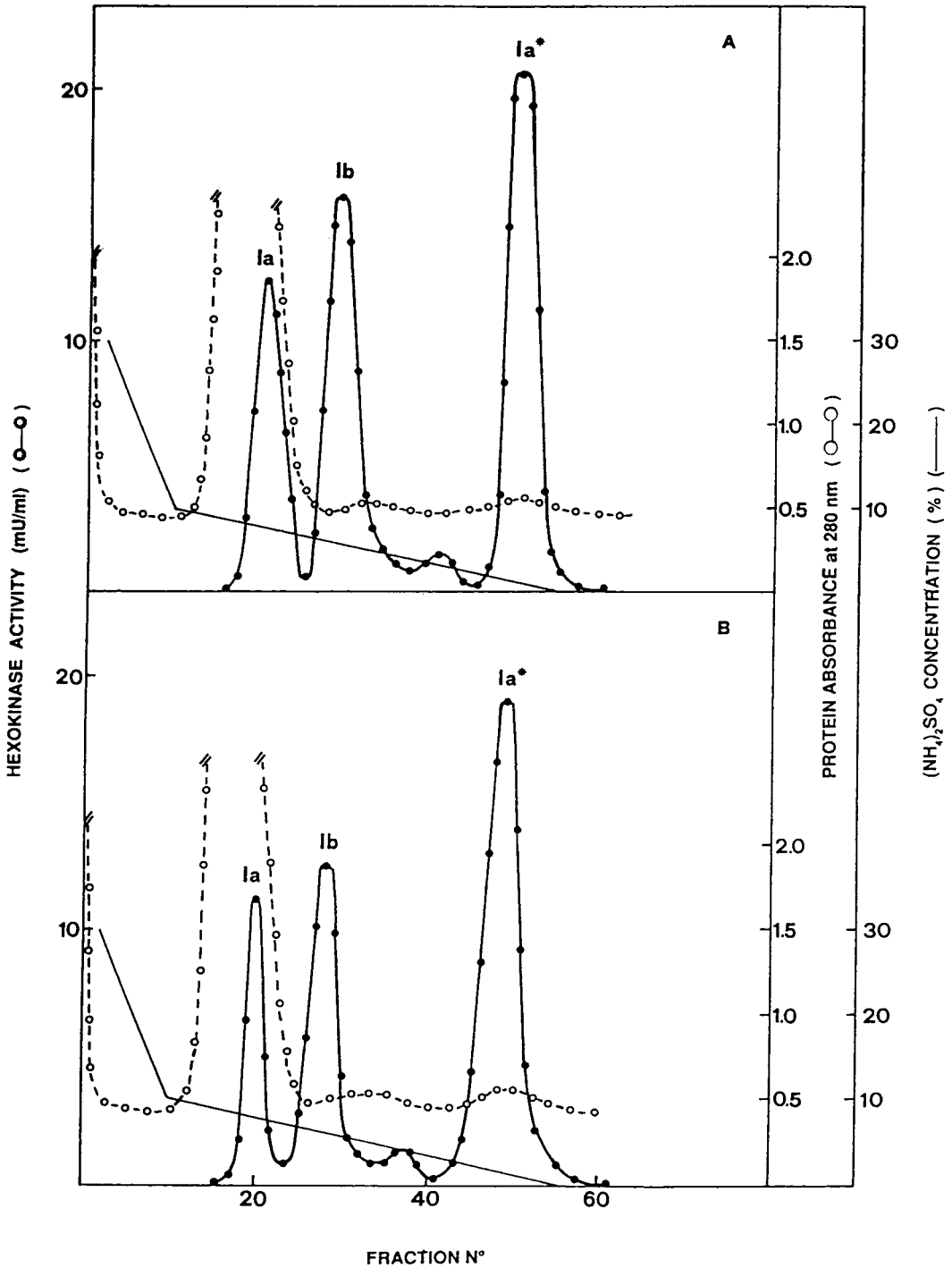

Fig. 4. Influence of flow-rates on the separation of multiple forms of hexokinase from rabbit reticulocytes. (A) Elution of hexokinase activity using the same experimental conditions as in Fig. 1B; (B) elution of hexokinase activity using a flow-rate of 1 ml/min; the descending gradient of ammonium sulphate was from 30 to 10% in 8 min and from 10 to 0% in 45 min.

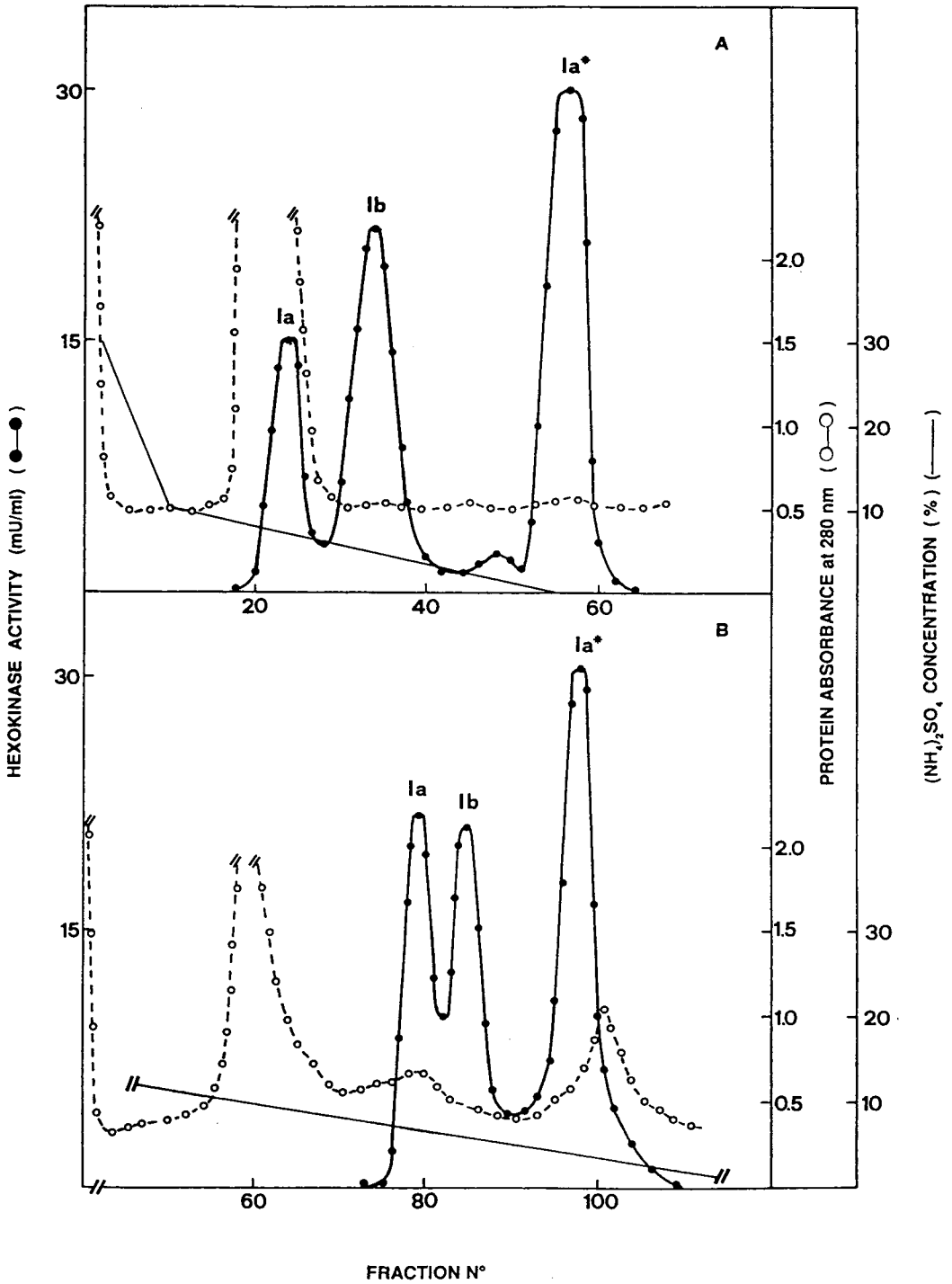

Fig. 5. Influence of the gradient on the separation of multiple forms of hexokinase from rabbit reticulocytes. (A) Elution of hexokinase activity using the same experimental conditions as in Fig. 4B; (B) elution of hexokinase activity using a one-step descending gradient from 30 to 0% ammonium sulphate in 120 min at a flow-rate of 1 ml/min.

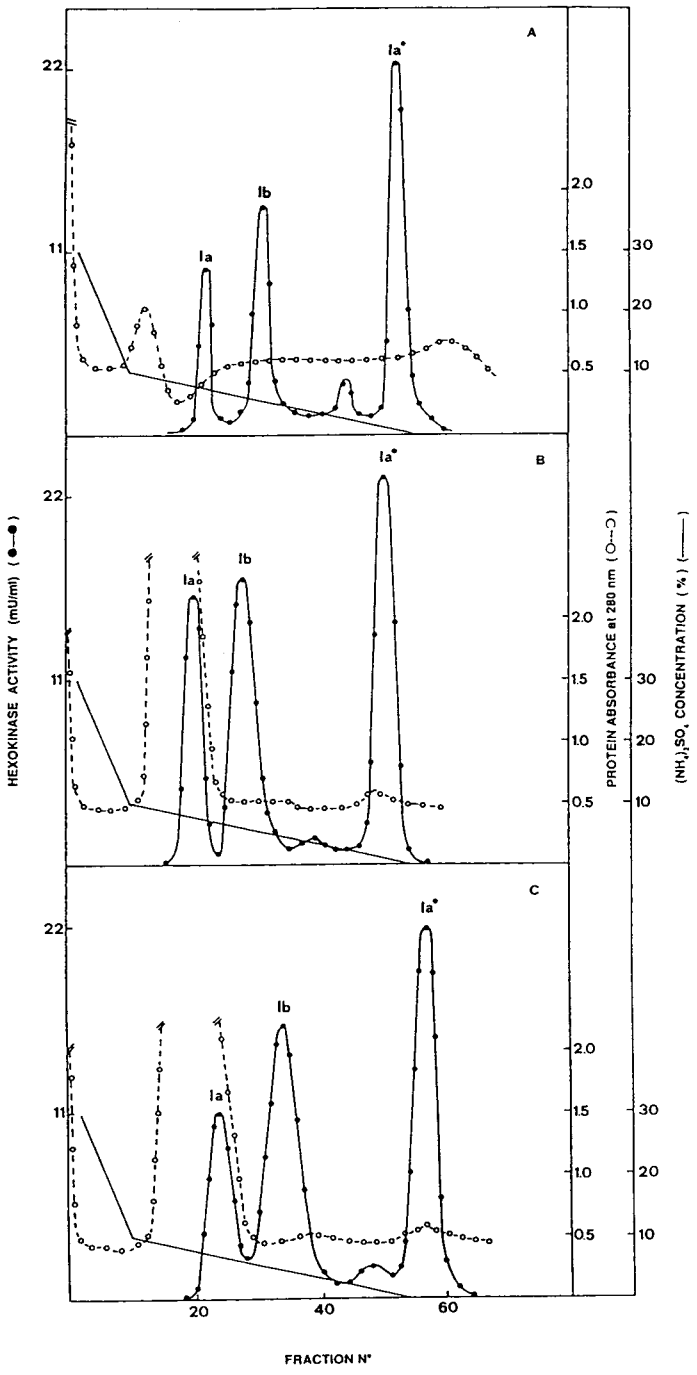

Fig. 6. Separation of multiple forms of hexokinase from rabbit reticulocytes using different chromatographic supports. (A) TSKgel Phenyl-5 PW (7.5 cm × 0.75 cm I.D.), particle size 10 μm; (B) Toyopearl Phenyl 650 S (5 cm × 1.2 cm I.D.), particle size 20–50 μm; (C) Toyopearl Phenyl 650 M (5 cm × 1.2 cm I.D.), particle size 40–90 μm. All chromatographic profiles were obtained using the same experimental conditions as in Fig. 4B.

100 to 500 μl. Further, after several injections of 500 μl of haemolysate, charged on to the column in separate aliquots of 100 μl, we observed a significant decrease in resolution due to the aspecific adsorption of material which remains bound to the column and is difficult to remove even by performing different regeneration procedures [0.1–0.2 *M* sodium hydroxide solution or 20–40% (v/v) acetic acid]. In order to overcome this inconvenience, we charged the haemolysate on to a guard column of TSKgel Phenyl-5 PW (1 cm × 0.6 cm I.D.). Under these conditions the hexokinase present in 500 μl of starting material is completely adsorbed, while most of the haemoglobin, which represents about 98% of the total proteins present in the haemolysate, is eluted using the equilibrating buffer. After removal of the bulk of the proteins, the guard column was connected to the analytical column and the elution of the distinct forms of hexokinase was obtained using a descending gradient of ammonium sulphate. Although this procedure prolongs the life of the analytical column, some proteins adsorbed on the guard column flow through the analytical column and, eventually, significantly affect the resolution. Given these results, it appears clear that the TSKgel Phenyl-5 PW HPLC column is very useful for analytical separations when injecting samples with low protein concentrations, whereas its use is not recommended when the starting material has a very high protein concentration (as with haemolysates, tissue homogenates, etc.).

In order to evaluate the influence of particle diameter on resolution, we compared the performance of Toyopearl Phenyl 650 S (20–50-μm particles) with that of Toyopearl Phenyl 650 M (40–90-μm particles). The chromatographic profile of rabbit reticulocyte hexokinase, shown in Fig. 6C, is very interesting, as the three molecular forms of hexokinase show a good resolution notwithstanding the fact that the peaks are slightly broader than those obtained using Toyopearl Phenyl 650 S (20–50 μm). The above results suggest that particle size does not significantly influence the resolution of hexokinase type I, even though Toyopearl Phenyl 650 S allows a better resolution with sharper peaks.

4. Conclusions

The use of Toyopearl Phenyl 650 S was found to allow a quicker and higher resolution of multiple forms of rabbit reticulocyte hexokinase Ia, Ia* and Ib than some other chromatographic methods [25]. The results reported in this paper also show that the low-pressure Toyopearl Phenyl 650 S support allows a resolution similar to that obtainable using a TSKgel Phenyl-5 PW HPLC column but with the advantage of charging higher amounts of starting material even with a very high protein concentration. These properties make this chromatographic support suitable for analytical and preparative purposes. Further, compared with other HIC supports, Toyopearl Phenyl 650 S allows the elution of different forms of hexokinase without the use of detergents or denaturing agents, thus allowing the recovery of proteins in their active form. A wide application of this technique in biochemical analysis and biotechnology is expected in the near future.

Acknowledgements

This work was supported by P.F. Chimica Fine II and Ingegneria Genetica, CNR.

References

[1] D.L. Purich, H.J. Fromm and F.B. Rudolph, *Adv. Enzymol.*, 39 (1973) 249.
[2] S.P. Colowick, in P.D. Boyer (Editor), *The Enzymes*, Vol. IX, Academic Press, New York, 1973, p. 1.
[3] V. Stocchi, M. Magnani, F. Canestrari, M. Dachà and G. Fornaini, *J. Biol. Chem.*, 257 (1982) 2357.
[4] G.M. Eaton, G.J. Brewer and R.E. Tashian, *Nature*, 212 (1966) 944.
[5] E.W. Holmes, J.I. Malone, A.I. Winegrad and F.A. Oski, *Science*, 156 (1967) 646.
[6] C. Altay, C.A. Alper and D.G. Nathan, *Blood*, 36 (1970) 219.
[7] J.C. Kaplan and E. Beutler, *Science* 159 (1968) 215.
[8] F.M. Gellerich and H.W. Augustin, *Acta Biol. Med. Ger.*, 38 (1979) 1091.
[9] W. Schröter and W. Tillmann, *Biochem. Biophys. Res. Commun.*, 31 (1968) 92.

[10] G.J. Brewer and C.A. Knutsen, *Science*, 159 (1968) 650.
[11] E.W. Holmes, J.I.Jr. Malone, I.A. Winegrad and F.A. Oski, *Science*, 159 (1968) 651.
[12] P.A. Rogers, R.A. Fischer and H. Harris, *Clin. Chim. Acta*, 65 (1975) 291.
[13] G. Rijksen, I. Schoop and G.E.J. Staal, *Clin. Chim. Acta*, 80 (1977) 193.
[14] M. Gahr, *Hoppe-Seyler's Z. Physiol. Chem.*, 361 (1980) 829.
[15] M. Gahr, *Br. J. Haematol.*, 46 (1980) 529.
[16] G. Fornaini, M. Magnani, M. Dachà, M. Bossù and V. Stocchi, *Mech. Ageing Dev.*, 8 (1978) 249.
[17] M. Magnani, V. Stocchi, M. Bossù, M. Dachà and G. Fornaini, *Mech. Ageing Dev.*, 11 (1979) 209.
[18] M. Magnani, V. Stocchi, M. Dachà, F. Canestrari and G. Fornaini, *FEBS Lett.*, 120 (1980) 264.
[19] V. Stocchi, M. Magnani, F. Canestrari, M. Dachà and G. Fornaini, *J. Biol. Chem.*, 256 (1981) 7856.
[20] V. Stocchi, M. Magnani, G. Piccoli and G. Fornaini, *Mol. Cell. Biochem.*, 79 (1988) 133.
[21] G. Fornaini, M. Dachà, M. Magnani and V. Stocchi, *Methods Enzymol.*, 90 (1982) 3.
[22] J.L. Fausnaugh, E. Pfannkoch, S. Gupta and F.E. Regnier, *Anal. Biochem.*, 137 (1984) 464.
[23] M. Magnani, M. Dachà, V. Stocchi, P. Ninfali and G. Fornaini, *J. Biol. Chem.*, 255 (1980) 1752.
[24] E. Beutler, in *Red Cell Metabolism*, Grune and Stratton Inc., New York, 3rd ed., 1984, p. 12.
[25] V. Stocchi, L. Masat, B. Biagiarelli, A. Accorsi, G. Piccoli, F. Palma, L. Cucchiarini and M. Dachà, *Prep. Biochem.*, 22 (1992) 11.
[26] H.M. Katzen, D.D. Soderman and C.E. Wilkey, *J. Biol. Chem.*, 245 (1970) 4081.
[27] D.P. Kasaw and I.A. Rose, *J. Biol. Chem.*, 243 (1968) 3623.
[28] J.E. Wilson, in R. Beiter (Editor), *Regulation of Carbohydrate Metabolism*, Vol. I, CRC Press, Boca Raton, FL, 1985, p. 45.
[29] R.K. Crane and A. Sols, *J. Biol. Chem.*, 203 (1953) 273.
[30] P.L. Felgner, J.L. Messer and J.E. Wilson, *J. Biol. Chem.*, 254 (1979) 4946.
[31] M. Lindèn, P. Gellerfors and B.D. Nelson, *FEBS Lett.*, 141 (1982) 189.
[32] P.G. Polakis and J.E. Wilson, *Arch. Biochem. Biophys.*, 236 (1985) 328.
[33] M. Magnani, V. Stocchi, M. Dachà and G. Fornaini, *Mol. Chem. Biochem.*, 63 (1984) 59.
[34] M. Kurokawa, K. Yokoyama, M. Kaneko and S. Ishibashi, *Biochem. Biophys. Res. Commun.*, 115 (1983) 1101.
[35] F. Ahmad and C.C. Bigelow, *J. Protein Chem.*, 5 (1986) 355.
[36] K. Benedek, S. Dong and B.L. Karger, *J. Chromatogr.*, 317 (1984) 227.
[37] J. Luiken, L. van der Zee and G.W. Welling, *J. Chromatogr.*, 284 (1984) 482.

ELSEVIER

Journal of Chromatography A, 676 (1994) 65–79

JOURNAL OF CHROMATOGRAPHY A

Coupled affinity–reversed-phase high-performance liquid chromatography systems for the measurement of glutathione S-transferases in human tissues

Jeffrey B. Wheatley*, Julie A. Montali, Donald E. Schmidt, Jr.

Terrapin Technologies, Inc., 750-H Gateway Boulevard, South San Francisco, CA 94080, USA

Abstract

HPLC affinity and reversed-phase modes were coupled for the direct measurement of glutathione S-transferases (GSTs) in cytosol extracts. Two coupling designs were examined. In the sequential configuration the affinity column served to extract the isoenzymes which were then eluted directly onto the reversed-phase column as a single fraction. Subsequent separation in the reversed-phase mode provided a GST profile based on the subunit composition of the isoenzymes as a whole. In the second configuration (rapid sampling configuration), gradient elution was performed in the affinity mode resulting in resolution of the intact isoenzymes. The eluate from the affinity separation was sampled in continuous, repetitive intervals and automatically subjected to ongoing reversed-phase analysis. This multidimensional approach provided information on the GST subunit content and also gave information about the distribution of the subunits among individual isoenzymes, thereby forming a basis for the determination of the actual isoenzymatic composition of the GSTs. In both configurations, events were automated and co-ordinated through the use of computer and multiport switching valves. Examples of GST separations from these procedures are shown for human lung and liver tissues. A comparison of the GST subunit analyses from normal and cancer lung tissue excised from the same patient showed substantial elevations of GSTs in the cancer sample. Two-dimensional affinity–reversed-phase analysis of a human liver sample illustrates the utility of the technique for determining the isoenzymatic organization of GST subunits. The criteria for extending two-dimensional analysis to more complex GST mixtures are discussed.

1. Introduction

Glutathione S-transferases (GSTs) are a widely occurring family of isoenzymes which show large compositional variations among different tissues in both type and amount [1–4]. Variations in the levels of individual isoenzymes and the overall GST enzymatic activity have also been found in cancer tissues in comparison with surrounding, normal tissue [5]. In addition, correlations have been reported between elevated GST levels and drug resistance in cells exposed to various cancer drugs *in vitro* [6]. Since alkylating agents used in cancer treatment are electrophilic compounds which are susceptible to GST-catalyzed glutathione conjugation, the presence of elevated GSTs in cancer tissue has been postulated as contributing to drug resistance which often develops in the course of chemotherapy [5,7,8]. Inhibition of GSTs has been proposed as a means of lowering drug resistance by reducing the GST metabolism of cancer drugs, thereby

* Corresponding author.

0021-9673/94/$07.00
SSDI 0021-9673(94)00200-S

rendering such drugs more effective [5,7,9,10]. This approach would have the added benefit of potentiating the action of the drug such that lower concentrations of these toxic compounds might be effective in cancer treatment.

Cytosolic GSTs are categorized according to four classes: Pi (P), Alpha (A), Mu (M) and Theta (T) [11,12]. The isoenzymes are comprised of two subunits with each subunit possessing one catalytic site which is involved in the conjugation of glutathione (L-γ-glutamyl-L-cysteinylglycine, GSH) to widely diverse classes of electrophilic compounds. Multiple subunit forms have been identified for some classes. These include A1 and A2 from Alpha; M1a, M1b, M2, M3, M4, and M5 from Mu; and T1 and T2 from Theta. Subunits within a class form both homodimers (A1-1, A2-2, M1a-1a, M1b-1b, M2-2, M3-3, etc.) and heterodimers (A1-2 and M1-2), but assembly of isoenzymes from different classes of subunits has not been observed to date. Pi is generally recognized as existing as a single isoenzyme, P1-1, although reports of Pi variants have also been published [3].

Analysis of GSTs has been performed most effectively by using reversed-phase HPLC following an affinity chromatography step to extract the enzymes from tissue homogenate [13,14]. The affinity step has usually been carried out with glutathione or S-hexylglutathione immobilized on agarose beads. GST extraction has also been performed using a commercially available HPLC column possessing immobilized glutathione [15]. We have recently developed an HPLC GST affinity packing in order to facilitate the extraction and separation of GSTs as part of a larger study concerned with selective inhibition of GST isoenzymes. In this context we also explored the unique selectivities obtained for isoenzyme separations generated from gradient elutions using structural variants of the GST substrate glutathione as the eluting ligand [16].

Reports have appeared in which coupled systems are described for affinity extractions followed by reversed-phase analysis [17–19] and for two-dimensional analysis using coupled modes exhibiting complementary selectivities [20–22]. The potential of and criteria for optimizing multidimensional separations have also been reviewed [23,24]. This report describes two system designs for coupling a GST affinity column, possessing an S-octylglutathione affinity ligand, to a reversed-phase column. The goal of one design, referred to as the sequential design, was to streamline the extraction and reversed-phase steps through coupling and automation. The reversed-phase separation, using this approach, provides information on the GST subunit content of the sample based on dissociation of GST isoenzymes into their subunits under reversed-phase conditions. The second design, referred to as rapid sampling, is multidimensional in that the eluate provided from a separation of GST isoenzymes in the affinity mode is subjected to repetitive analysis in the reversed-phase mode. The multidimensional approach provides an analysis of the subunit content of the GSTs and also gives information on how the subunits are organized into individual isoenzymes.

2. Experimental

2.1. Reagents

Iodobutane, iodooctane, sodium borohydride, ethanolamine and 1,4-butanediol diglycidyl ether were purchased from Aldrich (Milwaukee, WI, USA). Tris, EDTA, dithiothreitol, sodium chloride, glutathione, 1-chloro-2,4-dinitrobenzene (CDNB) and phenylmethylsulfonyl fluoride were purchased from Sigma (St. Louis, MO, USA). Sodium phosphate, HPLC-grade water and acetonitrile were from VWR Scientific (Brisbane, CA, USA). Trifluoroacetic acid was obtained from Pierce (Rockford, IL, USA). Recombinant GST (rGST) enzymes rA1-1, rP1-1, rM1a-1a, rM1b-1b and M2-2 were obtained from B. Mannervik (University of Uppsala, Uppsala, Sweden), and rA2-2 was obtained from A. Townsend (Bowman Gray School of Medicine, Winston-Salem, NC, USA).

2.2. Synthesis of peptides

S-Butylglutathione and S-octylglutathione

were synthesized by the method of Vince *et al.* [25]. The tripeptide γ-glutamyl-(*S*-benzyl) cysteinyl-β-alanine (TER106) was synthesized as previously reported [26]. All peptides had greater than 90% purity when analyzed by reversed-phase HPLC and had acceptable elemental analyses.

2.3. HPLC Apparatus

Model HPXL pumps, pump heads, a Rheodyne 7125-081 titanium injector, a 1.2-ml titanium dynamic mixer, Dynamax UV-C detectors, and Dynamax HPLC Method Manager for HPLC control and data acquisition were purchased from Rainin (Woburn, MA, USA). Eight-port high-pressure valves mounted on two-position electric actuators were obtained from Valco (Houston, TX, USA). Six-port low-pressure selection valves of polyether ether ketone (PEEK) construction, mounted on electric actuators, were obtained from Upchurch Scientific (Oak Harbor, WA, USA). A static mixing tee of PEEK construction and biocompatible 250 p.s.i. (1 p.s.i. = 6894.76 Pa) back-pressure regulators were obtained from Upchurch Scientific. For affinity chromatography all pathways in contact with the mobile phase were of either titanium or biocompatible polymer construction.

2.4. Tissue extraction

Human liver and lung samples were obtained from the Cooperative Human Tissue Network (Columbus, OH, USA and Birmingham, AL, USA) and stored at −80°C. Samples were slightly thawed, minced with scissors and homogenized in buffer (1 g per 4 ml total volume) containing 10 m*M* Tris hydrochloride (pH 7.8), 1 m*M* EDTA, 1 m*M* dithiothreitol and 0.10 m*M* phenylmethylsulfonyl fluoride using an OMNI stator generator homogenizer (Marietta, GA, USA). Cytosol was prepared by ultracentrifugation at 105 000 *g* for 35 min at 4°C in a Beckman Optima TL-100 tabletop ultracentrifuge (Fullerton, CA, USA). Protein concentrations were determined using a 96-well plate Coomassie dye binding assay (Bio-Rad, Richmond, CA, USA) read on a Tmax Plate Reader (Molecular Devices, Menlo Park, CA, USA) with bovine serum albumin as a standard [27].

2.5. Measurement of enzymatic activity

GST enzymatic activity was determined by measuring the conjugation of CDNB with glutathione at 340 nm with a Tmax Plate Reader. Aliquots (10 μl) of fractions from affinity chromatography were placed in the wells of a 96-well plate and mixed with 190 μl of a standard reaction solution. Standard reaction conditions were 200 m*M* sodium phosphate (pH 6.8) with 1 m*M* glutathione and 1 m*M* CDNB at 30°C [10].

2.6. HPLC columns

Reversed-phase analyses with the sequential design were carried out with a C_8, 5 μm, 250 × 4.6 mm column (7105-00) from Baker (VWR Scientific). Reversed-phase analyses with the rapid sampling design were performed with a C_{18}, 5 μm, 50 × 4.6 mm column (218ATP5405) from The Separations Group (Hesperia, CA, USA). HEMA BIO 1000 (Tessek 0001620005), a 10-μm polymeric HPLC support based on copolymerization of 2-hydroxymethacrylate and ethylene dimethacrylate, was obtained from Melcor Technologies (Sunnyvale, CA, USA).

The synthesis of the affinity matrix followed the general procedure of Sundberg and Porath [28]. The mixture HEMA BIO 1000–1,4-butanediol diglycidyl ether–0.6 *M* sodium hydroxide containing 2 mg/ml of sodium borohydride (0.03:1:1, w/v/v) was mixed overnight. The product was filtered and washed with water, ethanol and acetone. A 700-mg amount of the derivatized support was combined with a solution of S-octylglutathione (75 mg) dissolved in 3.5 ml of 0.5 *M* sodium carbonate and 60 μl of ethanolamine, pH 10.5. The suspension was mixed for approximately 90 h. After filtration the final product was washed with the following, in the order shown: 1 *M* sodium chloride in 0.1 *M* sodium phosphate (pH 9); 1 *M* sodium chloride in 0.1 *M* sodium acetate (pH 4.5); water; ethanol; and acetone.

A 90-mg amount of the affinity packing was slurried in 20 ml of water and packed at high pressure into stainless-steel columns, 30 × 2.1 mm. (Supelco, Bellefonte, PA, USA). The column frits were 2 μm (average pore diameter) titanium encased in a CTFE ring (Upchurch Scientific). A Haskell (Burbank, CA, USA) DSTV-122 liquid pump was used to provide the drive solvent (water) during the packing process. The columns were packed at 2000 p.s.i. (140 bar) with 50 ml of water and then 4000 p.s.i. (275 bar) with 50 ml of water.

2.7. HPLC system designs

The HPLC system design for the sequential configuration is shown in Fig. 1. Two pumps are associated with each column enabling gradient elution in both modes. Valve V1, a six-port selection valve mounted on an electric actuator, controls delivery of the loading, wash and regeneration solvents to the affinity column through pump P1. The affinity eluent is delivered through pump P2, and the affinity gradients are formed in the low-volume (3 μl) static mixing tee M1. The sample is introduced through the manual injection valve IN1. Reversed-phase solvents are delivered through pumps P3 and P4 which are mixed in the dynamic mixer M2 (1.2 ml). The affinity method is controlled from the computer. Since the software is not capable of exerting simultaneous control of affinity and reversed-phase pumps, the reversed-phase method is directed through (programmable) pump P3 with P4 subordinate to P3. A second manual injection valve, IN2, permits the option of introducing samples directly onto the reversed-phase column which can be used independently of the affinity system. Back-pressure regulators (250 p.s.i.) were installed in-line in order to insure proper function of the pumps' check valves at the low flow-rates existing at various times during the procedure.

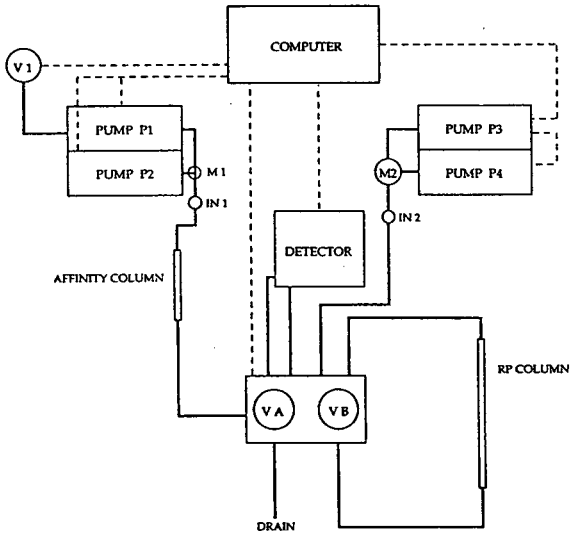

Fig. 1. HPLC design for sequential coupling of GST affinity and reversed-phase modes. M1 = Static low volume gradient mixer; M2 = dynamic gradient mixer; V1 = low pressure 6-port selection valve; IN1, IN2 = manual injection valves; VA, VB = 8-port, 2-position switching valves; solid lines = plumbing; broken lines = electrical connections. See text for complete description.

Valves VA and VB are two-position, eight-port, electrically actuated switching valves and co-ordinate changes in flow paths which occur during the procedure. The system plumbing in relation to VA and VB is shown in Fig. 2. Five of the eight ports from each valve were required for this design. The position of these valves and V1 is controlled from the computer which also signals initiation of the reversed-phase method stored in P3 and acquires data from the detector.

The HPLC system design for the rapid-sampling configuration, shown in Fig. 3, resembles the sequential configuration with a few fundamental differences. One switching valve and two detectors are required. Data from the detectors are acquired on two computer channels. The switching valve, shown in Fig. 4, is slightly modified from a design by Bushey and Jorgenson [20] in that one of the loops is incorporated into a manual injection valve thereby permitting independent sample introduction onto the reversed-phase column.

2.8. Chromatography

The determination of GST isoenzymes using the sequential design involves three stages: (1) extraction of the isoenzymes from the sample;

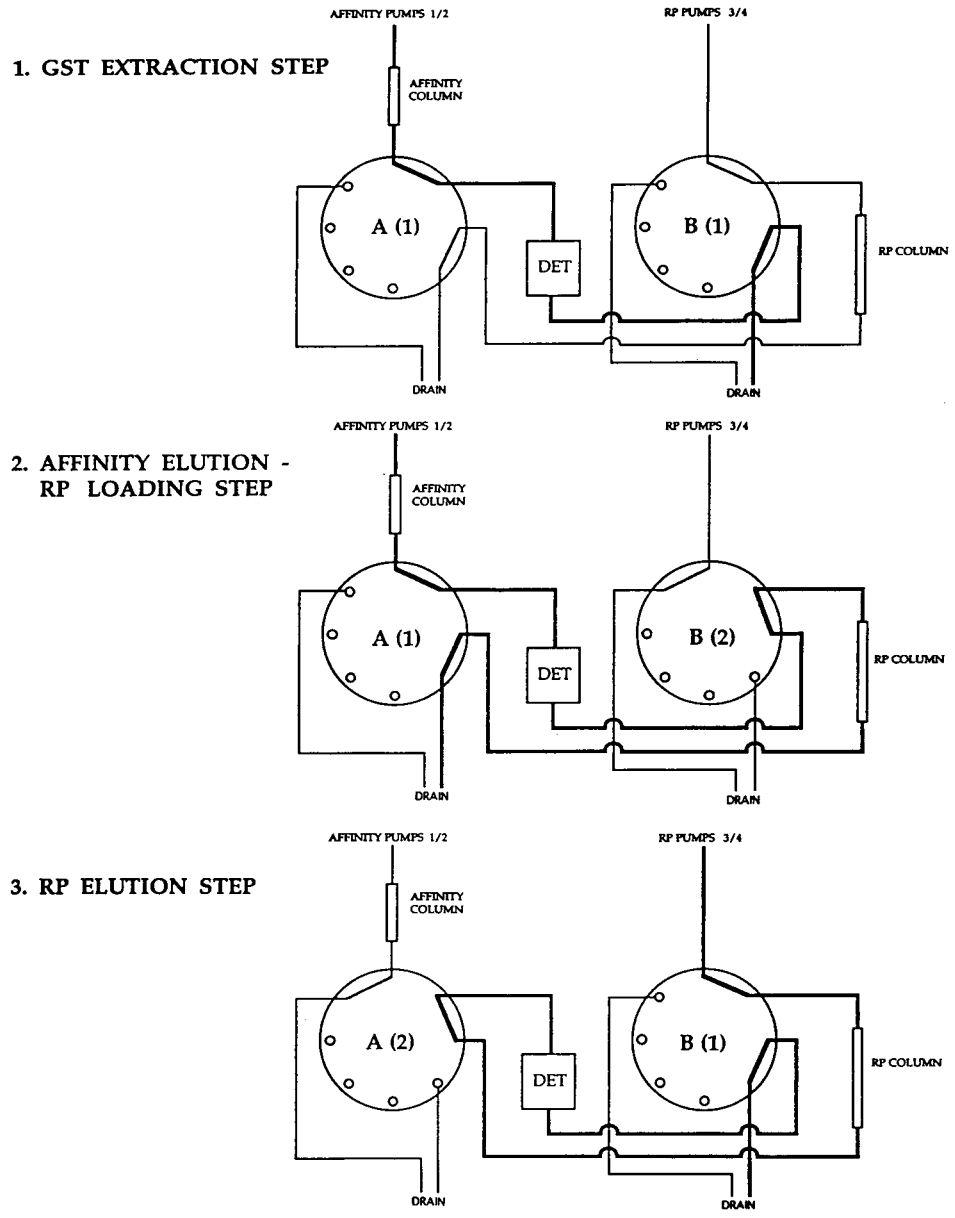

Fig. 2. Valve design for sequential coupling of GST affinity and reversed-phase modes. Positions of valves A and B are given for the three stages of the procedure. Use of a single detector permits acquisition of both affinity and reversed-phase data as a single chromatogram. DET = Detector. See text for detailed description.

(2) elution of the isoenzymes as a single fraction from the affinity column onto the reversed-phase column; (3) separation of the mixture of isoenzymes into their constituent subunits in the reversed-phase mode. These processes, which are co-ordinated by the positions of valves VA and VB, are summarized in Fig. 2 and described in detail by the method shown in Table 1.

During the first step, when valves VA and VB are both in position 1, the sample is introduced

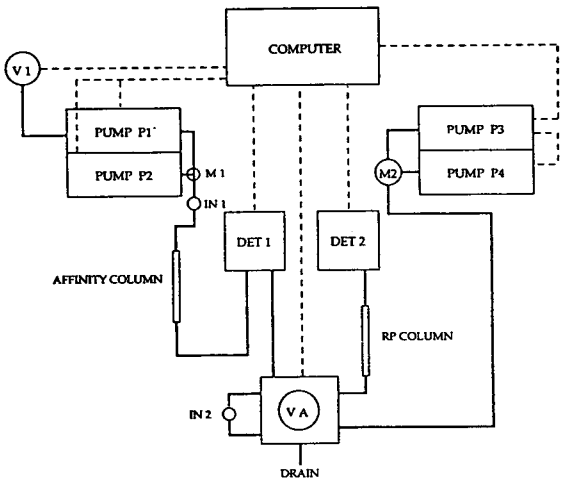

Fig. 3. HPLC design for rapid sampling coupling of GST affinity and reversed-phase modes. See Fig. 1 and text for description of components.

onto the affinity column in loading buffer A (solvent compositions are shown in Table 1) where the isoenzymes are extracted from the sample. Following a salt wash in buffer B, the isoenzymes are eluted from the affinity column with buffer C which, for this study, contained the affinity eluent S-butylglutathione. At about the same time valve VB is changed to position 2 which has the effect of directing the affinity eluate, containing the GST isoenzymes, onto the reversed-phase column. During the GST loading step the reversed-phase solvents from pumps P3 and P4 are diverted to drain. It is important to note that during the loading step the flow cell in the detector experiences back-pressure from the reversed-phase column. Consequently, the loading step was carried out at flow-rates consistent with pressure specifications of the flow cell.

Following the elution of the GSTs from the affinity column, which is monitored by the detector at 280 nm, VA and VB are simultaneously switched to positions 2 and 1, respectively. As a result the affinity and reversed-phase columns are de-coupled, and the effluent from the affinity column is diverted to drain. Also, the solvents from pumps P3 and P4 are redirected onto the reversed-phase column, and the effluent from the reversed-phase column replaces the affinity effluent in the detector flow cell. When the valves are switched a signal is also sent from the computer instructing pump P3 to initiate the reversed-phase method. About 2 min later the detector wavelength is changed to 214 nm and, subsequently, a signal is sent from the reversed-phase method to re-zero the detector.

During the reversed-phase separation (third stage of the analysis), the affinity column is subjected to a cleaning and regeneration procedure which is directed from the affinity method. At the conclusion of the reversed-phase gradient valve VA is returned to position 1, the detector wavelength is returned to 280 nm, and the regenerated affinity column is prepared to accept the next sample. The injection can be made prior to reversed-phase regeneration, which can be completed during the first part of the affinity procedure when the columns are de-coupled.

The affinity method for the rapid-sampling analysis resembles the sequential approach except that the GST elution is carried out using a long, shallow gradient. As the affinity eluate leaves the affinity column it passes into either loop 1 or loop 2 (1 ml volume), depending on the position of the switching valve, shown in Fig. 4. At regular intervals the valve position is changed as directed by the affinity program. When this occurs the reversed-phase flow path is directed through the most recently filled loop, sweeping the sample in that loop onto the reversed-phase column. At the same time the reversed-phase method, stored in pump P3, is initiated. While the reversed-phase analysis is performed, affinity eluate enters the other loop in preparation for the next reversed-phase analysis. The result is that all of the affinity eluate is collected as discrete fractions which are subjected to reversed-phase analysis. In order to obtain a detailed reversed-phase analysis of the affinity eluate, the reversed-phase analysis time must be fast. The cycle time in this study, including separation time and column regeneration, was 6 min. Since elution of GSTs from the affinity column was performed at 20 μl/min, the affinity eluate was sampled in continuous 120-μl fractions. The volume of the sampling loops (1 ml) was sufficient to insure complete capture of the affinity fractions.

VALVE POSITION 1 (FILL LOOP 1)

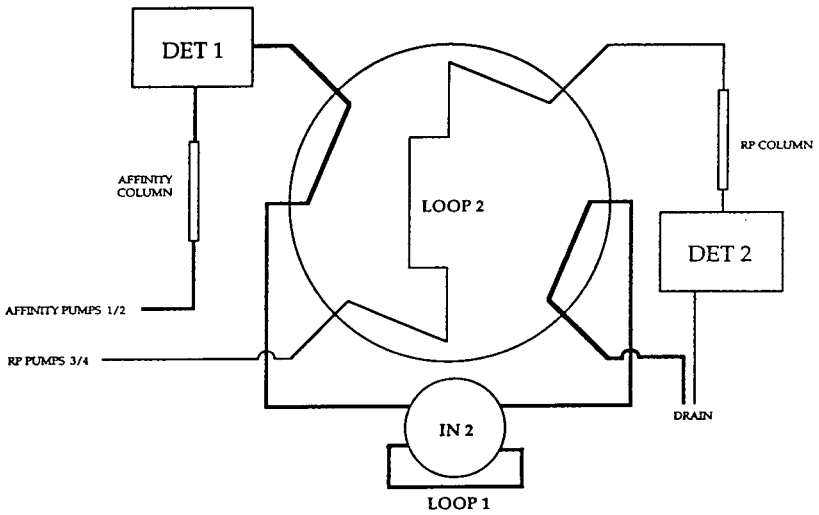

VALVE POSITION 2 (FILL LOOP 2)

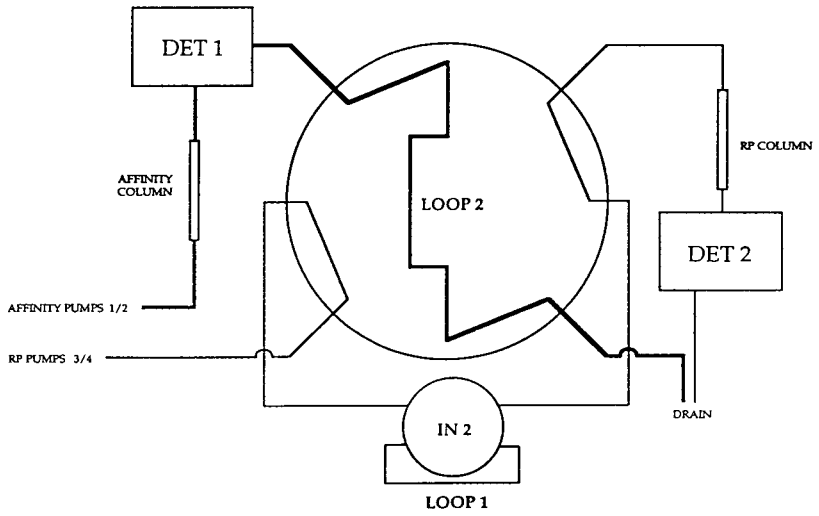

Fig. 4. Valve design for rapid sampling coupling of GST affinity and reversed-phase modes. Two valve positions permit continuous sampling of affinity eluate in loops 1 and 2 (volume 1 ml) and comprehensive reversed-phase analysis of fractionated isoenzymes. See text for details.

3. Results

The sequential design employs a single detector arranged such that the eluate from both affinity and reversed-phase columns passes through the flow cell. A similar feature, whereby

Table 1
HPLC method for coupled affinity–reversed-phase analysis of GSTs (sequential design)

Time (min)	VA[a]	VB[a]	Flow-rate (ml/min)[b]		Mobile phase	
			Affinity	RP	Affinity[c]	RP[d]
0	1	1	0.04	0.25	A	20.0% B′
5.00			0.04		B	
6.00			1.00			
17.00			1.00			
17.50			0.02			
20.00					B	
22.00		2				
26.00					C	
32.00					C	
32.02					B	
39.00[e]	2	1				
32.02			0.02	0.25	D	
39.50			1.00			
41.00				1.00		
42.00[f]						20.0% B′
47.00						42.0% B′
54.50					A	
59.50			1.00			
59.75			0.04			
93.00						50.7% B′
95.00	1		0.04			
95.50			1.00			
97.50			1.00			
98.00			0.04			

Mobile phase buffers, affinity column: A, 10 m*M* sodium phosphate, pH 6.0: B, 200 m*M* sodium chloride in A; C, 20 m*M* S-butylglutathione in B; D, 1.0 *M* sodium chloride in A. Mobile phase solvents, reversed-phase column: A′, 0.1% trifluoroacetic acid in water; B′, 0.1% trifluoroacetic acid in acetonitrile. Separate programs direct the flow of solvents through the affinity and reversed-phase columns and are controlled from the computer and pump P3, respectively. The GST extraction and wash occurs at 0–20 min. GST elution and reversed-phase loading occurs at 20–39 min, and the reversed-phase elution takes place at 39.02–95 min. See text for details.

[a] VA and VB represent 2-position, 8-port switching valves described in Fig. 2 and the text. The values 1 and 2 correspond to valve positions as shown in Fig. 2.

[b] Changes in flow-rate occur over a linear gradient between the times indicated.

[c] Mobile phases A, B and D were selected in a step at the times indicated. The change between B and C occurred in a linear gradient over 6 min.

[d] Changes in reversed-phase mobile phase occur over a linear gradient between the times indicated.

[e] At 39.00 min an output signal from the computer initiates the reversed-phase program stored in pump C. Reversed-phase mobile phase composition and flow-rate are controlled from this program.

[f] At 42.00 min an output signal is sent from the reversed-phase program stored in pump C to detector auto-zero.

data acquired from separations on two coupled columns are presented in a single chromatogram, was recently reported [29]. The first part of the chromatogram, obtained from the sequential design, depicts a separation of GST isoenzymes in the affinity mode, and the reversed-phase separation of GST subunits appears in the second part. Such a chromatogram, obtained from the injection of a standard mixture of five recombinant GST isoenzymes, is shown in Fig. 5. Peak assignments were made from individual injections of the isoenzymes in the mixture.

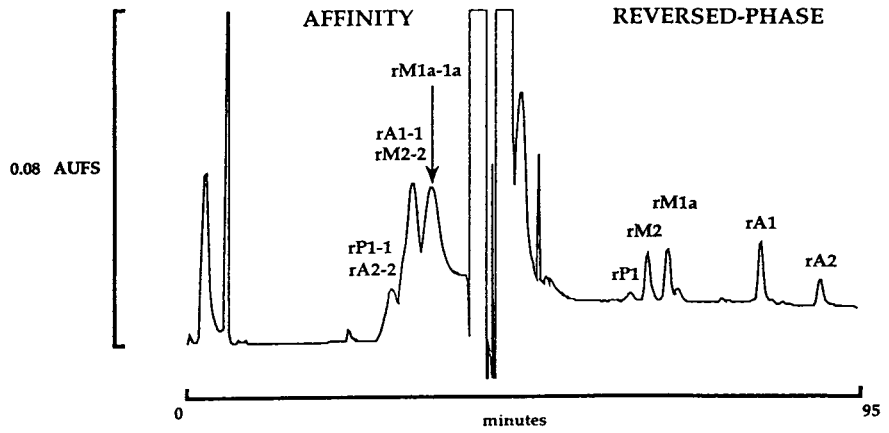

Fig. 5. Separation of a mixture of recombinant GST isoenzymes using the sequential design. Partial separation of the intact isoenzymes was achieved in the affinity mode, appearing in the first part of the chromatogram. Complete resolution of isoenzymatic subunits was achieved in the reversed-phase mode, shown in the second part of the chromatogram. Sample, 25 μl containing rP1-1 (2.3 μg), rM1a-1a (2.3 μg), rM2-2 (1.1 μg), rA1-1 (1.7 μg) and rA2-2 (1.7 μg); affinity column, S-octylglutathione immobilized onto a 10-μm polymeric support, 30 × 2.1 mm; reversed-phase column, Baker C_8, 5 μm, 250 × 4.6 mm; detection, 280 nm and 214 nm for affinity and reversed-phase, respectively. Mobile phases and the complete method program are given in Table 1.

Under the conditions of the affinity elution (0–20 m*M* S-butylglutathione over 6 min) only limited resolution of the intact isoenzymes was observed in the affinity mode. However, three distinct isoenzyme populations can be seen: an early eluting mixture of rA2-2 and rP1-1, a middle population containing rA1-1 and rM2-2, and a strongly retained band containing rM1a-1a. The small peak preceding the GST bands corresponds to the switch in the position of valve VB at 22 min. The strong absorption in the middle of the chromatogram results from an abrupt shift in mobile phase following the valve changes at 39.00 min (affinity to reversed-phase solvents) and from elution of S-butylglutathione from the reversed-phase column early in the method.

The peaks eluted from the reversed-phase column and appearing in the second part of the chromatogram represent rGST subunits generated from the isoenzymes observed in the affinity separation. Since the sample was comprised entirely of homodimeric isoenzymes, each of which dissociates into a single subunit under reversed-phase conditions, each subunit peak in the reversed-phase separation corresponds to one of the isoenzymes in the sample mixture. For example, rP1-1 generates a single rP1 peak in the reversed-phase chromatogram. The five subunit peaks are clearly resolved and easily distinguished.

Fig. 6 shows a comparison of chromatograms obtained from sequential GST analysis of lung tissue cytosols derived from cancer and normal tissue taken from the same patient. The peak areas are expressed as mV s mg^{-1} of injected cytosolic protein. In this case the sample protein concentrations were comparable (9.3 *versus* 9.4 mg protein per ml cytosol) so that the two chromatograms can be compared directly. It is clear from the reversed-phase profiles that the GST subunit content is substantially elevated for all components in the cancer sample compared to the normal sample. Both P1 and A2 subunits exist at greater than 2.5 × the normal concentrations. The concentrations of M1a and A1 are even more amplified in the cancer sample with M1a occurring at 30 × the normal concentration. The peak labeled X, the identity of which is under investigation, has been observed in this laboratory in other lung samples as well as in cytosol derived from breast tissue and in numerous cell lines grown in culture.

Fig. 7 shows the results of a GST analysis of

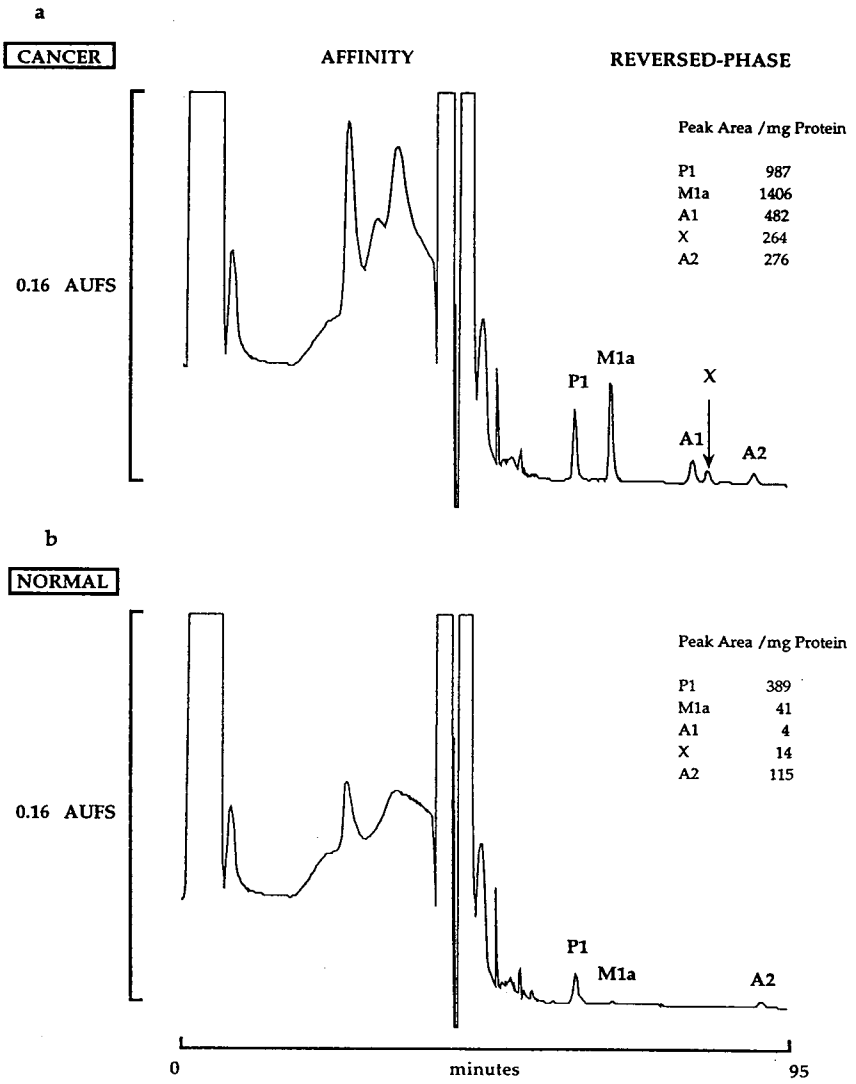

Fig. 6. Comparison of GST subunit analyses for cytosol derived from cancer (a) and normal (b) lung tissues excised from the same patient. The analyses were obtained from using the sequential design and are expressed as peak areas per mg of injected protein. The same amount of protein was injected from each sample permitting direct graphic comparison of peaks. A 200-μl volume of cytosol, diluted (1:2) in loading buffer, was injected. Other conditions as in Fig. 5. The peaks corresponding to A1 and X in the normal sample, which occur in very small amounts, are not apparent at this attenuation.

human liver cytosol, using the rapid sampling approach. The affinity separation is depicted vertically on the left, and the reversed-phase analysis of each 6-min fraction is shown horizontally alongside the corresponding affinity fraction. A reversed-phase chromatogram obtained for a standard mixture of rGSTs appears at the bottom. Three major bands appear in the affinity chromatogram, at about 25, 37 and 79 min. Reversed-phase analysis of the band at 25 min showed a single peak corresponding in retention to the A2 subunit, indicating that this affinity band represents the A2-2 homodimer. Reversed-phase analysis of the affinity eluate between 73

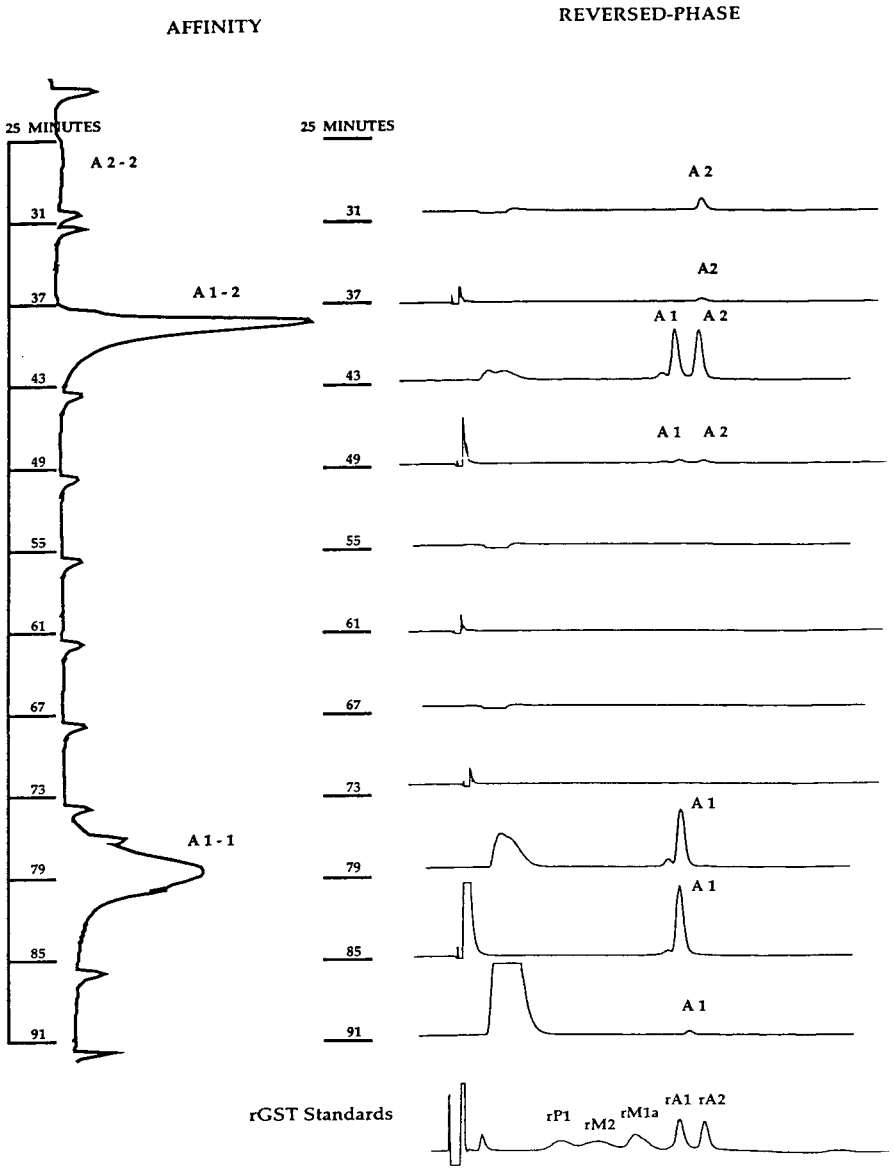

Fig. 7. Two-dimensional affinity, reversed-phase analysis of GSTs in human liver cytosol using the rapid sampling design. See text for description. Mobile phases, detection wavelengths and affinity column as in Fig. 5 and Table I. Reversed-phase column, Vydac C_{18}, 5 μm, 50 × 4.6 mm; sample volume 180 μl cytosol (17.4 mg protein/ml); affinity method: 0–2 min, A buffer (10 m*M* sodium phosphate, pH 6), 0.1 ml/min; 2–17 min, B buffer (200 m*M* sodium chloride in A); 17–20 min, B buffer, 0.02 ml/min; 20–127 min, 0–28% C buffer (20 m*M* S-butylglutathione in B), 0.02 ml/min. Reversed-phase method, 0–1 min, 44–45% B′ (0.1% trifluoroacetic acid in acetonitrile; A′ 0.1% trifluoroacetic acid in water); 1–4 min, 45–62% B′; 4–6 min, 44% B′; flow 2 ml/min. Reversed-phase analysis of affinity eluate was performed every 6 min beginning with affinity fraction 25–31 min.

and 91 min showed a single major GST peak, corresponding to subunit A1, suggesting that the affinity band represents the A1-1 isoenzyme.

Reversed-phase analysis of the affinity eluate between 37 and 49 min revealed two major peaks of approximately equal area, apparently

corresponding to the A1 and A2 subunits. Since these subunits originate from neither the A1-1 nor A2-2 isoenzymes, which were detected in separate affinity fractions, this affinity band must correspond to the A1-2 heterodimer. Equal areas would be anticipated for the pure A1-2 isoenzyme since their molar extinction coefficients are nearly the same. A minor, unidentified reversed-phase peak, eluting just prior to A1, also accompanies the A1 subunit wherever it appears and suggests some associated species distinct from the A2 subunit.

The bands eluting early in the reversed-phase chromatograms probably represent compounds in the affinity eluent, primarily S-butylglutathione. The regular alternations in the background, appearing near the beginning of the reversed-phase gradient, apparently depend on the position of the switching valve and could result from some difference in the two flow paths. Spikes appearing at regular intervals in the affinity chromatogram correspond to valve changes.

4. Discussion

The sequential approach for GST analysis essentially provides a reversed-phase analysis for the subunit content of a mixture of isoenzymes loaded onto the reversed-phase column as a single fraction. The coupled design represents a substantial improvement in comparison with methods employing separate agarose-based affinity extractions. The automated system, through computer control, streamlines all of the steps associated with the affinity extraction and efficiently transfers the extract to the reversed-phase column. As a result, handling errors are eliminated as is the labor associated with the individual manipulations inherent in a manual approach. The affinity and reversed-phase systems can also be used independently by decoupling the two columns (valves VA and VB positioned as described for step 1 or step 3 in Fig. 2). In the de-coupled configuration the affinity portion of the system may be used to purify GST isoenzymes for studies other than reversed-phase analysis. Conditions for achieving isoenzyme separations on this affinity column have been described elsewhere [16]. Also, the two independent gradient systems can also be used for other purposes so that the equipment need not be dedicated to GST analysis.

Relative standard deviations, determined for the retentions of P1, M1a, M1b, M2, A1 and A2 in the reversed-phase separation of the sequential design, indicated less than 5% overlap of the statistical envelopes surrounding the most closely eluting pairs of subunits in this group. Independent characterization of GST affinity eluate compositions, through immunochemical procedures and sodium dodecyl sulfate–polyacrylamide gel electrophoresis [16], was used to further corroborate the subunit identities. The efficacy of the affinity column for extracting GSTs was also examined. Injections of cytosol derived from 20 cell lines (containing mostly Pi GST) and 40 lung specimens showed, respectively, that an average of 1.8% and 5.9% of the enzymatic activity in the samples was unretained by the affinity column (data not shown). These measurements and those above indicate that efficient GST extractions are achieved on the affinity column and that the resolution obtained under the conditions described in Table 1 permit peak assignments with a high degree of confidence. From the samples examined thus far, we estimate that the GST content found in 1–2 mg of tissue should be easily detected, with variations expected according to tissue type and individual GST content. The amount of tissue obtained from a needle biopsy would thus prove sufficient for determination of GST analytical profiles using this procedure.

In reversed-phase separations of GSTs, the appearance of only one subunit from within a given GST class necessarily suggests its organization as the homodimeric isoenzyme. However, when two or more subunits from the same class are present, as is often the case, their distribution among isoenzymes cannot be deduced from the information obtained through the sequential approach. In order to determine the actual isoenzyme composition, the isoenzymes must first be at least partially separated from each

other. If this can be achieved the separated isoenzymes can then be identified through reversed-phase analysis. The rapid sampling design addresses this problem by co-ordinating a two-dimensional separation comprised of an affinity mode, by which isoenzymatic resolution is effected, and a reversed-phase mode for determining the subunit composition of the separated isoenzymes. This is illustrated in Fig. 7 for the separation of three A isoenzymes in liver cytosol. In this case the isoenzymes A1-1, A1-2 and A2-2 were fully resolved in the affinity mode and their identities confirmed by subunit analysis in the reversed-phase mode. Examination of this sample with the sequential design would have shown two peaks in the reversed-phase analysis corresponding to the total A1 and A2 subunit content but would have provided no information on the distribution of the subunits among the isoenzymes.

The GST isoenzyme content of the liver sample profiled in Fig. 7 is relatively simple, and the three A isoenzymes were easily separated. Often, however, more complex GST mixtures are encountered in which several Mu class subunits may be present in addition to the A1 and A2 subunits. We have observed mixtures containing various combinations of P1, A1, A2, M1a, M1b and M2, and several other Mu class subunits (M3, M4 and M5) have been reported elsewhere [6]. In addition to A1 and A2, we have also encountered samples containing a third A subunit, designated as Ax. In one sample these A subunits were distributed among five isoenzymes [16]. Adding to this complexity is the anticipation that new GST forms would be expected in any broad screening of the genetically diverse human population.

Although gradient separations of complex mixtures of GST isoenzymes in the affinity mode tend to produce overlapping bands, the identity of the overlapping isoenzymes can often be deduced from the subunit information obtained from the reversed-phase separation. For example, the subunit composition of an affinity fraction containing two isoenzymes of different classes necessarily suggests the identity of the isoenzymes. This is a consequence of isoenzymes assembling from among subunits within only the same class. In some cases isoenzyme content can be determined even when overlap of same class isoenzymes occurs. For the A mixture of Fig. 7, if affinity conditions were such that A1-2 and A2-2 overlapped (or even co-eluted) and the A1-1 band were still clearly distinguishable, reversed-phase analysis of the (distinct) A1-1 band would show a single peak for the A1 subunit. The A1 peak area for the A1-2, A2-2 mixture would then be attributable to heterodimeric association with an equal amount of A2, and the remaining A2 peak area would have to arise from the A2-2 homodimer.

In some cases, even with a two-dimensional analysis, failure to adequately resolve same-class isoenzymes in the affinity mode would prevent their identification. When this occurs, changing the eluting ligand for the affinity separation can improve resolution sufficiently for isoenzyme determination. As part of a larger study concerned with molecular recognition, this laboratory has measured dissociation constants for binding between GST isoenzymes and a variety of glutathione analogues [10]. Sets of dissociation constants for a collection of GST isoenzymes are distinct for each structural variant of glutathione. For chromatographic affinity systems which employ competitive inhibitors as immobilized and eluting ligands, retention of an enzyme represents a balance between the affinities displayed by the immobilized and free ligands for the enzyme [30]. The relative retentions (selectivity) for a mixture of isoenzymes in a defined system depends on the unique set of enzyme–ligand dissociation constants for that system, *e.g.*, a mixture of GST isoenzymes in the S-octylglutathione, S-butylglutathione system described here. By changing the eluting ligand, significant shifts in selectivity can be achieved commensurate with the relative changes in the binding constants between the isoenzymes in the mixture and the new ligand.

A potent shift in selectivity of this kind has been observed for liver samples which were found to contain five A isoenzymes: A1-1, A1-2, A2-2, and the previously unreported forms designated as A1-x and A2-x [16]. Affinity sepa-

rations, using S-butylglutathione as the eluting ligand under conditions similar to those described above (see affinity conditions in Fig. 7), failed to resolve A2-2 from A2-x and showed overlap of A1-2 with A1-x. Two-dimensional analysis based on this affinity separation would fail to provide the isoenzymatic distribution of subunits Ax and A2. By eluting with the glutathione analogue γ-glutamyl-(S-benzyl) cysteinyl-β-alanine instead of S-butylglutathione, all five isoenzymes were baseline resolved. Such an affinity separation would simplify subunit identification in a manner analogous to that described for the sample of Fig. 7.

Since all five Alpha isoenzymes in the above sample can be baseline resolved, they could, in principle, be distinguished on the basis of their separation in the affinity mode. It should be noted, however, that differentiation of isoenzymes in the affinity mode is complicated by several factors. Although data are limited at present, variations for retentions in the affinity mode appear to be wider than those in the reversed-phase mode. For example, single injections of cytosol from five different liver samples on the affinity column, using conditions similar to those of Fig. 7, gave a relative standard deviation for A1-1 of 4.6% (unpublished results) compared to 1.4% for retention of A1 on the reversed-phase column of Fig. 5 (10 injections from a single sample of liver cytosol). In addition, resolution in the affinity mode also appears to be limited by low peak capacities. Mu isoenzymes in particular tend to produce relatively wide bands in this affinity system [16]. These factors suggest that confident statistical differentiation of some isoenzymes may not be possible when based solely upon their retention times in the affinity mode. In addition, since peptide eluents interfere with detection at lower, more sensitive wavelengths, identification of minor isoenzymes, which may be present in low concentration, could be limited to subunit delineation from the reversed-phase separation.

The affinity and reversed-phases described in this report exhibit complementary selectivities such that the resolution provided by the 4-min reversed-phase separation (6 min with regeneration time) is sufficient for unequivocal differentiation of many of the subunit mixtures likely to be encountered in the affinity eluate. For example, P1-1 and A2-2, which exhibit similar selectivities in the affinity mode (see affinity separation of Fig. 5), would show widely separated P1 and A2 subunits under the reversed-phase conditions of Fig. 7. A1 and M2, whose homodimers also exhibit similar affinity selectivities, are also widely separated on the reversed phase. Some isoenzyme mixtures, however, could exhibit similar selectivities in the affinity mode and release subunits which also show similar retention on the reversed-phase. For example, subunit M1b, which elutes between M1a and A1 [16], would overlap with those subunits when the steep reversed-phase gradient described for Fig. 7 is used. Overlap of any of the isoenzymes in the affinity separation possessing the M1b subunit (M1b-1b or M1b-2, for example) with those possessing the M1a or A1 subunits could pose difficulty in obtaining confident identification of these subunits based on the reversed-phase separation. The GST subunits P1, M1a, M1b, M2, A1, A2 and Ax can be unequivocally resolved using shallower gradients like the one described for the sequential analysis in Fig. 5. However, if it is assumed that there are practical limits on the resolution obtainable in the affinity mode, as the reversed-phase analysis time increases, the number of affinity fractions that may be examined declines with a concomitant loss in definition. Also, the degree of resolution (and overall separation time) required in the affinity mode for reversed-phase identification of isoenzymes depends on the speed of the reversed-phase analysis. The importance of fast analysis time in the second mode for maximizing overall resolution in a two-dimensional separation has been discussed elsewhere [20]. In order to address these factors we are currently examining high-resolution, non-porous supports for speeding the reversed-phase analysis and other affinity eluents for producing diverse GST selectivities in the affinity mode.

In multidimensional chromatography, overall resolution improves as differences increase in the mechanisms by which separations occur in each

of the modes; the value of combining orthogonal modes in maximizing resolution has been discussed in detail [20,23,24,31,32]. By this measure, the combination of affinity and reversed-phase modes examined in this study provides an excellent basis for a two-dimensional separation since their respective chromatographic mechanisms are fundamentally different. We believe that these principles can be extended beyond the analysis of GST compositions for the elucidation of other complex mixtures of closely related isoenzymes. We are currently engaged in widespread screening of normal and cancer tissues for GST subunit compositions, using the sequential approach described in this study. The information obtained from the kinds of subunit mixtures encountered will provide the criteria for further development of two-dimensional separations based on the principles discussed above.

Acknowledgement

We wish to express our gratitude to Angela DeCarlo for the preparation of tissue homogenates and Dr. Lawrence Kauvar for valuable comments on the manuscript.

References

[1] Y. Soma, K. Satoh and K. Sato, *Biochim. Biophys. Acta*, 869 (1986) 247.
[2] D.L. Vander Jagt, L.A. Hunsaker, K.B. Garcia and R.E. Royer, *J. Biol. Chem.*, 280 (1985) 11 603.
[3] J. Carmichael, L.M. Forrester, A.D. Lewis, J.D. Hayes, P.C. Hayes and C.R. Wolf, *Carcinogenesis*, 9 (1988) 1617.
[4] A.G.J. van der Zee, B. van Ommen, C. Meijer, H. Hollema, P.J. van Bladeren and E.G.E. de Vries, *Br. J. Cancer*, 66 (1992) 930.
[5] K.D. Tew, P.J. Houghton and J.A. Houghton, *Preclinical and Clinical Modulation of Anticancer Drugs*, CRC Press, Boca Raton, FL, 1993, p. 49.
[6] X.Y. Hao, *Acta Univ. Ups., Abstr. Uppsala Diss. Fac. Sci.*, 469 (1993) 20.
[7] D.J. Waxman, *Cancer Res.*, 50 (1990) 6449.
[8] B. Coles and B. Ketterer, *Crit. Rev. Biochem. Mol. Biol.*, 25 (1990) 47.
[9] L.M. Kauvar, in K.D. Tew, C.B. Pickett, T.J. Mantle, B. Mannervik and J.D. Hayes (Editors), *Structure and Function of Glutathione S-Transferase*, CRC Press, Boca Raton, FL, 1993, p. 257.
[10] F.E. Flatgaard, K.E. Bauer and L.M. Kauvar, *Cancer Chemother. Pharmacol.*, 33 (1993) 63.
[11] B. Mannervik and U.H. Danielson, *Crit. Rev. Biochem.*, 23 (1988) 283.
[12] B. Mannervik, *Biochem. J.*, 282 (1992) 305.
[13] J.D. Hayes, L.A. Kerr and A.D. Cronshaw, *Biochem. J.*, 264 (1989) 437.
[14] B. van Ommen, J.J.P. Bogaards, W.H.M. Peters and B. Blaauboer and P.J. van Bladeren, *Biochem. J.*, 269 (1990) 609.
[15] F.P. La Creta, J.J. Olszewski and K.D. Tew, *J. Chromatogr.*, 434 (1988) 83.
[16] J.B. Wheatley, M.K. Kelley, J.A. Montali, C.O.A. Berry and D.E. Schmidt, Jr., *J. Chromatogr. A*, 663 (1994) 53.
[17] L. Hansson, M. Glad, C. Hansson, *J. Chromatogr.*, 265 (1983) 37.
[18] J. Fausnaugh-Pollitt, G. Thevenson, L. Janis and F.E. Regnier, *J. Chromatogr.*, 443 (1988) 221.
[19] M. de Frutos and F.E. Regnier, *Anal. Chem.*, 65 (1993) 17A.
[20] M.M. Bushey and J.W. Jorgenson, *Anal. Chem.*, 62 (1990) 161.
[21] G. Thevenon-Emeric and F.E. Regnier, *Anal. Chem.*, 63 (1991) 1114.
[22] S.A. Berkowitz, *Adv. Chromatogr.*, 29 (1989) 175.
[23] R.E. Majors, *J. Chromatogr. Sci.*, 18 (1980) 571.
[24] J.C. Giddings, *Anal. Chem.*, 56 (1984) 1259A.
[25] R. Vince, S. Daluge and W.B. Wadd, *J. Med. Chem.*, 14 (1971) 402.
[26] M.H. Lyttle, D.T. Aaron, M.D. Hocker and B.R. Hughes, *Pept. Res.*, 5 (1992) 336.
[27] V.M. Castro, M.K. Kelley, Å. Engqvist-Goldstein and L.M. Kauvar, *Biochem. J.*, 292 (1993) 371.
[28] L. Sundberg and J. Porath, *J. Chromatogr.*, 90 (1974) 87.
[29] F. Gimenez, C. Dumartin, I.W. Wainer and R. Farinotti, *J. Chromatogr.*, 619 (1993) 161.
[30] H.E. Swaisgood and I.M. Chaiken, in I.M. Chaiken (Editor), *Analytical Affinity Chromatography*, CRC Press, Boca Raton, FL, 1987, Ch. 2, p. 65.
[31] K. Benedek, A. Varkonyi, B. Hughes, K. Zabel and L.M. Kauvar, *J. Chromatogr.*, 627 (1992) 51.
[32] H.J. Cortes, *J. Chromatogr.*, 626 (1992) 3.

ELSEVIER

Journal of Chromatography A, 676 (1994) 81–90

JOURNAL OF CHROMATOGRAPHY A

Study of chromatographic parameters for glutathione S-transferases on an high-performance liquid chromatography affinity stationary phase

Jeffrey B. Wheatley, Betsy Hughes, Karin Bauer, Donald E. Schmidt, Jr.*

Terrapin Technologies, Inc., 750-H Gateway Blvd., South San Francisco, CA 94080, USA

Abstract

The chromatographic parameters were examined for recombinant glutathione S-transferases (GSTs) on a new HPLC affinity packing containing the immobilized ligand S-octylglutathione. The k' values of both rA1-1 and rP1-1 were determined under isocratic conditions with increasing concentrations of the mobile phase ligand S-butylglutathione. Plots of $1/k'$ vs. S-butylglutathione concentration were non-linear which is consistent with a bivalent model for the association of these dimeric enzymes and the stationary phase. Low flow-rates were found to be decisive in obtaining good resolution of the isoenzymes, and at 0.10 ml/min it was possible to obtain baseline resolution of rP1-1, rA1-1 and rM1a-1a using shallow, linear gradients of GST competitive inhibitors. Association constants were determined from solution phase kinetics assuming a rapid equilibrium random Bi Bi mechanism. Solution phase association constants provide an approximate guide for the selection of ligands useful in this affinity phase HPLC separation of GST isoenzymes. A good fit ($r^2 = 0.998$) for the rA1-1 binding data was obtained using the solution phase binding constant but this was not the case for rP1-1. A comparison of the selectivities for the separation of rP1-1, rA1-1 and rM1a-1a was made using the GST competitive inhibitors S-hexylglutathione, S-butylglutathione and γ-glutamyl-(S-hexyl)cysteinyl-phenylglycine as mobile phase modifiers. The association constants determined in solution did not always predict the elution order of the recombinant GSTs (rGSTs) using the mobile phase inhibitors. Yields of active rGSTs from the column were 90%, 88% and 61% for rP1-1, rA1-1 and rM1a-1a, respectively. This technique was used in the fractionation of GSTs in placental and liver cytosols.

1. Introduction

Glutathione S-transferases (GSTs, E.C. 2.5.1.18) are a group of cytosolic enzymes which catalyze the conjugation of electrophilic xenobiotics with glutathione via the free sulfhydryl group present in this abundant intracellular tripeptide [1]. This process generally leads to the detoxification of the xenobiotics since the resulting adducts are normally metabolized to mercapturates and excreted. These human cytosolic enzymes belong to a supergene family comprised of at least four multigene classes Alpha, Mu, Pi and Theta. The enzymes exist as dimers with monomeric molecular masses between 23 and 27 kD and have a range of isoelectric points from 4.8 to 8.9 [2].

* Corresponding author.

0021-9673/94/$07.00
SSDI 0021-9673(94)00230-7

These dimeric enzymes are named by class followed by an Arabic numeral designation of subunit composition. For example A1-1 designates a homodimer of the Alpha class consisting of two monomeric subunits of type A1 [3].

Current chemotherapy often fails due to the appearance of tumor cells resistant to chemotherapeutic agents [1,4]. In some cases elevated levels of the GSTs have been associated with the resistant state [5,6]. Because the expression of GSTs in cancerous and in normal human tissues varies widely in both level and type, techniques to examine isoenzyme profiles are needed for more accurate determination of the role of GSTs in drug resistance. Traditionally, the batch purification of GSTs is performed by affinity chromatography [7–9]. Affinity chromatography is also used to separate a range of GSTs by using isocratic and/or gradient elution with a counter ligand in the mobile phase. Partial resolution of GST homodimers and heterodimers has previously been accomplished using this technique with either S-hexylglutathione or glutathione as the affinity ligand bound to agarose [10–12]. In principle, the elution order of GSTs from an affinity column can be controlled by varying the type of counter ligand in the mobile phase [13–16]. Changes in selectivity resulting from a simple change in a mobile phase additive potentially make this a very powerful separation technique.

We recently developed an affinity HPLC stationary phase for the separation of GSTs using gradients of GST inhibitors [17]. In this report we study the interactions of recombinant GSTs (rGSTs) with this stationary phase in order to gain a better understanding of the parameters required to optimize chromatographic separation of GSTs. The parameters studied are the valence of interaction between the rGSTs and the stationary phase [14,15], and the effect of different mobile phase inhibitors [13–15,18], flow-rate and gradient steepness [14] on elution. These parameters are applied to optimize the separation of GSTs from two different human tissues.

2. Experimental

2.1. Reagents

Iodobutane, iodooctane, sodium borohydride, 1,4-butanediol diglycidyl ether and EDTA were purchased from the Aldrich (Milwaukee, WI, USA). Glutathione, dithiothreitol, 1-chloro-2,4-dinitrobenzene (CDNB), Tween-20 and phenylmethylsulfonyl fluoride were obtained from the Sigma (St. Louis, MO, USA). Recombinant GST enzymes rA1-1, rP1-1, and rM1a-1a were obtained from B. Mannervik (University of Uppsala, Sweden). HEMA BIO 1000 (10 μm) was purchased from Melcor Technologies (Sunnyvale, CA, USA)

2.2. Synthesis of peptides

S-butylglutathione and S-octylglutathione were synthesized by the method of Vince *et al.* [19]. The tripeptide γ-glutamyl-(S-hexyl)cysteinyl-phenylglycine (TER102) was synthesized as previously reported [20]. All peptides had greater than 90% purity when analyzed by reversed-phase HPLC and had acceptable elemental analyses.

2.3. Chromatography

The HPLC system consisted of one or two HPXL pumps equipped with 10 ml/min titanium pump heads, a Rheodyne 7125-081 titanium injector and a Dynamax UV-C detector (Rainin Instrument, Woburn, MA, USA). At the detection wavelength of 280 nm, an intensity of 1000 mV is equivalent to 1 OD unit. All pathways in contact with the mobile phase were of either titanium or biocompatible polymer construction.

For affinity chromatography a gradient was formed with a static mixing tee (Upchurch Scientific, Oak Harbor, WA, USA). When chromatography was performed in the isocratic mode, one port in the static mixing tee was plugged. A biocompatible 250 p.s.i. (1724 kPa) back-pressure regulator (Upchurch Scientific) was placed between the injector and the mixing tee. The

back-pressure regulator was placed in-line to insure proper function of the HPLC pump check valves at the low pressure generated at low flow-rates.

Fractions (0.8 min/fraction) were collected with a Gilson FC203 fraction collector (Rainin Instrument) into a polystyrene, 96-well plate (Costar, Cambridge, MA, USA, Catalog No. 9017). To reduce protein adsorption, the 96-well plate was pretreated with a solution of 0.1% Tween-20 for 16 h, washed with deionized water and air dried.

To determine the fraction of activity retained on the column, the unretained and retained protein peaks, as determined by absorbance at 280 nm, were collected in preweighed 1.5 ml polypropylene tubes. The volume of the fraction collected was determined by weight difference. Activities were then determined for the collected fractions.

2.4. Determination of valence of interaction

To determine the valence of binding of rA1-1 and rP1-1 to the affinity stationary phase, a series of zonal elution, isocratic runs were made at 0.1 ml/min with mobile phases containing 200 m*M* sodium chloride, 10 m*M* sodium phosphate (pH 6.0) and varying concentrations of the eluting ligand S-butylglutathione (Fig. 1). The column was equilibrated with at least 40 ml of a mobile phase containing S-butylglutathione before determining the elution times of rGSTs. The elution time of the recombinant protein (20 μl injection volume) was first determined in the mobile phase with the lowest concentration of S-butylglutathione. Subsequent elution times were determined with sequentially increasing concentrations of the eluting ligand. Capacity factors (k′) were calculated by using the elution time of ovalbumin as t_o.

2.5. CDNB conjugating activity

GST activity, as determined by the color change following conjugation of CDNB with glutathione, was measured at 340 nm with a Tmax Plate Reader (Molecular Devices, Menlo Park, CA, USA). Aliquots (5 or 10 μl) of fractions were placed in the wells of a 96-well plate and mixed with 190 μl of a standard reaction solution. Standard reaction conditions were 200 m*M* sodium phosphate (pH 6.8) with 1 m*M* glutathione and 1 m*M* CDNB at 32°C [21].

2.6. Determination of enzyme K_i values

The kinetic constants (K_i) for rP1-1, rA1-1 and rM1a-1a in the presence and absence of the inhibitors S-butylglutathione, S-hexylglutathione, TER102, or S-octylglutathione were determined from CDNB conjugating activity measurements at 10 m*M* sodium phosphate, 200 m*M* sodium chloride (pH 6) as described above and fitting the data using Hanes–Woolf plots [21].

The simplest mechanism for the conjugation of CDNB (A) and glutathione (B) by GST in the presence of an inhibitor (I) is shown below.

$$E + A \rightleftharpoons EA$$

$$E + B \rightleftharpoons EB$$

$$EA + B \rightleftharpoons EAB$$

$$EB + A \rightleftharpoons EAB$$

$$E + I \rightleftharpoons EI$$

$$EAB \rightharpoonup E + P$$

It is assumed that the binding of A and B are independent and that the inhibitor, I, is purely competitive with both A and B. The relevant dissociation constants based on these assumptions are $K_a = [E][A]/[EA] = [EB][A]/[EAB]$, $K_b = [E][B]/[EB] = [EA][B]/[EAB]$, and $K_i = [E][I]/[EI]$. Assuming steady-state kinetics, Eq. 1 can be derived for this rapid equilibrium random Bi Bi mechanism [22].

$$v = \frac{V_{max}[B]/(1 + K_a/[A])}{K_b\{1 + [I]/K_i(app)\} + [B]} \quad (1)$$

where

$$K_i(app) = K_i\frac{[A]}{K_a}(1 + K_a/[A]) \quad (2)$$

The apparent dissociation constant, K_i(app),

for an inhibitor was determined in the presence of an inhibitor by varying the glutathione concentration (B) and holding the CDNB (A) concentration constant at 1 m*M*. In a separate series of experiments the value of K_a was determined in the absence of inhibitor by varying the CDNB concentration while maintaining the glutathione concentration at 1 m*M*. The dissociation constants for CDNB were found to be 1.8 m*M*, 0.65 m*M* and 1.6 m*M* for rA1-1, rM1a-1a and rP1-1 respectively. The K_i values for the inhibitors were then calculated from the experimental values K_i(app), K_a and [A] = 1 m*M*. In Table 1 are listed the association constants K_{asso} (reciprocal of K_i) for the inhibitors. The inhibitors listed in Table 1 were found to be purely competitive with glutathione for all the rGSTs investigated and competitive with CDNB for rA1-1. All four inhibitors showed mixed inhibition with CDNB for rM1a-1a. All of the inhibitors were competitive with CDNB for rP1-1, except for TER102 which showed mixed inhibition.

2.7. Determination of activity retained on the affinity column

The percentage of activity retained was determined as a function of ionic strength of the loading buffer for the rGSTs. For these experiments the GST was diluted (1:5) in loading buffer (10 m*M* sodium phosphate, pH 6.0 with or without 200 m*M* sodium chloride) and injected onto the column (5 × 0.46 cm I.D.). Then the column was eluted for 5 min at 0.5 ml/min with loading buffer and the unretained protein collected. The flow-rate was increased to 1.0 ml/min with a mobile phase of 200 m*M* sodium chloride (10 m*M* sodium phosphate, pH 6). From 5 to 15 min a linear gradient of 5 m*M* S-hexylglutathione in 200 m*M* sodium chloride (10 m*M* sodium phosphate, pH 6) was used to elute retained GST from the column. The fraction containing eluted protein was collected and the activity determined. The percent of activity retained on the column was determined using the relationship: % activity retained = [activity retained/(activity retained + activity unretained)] × 100.

To determine the total recovery of protein from the column, injections were made in a mobile phase of 5 m*M* S-hexylglutathione, 200 m*M* sodium chloride and 10 m*M* sodium phosphate (pH 6.0). Under these conditions all the rGSTs were unretained. The area (280 nm) of the peak eluted in the 5 m*M* S-xylglutathione mobile phase was compared with the sum of the areas for the unretained and retained peaks described in the previous paragraph.

The amount of enzyme activity recovered after injection in 200 m*M* sodium chloride, 10 m*M* sodium phosphate (pH 6.0) from the affinity column was determined using the gradient previously described. A stock solution of the enzyme was prepared and one-half injected onto the column. Factions corresponding to the elution of protein were collected and the activity determined. The column was then disconnected, the injection loop filled using the other half of the enzyme stock solution and the enzyme collected in approximately the same volume of mobile phase as the other collected fractions. Again the activity was determined. The percent of activity recovered was calculated using the relationship: %activity recovered = activity eluted from the column/activity injected on the column.

Table 1
Solution phase association constants of ligands with GSTs

Ligand	K_{asso} (μM^{-1})		
	rA1-1	rM1a-1a	rP1-1
S-Hexylglutathione	1.3	1.2	0.17
S-Butylglutathione	0.02	0.11	0.07
TER102	0.34	0.08	6.3
S-Octylglutathione	4.0	4.0	0.65

2.8. Influence of eluting ligand

The three rGSTs were injected onto the column in a mobile phase of 10 m*M* sodium phosphate (pH 6.0). Gradients of S-hexylglutathione (0–5 m*M*), S-butylglutathione (0–20 m*M*) or TER102 (0–20 m*M*) as indicated in Fig. 2 were used to elute the rGSTs.

2.9. Influence of flow-rate and gradient steepness

Flow-rate and the gradient steepness were investigated to determine their influence on resolution of rP1-1 and rA1-1 (Fig. 3) using S-hexylglutathione (0–5 m*M*) gradients in 10 m*M* sodium phosphate (pH 6) and 200 m*M* sodium chloride. The gradient duration was varied inversely with the flow-rate so that their product (gradient steepness) was constant. For these flow-rate studies, the gradient duration was 25 min for measurements at 0.2 ml/min, 50 min at 0.1 ml/min and 167 min at 0.03 ml/min (Fig. 3a). Next the gradient steepness was varied while the flow-rate was maintained at 0.1 ml/min (Fig. 3b). For both studies the samples were loaded at 0.1 ml/min in 10 m*M* sodium phosphate (pH 6) for 9 min and the washing step was from 10–14 min with 10 m*M* sodium phosphate (pH 6) containing 200 m*M* sodium chloride. Gradients commenced at 15 min.

2.10. Tissue treatment

Human liver samples were obtained from the Cooperative Human Tissue Network (Columbus, OH and Birmingham, AL, USA) and stored at −80°C. Samples were slightly thawed, minced with scissors and homogenized at 25% (w/v) in buffer containing 10 m*M* Tris hydrochloride (pH 7.8), 1 m*M* EDTA, 1 m*M* dithiothreitol and 0.10 m*M* phenylmethylsulfonyl fluoride using an OMNI stator generator homogenizer (Marietta, GA, USA). Cytosol was prepared by ultracentrifugation at 105 000 *g* for 35 min at 4°C in a Beckman Optima TL-100 tabletop ultracentrifuge (Fullerton, CA, USA). Protein concentrations were determined using a 96-well plate Coomassie dye binding assay (Bio Rad, Richmond, CA, USA) read on a Tmax Plate Reader with bovine serum albumin as a standard [9].

2.11. Affinity matrix

The synthesis of the affinity matrix follows the general procedure of Sundberg and Porath [23]. HEMA BIO 1000, 1,4-butanediol diglycidyl ether and 0.6 *M* sodium hydroxide containing 2 mg/ml of sodium borohydride (0.03:1:1, w/v/v) were mixed overnight. The particles were filtered and washed with water, ethyl alcohol and acetone.

To 700 mg of the dried particles were added S-octylglutathione (75 mg) dissolved in 3.5 ml of 0.5 *M* sodium carbonate. The suspension was mixed for approximately 90 h. After filtration the particles were washed with (i) 1 *M* sodium chloride, 0.1 *M* sodium phosphate (pH 9), (ii) 1 *M* sodium chloride, 0.1 *M* sodium acetate (pH 4.5), (iii) water, (iv) ethyl alcohol and (v) acetone.

2.12. Packing of columns

The affinity material (650 mg) was slurried in 20 ml of water and was packed at high pressure into stainless-steel columns 5 × 0.46 cm I.D. or 3 cm (Supelco, Bellefonte, PA, USA). The column frits were 2 μm (average pore diameter) titanium encased in a CTFE ring (Upchurch Scientific, Oak Harbor, WA, USA). A Haskell (Burbank, CA, USA) DSTV122 liquid pump was used to provide the drive solvent (water) during the packing process. The columns were packed at 2000 p.s.i. (13 790 kPa) with 50 ml of water and then 4000 p.s.i. (27 579 kPa) with 50 ml of water. In some cases 5 × 0.3 cm I.D. Omni glass columns with stainless-steel frits (Rainin Instrument) were used. These columns were packed by connecting a 5-ml syringe to the outlet and pulling an aqueous slurry of the stationary phase into the column.

3. Results and discussion

Two models for the interaction of a GST with the stationary phase were considered. The first model assumes only monovalent interactions between a protein molecule and a ligand.

$$E + I \overset{K_1}{\rightleftharpoons} EI$$

$$E + L \overset{K_2}{\rightleftharpoons} EL$$

In this scheme E is the protein (GST), I is the mobile phase eluting ligand (S-butylglutathione) and L is the immobilized affinity ligand (S-octylglutathione). From the treatment of Walters [24,25] for this model, the inverse of the capacity factor as a function of mobile phase ligand concentration is given by:

$$\frac{1}{k'} = \frac{V_M}{K_2 m_L}(1 + K_1[I]) \quad (3)$$

In Eq. 3, $K_1 = [EI]/[E][I]$, $K_2 = \{EL\}/[E]\{L\}$, m_L = number of moles of affinity ligand in column and is the product of $A \cdot \{L\}$ and V_M is the total volume of mobile phase in the column. The symbol $\{\}$ indicates surface concentration and A is the column surface area [24,25]. Eq. 3 predicts that a plot of $1/k'$ *vs.* [I] should be a linear relationship. Clearly from Fig. 1, such a linear relationship is not exhibited for either rA1-1 or rP1-1.

The second model assumes that a protein molecule can interact with two molecules of ligand. This divalent model is represented as:

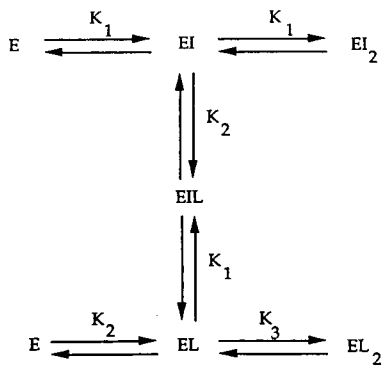

For the divalent model, the inverse of the capacity factor as a function of the mobile phase ligand concentration is given by [25].

$$\frac{1}{k'} = \frac{V_M}{K_2 m_L} \frac{(1 + K_1[I])^2}{2(1 + K_1[I]) + K_3\{L\}} \quad (4)$$

In this model an assumption is made that the two binding sites on the protein are identical and independent even when E is adsorbed on the stationary phase. The association constant K_1 is assumed, therefore, to be the same for the binding of I to E, EI and EL. The equilibrium constant K_3, which represents the equilibrium constant for the binding of EL to a second immobilized ligand, may be highly sensitive to steric effects. This condition is not necessary, however, and a divalent model has been proposed in which the equilibrium constant for the binding of the second immobilized affinity ligand is the same as for the first ligand [16]. The solid lines shown in Fig. 1 are computed based on Eq. 4. An association constant of $K_1 = 0.02\ \mu M^{-1}$ is used to generate the curve ($r^2 = 0.998$) for rA1-1. For the rP1-1 the curve ($r^2 = 0.976$) is generated using an association constant of $K_1 = 0.6\ \mu M^{-1}$.

The interaction of recombinant GSTs with this affinity stationary phase is best described by the divalent model. Several of the assumptions used in the derivation of Eq. 4 are reasonable for these enzymes. GSTs are known to be dimeric enzymes with each subunit containing one active site. Extensive kinetic data strongly suggest that the two active sites per dimer are kinetically independent [26]. Thus we propose that two affinity ligands (S-octylglutathione) bound to the stationary phase as well as two mobile phase ligands (S-butylglutathione) are able to interact with a GST dimer during the affinity chromatographic process.

The small deviations seen between the positions of the experimental points in Fig. 1 and the curves calculated from Eq. 4 may arise because of invalid assumptions used to derive this equation. In particular the assumption that K_1 best describes the binding of inhibitor to the EL complex may be incorrect. Enzymatic activities often decrease when the protein is attached to a surface [27,28] indicating that association constants may be different for the protein in solution than for the same protein attached to a surface.

In principle, the relevant association constants for mobile phase and stationary phase ligands can be calculated from kinetic inhibition constants. On the basis of the simple mechanistic model proposed here, the relevant association constants were determined (Table 1). The use of these experimentally determined association constants to calculate binding curves (Fig. 1) and to predict the elution order of proteins (Fig. 2) was

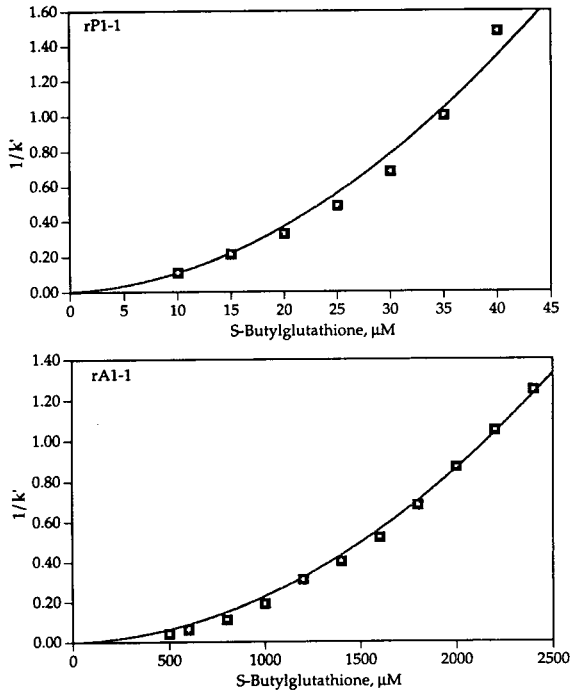

Fig. 1. $1/k'$ *vs.* S-butylglutathione concentration for rP1-1 and rA1-1. The k' values for the proteins were determined at increasing concentrations of S-butylglutathione in 10 m*M* sodium phosphate and 200 m*M* sodium chloride (pH 6). Flow-rate: 0.1 ml/min. Detection: 280 nm. Columns: 3 × 0.46 cm I.D. stainless steel for rP1-1, 5 × 0.46 cm I.D. stainless steel for rA1-1.

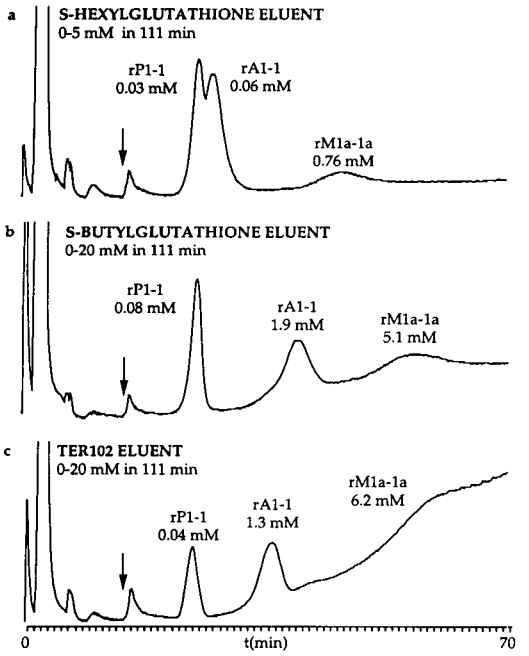

Fig. 2. Effect of eluting ligand on rGST elution. Gradients of S-hexylglutathione (a), S-butylglutathione (b) or TER102 (c) were used to elute the rGSTs. Mobile phases: A, 10 m*M* sodium phosphate (pH 6); B, 200 m*M* sodium chloride in A; C, S-hexylglutathione (5 m*M*), S-butylglutathione (20 m*M*) or TER102 (20 m*M*) in B. Gradient : 0–6 min, A, 0.1 ml/min; 7–14 min, B, 0.4 ml/min; 15–70 min, 0–57.3% C, 0.1 ml/min. Detection: 280 nm. Arrow marks the beginning of the eluent gradient. Column: 5 × 0.3 cm I.D. glass.

only partially successful. The curve for rA1-1 in Fig. 1 was calculated from the kinetically derived association constant and gave a good fit to the experimental points ($r^2 = 0.998$). The best fit curve for rP1-1 was calculated using an association constant of 0.6 μM^{-1} ($r^2 = 0.976$). Curves for rP1-1 data calculated using the kinetically derived association constant, 0.07 μM^{-1}, gave a very poor fit ($r^2 = 0.90$).

As expected, the ligand (S-hexylglutathione) which binds most strongly with the GSTs (Table 1) was the most effective ligand for the elution of the GSTs (Fig. 2). S-hexylglutathione eluted all three GSTs at concentrations less than 0.8 μM while the other two ligands required 5.1 μM (S-butylglutathione) or 6.2 μM (TER102). The order of rGST elution with S-hexylglutathione did not correspond, however, to the kinetically determined association constants. Examination of Table 1 indicates that rA1-1 and rM1a-1a exhibit equal solution phase association constants with S-hexylglutathione (the mobile phase ligand) and with S-octylglutathione (the stationary phase ligand). One might expect that these two rGSTs should nearly co-elute when S-hexylglutathione was used as the eluting ligand. The two proteins are clearly well separated using this mobile phase ligand (Fig. 2a). By a similar argument, rM1a-1a would be expected to be eluted before rA1-1 in a mobile phase containing S-butylglutathione but the order is in fact reversed (Fig. 2b). Interestingly, the order of elution using TER102 does correspond to that predicted from the kinetic association constants.

At least two reasons may be advanced to

explain the failure of kinetically derived solution phase association constants to predict chromatographically determined association constants or elution order. First the association constants of rGSTs with the immobilized S-octylglutathione may not be the same as those measured in solution. Because the immobilized S-octylglutathione imparts a net negative charge to the phase, the rGSTs see a different ionic environment when binding to an immobilized ligand than when binding to the ligand free in solution. The isoelectric points [2] of rP1-1 (p*I* 4.8), rM1a-1a (p*I* 6.6) and rA1-1 (p*I* 7.9) vary widely and at pH 6, the negatively charged rP1-1 will be repelled from the stationary phase while rA1-1 will be attracted. In addition, compared to binding in free solution, restricted orientation of the immobilized ligand could affect its ability to attain the same docking orientation in the catalytic site. The degree of restriction may vary between the various recombinant enzymes. Several investigators have found similar association constants for proteins to a ligand whether the ligand is free in solution or immobilized [15,18] while others have found differences of a factor of ten [29]. Second, the kinetically derived association constants may not be a valid measure of the true association constants. We have assumed the simplest mechanistic model for this complex enzymatic reaction. More complicated mechanisms have been proposed for the GSTs, and it has been postulated that mechanisms may vary among the isoenzymes [30,31]. Our observation that the four ligands studied showed mixed inhibition with CDNB for the GST rM1a-1a and competitive inhibition with rP1-1 and rA1-1 does support these mechanistic complexities. At best one may only use kinetically derived association constants for the qualitative prediction of elution order of GSTs.

Flow-rate and gradient steepness had a significant effect on this separation. The best separations were done at flow-rates considerably lower than are normally used in HPLC (Fig. 3). Low flow-rates are required due to a characteristic of affinity chromatography which relates to the slow dissociation rates of many protein–ligand complexes. Much faster kinetics are exhibited in other types of chromatography such as reversed-phase [14,32,33]. In addition, other

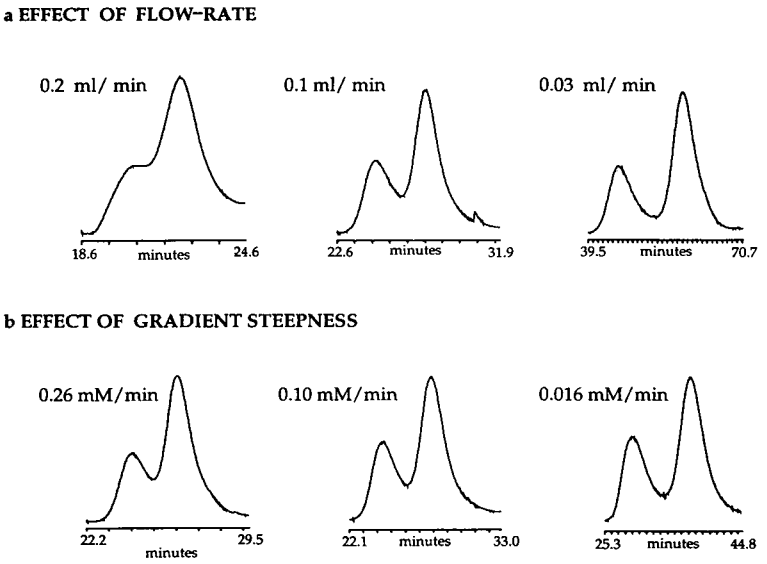

Fig. 3. Effect of flow-rate (a) and gradient steepness (b) on the separation of rP1-1 from rA1-1. Mobile phases: A, 10 m*M* sodium phosphate (pH 6); B, 200 m*M* sodium chloride in A; C, S-hexylglutathione (5 m*M*) in B. Samples were loaded in A, 0–9 min, 0.1 ml/min; washed in B, 10–14 min, 0.8 ml/min; and the gradient of 0–100% C commenced at 15 min. For gradient conditions see Experimental. Detection: 280 nm. Column: 5 × 0.3 cm I.D. glass.

diffusion-based processes responsible for band dispersion are sensitive to the molecular size of the analyte. Large molecules, such as proteins, produce large reduced velocities at normal HPLC flow-rates resulting in large plate heights [34]. Slow dissociation rates and high reduced velocities lead to large plate heights and relatively wide bands. At smaller reduced velocities these band widths can be minimized.

The slow dissociation rates of enzyme–stationary phase complexes can also be invoked to explain the increasing broadness of the peaks eluting later in the gradient (Fig. 2). Unlike gradients in reversed-phase chromatography where the peak width is generally constant regardless of the position in the gradient [35], here peak width increases with increasing retention. We postulate that M1a-1a elutes later in the gradient than rP1-1 because rM1a-1a binds more tightly to the affinity phase, and this difference in the association constants results from a smaller dissociation rate constant for the rM1a-1a/stationary phase complex than for the rP1-1/stationary phase complex. On the basis of this argument, at equal flow-rates the rM1a-1a peak will have a greater peak volume than the rP1-1 peak volume.

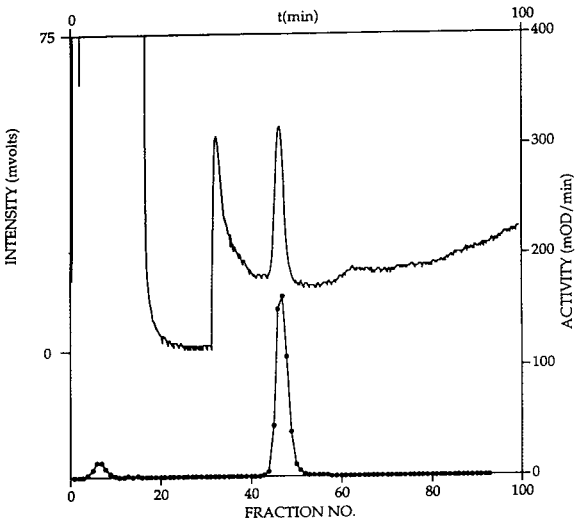

Fig. 4. Separation of GSTs from placental cytosol. Mobile phases: A, 10 m*M* sodium phosphate (pH 6); B, 200 m*M* sodium chloride in A; C, S-butylglutathione (20 m*M*) in B. Gradient : 0–12 min, A, 0.1 ml/min; 12–24 min, B, 0.4 ml/min; 24–116 min, 0–100% C, 0.1 ml/min. Detection: 280 nm (——). Activity (-O-). Column: 5 × 0.3 cm I.D. glass.

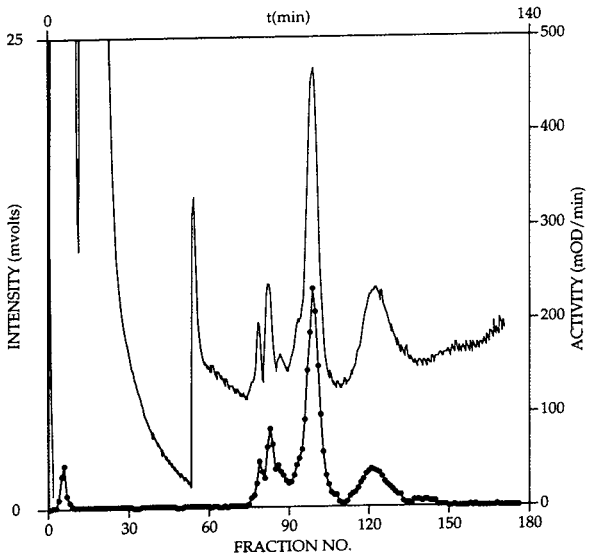

Fig. 5. Separation of GSTs from liver cytosol. Mobile phases: A, 10 m*M* sodium phosphate (pH 6); B, 200 m*M* sodium chloride in A; C, S-butylglutathione (20 m*M*) in B. Gradient : 0–5 min, A, 0.1 ml/min; 5–50 min, B, 0.4 ml/min; 50–146 min, 0–100% C, 0.1 ml/min. Detection: 280 nm (——). Activity (-O-). Column: 5 × 0.3 cm I.D. glass.

The ionic strength of the loading buffer had little effect upon the amount of rGST activity retained on the column. The activities retained for rP1-1, rM1a-1a and rA1-1 were 100%, 93% and 97%, respectively at low ionic strength (10 m*M* phosphate) and 100%, 99% and 95%, respectively at high ionic strength (200 m*M* sodium chloride, 10 m*M* phosphate). Yields as determined from peak areas at 280 nm of total protein eluted from the column were greater than 95% for the rGSTs. The percent activity eluted from the column under the higher ionic strength conditions were 90%, 88% and 61% for rP1-1, rA1-1 and rM1a-1a respectively.

Human cytosol obtained from human placenta and human liver was injected onto the affinity column and the GSTs in these samples fractionated. The separations were performed at the slow flow-rates and with gradients of S-butylglutathione found to be optimum for the model studies with rGSTs. For human placenta (Fig. 4) greater than 96% of the activity was eluted in

one peak which probably corresponds to the human P1-1. Previous investigators have shown that the GST in human placenta is predominately P1-1 [2]. For human liver (Fig. 5) greater than 97% of the activity was separated into at least four GST isoenzymes. Human liver is reported to contain multiple forms of GSTs [36].

In conclusion, solution phase inhibitory potency provides an approximate guide for selection of ligands useful in affinity HPLC separations of GST isoenzymes. Following empirical verification and adjustment, an optimized pair of immobilized and eluting ligands has been defined for resolving the major species of GSTs in human tissues.

Acknowledgements

The authors thank Larry M. Kauvar for comments on the manuscript and Angela DeCarlo for technical assistance.

References

[1] D.J. Waxman, *Cancer Res.*, 50 (1990) 6449.
[2] B. Ketterer, D.J. Meyer and A.G. Clark, in H. Sies and B. Ketterer (Editors), *Glutathione Conjugation, Mechanisms and Biological Significance*, Academic Press, London, 1988, p. 74.
[3] B. Mannervik, Y.C. Awasthi, P.G. Board, J.D. Hayes, C. Di Ilio, B. Ketterer, I. Listowsky, R. Morgenstern, M. Muramatsu, W.R. Pearson, C.B. Pickett, K. Sato, M. Widersten and C.R. Wolf, *Biochem. J.*, 282 (1992) 305.
[4] R.A. Kramer, J. Zakher and G. Kim, *Science*, 241 (1988) 694.
[5] R.B. Puchalski and W.E. Fahl, *Proc. Natl. Acad. Sci. U.S.A.*, 87 (1990) 2443.
[6] S.M. Black, J.D. Beggs, J.D. Hayes, A. Bartoszek, M. Muramatsu, M. Sakai and C.R. Wolf, *Biochem. J.*, 268 (1990) 309.
[7] B. Manervik and C. Guthengerg, *Methods Enzymol.*, 77 (1981) 231.
[8] W.H. Habig and W.B. Jakoby, *Methods Enzymol.*, 77 (1981) 398.
[9] V.M. Castro, M.K. Kelley, A. Engqvist-Goldstein and L.M. Kauvar, *Biochem. J.*, 292 (1993) 371.
[10] J.D. Hayes, *Biochem. J.*, 255 (1988) 913.
[11] J.D. Hayes, L.A. Kerr and A.D. Cronshaw, *Biochem. J.*, 264 (1989) 437.
[12] P.J. Dierickx, *J. Chromatogr.*, 530 (1990) 263.
[13] J.D. Hayes, in J.D. Hayes, C.B. Pickett and T.J. Mantle (Editors), *Glutathione S-Transferases and Drug Resistance*, Taylor and Francis, London, 1989, p. 17.
[14] P.-O. Larsson, M. Glad, L. Hansson, M.-O. Mansson, S. Ohlson and K. Mosbach, *Adv. Chromatogr.*, 21 (1983) 41.
[15] C. DeLisi and H.W. Hethcote, in I.M. Chaiken (Editor), *Analytical Affinity Chromatography*, CRC Press, Boca Raton, FL, 1987, p. 1.
[16] D.J. Winzor, *J. Chromatogr.*, 597 (1992) 67.
[17] J.B. Wheatley, M.K. Kelley, J.A. Montali, C.O.A. Berry and D.E. Schmidt, *J. Chromatogr. A*, 663 (1994) 53.
[18] H.E. Swaisgood and I.R. Chaiken, in I.M. Chaiken (Editor), *Analytical Affinity Chromatography*, CRC Press, Boca Raton, FL, 1987, p. 65.
[19] R. Vince, S. Daluge and W.B. Wadd, *J. Med. Chem.*, 14 (1971) 402.
[20] M.H. Lyttle, D.T. Aaron, M.D. Hocker and B.R. Hughes, *Peptide Res.*, 5 (1992) 336.
[21] J.E. Flatgaard, K.E. Bauer and L.M. Kauvar, *Cancer Chemother. Pharmacol.*, 33 (1993) 63.
[22] I.H. Segal, *Enzyme Kinetics*, Wiley, New York, NY, 1975, p. 302.
[23] L. Sundberg and J. Porath, *J. Chromatogr.*, 90 (1974) 87.
[24] R.R. Walters, in I.M. Chaiken (Editor), *Analytical Affinity Chromatography*, CRC Press, Boca Raton, FL, 1987, p. 117.
[25] D.J. Anderson and R.R. Walters, *J. Chromatogr.*, 331 (1985) 1.
[26] B. Mannervik and U.H. Danielson, *CRC Crit. Rev. Biochem.*, 23 (1988) 283.
[27] R.B. Van Breemen, M.G. Bartlett, Y. Tsou, C. Culver, H. Swaisgood and S.E. Unger, *Drug Metab. Dispos.*, 19 (1991) 683.
[28] G. Du Val, H.E. Swaisgood and H.R. Horton, *Biochemistry*, 24 (1985) 2067.
[29] K. Peters, S. Fittkau, A. Steinert and D. Strohl, *J. Chromatogr.*, 648 (1993) 91.
[30] K.M. Ivanetich, R.D. Goold and C.N.T. Sikakana, *Biochem. Pharmacol.*, 39 (1990) 1999.
[31] K.M. Ivanetich and R.D. Goold, *Biochim Biophys Acta*, 998 (1989) 7.
[32] M. Wikstrom and S. Ohlson, *J. Chromatogr.*, 597 (1992) 83.
[33] S. Ohlson, A Lundbald and D. Zopf, *Anal. Biochem.*, 169 (1988) 204.
[34] L.R. Snyder, in C. Horvath (Editor), *High Performance Liquid Chromatography*, Academic Press, New York, 1980, p. 207.
[35] L.R. Snyder and J.J. Kirkland, *Introduction to Modern Liquid Chromatography*, Wiley, 1979, p. 664.
[36] D.L. Vander Jagt, L.A. Hunsaker, K.B. Garcia and R.E. Boyer, *J. Biol. Chem.*, 260 (1986) 11603.

ELSEVIER

Journal of Chromatography A, 676 (1994) 91–98

JOURNAL OF CHROMATOGRAPHY A

Interaction of lysozyme with synthetic anti-lysozyme D1.3 antibody fragments studied by affinity chromatography and surface plasmon resonance

Edwin Lasonder*[,a], Wim Bloemhoff[b], Gjalt W. Welling[a]

[a] *Laboratory of Medical Microbiology, University of Groningen, Oostersingel 59, 9713 EZ Groningen, Netherlands*

[b] *Department of Organic Chemistry, Gorlaeus Laboratory, University of Leiden, P.O. Box 9502, 2300 RA Leiden, Netherlands*

Abstract

Synthetic antibody fragments of monoclonal anti-lysozyme antibody D1.3 have been tested on binding with hen egg white lysozyme using immunoaffinity chromatography and surface plasmon resonance. Upon immunoaffinity chromatography, peptides containing one or two complementarity determining regions (CDRs) of D1.3 show interaction with lysozyme. Surface plasmon resonance with immobilized CDR peptides showed that this interaction is not based on the antigen–antibody interaction. Nevertheless, these peptides could be useful as ligands for the purification of lysozyme from a mixture of proteins.

1. Introduction

The use of immobilized antibodies in immunoaffinity chromatography for purifications of antigens or the application in biosensors for detection of proteins is limited by the stability of the antibody. Size reduction of the antibody may improve the stability of an immobilized antibody. Antibodies ($M_r = 150\,000$) can easily be reduced to a fragment variable (Fv) ($M_r = 25\,000$) region without losing much of the specificity of the antibodies and in some cases to variable regions of the heavy chain (V_H) or light chain (V_L) ($M_r = 12\,500$) [1]. The specificity of antibody–antigen interactions is determined by three complementarity determining regions (CDRs) located at the variable region of the heavy chain and three CDRs at the variable region of the light chain. The Fv region of an antibody is the antigen binding site which consists of V_H and V_L regions. Further reduction in size results in peptides which contain one or two CDRs ($M = 1000$–4000) which may be able to bind the antigen. Synthetic CDR peptides have been found to bind an antigen or to inhibit binding of an antibody [2–8]. The advantage of small synthetic antibody fragments compared to an antibody is their stability and the possibility for large-scale production.

Selection of a CDR-containing fragment of an antibody for peptide synthesis is facilitated by tertiary structure information of well studied antibody–antigen complexes. For this reason we have chosen the monoclonal antibody (MAb) D1.3–hen egg white lysozyme (HEL) interaction as a model system to select antibody fragments for peptide synthesis and test them as immobilized ligands in immunoaffinity chromatography

* Corresponding author.

0021-9673/94/$07.00
SSDI 0021-9673(94)00125-S

and in surface plasmon resonance on binding lysozyme. X-Ray diffraction studies of the complex between Fab D1.3 and lysozyme revealed the contact residues of lysozyme and D1.3 [9,10]. The epitope of lysozyme which interacts with D1.3 consists of peptide 18–27 and peptide 116–129 of the linear sequence of lysozyme. The binding of D1.3 to lysozyme is based on hydrogen bonds, Van der Waals interactions and hydrophobic interactions but not on charge interactions (salt bridges). Upon binding, no changes in the conformation of D1.3 occur, except for a slight change in quaternary structure by a change of the "elbow bending" angle, the angle between V and C domain of Fab D1.3. The interacting surfaces of lysozyme and D1.3 are complementary; only a few amino acids residues of the contact area contribute directly to the binding energy. The contribution of the contact residues of Fv D1.3 to the binding of lysozyme has been calculated by Novotny *et al.* [11]. A much larger contribution to complex formation of the V_H domain (− 11.4 kcal; 1 cal = 4.1868 J) than of the V_L domain (− 2.5 kcal) was found. For this reason only peptides of the V_H domain were selected for synthesis (Table 1). In general, small synthetic peptides do not possess one stable preference conformation in solution. The CDR peptides of Table 1 will probably not have the same solution conformation as the conformation in D1.3. Some of these peptides (peptides 3 and 6) were cyclized to mimic the reverse turns present in the MAb D1.3. Another possibility to mimic the conformation of a peptide in the protein conformation is to enlarge the peptide to a "small protein" (peptide 7). H3D1.3 CDR peptides (peptides 1, 2 and 3 in Table 1) are potentially the most suitable synthetic antibody fragments, based on the number and the contribution to the binding of the contact residues.

First, the binding of the CDR peptides of D1.3 studied by immunoaffinity chromatography will be discussed. In previous studies it appeared that two CDR peptides of MAb Gloop2 (H2Gloop2 and L3Gloop2) directed against lysozyme could bind lysozyme in immunoaffinity chromatog-

Table 1
Selected peptides for synthesis based on structure information of the D1.3–lysozyme complex [9,10]

Peptide	CDR in D1.3	*M*	ΔG (kcal)	Amino acid sequence
1	H3D1.3 92–101	1356	− 6.8	H-ARERDYRLDY-NH_2 (xxxx)
2	H3D1.3 92–105	1784	− 6.8	H-ARERDYRLDYWGQG-NH_2 (xxxx)
3	cH3D1.3 98–103	1224	− 6.8	Ac-CERDYRLCK-NH_2 (xxxx)
4	H2D1.3 50–63	1708	− 2.0	Ac-(Nle)IWGDGNTDYNSALK-NH_2 (xxx)
5	H2D1.3 50–62	1538	− 2.0	H-(Nle)IWGDGNTDYNSAL-NH_2 (xxx)
6	cH2D1.3 51–57	1135	− 2.0	Ac-CIWGDGNTCK-NH_2 (xxx)
7	H1H2D1.3 28–63	3977	− 3.4	Ac-SLTGYGVNWVRQPPGKGLEWLG(Nle)IWGDGNTDYNSAL-NH_2 (xxx, xxx)

The CDR regions are underlined and the contact residues of the CDR are marked by an × sign. The contribution of the peptides to complex formation is given in Gibbs free energy ΔG [11]. Some of the peptides were acetylated at the N-terminus to prevent N-terminal coupling of the activated Sepharose in immunoaffinity chromatography or the activated dextran-coated sensorchip in a biosensor. Methionine was substituted by isosteric norleucine (Nle) to prevent oxidation of Met-containing peptides. A prefix c in column 2 indicates a cyclized peptide.

raphy [2,3]. Immunoaffinity chromatography of lysozyme on columns with D1.3 antibody fragments (Fv D1.3 and V_HD1.3 as ligands) was performed by Berry and co-workers [12–14]. A reduced specificity of the V_H column towards HEL was found. Separation of HEL from turkey lysozyme that could be accomplished on a Fv column was no longer possible on a V_H column.

Second, the results of the study of biospecific interaction of the synthetic antibody fragments by surface plasmon resonance (SPR) [15,16] will be given. Binding constants (K_a) of D1.3, Fv D1.3 and V_HD1.3 with immobilized HEL were determined with SPR by Borrebaeck *et al.* [17]. The published values of K_a were respectively $>10^{11}$, $5.9 \cdot 10^9$ and $0.1 \cdot 10^9\ M^{-1}$.

The aim of this study is to test the hypothesis whether it is possible to predict potential synthetic antibody fragments which may bind the antigen based on tertiary structure information of a antibody–antigen complex. The D1.3–lysozyme interaction is used as a model system for the selection and synthesis of such fragments.

2. Materials and methods

2.1. Peptide synthesis

The peptides were synthesized according to the solid-phase method with 9-fluorenylmethoxycarbonyl (Fmoc) amino acids [18]. The *in situ* activation of the Fmoc-amino acids was carried out by means of the benzotriazol-1-yloxytris-(dimethylamino) phosphonium hexafluorophosphate (BOP) reagent of Castro *et al.* [19]. BOP was purchased from Richelieu Biotechnologies (St. Hyacinthe, Canada). The peptides were synthesized as amides by the use of 4-(α-Fmoc-amino-2′,4′-dimethoxybenzyl) phenoxyacetic acid as a linkage agent [20], obtained from Novabiochem (Bubendorf, Switzerland). The linker was attached to Pepsyn K, purchased from MilliGen Biosearch (Etten-Leur, Netherlands). The Fmoc-amino acids were purchased from MilliGen Biosearch and Senn Chemicals (Dielsdorf, Switzerland). N,N-Dimethylacetamide (DMA), diisopropylethylamine (DIPEA), piperidine, trifluoroacetic acid (TFA), 1,2-ethanedithiol (EDT), thioanisole and phenol were obtained from Janssen (Geel, Belgium). Sidechain protection groups of the Fmoc-amino acids were: *tert.*-butyl for Asp, Glu, Ser, Thr and Tyr; *tert.*-butoxycarbonyl for Lys; Pmc (2,2,5,7,8-pentamethylchroman-6-sulfonyl) for Arg; Trt (trityl) for Gln and His. DMA was distilled under reduced nitrogen pressure, DIPEA was distilled from ninhydrin and piperidin was distilled from KOH before use. The peptides were synthesized with a laboratory-built automated peptide synthesizer [21]. The continuous flow synthesis was monitored at 304 nm. Each coupling was performed in DMA with 4 equivalents of *in situ* activated Fmoc-amino acids for 45 min. The Fmoc protecting group was deprotected by piperidine–DMA (20:80) for 9 min. Finally, the N-terminus was blocked by coupling with DMA–acetic anhydride (50:50) for 15 min. The peptides were cleaved from the resin with reagent K [22] (TFA–phenol–water–thioanisole–EDT, 82.5:5:5:5:2.5), precipitated in diethyl ether and washed with ether for five times and finally the peptides were lyophilized. The purity of the peptides was confirmed by RP-HPLC and by amino acid analysis performed by Eurosequence (Groningen, Netherlands). Cysteine-containing peptides were oxidized by stirring a solution of 0.1 mg/ml peptide pH 8 for at least 12 h at room temperature. Cyclisation of the peptides was followed with RP-HPLC. The peptides were lyophilized from a diluted acetic acid solution, followed by desalting on Sephadex G-25.

2.2. Immunoaffinity chromatography

The CDR peptides were tested on binding lysozyme using two different column materials, activated CH-Sepharose 4B obtained from Pharmacia (Uppsala, Sweden) and Affigel-10 obtained from Bio-Rad Labs. (Richmond, CA, USA). Coupling of the peptides was performed basically according to the protocols of the manufacturers. Briefly, 2 mg peptide (peptides 1, 2 and 4) in 2 ml coupling buffer (0.1 *M* $NaHCO_3$–Na_2CO_3, pH 8.2) were coupled to 0.5 g acti-

vated CH-Sepharose 4B during 2 h. The excess of unreacted active groups was blocked by 1 *M* ethanolamine in coupling buffer. Peptides were coupled to 2 ml Affigel-10 (4.5 mg peptide 7) and 1 ml Affigel-10 (7.5 mg peptide 4) in 2 ml coupling buffer (peptide 7 in coupling buffer with 40% ethanol) for 16 h at 4°C. The excess of reactive groups was blocked by 1 *M* ethanolamine in coupling buffer. Coupling percentages of the immobilized peptides were determined by comparison of peak heights in RP-HPLC of the coupling samples before and after coupling. The coupling percentages of the peptides were: peptide 1, >99%; peptide 2, 97%; peptide 4 to activated CH-Sepharose 4B 97%; peptide 4 to Affigel-10 75%; and peptide 7, 93%. Affinity chromatography was performed in columns of 1 cm diameter and a length of approximately 2 cm using an elution buffer of 0.05 *M* NaSCN (Fluka, Buchs, Switzerland) in 0.02 *M* Tris–HCl pH 7.4. A 1-ml volume of 1 mg/ml HEL (Boehringer Mannheim, Germany) was applied to the column at a flow-rate of 9 ml/h at room temperature. The flow-rate during chromatography was 18 ml/h. Regeneration of the columns was performed with 1 *M* NaSCN in 0.02 *M* Tris–HCl pH 7.4. The absorbance was measured at 278 nm. Chromatography was performed with a UV detection system from LKB (Bromma, Sweden), Model 2238 Uvicord SII and a Varioperpex II pump from LKB, Model 2120 and a recorder from LKB, Model 2210. Chemicals were obtained from Merck (Darmstadt, Germany) unless mentioned otherwise.

2.3. Surface plasmon resonance

SPR studies were carried out using the BIAcore system of Pharmacia Biosensor (Uppsala, Sweden). In all measurements a solution of 0.15 *M* NaCl, 50 m*M* Tris–HCl and 0.05% P20 (surfactant Tween 20 of Pharmacia) pH 8.0 was used as buffer solution with a flow-rate of 5 μl/min and a temperature of 25°C. Ligands were immobilized using standard procedures: (1) activation of the dextran layer by 35 μl 0.2 *M* N-ethyl-N′-(dimethylaminopropyl) carbodiimide–0.05 *M* N-hydroxysuccinimide mixture (coupling kit from manufacturer); (2) coupling of 35 μl 10 m*M* sodium acetate (NaAc) ligand solution; (3) 50 μl 1 *M* ethanolamine pH 8.5 (stock solution from manufacturer) and finally (4) regeneration with 15 μl 100 m*M* phosphoric acid.

Direct binding study

The CDR peptides of D1.3 and hLys6 (a humanized D1.3 antibody [23]) were immobilized at different dextran coated flow cells. The ligand solution of hLys6 was $2 \cdot 10^{-7}$ *M*, in 10 m*M* NaAc pH 5.0 resulting in 13 023 resonance units (RU) coupling. The ligand solution of the peptides and the amount of immobilization in RU were: peptide 1 in 3 mg/ml water, 174 RU; peptide 2 in 0.1 mg/ml 10 m*M* NaAc pH 4.0, 228 RU; peptide 3 in 1 mg/ml water, 234 RU; peptide 4 in 0.1 mg/ml 10 m*M* NaAc pH 6.0, 412 RU; peptide 5 in 1 mg/ml dimethyl sulphoxide (DMSO)–water (5:95), 283 RU; peptide 6 in 1.6 mg/ml DMSO–10 m*M* NaAc pH 6.0 (10:90), 160 RU and peptide 7 in 0.1 mg/ml DMSO–10 m*M* NaAc pH 6.0 (1:99), 192 RU. Binding of the peptides was tested by injecting 20 μl 1 mg/ml HEL into the flowcells.

Inhibition assay

HEL (10 ng/ml, $7.0 \cdot 10^{-10}$ *M*) was preincubated with a 0.1 mg/ml ($2.5 \cdot 10^{-5}$–$8.8 \cdot 10^{-5}$ *M*) peptide solution for 6 h. This lysozyme–peptide mixture was then injected into a 13 023 RU immobilized hLys6 channel. The same experiment was performed with peptide mixtures with a concentration of 0.1 mg/ml per peptide. Mixtures of H1H2D1.3 (peptide 6) with cyclic H3D1.3 (peptide 3), H1H2D1.3 (peptide 6) with H3D1.3 (peptide 2) and cyclic H2D1.3 (peptide 5) with H3D1.3 (peptide 2) were tested by this procedure. Chemicals were obtained from Merck unless mentioned otherwise.

3. Results and discussion

3.1. Affinity chromatography

Binding of lysozyme on immobilized CDR peptides of D1.3 was tested using two different

column materials, activated CH-Sepharose 4B and Affigel-10. The main difference between these two materials is the spacer attached to the solid phase. Activated CH-Sepharose 4B possesses a hydrophobic spacer and Affigel-10 a hydrophilic spacer. A blank column of Affigel-10 showed the least interaction with lysozyme (a very basic protein, p*I* 11) of these two materials. The results obtained from affinity chromatography of HEL with the tested peptides which showed interaction, are given in Fig. 1. Lysozyme was most retarded on columns with peptide 4 (H2D1.3) and peptide 7 (H1H2D1.3) compared to a blank ethanolamine column. Peptides of CDR 3 (peptides 1, 2 and 3) of the heavy chain of D1.3 showed much less interaction with lysozyme, although the contribution in binding energy of the Fv D1.3–lysozyme complex is about three times larger than that of peptide 7 and about two times larger than that of peptide 4 (see Table 1). This can only be explained by another interaction than that present in the tertiary structure of lysozyme and D1.3. Peptide 1 H3D1.3 92–101 has also been

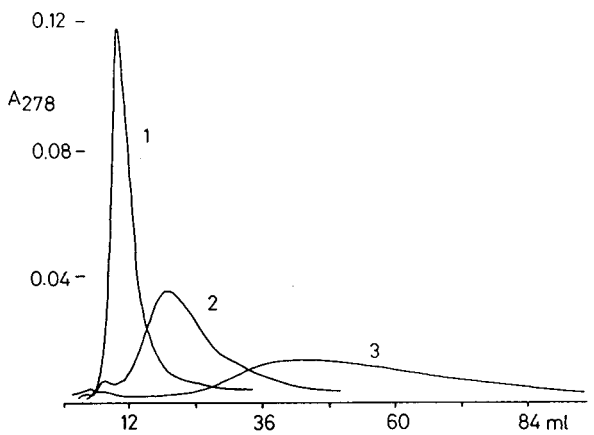

Fig. 1. Immunoaffinity chromatography of 1 ml 1 mg/ml hen egg white lysozyme. Lysozyme is eluted with 0.05 *M* NaSCN, 0.02 *M* Tris–HCl, pH 7.4 over peptides attached to Affigel-10 columns, flow-rate is 18 ml/h during elution. Column 1 is a 2-ml blank column (activated groups blocked by ethanolamine); column 2 is a 1-ml column of 5.6 mg/ml (3.3 m*M*) peptide 4 (H2D1.3 50–63); column 3 is a 2-ml column of 2.1 mg/ml (0.53 m*M*) peptide 7 (H1H2D1.3 28–63). The absorbance of lysozyme was measured at 278 nm at room temperature.

tested with cyanogen bromide-activated Sepharose 4B in immunoaffinity chromatography by Berry and Davies [13]. No binding of HEL could be detected.

3.2. Surface plasmon resonance

To prevent aspecific binding at a concentration of 1 mg/ml HEL with the dextran matrix the standard buffer in SPR studies with the BIAcore [10 m*M* 4-(2-hydroxyethyl)-1-piperazineethanesulphonic acid (HEPES), 0.15 *M* NaCl, 3.4 m*M* EDTA and 0.05% P20] had to be changed to a buffer solution containing 0.15 *M* NaCl, 50 m*M* Tris, 0.05% P20 pH 8.0. Direct binding studies of immobilized ligands with lysozyme were performed with 13 023 immobilized RU hLys6 as a positive control antibody (containing all 6 CDRs [23]), 174 RU peptide 1, 234 RU peptide 2, 228 RU peptide 3, 412 RU peptide 4, 283 RU peptide 5, 160 RU peptide 6 and 192 RU peptide 7. No binding curve was obtained after the injection of 20 μl 1 mg/ml lysozyme, therefore the immobilized CDR D1.3 peptides did not bind lysozyme. The humanized D1.3 antibody hLys6 did bind lysozyme as can be seen in Fig. 2. Kinetic parameters of the 13 023 RU immobilized hLys6 with lysozyme were determined from the binding curves: $k_{ass} = (4.7 \pm 0.2) \cdot 10^4\ M^{-1}\ s^{-1}$, $k_{diss} = (3.71 \pm 0.07) \cdot 10^{-3}\ s^{-1}$ and $K_a = (1.26 \pm 0.05) \cdot 10^7\ M^{-1}$.

Indirect binding of small ligands to proteins can be studied with the BIAcore instrument in an inhibition assay [24]. The analyte (lysozyme) is preincubated with a large excess of small ligand (synthetic peptide) before injecting the sample into the flowcell containing the immobilized antibody (hLys6). Only free, non-complexed analyte (lysozyme) will bind to immobilized hLys6, which can be seen as a binding curve. Disappearance of the binding curve at a large excess of small ligand (synthetic peptide) indicates interaction of peptide and lysozyme. The inhibition assays were performed on the 13 023 RU hLys6 channel. Preincubation of the CDR peptides (0.1 mg/ml, $2.5 \cdot 10^{-5}$–$8.8 \cdot 10^{-5}$ *M*) with lysozyme (10 ng/ml, $7.0 \cdot 10^{-10}$ *M*) and mixtures of the peptides (0.1 mg/ml) with

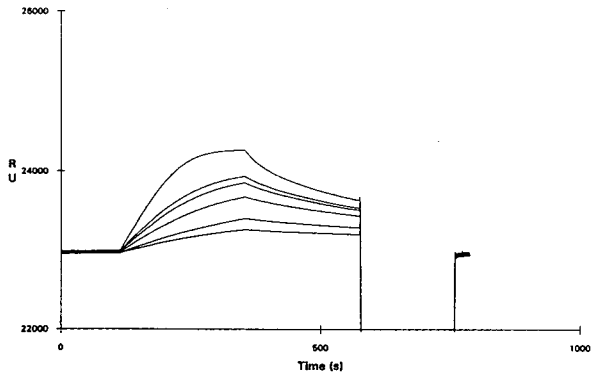

Fig. 2. Overlay plot of six different sensorgrams of different concentrations hen egg white lysozyme (0.2–2.0 μg/ml) with 13 023 RU immobilized hLys6 (a humanized D1.3 antibody [23]). Samples of 20 μl lysozyme solution in 50 m*M* Tris–HCl, 0.15 *M* NaCl, 0.05% surfactant P20 pH 8.0 were injected into the micro flow system with a flow-rate of 5 μl/min. The temperature was kept constant at 25°C during the measurements. The hLys6 flowcell was regenerated by injecting 15 μl 100 m*M* phosphoric acid. The association rate constant k_{ass} was determined from the six binding curves of lysozyme with immobilized hLys6 using the BIAlogue software as described [15,16,23]. Briefly, dR/dt *versus* R was plotted for each concentration. The obtained slopes were plotted against the lysozyme concentration. The association rate constant, $k_{ass} = (4.7 \pm 0.6) \cdot 10^4\ M^{-1}\ s^{-1}$ ($r^2 = 0.995$), was obtained from the slope of this straight line. The dissociation rate constant k_{diss} was obtained from datapoints of the dissociation (during the first 100 s) of bound lysozyme resulting from the injection of 20 μl lysozyme (2 μg/ml). A plot of ln (R_0/R_i) *versus* $t_i - t_0$ resulted in a straight line, which was used to determine k_{diss} [R_0 is signal in RU at the beginning (t_0) of dissociation; R_i is signal in RU at time t_i]. The dissociation rate constant value $k_{diss} = (3.7 \pm 0.7) \cdot 10^{-3}\ s^{-1}$ ($r^2 = 0.993$). The equilibrium constant K_a was calculated from the rate constants according to $K_a = k_{ass}/k_{diss}$. The determined K_a of the interaction of immobilized hLys6 with lysozyme is $(1.26 \pm 0.05) \cdot 10^7\ M^{-1}$.

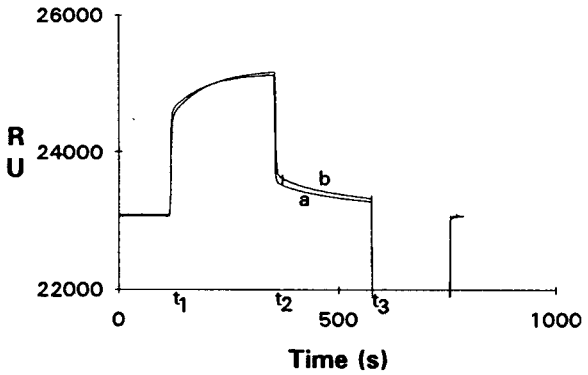

Fig. 3. Overlay plot of two sensorgrams of an inhibition assay of lysozyme with immobilized hLys6. Sensorgram a shows the binding curve of 20 μl 10 ng/ml ($0.7 \cdot 10^{-9}\ M$) hen egg white lysozyme with 13 023 RU immobilized hLys6. Sensorgram b shows the binding curve obtained after incubation of 10 ng/ml ($7.0 \cdot 10^{-10}\ M$) lysozyme with 0.1 mg/ml ($8.2 \cdot 10^{-5}\ M$) peptide 3 (cyclic H3D1.3 98–103) and 0.1 mg/ml ($2.5 \cdot 10^{-5}\ M$) peptide 7 (H1H2D1.3 28–63) for 6 h. The lysozyme samples of both sensorgrams contained 50 m*M* Tris–HCl, 0.15 *M* NaCl, 0.05% P20 pH 8.0 and 1% DMSO. The flow-rate during the measurements was 5 μl/min. Lysozyme (20 μl) was injected into the flowcell at t_1, dissociation of bound lysozyme started at t_2 followed by regeneration of the flowcell at t_3 with 15 μl 100 m*M* phosphoric acid. The large increase in signal at t_1 and large decrease in signal at t_2 was caused by the presence of 1% DMSO in the lysozyme sample, due to difference in refractive index of buffer and sample.

lysozyme for 6 h did not change the binding curve of lysozyme to hLys6. This is illustrated by one example of a mixture of cyclic H3D1.3 98–103 (peptide 3) and H1H2D1.3 28–63 (peptide 7) in Fig. 3. If the CDR peptides would have bound lysozyme specifically, then they should have blocked the antigen (lysozyme) at the contact residues, thereby disturbing the binding of lysozyme to immobilized hLys6, which should be seen as at least a less steeper binding curve or as no binding curve at all. Also, peptide mixtures of CDR peptides involving the three most important CDRs from the H chain should have inhibited binding of lysozyme to hLys6.

In BIAcore measurements it is very easy to reduce aspecific interaction of lysozyme to the dextran-coated gold layer. Raising the pH to 8 was sufficient to eliminate interaction of lysozyme with a blank channel. The solid phase in affinity chromatography mainly differs from the dextran layer of the sensorchip in the BIAcore instrument by the 10-atom spacer, which may partly cause aspecific interaction with lysozyme. The inhibition assay of lysozyme (measured with SPR) shows that the retardation of lysozyme shown in Fig. 1 is caused by other interaction than specific antibody–antigen interaction. However, such peptide columns might still be useful in the purification of lysozyme from a mixture of proteins.

The CDR peptides of the heavy chain of D1.3

do contain the most important contact residues for binding lysozyme. Nevertheless such peptides, even those containing several residues important for binding, did not bind lysozyme. Apparently it is not possible to reduce the V_H D1.3 fragment (3 CDRs) to smaller fragments without losing specificity towards hen egg white lysozyme. The large surface complementarity of D1.3 with lysozyme is also a major factor in the specific interaction of lysozyme with D1.3. In general, this suggests that Fv fragments are capable of binding antigens and that V_H or V_L fragments may bind antigens, but that these fragments will lose specificity. In some cases CDR peptides [2–8] may bind antigens, probably with much less specificity than the antibodies. Some of the reported CDR peptides [4–7] are derived from anti-idiotype antibodies and those CDR peptides are homologous with the linear epitope of the antigen. Inhibition of the antibody by the CDR peptide can be accomplished by competition of the antibody between the antigen and the CDR peptide, and not by binding of the CDR peptide with the antigen [7,25].

4. Conclusions

So far, the minimal lysozyme-binding part of monoclonal antibody D1.3 is the V_H region. Small synthetic fragments ($M = 1135–3977$) of the V_H region are not able to bind lysozyme specifically. This shows the difficulty to predict from tertiary structure information of antibody–antigen complexes whether CDR peptides may bind antigens. It also shows the importance of surface complementarity in antibody–antigen complexes besides the direct contact area in antibody–antigen interaction.

5. Acknowledgements

We thank Dr J. Foote (Cambridge, UK) for his generous gift of monoclonal antibody hLys6 and Dr. M.H.J. Ruiters of the Biomedical Technology Centre, University of Groningen for the use of the BIAcore instrument. This research was supported by the Technology Foundation (STW) grant No. GGN99.1924.

6. References

[1] D. Givol, *Molec. Immunol.*, 28 (1991) 1379.
[2] G.W. Welling, J. van Gorkum, R.A. Damhof, J.W. Drijfhout, W. Bloemhoff and S. Welling-Wester, *J. Chromatogr.*, 548 (1991) 235.
[3] G.W. Welling, Geurts, T., J. van Gorkum, R.A. Damhof, J.W. Drijfhout, W. Bloemhoff and S. Welling-Wester, *J. Chromatogr.*, 512 (1990) 337.
[4] W.V. Williams, T. Kieber-Emmons, J. VonFeldt, M.I. Greene and D.B. Weiner, *J. Biol. Chem.*, 266 (1991) 5182.
[5] W.V. Williams, D.A. Moss, T. Kieber-Emmons, J.A. Cohen, J.N. Myers, D.B. Weiner and M.I. Greene, *Proc. Natl. Acad. Sci. U.S.A.*, 86 (1989) 5537.
[6] W.V. Williams, D.B. Weiner, J.C. Cohen and M.I. Greene, *Biotechnology*, 7 (1989) 471.
[7] R. Taub and M.I. Greene, *Biochemistry*, 31 (1992) 7431.
[8] M. Levi, M. Sällberg, U. Ruden, D. Herlyn, H. Maruyama, H. Wigzell, J. Marks and B. Wahren, *Proc. Natl. Acad. Sci. U.S.A.*, 90 (1993) 4374.
[9] A.G. Amitt, R.A. Mariuzza, S.E.V. Phillips and R.J. Poljak, *Science*, 233 (1986) 747.
[10] T.O. Fischmann, G.A. Bentley, T.N. Bhat, G. Boulot, R.A. Mariuzza, S.E.V. Phillips, D. Tello and R.J. Poljak, *J. Biol. Chem.*, 266 (1991) 12 915.
[11] J. Novotny, R.E. Bruccoleri and F.A. Saul, *Biochemistry*, 28 (1989) 4735.
[12] M.J. Berry, J. Davies, C.G. Smith and I. Smith, *J. Chromatogr.*, 587 (1991) 161.
[13] M.J. Berry and J. Davies, *J. Chromatogr.*, 597 (1992) 239.
[14] M.J. Berry and J.J. Pierce, *J. Chromatogr.*, 629 (1993) 161.
[15] A.-C. Malmborg, A. Michaëlsson, M. Ohlin, B. Jansson and C.A.K. Borrebaeck, *Scand. J. Immunol.*, 35 (1992) 643.
[16] L.G. Fägerstam, Å. Frostell-Karlsson, R. Karlsson, B. Persson and I. Rönnberg, *J. Chromatogr.*, 597 (1992) 397.
[17] C.A.K. Borrebaeck, A.-C. Malmborg, C. Furebring, A. Michaelsson, S. Ward, L. Danielsson and M. Ohlin, *Biotechnology*, 10 (1992) 697.
[18] E.A. Atherton and R.C. Sheppard, *J. Chem. Soc., Chem. Commun.*, (1985) 165.
[19] B. Castro, J.R. Dormoy, G. Evin and C. Selve, *Tetrahedron Lett.*, 15 (1975) 1219.
[20] H. Rink, *Tetrahedron Lett.*, 28 (1987) 3787.

[21] J.W. Drijfhout, *Thesis*, University of Groningen, Groningen, 1989, p. 13.
[22] D.S. King, C.G. Fields and G.B. Fields, *Int. J. Pept. Prot. Res.*, 36 (1990) 255.
[23] J. Foote and G. Winter, *J. Mol. Biol.*, 224 (1992) 487.
[24] D. Altschuh, M.-C. Dubs, E. Weiss, G. Zeder-Lutz, M.H.V. Van Regenmortel, *Biochemistry*, 31 (1992) 6298.
[25] M.W. Pride, H. Shi, J.M. Anchin, D.S. Linthicum, P.T. LoVerde, A. Thakur and Y. Thanavala, *Proc. Natl. Acad. Sci. U.S.A.*, 89 (1992) 11900.

ELSEVIER

Journal of Chromatography A, 676 (1994) 99–112

JOURNAL OF CHROMATOGRAPHY A

High-performance liquid chromatography and photoaffinity crosslinking to explore the binding environment of nevirapine to reverse transcriptase of human immunodeficiency virus type-1

Deborah E.H. Palladino[a], Jerry L. Hopkins[a], Richard H. Ingraham*[a], Thomas C. Warren[b], Suresh R. Kapadia[c], Glenn J. Van Moffaert[c], Peter M. Grob[b], James M. Stevenson[a], Kenneth A. Cohen[a]

[a]*Department of Analytical Sciences, Boehringer Ingelheim Pharmaceuticals, Inc., Ridgefield, CT 06877-0368, USA*
[b]*Department of Biochemistry, Boehringer Ingelheim Pharmaceuticals, Inc., Ridgefield, CT 06877-0368, USA*
[c]*Department of Medicinal Chemistry, Boehringer Ingelheim Pharmaceuticals, Inc., Ridgefield, CT 06877-0368, USA*

Abstract

Nevirapine (BI-RG-587) is a potent inhibitor of the polymerase activity of reverse transcriptase of human immunodeficiency virus type-1. Nevirapine, as well as several other non-nucleoside compounds of various structural classes, bind strongly at a site which includes tyrosines 181 and 188 of the p66 subunit of reverse transcriptase. The chromatography which was utilized to explore this binding site is described. BI-RH-448 and BI-RJ-70, two tritiated photoaffinity azido analogues of nevirapine, are each crosslinked to reverse transcriptase. The use of several HPLC-based techniques employing different modes of detection makes it possible to demonstrate a dramatic difference between the two azido analogues in crosslinking behavior. In particular, by comparing HPLC tryptic peptide maps of the photoadducts formed between reverse transcriptase and each azido analogue, it can be shown that crosslinking with BI-RJ-70 but not with BI-RH-448 is more localized, stable, and hence exploitable for the identification of the specifically bonded amino acid residue(s). In addition, comparison of the tryptic maps also makes it feasible to assess which rings of the nevirapine structure are proximal or distal to amino acid side chains of reverse transcriptase. Finally, another feature of the HPLC peptide maps is the application of on-line detection by second order derivative UV absorbance spectroscopy to identify the crosslinked amino acid residue.

1. Introduction

Human immunodeficiency virus type-1 (HIV-1) is the causative agent of acquired immunodeficiency syndrome (AIDS). Reverse transcriptase, an enzyme of HIV-1, catalyzes the polymerization of proviral DNA and is essential to the replication of HIV-1. Hence drugs that inhibit reverse transcriptase represent potential therapies against AIDS (see ref. 1 and references cited therein).

In the USA the only three drugs approved for the treatment of AIDS are the nucleoside analogues 3′-azido-3′-deoxythymidine (AZT), 2′,3′-dideoxyinosine (ddI), and 2′,3′-dideoxycytosine (ddC) [2–4]. Nucleoside analogues inhibit re-

* Corresponding author.

0021-9673/94/$07.00
SSDI 0021-9673(94)00177-B

verse transcriptase by a complex mechanism that includes chain termination of the nascent nucleic acid in the process of reverse transcription [5,6]. Unfortunately, nucleoside analogues are associated with clinically significant side effects (*e.g.*, bone marrow suppression and peripheral neuropathy [7–9]).

Several non-nucleoside drugs, such as TIBO [10], L-697-661 [11], HEPT [12], BHAP [13], and nevirapine [14,15], also inhibit reverse transcriptase and are under investigation [16,17]. The mechanism of the non-nucleoside drugs does not involve chain termination and is specific for the polymerase activity of HIV-1 reverse transcriptase. Thus it is hoped that the non-nucleoside drugs will not inhibit polymerization of human DNA and that as a consequence fewer and/or less severe clinical side effects will be manifested [15].

Although the various non-nucleoside drugs are different in molecular structure, they evidently bind to a similar region of the p66 subunit of reverse transcriptase [18–22]. We were the first to report the identification of tyrosine residues 181 and 188 as important components of this critical region adjacent to the putative active site of reverse transcriptase [19]. Subsequent studies involving mutagenesis [20,21] and X-ray crystallography [22] corroborated the identification of the tyrosines and increased further an already intense interest in understanding the structure of the binding region of reverse transcriptase for non-nucleoside drugs [23].

In our earlier research, the identification of the tyrosine residues 181 and 188 was achieved through photoaffinity crosslinking of an azido analogue (BI-RJ-70) of nevirapine to reverse transcriptase [19]. The crosslinking was extensive and highly specific, as tryptic peptide mapping by HPLC and N-terminal peptide sequencing showed that approximately 75% of the starting amount of BI-RJ-70 covalently attached to the tyrosine residues 181 and 188.

The chromatography used with BI-RJ-70 is now described in detail in this paper. Furthermore, BI-RH-448, a new tritiated photoaffinity probe and azido analogue of nevirapine, is introduced and characterized. By using several HPLC-based techniques employing different modes of detection to compare BI-RH-448 with BI-RJ-70, a dramatic difference between the two azido analogues in crosslinking behavior can be demonstrated. In particular, a comparison of HPLC tryptic peptide maps of the photoadducts formed between reverse transcriptase and each azido analogue shows that crosslinking with BI-RJ-70 is more localized, stable, and hence more exploitable than with BI-RH-448 for the identification of the covalently modified amino acid residues.

Moreover, the tryptic maps are consistent with the A-ring of the nevirapine structure oriented proximal to the tyrosines, and with the C-ring oriented distal from the tyrosines as well as from other amino acids. This assessment was not possible previously [19]. Finally, another feature of the HPLC peptide maps is the novel application of on-line detection by second order derivative UV absorbance spectroscopy to identify the crosslinked amino acid residue.

2. Experimental

2.1. Photoaffinity crosslinking

Preparation of HIV-1 reverse transcriptase [18,19,24], synthesis of nevirapine and analogues [25,26], and photoaffinity crosslinking of azido analogue to reverse transcriptase [18,19,21] were described in detail previously.

2.2. Apparatus

A Hewlett-Packard 1090 (Avondale, PA, USA) high-performance liquid chromatograph integrated with a Hewlett-Packard 1040M diode array detector was used for HPLC. Zero-order UV absorbance spectra were collected on-line and reviewed with a Hewlett-Packard 98561A-300 series computer and 9153B disk drive. Hewlett-Packard revision 5.22 software was used to acquire and plot these spectra, as well as to convert them to second order derivative spectra. A C_{18} Delta-Pak column (150 × 2.1 mm) from Millipore-Waters (Milford, MA, USA) was used

for HPLC of reverse transcriptase, azido analogues, and tryptic digestions.

HPLC fractions were collected with a HeliFrac from Pharmacia LKB (Piscataway, NJ, USA), or with a 201 fraction collector from Gilson (Middleton, WI, USA). Sequences of amino acids of peptides in HPLC fractions were determined with a 477A pulsed-liquid protein sequencer from Applied Biosystems (Foster City, CA, USA). Radioactivity in HPLC fractions and in cycles of sequencing were measured with an LS 5000 TA scintillation counter from Beckman (Fullerton, CA, USA). Peptide synthesis was carried out on an Applied Biosystems 430A synthesizer.

2.3. Reagents and solvents

Trypsin treated with L-1-tosylamido-2-phenylethyl chloromethyl ketone was from Worthington (Freehold, NJ, USA). Water was HPLC-grade from a Milli-Q and Milli-RO system from Millipore (Milford, MA, USA). Acetonitrile was from Burdick and Jackson (Muskegon, MI, USA) and trifluoroacetic acid was sequenal grade from Pierce (Rockford, IL, USA). All other chemicals were reagent grade.

2.4. Procedures

Reverse transcriptase crosslinked to azido analogue was subjected to digestion by trypsin under denaturing conditions [19,27]. Briefly, to 35–250 μl of solution containing 40–1000 μg (0.34–8.5 nmol) of reverse transcriptase crosslinked to azido analogue, an approximately equal volume of 8 *M* urea in 400 m*M* ammonium bicarbonate (pH 7.8) was added. After vortexing, typically 2–4 volumes of water were then added. Next 10–25 μl of trypsin in water were added either all in one aliquot, or in two equal aliquots, the second aliquot following the first by 1.25 h. The final ratio of trypsin–reverse transcriptase was 1:25 or 1:12.5 (w/w).

Following a 2.5-h incubation at 37°C, the digest was frozen at −80°C, or treated with 1% trifluoroacetic acid to a final pH of 2, and/or injected onto the C_{18} reversed-phase HPLC column. Conditions for HPLC are given in legends of figures. Fractions of HPLC effluent of peptide maps were collected in intervals of 0.5–2.0 min corresponding to volumes of 100–400 μl. An aliquot of 5–20 μl of each collected fraction was sampled for liquid scintillation counting off-line, and the measurement of radioactivity was then adjusted and reported to reflect the radioactivity in the entire fraction.

After the aliquots were taken for liquid scintillation counting, 100–800 μl of the collected fractions of effluent of HPLC tryptic peptide mapping were applied to the protein sequencer. At the completion of each Edman cycle, a known percentage of the product was transferred on-line to an Applied Biosystems 120A PTH analyzer for identification of the amino acid in that cycle. The remaining percentage of product in each cycle was collected and measured off-line for radioactivity by liquid scintillation counting. The measured radioactivity was then adjusted and reported to reflect all the radioactivity of the entire product of each cycle.

Peptide synthesis was performed with small-scale rapid cycles and *tert.*-butoxycarbonyl chemistry followed by cleavage with hydrofluoric acid. Synthesized peptide was purified by semi-preparative HPLC employing conditions similar to those used for tryptic peptide mapping as described in the legend of Fig. 2.

3. Results and discussion

3.1. Crosslinking azido analogue to reverse transcriptase

Regions of reverse transcriptase accessible to nevirapine and other non-nucleoside drugs were explored by photoaffinity crosslinking by BI-RH-448 or BI-RJ-70, two structural and functional azido analogues of nevirapine [18,25,26]. The structures of BI-RH-448 and BI-RJ-70 (Fig. 1) were designed to achieve a bi-directional probing of reverse transcriptase, as the azido group was located on the C-ring of BI-RH-448 and on the A-ring of BI-RJ-70. To enhance detection, radioactive tritium was incorporated on the

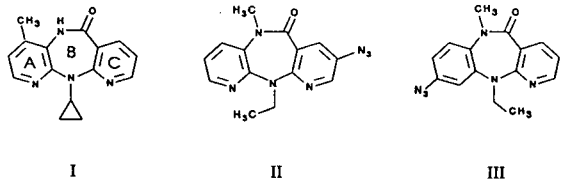

I II III

Fig. 1. Chemical structures of nevirapine (I), BI-RH-448 (II), and BI-RJ-70 (III). See text for position of tritium label.

methyl carbon at the 5-nitrogen of the B-ring of BI-RH-448 and on the 8-carbon of the C-ring of BI-RJ-70.

BI-RH-448 or BI-RJ-70 was separately crosslinked to reverse transcriptase. The crosslinking was effected by irradiating the azido analogue after binding to reverse transcriptase. At the start of irradiation the ratio of the molar concentration of azido analogue to that of reverse transcriptase was typically about 1:1 [18,19,21]. During irradiation the azide moiety was converted to a nitrene or other reactive intermediate that covalently bonded (crosslinked) the azido analogue to proximal backbone and/or side chains of the amino acid residues of reverse transcriptase [18,19,28,29]. The covalent attachment to reverse transcriptase abrogated its catalytic function [15,18].

3.2. Tryptic peptide mapping by HPLC of photoadduct

After irradiation the photoadduct formed between reverse transcriptase and BI-RH-448 or BI-RJ-70 was digested with trypsin, as was also a control of reverse transcriptase which had not been exposed to an azido analogue. The peptide fragments generated by digestion were resolved by reversed-phase HPLC (Fig. 2). At 210 nm approximately 70 major and minor peaks and shoulders were observed and exhibited generally comparable retentions and sizes in all three peptide maps (Fig. 2A, B, C). Seventy features in the maps were consistent with a prediction of 65 peptides if proteolysis of reverse transcriptase by trypsin was complete and specific at arginines and lysines. Another indication that the digestions were thorough was that little signal was observed in the retention window (125–135 min) of undigested reverse transcriptase.

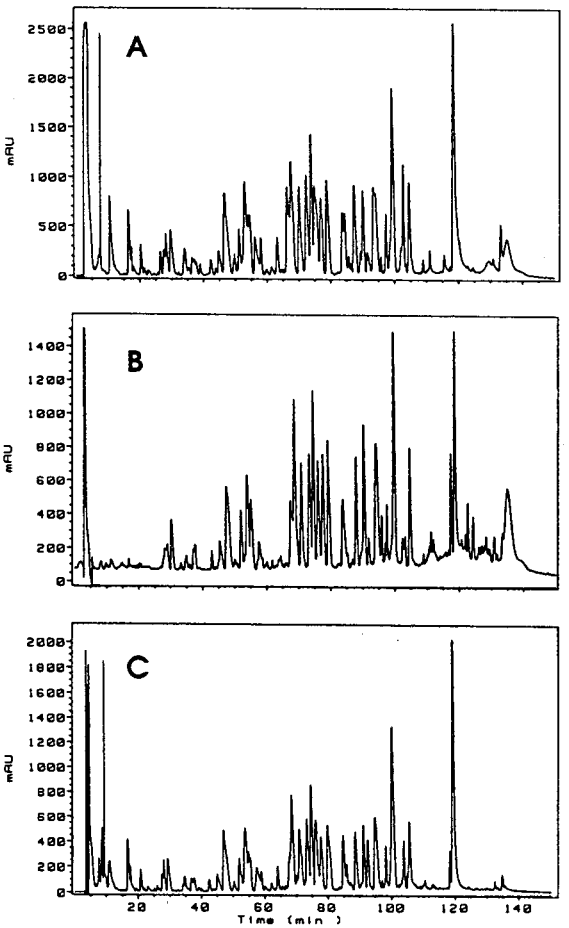

Fig. 2. Reversed-phase HPLC of tryptic peptides of 200–250 μg of reverse transcriptase. Solvent A was 0.06% (v/v) trifluoroacetic acid in water (pH 2.5) and solvent B was 0.052% (v/v) trifluoroacetic acid in water–acetonitrile (30:70, v/v). A gradient of 0–40% B in 90 min, 40–70% B in 40 min, 70–100% B in 20 min, 100% B for 5 min, 100–0% B in 15 min, and 0% B for 10 min was programmed with a flow-rate of 0.20 ml/min. Detection was by absorbance at 210 nm. (A) Reverse transcriptase exposed to no azido analogue. (B) Reverse transcriptase crosslinked to BI-RH-448 by irradiation. (C) Reverse transcriptase crosslinked to BI-RJ-70 by irradiation.

From one map to another in Fig. 2, a few differences in size and location of peaks were evident. The differences, however, were not

necessarily due to the presence or absence of azido analogue. Rather, the differences were often attributable to different conditions of the chromatography, such as amount and/or volume of sample injected onto the column [30], or the composition of solution containing the reverse transcriptase. Therefore, as in previous studies in which HPLC was utilized to locate the binding sites of proteins that were crosslinked to probes [31–47], a mode of detection more selective than absorbance at 210 nm in Fig. 2 was required to identify peaks that corresponded to peptide crosslinked to azido analogue.

3.3. Selective detection at 335 nm

A more selective spectroscopic method of detection was achieved from a comparison of the spectral properties of control reverse transcriptase and the azido analogues (Fig. 3). Reverse transcriptase which had not been irradiated eluted at 38 min under the HPLC conditions given in Fig. 3A. The spectrum of the protein peak was measured on-line via diode-array detection and exhibited a maximum in UV absorbance at approximately 278 nm (Fig. 3A), due to the presence of aromatic amino acid residues. Of note there was negligible absorbance at wavelengths greater than 320 nm.

When chromatographed, BI-RJ-70 which had not been irradiated eluted at 36 min (Fig. 3B). Unlike reverse transcriptase, however, BI-RJ-70 exhibited finite absorbance at wavelengths greater than 320 nm (Fig. 3B). BI-RH-448 also exhibited finite absorbance at wavelengths greater than 320 nm and eluted earlier than reverse transcriptase (data not shown).

Similarly, when BI-RJ-70 was irradiated in the presence of reverse transcriptase, the resulting photoadduct of BI-RJ-70 crosslinked to reverse transcriptase eluted at 38 min and exhibited finite absorbance at wavelengths greater than 320 nm (Fig. 3C). This absorbance was clearly due to the BI-RJ-70 component of the photoadduct. Not surprisingly, the crosslinking of BI-RJ-70 to reverse transcriptase had little effect on the retention of the reverse transcriptase (*cf.* Fig. 3A and C), as the molecular masses of reverse

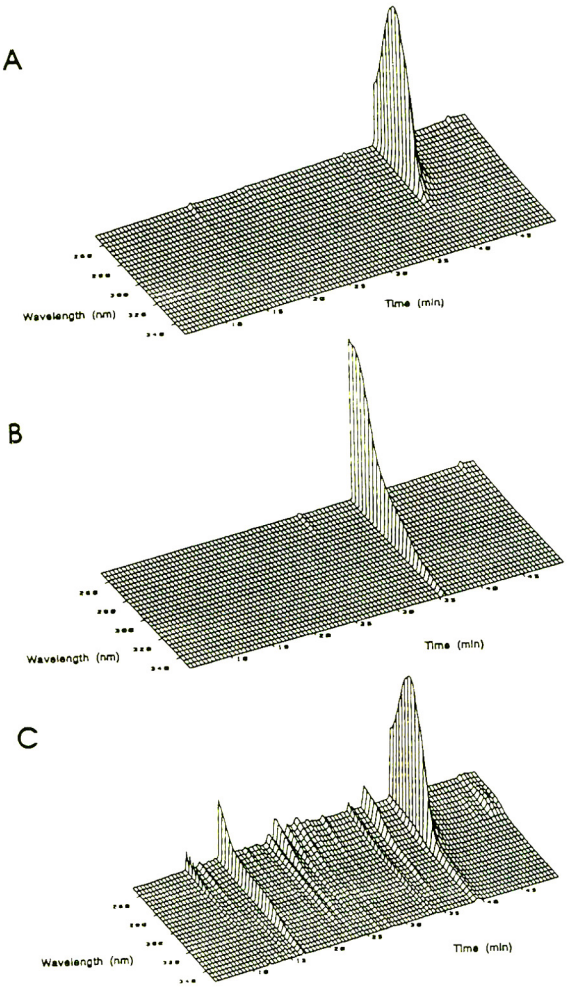

Fig. 3. Reversed-phase HPLC and on-line spectral scanning of reverse transcriptase, BI-RJ-70, their photoadduct, and photolytic derivatives of BI-RJ-70. Conditions were the same as those given in the legend of Fig. 2, except that the gradient was 0–70% B in 35 min, 70–100% B in 5 min, 100% B for 5 min, 100–0% B in 10 min, and 0% B for 10 min. (A) Reverse transcriptase exposed to no azido analogue and no irradiation. (B) BI-RJ-70 exposed to no reverse transcriptase and no irradiation. (C) Reverse transcriptase crosslinked to BI-RJ-70 by irradiation.

transcriptase and BI-RJ-70 were approximately 117 000 [24] and 294 [25], respectively.

In Fig. 3C numerous peaks that eluted earlier than the 36-min peak of unirradiated and uncrosslinked BI-RJ-70 (*cf.* Fig. 3B) were due to a molar excess (4:1) of BI-RJ-70 to reverse transcriptase at the start of irradiation. These peaks

were likely photolytic, derivative by-products of BI-RJ-70, because they were also produced when BI-RJ-70 was irradiated in the absence of reverse transcriptase (data not shown). The identities of the by-products were not determined, but of greater practical significance, all of them, like their precursor BI-RJ-70, exhibited finite absorbance at wavelengths greater than 320 nm (Fig. 3C).

From the data in Fig. 3 it followed that detection at a wavelength greater than 320 nm, *e.g.*, 335 nm, provided a means to locate selectively tryptic peptides of reverse transcriptase which were crosslinked to azido analogues and to render the remainder transparent. Thus the wavelength of 335 nm was exploited to pinpoint the locations of peptides crosslinked to BI-RH-448 or BI-RJ-70 in peptide maps.

3.4. Peptides crosslinked to azido analogue

The same analyses (*i.e.*, injections) illustrated with detection at 210 nm in Fig. 2 were replotted with detection at 335 nm in Fig. 4. In contrast to the three tryptic peptide maps in Fig. 2, the differences among the three chromatograms in Fig. 4 were striking. As there was no azido analogue present, no peaks corresponding to peptides crosslinked to analogue were observed for control reverse transcriptase in Fig. 4A. In Fig. 4B most of the peptides crosslinked to BI-RH-448 eluted within the 22-min retention window of 84–106 min, which was earlier than the 22-min retention window of 98–120 min that contained most of the peptides crosslinked to BI-RJ-70 in Fig. 4C.

Analogously, unirradiated BI-RH-448 eluted at 68 min, which was earlier than the elution time of 87 min for unirradiated BI-RJ-70 (data not shown). Irradiation of either azido analogue in the absence of reverse transcriptase yielded products that also absorbed at 335 nm and eluted earlier than the respective unirradiated azido analogue (data not shown, but *cf.* Fig. 3C). These findings corroborated that the peaks that eluted within 84–106 min in Fig. 4B and within 98–120 min in Fig. 4C corresponded to peptides

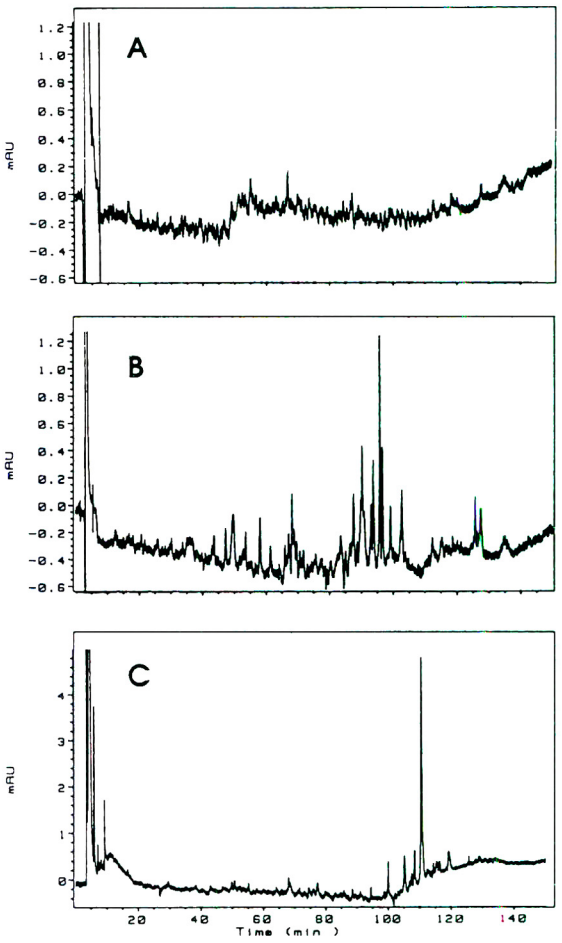

Fig. 4. Reversed-phase HPLC of tryptic peptides of 200–250 μg of reverse transcriptase. Conditions are identical to those given in the legend of Fig. 2, except detection was by absorbance at 335 nm. (A) Reverse transcriptase exposed to no azido analogue. (B) Reverse transcriptase crosslinked to BI-RH-448 by irradiation. (C) Reverse transcriptase crosslinked to BI-RJ-70 by irradiation.

crosslinked to analogue and not merely to non-peptide photolytic derivatives of azido analogue.

3.5. Crosslinking differences between BI-RH-448 and BI-RJ-70

Other differences between Fig. 4B and 4C were noteworthy. For instance in Fig. 4C one peak at 111 min predominated and was at least 5 times larger than any of the others. In com-

parison the largest peak (96 min) in Fig. 4B was no more than twice as large as several of the next largest peaks. Another difference was that there were many more additional peptides crosslinked to BI-RH-448 in Fig. 4B than there were peptides crosslinked to BI-RJ-70 in Fig. 4C.

Thus the HPLC profiles of Fig. 4B and 4C illustrated the dramatic difference between BI-RH-448 and BI-RJ-70 in their probing of the binding environment of reverse transcriptase. In addition, the profiles were also consistent with and diagnostic of a more specific, localized, and/or stable crosslinking of BI-RJ-70 than of BI-RH-448 to reverse transcriptase. Unlike other studies of crosslinking [28,29,31–47], our study takes advantage of tryptic peptide mapping by HPLC with selective detection for the purpose of comparing qualitatively the specificity, localization, and/or stability of the crosslinking of two photoaffinity azido analogues of a drug to its target protein.

3.6. Detection by radioactivity

The utility of detection at 335 nm in Fig. 4B and 4C was further corroborated by monitoring radioactivity in fractions of HPLC effluent collected from the two analyses. The radioactivities in the fractions of peptides crosslinked to BI-RH-448 in Fig. 5A and to BI-RJ-70 in Fig. 5B generally coeluted with their respective absorbances at 335 nm in Fig. 4B and 4C.

In Fig. 5B 75% of the radioactivity of BI-RJ-70 collected from the column was concentrated in the 22-min retention window 98–120 min containing most of the peptides crosslinked to BI-RJ-70 (*cf.* Fig. 4C). In contrast to Fig. 5B, in Fig. 5A only half that much or 38% of the radioactivity of BI-RH-448 collected from the column was concentrated in the 22-min retention window (84–106 min) containing most of the peptides crosslinked to BI-RH-448 (*cf.* Fig. 4B). Thus as was the case with absorbance at 335 nm in Fig. 4B and 4C, the profiles of radioactivities in the peptide maps showed a more specific, complete, and/or stable crosslinking of BI-RJ-70 (Fig. 5B) than of BI-RH-448 (Fig. 5A) to reverse transcriptase.

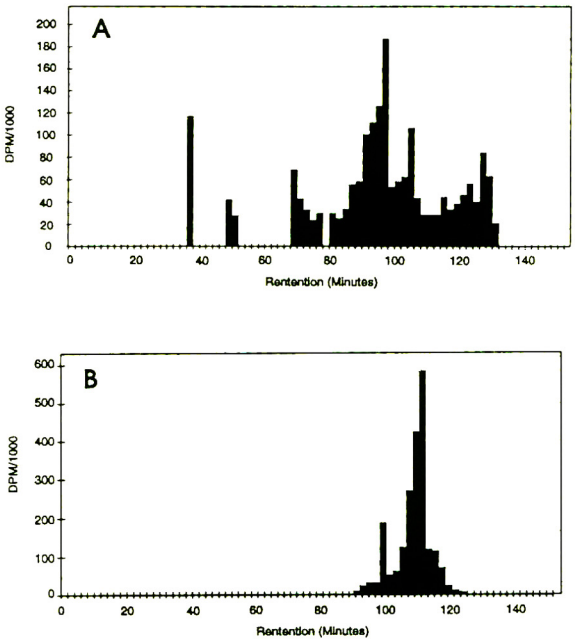

Fig. 5. Radiochromatograms of reversed-phase HPLC of tryptic peptides of 200–250 μg of reverse transcriptase. Conditions are identical to those given in the legend of Fig. 2, except detection was by measurement of radioactivity in fractions of HPLC effluent collected every 2 min. (A) Reverse transcriptase crosslinked to BI-RH-448 by irradiation. Approximately 4 million DPM were loaded onto and collected from the column. (B) Reverse transcriptase crosslinked to BI-RJ-70 by irradiation. Approximately 2 million DPM were loaded onto and collected from the column.

3.7. N-terminal sequencing of HPLC tryptic peptide fractions

The positions and identities of the amino acid residues that were crosslinked to azido analogue were determined by N-terminal protein sequencing. For amino acids crosslinked to BI-RH-448, 11 fractions of HPLC effluent within 84–106 min in Figs. 4B and 5A were analyzed. For amino acids crosslinked to BI-RJ-70, 11 fractions of HPLC effluent within 98–120 min in Figs. 4C and 5B were analyzed. At the conclusion of the chemistry of every cycle of Edman degradation and derivatization in sequence analysis, at least 60% of the volume of product was shunted off-line for measurement of radioactivity (Tables 1 and 2), while the remaining volume was directed

Table 1
Radioactivity (in DPM) in cycles of Edman sequencing of fractions of tryptic peptide map of reverse transcriptase crosslinked to BI-RH-448.

	Fraction[a]										
	84–86 2%	86–88 2%	88–90 4%	90–92 5%	92–94 5%	94–96 8%	96–98 2%	98–100 2%	100–102 2%	102–104 4%	104–106 2%
Cycle 1	568	864	573	369	258	492	319	639	337	371	521
2	–[b]	334	417	274	2328	6905	824	418	344	–	310
3	527	293	415	–	937	5034	260	305	272	–	–
4	332	420	–	–	1609	1941	–	–	258	–	–
5	–	321	2271	1376	1175	1469	263	392	314	–	–
6	449	404	1998	1268	1791	1346	–	369	331	–	260
7	–	889	1569	1122	2330	583	–	428	–	–	298
8	–	483	820	762	1389	465	–	294	–	–	254
9	–	–	505	540	936	689	–	1547	1036	1368	389
10	–	–	319	435	624	332	–	967	913	956	–
11	–	–	378	542	567	445	–	553	585	444	–
12	–	–	519	1277	443	291	–	431	417	442	–
13	–	–	752	1230	390	389	–	–	383	259	–
14	–	–	545	710	352	314	–	–	–	–	–
15	–	–	328	426	284	–	–	330	–	–	–
16	–	–	–	366	–	–	–	–	–	–	–
17	–	–	–	288	–	–	–	–	–	–	–
18	–	–	–	–	–	–	–	–	–	–	–
19	–	–	–	–	–	–	–	–	–	–	–
20	–	–	–	–	–	–	–	396	–	–	–

[a] First line (*e.g.* 84–86) indicates collection time (*e.g.* from 84 to 86 min) in the tryptic peptide map; second line (*e.g.* 2%) indicates percentage fraction accounted for (*e.g.* 2%) of total radioactivity collected in the tryptic peptide map.
[b] Radioactivity was less than background, which was defined as 250 DPM.

on-line for identification by HPLC of the phenylthiohydantoin (PTH) amino acid.

In such a manner radioactivity associated with specific amino acid positions was successfully captured. Successful capture of radioactivity has also been reported in a few other studies [32,37,46]. On the other hand, there have been numerous studies in which radioactivity was not captured [33–35,38,40,41,43–45], possibly because nucleotide analogues that were likely less hydrophobic than the azido analogues of nevirapine were employed as photoaffinity probes. Crosslinking nucleotide analogues to amino acids or their derivatives may have decreased solubility in the non-polar solvents utilized to extract the derivatized amino acids in the sequencer. Apparently and fortuitously, BI-RH-448 and BI-RJ-70 were hydrophobic enough not to prevent this solubilization of crosslinked amino acids and/or their derivatives.

The pattern of radioactivity associated with amino acid positions of peptides crosslinked to BI-RH-448 (Table 1) differed dramatically from that of BI-RJ-70 (Table 2). In the peptides crosslinked to BI-RH-448 (Table 1), each of 10 different cycles, including 2, 3, 4, 5, 6, 7, 9, 11, 12, and 13, were associated with radioactivity greater than that in the preceding cycle and thus not attributable to sequencer lag. Each of the 10 cycles likely corresponded to a different amino acid position, as the data in and the discussion of Fig. 2 suggested that the tryptic cleavages of reverse transcriptase were extensive and specific at arginines and lysines. Thus, the data of Table I implied that no fewer than 10 amino acids were crosslinked to BI-RH-448. In contrast to Table

Table 2
Radioactivity (DPM) in cycles of Edman sequencing of fractions of tryptic peptide map of reverse transcriptase crosslinked to BI-RJ-70.

	Fraction[a]										
	98–100 7%	100–102 1%	102–104 2%	104–106 4%	106–108 9%	108–110 15%	110–112 24%	112–114 4%	114–116 4%	116–118 3%	118–120 2%
Cycle 1	–[b]	–	–	–	–	–	–	818	–	–	–
2	–	–	–	–	–	–	–	–	–	–	–
3	–	–	–	–	–	–	–	–	–	–	–
4	–	–	–	–	–	–	–	–	–	–	–
5	–	–	–	–	–	–	–	–	–	–	–
6	–	–	–	–	–	–	–	–	–	–	–
7	–	–	–	–	–	–	–	–	–	–	–
8	3368	–	816	1324	9104	8080	25660	3238	8514	1842	1916
9	2488	–	548	634	7100	3620	7900	914	2316	744	624
10	1108	–	–	–	1394	960	2748	470	870	390	278
11	590	–	–	–	–	492	724	614	732	–	–
12	442	–	–	–	–	–	444	308	264	–	–
13	404	–	–	–	–	–	–	268	–	–	–
14	336	–	–	–	–	322	–	–	–	–	–
15	384	–	–	256	380	374	956	424	670	316	658
16	–	–	–	–	330	294	300	322	362	–	–
17	–	–	–	–	–	–	–	–	–	–	–
18	–	–	–	–	–	–	–	–	–	–	–
19	–	–	–	–	–	–	–	–	–	–	–
20	–	–	–	–	–	–	–	–	–	–	–

[a] First line (*e.g.* 98–100) indicates collection time (*e.g.* from 98 to 100 min) in the tryptic peptide map; second line (*e.g.* 7%) indicates percentage fraction accounted for (*e.g.* 7%) of total radioactivity collected in the tryptic peptide map.
[b] Radioactivity was less than background, which was defined as 250 DPM.

1, in the peptides crosslinked to BI-RJ-70 (Table 2), radioactivity greater than that in the preceding cycle was measured primarily in only two amino acid cycles, specifically 8 and 15, suggesting that amino acids at these two positions were crosslinked to BI-RJ-70.

Hence the data in Tables 1 and 2 again pointed to a more specific and localized crosslinking of BI-RJ-70 than of BI-RH-448 to reverse transcriptase. Furthermore, none of the 10 positions identified as containing amino acids crosslinked to BI-RH-448 was the same as the two positions, *i.e.*, 8 and 15, identified as containing amino acids crosslinked to BI-RJ-70. Therefore, none of the amino acids crosslinked to either azido analogue was crosslinked to the other azido analogue. Evidently, the two azido analogues probed different amino acids within the same region of reverse transcriptase, or probed two different regions. Because of the related structures of the azido analogues, it was more likely that the same region was probed. However, it could not be ruled out that different regions were probed as well, as discussed in the next sections.

3.8. Amino acids crosslinked to azido analogue

To identify the specific amino acids crosslinked to BI-RH-448 or to BI-RJ-70, peptides crosslinked to each azido analogue were isolated and then analyzed by protein sequencing. Isolation of the peptides crosslinked to azido analogue was achieved in high purity by modification of the HPLC conditions described for the tryptic peptide maps of Figs. 2 and 4.

For example in Fig. 4B the largest peak at 335 nm corresponding to peptide crosslinked to BI-RH-448 was at 95.5 min in the fraction collected at 94–96 min. Coeluting in the same fraction were also peptides which were not crosslinked to BI-RH-448 and which were likely at concentrations greater than that of the peptide at 95.5 min crosslinked to BI-RH-448 (*cf.* Figs. 2B and 4B). To isolate the peak at 95.5 min, four injections like that in Fig. 4B were made, and in each injection a 200-μl fraction was collected around 95.5 min. The four 200-μl fractions were pooled and subjected to a second HPLC step which employed pH 6.5 instead of the pH 2.5 employed in the first step (Fig. 4B). In the second HPLC step (Fig. 6), excellent resolution

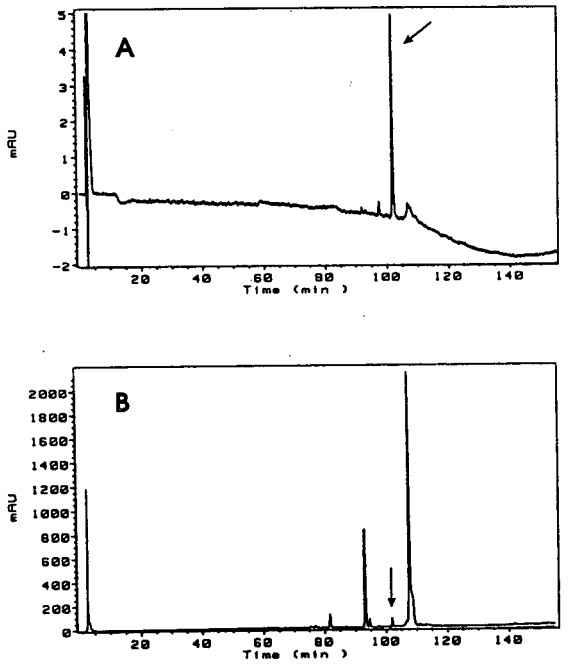

Fig. 6. Reversed-phase HPLC of a pool of four 200-μl fractions collected around 95.5 min in HPLC tryptic peptide maps comparable to that depicted in Figs. 2B and 4B. The pool of fractions was diluted to 1000 μl with water and then injected in 10 consecutive 100-μl loadings while the gradient was held at 100% A (0.05 *M* sodium phosphate, pH 6.5) and 0.20 ml/min. After injecting the 1000 μl a gradient identical to that described in the legend of Fig. 2 was applied, except solvent A was 0.05 *M* sodium phosphate and solvent B was 0.05 *M* sodium phosphate in water–acetonitrile (30:70, v/v). Detection was by UV absorbance. (A) 335 nm, (B) 210 nm.

of peptides crosslinked and not crosslinked to BI-RH-448 was obtained.

In Fig. 6A the HPLC fraction containing the largest peak (102 min) detected at 335 nm coeluted with the largest concentration of radioactivity (not shown) and did not appear to be contaminated with other peaks at 335 nm or 210 nm (Fig. 6B). Protein sequencing of this peak identified a peptide whose N-terminus started with leucine 425 of reverse transcriptase (Fig. 7). As illustrated in Fig. 7, tryptophan 426 corresponded to the amino acid residue released in cycle 2 of sequencing. The greatest level of radioactivity measured was also associated with cycle 2 of sequencing (Fig. 7), in agreement with the analysis of a comparable parent fraction (*cf.* fraction 94–96 min in Table 1). Thus it was concluded that BI-RH-448 was crosslinked to tryptophan 426.

In Fig. 6A fractions of other but smaller peaks at 335 nm and of smaller levels of radioactivity were analyzed by protein sequencing as well (data not shown). Again, peptides whose N-terminus started with leucine 425 were identified repeatedly whenever there was enough peptide to measure. Radioactivity was usually the greatest in amino acid position 2 corresponding to tryptophan 426, although for a few fractions of Fig. 6A levels of radioactivity too high to be attributable to sequencer lag were measured also in position 3, corresponding to tyrosine 427. In

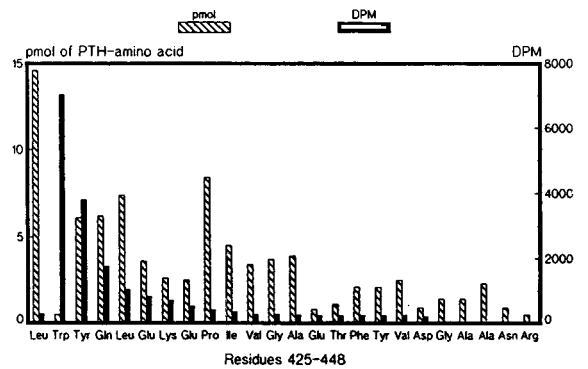

Fig. 7. Sequencing of the peptide corresponding to the peak indicated by the arrow at 102 min in Fig. 6. Conditions are given in the Experimental section.

Fig. 6A the different retentions of peptides all crosslinked to BI-RH-448 and all starting with leucine 425 at the N-terminus were due presumably to varying C-termini and/or to different atoms of tryptophan 426 and/or of tyrosine 427 to which BI-RH-448 was crosslinked.

3.9. Derivative UV absorbance spectroscopy

To corroborate that BI-RH-448 was crosslinked to tryptophan 426, on-line spectral scanning and second order derivative UV absorbance spectroscopy were carried out on the largest peak (102 min) at 335 nm in Fig. 6A. In the spectrum obtained (Fig. 8A), a minimum in absorbance was evident at 281–285 nm, which was indicative of the presence of tyrosine [48,49]. In the spectrum of Fig. 8B, which was of synthetic peptide not crosslinked to BI-RH-448 but otherwise of sequence of amino acids identical to the peptide in Fig. 8A, minima in absorbance were seen at 281–285 nm and at 288–292 nm, which were indicative of the presence of tyrosine and tryptophan, respectively [48,49]. In contrast, in Fig. 8A a minimum in absorbance at 288–292 nm was totally lacking, corroborating that BI-RH-448 was crosslinked to and thereby altered the spectrum of tryptophan 426.

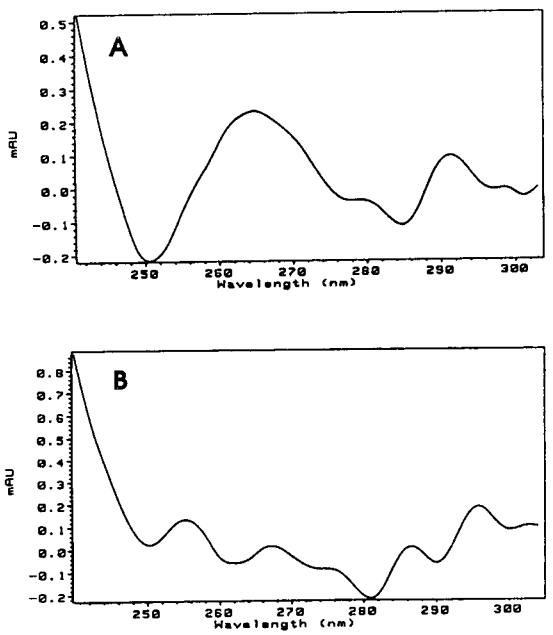

Fig. 8. Second order derivative UV absorbance spectra. Photodiode array detection was used to take spectra on-line at the apexes of eluting peptide peaks. (A) Peptide eluted at 102 min (Fig. 6A) was identified as amino acids 425–448, with tryptophan 426 crosslinked to BI-RH-448 (see text). (B) Synthetic peptide (amino acids 425–448) not crosslinked to BI-RH-448 eluted at 92 min (data not shown) under conditions of HPLC identical to that of Fig. 8A.

In fact in Fig. 8A the largest minimum in absorbance was observed at approximately 250 nm, which was characteristic of products of irradiated BI-RH-448. Such a dominant minimum was not seen in Fig. 8B, as the synthetic peptide was never exposed to BI-RH-448. Other studies like ours have used on-line spectral scanning to locate in HPLC peptide maps peaks that corresponded to peptides crosslinked to azido reagents [33–35,38,40]. Our study, however, is the first to exploit on-line derivative spectroscopy to identify the precise amino acid to which the azido reagent was crosslinked.

By similar approaches attempts were made to elucidate the other amino acids that were crosslinked to BI-RH-448 and that corresponded to amino acid positions 4, 5, 6, 7, 9, 11, 12, and 13, in which radioactivity was measured in protein sequencing (Table 1). However, the peptides associated with the radioactivities in these positions were distributed so widely in Fig. 4B and were of concentrations so low that unambiguous identification has not been achieved to date. This was unfortunate, because these identifications potentially offer additional information about the binding environment of reverse transcriptase for nevirapine and its analogues.

3.10. Correlations to techniques other than HPLC

The amino acid residues which crosslinked to BI-RJ-70 and which corresponded to amino acid positions 8 and 15 (Table 2) were successfully identified as tyrosines 181 and 188, as reported previously [19]. The identifications of the tyrosines were supported by subsequent studies involving mutagenesis of reverse transcriptase. For instance the potency of nevirapine decreased

300–800 fold when tyrosine at position 181 or 188 or both was substituted with other amino acids [20,21]. Moreover a recent report in which the structure of reverse transcriptase co-crystallized with nevirapine was studied by X-ray crystallography showed that nevirapine was proximal to tyrosines 181 and 188 [22].

In comparison, mutagenesis studies performed in conjunction with the BI-RH-448 crosslinking experiments showed a far less dramatic decrease in the potency of nevirapine or its analogues. When tryptophan 426 or tyrosine 427 or glutamine 428 was substituted with the respective residue (alanine, phenylalanine, asparagine) from HIV-2 reverse transcriptase, the losses in inhibitory activity were only 2–6 fold [50]. Also, crystallographic studies of reverse transcriptase showed that tryptophan 426 was not proximal to nevirapine [22]. Indeed, based on other studies involving mutagenesis of reverse transcriptase, it was speculated that tryptophan 426 was in a region near the surface of reverse transcriptase [51]. This hypothesis was consistent with several of our findings: (i) tryptophan 426 was accessible to BI-RH-448, (ii) the effect of tryptophan 426 on the binding of nevirapine and its analogues to reverse transcriptase was modest at best, and (iii) the levels of tryptophan 426 crosslinked to BI-RH-448 were measurably smaller than that of tyrosines 181 and 188 crosslinked to BI-RJ-70.

Although the role, if any, which tryptophan 426 and tyrosine 427 played in binding nevirapine and its analogues was not clear, the use of BI-RH-448 contributed to our understanding of how non-nucleoside drugs bind to reverse transcriptase. For instance, the dramatic difference between BI-RH-448 and BI-RJ-70 in crosslinking behavior was consistent with the two analogues orienting with a similar directionality into the binding pocket. Furthermore, as nevirapine, BI-RH-448, and BI-RJ-70 exhibited comparable inhibition (IC50 90 n*M*, 150 n*M*, and 160 n*M*, respectively) against the polymerase activity of reverse transcriptase [14,18], the relatively diffuse crosslinking of BI-RH-448 to reverse transcriptase strongly suggested that immediately proximal to the C-ring of nevirapine or its analogues there were no amino acid side chains with high reactivity towards nitrenes or other intermediates. The testing of this observation has not been possible by X-ray crystallography because of insufficient resolution to date [22,52].

4. Conclusions

HPLC-based techniques, most notably tryptic peptide mapping, on-line derivative UV absorbance spectroscopy, and off-line protein sequencing, were employed to demonstrate that two azido analogues of nevirapine differed markedly in their crosslinking behavior to reverse transcriptase of HIV-1. The HPLC techniques made it possible to carry out the unique comparison of BI-RH-448 and BI-RJ-70, and as a result to define better the structure of the binding pocket of reverse transcriptase for non-nucleoside inhibitors. For instance, the HPLC techniques made it feasible to show that tyrosines 181 and 188 were crucial components of the binding pocket, that the A-ring of nevirapine was oriented proximal to the tyrosines, and that the C-ring was likely oriented distal from the tyrosines as well as from other amino acids.

The identification of the tyrosines was subsequently used to assist in the design of mutant reverse transcriptase in mutagenesis studies [21], and in the assignment of amino acid positions in X-ray crystallography studies [22]. Both of these non-HPLC techniques were then able to corroborate the tyrosines 181 and 188 initially identified with the HPLC approach [19]. However, the finding that the C-ring of the azido analogues of nevirapine was oriented not proximal to the tyrosines, or for that matter, not proximal to any other amino acids in the binding pocket of reverse transcriptase for nevirapine analogues, remains achievable so far by HPLC methodology only. Testing of this finding by other techniques (*e.g.*, mutagenesis or X-ray crystallography) is eagerly awaited. Finally, as a practical note, the results reported demonstrate that all azido analogues of a given inhibitor may not be of equivalent utility in identifying amino acid residues located at the binding site. There-

fore, an accurate and/or complete definition of a binding site may demand the use of more than one azido analogue.

5. Acknowledgements

The insightful discussions and/or research of C.-K. Cheng, J. Rose, J. Wu, K. Hargrave, C. Perry, J. Adams, and P. Farina are gratefully acknowledged. Also gratefully acknowledged are the assistance of M. Folderauer in preparation of the manuscript and of D. Ligi and L. Rondano in preparation of figures.

6. References

[1] E. Gilboa, S.W. Mitra, S. Goff and D. Baltimore, *Cell*, 18 (1989) 93.

[2] M.H. St. Clair, J.L. Martin, G. Tudor-Williams, M.C. Bach, C.L. Vavro, D.M. King, P. Kellam, S.D. Kemp and B.A. Larder, *Science*, 253 (1991) 1557.

[3] J.S. Lambert, M. Seiden, R.C. Reichman, C.S. Plank, M. Laverty, G.D. Morse, C. Knupp, C. McLauren, C. Pettinelli, F.T. Valentine and R. Dolin, *N. Engl. J. Med.*, 322 (1990) 1333.

[4] T.C. Merigan, G. Skowron, S.A. Bozzette, D. Richman, R. Uttamchandani, M. Fischl, R. Schooley, M. Hirsch, W. Soo, C. Pettinelli, H. Schaumburg and the ddC Study Group of the AIDS Clinical Trials Group, *Ann. Intern. Med.*, 110 (1989) 189.

[5] P.S. Kedar, J. Abbots, T. Kovacs, K. Lesiak, P. Torrence and S.H. Wilson, *Biochemistry*, 29 (1990) 3603.

[6] P. Huang, D. Farquhar and W. Plunkett, *J. Biol. Chem.*, 265 (1990) 11914.

[7] D.D. Richman, M.A. Fischl, M.H. Grieco, M.S. Gottlieb, P.A. Volberding, O.L. Laskin, J.M. Leedom, J.E. Groopman, D. Mildvan, M. Hirsch, G.G. Jackson, D.T. Durack and S.N. Nusinoff-Lehrman, *N. Engl. J. Med.*, 317 (1987) 192.

[8] M.C. Dalakas, I. Illa, G.H. Pezeshkpour, J.P. Laukaitis, B. Cohen and J.L. Griffin, *N. Engl. J. Med.*, 322 (1990) 1098.

[9] J.S. Lambert, M. Seidlin, R.C. Reichman, C.S. Plank, M. Laverty, G.D. Morse, C. Knupp, C. McLaren, C. Pettinelli, F.T. Valentine and R. Dolin, *N. Engl. J. Med.*, 322 (1990) 1333.

[10] R. Pauwels, K. Andries, J. Desmyter, D. Schols, M.J. Kukla, H.J. Breslin, A. Raeymaeckers, J. VanGelder, R. Woesteinborghs, J. Heykants, K. Schellekens, M.A. Janssen, E. DeClercq and P.A. Janssen, *Nature*, 343 (1990) 470.

[11] M.E. Goldman, J.H. Nunberg, J.A. O'Brien, J.C. Quintero, W.A. Schleif, K.F. Freund, S.I. Gaul, W.S. Saari, J.S. Wai, J.M. Hoffman, P.S. Anderson, D.J. Hupe, E.A. Emini and A.M. Stern, *Proc. Natl. Acad. Sci. U.S.A.*, 88 (1991) 6863.

[12] M. Baba, E. DeClercq, H. Tanaka, M. Ubasawa, H. Takashima, K. Sekiya, I. Nitta, K. Umezu, H. Nakashima, S. Mori, S. Shigeta, R.T. Walker and T. Miyasaka, *Proc. Natl. Acad. Sci. U.S.A.*, 88 (1991) 2356.

[13] T.J. Dueweke, F.J. Kezdy, G.A. Waszak, M.R. Deibel, Jr. and W.G. Tarpley, *J. Biol. Chem.*, 267 (1992) 27.

[14] V.J. Merluzzi, K.D. Hargrave, M. Labadia, K. Grozinger, M. Skoog, J.C. Wu, C.-K. Shih, K. Eckner, S. Hattox, J. Adams, A.S. Rosenthal, R. Faanes, R.J. Eckner, R.A. Koup and J.L. Sullivan, *Science*, 250 (1990) 1411.

[15] P.M. Grob, J.C. Wu, K.A. Cohen, R.H. Ingraham, C.-K. Shih, K.D. Hargrave, T.L. McTague and V.J. Merluzzi, *AIDS Res. Hum. Retroviruses*, 8 (1992) 145.

[16] Y.-K. Chow, M.S. Hirsch, D.P. Merrill, L.J. Bechtel, J.J. Eron, J.C. Kaplan and R.T. D'Aquila, *Nature*, 361 (1993) 650.

[17] J. Balzarini, A. Karlsson, M.-J. Perez-Perez, M.-J. Camarasa and E. De Clercq, *Virology*, 196 (1993) 576.

[18] J.C. Wu, T.C. Warren, J. Adams, J. Proudfoot, J. Skiles, P. Raghavan, C. Perry, I. Potocki, P.R. Farina and P.M. Grob, *Biochemistry*, 30 (1991) 2022.

[19] K.A. Cohen, J. Hopkins, R.I. Ingraham, C. Pargellis, J.C. Wu, D.E.H. Palladino, P. Kinkade, T.C. Warren, S. Rogers, J. Adams, P.R. Farina and P. Grob, *J. Biol. Chem.*, 266 (1991) 14670.

[20] J.H. Nunberg, W.A. Schleif, E.J. Boots, J.A. O'Brien, J.C. Quintero, J.M. Hoffman, E.A. Emini and M.E. Goldman, *J. Virol.*, 65 (1991) 4887.

[21] C.-K. Shih, J.M. Rose, G.L. Hansen, J.C. Wu, A. Bacolla and J.A. Griffin, *Proc. Natl. Acad. Sci. U.S.A.*, 88 (1991) 9878.

[22] L.A. Kohlstaedt, J. Wang, J.M. Friedman, P.A. Rice and T.A. Steitz, *Science*, 256 (1992) 1783.

[23] A. Wlodawer, *Science*, 256 (1992) 1765.

[24] T.C. Warren, J.J. Miglietta, A. Shrutkowski, J.M. Rose, S.L. Rogers, K. Lubbe, C.-K. Shih, G.O. Caviness, R. Ingraham, D.E.H. Palladino, E. David, G.C. Chow, E.B. Kopp, K.A. Cohen, J.A. Glinski, P.R. Farina and P.M. Grob, *Protein Expression and Purification*, 3 (1992) 479.

[25] K.D. Hargrave, J.R. Proudfoot, K.G. Grozinger, E. Cullen, S.R. Kapadia, U.R. Patel, V.U. Fuchs, S.C. Mauldin, J. Vitous, M.L. Behnke, J.M. Klunder, K. Pal, J.W. Skiles, D.W. McNeil, J.M. Rose, G.C. Chow, M.T. Skoog, J.C. Wu, G. Schmidt, W.W. Engel, W.C. Eberlein, T.D. Saboe, S.J. Campbell, A.S. Rosenthal and J. Adams, *J. Med. Chem.*, 34 (1991) 2231.

[26] J.M. Klunder, K.D. Hargrave, M. West, E. Cullen, K. Pal, M.L. Behnke, S.R. Kapadia, D.W. McNeil, J.C. Wu, G.C. Chow and J. Adams, *J. Med. Chem.*, 35 (1992) 1887.

[27] K.L. Stone and K.R. Williams, *J. Chromatogr.*, 359 (1986) 203.
[28] S.M. King, H. Kim and B.E. Haley, *Methods Enzymol.*, 196 (1991) 449.
[29] H. Bayley, in T.S. Work and R.H. Burdon (Editors), *Laboratory Techniques in Biochemistry and Molecular Biology*, Elsevier, Amsterdam, 1983, Vol. 12, p. 11.
[30] K.L. Stone, J.I. Elliott, G. Peterson, W. McMurray and K.R. Williams, *Methods Enzymol.*, 193 (1990) 389.
[31] R. Benesch, R.E. Benesch, S. Kwong, A.S. Acharya and J.M. Manning, *J. Biol. Chem.*, 257 (1982) 1320.
[32] Y. Okamoto and R.G. Yount, *Proc. Natl. Acad. Sci. U.S.A.*, 82 (1985) 1575.
[33] A. Basu and M.J. Modak, *Biochemistry*, 26 (1987) 1704.
[34] A. Basu, V.B. Nanduri, G.F. Gerard and M.J. Modak, *J. Biol. Chem.*, 263 (1988) 1648.
[35] S. Basu, A. Basu and M.J. Modak, *Biochemistry*, 27 (1988) 6710.
[36] M.P. Kavanugh, D.T.-B. Shih and R.T. Jones, *Biochemistry*, 27 (1988) 1804.
[37] R. Mahmood, M. Elzinga and R.G. Yount, *Biochemistry*, 28 (1989) 3989.
[38] A. Basu, R.S. Tirumalai and M.J. Modak, *J. Biol. Chem.*, 264 (1989) 8746.
[39] V.B. Nanduri and M.J. Modak, *Biochemistry*, 29 (1990) 5258.
[40] J. Inglese, J.M. Smith and S.J. Benkovic, *Biochemistry*, 29 (1990) 6678.
[41] J. Rush and W.H. Konigsberg, *J. Biol. Chem.*, 265 (1990) 4821.
[42] G. Reddy, V.B. Nanduri, A. Basu and M.J. Modak, *Biochemistry*, 30 (1991) 8195.
[43] R.S. Tirumalai and M.J. Modak, *Biochemistry*, 30 (1991) 6436.
[44] A. Basu, K.K. Ahluwalia, S. Basu and M.J. Modak, *Biochemistry*, 31 (1992) 616.
[45] M.E. Salvucci, A.J. Chavan and B.E. Haley, *Biochemistry*, 31 (1992) 4479.
[46] L.L.W. Mitchell and B.S. Cooperman, *Biochemistry*, 31 (1992) 7707.
[47] C.-P.H. Yang, W. Mellado and S.B. Horwitz, *Biochem. Pharmacol.*, 37 (1988) 1417.
[48] B. Grego, E.C. Nice and R.J. Simpson, *J. Chromatgr.*, 352 (1986) 359.
[49] D.E.H. Palladino and K.A.Cohen, *J. Chromatogr. Sci.*, 29 (1991) 91.
[50] C.-K. Shih and J.M. Rose, unpublished results
[51] A. Jacobo-Molina and E. Arnold, *Biochemistry*, 30 (1991) 6351.
[52] A. Jacobo-Molina, J. Ding, R.G. Nanni, A.D. Clark, Jr., X. Lu, C. Tantillo, R.L. Williams, G. Kamer, A.L. Ferris, P. Clark, A. Hizi, S.H. Hughes and E. Arnold, *Proc. Natl. Acad. Sci. U.S.A.*, 90 (1993) 6320.

ELSEVIER

Journal of Chromatography A, 676 (1994) 113–120

JOURNAL OF CHROMATOGRAPHY A

Nitrogen-specific detection of peptides in liquid chromatography with a chemiluminescent nitrogen detector

Eugene M. Fujinari*[,a], J. Damon Manes[b]

[a]*Antek Instruments Inc., 300 Bammel Westfield Road, Houston, TX 77090, USA*
[b]*Bristol-Myers/Squibb, 2400 W. Lloyd Expressway, Evansville, IN 47721, USA*

Abstract

High-performance liquid chromatography with chemiluminescent nitrogen detection (HPLC–CLND) in the reversed-phase mode was used to quantitate peptides that were isolated from casein hydrolysate. When CLND is used simultaneously with a UV detector in peptide mapping, unique quantitative information about the nitrogen distribution of the sample is obtained. Nitrogenous compounds without UV chromophores are easily detected by CLND without pre- or post-column derivatization. Of further significance, the non-nitrogenous compounds in the sample matrix are transparent to the detector. This paper will focus primarily on the analysis of two peptides, identified as **1** and **2**. The UV peptide map showed peptide **2** as the largest component. On the other hand, the CLND results indicated that peptide **1** was the major peak. RP-HPLC amino acid analysis of the peptides **1** and **2** confirmed the CLND results. This analysis shows that peptide **1** was the major component and did not contain aromatic amino acid residues. Peptide **2** however, contained aromatic groups with strong chromophores, thereby explaining the UV response.

1. Introduction

Peptide mapping with RP-HPLC is an established procedure that is routinely used in biotechnology for sequencing and protein identification. Typically, the standard RP-HPLC system for peptide mapping uses columns with either a C8 or C18 stationary phase, acetonitrile–water + 0.1% TFA binary gradient for peptide elution followed by UV detection. However, direct quantitation of eluted peptides is not possible with UV detection because of the differential UV absorption properties between peptides with aromatic functional groups and those containing primarily non-aromatic amino acid residues. Recently, a novel HPLC–chemiluminescent nitrogen detection (HPLC–CLND) system was described [1]. This detector was designed primarily as a means for direct quantitation of nitrogen containing analytes.

Acetonitrile because of its low UV cutoff is an excellent solvent for UV detection. However, due to its nitrogen moiety, acetonitrile interferes with CLND. Alcohols, both methanol and isopropanol, can be substituted for acetonitrile in RP-HPLC peptide mapping [2–8]. Alcohols offer additional advantages to the chromatographer besides CLND compatibility: (1) many peptides are more soluble in alcohols, particularly isopropanol; (2) retention of peptide tertiary structures and therefore biological activity is much less affected; and (3) environmental

* Corresponding author.

0021-9673/94/$07.00
SSDI 0021-9673(94)00335-7

concerns are lessened with alcohols as compared to acetonitrile, including the disposal of these solvents. Direct quantitation of peptides separated by RP-HPLC is needed by researchers in the pharmaceutical, bioanalytical, immunochemical, and food chemistry to assess purity or yield. Fujinari *et al.* reported the use of a CLND system in the RP-HPLC separations of peptides [9]. We now present a new binary gradient RP-HPLC method for the separation and quantitation of peptides isolated from casein hydrolysate using the nitrogen specific detection capabilities of the CLND system [10]. This study demonstrates that peptides can be separated and quantitated using standard RP-HPLC columns, solvents and the HPLC–CLND system. Optimization of the column, mobile phase and CLND operating conditions is also presented.

2. Experimental

2.1. Apparatus

All HPLC mobile phases were filtered through a Millipore (Bedford, MA, USA) HV filter with a pore size of 0.45 μm. RP-HPLC peptide analysis was performed on a Waters Model 625 pump with an analytical pumphead, Model 490 UV detector purchased from Waters Associates (Milford, MA, USA) and Model 7000 HPLC–CLND nitrogen-specific detector from Antek Instruments (Houston, TX, USA). Sample injection was performed with a Model 9125-080 sample valve with a 50 μl loop from Rheodyne (Cotati, CA, USA) onto the analytical HPLC column from Vydac (Hesperia, CA, USA), and the eluate passed through a GC capillary splitter from SGE (Austin, TX, USA) to split the mobile phase flow rate to the two detectors. A rotary evaporator Model Speed-Vac Plus from Savant (Farmingdale, NY, USA) and microwave digestion apparatus Model MDS 2000 from CEM (Matthews, NC, USA) were used. Amino acid analysis was performed by RP-HPLC using Waters Pico-Tag reagents, column, and Model 625 pump. The chromatographic data were collected and analyzed with Waters Millennium Sample Information software operating on a NEC Power Mate 486 computer.

RP-HPLC analysis of piperazine and 2,3-diethylpyrazine was accomplished on a Micromeritics Model 760 pump with a microbore pumphead purchased from Alcott Chromatography (Norcross, GA, USA) with an Antek Model 7000 HPLC–CLND nitrogen-specific detector, then analyzed separately with Model 770 UV detector from Spectra-Physics (Santa Clara, CA, USA). Sample was injected into a Model 8126 sample valve with a 5-μl loop from Rheodyne and chromatographed on a microbore HPLC column from Keystone Scientific (Bellefonte, PA, USA). Data were stored and analyzed on the Delta chromatography software (Digital Solutions, Margate, Australia) on an IBM 486 compatible computer.

2.2. Reagents and standards

Casein, Gly–Gly–Leu, glycine, HPLC peptide standard mixture (approximately 0.125 mg Gly–Tyr and approximately 0.5 mg each of Val–Tyr–Val, methionine enkephalin, leucine enkephalin, and angiotensin II) were purchased from Sigma Chemical Co. (St. Louis, MO, USA). Immobilized polyclonal, anti-casein antibodies (GTA disk) produced by Lampire Biological (Pipersville, PA, USA) and FMC (Pine Brook, NJ, USA), HCl, phenylisothiocyanate, Mix H amino acid standard, methanol, and TFA were purchased from Pierce Chemical (Rockford, IL, USA). RO/deionized water was obtained from a Model Milli-QUV Plus from Millipore.

2.3. Standard preparation and analytical method

The stock standard solution with 6 peptide components was prepared by adding 0.1 mg of Gly–Gly–Leu to the dry Sigma HPLC standard mixture and dissolving in 1 ml of water. Sequential partially filled injections (1, 2.5, 5, and 10 μl of the stock standard solution) were made into a 50-μl sample loop of the HPLC system. Casein hydrolysate was also analyzed by RP-HPLC (250 mm × 4.6 mm I.D., 90 Å pore size, 5 μm particle size) Vydac C18 column at 25°C. Mobile

phases: 0.1% TFA in water (A) and 0.1% TFA in methanol (B), flow rate of 650 μl/min, a gradient elution: 0 min 0%B, 50 min 50%B, 55 min 50%B, 60 min 0%B, and 65 min 0%B. The flow rate was split after the column using the SGE capillary splitter where 150 μl/min was directed to the CLND and 500 μl/min to the UV detector. Peptides **1** and **2** were collected from the exit end of the UV detector and evaporated to dryness. CLND conditions: 1050°C pyrolysis temperature, PMT voltage 700 V, range 25×, and detector output of 1 V; UV conditions: at 214 nm, range 0.2 AUFS. Alpha-amino butyric acid (1.74 μg) was added as internal standard to a 5-μl aliquot of the Mix H amino acid standard solution (Pierce Chemical). The same amount of internal standard was added to the hydrolyzed peptide fractions. The Waters Pico-Tag method was followed for the derivatization and amino acid analysis.

Piperazine (191 mg) and 2,3-diethylpyrazine (171 mg) were dissolved in 25 ml of water. A 2-μl partially filled injection of the standard mixture was made into a 5-μl sample loop and analyzed by RP-HPLC (150 mm × 2.0 mm I.D., 120 Å pore size, 5 μm particle size) BDS Hypersil C18 column at 25°C. Mobile phase: 0.1% TFA in methanol–water (50:50, v/v) was utilized at a flow rate of 200 μl/min, CLND conditions: 1050°C pyrolysis temperature, PMT voltage 760 V, range 10×, and detector output 1 V; UV conditions: at 254 nm, range 0.1 AUFS. The CLND and UV detection were performed separately.

3. Results and discussion

Direct quantitation by reversed-phase HPLC–CLND of peptides isolated from a casein hydrolysate is presented. Casein is a phosphoprotein that is one of the major constituents in milk and is an essential ingredient in cheese. Casein hydrolysates are used in food industry and in particular as the protein source in hypoallergenic infant formulas. Using this detector, a new, innovative and useful approach to analyze peptides was accomplished.

The chemiluminescence nitrogen detection mechanism is shown: as each nitrogen containing analyte is eluted from the column, it undergoes high-temperature oxidation (1000–1100°C). All chemically bound nitrogen compounds, except diatomic nitrogen (N_2), are converted to nitric oxide (NO).

$$R_3N + O_2 \xrightarrow{>1000^\circ C} H_2O + \cdot NO + \text{other oxides}$$

$$\cdot NO + O_3 \longrightarrow {}^{*}NO_2 \longrightarrow NO_2 + h\nu$$

The gases are dried and mixed with ozone in the reaction chamber. Nitrogen dioxide (NO_2^*) in the excited state is formed. As the NO_2^* molecule reaches the stable ground state (NO_2), light ($h\nu$) is emitted and is detected by a photomultiplier tube (PMT). The signal from the chemiluminescence reaction is amplified and data stored on a computer for analysis and report generation.

A standard mixture of 6 peptides (peaks: 1 = Gly–Tyr, 2 = Gly–Gly–Leu, 3 = Val–Tyr–Val, 4 = methionine enkephalin, 5 = leucine enkephalin, and 6 = angiotensin II) was chromatographed by RP-HPLC. A simultaneous CLND and UV detection is shown in Fig. 1. One of the most important advantages of HPLC–CLND is the realization of an order of magnitude sensitivity enhancement over UV detection, in some cases, as demonstrated in Fig. 1. Gly–Gly–Leu, a tripeptide with no aromatic UV chromophore, produces at least 10 times more signal using HPLC–CLND than was produced by UV detection. This enhanced sensitivity is particularly important in the analysis of low molecular weight peptides. An optimum UV response at 214 nm for the compounds of interest was achieved using our chromatographic conditions. The upward baseline shift due to the TFA in the mobile phase was minimized at this wavelength. A linear detector response for each of the 6 peptide standards was observed for CLND. Four-point calibration curves using the linear regression

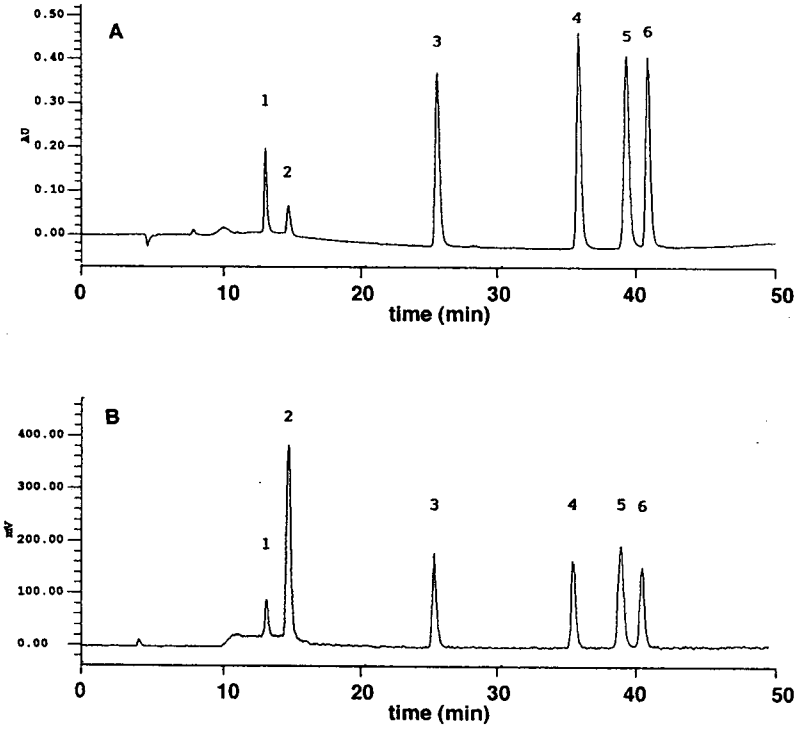

Fig. 1. RP-HPLC chromatograms of the 6-peptide standard mixture. Peaks: 1 = Gly–Tyr, 2 = Gly–Gly–Leu, 3 = Val–Tyr–Val, 4 = methionine enkephalin, 5 = leucine enkephalin, 6 = angiotensin II. (A) UV detection at 214 nm, (B) HPLC–CLND.

analysis (where r = correlation coefficient, m = slope and b = y-intercept) were obtained: Gly–Tyr ($r = 0.99450$, $m = 0.00003$, $b = 0.96929$), Gly–Gly–Leu ($r = 0.99733$, $m = 0.00002$, $b = 0.80865$), Val–Tyr–Val ($r = 0.99921$, $m = 0.00004$, $b = 3.65512$), methionine enkephalin ($r = 0.99895$, $m = 0.00003$, $b = 4.47127$), angiotensin II ($r = 0.99806$, $m = 0.00004$, $b = 0.07473$), and leucine enkephalin ($r = 0.99092$, $m = 0.00004$, $b = -4.00664$). The resulting slopes obtained using CLND were all very similar from the dipeptide, Gly–Tyr, to the larger peptides such as leucine enkephalin since the detector responded to the amount of nitrogen in each of these nitrogen bearing compounds. The HPLC–CLND responded equally to both aromatic and non-aromatic peptides. This suggests that detection and quantitation using a single compound calibration for the nitrogen quantification in a given sample is feasible. The UV detector on the other hand, responds to the presence of chromophores on the analytes. Gly–Gly–Leu, due to the absence of a strong aromatic chromophore, displayed a low UV detector response ($r = 0.99752$, $m = 0.00147$, $b = 5.93881$) and consequently a slope much different from the standard calibration curves generated by the CLND.

This paper will focus primarily on two peptides, **1** and **2**, which were isolated from casein hydrolysate using immobilized antibodies followed by RP-HPLC chromatographic determination with simultaneous CLND and UV detection. Several brand name columns (Vydac C18 with 90 and 300 Å pore; Waters C8 and C18 NovaPak; Hamilton RP1 and RP3; Sigma Nucleosil C18; Supelco LC 18 DB; and SGE 100 GL2-ODS2 2 × 100 mm) were evaluated on the basis of separation of the 6-peptide standard mixture. A Vydac C18 (90 Å) column was selected for the following reasons: it showed minimum tailing, optimum separation of the L- and M-

enkephalins, and consistent retention times from day to day operation. The peptide peaks **1** and **2** were isolated using immobilized polyclonal, anti-casein antibodies (GTA disk) and eluted with 0.10 *M* glycine with HCl (at pH = 2.7). Peptide 1 (t_R = 20.8 min) did not contain any significant chromophore and was not observed at 254 nor 280 nm UV detection. Peptide 2 (t_R = 38.2 min) however, showed a strong absorption at 280 nm. The UV (214 nm) chromatogram, Fig. 2, showed peptide **1** as the minor peak as compared to peptide **2**. In contrast, the nitrogen-specific detector, HPLC–CLND, showed peptide **1** as the major peak. The two peptides (**1** and **2**) were isolated by collecting each fraction from the post UV-eluent and dried by rotary evaporation. Each peptide fraction was then hydrolyzed by HCl gas phase microwave digestion [11], derivatized with phenylisothiocyanate and the amino acid composition determined by reversed-phase HPLC. From the results of the amino acid analysis, peptides **1** and **2** were calculated as 7.81 μg and 1.84 μg, respectively (see Tables 1 and 2). Peptide **1** did not contain amino acids with aromatic functional groups such as F, W, or Y. On the other hand, Tyrosine (Tyr or Y) contains aromaticity and was present in peptide **2**. This explains why peak **2** showed a strong UV absorbance. Both peptides were quantitated by HPLC–CLND based on the N response of the standard peptides: peptide **1** (10.7 μg) and peptide **2** (0.80 μg). These data agree with the relative amounts of peptides **1** and **2** found by the amino acid analysis. The significance of the CLND data is that peak **1** was found to be the major peptide based on the nitrogen content of the sample. Direct nitrogen quantitation (*i.e.* of peptides) is important to those who synthesize biologically active peptides as well as other nitrogen containing compounds. Nitrogenous

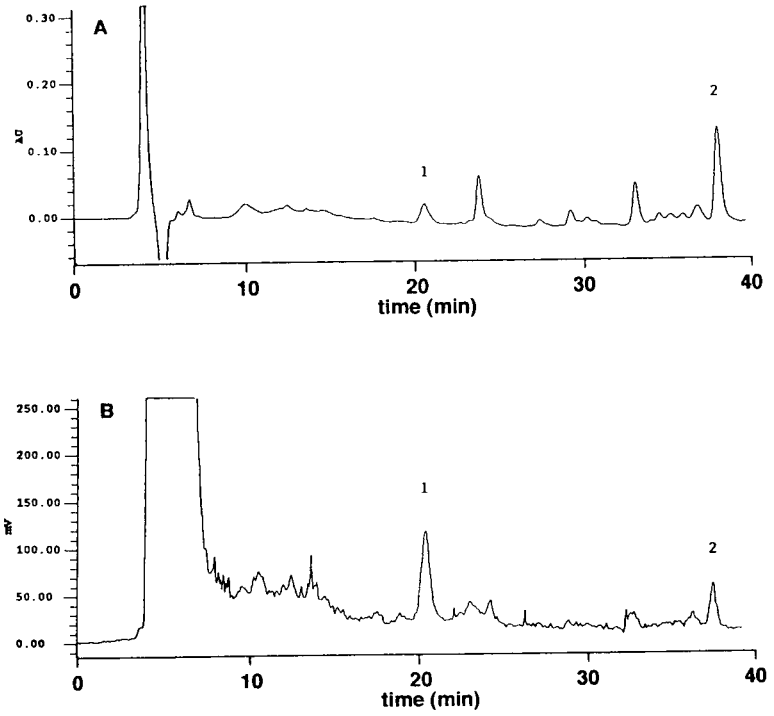

Fig. 2. RP-HPLC chromatograms of casein hydrolysate. Peaks: 1 = peptide with no aromatic UV chromophore, 2 = peptide with aromatic UV chromophore. (A) UV detection at 214 nm, (B) HPLC–CLND.

Table 1
Determination of amino acid (AA) composition of peptide **1** isolated from a casein hydrolysate sample

AA type	AA composition	No/mol	Peptide peak	AA data calculated (μg)	HPLC–CLND value (μg)
GLx	E/Q	4			
Ser	S	4			
Gly	G	1			
Ala	A	1			
Leu	L	2			
			Peptide **1**	7.81	10.7

Please note the absence of amino acids with aromatic functional groups such as F, W, or Y.

compounds without a UV chromophore are easily detected by CLND without the need of pre- or post-column derivatization. In addition, the non-nitrogenous compounds in the sample are transparent to the CLND. Our analytical approach enables other researchers to detect and focus on major nitrogen containing components in their samples.

Aromatic compounds such as 2,3-diethylpyrazine are easily detected by UV at 254 nm. Compounds with no chromophores such as piperazine are not detected by UV, and consequently can be overlooked. However, piperazine (peak **1**) is detected by the CLND without derivatization along with 2,3-diethylpyrazine (peak **2**) as depicted in Fig. 3. RP separation of nucleotides, nucleosides, and their bases with HPLC–CLND detection have been reported [12]. The sensitivity of HPLC–CLND is 0.4 ng N with signal-to-noise ratio of greater than 2:1. The high sensitivity of the nitrogen detector makes CLND a good candidate for capillary electrophoresis (CE) separations of complex molecules and biochemicals. HPLC–CLND study of peptides and food grade protein hydrolysates by size exclusion chromatography (SEC) has been completed and will be presented in the near future [13].

4. Conclusion

A new HPLC–CLND method for the analysis of peptides in a casein hydrolysate was achieved with a binary gradient reversed-phase elution. Peptides **1** and **2** were isolated and amino acid

Table 2
Determination of Amino Acid (AA) composition of peptide **2** isolated from a casein hydrolysate sample

AA type	AA composition	No/mol	Peptide peak	AA data calculated (μg)	HPLC–CLND value (μg)
GLx	E/Q	2			
ASx	D/N	1			
Ser	S	2			
Avg	R	1			
Pro	P	1			
Gly	G	1			
Tyr	Y	4			
			Peptide **2**	1.84	0.80

Please note the presence of amino acids with aromatic functional groups such as Y

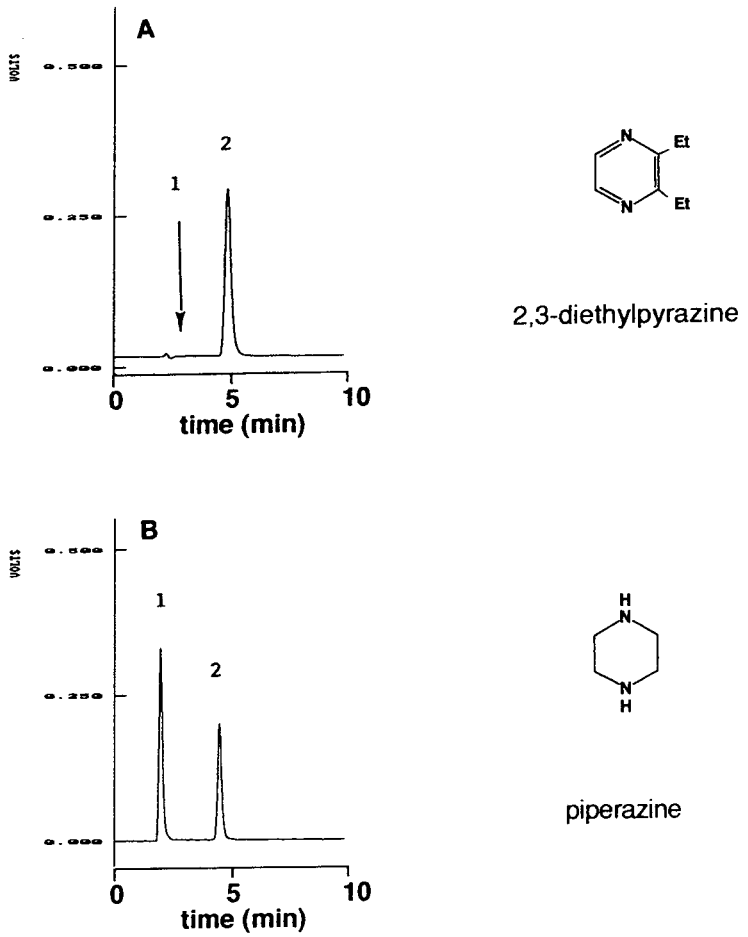

Fig. 3. RP-HPLC chromatograms of a 2-standard mixture. Peaks: 1 = piperazine which does not have a UV chromophore, 2 = 2,3-diethylpyrazine. (A) UV detection at 254 nm, (B) HPLC–CLND.

composition determined. The significance of utilizing HPLC–CLND is that peak integration of the peptides based on nitrogen content is obtained. Non-nitrogenous peaks detected by UV are not seen by CLND, thus simplifying interpretation of the chromatographic results. Other nitrogen containing compounds (*i.e.* piperazine) without a UV chromophore are easily detected by CLND without derivatization. A 6-component peptide standard mixture was used to show linearity of the HPLC–CLND. When this instrument is coupled to the UV detector, CLND provides additional useful data to enhance ones research. For example, by reversed-phase HPLC–CLND, one can achieve "total N" peptide mapping, selective isolation of modified peptides, direct peptide quantitation, and most important, purity analysis of bioactive peptides and other nitrogen bearing compounds.

References

[1] E.M. Fujinari and L.O. Courthaudon, *J. Chromatogr.*, 592 (1992) 209.
[2] W.C. Mahoney and M.A. Hermodson, *J. Biol. Chem.*, 255 (1980) 11199.
[3] K.J. Wilson, A. Honegger, R.P. Stotzel and G.J. Hughes, *Biochem. J.*, 199 (1981) 31.

[4] M. Hermodson and W.C. Mahoney, *Methods Enzymol.*, 91 (1983) 352.
[5] C.T. Mant and R.S. Hodges (Editors), *High Performance Liquid Chromatography of Peptides and Proteins: Separation, Analysis and Conformation*, CRC Press, Boca Raton, FL, 1991, p. 289.
[6] J. Heukeshoven and R. Dernick, *J. Chromatogr.*, 326 (1985) 91.
[7] M.R. Sussman, R.P. Stotzel and G.J. Hughes, *Anal. Biochem.*, 169 (1988) 395.
[8] K. Titani, T. Sasagawa, K. Resing and K.A. Walsh, *Anal. Biochem.*, 123 (1982) 408.
[9] E.M. Fujinari, E. Ribble and M.V. Piserchio, in G. Charalambous (Editor), *Food Flavors, Ingredients and Composition*, Elsevier, Amsterdam, 1993, p. 75.
[10] E.M. Fujinari and J.D. Manes, presented at the *13th International Symposium on HPLC of Proteins, Peptides and Polynucleotides, San Francisco, CA, November 30–December 3, 1993.*
[11] C. Woodward, L.D. Gilman and W.G. Engelhart, presented at the *9th International Symposium on HPLC of Proteins, Peptides and Polynucleotides, Philadelphia, PA, November 7, 1989.*
[12] E.M. Fujinari and J.D. Manes, presented at the *32nd Eastern Analytical Symposium and Exposition, Somerset, NJ, November 15–19, 1993.*
[13] E.M. Fujinari and J.D. Manes, presented at the *45th Pittsburgh Conference and Exposition, Session: Bioanalytical Chemistry Mini-Conference–Food Analysis, Chicago, IL, February 28–March 4, 1994.*

ELSEVIER

Journal of Chromatography A, 676 (1994) 121–137

JOURNAL OF CHROMATOGRAPHY A

Microbore reversed-phase high-performance liquid chromatographic purification of peptides for combined chemical sequencing–laser-desorption mass spectrometric analysis

Christopher Elicone, Mary Lui, Scott Geromanos, Hediye Erdjument-Bromage, Paul Tempst*

Molecular Biology Program and Protein Chemistry Laboratory, Memorial Sloan-Kettering Cancer Center (Box 137), 1275 York Avenue, New York, NY 10021, USA

Abstract

An optimized microbore RP-HPLC system (1.0 mm I.D. columns) for the purification of low picomole amounts (< 5 pmol) of peptides is described. It is comprised of commercially available columns, instrument components and parts. These were selected on the basis of a comparative evaluation and to yield the highest resolution and most efficient peak collection. The sensitivity of this system equals, probably surpasses, that of advanced chemical microsequencing for which 2–4 pmol of peptide are minimally required. As an automated sequencer cannot be "on-line" connected with a micro-preparative HPLC system, fractions must be collected and transferred. With a typical flow of 30 μl, efficient manual collection is possible and fractions (about 20 μl in volume) can still be handled without unacceptable losses, albeit with great precaution. Furthermore, major difficulties were encountered to efficiently and quantitatively load low- or sub-picomole amounts of peptide mixtures onto the RP-HPLC column for separation. Discipline and rigorous adherence to sample handling protocols are thus on order when working at those levels of sensitivity. With adequate instrumentation and handling procedures in place, we demonstrate that low picomole amounts of peptides can now be routinely prepared for analysis by combined Edman-chemical sequencing–matrix-assisted laser-desorption mass spectrometry (MALDI-MS). The integrated method was applied to covalent structural characterization of minute quantities of a gel-purified protein of known biological function but unknown identity. The results allowed unambiguous identification and illustrated the power of MALDI-MS-aided interpretation of chemical sequencing data: accurate peptide masses were crucial for (i) confirmation of the results, (ii) deconvolution of mixed sequences, (iii) proposal of complete structures on the basis of partial sequences, and (iv) confirmation of protein identification (obtained by database search with a single, small stretch of peptide sequence) by "mass matching" of several more peptides with predicted proteolytic fragments.

1. Introduction

As part of the sequencing process, proteolysis of proteins is often necessitated to cope with blocked N-termini and desirable to facilitate later gene cloning experiments [1,2]. Owing to low abundance and/or source limitations, these studies must frequently be done on small

* Corresponding author.

0021-9673/94/$07.00
SSDI 0021-9673(94)00089-R

amounts (10–20 pmol); additional steps, such as two-dimensional gel purification and *in situ* proteolysis will reduce analyte levels even more [1,3]. Regardless of digest technique, liquid chromatographic (LC) fractionation of the resulting peptide pool is required before further analysis can be attempted.

Covalent structural analysis of peptides usually involves, at least in part, Edman-chemical sequencing [4–6]. However, automated chemical sequencing, when carried out at low picomole levels (initial yields <2 pmol), does have its shortcomings [7,8]. For instance, ambiguous calls in the first two cycles, gaps in sequences and inability to identify the C-terminal Lys or Arg (of tryptic peptides) are a frequent occurrence. In addition, micro-heterogeneities (*e.g.* isoforms) exist among naturally occurring peptides, that may also have ragged ends. Furthermore, most modified amino acids (*e.g.* phospho-, glyco-, etc.) cannot be directly identified. Accurate mass measurements could greatly facilitate interpretation of such complex and/or incomplete chemical peptide micro sequencing data. Matrix-assisted laser-desorption time-of-flight mass spectrometry (MALDI-TOF-MS) has emerged as a popular choice in this regard for reasons of high sensitivity, accuracy and ease of operation [9–11].

As chemical sequencing [7,8,12] and MALDI-MS [13,14] have become increasingly more sensitive, it seems clear that the LC technique providing the highest sensitivity would be ideally suited for peptide separation. Luckily, progress in micro-preparative RP-HPLC during the last decade has been phenomenal. Through down-sizing of column I.D. from the once customary 4.6 mm [15,16] to well below 1 mm [17,18], purifiable amounts of peptide and corresponding peak elution volumes have decreased by almost three orders of magnitude [19–21]. However, Edman-sequencing and MALDI-MS are not easily "on-line" coupled to LC. Therefore, samples must be collected, stored and transferred.

It has been noted that those sample handling routines, using laboratory techniques and supplies from the "nanomole" era of protein chemistry, have become increasingly inefficient [7,20]. Clumsy sample handling may very well be the real reason for failure of numerous high-sensitivity sequencing projects (*i.e.* those carried out at levels approaching femtomoles). The protein chemistry community is currently struggling to come to grips with this problem, let alone solving it quickly. It can be argued that the multi-step process of protein isolation, digestion, peptide LC purification and chemical sequencing, including the required sample transfers, is only going to be as good as the proverbial "weakest-link-in-the-chain". Femtomole-level capillary LC of peptides seems therefore to be of somewhat excessive power, unless "on-line" connected to a femtomole-level analytical technique (*e.g.* LC–MS).

In this report, we present the results of an investigation of various microbore (columns of 1.0 mm I.D.) RP-HPLC components and experimental variables. Great attention was given to the specific aspects of processing *in situ* digest peptide mixtures for analysis by combined chemical sequencing–MALDI-MS. By also applying rigorous sample handling routines and peak selection criteria, protocols are now available for micro-digestions/separations at high volumes (*e.g.* core facility settings) and without jeopardizing quality.

2. Experimental

2.1. Materials

SKI PepMix6 is a mixture of 14 synthetic peptides, ranging in size from 9 to 26 amino acids, as listed in Table 1. Syntheses were carried out at the MSKCC Microchemistry Facility by Ms. Deborah Desrouilleres. The mix (on the average, 200 pmol per peptide per μl water) was periodically remade from separate stock solutions that, each time, had been requantitated by amino acid composition analysis. Peptides were represented in the mix in slightly varying molar ratios (see Table 1) to yield a RP-HPLC profile with roughly equal sized peaks. With the average peptide concentration being assigned the arbitrary value of 1.0, concentrations of constituent

Table 1
Components of SKI PepMix6

No.	Sequence	Length	Net charge	Aromatic amino acids	Molar ratio
1	SIINFEKLT	9	0	F	1.3
2	WFRKRGSQQP Q	11	+3	FW	0.65
3	HHQKLVFFAE D	11	+1	FF	0.45
4	DAEFRHDAGY EV	12	−2	FY	1.1
5	LQYTEHQQLE GWK	13	0	YW	0.65
6	QGMLPEDLSS VIR	13	−1	–	1.8
7	QLQKDKQVYR ATHR	14	+4	Y	1.05
8	TPTPNPPTTE EEKTE	15	−3	–	1.05
9	NISPKSYDDF ISRNK	15	+1	Y	0.8
10	RAGGTQRVEV LEGRT-amid	15	+2	–	1.75
11	ELVEPLTPSG EAPNQALLR	19	−2	–	1.25
12	TPYSWDLPEP RSRSAKIRVH PR	22	+4	YW	0.6
13	ISCWAQIGKE PITFEHINYE RVSDR	25	+1	FYWpC	1.05
14	KDELPQLVTL PHPNLHGPEI LDVPST	26	−1	–	0.6

Peptides were synthesized, purified and quantitated at the MSKCC Microchemistry Facility. Length and net charge are listed. Molar ratio indicates the correction factor to be applied for calculation of the "real" molar amount of each peptide in the mixture; when, for instance, it is stated that 5 pmol mix was used, molar ratios of 1.3 or 0.65 indicate 6.5 or 3.25 pmol, respectively.

peptides ranged in value from 0.45 to 1.75. Aliquots of 5 μl (1 nmol per peptide, on the average) were stored at −70°C for one-time use.

Preparative tryptic (trypsin from Boehringer, Indianapolis, IN, USA) digestion of horse cytochrome *c* (Sigma, St. Louis, MO, USA) was carried out as described [15] and a stock solution (in water) of 48 pmol/μl (by amino acid composition analysis) was aliquoted in 20 μl volumes (960 pmol total) and stored at −70°C for one-time use.

Proteins used in the various applications described in this report were studied under collaborative agreements or were submitted to the MSKCC Microchemistry Facility for covalent structural analysis. As the results have not yet been published, protein sources and biological functions are subject to confidentiality agreements. All "unknown" proteins were prepared by SDS-polyacrylamide gel electrophoresis (PAGE), electroblotted onto nitrocellulose (Schleicher and Schuell, Keene, NH, USA) and visualized by amido black (Serva, Paramus, NJ, USA) staining. Bands of interest were excised, digested *in situ* with 1 μg trypsin (sequencing grade from Boehringer), and the resulting peptide mixture reduced and S-alkylated with, respectively, β-mercaptoethanol (BioRad, Richmond, CA, USA) and 4-vinylpyridine (Aldrich, Milwaukee, WI, USA), all as described [1]. Trypsin blanks were prepared as controls.

All other chemicals, supplies, equipment and parts were as indicated elsewhere in this Experimental section.

2.2. Microbore RP-HPLC assembly

The microbore system used in this study was based on a previously described narrow-bore HPLC design/assembly [1]. In the current configuration we have used a 140B Solvent Delivery System equipped with a 75-μl dynamic mixer (Applied Biosystems, Foster City, CA, USA). A precolumn filter with a 0.5-μm frit (Upchurch Scientific, Oak Harbor, WA, USA) was plumbed between the mixer and a Rheodyne 7125 injector (Rainin, Ridgefield, NJ, USA) using two pieces [27 cm × 0.007 in. I.D. (1 in. = 2.54 cm)] of polyetheretherketone (PEEK) tubing (Upchurch). The injector was fitted with a 50-μl loop and connected to the column inlet with PEEK tubing (30 cm × 0.005 in.). Total pre-column

volume (including mixer and loop) was therefore 145 μl. The outlet of the column was connected directly to a glass capillary (20 cm × 280 μm O.D./75 μm I.D.; 0.88 μl) (LC Packings, San Francisco, CA, USA) with the appropriate PEEK sleeve (Upchurch) and stainless-steel fitting. By swaging a stainless-steel fitting to the PEEK sleeve the capillary can be held tightly and then adjusted to avoid dead volume; the final assembly to the column outlet is then made. The back-end of the glass capillary was connected to the flow cell of an Applied Biosystems (AB) 783 detector with the appropriate hardware and in the same manner as the front-end. The flow cells used were as follows: AB "straight-shaped" with 2.4 μl volume/6 mm pathlength (AB P/N:2900-0197) and 0.5 μl volume/1 mm pathlength (AB P/N:2900-0034), AB "L-shaped" with 2.4 μl volume/6 mm pathlength (AB P/N:2900-0195), and LC Packings U-Z View 35 nl volume/8 mm pathlength (Kratos compatible). The outlet tubing of the AB flow cells was a 15 cm long, 75 μm I.D. glass capillary. When installing the LC Packings capillary flow cell, the outlet of the column was plumbed directly to the leading portion of the capillary; the trailing portion of the capillary cell was trimmed to a 15 cm length and threaded out of the detector head. In all cases, the 15 cm length resulted in a post flow cell volume of 0.66 μl and a collection delay of only 1.3 s at a flow-rate of 30 μl/min; this allowed real time collection of peaks. The SGE columns required zero dead volume (ZDV) unions (Valco Instrument, Houston, TX, USA) to mate their 1/16 in. O.D./50 μm I.D. Polysil tubing to the PEEK inlet tubing and glass capillary outlet tubing. Analog signals from the 783 detector were registered with a Kipp and Zonen Model BD 41 dual pen stripchart recorder (VWR, Piscataway, NJ, USA); signals were also sent to a Model 970 A/D converter (PE Nelson, Cupertino, CA, USA) and chromatograms analyzed and plotted using PE Nelson Turbochrom 3 (version 3.2) software.

Columns used in this study were: Vydac 218TP5115 C_{18} (5-μm particles, 300 Å pore size; 150 × 1 mm column dimension) and 214TP5115 C_4 (5 μm, 300 Å; 150 × 1 mm) from The Separations Group (Hesperia, CA, USA), SGE Inertsil 100GL-1-ODS-I10/5 C_{18} (5 μm, 150 Å; 100 × 1 mm) and SGE ODS-2 C_{18} (5 μm, 300 Å; 100 × 1 mm) from Scientific Glass Engineering (Austin, TX, USA), and Brownlee Aquapore RP-300 C_8 (7 μm, 300 Å; 250 × 1 mm) and Aquapore OD-300 C_{18} (7 μm, 300 Å; 100 × 1 mm) from Applied Biosystems (purchased from Rainin, Woburn, MA, USA).

2.3. RP-HPLC operation and sample handling

All columns were operated at a flow-rate of 30 μl/min and at ambient temperature, except where indicated. Solvent A consisted of 0.1% trifluoroacetic acid (TFA) (Pierce, Rockford, IL, USA) in fresh Milli Q water and solvent B was 0.09% TFA in 70% aqueous acetonitrile (Burdick and Jackson, Muskegon, WI, USA); solvents were always made in dedicated glass measuring cylinders, mixed thoroughly and sonicated (Branson Ultrasonics, Danbury, CT, USA) for 5 min before use. Gradient elution of peptides was typically done by linear increase of solvent B at a rate of 1 or 2% per min (5–50%B/45 min or 5–50%B/22.5 min), except were indicated.

Frozen aliquots of PepMix6 (1 nmol of each peptide per 5 μl) or cytochrome *c*/tryptic peptides (960 pmol per peptide in 20 μl) were diluted with 2% TFA (Pierce) to give a volume of 100 or 96 μl, respectively. Further serial dilutions were then made in 2% TFA (or 20% in some experiments) to yield 5, 2.5, 1.25 and 0.625 pmol amounts of peptide mix per 50 μl solvent (typically in a much larger volume to allow overfilling of the loop). In case of *in situ* digests, nitrocellulose was removed by centrifugation and rinsed once with 25 μl 5% acetonitrile (Burdick and Jackson)–100 m*M* ammonia bicarbonate, under sonication. Supernatants were pooled, and reduced and alkylated (see Materials). In every instance, the samples were injected immediately after they had been prepared, except where noted.

Samples were then introduced in the injector, either by overfilling an empty loop or by careful displacement of solvent A from the loop to

guarantee, respectively, accurate injections of defined quantities of the standards or introduction of 100% of the "unknown" peptide mixtures. After injection, columns were eluted isocratically (at 5%B) until the void peaks had passed and the baseline was back to its pre-injection level; at this point, the gradient was started manually as was the data acquisition (time zero).

Column peak fractions (typically about 20 μl) were collected by hand in 0.5-ml polypropylene Eppendorf tubes (National Scientific Supply Co., San Rafael, CA, USA) and kept on ice until the end of the experiment. Aliquots were then withdrawn for mass analysis and the rest frozen at −70°C until chemical sequencing. Fractions were never dried or concentrated. For repurifications, fractions were acidified with 5 μl TFA and then two-fold diluted with solvent A before injection (by two succesive injections of about 25 μl each).

2.4. Edman-chemical sequencing of peptides

Purified peptides were sequenced with the aid of an AB Model 477A automated sequenator, operated according to the principles outlined by Hewick *et al.* [4]. Stepwise liberated phenylthiohydantoin (PTH)–amino acids were identified using an "on-line" 120A HPLC system equipped with a PTH C_{18} (220 × 2.1 mm; 5 μm particle size) column (AB). The standard AB method was optimized for sub-picomole PTH–amino acid analysis, as described by members of our laboratory [7,12]. After storage, column fractions were always supplemented with neat TFA (to give a final concentration of 10%) before loading onto the sequencing disc as it has been shown that this increases recoveries from the test tube for most peptides [7].

2.5. Mass spectrometry of peptides

Peptide mass analysis was carried out by MALDI-TOF-MS using a Vestec (Houston, TX, USA) LaserTec ResearcH instrument, with a 337-nm output nitrogen laser and a 1.2-m flight tube, operated according to published principles [9,22]; 28-kV ion acceleration and 4.3-kV multiplier voltage were used. The instrument has a built-in video camera for real-time inspection of the laser beam impact on the target area. Tektronix (Beaverton, OR, USA) Model 2225 single-channel analog (50 MHz, real time) and Model TDS520 dual-channel digitizing (500 MHz:500 Ms/s, averaging) oscilloscopes are connected in parallel to the detector for data acquisition; digitized spectra are downloaded to a ZEOS 486 33Mz computer. *m/z* Spectra are generated using the GRAMS (Galactic Ind., Salem, NH, USA) data analysis software.

Steel probe tips (pins) were cleaned by sonication in 5% acetic acid for 5 min, followed by washing with water and acetonitrile, and air drying. Matrix solution was prepared freshly by dissolving 10 mg α-cyano-4-hydroxycinnamic acid (ACCA) (Sigma) in 1 ml of a 0.1% TFA–33% aqueous acetonitrile solution, followed by vigorous vortexing and brief centrifugation (Eppendorf); only the supernatant was used for sample preparation. Working stocks of calibrants [peptides Apid ($MH^+ = 2109.45$) and Ova ($MH^+ = 980.00$)] were stored in 25 μl aliquots at − 20°C for one-time use; concentrations were: 1 pmol Apid + 2 pmol Ova per μl of 0.1% aqueous TFA. Just prior to use they were either 4-fold or 20-fold diluted (depending on estimated amounts of analyte) by addition of, respectively, 75 μl or 475 μl of 2% TFA–33% aqueous MeCN, and kept on ice. In this order, matrix (1 μl), analyte (1 μl) and calibrant mixture (0.5 μl) were spotted on the pin, using separate pipette tips, and mixed *in situ* by pipetting up and down (3 times). Samples were then air-dried at room temperature for 30 min. For more details and a full description of the actual laser-desorption MS experiments (acquiring data), analyte/calibrant adjustments and final data analysis, we refer to an earlier publication [10].

3. Results and discussion

3.1. Why use 1.0 mm I.D. columns for micro-preparative peptide purification?

There are two aspects to the LC miniaturization trend of the last decade, namely pioneering

of new technology and then applying it to biological/medical research. Columns of ever narrower I.D. (bore) were introduced and shown, through the use of chromatographic standards, to be of substantial promise. General applications however, must always await commercial availability of (i) optimally packed columns and (ii) special hardware components and parts required to upgrade existing HPLC systems. By the time the user community has widely adopted a new, more sensitive level of LC experimentation, pioneering laboratories have already reached the next (or several) level(s) down.

Even though the aims of LC development are (or should be) to extend the realm of applications, both areas are quite specialized, come with their own set of rules and, most importantly, should not be confused with one another. For example, when it is obvious that a certain level of LC-sophistication is either unnecessary, inefficient or extremely impractical (or all of the above) for a specific application, then why use it?

New developments have been introduced at a fast pace and it has been clear for some years now that molecular separations in packed 50 μm I.D. columns are certainly feasible [17,18]. However, for every down-sizing step (from 4.6 to 2.1 to 1.0 to sub-1 mm I.D.), manufacturers have struggled somewhat (to very seriously) to produce columns at high volume, and with uncompromised chromatographic performance as compared to the wider-bore predecessors. While 2.1 mm columns [1,6,23] have succesfully replaced the 4.6 mm ones [16,24] for micropreparation of peptides, 1.0 mm (microbore) columns are not yet widely used for this purpose; this, despite the fact that they have been commercially available for years. When, some three years ago, this laboratory tried to switch to microbore columns for peptide applications, we failed; peak resolution was unacceptable [38]. Because of these observations and similar ones made in other laboratories, and with the sharp rise in fame of home-made capillary (sub-mm I.D.) columns during the last three to four years [19–21,25], there has been a movement to just skip the 1.0 mm level.

Recently however, we became aware of the commercial availability of a newer generation of microbore columns; actually, they contained the same packing materials that have been successfully used by some of the authors for years [1,16]. As covalent structural analysis of peptides is practiced exclusively by chemical sequencing in our laboratory, and for the reasons already discussed, we felt that 1.0 mm I.D. columns should be reevaluated. This report describes these studies and subsequent applications.

3.2. Instrument assembly and operation

As microbore LC can be considered to be at the extreme lower end of classical HPLC, there was no need for specialized components such as flow splitters etc. [20,21], just standard hardware. This allowed us to draw heavily from our earlier experiences with HPLC configuration-design and assembly [1]. The guiding principle then was to minimize total dead-volumes, from mixing-T to column, and certainly post-column. To allow "real-time" manual collection (*i.e.* by visually monitoring the analog peak signals on a stripchart recorder), lag time should be near zero. With a post-flow cell volume of only 0.66 μl and a flow of 30 μl/min, collection delay is a negligible 1.3 s. Description of the entire microbore HPLC assembly can be found under Experimental; the choice of flow cell was made after a comparative study (see below).

In the past, we have satisfactorily operated 2.1 mm columns at flows of 100 μl/min, typically with gradients of 0.7% acetonitrile increase per min [1]. For a scaled-down column, the flow should be decreased proportionally to the square of the inside column radius; *i.e.* for 1.0 mm I.D. this would then become 22.7 μl/min. Systematic investigation of such typical operating variables as flow, gradient slope and temperature indicated that peptide retention, peak shape and height were all affected (data not shown) exactly as predicted from the long established ground-rules of standard-bore RP-HPLC (for review of those, see ref. 26). While it appeared that a flow of 23 μl/min may indeed have been chromatographically optimal, practical considerations such as reproducibility (shaky gradients) and time

(long experiments) eventually mandated a routine flow of 30 μl/min. This has since been shown adequate in several dozens of applications [see Figs. 6 and 8, and unpublished observations (1993)]. We have also maintained our previous gradient conditions at ambient temperature.

Injection volumes of up to 200 μl (containing less than 10% acetonitrile and less than 3% TFA) can easily be tolerated (data not shown). Standard, we have used a 50-μl injector loop as that was sufficient for nearly all applications. Chromatographic effects of high concentrations TFA in the sample are discussed further in this text.

3.3. Column evaluation

Six different columns were chosen for evaluation. The non-arbitrary selection was the result of our previous experiences with the same packings in bigger columns. Two carefully quantitated peptides mixtures were prepared for these investigations: cytochrome *c* tryptic peptide mix [15] and an artificial mixture of 14 synthetic peptides (SKI PepMix6), ranging in size from 9 to 26 amino acids (listed in Table 1). Sizes were specifically chosen to reflect the mass distribution of the pertinent peptides in an "average" tryptic digest; bigger peptides usually do not recover all that well from reversed-phase supports and smaller ones, albeit well recovered, are essentially uninteresting for most of our studies (aimed at providing the information for protein identification or gene cloning experiments).

RP-HPLC separation profiles of 5 pmol PepMix6 (average for the 14 peptides, with distribution ranging from 2.25 to 8.75 pmol) and 2.5 pmol cytochrome *c* tryptics are shown in Fig. 1. Even though no efforts have been made to identify all peaks or align the chromatograms, it appears that the profiles are reasonably comparable and generally satisfactory. All 14 PepMix6 peptides are accounted for on the Vydac C_4 profile only (although two late eluting peaks have almost merged). This may have been just a lucky coincidence as overall resolution on the Vydac C_4/C_{18}, Inertsil C_{18} and SGE ODS-2 columns was essentially the same. It should also

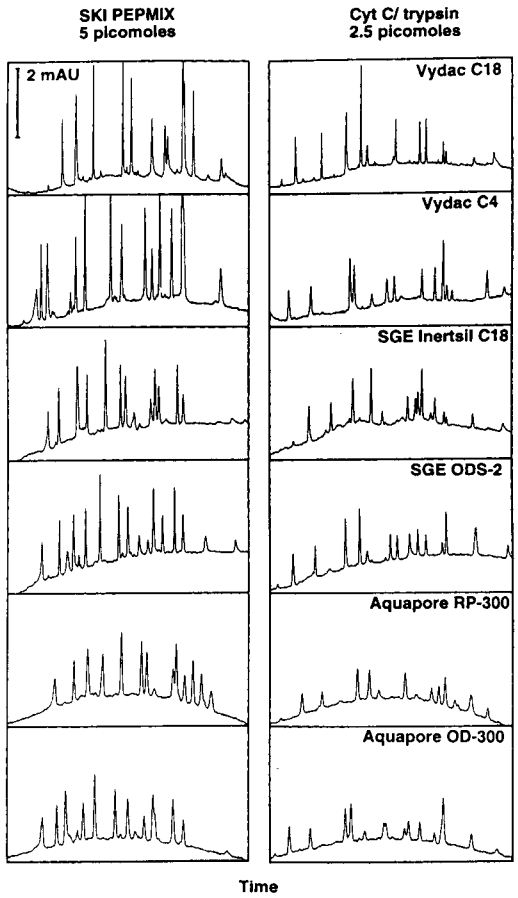

Fig. 1. Comparison of 1.0 mm I.D. reversed-phase columns for peptide separation. RP-HPLC profiles of 5 pmol PepMix6 (composition listed in Table 1) and 2.5 pmol cytochrome *c* tryptic peptides are shown. HPLC configuration was as described under Experimental; an LC packings U-Z view flow cell was used. Columns are indicated on each panel; column specifications can be found under Experimental. Chromatographic conditions were: a linear two-step acetonitrile gradient (in 0.1% TFA) of 3.5–35%/45 min, 35–70%/22.5 min at a flow-rate of 30 μl/min and at ambient temperature; samples were injected in 50 μl of 2% TFA. Full scale on each panel corresponds to 0.004 AU at 214 nm; time scale is from 15 to 50 min.

be noted that elution profiles of the peptide mixtures were near identical between 1.0 and 2.1 mm I.D. columns filled with the same Vydac packings (dat not shown). In keeping with earlier observations [16,26], late eluting peptides also recovered well from the C_4 support here; this should be kept in mind when designing LC

experiments. The Aquapore resins consistently showed wider peaks, most likely related to their bigger particle size (7 μm). Although we have no strong preference as yet for any particular column packing, we assume that Vydac and SGE microbore columns may be logical partners for high-resolution two-dimensional RP-HPLC separations. A minor disadvantage of SGE columns, in our view, are the unusual endfittings, requiring adaptors (Valco ZDV unions) to connect them to our standard plumbings.

3.4. Detector flow cells and wavelength

Flow cells that come standard with the Applied Biosystems (AB) microbore LC package have a 6 mm path length and a 2.4 μl volume. Therefore, at a flow of 30 μl/min, it takes nearly 5 s for the void volume to be completely displaced, while during all that time mixing occurs. This raises legitimate questions about peak broadening and remixing of closely eluting peptides.

As flow cells can be easily interchanged in the AB 783 detector, we evaluated two different sub-μl volume models, the 1 mm path length (0.5 μl volume) type from the same manufacturer and a longitudinal capillary cell from LC packings (Model U-Z view). Whereas the former is still an assembly of the classical housing with two windows and in/out fittings, the newer type cell consists of a 75 μm I.D. glass capillary, bent in a U-shape and held by a metal template to align the 6 mm long center portion of the U with the optical axis [27]. As the U-Z cell is nothing else but a capillary, no mixing or band-spreading should occur. The chromatograms shown in Fig. 2, generated by separation of 5 pmol cytochrome *c* tryptics on a Vydac 1.0 mm I.D. C_{18} column operated in our LC system but using different flow cells, seem to confirm this presumption. However, whereas peak heights obtained with the U-Z cell were clearly larger than with the 1 mm path length cell, they were about three-fold smaller than those with the 6-mm AB cells. In addition, at 5 pmol analyte levels, peak signal-to-noise ratios were 636, 358, 252 and 49 for, respectively, the 6-mm AB (straight), 6-mm AB (L-shaped), 1-mm AB and the U-Z view cells. Nonetheless, we have opted for the U-Z view cell as standard feature in our microbore LC systems for the reasons discussed below.

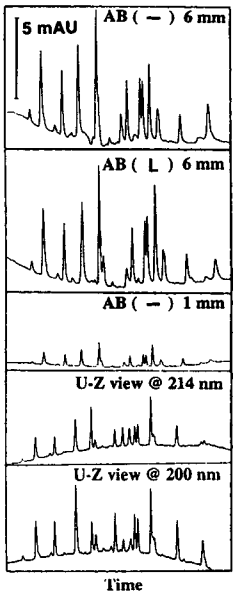

Fig. 2. Comparison of detector flow cells and wavelengths for peptide detection in microbore RP-HPLC. RP-HPLC profiles of 5 pmol cytochrome *c* tryptic peptides are shown. HPLC configuration was as described under Experimental; a 1.0 mm I.D. Vydac 218 TP5115 C_{18} column was used. Flow cell type is indicated on the panels and their specifications can be found under Experimental; symbols: — = straight shaped flow path; L = L-shaped flow path. Chromatographic conditions were: a linear two-step acetonitrile gradient (in 0.1% TFA) of 3.5–35%/22.5 min, 35–70%/12.5 min at a flow-rate of 30 μl/min and at ambient temperature; samples were injected in 50 μl of 2% TFA. Scale of absorbance units at 214 nm (or 200 nm in the bottom panel) is indicated by the vertical bar (0.005 AU) and applies to all panels; the time scale is from 12 to 33 min. Peak signal-to-noise ratios were (from top panel to bottom panel): 636, 358, 252, 49 and 52.

Even though the incentive for evaluating 1.0 mm I.D. columns was increased sensitivity, it should not be forgotten that the purpose of the LC experiment is to provide peptides, sufficiently homogeneous to yield interpretable chemical sequencing data. As conclusive sequencing results are the sole objective of the applications laboratory, resolving power of the micro-preparative LC system should be safeguarded in an uncompromising way. Unquestionably, this was

best accomplished when the detector was fitted with the U-Z view flow cell (Fig. 2). Our conclusion was subsequently validated by the results of several hundred sequencing experiments that showed a significantly lower incidence of mixed sequences, thus indicating absence of peptide cross-contaminations.

The three-fold reduction in peptide detection sensitivity, as compared to the AB 6 mm path length flow cell, can be partially offset in two ways. First, we found that the most sensitive detector AUFS settings (*i.e.* what the operator sees on the stripchart recorder while collecting fractions) that could be routinely obtained were about two-fold better for the U-Z view flow cell (10 mAUFS *versus* 20 mAUFS for the AB 6-mm cell). Through meticulous, but time consuming, baseline optimization, the absolute AUFS values could be further reduced for both cells, but the ratios remained unchanged (*e.g.* 5 *versus* 10 mAUFS). Second, as had already been demonstrated [20,21], enhanced sensitivity of peptide detection can be attained using an U-Z view cell and at a wavelength of 195 nm. A quick investigation in our laboratory confirmed these findings but also resulted in the following additional observations. At a 0.01 AUFS detector setting, (i) 200 nm is really the practical lower limit as at 195 nm the baseline is nearly uncontrollable, and (ii) using an AB 6-mm flow cell, detection at wavelengths below 210 nm is essentially impossible for the same reasons. Thus, for all practical purposes, real-time sensitivity of U-Z flow cells approaches that of the classical 6-mm types. On the other hand, a previously reported drawback of the U-Z view cell, namely its limited dynamic range (*i.e.* signal saturation at 50 pmol level [21]), is not a real concern as these amounts of peptide are very seldom chromatographed in our laboratory.

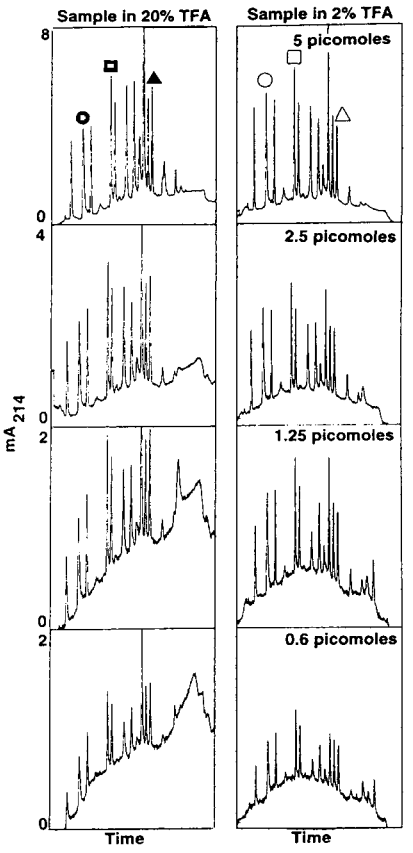

Fig. 3. Sensitivity of peptide detection in microbore RP-HPLC. RP-HPLC profiles of various quantities of PepMix6 (composition listed in Table 1) are shown. HPLC configuration was as described under Experimental; a 1.0 mm I.D. Vydac 218 TP5115 C_{18} column and an LC packings U-Z view flow cell were used. Amounts of PepMix6 are indicated on the panels; samples were injected in 50 μl of 2 or 20% TFA (indicated). Chromatographic conditions were: a linear two-step acetonitrile gradient (in 0.1% TFA) of 3.5–35%/22.5 min, 35–70%/12.5 min at a flow-rate of 30 μl/min and at ambient temperature. Time scale is from 15 to 32 min; AUFS values vary between panels, as indicated. Symbols: ○, □, and △ indicate the peaks corresponding to peptides 7, 4 and 13, respectively (sequences listed in Table 1).

3.5. Peptide detection sensitivity

With our microbore LC configuration established, we carried chromatographic separations of increasingly reduced quantities of PepMix6 (from 5 pmol down to 625 fmol); the results are shown in Fig. 3. It appeared that, under ideal conditions, peptides could be satisfactorily separated and collected at the 1–2 pmol level and analytical experiments with 625 fmol of peptide mix still yielded clearly discernible peaks.

In the course of the present studies we made the very important observation, essentially confirming limited data described in an earlier

report [7], that at dilute concentrations, low picomole amounts of many peptides tend to "disappear" from the solutions. As the protein chemistry community is just brushing femtomole level polypeptide isolation and sequencing, the problem of minute peptide losses during preparation, storage and transfer has either not been fully recognized or has been blamed on unrelated factors. Several studies on femtomole level peptide chromatography have indeed been performed by injecting very small volumes (1–5 μl) of rather concentrated stock solutions; in the other cases, where large volumes (50 μl or more) of dilute stocks were injected, poor recoveries have typically been blamed on column losses, an often abused term for lack of any other reasonable explanation (as for instance in ref. 1). We show here that these column losses are minimal.

High losses during sample handling can be satisfactorily reduced in the presence of 20% TFA, with 2% being the lowest TFA concentration to yield a significant effect [7]. When serial dilutions of PepMix6 were prepared in either 2 or 20% TFA for chromatographic injection, a near linear relationship was found between peak detection signals and the amount of peptide (Fig. 4); in water, most peptides were poorly recovered, or not at all, once below the 10 pmol level (data not shown). The presence of high acid concentrations is mostly required for large size (> 20 amino acids) and/or hydrophobic peptides; *i.e.* those that typically elute late

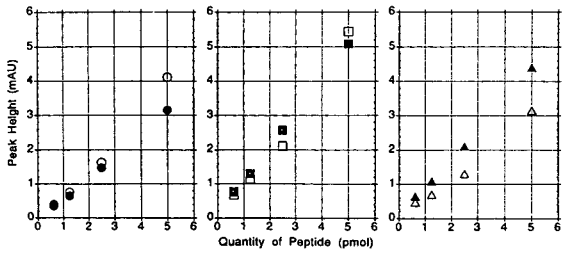

Fig. 4. Molar sensitivities of peptide detection in microbore RP-HPLC. The data are taken from the chromatographic experiments shown in Fig. 3. Symbols as in Fig. 3; open and closed symbols indicate TFA concentrations in the injected sample (50 μl) of 2 and 20%, respectively. Precise amounts of peptides were calculated using the molar ratios listed in Table 1.

from reversed-phase supports. Figs. 3 and 4 clearly illustrate that, while peptides eluting in the early-to-mid section of the chromatogram are well recovered when injected in 2% acid, dramatic reduction of peak heights in the late portion resulted from sample preparation in 2% TFA, as compared to 20% acid. Drawbacks of injecting peptide mixtures in high acid concentrations are (i) the enormous void peak that takes at least 30 min to pass the detector, and (ii) broadening of the early peaks with concomitant reduction in size (Fig. 4). The latter is not really a consideration for most applications; unfortunately, the long wait at the beginning of the chromatographic run will be a necessary inconvenience until alternative remedies can be recommended.

Finally, if the specifics of an experiment should call for low acid concentrations, it is recommended to immediately (*i.e.* within 1 min) inject the sample onto the column. The value of this advisory can not be better illustrated than by the chromatographic data shown in Fig. 5. Two peptide mixtures (2.5 pmol each; prepared by two-way splitting of one 5-pmol sample) diluted in 50 μl of 2% TFA were analyzed, the first immediately after preparation, and the second after keeping the vial on the bench for 4 h. In the latter experiment, half of the peaks were gone and the others had decreased substantially.

When using appropriate sample handling routines, it is clear that the practical (*i.e.* routine operation) sensitivity of the LC system described in this report equals, probably surpasses, that of advanced chemical microsequencing (2 pmol minimally required; for example, see Fig. 7). We feel that it is certainly adequate at this time.

3.6. Practical peptide preparation

As already alluded to, a major obstacle in chemical microsequencing is the frequent occurrence of post-translationally modified N-termini (mostly acetylated). This renders the affected proteins inaccessible for cyclic chemical degradation, a condition well know under the term "blocked". In the absence of an adequate remedy (*i.e.* efficient deblocking), internal se-

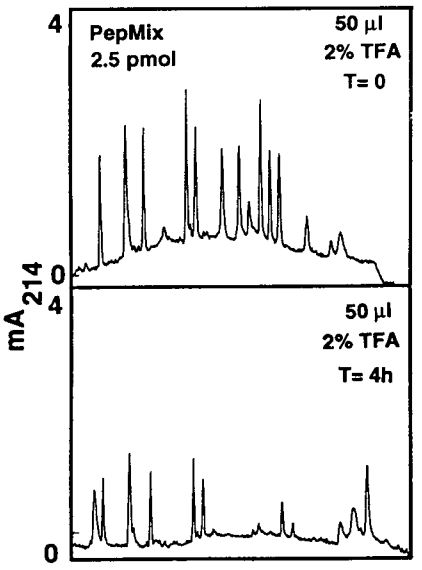

Fig. 5. Effects of storage on recovery of low picomole amounts of diluted peptides. RP-HPLC profiles of 2.5 pmol PepMix6 (composition listed in Table 1) are shown; two samples (2.5 pmol each; prepared by two-way splitting of one 5 pmol sample) were diluted into 50 µl of 2% TFA and injected, the first (shown in top panel) immediately after preparation, and the second (bottom panel) after keeping the vial on the bench for 4 h. HPLC configuration was as described under Experimental; a 1.0 mm I.D. Vydac 218 TP5115 C_{18} column and an LC packings U-Z view flow cell were used. Chromatographic conditions were: a linear two-step acetonitrile gradient (in 0.1% TFA) of 3.5–35%/22.5 min, 35–70%/12.5 min at a flow-rate of 30 µl/min and at ambient temperature. Full scale on each panel corresponds to 0.004 AU at 214 nm; time scale is from 15 to 32 min.

quence analysis is the only alternative. This requires cleavage of the protein and separation of the resulting peptides. Different techniques, including for proteins separated on gels, have been developed for this purpose [1,28–31]. A blocked protein should, therefore, no longer serve as a cheap excuse for failure, nor be the reason for abandoning a preferred research strategy. In our laboratory, we have selected the Aebersold method [28] for *in situ* proteolysis and adapted it for routine use at the 10–20 picomole level [1]. Current efforts to further improve on this technique require the use of microbore RP-HPLC (this study) and implementation of various new precautions, in addition to the ones discussed in the previous section, to guarantee acceptable recoveries at every step.

Since it is not the topic of this paper, we will only briefly touch on the major categories of micro-preparative "rules" that have not yet been discussed: (i) low picomole level sequencing cannot be done in a dirty laboratory crowded with people that are not strictly needed there; (ii) sophisticated HPLC systems should be operated and maintained with great care and discipline, including daily chromatography of several control standards and blanks; (iii) formulation of peak selection criteria have been necessitated by a growing volume of digests while trying to limit the number of wasted sequencing runs on protease-derived peptides (from autolysis), peptide mixtures and ghost peaks. MALDI-MS now features a prominent role in these pre-Edman routines (see further). A detailed account on the practical aspects of micro-preparation will be published elsewhere. The importance of the sample preparation for successful sequencing cannot be sufficiently emphasized. Without it, sophisticated microsequencer and mass spectrometry improvements, no matter how well thought of, are essentially useless.

Two issues directly related to microbore RP-HPLC deserve further comment, fraction collection and peptide rechromatography. At a flow of 30 µl/min, peaks will typically elute in 20–30 µl of solvent. This volume is about equal to the small drops forming at the end of the glass capillary outlet tubing. When the beginning of a peak is observed, the forming droplet is quickly removed with a kimwipe and the fraction collected by holding the end of the capillary, so that it just touches the wall of the micro-Eppendorf tube. The delay time of 1.3 s conveniently allows for this little manipulation. The acetonitrile-containing solvent has a low viscosity and flows easily to the tip of the tube. No droplet is formed; this limits the collection volume and allows efficient collection of closely eluting peaks. Tedious as this manual collection may be, by comparison, so called "smart" automated fraction collectors are totally inadequate.

For repurifications, fractions (20 µl) should be acidified with 5 µl TFA (for reasons discussed

earlier) and then diluted two-fold with solvent A before injection. We have not yet worked out the details for optimal microbore two-dimensional HPLC column combinations. Our only experiences to date have been with rechromatographies of peptides eluted from an Inertsil C_{18} column on the same column but using a shallower gradient (typically 0.35% acetonitrile per min). As the example of a real-life sample in Fig. 6 shows, recoveries after such rechromatographies were on the order of 40–60% (as determined from peak heights); repurified peptides proved to be homogeneous (by sequencing analysis). Care should be taken to dilute early eluting peaks more than average to avoid peak broadening (as sadly illustrated for peak T17 in Fig. 6).

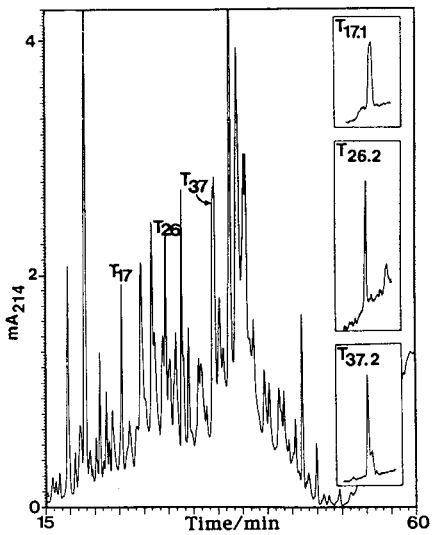

Fig. 6. Repurification of peptide peaks obtained from microbore RP-HPLC. RP-HPLC profile of a peptide mixture, obtained after *in situ* tryptic digestion of protein CM-CRKAp110; precise amount of protein was not known but estimated, from amido black staining of the nitrocellulose blot, to be about 10 to 15 pmol. Peaks T17, T26, and T37 (indicated) were rechromatographed on the same column after addition of 5 μl neat TFA and two-fold dilution with water; results are shown in the insets. HPLC configuration was as described under Experimental; a 1.0 mm I.D. SGE Inertsil 100 GL-1-ODS-I10/5 C_{18} column and an LC packings U-Z view flow cell were used. Chromatographic conditions were: a linear two-step acetonitrile gradient (in 0.1% TFA) of 3.5–35%/45 min, 35–70%/22.5 min at a flow-rate of 30 μl/min and at ambient temperature, for the primary separation; gradient during each rechromatography was 3.5–35%/90 min. Full scale corresponds to 0.004 AU at 214 nm; the same absolute scale also applies to the sections of the secondary chromatograms (insets).

3.7. Micro-chemical sequencing of peptides

As shown, microbore RP-HPLC allows the recovery of 2–3 pmol of peptides, which can be used for direct sequencing. The initial coupling yields during chemical analysis could then be 1–2 pmol or less. Subpicomole PTH–amino acid identification is therefore required; in general, the method of choice is "on-line" narrow-bore HPLC. Rare examples have appeared in the literature where subpicomole sequencing was done and even fewer described how the sequence calls were actually made [1,3,32,33]. This can be explained, in part, by the fact that in biological research papers short thrift is usually given to the details of peptide sequencing experiments, as they were done *in the core facility* and, apparently, the fee-for-service status degrades this integral part of the research process to the level of purchasing a chemical. Nonetheless, it is fair to state that, until recently, peptide sequencing with femtomole level signals was very difficult.

This laboratory has had a longstanding interest in development and application of high-sensitivity sequencing techniques; details of these studies, technical and biological, are beyond the scope of this report and can be found elsewhere [1,7,12,23,32–35]. However, considering the fact that these accomplishments were made possible for a large part by the progress of HPLC technology (both for peptide and PTH separations), it may be of interest to the reader/chromatographer to view an example of an extended sequencing run carried out on an estimated 2 pmol (by peak height) of an unknown polypeptide. Fig. 7 contains the chromatograms of 23 consecutive cycles of PTH–amino acid identification of peptide JE-HAIICK-T51.3, isolated from a digest mixture by two rounds of microbore LC, all with signals in the femtomole range.

To specifically prepare the sequencer/analyzer instruments for an experiment as shown in Fig. 7 may take several days of meticulous optimizations and tests, at least in our hands. Still, in all

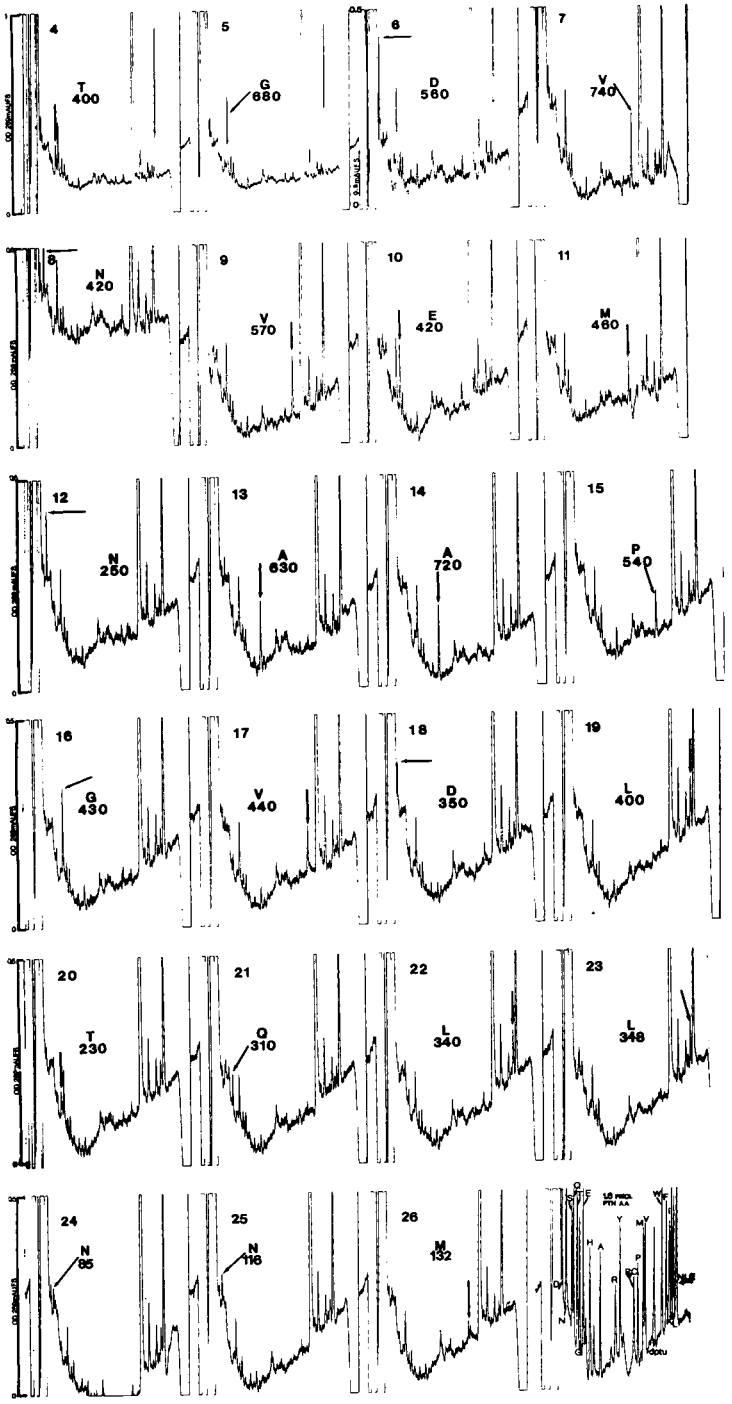

Fig. 7. Micro-chemical peptide sequence analysis. Amino acid sequence analysis of a tryptic peptide, isolated by microbore RP-HPLC from an *in situ* digest of electrophoretically separated (and blotted) protein JE-HAIICK. Sequencing conditions were as listed under Experimental. Starting amount of peptide was estimated to be 2 pmol (from LC peak height). Chromatograms 4–26 are shown; full scale corresponds to 0.001 AUFS for cycles 4 and 5 and 0.0005 AUFS for cycles 6–26. PTH–amino acid peaks are indicated with an arrow and the femtomolar quantities shown. A chromatographic standard (1.6 pmol of each amino acid in the sequencer flask) is shown at the bottom right; scale of the standard is 0.001 AUFS at 269 nm.

too many cases, high-sensitivity chemical sequencing data turn out to be non-ideal, *i.e.* complex and/or incomplete. For instance, ambiguous calls in the first two cycles (due to amino acid contaminants), gaps in sequences (associated with PTH–W,–C,–H,–R,–S etc. at levels below 200–500 fmol) and inability to identify the C-terminal Lys or Arg (of tryptic peptides) are a frequent occurrence. In addition, mixed peptides yield mixed sequences. An additional, complimentary, analytical technique was therefore required for error-free gap-filling and deconvolution of sequence data.

3.8. Combined Edman-chemical–MALDI-MS peptide sequencing

If MS is going to be routinely used in combination with Edman-chemical sequencing, one should be able to cope with a wide array of applications and diversity of situations (*e.g.* varying peptide quantities, sizes, mixtures, etc.), especially in a core facility setting where throughput is an issue as well. High throughput does not leave much room for improvization or unlimited trial and error. Thus, a generally applicable protocol needed to be developed for facile, reproducible mass analysis. It is imperative that for combined Edman–MS sequencing to be successful, (i) accuracy of the mass measurements must be within 1 u (for peptides up to 4000 dalton) and (ii) peptide consumption for MS must be kept to the absolute minimum. A bonus from routine mass spectrometric prescreening of peptides is that mixtures and artefacts (*e.g.* trypsin autolytic products, chemical background) can be weeded out to save valuable sequencing time and expenditure.

Both electrospray-MS [36] and MALDI-MS [10] have recently been shown to be of practical utility in this regard, but to date, no careful comparative studies have been conducted to evaluate the preferred use of one or the other technique in any particular situation. As a more theoretical treatise of MALDI *versus* electrospray ionization is outside the scope of this report, the most obvious practical difference is the suitability of the latter for "on-line" connection with LC. Although this may offer an advantage in terms of MS analysis automation, column eluates need to be split for "on-line" MS and "off-line" sequencing, still mandating fraction collection. During LC–MS, the mass analyzer is also dedicated to a single HPLC system. In contrast, "off-line" MALDI-TOF-MS accommodates post-run analysis of peak fractions from several LC experiments carried out concurrently, a frequently occurring situation in our laboratory. Since there is usually no pressing need to analyze each and every peak of a digest, we feel that MALDI-MS is certainly adequate. Here, we will present a case study, illustrating the capabilities of Edman–MALDI-MS sequencing.

In collaboration with the laboratory of Dr. F. Ulrich Hartl (MSKCC), protein JF-HSP75 was purified by SDS-PAGE, electroblotted onto nitrocellulose, stained with amido black, the band excised and digested *in situ* with trypsin, all as described [1]. Peptide fragments were separated by microbore RP-HPLC; the resulting chromatogram is shown in the top panel of Fig. 8. Peptide T54, because of its position in the late part of the chromatogram, was analyzed first. MALDI-MS (bottom panel of Fig. 8) indicated the presence of a single peptide of about 23–25 amino acids in length. Some 20 residues could be sequenced (Table 2), allowing a Genbank search, which turned up an excellent match with the sequence of yeast HSP70 [37]. The m/z value for T54 (2628.4) was in excellent agreement with the value ($MH^+ = 2627.92$) for the predicted tryptic peptide (residues 572–596) which contains the limited sequence, so confirming the identity of the entire peptide.

The identification of protein HSP70 was then confirmed by matching experimental m/z values of several more peptides with theoretical values of predicted tryptic fragments. Theoretical average isotopic masses were calculated from the published sequence [37] using ProComp version 1.2 software (obtained from Dr. P.C. Andrews, University of Michigan, Ann Arbor, MI, USA). Examples (peptides T18, T46 and T51) are given in Table 2; in all cases, discrepancies between m/z and theoretical [MH^+] were less than 0.6 dalton.

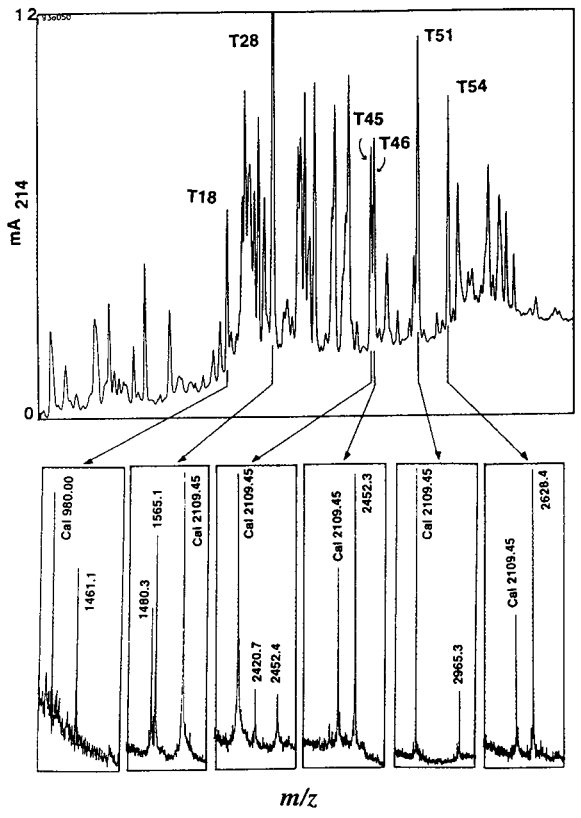

Fig. 8. Peptide microbore RP-HPLC with MALDI-MS analysis. Protein JF-HSP75 was purified by SDS-PAGE, electroblotted onto nitrocellulose, stained with amido black, the band excised and digested *in situ* with trypsin, all as described [1]. Peptide fragments were separated by microbore RP-HPLC; the resulting chromatogram is shown in the top panel, with a time scale from 20 to 65 min. HPLC configuration and conditions were the same as described under Fig. 6. Portions (1 μl) of selected peak fractions were taken for MALDI-TOF analysis using a Vestec LaserTec ResearcH instrument; conditions were as described under Experimental. Relevant sections of the mass spectra are shown (bottom panel); m/z values are listed for all peaks, including the calibrants (cal).

As this study was one of the first examples of mass-aided protein identification in our laboratory, additional peptide peaks were analyzed by chemical sequencing to confirm the result. Peptide T45 (Fig. 8) yielded two peak m/z values, one of them near identical to the single peak m/z value found for partially co-eluting peak T46. However, sequence analysis of T45 indicated a major and a very minor sequence (Table 2) that could easily be separated. As sequencing yields are indicative for the amounts of peptides applied, this clearly shows that no quantitative conclusions can be drawn from the equal sized m/z peaks observed during MALDI-MS analysis (Fig. 8, bottom panel).

The major sequence obtained for T45, however, was not perfect. Ser was only tentatively identified in cycle one due to the presence of various other (contaminating) amino acids; a misinjection occurred during analysis of the PTH-residue in cycle 10. The mass summed from the identified residues fell 272.9 short of the experimental m/z (Table 2). Assuming a Ser in position one and a Lys at the end (obligatory C-terminal Lys or Arg for all tryptic peptides), a mass discrepancy of 57.6 was still unaccounted for. This value was sufficiently close to the average isotopic mass of Gly (57.05) and far enough removed from the second nearest amino acid mass (Ala at 71.08) to reliably position the former residue at cycle ten (as confirmed by the published sequence [37]).

A similar analysis was carried out for peptide T28 (Table 2). Again, a major and minor sequence were observed, as were two peak m/z values. The major sequence differed from the expected mass (m/z = 1565.1) by 155.5, allowing the positioning of Arg (average isotopic mass = 156.19) at the C-terminus. The mass summed from the minor sequence was 455.1 less than expected. Assuming that the two tentative assignments (Val at cycle 6; Glu at cycle 12) were correct and an Arg at the C-terminus, 70.66 was still unaccounted for, leading us to assign Ala (average isotopic mass = 71.08) to cycle 7. Thus, complete structures of peptides could be proposed on the basis of incomplete sequence and accurate mass.

3.9. Conclusions

We have described the optimized configuration of a microbore RP-HPLC system for the purification of low picomole quantities of peptides. This required evaluation and selection of appro-

Table 2
Tryptic peptide analysis by combined chemical sequencing–laser-desorption mass spectrometry

Peptide	Sequence	$[MH^+]$ part. seq.	m/z	Difference/ a.a. assigned	Position HSP-75	$[MH^+]$ HSP-75
T18	ND	NA	1461.1	NA	332–345	1460.63
T28(a)	AVITVPAYFNDAQ.. (major)	1409.6	1565.1	$155.5/R_{14}$	144–157	1565.78
(b)	VTPSF(v)xFTPE(e).. (minor)	1025.2	1480.3	$455.1/V_6A_7E_{12}R_{13}$	39–51	1480.67
T45(a)	(s)TSGNTHLGx#QDFDTNLLEHF..	2147.8	2420.7	$272.9/S_1G_{10}K_{22}$	224–245	2420.10
(b)	QxLExYVA.. (very minor)	722.8	2452.4	1729.6/none	544–565	2451.75
T46	ND	NA	2452.3	NA	544–565	2451.75
T51	ND	NA	2965.3	NA	276–302	2965.17
T54	xKIEAALSDALAALQIE(d)PxA..	1825.1	2628.4	803.3/none	572–596	2627.92

Selected peak fractions from the chromatographic separation shown in Fig. 8 were analyzed by chemical sequencing (Sequence) and by MALDI-MS (m/z; see also Fig. 8, bottom panel). Symbols (used in sequences): amino acids printed in lower case (and in parentheses) were assigned with a lower level of confidence; x = no amino acid assigned; $x^{\#}$ = no assignment due to instrument failure; .. = no further sequence calls but unlikely to be the C-terminus. ND = not done; NA = not applicable. $[MH^+]$ part. seq. denotes the mass values calculated by summing the average isotopic masses of all amino acids that were positively identified during chemical sequencing. Difference/a.a. indicates the difference between experimental mass (m/z) and the calculated mass of the partial sequence (MH^+ part. seq.), and the amino acids assigned to the gaps as to yield a perfect match between calculated and experimental masses. Position HSP-75 indicates the location of the peptide in the published sequence [37] that was retrieved by searching Genbank. $[MH^+]$ HSP-75 denotes the theoretical average isotopic mass of the peptide, calculated from the published sequence using ProComp software.

priate columns (1.0 mm I.D.), detector flow cells and wavelengths, and overall assembly with minimal dead volume. We found that the sensitivity of our system equalled, probably surpassed, that of advanced chemical micro-sequencing (2–4 pmol minimally required [3,7]).

As a chemical sequencer cannot be "on-line" connected with a micro-preparative HPLC system, fractions must be collected and transferred. With a typical flow of 30 μl, efficient manual collection is possible and fractions (about 20 μl in volume) can still be handled without unacceptable losses, albeit with great precautions. Furthermore, major difficulties were encountered to quantitatively load low- or sub-picomole amounts of peptide mixtures efficiently onto the RP-HPLC column for separation. Discipline and rigorous adherence to sample handling protocols are thus on order when working at those levels of sensitivity.

With adequate instrumentation and handling procedures in place, low-picomole amounts of peptides (< 5 pmol) could be easily prepared for analysis by combined chemical sequencing–MALDI-MS. The power of this approach resides in the complementarity of these two analytical techniques. Aside from the fact that MS provides a simple and ultra-sensitive way to pre-screen peptides for sequencing, mass-aided interpretation of Edman-chemical sequencing data has allowed (i) confirmation of the results, (ii) deconvolution of mixed sequences, (iii) proposal of complete structures on the basis of partial sequences, and (iv) confirmation of protein identification (obtained by database search with a single, small stretch of peptide sequence) by mass-matching of several more peptides with predicted proteolytic fragments.

4. Acknowledgements

The authors are indebted to Deborah Desrouilleres for synthesis of the peptides used in this study. The frequent help of Lynne Lacomis, Eileen Kelly and Mike Powell, with experiments and instruments, is also greatly appreciated. We thank The Separations Group (Hesperia, CA, USA) for letting us evaluate their microbore columns. The MSKCC Microchemistry Facility is

supported by NCI Core Grant 5 P30 CA08748-29.

5. References

[1] P. Tempst, A.J. Link, L.R. Riviere, M. Fleming and C. Elicone, *Electrophoresis*, 11 (1990) 537–553.

[2] R. Aebersold, in A. Chrambach, M.J. Dunn and B.J. Radola (Editors), *Advances in Electrophoresis*, Vol. 4, VCH, New York, NY, 1991, pp. 81–168.

[3] S.W. Wong, C. Grimley, A. Padua, J.H. Bourell and W.J. Henzel, in R.H. Angeletti (Editor), *Techniques in Protein Chemistry IV*, Academic Press, San Diego, CA, 1993, pp. 371–378.

[4] R.M. Hewick, M.W. Hunkapiller, L.E. Hood and W.J. Dreyer, *J. Biol. Chem.*, 256 (1981) 7990–7997.

[5] J.E. Shively, R.J. Paxton and T.D. Lee, *Trends Biochem. Sci.*, 14 (1989) 246–255.

[6] R.J. Simpson, R.L. Moritz, G.S. Begg, M.R. Rubira and E.C. Nice, *Anal. Biochem.*, 177 (1989) 221–236.

[7] H. Erdjument-Bromage, S. Geromanos, A. Chodera and P. Tempst, in R.H. Angeletti (Editor), *Techniques in Protein Chemistry IV*, Academic Press, San Diego, CA, 1993, pp. 419–426.

[8] S.M. Mische, K.U. Yuksel, L.M. Mende-Mueller, P. Matsudaira, D.L. Crimmins and P.C. Andrews, in R.H. Angeletti (Editor), *Techniques in Protein Chemistry IV*, Academic Press, San Diego, CA, 1993, pp. 453–461.

[9] F. Hillenkamp, M. Karas, R.C. Beavis and B.T. Chait, *Anal. Chem.*, 63 (1991) 1193A–1203A.

[10] S. Geromanos, P. Casteels, C. Elicone, M. Powell and P. Tempst, in J.W. Crabb (Editor), *Techniques in Protein Chemistry V*, Academic Press, San Diego, CA, 1994, pp. 143–150.

[11] K. Williams, R. Kobayashi, W. Lane and P. Tempst, *ABRF News*, 4 (4) (1993) 7–12.

[12] P. Tempst and L. Riviere, *Anal. Biochem.*, 183 (1989) 290–300.

[13] B.T. Chait, R. Wang, R.C. Beavis and S.B.H. Kent, *Science*, 262 (1993) 89–92.

[14] T.M. Billeci and J.T. Stults, *Anal. Chem.*, 65 (1993) 1709–1716.

[15] P. Tempst, M.W. Hunkapiller and L.E. Hood, *Anal. Biochem.*, 137 (1984) 188–195.

[16] P. Tempst, D.D.L. Woo, D.B. Teplow, R. Aebersold, L.E. Hood and S.B.H. Kent, *J. Chromatogr.*, 359 (1986) 403–412.

[17] M. Novotny, *Anal. Chem.*, 60 (1988) 500A–510A.

[18] K.E. Cobb and M. Novotny, *Anal. Chem.*, 61 (1989) 2226–2231.

[19] W.J. Henzel, J.H. Bourell and J.T. Stults, *Anal. Biochem.*, 187 (1990) 228–233.

[20] R.L. Moritz and R.J. Simpson, *J. Chromatogr.*, 599 (1992) 119–130.

[21] M.T. Davis and T.D. Lee, *Protein Science*, 1 (1992) 935–944.

[22] R.C. Beavis, T. Chaudhary and B.T. Chait, *Org. Mass Spectrom.*, 27 (1991) 156–158.

[23] T. Sollner, S.W. Whiteheart, M. Brunner, H. Erdjument-Bromage, S. Geromanos, P. Tempst and J.E. Rothman, *Nature*, 362 (1993) 318–324.

[24] P. Parker, L. Coussens, N. Totty, L. Rhee, S. Young, E. Chen, S. Stabel, M.D. Waterfield and A. Ullrich, *Science*, 233 (1986) 853–859.

[25] D.F. Hunt, R.A. Henderson, J. Shabanowitz, K. Sakaguchi, H. Michel, N. Sevilir, A.L. Cox, E. Appella and V.H. Engelhard, *Science*, 255 (1992) 1261–1266.

[26] P. Tempst, L.E. Hood and S.B.H. Kent, in H.F. Linskens and J.F. Jackson (Editors), *Modern Methods of Plant Analysis*, Vol. 5, Springer, Heidelberg, pp. 170–208.

[27] J.P. Chervet, M. Ursem, J.P. Salzmann and R.W. Vannoort, *J. High Resolut. Chromatogr.*, 12 (1989) 278–281.

[28] R.H. Aebersold, J. Laevitt, R.A. Saavedra, L.E. Hood and S.B.H. Kent, *Proc. Natl. Acad. Sci. USA*, 84 (1987) 6970–6974.

[29] C. Eckerskorn and F. Lottspeich, *Chromatographia*, 28 (1989) 92–94.

[30] J. Fernandez, M. DeMott, D. Atherton and S.M. Mische, *Anal. Biochem.*, 201 (1992) 255–264.

[31] J. Rosenfeld, J. Capdevielle, J.C. Guillemot and P. Ferrara, *Anal. Biochem.*, 203 (1992) 173–179.

[32] T. Jayaraman, A.M. Brillantes, A.T. Timerman, S. Fleischer, H. Erdjument-Bromage, P. Tempst and A.R. Marks, *J. Biol. Chem.*, 267 (1992) 9474–9477.

[33] N.C. Andrews, H. Erdjument-Bromage, M.B. Davidson, P. Tempst and S.H. Orkin, *Nature*, 362 (1993) 722–728.

[34] S. Ghosh, A.M. Gifford, L.R. Riviere, P. Tempst, G.P. Nolan and D. Baltimore, *Cell*, 62 (1990) 1019–1029.

[35] G.P. Nolan, S. Ghosh, H.C. Liou, P. Tempst and D. Baltimore, *Cell*, 64 (1991) 961–969.

[36] D. Hess, T.C. Covey, R. Winz, R.W. Brownsey and R. Aebersold, *Protein Science*, 2 (1993) 1342–1351.

[37] M.R. Slater and E.A. Craig, *Nucleic Acids Res.*, 17 (1989) 4891.

[38] C. Elicone and P. Tempst, unpublished results (1990).

ELSEVIER

Journal of Chromatography A, 676 (1994) 139–153

JOURNAL OF CHROMATOGRAPHY A

Reversed-phase chromatography of synthetic amphipathic α-helical peptides as a model for ligand/receptor interactions Effect of changing hydrophobic environment on the relative hydrophilicity/hydrophobicity of amino acid side-chains

Terrance J. Sereda[a], Colin T. Mant[a], Frank D. Sönnichsen[b], Robert S. Hodges*,[a]

[a]*Department of Biochemistry and the Medical Research Council of Canada Group in Protein Structure and Function, University of Alberta, Edmonton, Alberta T6G 2H7, Canada*

[b]*Protein Engineering Network of Centres of Excellence, University of Alberta, Edmonton, Alberta T6G 2H7, Canada*

Abstract

To mimic a hydrophobic protein binding domain, which is a region on the surface of a protein that has a preference or a specificity to interact with a complementary surface, we have designed amphipathic α-helical peptides where the non-polar face interacts with the non-polar surface of a reversed-phase stationary phase. Two series of potentially amphipathic α-helical peptides, a native Ala peptide (AA9) and a native Leu peptide (LL9), were designed where the native peptide contains 7 residues of either Ala or Leu, respectively, in its non-polar face. This design results in an overall hydrophobicity of the non-polar face of the Leu peptide that is greater than that of the non-polar face of the native Ala peptide. Mutants of the native Ala-face peptide, AX9, and the native Leu-face peptide, LX9, were designed by replacing one residue in the centre of the non-polar face in both series of peptides. Therefore, by changing the hydrophobicity of the environment surrounding the mutated amino acid side-chain, the effect on the hydrophilicity/hydrophobicity of each amino acid side-chain could be determined. Using the substitutions Ala, Leu, Lys and Glu, it was shown that the maximum hydrophilicity of these amino acid side-chains could be determined when the environment surrounding the mutation is maximally hydrophobic; whereas its maximum hydrophobicity can be determined when the environment surrounding the mutation is minimally hydrophobic. This procedure was further extended to the remaining amino acids commonly found in proteins and it was determined that this general principle applies to all 20 amino acids. These results have major implications to understanding the hydrophilicity/hydrophobicity of amino acid side-chains and the role side-chains play in the folding and stability of proteins.

1. Introduction

One of the most interesting developments of liquid chromatography analysis lies in the employment of reversed-phase liquid chromatography (RPLC) as a physicochemical model of biological systems. Studies in this area have generally centred on attempting to correlate the retention behaviour of peptides [1] or proteins [2–6] during RPLC with their conformational stability; the rationale behind this approach lies

* Corresponding author.

0021-9673/94/$07.00
SSDI 0021-9673(94)00371-F

in the assumption that the hydrophobic interactions between peptides and proteins with the non-polar stationary phase characteristic of RPLC [7] reflects the interactions between non-polar residues which are the major driving force for protein folding and stability. A recent report [8] also suggested that the hydrophobic stationary phase in RPLC may be a reasonable mimic for the hydrophobic environment created internally by proteins, e.g., as a probe of how the pK_a values of potentially ionizable side-chains in the hydrophobic interior of a protein, frequently important in catalytic groups, are influenced by their environment. Indeed, RPLC provides an excellent example of the way the original purpose for method development of a particular chromatographic mode may be transcended by its employment in a different field.

Another area of profound biological importance where RPLC is likely to be a good model is that of ligand–receptor interactions. A ligand binding domain may be defined as the region on the surface of a receptor protein that has a preference or specificity to interact with a complementary surface. In addition, this region may be a protrusion, depression or groove that is surface exposed. The complementary surface to such a receptor binding domain may be another protein, peptide, macromolecule or other non-protein surface. In a similar manner to their importance in folding and stabilization of proteins, hydrophobic interactions also play a key role in the binding of such ligands to their receptors. Although the concept of employing RPLC as a mimic of such ligand–receptor interactions is not new, little has been reported to date to verify the potential of this approach mainly due, in the authors view, to the lack of a flexible and well defined model system.

Horváth et al. [9] postulated 18 years ago that the hydrophobic surface characteristic of the stationary phase of reversed-phase packings may be a useful probe of amphipathic helices induced or stabilized in hydrophobic environments. Indeed, this structural motif has much to recommend it as a part of a ligand–receptor model system, in terms of practical considerations and biological relevance. From the latter perspective, amphipathic α-helical structures are an important determinant of the biochemical and/or pharmacological properties of peptide hormones and neurotransmitters [10–13]; a whole class of cytotoxic peptides, including bee or wasp venom peptides such as melittin or one of the mastoparans, are capable of forming amphipathic α-helices upon binding to hydrophobic surfaces [14–20]; amphipathic helices putatively have a role in the activation of G proteins (trimeric GTP-binding regulatory proteins) by membrane receptors and peptides [21,22], including mastoparan [23]; the high amphipathic helical content of the antibiotic family of peptides known as magainins enables them to interact strongly with bacterial and acidic model membranes [24,25]; finally, other functions of amphipathic helices in ligand–receptor interaction include their involvement in T-cell recognition [26], lipid-associating domains of apolipoproteins and lipoproteins [27,28] and the hydrophobic domains of coiled-coil proteins that bind to DNA (the so-called leucine-zipper proteins) [29,30]. From a practical point of view, model single-stranded amphipathic α-helices have much to offer in terms of both stable three-dimensional structure capable of tolerating sequence changes, as well as relatively straightforward chemical synthesis of analogues [31,32]. In addition, since the hydrophobic domain of these model amphipathic helices will bind preferentially to a hydrophobic stationary phase, even subtle environmental variations within this domain may well be expressed as a variation in RPLC retention behaviour.

In the present study, we describe a simple model ligand–receptor system based on observing the retention behaviour during RPLC of de novo designed single-stranded amphipathic α-helical peptides. In addition, as an initial evaluation of this system, we set out to determine whether, and to what extent, the relative hydrophilicity/hydrophobicity of a centrally located side-chain in the hydrophobic domain of the amphipathic helix was determined by its environment.

2. Experimental

2.1. Materials

HPLC-grade water and acetonitrile were obtained from BDH (Poole, UK). Trifluoroacetic acid (TFA) was obtained from Aldrich (Milwaukee, WI, USA). Trifluoroethanol (TFE) was obtained from Sigma (St. Louis, MO, USA).

2.2. Instrumentation

Peptide synthesis was carried out on an Applied Biosystems peptide synthesizer Model 430 (Foster City, CA, USA). Crude peptides were purified by an Applied Biosystems 400 solvent-delivery system connected to a 783A programmable absorbance detector.

The analytical HPLC system consisted of an HP1090 liquid chromatograph (Hewlett-Packard, Avondale, PA, USA), coupled to an HP 1040A detection system, HP9000 series 300 computer, HP9133 disc drive, HP2225A Thinkjet printer and HP7460A plotter.

Amino acid analyses of purified peptides were carried out on a Beckman Model 6300 amino acid analyser (Beckman Instruments, Fullerton, CA, USA).

The correct primary ion molecular masses of peptides were confirmed by time-of-flight mass spectroscopy on a BIOION-20 Nordic (Uppsala, Sweden).

Circular dichroism (CD) spectra were recorded on a JASCO J-500C spectropolarimeter (Easton, MD, USA) attached to a JASCO DP-500N data processor and a Lauda (Model RMS) water bath (Brinkman Instruments, Rexdale, Canada) used to control the temperature of the cell. The instrument was routinely calibrated with an aqueous solution of recrystallized *d*-camphorsulphonic acid at 290 nm. Constant nitrogen flushing was employed.

2.3. Peptide synthesis

Peptides were synthesized by the solid-phase technique (SPPS) on co-poly(styrene–1% divinylbenzene) benzhydrylamine–hydrochloride resin (0.92 mmol/g resin) as previously described [8]. The cleaved peptide–resin mixtures were washed with diethyl ether (3 × 25 ml) and the peptides extracted with neat acetic acid (3 × 25 ml). The resulting peptide solutions were then lyophilized prior to purification.

2.4. Columns and HPLC conditions

Crude peptides were purified on a semi-preparative Synchropak RP-P C_{18} reversed-phase column (250 × 10 mm I.D., 6.5-μm particle size, 300-Å pore size) from Synchrom, Lafayette, IN, USA. The peptides were purified at pH 2 by linear AB gradient elution (0.5% B/min) at a flow-rate of 5 ml/min, where eluent A is 0.1% aqueous TFA and eluent B is 0.1% TFA in acetonitrile.

Analytical runs were carried out on an Aquapore RP-300 C_8 reversed-phase column (220 × 4.6 mm I.D., 7-μm particle size, 300-Å pore size) from Applied Biosystems, by employing linear AB gradient elution (1% B/min) at a flow-rate of 1 ml/min, using the same eluents as above.

2.5. Calculation of accessible surface areas

All peptide structures were generated in an idealized conformation using equilibrium bond lengths, and angles and dihedral angles (Insight II, Biosym Technologies, San Diego, CA, USA). Backbone dihedral angles were set to ideal α-helical values of -67 for ϕ and -44 for ψ [33]. The structures were subsequently relaxed by conducting 100 steps of steepest descent and 2000 steps of conjugate gradient minimization in vacuum using a distance-dependent dielectric model [34]. The minimizations were performed with Discover (Biosym) and the consistent valence force field (CVFF) on a Silicon Graphics Crimson Elan workstation. The solvent-accessible surface areas of the minimized peptides were calculated using a 1.4-Å solvent probe in the program Anarea [35]. Individual surface areas

per atom were summed to yield hydrophobic, hydrophilic and charged surface areas according to the definition by Eisenberg and McLachlan [36].

3. Results and discussion

3.1. Design of ligand–receptor model system

We wished to pursue an incremental approach to assessing factors involved in ligand–receptor interactions. By reducing the number of variables in a defined model system, it was felt that both interpretation of results and their extrapolation to biological systems would be simplified. Since a minimum of two hydrophobic surfaces are involved in ligand–receptor interactions, the basic requirements for a flexible model system are: (1) the hydrophobic surface representing the protein receptor may remain constant, whilst that representing the ligand is varied; (2) conversely, the surface representing the protein receptor is varied, whilst that representing the ligand remains constant; (3) finally, the relative hydrophobicity of the surfaces representing both the ligand and receptor are varied concomitantly.

For this initial study, only one surface was varied. Thus, option 1 was selected, i.e., it was decided to vary the hydrophobic surface of the ligand, represented by the hydrophobic face of the synthetic amphipatic α-helical peptide analogues; the non-variable hydrophobic surface of the receptor was represented by the stationary phase of the reversed-phase column.

As noted by Opella et al. [37], relatively short polypeptide sequences perform functional roles as isolated molecules, as oligomers and as domains of large proteins. Indeed, many of the physical (and chemical) properties of large proteins are retained by synthetic oligomeric analogues. Thus, the results of working with a defined model peptide representing a ligand binding to a protein receptor may potentially be directly applied to naturally occurring ligands of similar size; alternatively, such results may be extrapolated to amphipathic sequences within larger polypeptides and proteins responsible for binding to a protein receptor.

3.2. Design of model "native" synthetic amphipatic α-helical peptide

We have designed and synthesized an 18-residue peptide ligand for our model ligand–receptor model system. The amino acid sequence is Ac–Glu–Leu–Glu–Lys–Leu–Leu–Lys–Glu–Leu–Glu–Lys–Leu–Leu–Lys–Glu–Leu–Glu–Lys–amide, which has a high potential to form an amphipathic helix (Fig. 1, right). In the design of this peptide, leucine, glutamic acid and lysine residues were selected in light of their highly intrinsic helical propensities [38–40]; leucine as a non-polar aliphatic residue and glutamic acid and lysine as, respectively, potentially negatively charged and positively charged residues, depending on pH.

The amino acid sequences of amphipathic α-helices tend to have a strong periodic distribution of hydrophobic amino acids along the chain with three to four residue repeats [41–43] and this is reflected in the design of the "native" model peptide ligand. In addition, the glutamic acid/lysine pairs located in i and $i+3$ or i and $i+4$ positions along the sequence could provide additional stability to the α-helical structure by intra-chain side-chain electrostatic interactions [44,45] at neutral pH values.

Fig. 1 (right) represents this "native" sequence as an α-helical net, with the hydrophobic face of the helix consisting of leucine residues and the opposite hydrophilic face of the helix consisting of lysine and glutamic acid residues. It should be noted that the width of the hydrophobic face, involving 7 hydrophobic residues at positions 2, 5, 6, 9, 12, 13 and 16 (between the solid lines), as expressed in this helical net representation is wider than the relatively narrow hydrophobic face (between the dotted line and the right-hand solid line) of amphipathic α-helices making up two-stranded α-helical coiled-coil structures in which there is a 3–4 hydrophobic repeat [32,41,46–48], involving 5 hydrophobic residues at positions 2, 5, 9, 12 and 16. It was felt that the wider hydrophobic face of our model peptide

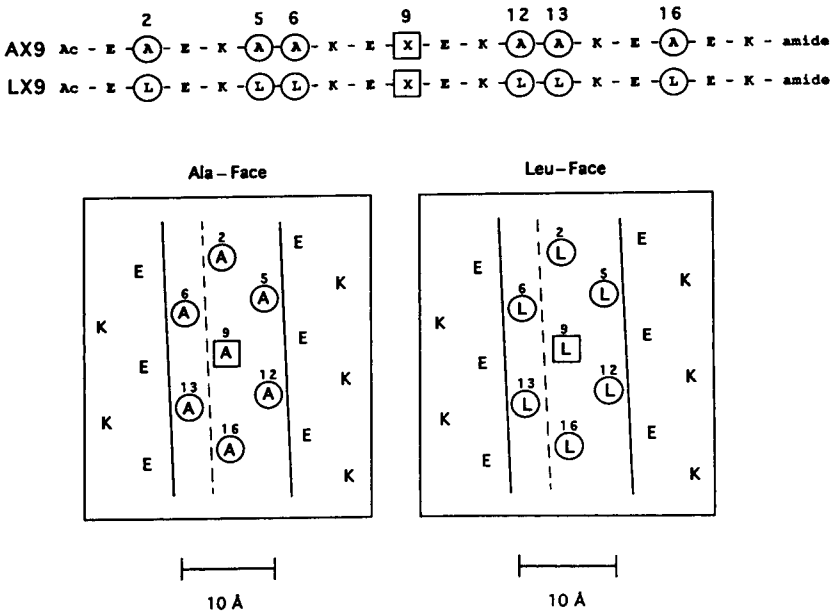

Fig. 1. Design of model synthetic peptides. Top: sequence of mutant peptides, AX9 and LX9, where the first letter represents amino acid residues used in the hydrophobic face of the peptide, the X represents each of the 20 amino acids (boxed) (single letter code given in Table 1) substituted at position 9. The residues that are circled or boxed and labelled 2, 5, 6, 9, 12, 13 and 16 are in the hydrophobic face of the amphipathic α-helical peptides. Lysine and glutamic acid residues make up the hydrophilic face of the amphipathic helix. Bottom: "native" Ala-face (AA9, left) and Leu-face (LL9, right) model peptides represented as α-helical nets. The radius of the α-helix is taken as 2.5 Å with 3.6 residues per turn, a residue translation of 1.5 Å and thus a pitch of 5.4 Å. The area between the solid lines on the α-helical nets represents the wide hydrophobic face of the peptides. The area between the dotted line and the right-hand solid line in the α-helical net representations of the "native" peptides represents the narrower hydrophobic face (made up of a 3–4 or 4–3 hydrophobic repeat) characteristic of coiled-coil peptides (see text for details).

would have more validity as a general mimic of the non-polar face of ligands from a wide variety of sources than the relatively narrow hydrophobic face characteristic of amphipathic α-helices present in coiled-coil systems. Other advantages of this wide hydrophobic face will become apparent below.

3.3. Conformation and helicity of model peptide ligands

The α-helicity of the "native" peptide ligands was determined by CD, with the CD spectrum measured in 0.1 *M* KCl + 50 m*M* potassium phosphate buffer (pH 5.2)–TFE (1:1, v/v), a solvent that induces helicity in single-chain potentially α-helical peptides [49,50]. Studies [51,52] have shown that the presence of 50% TFE will ensure that the high amphipathicity of a peptide, such as our model ligands, does not lead to aggregation in aqueous solution through intermolecular hydrophobic interactions. The observed ellipticity of −26 640 degree cm^2/dmol for the model peptide (LL9) in 50% TFE yielded an estimate of 86% α-helix in solution, based on a value of −31 060 degree cm^2/dmol calculated for a 100% α-helical 18-residue peptide [53].

3.4. Choice of hydrophobic stationary phase

As noted above, in this initial study, the non-polar stationary phase of a reversed-phase packing represents the hydrophobic binding region of

a protein receptor. However, although the hydrophobicity of a specific reversed-phase packing is constant, as required for the present study, we still wished there to be a scope for a variation in overall stationary phase hydrophobicity for future investigations, i.e., it was deemed important to retain flexibility in the characteristics of the second component of our ligand–receptor model. A silica-based stationary phase was chosen for the following reasons: (1) the stability (particularly at low pH) and efficiency of such columns makes them particularly advantageous for peptide separations [7]; (2) the nature of the functional group attached to the silica matrix (e.g., C_1, C_3, C_8, C_{18}, CN, phenyl) offers a wide choice of stationary phase hydrophobicity and (3) the ligand density may be varied, also offering a range of stationary phase hydrophobicity. Concerning points 2 and 3, it is possible to prepare and pack silica-based stationary phases of varying functional group and/or ligand density in the laboratory [54]; thus, the potential for tailored stationary phases then becomes an option, considerably enhancing the flexibility of the ligand–receptor model.

For this initial study, a C_8 packing was used. In addition to the common usage of such columns for peptide separations [7], the specific column employed has, in our hands, proved to be reliably stable and efficient.

3.5. Retention behaviour of amphipathic α-helices during RPLC

On binding to a reversed-phase column, the high hydrophobicity of the stationary phase stabilizes secondary (α-helical) structure, mimicking, in fact, the effect of TFE when the peptide is in solution. Indeed, Zhou et al. [52] demonstrated that amphipathic peptides remain α-helical when bound to a reversed-phase column and, due to the preferred binding domain created by the non-polar face of the α-helix, are considerably more retentive than peptides of the same composition but lacking the preferred binding domain.

3.6. Effect of environment on relative hydrophobicity/hydrophilicity of amino acid side-chains

It is known that amino acid side-chain hydrophobicities are influenced by the proximity of other polar or charged atoms [55]. Thus, it is not unreasonable to assume that the proximity of non-polar groups may have a similar fundamental effect on the relative hydrophilicity/hydrophobicity of amino acid side-chains. Such an effect would have profound implications for side-chains involved in biologically important hydrophobic interactions such as those which characterize ligand–receptor interactions. Thus, the model ligand–receptor system presented in this study was now applied to the question of whether and how the hydrophilic/hydrophobic characteristics of an amino acid side-chain are affected by a varying local hydrophobic environment of the ligand (non-polar face of an amphipathic α-helix).

3.7. Design of model peptide series exhibiting varying hydrophobic environment

Two series of synthetic amphipathic peptide analogues were prepared, with their non-polar faces representing homogeneous hydrophobic domains of very different hydrophobicities (Fig. 1). The most hydrophobic series of analogues was based on the "native" model peptide described above (Fig. 1, right), with leucine at all of the hydrophobic positions along the sequence: the "leucine domain" or "Leu-face". The 20 amino acids found in proteins are substituted at residue 9 (the central boxed residue in the helical net presentation; Fig. 1, right). The second series of analogues was based on a peptide with alanine at all of the hydrophobic positions: the "alanine domain" or "Ala-face" (Fig. 1, left). In a similar manner to the "Leu-face" series, the central residue at position 9 is substituted by the 20 amino acids found in proteins.

The choice of alanine as the non-polar residue making up the hydrophobic face of an amphipathic helix was based on two major consid-

erations: (1) alanine, like leucine, has a high intrinsic helical propensity [38–40]; (2) alanine is considerably less non-polar than leucine [56], resulting in an excellent contrast between the very hydrophobic environment represented by the "Leu-face" and the much less hydrophobic environment created in the "Ala-face".

From the helical net representation of the peptide analogues shown in Fig. 1, it can be seen that the 18-residue length of the peptides, coupled with the wide-face design of the hydrophobic domains of the helices, allowed a central residue (position 9, boxed) to be completely surrounded by identical hydrophobic residues at positions 2, 5, 6, 12, 13 and 16 (circled residues).

The general denotion of the Ala-face series is AX9 (Fig. 1, top), with X referring to the central residue at position 9; the peptide with alanine at this position, and which can be viewed as the "native" peptide of this series, is thus denoted AA9 (Fig. 1, left); with glycine at this position, it is denoted AG9, etc. The same general terminology was also used for the series of analogues based on leucine (general designation LX9), i.e., LL9 for the "native" peptide (Fig. 1, right), LG9 for the analogue substituted by glycine at mutant position 9, etc. For the sake of brevity, the number "9" is frequently omitted from these designations, e.g., LL9 becomes simply LL, AE9 becomes AE, etc.

3.8. Conformation and helicity of model peptide analogues

The α-helicities of the peptide analogues of the Ala-face series were determined by CD (in 50% TFE) as described above. With the exception of the proline-substituted analogue (AP9), all of the peptide analogues were shown to exhibit high and similar α-helicity, e.g., an average ellipticity value of $-28\,196 \pm 510$ for the Ala-face series, excluding peptide AP9; in addition, analogues of the Leu-face were also shown to exhibit similar high α-helicity. In addition, when Eisenberg and co-workers' [57,58] mean helical hydrophobic moment was used to express the helical amphipathicity of the "native" Ala- and Leu-face peptides, values of 0.59 and 0.73, respectively, were obtained when calculated using a normalized consensus hydrophobicity scale [58]. Native amphipathic α-helices in peptides/proteins have amphipathicity values over the range: coiled-coil proteins, e.g., myosin c-β, residues 449–465, 0.28; transmembrane proteins, e.g., bacteriorhodopsin helix C, residues 1–17, 0.31; apolipoproteins, e.g., C-III, residues 40–67, 0.39; globular proteins, e.g., worm myohemerythrin helix, residues 20–36, 0.47; lytic polypeptides, e.g., bombolitin I, residues 1–17, 0.55; calmodulin regulated protein kinases, e.g., rabbit smooth muscle myosin light chain kinase, residues 1–16, 0.60; and polypeptide hormones, e.g., pancreatic polypeptide, residues 24–34, 0.84. Thus, these model amphipathic peptides used in this study clearly have considerable amphipathic character. It has also been shown independently by ^{1}H NMR that the α-helical structure extends along the entire peptide chain, except for the terminal residues, for peptides AG9, AA9, AL9, LG9, LA9 and LL9 [31,59]. Further, these peptides have been shown, by size-exclusion chromatography, to be monomeric when the TFE concentration in solution is greater than 25% (v/v) [60]. Thus, it can be confidently expected that the peptides will bind to a reversed-phase column as monomers at their preferred hydrophobic binding domains. The substituted residue at position 9 in the centre of the hydrophobic face of the amphipathic α-helices will, thus, be interacting intimately with the stationary phase. As indicated above, the proline-substituted analogues were the exception to the high α-helical character of the peptide series, e.g., AP9 showed an ellipticity of $-14\,600$, about 50% that of the average value for the other analogues. Proline is well recognized as a helix-disrupting residue, making the relatively low helical character of AP9 and LP9 unsurprising. Though Gly has been considered as a helix-perturbing residue, this mutation in the peptide sequence used in this study does not affect the helicity of the peptide in a non-polar environment as shown above. In addition, we have previously shown that α-heli-

cal peptides with Gly residues every seventh residue can still be completely α-helical even in benign medium in two-stranded α-helical coiled-coils [61]. The strong interhelical hydrophobic interactions stabilizing the coiled-coil override the destabilizing effect of Gly due to its intrinsic low helical propensity value [61].

3.9. Reversed-phase chromatography of synthetic peptide analogues

Fig. 2 shows the reversed-phase separation at pH 2 of selected peptide analogues. At this pH value, all of the glutamic acid (and aspartic acid) residues will be protonated, i.e., only the lysine residues in the hydrophilic face (and the arginine and lysine residues substituted at position 9 of the hydrophobic face) of the amphipathic helices will be (positively) charged. From Fig. 2A, it can be seen that the native leucine peptide (LL9) is, as expected, more retentive than the native Ala peptide (AA9). In fact, the magnitude of the retention time difference between the two peptides (26.1 min) is further evidence that the peptide is interacting with the stationary phase through preferential binding with their hydrophobic faces. Also from Fig. 2A, the hydrophobicity of the leucine side-chain was determined relative to glycine in the Ala-face and Leu-face, where the glycine analogues (LG9 and AG9) represent the situation where there is no side-chain present at position 9. Thus, in the Ala-face, the hydrophobicity of leucine may be expressed as $t_{R,AL9}$ minus $t_{R,AG9}$, i.e., a retention time difference of 8.5 min; in the Leu-face, this value is $t_{R,LL9}$ minus $t_{R,LG9}$, i.e., 5.01 min. Hence, there is a substantial decrease in apparent hydrophobicity of the leucine side-chain in the Leu-face compared to the less hydrophobic Ala-face.

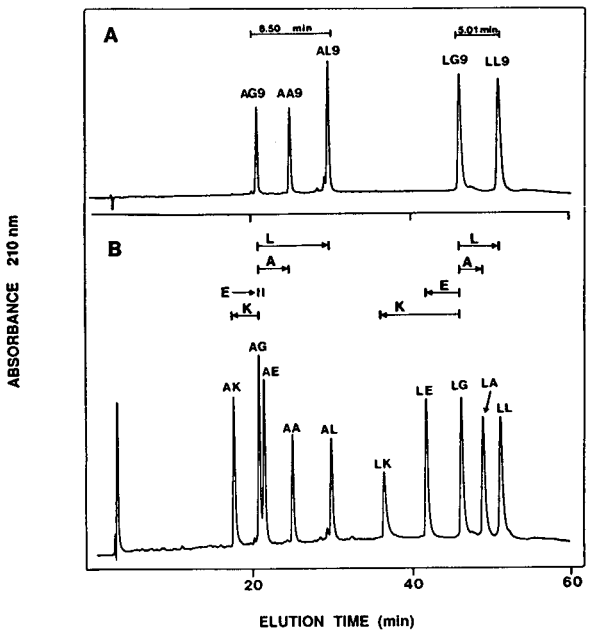

Fig. 2. RPLC of model synthetic peptides. (A) Separation of the "native" Ala-face peptide (AA9) and the "native" Leu-face peptide (LL9) from mutant peptides AG9, AL9 and LG9. (B) separation of the "native" Ala-face (AA) and the "native" Leu-face peptide (LL) from selected mutant analogues [since all residue substituitions were made at the same position in the peptide sequence (see Fig. 1) the number "9" has been omitted from the peptide designations for the sake of clarity]. The bars above the peptides in (B) represent an increase or decrease in peptide hydrophobicity relative to the glycine-substituted analogue. HPLC column, instrumentation and conditions: see Experimental. The peptide designations are described in the text.

Fig. 2B, shows the effect of alanine, leucine, lysine and glutamic acid substitutions relative to the glycine-substituted analogues. The bars above each series of peptides represents an increase or decrease in apparent hydrophobicity of the side-chain relative to the glycine mutant. The relative hydrophilicity/hydrophobicity of the side-chains shown is clearly dependent on the hydrophobicity of the environment surrounding the site of mutation. This observation not only applies to non-polar residues such as alanine and leucine, where the hydrophobicities of these side-chains relative to glycine (peptides AG and LG) are of lesser magnitude in the Leu-face (peptides LA and LL) compared to the less hydrophobic Ala-face (peptides AA and AL), but also to a charged residue such as lysine which is much more hydrophilic in the Leu-face (peptide LK) compared to the Ala-face (peptide AK). It is interesting to note that, in the Leu-face peptide (LE), the protonated glutamic acid residue is more hydrophilic relative to glycine (peptide LG); in contrast, in the Ala-face pep-

tide (AE), glutamic acid is more hydrophobic compared to glycine (peptide AG).

Table 1 summarizes the reversed-phase retention behaviour of all 40 peptide analogues. The retention times of the Ala-face peptides (column denoted $t_{R,AX}$ in Table 1) were now plotted against those of the Leu-face peptides (column denoted $t_{R,LX}$ in Table 1). From Fig. 3, there is a good correlation ($r = 0.920$) between the two sets of data, suggesting that though the magnitude of the hydrophilicity/hydrophobicity values for the side-chains are different in the Ala- and Leu-face the directional effect on all side-chains is similar when changing the hydrophobicity of the environment surrounding the mutation. Thus, it is the hydrophobic environment surrounding the mutation site that is the major factor in determining the contribution of the mutation to the retention behaviour of the peptide.

The order of amino acid substitutions shown in Table 1 was based on decreasing retention time of the Ala-face mutants ($t_{R,AX}$), starting with the highest retention time for the leucine-substituted analogue (AL; 29.32 min) and ending with the least retained proline-substituted analogue (AP; 16.95 min). When the retention time of the glycine analogue (AG; 20.82 min) has been subtracted from the retention times of the other 19 analogues (AX − AG in Table 1), the resulting numbers represent a series of coefficients expressing side-chain hydrophobicity (values > 0) or hydrophilicity (values < 0) relative to glycine. Interestingly, the order and magnitude of these values match very closely the side-chain hydrophobicity coefficients derived from the

Table 1
RPLC retention times of Ala- and Leu-face mutant peptides

Amino acid[a] substitution	Ala-face mutants		Leu-face mutants	
	$t_{R,AX}$ (min)[b]	$\Delta t_{R,AX-AG}$ (min)[c]	$t_{R,LX}$ (min)[b]	$\Delta t_{R,LX-LG}$ (min)[c]
Leu (L)	29.32	8.50	50.83	5.01
Ile (I)	29.32	8.50	51.22	5.40
Phe (F)	28.68	7.86	49.80	3.98
Trp (W)	27.92	7.10	47.37	1.55
Val (V)	27.56	6.74	50.71	4.89
Met (M)	27.15	6.33	48.82	3.00
Cys (C)	25.21	4.39	48.86	3.04
Tyr (Y)	24.98	4.16	44.90	−0.92
Ala (A)	24.78	3.96	48.84	3.02
Thr (T)	21.91	1.09	46.36	0.54
Glu (E)	21.51	0.69	41.89	−3.93
Gly (G)	20.82	0.00	45.82	0.00
Ser (S)	20.23	−0.59	44.67	−1.15
Asp (D)	19.29	−1.53	41.42	−4.40
Gln (Q)	19.29	−1.53	40.06	−5.76
Arg (R)	18.65	−2.17	37.53	−8.29
Lys (K)	17.68	−3.14	36.59	−9.23
Asn (N)	17.36	−3.46	39.99	−5.83
His (H)	17.25	−3.57	37.21	−8.61
Pro (P)	16.95	−3.88	40.84	−4.98

[a] Three-letter code and single-letter code for the 20 amino acids commonly found in proteins. Amino acid substitutions in either the Ala- or Leu-face at position 9 of the sequence (Fig. 1).
[b] Linear AB gradient, where eluent A is 0.1% aqueous TFA and eluent B is 0.1% TFA in acetonitrile with a gradient rate of 1% acetonitrile/min at a flow-rate of 1 ml/min.
[c] Retention time difference between the mutant peptide and the Gly-substituted peptide (i.e., AG or LG).

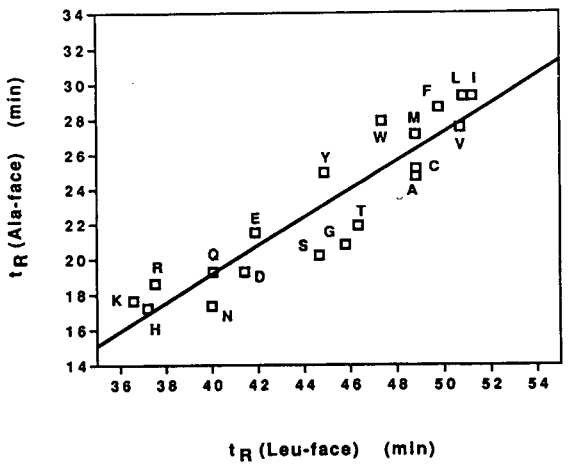

Fig. 3. Plot of $t_{R,AX}$ vs. $t_{R,LX}$, where AX and LX represent mutants of either the Ala- or Leu-face peptides. Retention time (t_R) data taken from Table 1. The single-letter code represents the amino acid substitution at position 9 of the peptide sequence (see Fig. 1).

observed reversed-phase retention behaviour of a series of octapeptide analogues reported by Guo et al. [56]. The one exception is the proline-substituted analogue (AP) which these workers reported to have a hydrophobicity similar to that of alanine. In the present study, the proline side-chain is exhibiting the most hydrophilic characteristics relative to glycine (AP − AG = − 3.88 min). As noted above, the presence of proline at position 9 of the 18-residue peptide sequence seriously disrupts the α-helical structure of peptide AP compared to the other 19 analogues of the Ala-face. This disruption of the amphipathic α-helix of peptide AP and, hence, modification of the hydrophobic face of this peptide, is presumably affecting the magnitude of interaction of AP with the hydrophobic stationary phase. Thus, it would not be surprising that a value denoting hydrophilicity/hydrophobicity of a proline side-chain relative to other side-chains may be substantially different when calculating this value from the observed retention times of amphipathic α-helical peptides (the present study) compared to the value derived from the retention behaviour of non-amphipathic peptides analogues [56].

From Table 1, for the Leu-face mutants, there is a decrease in $\Delta t_{R,LX-LG}$ for all 19 amino acids compared to the Ala-face mutants. This suggests that the side-chains of all 19 amino acids decrease in hydrophobicity when surrounded by a more hydrophobic environment. Interesting amino acid side-chains are those of tyrosine and glutamic acid (also see Fig. 2) which are hydrophobic relative to glycine in the Ala-face and hydrophilic relative to glycine in the Leu-face. The proline-substituted analogues, AP and LP, have been excluded from the remainder of this study, based on the conviction that HPLC data derived from these mutants would not be directly comparable to the retention behaviour of the other model peptides.

In order to visualize more easily the variation in hydrophobicity of the hydrophobic side-chains between the Ala- and Leu-domains, the positive Δt_R values reported in Table 1 were normalized, the value for maximum side-chain hydrophobicity (leucine in the Ala-face, where $\Delta t_{R,AX-AG} = 8.50$ min) being denoted 1.00 and the glycine mutant being assigned a value of 0.0. Table 2 compares the relative hydrophobicity of the side-chains of hydrophobic residues (i.e., defined as those which are more hydrophobic than glycine) following this normalization procedure. Clearly, these 11 amino acid side-chains vary considerably in hydrophobicity between the two non-polar faces, expressing their maximum hydrophobic characteristics in the Ala-face and their minimum hydrophobicity in the Leu-face, i.e., when there is an increase in hydrophobicity of the environment around the mutation, the apparent hydrophobicity of the side-chain decreases significantly.

The normalization procedure was now applied to comparing the hydrophilicity of the hydrophilic side-chains between the Ala- and Leu-domains. Thus, the negative Δt_R values from Table 1 were now normalized, the maximum value for side-chain hydrophilicity (lysine in the Leu-face, where $\Delta t_{R,LX-LG} = -9.23$ min) being denoted −1.00 and the glycine mutant again being assigned a value of 0.0. Table 3 compares the resulting relative hydrophilicities of these hydrophilic side-chains (i.e., defined as those

Table 2
Relative hydrophobicity of hydrophobic amino acid side-chains

Hydrophobic amino acid side-chains[a]	Maximum relative hydrophobicity (Ala-face)[b]	Minimum relative hydrophobicity (Leu-face)[c]
Leu	1.00	0.59
Ile	1.00	0.64
Phe	0.92	0.47
Trp	0.84	0.18
Val	0.79	0.58
Met	0.74	0.35
Cys	0.52	0.36
Tyr	0.49	–[d]
Ala	0.47	0.35
Thr	0.13	0.06
Glu	0.08	–[d]
Gly	0.00	0.00

[a] Hydrophobic amino acid side-chains are defined as side-chains resulting in an increase in peptide retention time relative to the mutant Gly-substituted peptide (i.e., AG or LG).
[b] The maximum relative hydrophobicity is defined as the ratio of $\Delta t_{R,AX-AG}$ values for the hydrophobic amino acid side-chains obtained from the Ala-face mutants and the maximum hydrophobicity value obtained for a side-chain in the Ala-face (Leu = 8.5 min, Table 1).
[c] The minimum relative hydrophobicity is defined as the ratio of $\Delta t_{R,LX-LG}$ values for the hydrophobic amino acid side-chains obtained from the Leu-face mutants and the maximum hydrophobicity value obtained for a side-chain in the Ala-face (Leu = 8.5 min, Table 1).
[d] Glu and Tyr side-chains are not hydrophobic relative to Gly in the Leu-face peptide and, therefore, they do not have a minimum relative hydrophobicity by our definition. From Table 1 these two residues behave in a similar fashion to the other hydrophobic residues by showing a decrease in hydrophobicity in the Leu-face compared to the Ala-face. However, these residues become less hydrophobic than Gly in the Leu-face.

Table 3
Relative hydrophilicity of hydrophilic amino acid side-chains

Hydrophilic amino acid side-chains[a]	Maximum relative hydrophilicity (Leu-face)[b]	Minimum relative hydrophilicity (Ala-face)[c]
Gly	0.00	0.00
Tyr	−0.10	–[d]
Ser	−0.12	−0.06
Glu	−0.43	–[d]
Asp	−0.48	−0.17
Gln	−0.62	−0.17
Asn	−0.63	−0.37
Arg	−0.90	−0.24
His	−0.93	−0.39
Lys	−1.00	−0.34

[a] Hydrophilic amino acid side-chains are defined as side-chains resulting in a decrease in peptide retention time relative to the mutant Gly peptide (i.e., AG or LG).
[b] The maximum relative hydrophilicity is defined as the ratio of $\Delta t_{R,LX-LG}$ values for the hydrophilic amino acid side-chains obtained from the Leu-face mutants and the maximum hydrophilicity value obtained for a side-chain in the Leu-face in absolute terms (Lys = 9.23 min, Table 1).
[c] The minimum relative hydrophilicity is defined as the ratio of $\Delta t_{R,AX-AG}$ values for the hydrophilic amino acid side-chains obtained from the Ala-face mutants and the maximum hydrophilicity value obtained for a side-chain in the Leu-face in absolute terms (Lys = 9.23 min, Table 1).
[d] Glu and Tyr side-chains are not hydrophilic relative to Gly in the Ala-face peptide and, therefore, they do not have a minimum relative hydrophilicity by our definition. From Table 1 these two residues behave in a similar fashion to the other hydrophilic residues by showing an increase in hydrophilicity in the Leu-face compared to the Ala-face. However, these residues become more hydrophobic than Gly in the Ala-face.

which are more hydrophilic than glycine). In a similar manner to the observed behaviour of the hydrophobic residues (Table 2), there is a clear and substantial variation in hydrophilicity of these 9 side-chains between the two non-polar faces. These side-chains express their maximum hydrophilic characteristics in the Leu-face and their minimum hydrophilicity in the Ala-face, i.e., when there is an increase in hydrophobicity of the environment around the mutation, the apparent hydrophilicity of the side-chain increases significantly.

3.10. Correlation of RPLC retention behaviour with non-polar accessible surface area of model peptides

Computer modeling was used to study the α-helices of all analogues of the native Ala- and Leu-face. The side-chains were energy minimized and the non-polar accessible surface area

Table 4
Accessible surface area of peptides AA9 and LL9

Peptide	Non-polar (A) ($Å^2$)	Polar (B) ($Å^2$)	Net (A − B)	$t_R - t_g$ [a] (min)
AA9	442	47	395	23.85
LL9	810	31	779	49.90
Ratio LL9/AA9	1.83	–	1.97	2.09

[a] t_g denotes gradient delay time, i.e., the time for the solvent front to travel from the solvent mixer to the top of the column (0.93 min at 1 ml/min). At a gradient rate of 1% acetonitrile/min, $t_R - t_g$ is then equal to the % acetonitrile required to elute the peptide from the column.

(NPASA) was calculated for the non-polar face of these peptides. From Table 4, the ratio of the NPASA of LL9 (810 $Å^2$) to AA9 (442 $Å^2$) is 1.83. The similar ratio of 2.09 (LL9/AA9) for the % acetonitrile required to elute these peptides from the column strongly suggested a correlation between the increase in retentiveness of LL9 by the column relative to AA9 and the concomitant increase in NPASA. This correlation becomes even clearer when allowance is made for the small polar surface areas on the hydrophobic faces of LL9 (31 $Å^2$) and AA9 (47 $Å^2$) which may offset to a small extent the non-polar contribution to retention. From Table 4, once these polar contributions have been subtracted from their non-polar counterparts, the resulting ratio of modified NPASA of LL9 to AA9 (779 $Å^2$/395 $Å^2$ = 1.97) is now in excellent agreement with the % acetonitrile ratio of 2.09.

The results of Table 4 suggested that the non-polar accessible surface area is a major factor in determining the retention behaviour of our model peptides. Taking this further, we now wished to determine whether the change in apparent hydrophilicity/hydrophobicity of a specific side-chain in the centre of one hydrophobic domain compared to another, e.g., between a side-chain in the Ala-face compared to the Leu-face, was related to a corresponding change in non-polar accessible surface area between these domains. The NPASA values for 14 of the analogues in both series are shown in Table 5. The NPASA values for the glycine mutant in both the Ala-face and Leu-face peptides were now subtracted from each of the values for the remaining residues (ΔNPASA), to produce a designated NPASA value for the substituted side-chain at mutant position 9 only. From the results shown in Table 5, it can be seen that, in an analogous manner to the calculated apparent side-chain hydrophilicity/hydrophobicity values (or coefficients) reported in Table 1 ($\Delta t_{R,AX-AG}$ and $\Delta t_{R,LX-LG}$), the ΔNPASA of each side-chain was lower in the more hydrophobic Leu-face compared to the Ala-face.

Fig. 4 plots the difference between the ΔNPASA values of 13 side-chains in the two hydrophobic domains (Ala-face values minus Leu-face values, denoted ΔΔNPASA in Table 5 and Fig. 4) versus the difference in apparent side-chain hydrophilicity/hydrophobicity of the side-chains in these domains (Ala-face minus Leu-face values, denoted $\Delta\Delta t_R$ in Table 5 from Δt_R values reported in Table 1). From Fig. 4, it can be seen that there is an excellent correlation ($r = 0.967$) between these two parameters for most of the amino acid side-chains. These results suggest strongly that the change in apparent hydrophilicity/hydrophobicity of a specific side-chain in environments of varying hydrophobicity is directly related to the concomitant change in non-polar accessible surface area expressed by the side-chain. Interestingly, the values for the acidic (glutamic acid, aspartic acid) and basic (lysine, arginine, histidine) side-chains did not correlate well. It is possible that the polar constituents in these side-chains are sterically shielding the non-polar accessible surface areas

Table 5
Comparison of the non-polar accessible surface area in the Ala- and Leu-face peptides

Amino acid substitution[a]	Non-polar accessible surface area (NPASA) (Å^2)					
	Ala-face		Leu-face		ΔΔNPASA[c]	$\Delta\Delta t_R$ [d]
	NPASA	ΔNPASA[b]	NPASA	ΔNPASA[b]		
Leu	499	79	810	45	34	3.49
Ile	494	74	797	32	42	3.10
Phe	493	73	792	27	46	3.88
Trp	501	81	786	21	60	5.55
Val	486	66	802	37	29	1.85
Met[e]	493	73	808	43	30	3.33
Cys[e]	466	46	784	19	27	1.35
Tyr	464	44	770	5	39	3.24
Ala	442	22	780	15	7	0.94
Thr	455	35	773	8	27	0.55
Gly	420	0	765	0	0	0.00
Ser	430	10	769	4	6	−0.56
Gln	418	−2	727	−38	−36	−4.23
Asn	410	−10	740	−25	−15	−2.37

[a] Represents the amino acid substituted into position 9 of either the Ala- or Leu-face mutants (Fig. 1).
[b] Non-polar surface area of amino acid side-chain in either the Ala- or Leu-face, obtained by subtracting the non-polar surface area of the Gly-substituted peptide from the corresponding mutant peptide.
[c] Non-polar surface area change in the amino acid side-chain that occurs when the side-chain is substituted from the Ala-face to the Leu-face. Value is obtained by subtracting the non-polar surface area of the side-chain in the Leu-face, i.e. ΔNPASA, from the non-polar surface area of the side-chain in the Ala-face, i.e. ΔNPASA. Since the ΔNPASA values of Gln and Asn are negative in both the Ala- and Leu-face, the absolute value of each ΔNPASA is taken before the subtraction.
[d] The change in retention time that is observed for a substitution in going from the Ala-face to the Leu-face. The value is obtained by subtracting the absolute value of the retention time (Δt_R) of the peptide, relative to the Gly peptide, in the Leu-face, i.e. LX − LG, from the retention time of the peptide, relative to the Gly peptide, in the Ala-face, i.e. AX − AG; Table 1.
[e] The sulphur atom of Met and Cys is calculated as a non-polar atom [36].

of these residues [62], thus reducing the expected magnitude of interaction of these side-chains with the reversed-phase matrix.

4. Conclusions

The present study describes the design and development of a chromatographic model for studying the hydrophobic interactions which characterize the way a ligand binds to its receptor. This model is based on observing the reversed-phase retention behaviour of de novo designed model amphipathic α-helical peptides representing the hydrophobic binding domain of a receptor protein and/or ligand. In this initial appraisal of the ligand–receptor model system, we have shown that the hydrophobicity of the environment surrounding a site in the interface of a binding domain affects the apparent hydrophilicity/hydrophobicity of the amino acid side-chain substituted into the site. In addition, our results suggest that this effect is related to a variation of non-polar accessible surface area expressed by the side-chains in different hydrophobic environments. Such results may have major implications in understanding protein folding and stability, as well as ligand–protein binding and protein–protein interactions, by delineating the role that individual side-chains play in these systems. Thus, the model system described here should prove to be useful not only as a mimic of ligand–receptor interactions, but also as a general chromatographic probe of

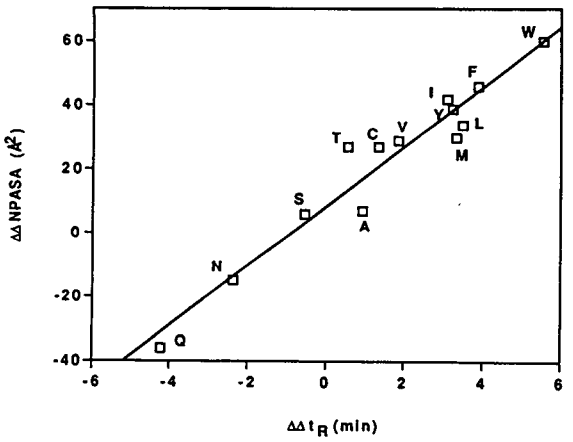

Fig. 4. Plot of ΔΔNPASA vs. $\Delta\Delta t_R$ (see Table 5) for amino acid side-chains. The single-letter code represents the amino acid substitution at position 9 of the peptide sequence (see Fig. 1).

hydrophobic interactions involved in protein folding and stability.

Acknowledgements

This work was supported by the Medical Research Council of Canada Group in Protein Structure and Function and by the Protein Engineering Network of Centres of Excellence programme supported by the Government of Canada. We thank Paul Semchuck for synthesizing the peptides used in this study.

References

[1] A.W. Purcell, M.I. Aguilar and M.T.W. Hearn, *J. Chromatogr.*, 593 (1992) 103.
[2] S.A Cohen, K. Benedek, Y. Tapuhi, J.C. Ford and B.L. Karger, *Anal. Biochem*, 144 (1985) 275.
[3] R.H. Ingraham, S.Y.M. Lau, A.K. Taneja and R.S. Hodges, *J. Chromatogr.*, 327 (1985) 77.
[4] E. Watson and W.-C. Kenney, *J. Chromatogr.*, 606 (1992) 165.
[5] R. Rosenfeld and K. Benedek, *J. Chromatogr.*, 632 (1993) 29.
[6] K. Benedek, *J. Chromatogr.*, 646 (1993) 91.
[7] C.T. Mant and R.S. Hodges (Editors), *High Performance Liquid Chromatography of Peptides and Proteins: Separation, Analysis and Conformation,* CRC Press, Boca Raton, FL, 1991.
[8] T.J. Sereda, C.T. Mant, A.M. Quinn and R.S. Hodges, *J. Chromatogr.*, 646 (1993) 17.
[9] Cs. Horváth, W. Melander and I. Molnár, *J. Chromatogr.*, 125 (1976) 129.
[10] J.W. Taylor, D.G. Osterman, R.J. Miller and E.T. Kaiser, *J. Am. Chem. Soc.*, 103 (1981) 6965.
[11] E.T. Kaiser and F.J. Kezdy, *Science*, 223 (1984) 249.
[12] J.W. Taylor and E.T. Kaiser, *Pharmacol. Rev.*, 38 (1986) 291.
[13] J.W. Taylor, in R.E. Epand (Editor), *The Amphipathic Helix,* CRC Press, Boca Raton, FL, 1993, p. 285.
[14] M. Thelestam and R. Möllby, *Biochim. Biophys. Acta*, 557 (1979) 156.
[15] J.A. Cox, M. Comte, J.E. Fitton and W.F. DeGrado, *J. Biol. Chem.*, 260 (1985) 2527.
[16] L. McDowell, G. Sanyal and F.G. Prendergast, *Biochemistry*, 24 (1985) 2979.
[17] P.J. Cachia, J. Van Eyk, R.H. Ingraham, W.D. McCubbin, C.M. Kay and R.S. Hodges, *Biochemistry*, 25 (1986) 3553.
[18] A.W. Berheimer and B. Rudy, *Biochim. Biophys. Acta*, 864 (1986) 123.
[19] R.M. Kini and H.J. Evans, *Int. J. Pept. Protein Res.*, 34 (1989) 277.
[20] I. Cornut, E. Thiaudière and J. Dufourcq, in R.E. Epand (Editor), *The Amphipathic Helix*, CRC Press, Boca Raton, FL, 1993, p. 173.
[21] A.M. Spiegel, P.S. Backlund, J.E. Butrynski, T.L.Z. Jones and W.F. Simonds, *Trends Biochem. Sci.*, 16 (1991) 339.
[22] M. Mousli and Y. Landry, in R.E. Epand (Editor), *The Amphipathic Helix*, CRC Press, Boca Raton, FL, 1993, p. 313.
[23] T. Higashijima, S. Vzu, T. Nakajima and E.M. Ross, *J. Biol. Chem.*, 263 (1988) 6491.
[24] M. Zasloff, *Proc. Natl. Acad. Sci. U.S.A.*, 84 (1987) 5449.
[25] D. Marion, M. Zasloff and A. Bax, *FEBS Lett.*, 227 (1989) 21.
[26] C. DeLisi and J.A. Berzofsky, *Proc. Natl. Acad. Sci. U.S.A.*, 82 (1985) 7048.
[27] G.M. Anantharamaiah, *Methods Enzymol.*, 128 (1986) 626.
[28] J.P. Segrest, M.K. Jones, H. De Loof, C.G. Brouillette, Y.V. Venkatachalapathi and G.M. Anantharamaiah, *J. Lipid Res.*, 33 (1992) 141.
[29] W.H. Landschultz, P.F. Johnson and S.C. McKnight, *Science*, 240 (1988) 1759.
[30] C.R. Vinson, P.B. Sigler and S.L. McKnight, *Science*, 246 (1989) 911.
[31] N.E. Zhou, C.M. Kay, B.D. Sykes and R.S. Hodges, *Biochemistry*, 32 (1993) 6190.

[32] C.T. Mant, N.E. Zhou and R.S. Hodges, in R.E. Epand (Editor), *The Amphipathic Helix*, CRC Press, Boca Raton, FL, 1993, p. 39.
[33] G.N. Ramachandran, C. Ramakrishnan and V. Sasisekharan, *J. Mol. Biol.*, 7 (1963) 95.
[34] B.R. Brooks, R.E. Bruccoleri, B.D. Olafson, D.Y. States, S. Swaminathan and M. Karplus, *J. Comp. Chem.*, 4 (1983) 187.
[35] T.Y. Richmond, *J. Mol. Biol.*, 178 (1983) 63.
[36] D. Eisenberg and A.D. McLachlan, *Nature*, 319 (1986) 199.
[37] S.J. Opella, J. Gesell and B. Bechinger, in R.E. Epand (Editor), *The Amphipathic Helix*, CRC Press, Boca Raton, FL, 1993, p. 87.
[38] P.Y. Chou and G D. Fasman, *Ann. Rev. Biochem.*, 47 (1978) 251.
[39] M. Sueki, S. Lee, S.P. Powers, J.B. Denton, Y. Konishi and H.A. Scheraga, *Macromolecules*, 17 (1984) 148.
[40] H.A. Scheraga, *Pure Appl. Chem.*, 50 (1978) 315.
[41] J.A. Talbot and R.S. Hodges, *Acc. Chem. Res.*, 15 (1982) 224.
[42] D. Eisenberg, R.M. Weiss and T.C. Terwilliger, *Proc. Natl. Acad. Sci. U.S.A.*, 81 (1984) 140.
[43] R.R. Torgerson, R.A. Lew, V.A. Reges, L. Hardy and R.E. Humphreys, *J. Biol. Chem.*, 266 (1991) 5521.
[44] S. Marqusee and R.L. Baldwin, *Proc. Natl. Acad. Sci. U.S.A.*, 84 (1987) 8898.
[45] G. Merutka and E. Stellwagen, *Biochemistry*, 30 (1991) 1591.
[46] R.S. Hodges, P.D. Semchuk, A.J. Taneja, C.M. Kay, J.M.R. Parker and C.T. Mant, *Pept. Res.*, 1 (1988) 19.
[47] R.S. Hodges, N.E. Zhou, C.M. Kay and P.D. Semchuk, *Pept. Res.*, 3 (1990) 123.
[48] R.S. Hodges, *Curr. Biol.*, 2 (1992) 122.
[49] J.W. Nelson and N.R. Kallenbach, *Proteins*, 1 (1986) 211.
[50] J.W. Nelson and N.R. Kallenbach, *Biochemistry*, 28 (1989) 5256.
[51] S.Y.M. Lau, A.K. Taneja and R.S. Hodges, *J. Chromatogr.*, 317 (1984) 129.
[52] N.E. Zhou, C.T. Mant and R.S. Hodges, *Pept. Res.*, 3 (1990) 8.
[53] Y.-H. Chen, T.J. Yang and K.H. Chau, *Biochemistry*, 13 (1974) 3350.
[54] C.T. Mant and R.S. Hodges, *J. Chromatogr.*, 409 (1987) 155.
[55] D.J. Abraham and A.J. Leo, *Proteins: Struct. Funct. Genet.*, 2 (1987) 130.
[56] D. Guo, C.T. Mant, A.K. Taneja, J.M.R. Parker and R.S. Hodges, *J. Chromatogr.*, 359 (1986) 499.
[57] D. Eisenberg, R.M. Weiss and T.C. Terwilliger, *Nature*, 299 (1982) 371.
[58] D. Eisenberg, E. Schwartz, M. Komaromy and R. Wall, *J. Mol. Biol.*, 179 (1984) 125.
[59] N.E. Zhou, B.-Y. Zhu, B.D. Sykes and R.S. Hodges, *J. Am. Chem. Soc.*, 114 (1992) 4320.
[60] N.E. Zhou, unpublished results.
[61] R.S. Hodges, A.K. Saund, P.C.S. Chong, S.A. St. Pierre and R.E. Reid, *J. Biol. Chem.*, 256 (1981) 1214.
[62] G.J. Lesser and G.D. Rose, *Proteins: Struct. Funct. Genet.*, 8 (1990) 6.

ELSEVIER

Journal of Chromatography A, 676 (1994) 155–160

JOURNAL OF CHROMATOGRAPHY A

Reversed-phase high-performance liquid chromatography for the determination of haemorphin-like immunoreactivity in human cerebrospinal fluid

Katarina Sanderson, Madeleine Thörnwall, Greger Nyberg, Eva-Lena Glämsta, Fred Nyberg*

Department of Pharmaceutical Biosciences, Division of Biological Research on Drug Dependence, Uppsala University, P.O. Box 591, S-751 24 Uppsala, Sweden

Abstract

The haemorphins are opioid peptides derived form the blood protein haemoglobin. This study was focused on the detection and determination of haemorphin-like immunoreactivity in human cerebrospinal fluid (CSF) by reversed-phase HPLC. For this purpose a SMART System, optimized for micropurification, was applied. Prior to application to HPLC, the peptide fraction of the CSF sample was extracted using a reversed-phase silica gel cartridge (Sep-Pak C_{18}). In the HPLC separation, the peptide-like material associated with haemorphin-7 immunoreactivity was recovered and determined using a UV detector. The tryptophan residue present in the haemorphin sequence allowed UV detection at wavelengths (e.g., 276 nm) where interference with other co-eluting peptides lacking this residue is minimized. Recorded levels of haemorphin-like immunoreactivity were compared with those detected by radioimmunoassay.

1. Introduction

The haemorphins are recently identified peptides with opioid activity, which are enzymatically released from the blood protein haemoglobin [1,2]. In contrast to the "classical" endorphins (e.g., the enkephalins), the haemorphins exhibit a relatively high metabolic stability [3], probably owing to the proline residue next to the N-terminal tyrosine (Table 1). The haemorphins also differ from the enkephalins with regard to their receptor activation profile. Whereas the enkephalins preferentially bind to delta-opioid receptors, the haemorphins are selective for both delta- and mu-receptors [4,5]. In addition, the haemorphins also have affinity for sigma-receptors (2).

An opioid active decapeptide (LVV-haemorphin-7), identical with the sequence 32–41 of the β-chain of haemoglobin, was previously isolated from human ventricular cerebrospinal fluid (CSF) [6,7]. In a recent study, a shorter active fragment of this peptide, haemorphin-7 (Tyr–Pro–Trp–Thr–Gln–Arg–Phe), was tentatively identified in human plasma [8]. Haemorphin-7 was found to increase in the circulation following long-distance running. This increase was paralleled by elevated levels of circulating β-endorphin-

* Corresponding author.

0021-9673/94/$07.00
SSDI 0021-9673(94)00432-9

Table 1
Structures of the haemorphins and related peptides

Compound	Structure
Haemorphin-4	Tyr–Pro–Trp–Thr
Haemorphin-7	Tyr–Pro–Trp–Thr–Gln–Arg–Phe
LVV-haemorphin-4	Leu–Val–Val–Tyr–Pro–Trp–Thr
LVV-haemorphin-7	Leu–Val–Val–Tyr–Pro–Trp–Thr–Gln–Arg–Phe
Leu-enkephalin	Tyr–Gly–Gly–Phe–Leu
Met-enkephalin	Tyr–Gly–Gly–Phe–Met

like immunoreactivity [8]. In animal experiments, the haemorphins were shown to lower the blood pressure, probably through a mechanism where the activity of angiotensin-converting enzyme is inhibited [3].

To explore further the physiological relevance of the haemorphins, the use of highly efficient techniques for their detection and determination is essential. In this study, we applied a new chromatographic system, the SMART System, to detect and determine these peptides in cerebrospinal fluid (CSF). Detected levels of haemorphin-like peptide material in CSF collected from patients with cerebrovascular bleeding were compared with those in control samples. Levels calculated from the HPLC results were compared with those recorded by radioimmunoassay (RIA).

2. Experimental

2.1. Peptides and chemicals

Synthetic haemorphins were prepared by Dr. G. Lindeberg (Department of Medical Immunology, Uppsala University, Sweden), except for haemorphin-4, which was a gift from Dr. V. Brantl (Schlingen, Germany). Prior to use, the synthetic peptides were purified by HPLC [8]. Sep-Pak C_{18} silica gel cartridges were purchased from Waters (Milford, MA, USA). All other chemicals and solvents were of analytical-reagent grade from commercial sources.

2.2. Cerebrospinal fluid material

Ventricular CSF from patients with cerebrovascular bleeding was obtained from the Department of Neurosurgery, Karolinska Hospital (Stockholm, Sweden) and lumbar CSF from controls without cerebral disease was obtained from the Department of Neurology, Umeå University (Umeå, Sweden). Prior to analysis, the CSF samples were stored at −70°C.

2.3. Sample preparation

CSF samples (10 ml) were thawed (the samples were kept in a cold room at 5°C) and eluted through Sep-Pak C_{18} cartridges for reversed-phase (RP) extraction. Prior to sample application, the cartridge was successively washed with 5 ml of methanol, 5 ml of methanol containing 0.04% trifluoroacetic acid (TFA) and finally with 10 ml of distilled water containing 0.04% TFA. Following sample application, the cartridge was washed with 4 ml of distilled water and subsequently with 4 ml of 20% methanol before elution with 4 ml of 60% methanol (all solutions containing 0.04% TFA). The eluate obtained at a methanol concentration of 60% was evaporated in a vacuum concentrator (Savant Vac, Hicksville, NY, USA) and collected for further analysis by HPLC or radioimmunoassay. In calibration elutions, synthetic haemorphins were added to control CSF and subjected to the same extraction procedure.

2.4. Chromatography

RP-HPLC was performed using a SMART System (Pharmacia–LKB Biotechnology, Uppsala, Sweden). The computer-controlled system was equipped with a micro-precision pump, SepUnit, micro-fraction collector and built-in detector cells for UV (μPeak Monitor with variable-wavelength monitor) and conductivity measurements. The conductivity scale was set by calibration with eluent A (100%) and eluent B (0%): A, 0.14% TFA; B, 0.13% TFA in 60% acetonitrile. The column used was a μRPC C_2/C_{18} SC 2.1/10 (particle size 3 μm, 120 Å) (100 mm × 2.1 mm I.D.). Elution was carried out with a gradient of acetonitrile (0–60% over 40 min) maintaining a flow-rate of 100 μl/min. Prior to injection, the sample (100 μl) was centrifuged at 10 000 *g* for 1 min. Collected fractions (100 μl) were dried in a Savant Vac concentrator and assayed by RIA.

2.5. Radioimmunoassay

The RIA for haemorphin-7 was based on the charcoal adsorption technique and was conducted as described in a previous paper [8]. Briefly, antibodies were raised in rabbits and the iodinated petide was used as a tracer. Cross-reaction in the RIA and LVV-haemorphin-7 was 100% and for LVV-haemorphin-6 and shorter fragments of the peptide it was less than 1%. The detection limit of the RIA was 4 fmol per tube.

3. Results

The SMART System used in this study for RP-HPLC, was optimized for the separation of various haemorphin structures. As shown in Fig. 1, the technique appeared to be highly efficient for resolving the synthetic haemorphin-4 and haemorphin-7 and also their N-terminal elongations LVV-haemorphin-4 and LVV-haemorphin-7, respectively.

Prior to HPLC of haemorphin-like peptide material in CSF, the samples were extracted on Sep-Pak C_{18} cartridges. In calibration elutions the synthetic peptides were added at different concentrations (0.01, 0.05, 0.1 and 0.2 μg/ml) to a control CSF sample (10 ml) containing no or negligible amounts of the native peptides. By this approach, it was possible to determine the recovery of the extraction procedure. Table 2 summarizes data obtained from these recovery studies. It was found that on adding synthetic peptides in concentrations of 0.1 μg/ml (total amount 1 μg), their recovery following HPLC ranged from 44 to 76%. The recovery seems relatively low, but it is known from several

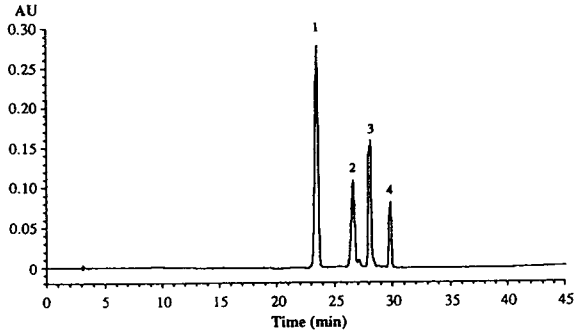

Fig. 1. RP-HPLC using the SMART System of synthetic haemorphins. Elution was carried out using a linear gradient of acetonitrile (0–60% over 40 min) at a flow-rate of 100 μl/min. The UV absorbance was recorded at 276 nm. For further details, see text. Peaks: 1 = haemorphin-4 (1 μg); 2 = haemorphin-7 (1 μg); 3 = LVV-haemorphin-4 (4 μg); 4 = LVV-haemorphin 7 (1 μg).

Table 2
Recovery of synthetic haemorphins added to control CSF (1 μg in 10 ml) following Sep-Pak C_{18} extraction and RP-HPLC

Peptide	Recovery (%)[a]
Haemorphin-4	44
Haemorphin-7	56
LVV-haemorphin-4	52
LVV-haemorphin-7	76

[a] Values are means from three separate experiments.

studies that losses of hydrophobic peptides often occur during Sep-Pak extraction [9].

In studies of CSF samples from patients with cerebrovascular bleedings, the content of haemorphin-like immunoreactivity varied depending on the individual diagnosis. A patient with a subdural haematoma exhibited comparatively higher levels of peptides co-eluting with haemorphin-4, haemorphin-7 and LVV-haemorphin-4 (Fig. 2), whereas one patient with subarachnoid bleeding only showed a modest increase in UV-absorbing material co-eluting with LVV-haemorphin-7 (Fig. 3). This latter UV peak or shoulder was also found to be associated with LVV-haemorphin-7-like immunoreactivity, although its peak was seen at a retention time of 29.6 min instead of the 29.8 min found for the synthetic LVV-haemorphin-7. However, repetitive chromatography showed that these divergences were within the precision of the instrument. Analysis of samples from other patients with identical diagnosis gave similar HPLC patterns to those shown in Figs. 2 and 3 (data not shown). In control patients, the levels of haemorphins were very low, although detectable at least in one patient (Fig. 4). In both Figs. 3 and 4 it was possible to observe UV-absorbing peaks associated with haemorphin-like material only when the chromatograms were expanded.

The level of the separated haemorphin-like

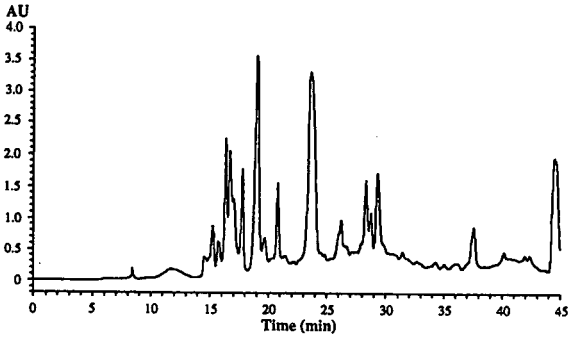

Fig. 2. RP-HPLC of a concentrated CSF sample (10 ml) from a patient with a subdural haematoma. Separation conditions as in Fig. 1. The UV absorbtion at 276 nm was recorded and 100-μl fractions were collected and dried for RIA. Haemorphin-7-like immunoreactivity and LVV-haemorphin-7-like immunoreactivity were eluted in fractions 27 and 30, respectively. For further details, see text.

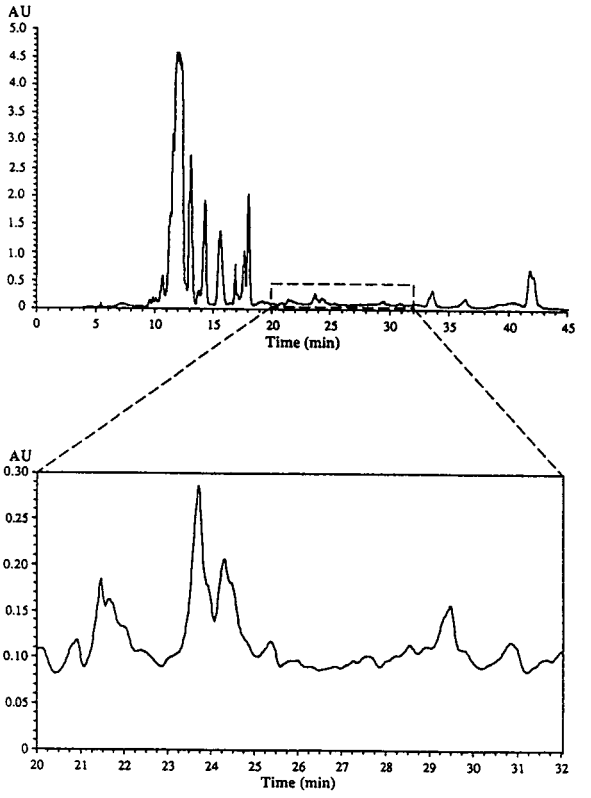

Fig. 3. RP-HPLC using the SMART System of a concentrated CSF sample (10 ml) from a patient with subarachnoid bleeding. Conditions as in Figs. 1 and 2. Fractions of 100 μl were collected and dried before testing by RIA. Haemorphin-7-like immunoreactivity and LVV-haemorphin-7-like immunoreactivity were eluted in fractions 27 and 30, respectively. At the bottom, part of the chromatogram is expanded to shown peaks in the area were the synthetic haemorphins were observed to elute.

CSF components (Figs. 2–4) was determined by recording the area under the curve (AUC). A calibration graph was established for each synthetic peptide, which was added to a control CSF sample at different concentrations. A sample for each peptide concentration was run through the Sep-Pak C_{18} cartridge and analysed by HPLC, where the AUC was recorded.

Data obtained by RIA confirmed the results showed in Figs. 2–4. Thus, haemorphin-7 was confirmed as a major component in the patient with a subdural haematoma. This patient exhibited comparatively low levels of LVV-haemor-

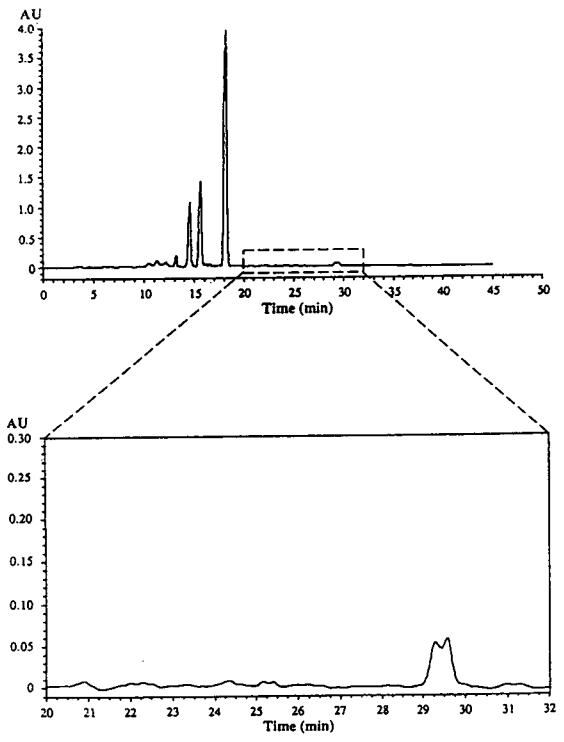

Fig. 4. RP-HPLC using the SMART System of a concentrated control CSF sample (10 ml). Conditions as in Figs. 1–3. Fractions of 100 μl were dried and taken for analysis by RIA. Haemorphin-7 and LVV-haemorphin-7-like immunoreactivity were eluted in fractions 27 and 30, respectively.

phin-7. The patients with subarachnoid bleeding, shown in Fig. 3, and the control subject contained the highest levels of haemorphin-7-like immunoreactivity, although in control samples immunoreactive material co-eluting with LVV-haemorphin-7 was also found. No RIA recognizing haemorphin-4 or LVV-haemorphin-4 was used in this study.

4. Discussion

RP-HPLC is frequently applied in studies of neuroactive peptides. However, so far very few studies have been published in which the technique combined with UV detection has been successfully used for the determination of peptides present in the CSF. One major reason for this may be that the level of these peptides in this fluid is very low and the procedure has to be combined with RIA or radioreceptor assay [9]. Another reason is that most instruments used for HPLC do not allow the recovery and detection of any peptide below certain levels. The SMART System is a recently developed chromatographic technique that fulfils some important requirements for efficient peptide separation and recovery. With this system, peptides and other biological molecules can be detected at levels below 5 pmol [10]. In previous studies in our laboratory this system was applied to probe molecular components in CSF from pregnant and puerperal women [10]. The technique was also useful for the separation and detection of monoamines and their metabolites. The system was further applied to determine CSF peptides and proteins in the rat [11]. In a recent study, we were able to isolate an opioid peptide for sequence determination from human milk [12].

This study indicates the potential of this HPLC system for the determination of the haemorphin-like immunoreactivity in human CSF. Although in this work the number of patients studied was limited, we believe that this approach may be useful as a complement to the clinical scores used in the diagnosis of patients with cerebrovascular bleeding. Further, the appearance of peptides known to act on opioid receptors is of interest with regard to some of the symptoms related to patients with the actual disorder. The presence of haemorphin-7 [13], LVV-haemorphin-4 [14], LVV-haemorphin-6 [2] and LVV-haemorphin-7 [6,7] in tissue extracts and body fluids suggests a sequential degradation of the β-chain of the blood protein haemoglobin. The release of LVV-haemorphin-7 is indicative of the action of a chymotrypsin-like enzyme. The shorter haemorphin structures may result from further degradation of this peptide as indicated in a previous study [3].

In conclusion, the study has demonstrated the usefulness of the SMART System for the recovery and determination of haemorphin-7-like material in CSF from patients with cerebrovascular bleeding. The technique may be applicable not only to the determination of the haemor-

phins in CSF, but possibly also to the determination of these compounds in plasma, where they are known to be released during certain physiological [8] or perhaps also pathophysiological conditions.

Acknowledgements

This study was supported by the Swedish Medical Research Council (Grant 9459), the Swedish Board for Technical Development (NUTEC) and Pharmacia–LKB Biotechnology.

References

[1] V. Brantl, C. Gramsch, F. Lottspeich, R. Mertz, K.H. Jaeger and A. Herz, *Eur. J. Pharmacol.*, 125 (1986) 309–310.
[2] E.-L. Glämsta, A. Marklund, U. Hellman, C. Wernstedt, L. Terenius and F. Nyberg, *Regul. Pept.*, 34 (1991) 169–179.
[3] I. Lantz, E.-L. Glämsta, L. Talback and F. Nyberg, *FEBS Lett.*, 287 (1991) 39–41.
[4] C. Liebmann, U. Schrader and V. Brantl, *Eur. J. Pharmacol.*, 166 (1989) 523–526.
[5] R. Yukhananov, E.-L. Glämsta and F. Nyberg, *Regul. Pept.*, Suppl. 1 (1994) 239–242.
[6] E.-L. Glämsta, B. Meyerson, J. Silberring, L. Terenius and F. Nyberg, *Biochem. Biophys. Res. Commun.*, 184 (1992) 1060–1066.
[7] E.-L. Glämsta, F. Nyberg and J. Silberring, *Rapid Commun. Mass. Spectrom.*, 6 (1992) 777–780.
[8] E.-L. Glämsta, L. Mörkrid, I. Lantz and F. Nyberg, *Regul. Pept.*, 49 (1993) 9–18.
[9] F. Nyberg, I. Christensson-Nylander and L. Terenius, *Handb. Exp. Pharmacol.*, 82 (1987) 227–253.
[10] F. Nyberg, S. Lyrenäs and A. Danielsson, *J. Chromatogr.*, 548 (1991) 311–318.
[11] S. Persson, C. Post, R. Holmdahl and F. Nyberg, *Brain Res.*, 581 (1992) 273–282.
[12] S. Renlund, I. Erlandsson, J. Silberring, L. Lindström and F. Nyberg, *Peptides*, 14 (1993) 1125–1132.
[13] J.-M. Piot, D. Guillochon, G. Ricart and D. Thomas, *Biochem. Biophys. Res. Commun.*, 189 (1992) 101–110.
[14] K. Nishimura and T. Hazato, *Biochem. Biophys. Res. Commun.*, 194 (1993) 713–719.

ELSEVIER

Journal of Chromatography A, 676 (1994) 161–167

JOURNAL OF CHROMATOGRAPHY A

Determination of a novel hematoregulatory peptide in dog plasma by reversed-phase high-performance liquid chromatography and an amine-selective *o*-phthaldialdehyde–thiol post-column reaction with fluorescence detection

Venkata K. Boppana*, Cynthia Miller-Stein

Department of Drug Metabolism and Pharmacokinetics, SmithKline Beecham Pharmaceuticals, P.O. Box. 1539, King of Prussia, PA-19406, USA

Abstract

A sensitive and selective high-performance liquid chromatographic method was developed for the determination of SB 107647 (**I**), a novel synthetic hematoregulatory peptide, in plasma samples of dog and rat. The method involves isolation of **I** and the internal standard (SB 203285, IS) from plasma by a solid-phase anion-exchange extraction column prior to reversed-phase ion-pair chromatographic separation on an octyl silica column. Following separation, a selective post-column reaction of the ϵ-amino groups of the lysine moieties of the peptide with *o*-phthaldialdehyde and a thiol under basic conditions was used to generate a highly fluorescent isoindole product, which was subsequently detected on-line with a fluorometer. Optimization of chromatographic conditions resulted in an on-column detection limit of 1 ng. The recovery of **I** from dog plasma at 20 and 4000 ng/ml was 50.0 ± 5.94 and $56.6 \pm 1.45\%$ (Mean $\pm$ S.D.), respectively. The limit of quantification for **I**, for 0.25-ml plasma samples, was 20 ng/ml. Linear response was observed for concentrations of **I** ranging from 20 to 4000 ng/ml of plasma. The assay was sufficiently sensitive, accurate and precise to support toxicokinetic studies in animal species.

1. Introduction

SB 107647 {**I**, Fig. 1; (S)-5-oxo-L-prolyl-L-α-glutamyl-L-α-aspartyl-N8-(5-amino-1-carboxypentyl)-8-oxo-N7-[N-[N-(5-oxo-L-prolyl)-L-α-glutamyl]-L-α-aspartyl]-L-*threo*-2,7,8-triaminooctanoyl-L-lysine} is a novel synthetic hematoregulatory peptide [1–3]. It selectively stimulates cytokinin production by stromal cells, particularly fibroblasts, at an early stage of hematopoiesis relative to the colony stimulating factors (CSFs).

Since **I** lacks appreciable absorbance in the ultraviolet region, development of a sensitive and specific HPLC method to support toxicokinetic studies was impractical using conventional HPLC detectors. However, the ϵ-amino groups of the lysine moieties of the peptide provided potential sites for chemical modification in order to improve detectability of **I** for development of a selective HPLC methodology with fluorescence detection. This report describes a rapid, selective and sensitive HPLC method for quantification of **I** in dog and rat plasma samples. The method involves isolation of **I** and the internal standard (IS) from plasma by solid-phase extraction prior to reversed-phase ion-pair chromatographic separation on an octyl

* Corresponding author.

0021-9673/94/$07.00
SSDI 0021-9673(94)00130-2

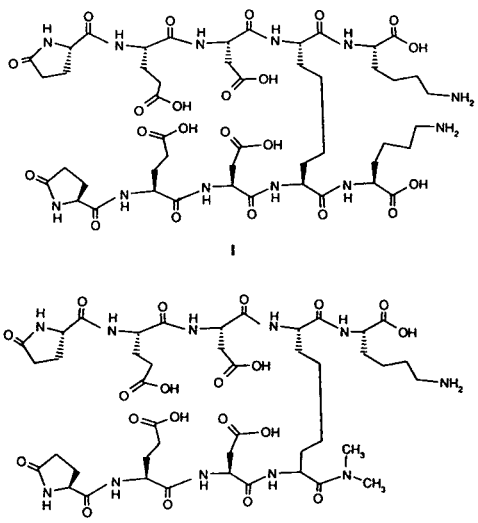

Fig. 1. Structures of I and internal standard (IS).

silica column. Following separation, a selective post-column reaction of the ϵ-amino groups of the lysine moieties of the peptide with *o*-phthaldialdehyde and a thiol under basic conditions was used to generate a highly fluorescent isoindole product which was subsequently detected on-line with a fluorometer.

2. Materials and methods

2.1. Chemicals

SB 107647 (I) and the internal standard (SB 203285, IS) were supplied by Central Supply and Investigational Materials, SmithKline Beecham Pharmaceuticals (Swedeland, PA, USA). Glacial acetic acid and monochloroacetic acid were obtained from Mallinckrodt Chemical Company (Paris, KY, USA). Citric acid monohydrate, sodium hydroxide, HPLC-grade methanol and acetonitrile were obtained from J.T. Baker Chemical Company (Phillipsburg, NJ, USA). Disodium EDTA was obtained from E.M. Science (Cherry Hill, NJ, USA). Sodium salt of 1-octanesulfonate was purchased from Regis Chemical Company (Morton Grove, IL, USA). Thiofluor (N,N-dimethyl-2-mercapto ethylamine hydrochloride) was purchased from Pickering Laboratories (Mountain View, CA, USA). *o*-Phthaldialdehyde was purchased from Fluka Chemical Corporation (Ronkonkoma, NY, USA). Strong anion exchange (SAX) solid-phase extraction cartridges (100 mg, 1 ml) and the Vac-Elut manifold were purchased from Analytichem International (Harbor City, CA, USA).

2.2. Reagents

0.3 M Monochloroacetate (MCA) buffer

28.3 g of monochloroacetic acid, 9.8 g of sodium hydroxide and 1.0 g of disodium EDTA were dissolved in 1 l of HPLC-grade water. The final pH of the solution was 3.2.

Mobile phase buffer

Sodium salt of 1-octane sulfonate (10 m*M*, 2.16 g) was dissolved in 100 ml of 0.3 *M* monochloroacetate buffer, pH 3.2 and 900 ml of HPLC-grade water. The solution was filtered through a 0.45-μm membrane filter (type HA, Millipore, USA).

o-Phthaldialdehyde (OPA) reagent solution

Sodium hydroxide (1.0 g) was first dissolved in 500 ml of HPLC-grade water and filtered through a 0.45-μm membrane filter (type HA, Millipore). The solution was sonicated for approximately 10 min and then sparged with helium for approximately 10 min. To this alkaline solution, 2 ml of freshly prepared methanolic solution of *o*-phthaldialdehyde (OPA, 2 mg/ml) and 80 mg of thiofluor were added and the contents were mixed by swirling. The solution was sparged continuously with helium during its use as post-column reagent. The solution was stable for 48 h.

Stock standard solutions

The stock standard solutions of **I** and IS were prepared by dissolving appropriate amounts of the peptide in 0.05 *M* acetic acid to give a final solution concentration of 1 mg/ml. These stock solutions were stable for 2 months when stored at 4°C. Appropriate dilutions of the stock solution of **I** were made fresh every day with 0.05 *M*

acetic acid solution to generate a series of working standard solutions (100, 10, 1 and 0.1 μg/ml). The stock solution of IS was diluted 1:200 with 0.05 *M* acetic acid to give a solution concentration of 5 μg/ml. The working internal standard solution was stable for 2 months when stored at 4°C.

2.3. Calibration

A set of plasma calibration standards (concentrations of **I**: 20, 40, 100, 200, 400, 1000, 2000, 4000 ng/ml) was analyzed with every determination of **I** in plasma samples of unknown concentration, by adding appropriate volumes of the working standards of **I** to 0.25 ml of plasma. A weighted $(1/y)$ linear regression was used to construct a calibration curve for the peak height ratio of analyte to internal standard *vs.* analyte concentration. The concentration of **I** in plasma samples was then calculated using the equation $y = bx + a$, where b = slope of regression line, a = y-intercept of regression line, x = concentration of **I** in ng/ml and y = peak height of **I** in millivolts (mV)/peak height of IS in millivolts (mV)

2.4. Extraction of I from plasma

An aliquot of heparinized plasma (0.25 ml) mixed with 200 μl of 0.05 *M* acetic acid (contains standards when preparing standard curve) and 50 μl of internal standard solution (5 μg/ml, IS) was added to 500 μl of acetonitrile in a 75 × 12 mm borosilicate tube in order to precipitate plasma proteins. The sample was then centrifuged at approximately 2000 *g* for 5 min. An SAX extraction column was conditioned by successive washings with 1 ml of methanol and 1 ml of water. The deproteinated plasma sample was then applied onto the SAX column under reduced pressure at 1–2 in. of Hg (1 in. Hg ≈ 3386 Pa). After passage of the sample through the column, the vacuum was increased to 10–15 in. of Hg to remove any traces of plasma from the extraction column. The column was then washed with 1 ml of water and the washing solvent was completely removed from the sorbent bed prior to elution of analytes. The analytes were then eluted from the column with 0.25 ml of citric acid (0.1 *M*, pH 2.2) under reduced pressure (1–2 in. of Hg) and the eluate was collected into a 1.5 ml polypropylene Eppendorf micro centrifuge tube (Brinkmann Instruments, Westbury, NY, USA). The sample was centrifuged in a micro-centrifuge (Model microfuge E, Beckman Instruments, Palo Alto, CA, USA) at approximately 2000 *g* for 5 min and the supernatant was transferred to an autosampler vial. A portion of the extract (25–130 μl) was injected into the HPLC system for analysis.

2.5. High-performance liquid chromatography

The HPLC system consisted of a 665A-12 high pressure gradient semi-micro solvent delivery system (Hitachi Instruments, Danbury, CT, USA), an autoinjector (WISP, Model 710B; Waters Assoc., Millford, MA, USA), a 1 ml post-column reaction coil (ABI Analytical, Ramsey, NJ, USA) and a FL-750B fluorescence detector (McPherson, Acton, MA, USA). Chromatographic separations were carried out on a 15 cm × 2.1 mm I.D. Zorbax Rx 5 μm octyl silica column (Mac Mod Analytical, Chadds Ford, PA, USA) which was preceded by a 3 cm × 2.1 mm I.D. C_8 guard column (ABI Analytical). The column was maintained at 40°C with a column heater (Model 725-1010, Rainin Instruments, Woburn, MA, USA). Standard HPLC tubing (0.007 in. I.D. × 1/8 in. O.D.) was used to connect the various components of the HPLC system. The isocratic mobile phase was composed of 30 m*M* MCA buffer with 10 m*M* octane sulfonate, pH 3.2, and methanol mixed on-line at a ratio of 80:20 (v/v) and pumped at 300 μl/min. An additional pump (Model 114, Beckman) was utilized to deliver the OPA reagent solution at a flow-rate of 100 μl/min to the post column reaction coil (1 ml), where it was mixed with the column effluent utilizing a low dead-volume 10 μl Visco Mixer (The Lee Company, Westbrook, CT, USA). The resulting fluorescent reaction product was detected with the fluorome-

ter. The fluorescence detector was equipped with a High Sensitivity Accessory (HSA) and utilized a 200 W xenon–mercury lamp. The xenon–mercury lamp allowed optimum signal-to-noise (S/N) ratio via use of the lamp emission maxima instead of compound extinction maxima. Since the mercury line emission maximum spans a relatively narrow range which is within the range where the fluorescence of the peptide derivative is excited, an increase in sensitivity for **I** was observed. The excitation wavelength was set approximately 336 nm (the mercury emission line may vary slightly depending on the lamp). A band pass filter (UT-1), which transmits the light between 250 and 400 nm, was also installed on the excitation side of the monochromator. The fluorescence emission was monitored at HSA utilizing an 400 nm cut-off filter. An automated laboratory system (PE/Nelson Access Chrom, Version 1.8, Cupertino, CA, USA) was used for data acquisition and processing. Chromatographic peak height data were collected and used for the generation of standard curves.

2.6. Validation procedures

Four pools of plasma precision samples containing 20, 40, 400 and 4000 ng/ml of **I** were prepared by adding appropriate volumes of standard solutions to drug-free dog plasma. These plasma samples were stored at − 80°C until analysis was performed. Six replicate samples from each pool were extracted and analyzed on three separate days. Concentrations were determined by comparison with a calibration curve prepared on the day of analysis. From the data obtained, intra-day precision (determined as the mean of the daily relative standard deviations, R.S.D.s), inter-day precision (determined as the R.S.D. of the daily means) and mean accuracy were calculated.

2.7. Absolute recovery

Known amounts of **I** and the internal standard were dissolved in drug-free plasma samples (n = 6) and processed according to the methods described earlier. In order to estimate recovery, the peak heights observed were compared with those obtained by direct injection in triplicate of known amounts of the two compounds equivalent to 100% recovery. Recovery of **I** and internal standard was expressed as a percent value relative to the peak height observed following direct injection.

3. Results and discussion

The need to measure endogenous bioactive peptides and their synthetic analogs in biological fluids requires a highly sensitive and specific analytical methodology. The application of HPLC to such a problem typically requires chemical derivatization in order to improve the native detectability of the peptide analyte. For many peptide analytes containing an α- or ϵ-amino group, derivatization with one of the many fluorescent reagents available for primary amines is an attractive approach to high sensitivity detection by HPLC. Of the several fluorescent reagents [4–7] available for the derivatization of primary amines, only *o*-phthaldialdehyde (OPA) reacted readily with ϵ-amino group of the lysine moiety of **I**, in presence of a thiol and base, and yielded a highly fluorescent substituted isoindole product. Since pre-column derivatization of **I** with OPA–thiol was precluded due to presence of multiple sites of reaction and limited stability of the peptide in base, the reaction was carried out in the post-column mode following chromatographic separation on a reversed-phase column.

In order to optimize the reaction conditions for the 2.0 mm I.D. reversed-phase columns used here, several post-column reaction parameters were examined using **I** as a substrate. The post-column reaction conditions were optimized for reagent flow-rate, base concentration, concentration of OPA and thiol, and reaction time by injecting 100 ng of **I** onto the column and monitoring the intensity of the fluorescence signal obtained. Results from these experiments led to the development of a post-column reagent that contains 8 mg of OPA and 160 mg of thiofluor in 1 l of 0.05 *M* sodium hydroxide

solution. Use of sodium hydroxide in place of the traditionally used borate buffer to prepare the OPA–thiol reagent solution not only improved the sensitivity of the method by reducing the volume of post-column reagent needed but also reduced the fluorescence background and noise. Optimum results were obtained when this OPA–thiol reagent was pumped at a flow-rate of 100 μl/min and the reaction was allowed to take place for 2.5 min in a 1 ml reaction coil at room temperature. Fig. 2 displays a chromatogram of a standard solution of **I** and the internal standard (IS). Application of this methodology provided a sensitive assay to determine **I** concentrations in dog and rat plasma samples. The assay involved anion-exchange solid-phase extraction of the peptide from deproteinated plasma, as a preliminary isolation step, followed by ion-pair chromatographic separation on a reversed-phase column and post-column reaction detection.

3.1. Recovery and stability

Due to presence of several carboxyl groups in the peptide chains, both **I** and the internal standard are well retained on a strong anion-exchange solid phase extraction column and provide a highly selective method of isolation of these analytes from the acidified and deproteinated plasma. Deproteination of plasma with acetonitrile is essential in order to retain the peptide analytes on SAX column. Use of other deproteinating agents such as trichloroacetic acid in place of acetonitrile significantly reduced the recovery of these peptides. Following the application of a deproteinated plasma sample onto the SAX column, the analytes are eluted with a minimum volume of dilute aqueous (0.1 *M*) citric acid. The recovery of **I** from dog plasma at 20 and 4000 ng/ml was 50.0 ± 5.94 and 56.6 ± 1.45% (mean ± S.D.), respectively. The recovery of the internal standard from plasma at a concentration of 250 ng/ml was 72.6 ± 3.28% (mean ± S.D.). Elution of the peptide analytes from the SAX column with excess 0.1 *M* methanolic citric acid (1 ml) followed by removal of methanol by evaporation, greatly decreased the recovery of these peptides. Although the recovery of **I** from the SAX column was improved through the use of higher molar concentrations of aqueous citric acid (0.5 to 1.0 *M*), the analytical column life was greatly reduced when these extracts were injected onto the column during routine use. Both **I** and the internal standard were stable in the final extract for at least 48 h.

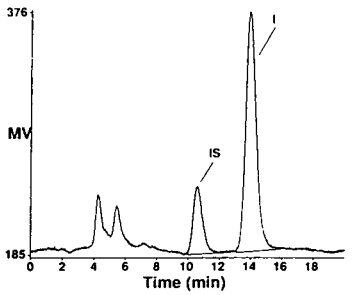

Fig. 2. Chromatogram of aqueous standard solution of **I** and IS. 100 ng of **I** and 25 ng of IS injected on column. Chromatographic conditions: column, 150 × 2.1 mm Zorbax Rx C_8 silica maintained at 40°C; mobile phase, 30 m*M* MCA buffer with 10 m*M* octane sulfonate, pH 3.2 and methanol (80:20, v/v); flow-rate, 300 μl/min; injection volume, 130 μl.

3.2. Sensitivity, linearity and selectivity

By utilizing a 2.1 mm I.D. HPLC column, the on-column limit of detection of **I** (signal-to-noise ratio 3) was 1 ng. The limit of detection and quantification for **I** in 0.25 ml plasma samples was 10 and 20 ng/ml, respectively. The calibration curves were linear over the range of 20–4000 ng/ml of **I**. Based on the analysis of drug-free plasma samples, endogenous plasma components did not interfere with the drug and the internal standard over the concentration range described here. Weighted ($1/y$) linear regression analysis of calibration curves provided the equation $y = 0.00093\,x + 0.001443$ and a correlation coefficient greater than 0.99. The calibration curves were highly reproducible. The precision, as measured by the relative standard deviations at each of the spiked concentrations, and accuracy, evaluated by the average concentration back-calculated from the respective standard curves, are shown in Table 1.

Table 1
Back calculated standard curve concentrations for I

	Nominal concentrations of I in plasma (ng/ml)							
	20	40	100	200	400	1000	2000	4000
Day 1	17.31	53.72	93.38	195.75	391.89	947.02	2079.28	4199.90
Day 2	22.75	42.67	94.07	192.37	394.20	967.95	1952.82	4099.56
Day 3	23.38	38.37	105.13	189.91	370.07	876.97	2037.38	4146.24
Mean	21.15	44.92	97.53	192.68	385.39	930.65	2023.16	4148.57
S.D.	3.34	7.92	6.59	2.93	13.32	47.65	64.42	50.21
R.S.D. (%)	15.79	17.60	6.76	1.52	3.46	5.12	3.18	1.21
Accuracy	105.75	112.30	97.53	96.34	96.35	93.07	101.16	103.71

3.3. Accuracy and precision

Table 2 summarizes the results obtained from a three-day dog plasma validation study in which six replicate spiked standards at four concentrations, 20, 40, 400 and 4000 ng/ml, were analyzed by this methodology. The mean accuracy of the assay at these concentrations ranged from 91.61 to 106.95%, whereas the intra-day precision, indicated by the mean of the daily R.S.D.s, ranged from 4.46 to 17.72%. The inter-day precision, indicated by the R.S.D.s of the daily means, ranged from 5.3 to 14.44%. The inter-day R.S.D.s of the method were also calculated by analyzing three pools of quality control dog plasma samples spiked with 40, 400 and 4000 ng/ml of I over period of 10 days. The inter-day R.S.D.s from the analysis of these samples (n = 19) were found to be 8.04, 12.26 and 10.14%, respectively. A one-day validation of the method was also carried out in rat plasma in order to check the suitability of this methodology for the analysis of rat plasma samples. At I concentrations of 20, 40, 400 and 4000 ng/ml of plasma,

Table 2
Accuracy and precision data for I in dog plasma

Parameter	Nominal concentrations of I in plasma (ng/ml)			
	20	40	400	4000
R.S.D				
Day 1	17.25	18.19	3.92	3.02
Day 2	15.45	7.43	1.98	3.25
Day 3	20.47	6.19	13.05	7.09
Error (%) [a]				
Day 1	+2.30	+2.41	−18.87	−6.27
Day 2	+1.27	+5.03	+4.07	+18.51
Day 3	−7.24	+13.42	−10.36	−7.49
Inter-day R.S.D. [b]	5.30	5.38	12.66	14.44
Intra-day R.S.D. [c]	17.72	10.60	6.32	4.46
Mean accuracy (%)	98.78	106.95	91.61	101.58

[a] (Calculated concentration − actual concentration)/actual concentration × 100.
[b] Coefficients of variation of daily means.
[c] Mean of the daily R.S.D.s.

the intra-day R.S.D.s were found to be 13.75, 8.11, 4.35 and 6.01%, respectively. The accuracy of the method in this study was found to be 101.3, 109.2, 97.3 and 94.3%, respectively.

3.4. Application of the procedure to plasma samples

The quantitative HPLC methodology described here provides a selective and sensitive detection of **I** in dog and rat plasma samples. A typical chromatogram of a plasma extract obtained from drug free dog plasma and a plasma sample spiked with 100 ng/ml of **I** is shown in Fig. 3. The chromatography was highly reproducible and provided a retention time for **I** and IS of 11.5 and 14.5 min, respectively. To date the method has been used successfully in the analysis of plasma samples from pre-clinical studies in dogs and rats. In conclusion, a sensitive and selective high-performance liquid chromatographic method has been developed for the determination of **I** in dog and rat plasma samples. The assay performed acceptably in a three-day validation over a concentration range of 20 to 4000 ng/ml, sufficiently accurate and precise to support toxicokinetic studies for **I** in dogs and rats.

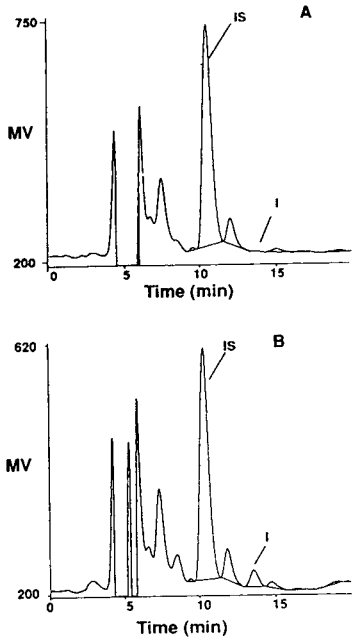

Fig. 3. Chromatograms of plasma extracts from dog plasma spiked with 250 ng/ml of IS (A) and plasma sample spiked with 250 ng/ml of IS and 100 ng/ml of **I** (B). See Fig. 2 for chromatographic conditions. Injection volume, 130 μl.

4. References

[1] A.G. King, P. Bhatnagar, J. Balcarek and L.M. Pelus, *Exp. Hematol.*, 19 (1991) 481.
[2] L.M. Pelus, P. Bhatnagar, C. Frey, P. DeMarsh and A.G. King, *Exp. Hematol.*, 19 (1991) 481.
[3] P. DeMarsh, P. Bhatnagar, R.A. Levin, L.M. Pelus and S.R. Petteway, *Exp. Hematol.*, 20 (1992) 726.
[4] V.K. Boppana, C Miller-Stein, J. Politowski and G.R. Rhodes, *J. Chromatogr.*, 548 (1991) 327.
[5] V.K. Boppana, R.C. Simpson, K. Anderson, C Miller-Stein, T.J.A. Blake, B.Y-H. Hwang and G.R. Rhodes, *J. Chromatogr.*, 593 (1992) 29.
[6] W.F. Kline, B.K. Matuszewski and J.Y.-K. Hsieh, *J. Chromatogr.*, 578 (1992) 31.
[7] S. Einarsson, B. Josefsson and S. Lagerkvist, *J. Chromatogr.*, 282 (1983) 609.

ELSEVIER

Journal of Chromatography A, 676 (1994) 169–176

JOURNAL OF CHROMATOGRAPHY A

Comparative and optimized dabsyl-amino acid analysis of synthetic phosphopeptides and glycopeptides

Livia Gorbics, Laszlo Urge, Laszlo Otvos, Jr.*

Wistar Institute of Anatomy and Biology, 3601 Spruce Street, Philadelphia, PA 19104-4268, USA

Abstract

The optimal conditions for amino acid analysis of phosphopeptides and N-acetylglucosamine- and N-acetylgalactosamine-containing glycopeptides were investigated by dabsyl-Cl derivatization and reversed-phase high-performance liquid chromatographic separation. By comparing the chromatographic behaviour of the dabsylated phosphoamino acids and dabsylated aminosugars on three different columns, it appears that the mechanism of binding to the column is different for the two modified dabsyl derivatives. The acid sensitivities of sugar and phosphate groups were also investigated. We found that while the optimal hydrolysis conditions for phosphopeptide analysis are peptide sequence-dependent, there is generally an applicable condition for the highest recovery of glycopeptides. A 1-h gas-phase hydrolysis time seems to be appropriate for the majority of glycopeptides and 1.5 h is suitable for the majority of phosphopeptides. The analysis was extended to the successful verification of the presence of the N-acetylglucosamine and the N-acetylgalactosamine moieties when these sugars were incorporated as parts of a disaccharide side chain of glycopeptides.

1. Introduction

Although codons for only 20 amino acids are found in the genome (and are used in protein synthesis), 140 modified amino acids exist in various proteins [1]. These posttranslationally modified proteins are known to play a crucial role in many recognition processes. The two most frequent forms of posttranslational modifications are the phosphorylation of hydroxyamino acids and the glycosylation of the asparagine, serine and threonine residues. Both the oligosaccharide antennae and the negatively charged phosphoryl groups are located on the surface of the proteins and, therefore, can easily participate in numerous recognition processes. The structure and the biological significance of glycosylated and phosphorylated proteins have been discussed in a great variety of review articles [2–8].

Small- and medium-sized glycopeptides and phosphopeptides are appropriate models for biological studies so the improvement of their synthesis has become the focus of interest. Since the basic methodology of glycopeptide synthesis has been developed, the current study addresses the incorporation of more complex sugar systems [9]. As a result of this improvement longer oligosaccharide chains can be attached to a model peptide, where the first sugar moiety is N-acetylglucosamine (GlcNAc, 2-acetamido-2-deoxy-D-glucose) or N-acetylgalactosamine (GalNAc, 2-acetamido-2-deoxy-D-galactose) in almost all cases [10].

* Corresponding author.

0021-9673/94/$07.00
SSDI 0021-9673(94)00176-A

Recognition of the increasing importance of model glycopeptides and phosphopeptides demanded the development of appropriate analytical methods [11,12]. Among the standard procedures of amino acid analysis the use of 4-dimethylaminoazobenzene-4′-sulphonyl chloride (dabsyl-Cl) is the most appropriate for analysis of acid-sensitive phosphopeptides and glycopeptides [13,14]. Partial hydrolysis, the stability of dabsyl-phosphoamino acids and dabsyl-aminosugars, and the usage of visible wavelength are the advantages of this analysis method. Recently, we reported the application of the dabsyl-Cl amino acid analysis for the compositional study of synthetic glycopeptides [13] and phosphopeptides [14].

In this paper we further investigate the optimal hydrolysis and chromatographic conditions of the similarly acid-sensitive glycopeptides and phosphopeptides and extend the amino acid analysis of glycopeptides to those disaccharide-containing units of the natural glycoprotein antennae.

2. Experimental

2.1. Chemicals

The unmodified and modified peptides were synthesized in our laboratory [15,16] and their composition was verified (including mass spectroscopy). Phosphoamino acid standards, O-phospho-L-serine (L-2-amino-3-hydroxypropanoic acid 3-phosphate), O-phospho-L-threonine (L-2-amino-3-hydroxybutanoic acid 3-phosphate), O-phospho-L-tyrosine [L-3-(4-hydroxyphenyl)alanine 4′-phosphate], were purchased from Sigma (St. Louis, MO, USA). Sugar standards glucosamine (2-amino-2-deoxy-D-glucopyranose), galactosamine (2-amino-2-deoxy-D-galactopyranose), mannosamine (2-amino-2-deoxy-D-mannopyranose), GlcNAc and GalNAc were purchased from Sigma. Gal(β1–3)GalNAc (Gal = galactose) standard was purchased from Bachem (Torrance, CA, USA), Fmoc-Asn(O-tBu)-Gal(β1-3)GlcNAc (Fmoc = 9-fluorenylmethoxycarbonyl; tBu = *tert.*-butyl) was synthesized in our laboratory [17]. Hydrolysis and dabsylating reagents were purchased from Beckman (Fullerton, CA, USA), HPLC solvents and all the rest of the chemicals were from Aldrich (Milwaukee, WI, USA).

2.2. Gas-phase hydrolysis

Lyophilized samples (twelve in 600-μl vials) and 700 μl of 6 *M* HCl were placed in a hydrolysis vessel (provided by Beckman; volume 113 ml), and then flushed with argon and evacuated at 0.1 mbar for 1–2 min. The vessels were placed in a drying oven at 110°C for 1 or more h (see details in Results and discussion section).

2.3. Dabsylation

The amino acid mixture —the result of hydrolysis of 2–5 nmol peptide or phosphoamino acid standards— was dissolved in 20 μl $NaHCO_3$–NaOH buffer (pH 8.3) and to that mixture 40 μl dabsyl-Cl solution (40 μg in 40 μl acetonitrile) was added [18–20]. The vials were closed and placed in a drying oven at 70°C for 12–14 min. After derivatization, samples were diluted with 440 μl of ethanol–water (1:1), and 8% of the diluted sample was injected for HPLC analysis.

2.4. HPLC

The Beckman System Gold HPLC apparatus consisted of a 126 programmable solvent delivery module, a 167 scanning UV–visible detector module operating at 436 nm, a Rheodyne 7725i injector, and a C_{18} column. Three different columns were used: a Beckman Ultrasphere-dabsyl C_{18} column (250 × 4.6 mm), a Merck LiChrospher 100 RP-18 column (Gibbstown, NJ, USA) (5 μm; 250 × 4.0 mm) and an Alltech Econosphere analytical column (Deerfield, IL, USA) (5 μm; 250 × 4.6 mm). The columns were installed as follows: the columns were rinsed with 30% acetonitrile in water for 30 min at 1 ml/min then rinsed with an installation buffer for 30 min at 1 ml/min. The installation buffer was a

Table 1
Solvent composition during RP-HPLC

Gradient	Time (min)	Solvent		Duration (min)
		A (%)	B (%)	
1	Start	71	29	
	0	49	51	24
	24	14	86	10
	40	0	100	1
	47	71	29	0.25
	55			End of run
2	Start	71	29	
	0	49	51	12
	12	14	86	5
	20	0	100	1
	27	71	29	0.25
	35			End of run

solution of 100 m*M* citric acid, pH 3.5 containing 20% N,N-dimethylformamide (DMF). After this procedure the columns were rinsed with solution A and solution B (see below) until the baseline stabilized.

The HPLC system was controlled by an IBM system 2 Model 55SX personal computer with Beckman System Gold Personal Chromatography software version 6.0. The chromatographic conditions were as follows: solution A (final pH 6.50 ± 0.05) contained 100 ml of 0.11 *M* sodium citrate (pH 6.51), 860 ml HPLC water and 40 ml DMF. Solution B contained 300 ml solution A, 672 ml acetonitrile and 28 ml DMF. The flow-rate was 1.4 ml/min. The gradient conditions were as listed in Table 1. The solution vessels were continuously flushed with argon. All runs were done at room temperature.

3. Results and discussion

The main goal of our study was to investigate the influence of the identity of the chromatographic column, the influence of the extension of sugar chain, and the influence of changes of the partial hydrolysis conditions on our analysis method.

3.1. Chromatographic behaviour of dabsylated phosphoamino acids and aminosugars

Three different columns were used in order to compare the elution properties of dabsylated phosphoamino acids and aminosugars. (2-Aminosugars were found as the only derivatizable species after hydrolysis of GlcNAc and GalNAc [13].) The columns used were manufactured by Beckman, Merck and Alltech. Using the same elution conditions we observed slight differences among the resolution of the three columns. The three phosphoamino acids (phosphoserine, phosphothreonine and phosphotyrosine) eluted in the same order on all columns (Table 2). Comparison of the retention times show that on the Alltech column the hydrophilic amino acids eluted very early. Dabsyl-aminosugars were eluted from all three columns in the following order: galactosamine, glucosamine and mannosamine (Fig. 1A). The absolute retention times of the aminosugars were very similar on each column (Table 2). The retention times of the other peaks (phosphoamino acids and dabsyl-OH) however, were shorter on the Alltech column than on the other two indicating the possibility that dabsyl-aminosugars bound to the Alltech column by a differ-

Table 2
Comparison of retention time of dabsyl-phosphoamino acids and dabsyl-amino sugar standards

Column	Retention time (min)					
	Phosphoserine	Phosphothreonine	Phosphotyrosine	Galactosamine	Glucosamine	Mannosamine
Beckman	7.48	8.26	9.10	19.39	20.08	20.75
Merck	7.37	8.11	9.09	20.36	21.11	21.85
Alltech	5.62	6.20	6.80	19.94	20.65	21.38

ent mechanism than the other derivatized species.

When a dabsyl-amino acid standard mixture was injected into each column we found that the separation properties of Beckman and Merck columns were similar, while on the Alltech column the peaks eluted much earlier.

Chromatograms made after coinjection of the amino acid standards, phosphoamino acids and aminosugars provided the best comparison of the elution properties from the different columns (Fig. 1C). Phosphopeptides eluted separately from the hydrophilic amino acids (aspartic, glutamic) on the Beckman and Merck columns, while they could not be separated on the Alltech column. Glucosamine eluted between the proline and valine peaks, galactosamine coeluted with the proline, and mannosamine coeluted with the valine. (In our previous study [13] using gradient 2 we could separate proline from galactosamine.)

In summary, the strongly hydrophilic feature of the phosphate group equally shifted the retention time of the corresponding unmodified dabsyl-amino acids as was expected and did not change the order of the peaks. In addition, no major difference was found in the elution profile of phosphoamino acids from the different columns. Good separation of phosphoamino acids from the other amino acids can be achieved by modifying the gradient or the pH of the eluents in each of the columns tested. Derivatized aminosugars were eluted later than it was predicted by their hydrophilic properties. While the reversed-phase chromatographic behaviour of the glycopeptides was dependent upon the conformation of both the peptide and the sugar, the incorporation of phosphate group decreased the retention time of the non-phosphorylated analogues independent of the peptide sequence [21]. Our findings concern both the separation of

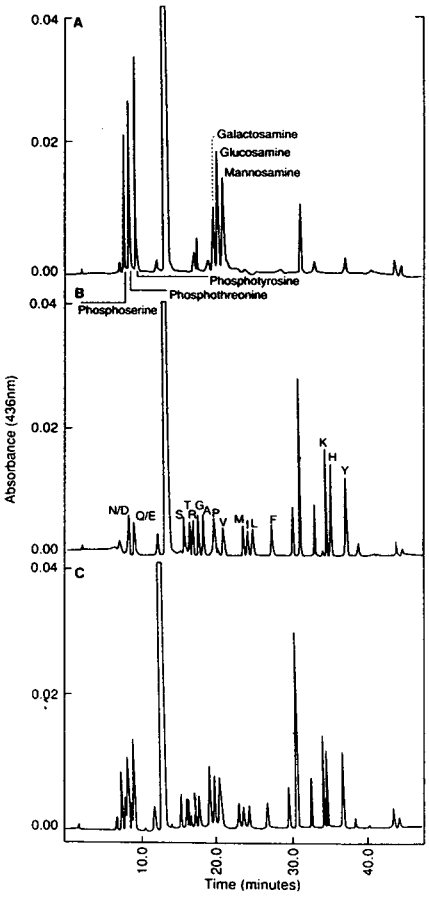

Fig. 1. Chromatographic separation of dabsyl-phosphoamino acids and dabsyl-aminosugars (A), dabsyl-amino acids (B) and a mixture of dabsyl-phosphoamino acids, amino acids and aminosugars (C). The separation was carried on a Beckman column using gradient 1 (Table 1).

phosphopeptides/glycopeptides, and the chromatographic behaviour of dabsyl-phosphoamino acid standards or dabsyl-aminosugars. These results emphasize the importance of not only the hydrolysis or derivatization conditions, but also the identity of chromatographic columns for finding appropriate conditions for successful aminosugar or phosphate analysis.

3.2. Analysis of disaccharide-containing glycopeptides

The ultimate goal of our study was to extend the analysis of glycopeptides from monosaccharide- to oligosaccharide-containing glycopeptides. GlcNAc and GalNAc were the first sugar moieties found in natural glycoproteins, therefore their presence in protein hydrolysates is a clear indication of the presence of glycosylated protein backbone. Most of the synthetic glycopeptide models also contain these sugar residues, so that analysis of GlcNAc and GalNAc can indicate the success of glycopeptide synthesis. In our previous study [13] we reported the development of a dabsyl-amino acid analysis method to verify the presence of the GlcNAc and GalNAc in glycopeptides. These sugar residues can be hydrolyzed by selective hydrolysis to glucosamine and galactosamine, and these intermediate products can be derivatized in a manner similar to that used for amino acids. These glycopeptides contained only monosaccharide units. In the current study we extended our analysis method to glycopeptides in which the sugar moiety is a disaccharide.

First, we investigated if our method could be used for disaccharide standards. We hydrolysed a Gal(β1–3)GalNAc standard for 1 h, dabsylated it, and analyzed it with gradient 2 (Table 1) using the Beckman column. Fig. 2A shows the chromatogram of this analysis. The peak at 14.22 min (labeled with an asterisk) eluted at the same position as the previously studied galactosamine from the GalNAc monosaccharide standard. This result indicated that the presence of a GalNAc moiety can be detected not only for the monosaccharide, but also as a part of a disaccharide. The utility of the strategy was tested

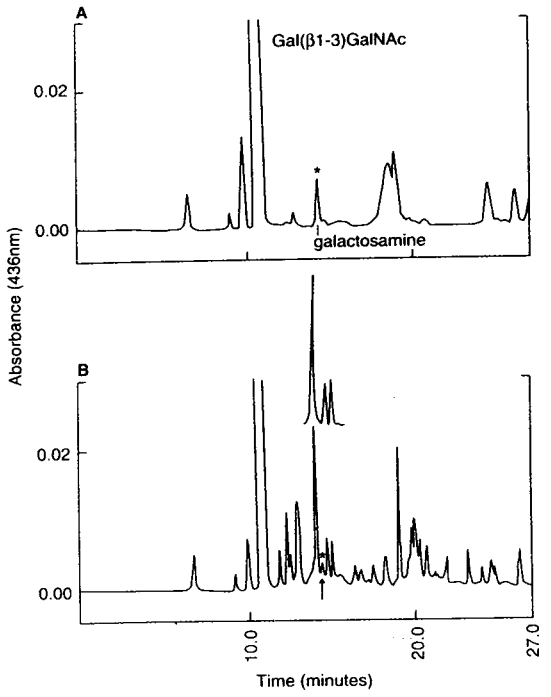

Fig. 2. Chromatograms of the analysis of Gal(β1–3)GalNAc standard (A) and a *Drosophila*-originated O-glycosylated glycopeptide (B), GKPRPYSPRPT[Gal(β1–3)GalNAc]SHPRPIRV after 1 h hydrolysis and derivatization. For chromatographic analysis we used gradient 2 (Table 1).

on two O-glycosylated peptides. Using the same conditions for the hydrolysis and for the analysis we could easily detect the presence of sugar on peptide 31DS {sequence: T[Gal(β1–3)GalNAc]RIMMNGGR}. This sequence does not contain proline or valine residues (neighbouring dabsyl derivatives) so that the separation of dabsyl-galactosamine from the dabsyl-amino acid peaks was unambiguous. An extra peak at the position of dabsyl-galactosamine verified the presence of GalNAc (data not shown). We tested our method on a *Drosophila*-originated peptide [22], GKPRPYSPRPT[Gal(β1 – 3)GalNAc]SHPRPIRV. The difficulty level of this analysis was particularly high, since the sequence contained six prolines and one valine. Fig. 2B illustrates the result of the analysis. An extra peak was found at 14.20 min (labeled with an asterisk). The chromatogram of the non-glycosylated pep-

tide (processed exactly the same way) did not contain this peak (see insert), indicating that the extra peak on the chromatogram of the glycosylated peptide can be assigned to the sugar (GalNAc), and that the peak was not an intermediate of the partial hydrolysis of the peptide bonds.

To test whether the presence of GlcNAc in a disaccharide can be detected, we synthesized an Fmoc-Asn(OtBu)-[Gal(β1–3)GlcNAc] standard [17]. After a 1-h acidic hydrolysis and derivatization we analyzed it with gradient 1 (Table 1) on a Beckman column. Fig. 3A shows the chromatogram of this analysis where we found an extra peak at the position of the dabsyl-glucosamine peak (20.70 min). This result indicates that the presence of GlcNAc as a part of a disaccharide side chain can be analyzed in the same way as a monosaccharide GlcNAc linked to a peptide chain. The utility of the method was tested on an N-glycosylated peptide, N[Gal(β1–3)GlcNAc]HSGKRELSAEK. Fig. 3B shows the chromatogram of the analysis of this peptide. The peak at 20.12 min (labeled with an asterisk) coeluting with the GlcNAc standard verified the presence of the sugar. (The shift in the retention times compared to those in Fig. 3A is similarly observable for the other peaks and reflects aging of the column [23].)

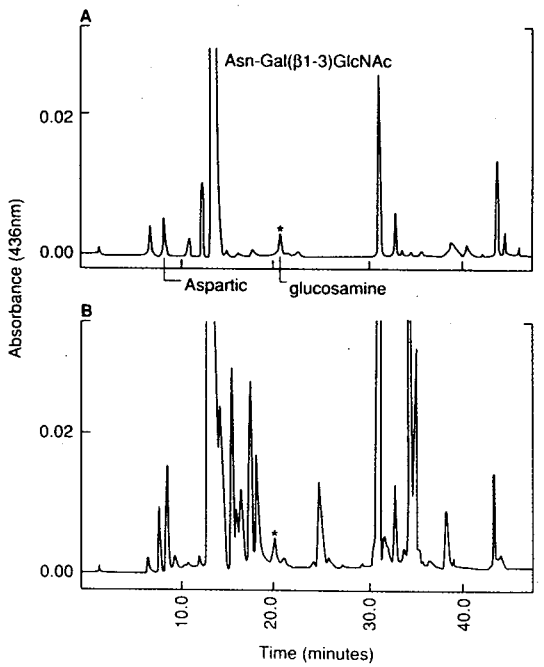

Fig. 3. Chromatograms of the analysis of Fmoc-Asn(O-tBu)Gal(β1–3)GlcNAc standard (A) and a N-glycosylated glycopeptide (B), N[Gal(β1–3)GlcNAc]HSGKRELSAEK after 1 h hydrolysis and derivatization. For chromatographic analysis we used gradient 1 (Table 1).

In summary, our previously developed analysis method, using standard dabsyl-Cl amino acid analysis for verifying the presence of GalNAc or GlcNAc on synthetic glycopeptides, is suitable when a disaccharide is attached to the peptide chain with either O- or N-glycosydic linkages. GlcNAc and GalNAc are the first sugar residues in natural glycoproteins, and thus, verification of their presence is a clear indication of a successful glycosylation not only in synthetic glycopeptides, but in protein hydrolysates as well.

3.3. Comparison of partial hydrolysis conditions of glycopeptides and phosphopeptides

Both sugars and phosphoamino acids are labile during standard acidic hydrolysis, but partial hydrolysis can offer a viable alternative for their analysis [13,14,24]. Partial hydrolysis conditions are, however, found to be inappropriate for qualitative analysis of both amino acids and modified derivatives. Nevertheless, verification of the presence of phosphate groups, as well as sugars, is an important task for peptide synthesis laboratories. Instrumentation for a standard amino acid analysis is available in almost all peptide or protein laboratories; therefore, partial hydrolysis combined with a standard derivatization procedure offers a quick, inexpensive, and unambiguous checking method.

In order to study partial hydrolysis conditions, a phosphoserine standard, two phosphopeptides, a GlcNAc standard and two glycopeptides were partially hydrolysed using different hydrolysis times. Our goal was to find optimal hydrolysis times for these acid-sensitive residues. The sequence of these peptides were: GDS(Ph)KG, GDRS(Ph)G, N(GlcNAc)TTNYT, and DELLQKEQN(GlcNAc)YSDDVLA.

Table 3 illustrates that less glucosamine was

Table 3
Yield (recovery) of glucosamine or phosphoserine hydrolyzing GlcNAc or phosphoserine standards as well as glycopeptides or phosphopeptides

Sample	Yield (%) after hydrolysis time of			
	1 h	2 h	3 h	4 h
GlcNAc	17	8	5	
N(GlcNAc)TTNYT	22	12	10	
DELLQKEQN(GlcNAc)YSDDVLA	24	20	11	
Phosphoserine	77	53	21	15
GDS(phospho)KG	7	12	4	4
GDRS(phospho)G	10	9	3	2

recovered from the GlcNAc standard as the hydrolysis time increased. A 1-h hydrolysis gave the highest recovery of glucosamine from GlcNAc. As we reported earlier [13], less than 1 h hydrolysis decreases the recovery of glucosamine from GlcNAc, because the hydrolysis of the acetamido group requires some time. Similarly, a 1-h hydrolysis was found to be the optimum for glycopeptides (Table 3). As the hydrolysis time increased the recovery of the sugar slowly decreased. It is important to note that 1 h hydrolysis was found reliable not only for these two glycopeptides, but for several other glycopeptides that were analyzed earlier [13]. In our experience, the analysis of glycopeptides with partial acid hydrolysis does not seem to be peptide sequence-dependent.

Similar experiments with phosphoserine and phosphopeptides (Table 3) demonstrated that a longer period of hydrolysis resulted in a dramatic decrease in the recovery of phosphoserine. A 1-h hydrolysis gave the best results. Under the same conditions, using phosphopeptides, 2 h hydrolysis increased, or at least did not decrease the recovery of phosphoserine. The recovery of phosphoserine is far less from the phosphopeptides than from the phosphoserine standard clearly indicating that analysis of phosphoserine from phosphopeptides is much more difficult. Furthermore, our results indicated that general hydrolysis conditions are not applicable to phosphopeptides because the recovery of phosphoserine is sequence-dependent. This is in good agreement with our previous phosphopeptide analysis experience [14]. Other laboratories using liquid-phase hydrolysis have found the detection of phosphoserine to be similarly peptide sequence-dependent [24]. We expected that the milder conditions of gas-phase hydrolysis might offer a generally more reliable hydrolysis condition, but the acid sensitivity of the phosphoserine is higher than we expected. The result that the recovery of phosphoserine from phosphopeptides is high enough when the hydrolysis period is more than 1 h and less than 2 h, combined with our previous study [14], which shows that the 1.5 h hydrolysis time was found to be appropriate for most of the analyzed phosphopeptides [14], indicates that a 1.5-h hydrolysis time is suitable for the majority of phosphopeptides.

4. Acknowledgements

The authors thank Shirley Peterson and Dr. Hildegund Ertl for their critical reading of the manuscript. This work was supported by research grants AG10670 and GM45011 from the National Institutes of Health.

5. References

[1] F. Wold, *Ann. Rev. Biochem.*, 50 (1981) 783.
[2] A. Varki, *Glycobiology*, 3 (1993) 97.
[3] R. Kornfeld and S. Kornfeld, *Annu. Rev. Biochem.*, 54 (1985) 631.

[4] P.L. Mollison, in C.P. Engelfriet and M. Contreras (Editors), *Blood Transfusion in Clinical Medicine*, Blackwell, Oxford, 1987, p. 269.
[5] E.A. Kabat, in J.D. Ebert, A.G. Loewy and H.A. Schneiderman (Editors), *Structural Concepts in Immunology and Immunochemistry*, Holt, Rinehart & Winston, New York, 1987, p. 269.
[6] G. Thomas, E.J. Podesta and J. Gordon (Editors), *Protein Phosphorylation and Bio-Regulation*, S. Karger, Basel, 1980.
[7] S. Shenolikar, *J. Cyclic Nucleotide Protein Phosphorylation Res.*, 11 (1986–1987) 531.
[8] A.W. Frank, *CRC Crit. Rev. Biochem.*, 16 (1984) 51.
[9] K.B. Reimer, M. Meldal, S. Kusumoto, K. Fukase and K. Bock, *J. Chem. Soc.*, 1 (1993) 925.
[10] A. Kobata, in V. Ginsburg and P. Robbins (Editors), *Biology of Carbohydrates*, Vol. 2, Wiley, New York, 1984, p. 87.
[11] D.E.H. Palladino, R.M. House and K.A. Cohen, *J. Chromatogr.*, 599 (1992) 3.
[12] F. Altmann, *Anal. Biochem.*, 204 (1992) 215.
[13] L. Gorbics, L. Urge, E. Otvos-Papp and L. Otvos, Jr., *J. Chromatogr.*, 637 (1993) 43.
[14] L. Gorbics, L. Urge, E. Lang, G.I. Szendrei and L. Otvos, Jr., *J. Liq. Chromatogr.*, 17 (1994) 175.
[15] L. Otvos, Jr., I. Elekes and V.M.-Y. Lee, *Int. J. Peptide Protein Res.*, 34 (1989) 129.
[16] L. Urge, E. Kollat, M. Hollosi, I. Laczko, K. Wroblewski, J. Thurin and L. Otvos, Jr., *Tetrahedron Lett.*, 32 (1991) 3445.
[17] L. Urge, L. Otvos, Jr., E. Lang, K. Wroblewski, I. Laczko and M. Hollosi, *Carbohydr. Res.*, 235 (1992) 83.
[18] J.-Y. Chang, R. Knecht and D.G. Braun, *Biochem. J.*, 199 (1981) 547.
[19] J.-Y. Chang, R. Knecht and D.G. Braun, *Biochem. J.*, 203 (1982) 803.
[20] R. Knecht and J.-Y. Chang, *Anal. Chem.*, 58 (1986) 2375.
[21] L. Otvos, L. Urge and J. Thurin, *J. Chromatogr.*, 599 (1992) 43.
[22] P. Bulet, J.L. Dimarcq, C. Hetru, M. Lagueux, M. Charlet, G. Hegy, A. Van Dorsselaer and J.A. Hoffmann, *J. Biol. Chem.*, 268 (1993) 14 893.
[23] C.T. Mant and R.S. Hodges (Editors), *High-Performance Liquid Chromatography of Peptides and Proteins: Separation, Analysis and Conformation*, CRC Press, Boca Raton, FL, 1991, p. 289.
[24] D.B. Bylund and T.-S. Huang, *Anal. Biochem.*, 73 (1991) 477.

ELSEVIER

Journal of Chromatography A, 676 (1994) 177–183

JOURNAL OF CHROMATOGRAPHY A

Identification of proteinaceous binding media in paintings by amino acid analysis using 9-fluorenylmethyl chloroformate derivatization and reversed-phase high-performance liquid chromatography

Cecily M. Grzywacz

The Getty Conservation Institute, 4503 Glencoe Avenue, Marina del Rey, CA 90292, USA

Abstract

Identification of binding medium, the vehicle which adheres pigment particles to each other and to a backing or substrate, is important to both art conservators and curators. Proteinaceous binders such as egg, glue and milk casein have been widely used by artists. A protocol for the identification of different proteinaceous binding media in paintings was developed using HPLC analysis with fluorescent detection of 9-fluorenylmethyl chloroformate (FMOC-Cl) derivatives of amino acids.

A scheme based on peak area ratios of FMOC-amino acid derivatives was developed and successfully used on museum samples. The sample preparation techniques, identification scheme and museum applications are discussed.

1. Introduction

Quantitative amino acid analysis has been used to distinguish proteinaceous binding media in cultural property since the late 1960s [1,2]. However, the quantity of sample required, 1–4 mg, frequently prohibited sample collection; imagine the visible damage to a painting if 1–4 mg were scraped from its surface. Typical sample sizes currently routinely taken from art objects are only a few micrograms to at most one-half a milligram. Recent advances in HPLC detectors and columns have led to increased sensitivity and a drastic reduction in required sample size [3] increasing the feasibility of amino acid analysis of paint layers.

The Waters Pico-Tag method (Millipore, Milford, MA, USA) has been used to identify binding media [4,5]. However, there have been literature reports of variable recoveries of lysine, aspartic acid and glutamic acid due to matrix interferences from the presence of salts and/or metal ions in the samples [6]. Accurate quantification of these amino acids is critical to identification of proteinaceous binding media.

9-Fluorenylmethyl chloroformate (FMOC-Cl) precolumn derivatization was selected because of its high sensitivity, good derivative stability and

0021-9673/94/$07.00
SSDI 0021-9673(94)00421-5

low potential for interferences from sample matrices, such as pigments, substrates, ground layers, varnishes, glazes, etc. [7–10].

2. Background

Popular forms of cultural objects are painted objects such as paintings, polychrome sculptures and wall painting fragments. Museum visitors enjoy painted artifacts aesthetically, admiring shape, colors and imagery. Conservation scientists scrutinized art objects more closely, investigating the specific materials used to create the painting, including but not limited to pigments and binding media.

The function of binding media is fourfold: (1) a binder coats each pigment particle and holds the pigment particles in suspension, (2) adheres the paint layer to a substrate, (3) imparts optical properties that intensify the natural color of pigments and (4) protects pigment particles from the potentially damaging effects of the environment. Identification of binding medium can assist curators and art historians in the provenance of painted objects. Throughout the ages artists have been experimenting with different binders. A timetable of binding media use can be created and used to confirm the period of the artifact. Binding media is important in the study of artists' techniques as well. Artists have used a variety of binder recipes depending upon how they wished to modify the handling and/or optical properties of paint. Many choices of binding media have led to non-durable binders which has resulted in early degradation of the pigment layer requiring conservation. By understanding the composition of the binder in paint layers, conservation scientists are better able to offer advice for restoration and preservation of painted objects.

Casein, egg and collagen are proteinaceous materials used as binding media. Animal and fish collagen products are used as a strong adhesive for wood, as a paint binding medium and most often as a binder in ground layers of paintings. Ground layers are a paste of fine chalk or gypsum and an adhesive which is applied over a canvas fabric or wood panel to create a smooth surface before the application of paint layers. The painting technique tempera uses whole egg or egg yolk as binders; egg yolk provides a richer binding medium. Glair is the use of only egg white, and it is used as a temporary varnish or as a sealant between ground layers and paint layers [1,11,12]. Milk curds, whey or whole milk have been identified in binders based on the presence of milk protein, casein [1,13].

3. Experimental

3.1. Sample weighing and transfer techniques

Samples removed from museum objects typically weighed 10–200 μg. Sample particles were transferred with a dissecting needle using static electricity attractive forces. A particle was carefully transported by gently touching it with a dissecting needle. Extreme care was used throughout this procedure as too much pressure on the particles would cause them to flip away and be lost. Particles were weighed and transferred to a 1.0-ml vacuum hydrolysis tube (Pierce, Rockford, IL, USA) by depositing them in the tip of a 9-in. (1 in. = 2.54 cm) pre-cleaned Pasteur pipette with the dissecting needle. The pipette was inserted into the hydrolysis tube and the sample was delivered to the bottom. A predetermined amount of norleucine as an internal standard (Sigma, St. Louis, MO, USA) was delivered to the tip of a 9-in. Pasteur pipette. The tip of the pipette was suspended 2 cm above the bottom of the hydrolysis tube and the norleucine was flushed into the tube by adding 300–400 μl of 6 *M* constant-boiling sequanal-grade HCl (Pierce) to the top opening of the Pasteur pipette. This method of transferring samples and adding small volumes of reagents was necessary to guarantee successful sample preparation of the μg samples.

3.2. Hydrolysis

The hydrolysis step was critical due to the small sample size. Samples of 10–200 μg were

transferred to the 1.0-ml hydrolysis vacuum tubes, 1 μg norleucine per 10 μg sample was added as an internal standard and 300 μl of constant-boiling 6 *M* HCl was added to the tube. Tubes were placed in a Reacti-Therm module (Pierce) adjusted to 110°C for 20–24 h. The samples were cooled and heated to dryness under a nitrogen stream. The dried samples were taken up in 50–300 μl borate buffer at pH 8.5.

3.3. FMOC Derivatization

A 2-μl volume of a collagen hydrolysate standard (Sigma A-9531) or 5–50 μl of a hydrolyzed protein sample in borate buffer was diluted with borate buffer to 50 μl total volume in a 300-μl glass vial. Samples were derivatized using the method of Haynes et al. [7].

3.4. HPLC Analysis

The analytical system consisted of two Waters (Millipore) 510 pumps controlled by a DEC Pro 380 mini-computer using Waters Expert software version 6.21. Samples were introduced to the system via a Waters WISP 712 autosampler. The syringe motor rate was reduced to 1.85 μl s^{-1} to improve reproducibility. The analytical column was a Phenomenex (Torrance, CA, USA) Spherex 3 μm C_{18} (ODS) 150 × 4.6 mm column, with a 2-μm precolumn filter and a Spherex 3 μm C_{18} (ODS) 50 × 4.6 mm guard column. A Hewlett-Packard (Wilmington, DE, USA) 1046A detector was set for fluorescence with the photomultiplier tube detector gain setting at 10 and adjusted as needed based on the sample concentration. The excitation wavelength was 265 nm with emission detection at 315 nm. The column temperature was maintained at 43°C.

The FMOC-amino acid derivatives were separated with binary gradient elution based on the method developed by Haynes et al. [7] The gradient profile is graphically displayed in Fig. 1. The two eluents, (A) 50 m*M* sodium acetate and 7 m*M* triethylammonium acetate (TEAA) with 10% acetonitrile adjusted to pH 6.5 with acetic acid and (B) acetonitrile–water (90:10, v/v), were filtered and degassed under a helium sparge. The flow-rate was 1 ml min^{-1}. Injection volumes ranged from 2–20 μl depending upon sample concentration. A more concentrated sample was prepared if 20 μl did not give sufficient detector response. The total analysis time was 45 min.

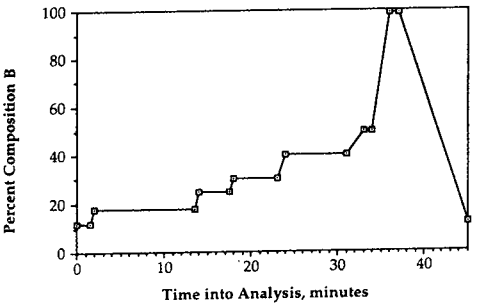

Fig. 1. Gradient profile: sodium acetate–acetonitrile–TEAA buffer system. (A) 50 m*M* Sodium acetate and 7 m*M* TEAA with 10% acetonitrile adjusted to pH 6.5 with acetic acid and (B) acetonitrile–water (90:10, v/v) at 1 ml min^{-1}.

4. Results and discussion

4.1. Analysis of standard binding media materials

Known binding media standard materials from The Getty Conservation Institute's Binding Media Reference Collection were analyzed to validate the identification protocol. Samples of rabbit skin glue, casein, whole egg, egg white and egg yolk were hydrolyzed, derivatized with FMOC-Cl, and analyzed to determine which ratios of amino acids were best suited for distinguishing between proteinaceous binding media. Chromatograms for glue, casein and egg materials are shown in Fig. 2. Each material had a distinct amino acid profile. A scheme was developed to differentiate proteinaceous binders based on FMOC-amino acid peak area ratios. Identification was based on the following distinctions: hydroxyproline was only present in collagen-based glues which also had a very large glycine peak; aspartic acid and glutamic acid peaks in collagen glues were large and nearly equal; casein had a very large glutamic acid peak

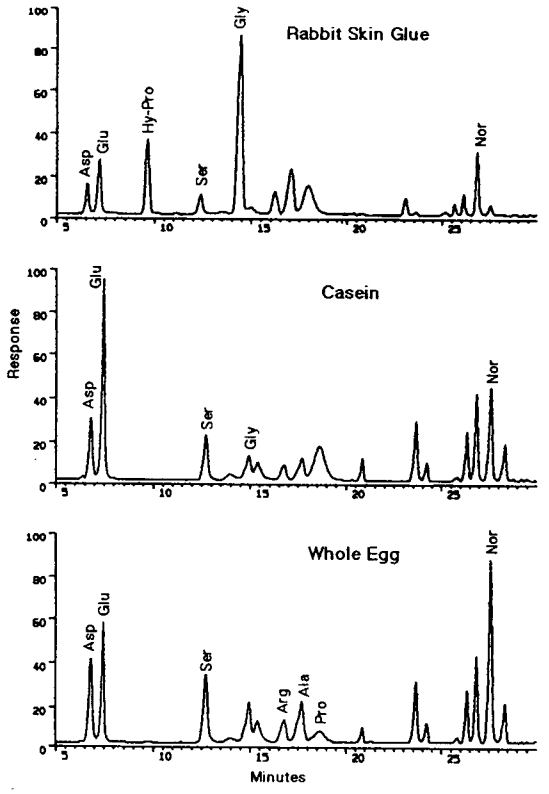

Fig. 2. Amino acid analysis of different proteinaceous binding media: rabbit skin glue, casein and egg.

which was two to three times greater than the aspartic acid peak; and egg components had nearly equal amounts of glycine, aspartic acid and glutamic acid. The differences between egg components were more subtle and peak areas differed by only a few percent. For very important, critical samples, it was necessary to use confirmation techniques. For example, the presence of phosphorus confirmed casein identification and cholesterol differentiated egg yolk from egg white or glair. Fatty acid profiles can also be used to distinguish between the various egg components [1].

4.2. Analytical strategy for identification of proteinaceous binding media

Amino acid analysis applied by conservation scientists to identify protein binding media use molar percent ratios of all amino acids present [1–3,5,14–16]. This technique is feasible when larger sample sizes are available and quantification of all amino acids present is guaranteed. However, when dealing with microgram quantities, not all of the amino acids may be detected due to amino acid degradation as well as isolation difficulties or incomplete binding-medium extraction from the paint layer. These factors make it hard to correlate contemporary egg, casein and collagen standards with older, aged paint layer samples.

The continuous degradation of the C_{18} column from the repeated exposure to basic FMOC-amino acid samples affected the ability to identify all amino acids in proteinaceous binding media. The gradient was adjusted to accommodate changes in column resolution. Also, by using ratios of peak areas rather than percent molar quantities, the small losses in resolution were not critical. Minor peaks which were not well resolved were eliminated in the identification scheme.

A number of critical amino acid ratios were chosen for identification of protein binding media (Table 1). The detection of hydroxyproline distinguished collagen-based glues from the other proteinaceous binders. A 3:1 ratio of glycine to hydroxyproline was an important secondary confirmation. Casein binders were determined by a 3:1 ratio of glutamic acid to aspartic acid, other protein binders had a glutamic acid:aspartic acid ratio of less than 2. Egg binders were identified by the absence of hydroxyproline and the presence of equal amounts of glycine, glutamic acid and aspartic acid. To distinguish egg yolk from egg white from whole egg, it was necessary to use more than one amino acid peak area ratio as the compositions were similar. The ratios to distinguish between the egg components were alanine:proline, glutamic acid:serine, proline:aspartic acid and aspartic acid:serine. To distinguish whole egg from egg white, the ratios of glutamic acid:serine and aspartic acid:serine were used. The systematic identification scheme for proteinaceous binders developed is shown in Fig. 3. To corroborate the identity of binding

Table 1
FMOC-Amino acid peak area ratios for the identification of proteinaceous binding media (single-letter codes for amino acids)

Amino acid ratio	Glues	Casein	Whole egg	Egg white	Egg yolk
Hydroxyproline:serine	>1.5	<1.5	<1.5	<1.5	<1.5
Hydroxyproline:glycine	>0.2	<0.2	<0.2	<0.2	<0.2
Glutamic acid:aspartic acid	<2.0	>2.0	<2.0	<2.0	<2.0
Glutamic acid:glycine	<1.0	>3.0	1.0 < (E/D) < 3.0	1.0 < (E/D) < 3.0	1.0 < (E/D) < 3.0
Glutamic acid:alanine	<0.8	>3.0	1.0 < (D/A) < 3.0	1.0 < (D/A) < 3.0	1.0 < (D/A) < 3.0
Alanine:proline	0.5 < (A/P) < 1.5	<0.5	>1.8	>1.8	<1.8
Glutamic acid:serine	1.5 < (E/S) < 2.5	>2.5	1.0 < (E/S) < 1.2	>1.2	<1.0
Valine:glutamic acid	<0.5	<0.5	>0.5	>0.5	>0.5
Aspartic acid:serine	>1.0	>0.8	<1.0	>1.0	<0.9
Aspartic acid:threonine	>2.0	<2.0	>1.5	>1.9	<1.9
Serine:tyrosine	>1.7	<1.7	>1.7	>1.7	>1.7
Methionine:threonine	>1.0	<1.0	0.8 < (M/Y) < 1.5	>1.5	<1.0
Proline:aspartic acid	>2.0	>1.5	<0.5	<0.5	>0.5
Proline:alanine	0.5 < (P/A) < 1.5	>2.0	>0.5	>0.5	>0.5
Leucine:alanine	<0.5	>1.5	0.8 < (L/A) < 1.0	<1.0	>1.0

media in paint samples, the scheme in Fig. 3 should be used in conjunction with the confirmation ratios presented in Table 1.

4.3. *Analysis of museum samples*

The analysis scheme and confirmation FMOC-amino acid peak area ratios were applied to samples of unknown binding media obtained from cultural properties. For several samples the HPLC identifications were confirmed with other techniques. Five analysis results are described.

Yungang grotto Chinese wall painting

The Getty Conservation Institute (GCI) and China, with assistance from UNESCO, are col-

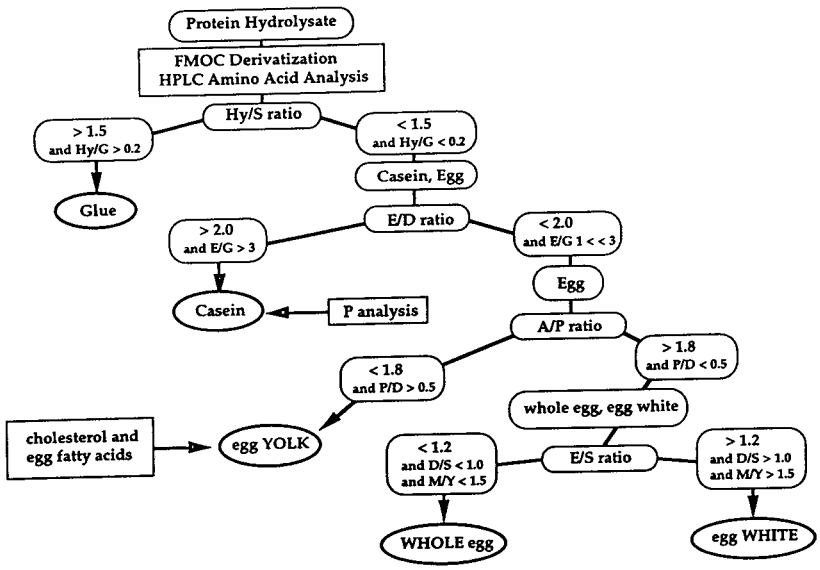

Fig. 3. Flowchart diagram for the identification of binding media. Single-letter codes for amino acids; Hy = hydroxyproline and P analysis = phosphorus analysis.

laborating on the conservation of two of China's most important cultural sites, the ancient rock temples of the Mogao grottoes located near Dunhuang on the edge of the Gobi Desert and the Yungang grottoes near Datong, located approximately 270 km due west of Beijing. The Dunhuang site is inscribed in the World Heritage List; the Yungang caves are in the process of inscription. These two great ancient sites of mankind record the patterns of interchange of civilization, trade, and Buddhist art along the Silk Road into China. Both sites are national treasures [17].

A mg sample was removed from an existing crack in the restored plaster of a historic wall painting at one of the Yungang grottoes and analyzed. From the chromatogram in Fig. 4 and the scheme in Fig. 3, it was determined that the binder was an animal glue based on the relative amounts of hydroxyproline and glycine which are indicative of collagen animal glue binders.

Rembrandt's "The Raising of Lazarus"

The curator of the Paintings Department at the Los Angeles County Museum of Art was interested in identifying the binder in the various layers of Rembrandt's "The Raising of Lazarus". A cross-section was carefully removed and examined by a number of analytical techniques. Infrared microspectroscopy indicated that the binding medium in both the ground and paint layers contained oil, natural resin and protein. GC–MS analysis determined that the paint layer binding medium was linseed oil mixed with whole egg or egg yolk; the ground layer contained linseed oil with no indication of egg. A paint layer and ground layer sample were prepared for HPLC analysis to confirm the proteinaceous binders.

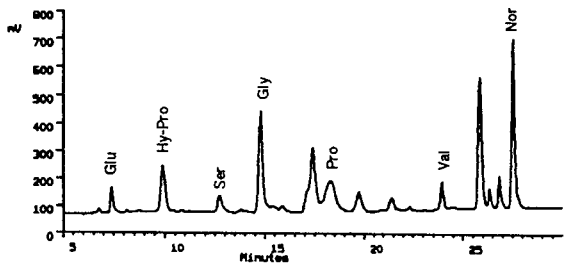

Fig. 4. Amino acid analysis chromatogram of Yungang Chinese wall painting glue sample.

The binder in the ground layer was a mixture of proteinaceous binding media based on the ratios of FMOC-amino acid derivatives. One component was identified as glue because of the significant amount of hydroxyproline. The GC–MS analysis did not find evidence of egg yolk; thus, the second binder was egg white. The binder in the pink paint layer was determined to be egg yolk, based on the ratios of alanine, proline and lysine to each other.

Mantegna's "Presentation in the Temple"

Samples of Andrea Mantegna's "Presentation in the Temple" from the Staatliches Museum in Berlin were received for analysis. Protein was identified in all of the samples by IR spectroscopy. GC–MS cholesterol analysis indicated that egg yolk was not present in concentrations greater than 1% (w/w) of the paint sample. Scanning electron microprobe analysis indicated that some phosphorus was present in one sample while another sample showed no indications of phosphorus. The HPLC analysis of both samples indicated that glue was the binding medium because of the presence of hydroxyproline and high amounts of glycine. This is in agreement with the techniques known to have been used by Andrea Mantegna.

Mantegna's "Cardinal Trevisano"

A paint sample from "Cardinal Trevisano" painted by Andrea Mantegna was analyzed by HPLC. From the large amounts of hydroxyproline and glycine seen in Fig. 5, the binder was determined to contain collagen-based glue.

Czechoslovakian panel painting, "Master of Vysebrotsky Altar"

Samples from the green ground layer of a Czechoslovakian panel painting, "Master of Vysebrotsky Altar", were obtained for HPLC analysis. Hydroxyproline and a large amount of glycine indicated that a collagen-based glue was used.

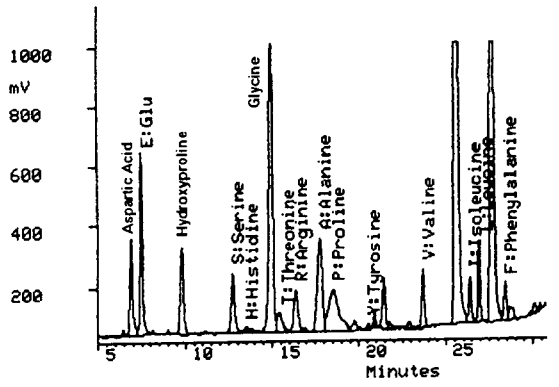

Fig. 5. Amino acid analysis of Mantegna's "Cardinal Trevisano".

5. Conclusions

The use of FMOC-amino acid peak area ratios proved to be the best method to distinguish between proteinaceous binding media. By using peak areas rather than molar percent compositions of amino acids, small losses of resolution due to column degradation were not critical. The analytical scheme presented in Fig. 3, along with the use of confirmation peak area ratios listed in Table 1, successfully identified binding media in museum samples.

References

[1] R. White, *Natl. Gallery Tech. Bull.*, 8 (1984) 5.
[2] S. Keck and T. Peters, Jr., *Stud. Conserv.*, 14 (1969) 75.
[3] S.M. Halpine, *Stud. Conserv.*, 37 (1992) 22.
[4] P.K. Hupe, *LC · GC*, 10 (1992) 211.
[5] J.-S. Tsang, *Final Report: HPLC of Binding Media*, The Getty Conservation Institute, Marina del Rey, CA, 1986.
[6] A.J. Smith and J.M. Presley, in T.E. Hugli (Editor), *Techniques in Protein Chemistry*, Academic Press, San Diego, CA, 1989, Ch. 25, p. 255.
[7] P.A. Haynes, D. Sheumack, J. Kibby and J.W. Redmond, *J. Chromatogr.*, 540 (1991) 177.
[8] J.E. Carlton and W.T. Morgan, in T.E. Hugli (Editor), *Techniques in Protein Chemistry*, Academic Press, San Diego, CA, 1989, Ch. 26, p. 266.
[9] T. Näsholm, G. Sandberg and A. Ericsson, *J. Chromatogr.*, 396 (1987) 225.
[10] S. Einarsson, B. Josefsson and S. Lagerkvist, *J. Chromatogr.*, 282 (1983) 609.
[11] J.S. Mills and R. White, *Natl. Gallery Tech. Bull.*, 4 (1980) 3.
[12] J.S. Mills and R. White, *Stud. Conserv.*, 20 (1975) 176.
[13] L. Masschelein-Kleiner, *PACT Sci. Exam. Easel Paintings*, 13 (1986) 185.
[14] M. Johnson and E. Packard, *Stud. Conserv.*, 16 (1971) 145.
[15] L. Masschelein-Kleiner, in N. Brommelle and P. Smith (Editors), *Conservation and Restoration of Pictorial Art*, Butterworths, London, 1976, Ch. 11, p. 84.
[16] J. Mills and R. White, *Natl. Gallery Tech. Bull.*, 2 (1978) 71.
[17] *Getty Conserv. Inst. Newsl.*, 4 (1989) 1.

ELSEVIER

Journal of Chromatography A, 676 (1994) 185–189

JOURNAL OF CHROMATOGRAPHY A

Molecular size determinations of DNA restriction fragments and polymerase chain reaction products using capillary gel electrophoresis

Michael A. Marino*, Lisa A. Turni, Susie A. Del Rio, Patrick E. Williams

Developmental Laboratory, Armed Forces DNA Identification Laboratory, Armed Forces Institute of Pathology, Washington, DC 20306-6000, USA

Abstract

Commercially available capillary electrophoresis (CE) systems offer advantages over traditional slab gel methodologies. The capillary format allows the use of higher voltages (225 V/cm), which results in faster migration, higher resolution and greater efficiency without excessive heating. The ability to automate the system increases the unattended sample analysis throughput. For this study, the CE system was configured with a μPAGE 3% T, 3% C polyacrylamide gel capillary with an effective length of 40 cm and μPAGE Tris–borate urea buffer system. The analysis of DNA restriction fragments and polymerase chain reaction products, with an internal standard of Boehringer Mannheim DNA marker XI were completed in less than 70 min. All samples were analyzed at 260 nm. The data establishes automated capillary gel electrophoresis as a high-resolution, reproducible method for analysis of samples under 1000 base pairs.

1. Introduction

DNA is found in virtually every cell of the human body and is unique to the individual. By analyzing the DNA it is possible to identify suspects, victims of crime, and casualties of mass disaster. In some cases, identification is completed by using DNA extracted from samples of tissue, bone, semen, blood or hair.

One general approach to DNA profiling uses markers that are based upon restriction fragment length polymorphism (RFLP) [1]. As originally conceived, variation in the length of target DNA fragments is based upon differences in the presence or absence of endonuclease restriction sites. Two drawbacks often associated with the detection of RFLP markers is the necessity of a relatively large DNA sample (20–100 ng) and detection using radioactive ^{32}P labels.

In humans, RFLP loci with as many as 80 different alleles [2] have been reported. Such loci, referred to as variable number tandem repeat (VNTR) loci [3] consist of sets of tandemly repeated oligonucleotide core sequences and were termed "minisatellites" by Jeffreys *et al.* [4]. The core sequence vary in length from 11 to 60 base pairs and the repetitive region is flanked by conserved endonuclease restriction sites. Thus, the length of the restriction fragment produced by this type of genetic locus is proportional to the number of oligonucleotides core units it contains. Alleles at these loci are visual-

* Corresponding author.

0021-9673/94/$07.00
SSDI 0021-9673(94)00119-T

ized via Southern hybridization. Theoretically, hundreds of alleles varying in length from 9 to 30 base pairs can be identified at such a loci. Hybridizing bands on a Southern blot varying in length by only a few core sequences are extremely difficult to differentiate. This difficulty, combined with the possibility of band shifting, have caused concern with the accuracy of human DNA fingerprinting [5].

A new type of genetic marker that allows more exact determination of allelic profiles was suggested in 1989 [6–8]. Rather than repeat units in the range of 11 to 60 base pairs in length, these workers suggested that high levels of length polymorphism exist in dinucleotide tandem repeat sequences. A dinucleotide repeat such as $(C–A)_n$ were reported to occur in human genome as many as 50 000 times with n varying from 10 to 60. These reiterated sequences have been referred to as microsatellites, simple sequence repeats (SSR) [9], simple sequence length polymorphism (SSLP) [10] or short tandem repeats (STR) [7,11,12]. The detection of STRs is based upon variations in the length of polymerase chain reaction (PCR) products [13]. The PCR basis of the system reduces the DNA required for detection a number of orders of magnitude below that of RFLP-based procedures.

The DNA restriction fragments and PCR products are traditionally separated by conventional slab gel electrophoresis, but the fragments have similar charge-to-mass ratios, and thus are separated by length-induced drag. Capillary gel electrophoresis (CGE) is a new technique used in molecular biological analysis which offers advantages over conventional slab gel methodology [14]. CE, using a thin walled capillary of 50–150 μm I.D., provides excellent heat transport, thus allowing higher applied voltages to produce quicker separations. The recent development of polyacrylamide gel capillary and buffer systems have sufficient resolving power to separate these alleles. CGE also uses a smaller sample volume, generally 5 ng sample per injection. The system detector is on-column, which increases sensitivity [14,15]. Consequently, DNA fragments can be detected at 260 nm without radioactive labels.

The purpose of this study was to apply the speed and resolution of CGE to DNA analysis of PCR products and DNA restriction fragments. This study includes examples of PCR products such as soybean STRs and DNA restriction fragments of ΦX174/Hinf1.

2. Materials and methods

2.1. Instrumentation

All analyses used the Dionex CE system CES-1 (Sunnyvale, CA, USA). Separations were performed using μPAGE (3% C, 3% T[a]) polyacrylamide gel electrophoresis column from J & W Scientific (Folsom, CA, USA). The effective column length was 40 cm, and the applied voltage was −225 V/cm. The DNA fragments were detected at 260 nm. The data were collected by the Dionex AI 450 software package (version 3.31) on a ZEOS 486DX (MS-DOS 5.00 and Windows 3.10).

2.2. Reagents

All water used in this study was reagent-grade HPLC water. The buffer used was μPAGE Tris–borate and urea buffer supplied by J & W Scientific with 10 μM ethidium bromide. The standard DNA ladder, DNA molecular mass marker XI (Boehringer Mannheim, Indianapolis, IN, USA) and DNA restriction digest, ΦX174/Hinf1 (BRL 9; Gibco, Gaithersburg, MD, USA) were prepared using a 20-ml aliquot. After dialysis on a MF-Millipore membrane filter (Millipore, Bedford, MA, USA) for 15 min, 20 μl of the ladder were added to 20 μl of dialyzed sample.

2.3. Sample preparation

The PCR products and allelic ladders used in this study were prepared by Ms. Rhonda Roby, Ms. Demeris Lee and Dr. Mitchell Holland from our institute according to standard amplification

[a] C = g N,N′-methylenebisacrylamide (Bis)/%T; T = (g acrylamide + g Bis)/100 ml solution.

procedures as described by Roche Molecular Systems (Alameda, CA, USA). The PCR products of soybeans used were prepared by Dr. Perry Cregan (Soybean & Alfalfa Research Laboratory, US Department of Agriculture, Agricultural Research Service, Beltsville, MD, USA).

3. Results and discussion

The study started with the analysis of DNA molecular mass marker XI. The marker contains double stranded, non-phosphorylated, blunt-ended DNA fragments of 50, 100, 200, 300, 400, 500, 700 and 1000 base pairs (see Fig. 1.). The method used for size determination of a DNA restriction fragment or PCR product was based on the production of a calibration plot. In this method the DNA fragments of known size were separated by CGE and the corresponding retention time were plotted. Fig. 2. is a calibration curve generated from the analysis of the molecular mass ladder.

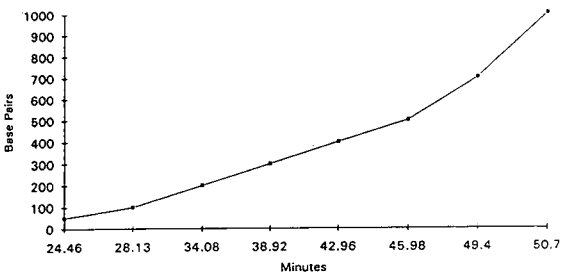

Fig. 2. A calibration curve generated from the analysis in Fig. 1.

The high resolution and reproducibility of CGE gives this technique the potential to perform routine DNA analysis. Fig. 3. shows the analysis of the mitochondrial dinucleotide repeat. The STR is a two-base pair repeat (AC) at location 514 in the D-Loop of the mitochondria [11,16]. CGE has the resolution capable of sizing the PCR products which are a single repeat apart (two base pairs). The size of the mitochondrial repeat was confirmed by direct DNA sequencing of the PCR product.

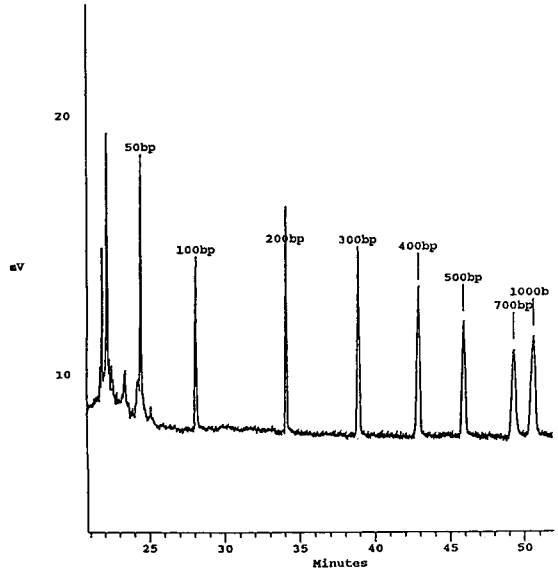

Fig. 1. Analysis of DNA molecular mass marker XI (Boehringer Mannheim) with size as indicated (bp = base pairs). Conditions: μPAGE (3% C, 3% T) polyacrylamide gel electrophoresis column from J & W Scientific. The effective column length was 40 cm. Injection of standard was at −7 kV for 9 s. Run voltage was −225 V/cm. System detector was set at 260 nm.

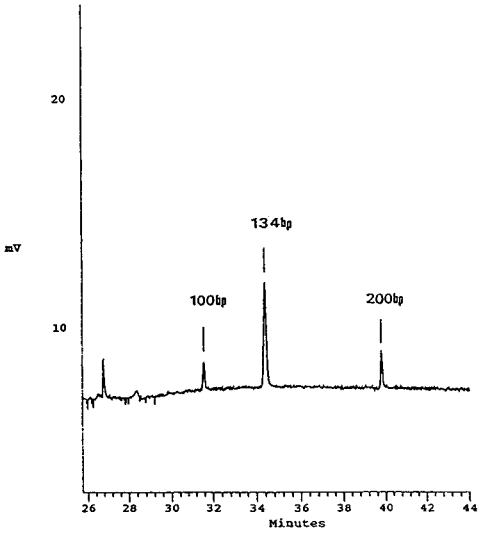

Fig. 3. Analysis of STR at location 514 in the D-loop of the mitochondria. Conditions: μPAGE (3% C, 3% T) polyacrylamide gel electrophoresis column from J & W Scientific. The effective column length was 40 cm. Injection of sample was at −7 kV for 9 s. Run voltage was −225 V/cm. System detector was set at 260 nm.

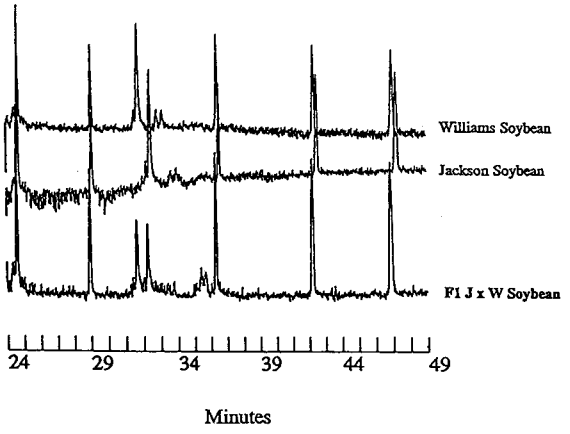

Fig. 4. Analysis of the parental genotypes Jackson and Williams and their using the same conditions as Fig. 1. The molecular mass markers 100 and 200 base pairs are at 29 and 36 min, respectively. The SSR-containing fragments for the genotypes are found between 30 and 33 min. F1 generation is heterozygous.

Analyses of STR-containing PCR products were also performed using soybean genotype [17,18]. Fig. 4. is the electropherograms of parents and the F_1 generation. The allelic STRs are located between 30 and 33 min (flanked by the molecular mass marker). Notice the F_1 generation is a heterozygote, containing the alleles of both parent genotypes.

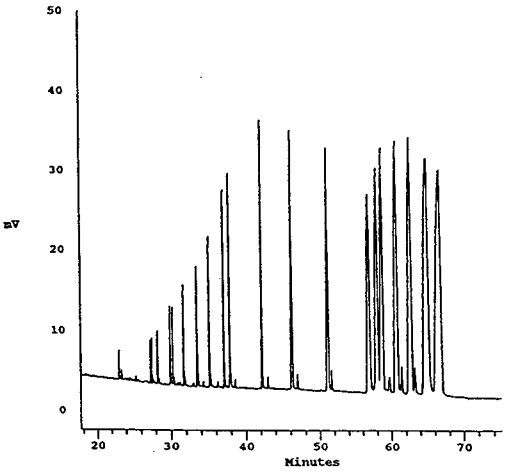

Fig. 5. ΦX174/HinfI restriction fragment digest containing 22 fragments from 22 to 726 base pairs in size (conditions as in Fig. 1).

An example of the separation the ΦX174/HinfI restriction fragment digest is found in Fig. 5. The resolution of the CGE separates all 22 restriction fragments from 22 to 726 base pairs in size. This system also provides 4-base pair resolution between 413–417 base pair fragments. This separation is complete within 60 min and is superior to the traditional slab gel methods.

4. Conclusions

It is possible to analyze and determine the allelic profile of plants and humans using CGE. The method requires a reference sample and molecular mass markers or internal reference marker. This method is rapid, sensitive and reproducible. Advances in the gel capillary production have greatly increased their life expectancy (over 160 h at 225 V/cm). The automation of the CE allows for continual unattended operation. These advantages make this analysis desirable for many biological studies.

5. Disclaimer

The opinions or assertions herein are those of the author and do not necessarily reflect the views of the Department of Army of the Department of Defense.

6. References

[1] D. Botstein, R.L. White, M. Skolnick and R.W. Davis., *Am. J. Hum. Genet.*, 32 (1980) 314–331.
[2] I. Balazs, M. Baird, M. Clyne and E. Meade, *Am. J. Hum. Genet.*, 44 (1989) 182–190.
[3] Y. Nakamura, M. Leppert, P. O'Connell, R. Wolff, T. Holm, M. Culver, C. Martin, E. Fujimoto, M. Hoff, E. Kumlin and R. White, *Science*, 235 (1987) 1616–1622.
[4] A.J. Jeffreys, V. Wilson and S.L. Thein, *Nature*, 314 (1985) 67–73.
[5] R. Chakraborty, R. and K.K. Kidd, *Science*, 254 (1991) 1735–1739.
[6] M. Litt and J.A. Luty, *Am. J. Hum. Genet.*, 44 (1989) 397–401.
[7] J.L. Weber and P.E. May, *Am. J. Hum. Genet.*, 44 (1989) 388–396.

[8] D. Tautz, *Nucleic Acids Res.*, 17 (1989) 6463–6471.
[9] H.J. Jacob, K. Lindpaintner, S.E. Lincoln, K. Kusumi, R.K. Bunker, Y.-P. Mao, D. Ganten, V.J. Dzau and E.S. Lander, *Cell*, 67 (1991) 213–224.
[10] N.G. Copeland, N.A. Jenkins, D.J. Gilbert, J.T. Eppig, L.T. Maltais, J.C. Miller, W.F. Deitrick, A. Weaver, S.E. Lincoln, R.G. Steen, L.D. Stein, J.H. Nadeau and E.S. Landers, *Science*, 262 (1993) 57–66.
[11] A. Bodenteich, L. Mitchell, M. Polymeropoulos and C. Merril, *Molec. Gen.*, 1 (1992) 40.
[12] A. Edwards, A. Civitella, H. Hammond and C.T. Caskey, *Am. J. Hum. Genet.*, 44 (1991) 746–756.
[13] K. Mullis, F. Faloona, S. Scharft, R. Saiki, G. Horn and H. Erlich, *Quant. Biol.*, 51 (1986) 263–275.
[14] I.S. Krull and J.R. Mazzeo, *Nature*, 357 (1992) 92–94.
[15] L.M. Smith, *Nature*, 349 (1991) 812–813.
[16] P.E. Williams and K. Turner, *Crime Lab. Digest.*, (1994) in press.
[17] M.A. Marino, L.A. Turni, S.A. Del Rio, P.E. Williams and P.B. Cregan, *Appl. Theoret. Electrophoresis*, submitted for publication.
[18] M.S. Akkaya, A.A. Bhagwat and P.B. Cregan, *Genetics*, 132 (1992) 1131–1139.

ELSEVIER

Journal of Chromatography A, 676 (1994) 191–202

JOURNAL OF CHROMATOGRAPHY A

Hydrophilic-interaction chromatography of complex carbohydrates

Andrew J. Alpert*[,a], Mukta Shukla[a], Ashok K. Shukla[b], Lynn R. Zieske[c], Sylvia W. Yuen[c], Michael A.J. Ferguson[d], Angela Mehlert[d], Markus Pauly[e], Ron Orlando[e]

[a]*PolyLC Inc., 9151 Rumsey Road, Suite 180, Columbia, MD 21045, USA*
[b]*Sialomed, Inc., 8980F Oakland Center, Rt. 108, Columbia, MD 21045, USA*
[c]*Applied Biosystems Division of Perkin-Elmer Corp., 850 Lincoln Centre Drive, Foster City, CA 94404, USA*
[d]*Department of Biochemistry, University of Dundee, Dundee DD1 4HN, UK*
[e]*Complex Carbohydrate Research Center, University of Georgia, Athens, GA 30602, USA*

Abstract

Complex carbohydrates can frequently be separated using hydrophilic-interaction chromatography (HILIC). The mechanism was investigated using small oligosaccharides and a new column, PolyGLYCOPLEX. Some carbohydrates exhibited anomer separation, which made it possible to determine the orientation of the reducing end relative to the stationary phase. Amide sugars were consistently good contact regions. Relative to amide sugars, sialic acids and neutral hexoses were better contact regions at lower levels of organic solvents than at higher levels. HILIC readily resolved carbohydrates differing in residue composition and position of linkage.

Complex carbohydrate mixtures could be resolved using volatile mobile phases. This was evaluated with native glycans and with glycans derivatized with 2-aminopyridine or a nitrobenzene derivative. Both asialo- and sialylated glycans could be resolved using the same set of conditions. With derivatized carbohydrates, detection was possible at the picomole level by UV detection or on-line electrospray mass spectrometry. Selectivity compared favorably with that of other modes of HPLC. HILIC is promising for a variety of analytical and preparative applications.

1. Introduction

Many proteins and lipids of higher organisms are glycosylated. Recently, interest in the free carbohydrate chains has mounted with the discovery that they can be involved in very specific interactions with receptor proteins (e.g., lectins) and intact cells. This can control cell adhesion, which is involved in such phenomena as inflammation or microbial activity [1–3].

The carbohydrate moieties of mammalian proteins and lipids can be complex. Typically, they are composed of the following sugars: the amide sugars N-acetylglucosamine (GlcNAc) and N-acetylgalactosamine (GalNAc); the neutral hexoses glucose (Glc) (rare in mammalian glycoproteins), galactose (Gal), mannose (Man) and fucose (Fuc); and sialic acids (of which over 30 are known from natural sources [1]). The method of linkage can vary in three respects: (1) linkage via the α- or β-anomer; (2) position of linkage ($1\rightarrow6$; $2\rightarrow3$; $1\rightarrow4$; etc.); (3) branching

* Corresponding author.

0021-9673/94/$07.00
SSDI 0021-9673(94)00467-N

(i.e., linkage of more than one sugar to a residue). All of these factors are important in determining the biological activity of a complex carbohydrate. Chromatographic methods for this class of solutes should be sensitive to these differences.

Various methods have been used for chromatography of complex carbohydrates. Some of the more widely used methods are as follows:

Anion-exchange chromatography (conventional) [4]. This works only with carbohydrates containing acidic residues (e.g., sialic acid or phosphate groups).

Reversed-phase (RP) HPLC. Usually this involves attachment of a hydrophobic chromophore or fluorophore to the reducing end by reductive amination; derivatives of 2-aminopyridine (PA) are increasingly being used for this purpose [5,6]. The eluting carbohydrates are easy to detect using conventional HPLC detectors, and can be analyzed by mass spectrometry (MS). Recently, RP-HPLC of underivatized carbohydrates has been performed with a Hypercarb S column [7].

Size-exclusion chromatography. This mode is useful in combination with other modes [8].

High-performance anion-exchange chromatography (HPAEC). This subset of anion exchange was developed by Hardy and Townsend [9,10]. The mobile phases contain 0.1 *M* NaOH; sugar hydroxyl groups ionize at the high pH and adsorb to anion-exchange resins, from which they can be eluted with a salt gradient (e.g., sodium acetate). HPAEC has excellent selectivity for linkage and composition variations in complex carbohydrates. Upon elution, carbohydrates can be detected at the picomole level with pulsed amperometric detection (PAD). The salts in the mobile phase are sometimes inconvenient when other detection methods are used, or in preparative applications.

Hydrophilic-interaction chromatography (HILIC). This features a "normal-phase" combination of a hydrophilic stationary phase and a hydrophobic (mostly organic) mobile phase [11]. A partition mechanism is probably involved [11–14] (rather than "hydrogen bonding", as stated in some reports). Elution is in order of least to most polar. Amino-silica columns, widely used for analysis of neutral sugars, have also been evaluated with complex carbohydrates [15,16]. Elution of sialylated oligosaccharides from these columns requires a significant level of salt in the mobile phase [17], reflecting the superimposition of electrostatic attraction on the hydrophilic interaction. Neutral materials used in this mode include TSKgel Amide-80, which has been used in two-dimensional HPLC of PA-derivatized carbohydrates along with RP-HPLC [3,18], and GlycoPAK N, which has been used with native glycans [19].

HILIC is a rational mode to develop for carbohydrates, which are polar solutes. Earlier, a neutral material, poly(2-hydroxyethyl aspartamide)-silica, was developed for general HILIC of polar solutes [11]. This material works well with glycopeptides and homologous oligomers of carbohydrates, but retention of complex carbohydrates is inadequate. Accordingly, a new material, PolyGLYCOPLEX, has been developed for such applications. This material was used here to study the utility of HILIC for topical carbohydrate separations, and to explore the mechanisms governing selectivity in this mode.

2. Materials and methods

2.1. Reagents

The complex carbohydrate library from native bovine fetuin was a gift of Dr. Rao Thotakura (NIH, Bethesda, MD, USA). It was obtained via hydrazinolysis with a GlycoPrep 1000 system from Oxford GlycoSystems (Abingdon, UK).

Biantennary oligosaccharides (Figs. 7 and 8) were released enzymatically from human apotransferrin (Sigma, St. Louis, MO, USA) using PNGase F. Reductive amination with 2-aminopyridine was performed using borane–dimethylamine complex, as per the improved method of Hase et al. [20]. The products were purified using column chromatography and characterized using LDMS, electrospray MS, and 300 MHz ^{1}H NMR.

The GPI anchor glycans were isolated from

purified VSG (variant surface glycoprotein) of *Trypanosoma brucei brucei* by aqueous HF dephosphorylation, then re-N-acetylation using [^{14}C]acetic anhydride (Amersham, UK) [21,22]. The resulting neutral glycans are labelled in the GlcNAc residue proximal to the terminal inositol residue (cf. Fig. 9).

Xyloglucans were obtained from tamarind seeds (*Tamarindus indica*) using a published method [23], and from pea root (*Pisum sativum*) cell walls by extraction with an *endo*-β-1,4-glucanase [24]. The reducing ends were derivatized with a *p*-nitrobenzene derivative; the procedure is described elsewhere [25,26].

The sialic acids were from Sialomed (Baltimore, MD, USA).

All other carbohydrates were purchased from Sigma.

2.2. HPLC columns and apparatus

PolyGLYCOPLEX columns were prepared by PolyLC (Columbia, MD, USA). The neutral, hydrophilic material is derived from silica with a covalent coating of polysuccinimide, using a procedure similar to that detailed in previous papers [11,27]. The amount of residual charge is quite low, but not absent. HPAEC was performed with HPLC systems, PAD detectors, and CarboPac PA1 columns from Dionex (Sunnyvale, CA, USA). RP-HPLC (Fig. 14) was performed with a Spherisorb 5 ODS1 column, 250 × 4.6 mm (Phase Separations, Norwalk, CT, USA). Radioactivity detection was performed on-line with a Raytest Ramona detector equipped with a 200-μl X-cell solid scintillator flow cell (Raytest Instruments, Sheffield, UK).

2.3. Apparatus for MS and narrow-bore and microbore HPLC

In Fig. 8, the HPLC system was Model 172 from Applied Biosystems Division of Perkin-Elmer (Foster City, CA, USA). Microbore LC–MS (Figs. 11–13) was performed with HPLC system Model 140B from Applied Biosystems with a 5-μl sample loop. Post-column addition of 0.1% acetic acid at 8 μl/min was accomplished through an Upchurch low-dead-volume tee (Upchurch Scientific, Oak Harbor, WA, USA) connected by fused-silica tubing (50 μm I.D.) to a Harvard Apparatus (South Natick, MA, USA) Model 22 syringe pump. The combined effluent was again split using an Upchurch low-dead-volume tee. A length of fused silica (50 μm I.D.) from one outlet went directly to the tip of the ion spray needle of the mass spectrometer. The other outlet of the tee was connected to the UV detector by a length of 100 μm I.D. fused-silica tubing. The split ratio of 1:9 (MS:UV detector) was accomplished by adjusting the lengths of the fused-silica tubing. UV detection at 275 nm was accomplished with a Applied Biosystems Model 785A detector with a 2.4-μl flow cell.

MS detection was accomplished with a Sciex API-III triple quadrupole mass spectrometer fitted with an ion spray source (PE Sciex, Canada). The mass analyzing quadrupole (Q1) was scanned over a m/z range of 1214–1542, at a scan rate of 2.85 s/scan in steps of 0.5 u. The orifice potential was set at 50 V. The mass spectrometer was calibrated with a mixture of polypropylene glycols 425, 1000 and 2000 ($3.3 \cdot 10^{-5}$, $1 \cdot 10^{-4}$ and $2 \cdot 10^{-4}$ *M*, respectively), dissolved in water–methanol–formic acid (50:50:0.1), with 1 m*M* NH_4OAc. Q1 was adjusted for unit mass resolution (approx. 50% peak valley). All data were recorded by Sciex data acquisition software (Tune 2.1.2) on a Macintosh IIfx computer.

3. Results

3.1. HILIC of small carbohydrates

Initially, HILIC was performed with small oligosaccharides. These small solutes might be expected to have fewer interactions with the stationary phase than larger oligosaccharides, facilitating the interpretation of the data. While uncharged oligosaccharides were retained when the mobile phase contained only MeCN and water, sialic acids and small sialylated oligosaccharides (e.g., sialyllactose) eluted in the void volume (data not shown), owing to ion-exclusion

effects. This phenomenon has been noted before [28]. Accordingly, 10 m*M* triethylamine phosphate (TEAP) [11] was included in the mobile phases for the initial studies.

Figs. 1 and 2 show that sialic acids and small oligosaccharides can be resolved by HILIC on the PolyGLYCOPLEX column. The resolution of the sialic acids is at least as good as any currently in the literature. The position of linkage affects retention as much as residue composition; an oligosaccharide with a (1→6) or (2→6) link is better retained than one with a (1→4) or (2→3) link. This confirms earlier observations with HILIC columns [15,17]. From Figs. 1 and 2,

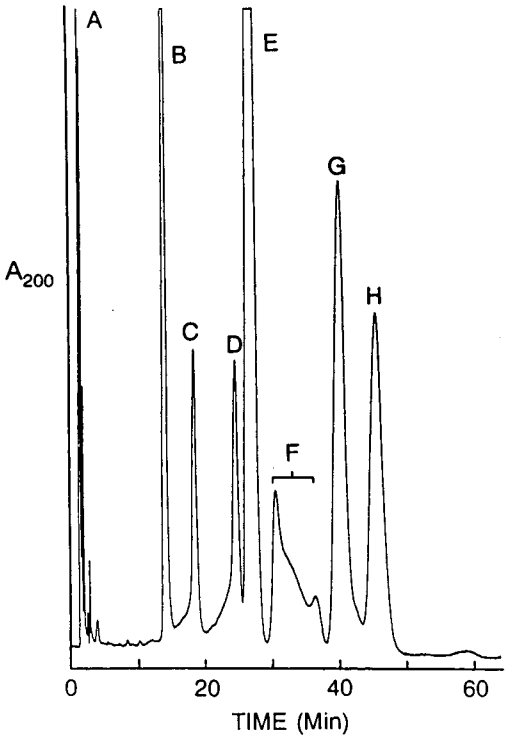

Fig. 1. HILIC of small carbohydrates. Column: PolyGLYCOPLEX, 200 × 4.6 mm (5 μm). Mobile phase (isocratic): 10 m*M* TEAP, pH 4.4, in MeCN–water (80:20, v/v). Flow-rate: 1.0 ml/min. Detection: A_{200} = 0.05 AUFS. Peaks: A = monosaccharides; B = 2,3-didehydro-2,6-anhydro-N-acetylneuraminic acid (Neu5Ac2en); C = N-acetylneuraminic acid (Neu5Ac); D = N-glycolylneuraminic acid (Neu5Gc); E = sialyl(2→3)lactose; F = sialyl(2→6)-N-acetyllactosamine; G = sialyl(2→6)lactose; H = disialyllactose.

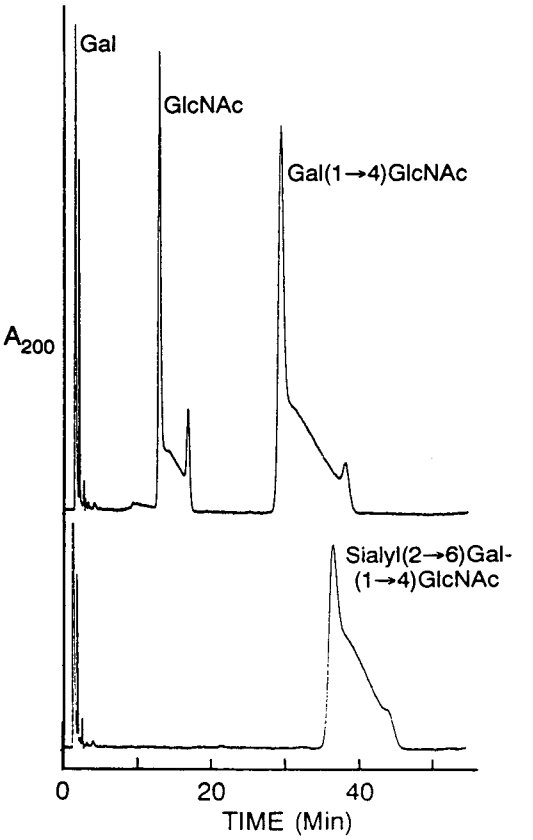

Fig. 2. HILIC of GlcNAC-containing carbohydrates. Conditions as in Fig. 1.

it is evident that either amide sugar or sialic acid residues promote retention of a carbohydrate through hydrophilic interactions. Upon comparing peaks F and G in Fig. 1, one could conclude that a neutral hexose at the reducing end promotes retention more than an amide sugar, again in accordance with previous observations [15,16]. Oligosaccharides with an amide sugar at the reducing end (Fig. 1, peak F, and Fig. 2), and GlcNAc itself, are resolved into separate peaks for the α- and β-anomers, linked by a continuum of the intermediate forms. This separation of anomers also accounts for the tailing peaks for Neu5Ac and Neu5Gc; Neu5Ac2en, which does not form anomers, elutes as a symmetrical peak. This phenomenon has been noted before when neutral stationary phases were used for HILIC

[19,29]; mutarotation is slow on the time scale of HPLC with these mobile phases. Mutarotation is accelerated by high pH. Thus, addition of 0.1% organic amine to the mobile phase can collapse the anomer doublets when a neutral column is used [29]. Similarly, anomer separation is normally not observed in HILIC with amino-silica columns, owing to the basicity of this stationary phase (although even these columns will resolve anomers if the mobile phase is sufficiently acidic [30]).

In some chromatographic separations, a solute can be oriented in such a manner that a particular "contact region" [31] is favored for interaction with the stationary phase surface. This phenomenon is not limited to partition modes. If a carbohydrate displays anomer separation, the implication is that the reducing end is a good contact region. Lack of an anomer effect implies that the reducing end is not the preferred contact region. Anomer separation can thus serve as a reporter function for solute orientation during chromatography. Fig. 3 is a schematic of such oriented contact; orientation is determined by the position of the amide sugar, which is the preferred contact region. This hypothesis on orientation is falsifiable. It was tested by inverting the sequence of amidated sugar and neutral hexose. GlcNAc(1→6)Gal does exhibit a symmetrical peak in Fig. 4, which would seem to confirm the hypothesis. However, at lower levels of acetonitrile (MeCN) in the mobile phase (inset), a small amount of anomer separation becomes evident with this compound too. This

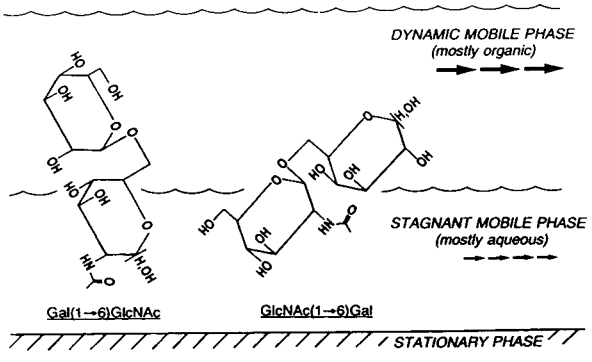

Fig. 3. Contact orientation and anomer effects in HILIC.

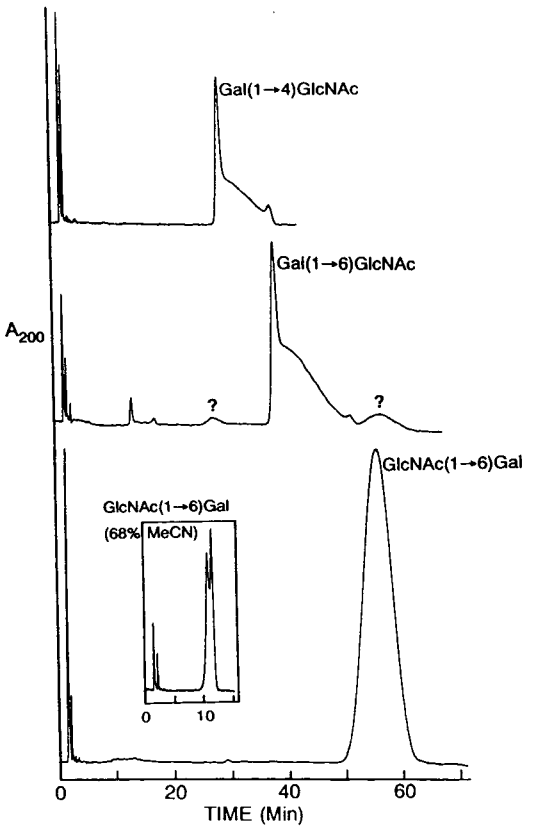

Fig. 4. Effect of sequence on anomer separation. Conditions as in Fig. 1, except for the inset, where MeCN–water ratio is 68:22 (v/v).

implies that the selectivity of the column changes somewhat with MeCN concentration; at lower levels of MeCN, neutral sugars serve as contact regions to a limited extent. At higher levels, amidated sugars dominate the chromatography.

Fig. 5 presents this shift in retention and selectivity for a number of carbohydrates. At relatively low levels of MeCN, sialic acids are very good contact regions. As the MeCN concentration increases, their role as contact regions diminishes relative to other sugars. Thus, the best separation of disialyllactose from the other carbohydrates is observed at the lowest level of MeCN in this study. Additive effects are evident in some cases [Gal(1→4)GlcNAc vs. GlcNAc] but not in others [sialyl(2→3)lactose vs. Gal(1→4)GlcNAc]. Fig. 2 confirms that the

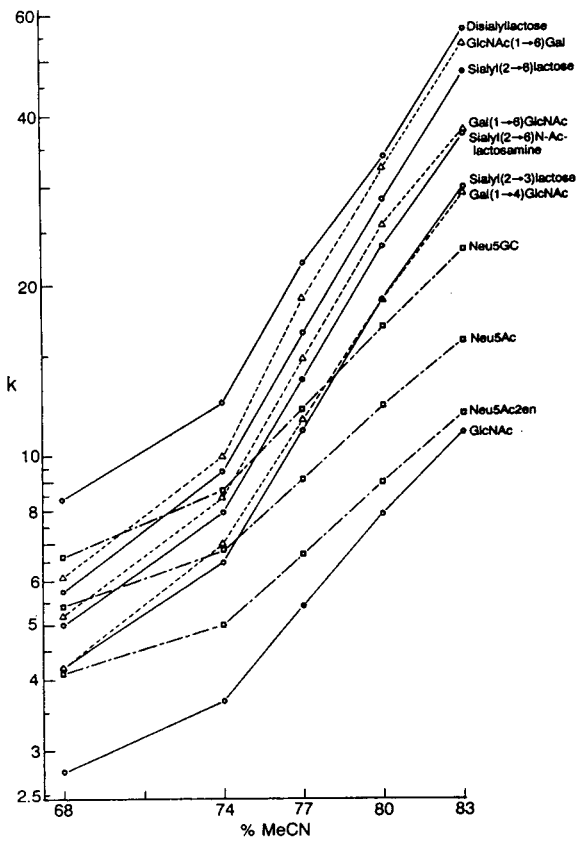

Fig. 5. Retention and selectivity vs. %MeCN. Conditions as in Fig. 1. The retention factor was determined from the formula $k = (t_R - t_0)/t_0$, where t_0 is the elution time for toluene, a non-retained solute, at a given flow-rate (*Note*: this replaces the expression for capacity factor, as per the new IUPAC nomenclature for chromatography).

addition of a sialyl residue has little effect on the orientation of contact as well as on the degree of retention; the amidated sugar is clearly the preferred contact region.

It seems counterintuitive that replacement of a residue which is a poor contact region with a better one (e.g., GlcNAc for Glc) results in a shorter retention time. The results probably reflect the partition nature of the HILIC mode. Retention is proportional to the degree to which a solute partitions into the stagnant aqueous layer on the surface of the stationary phase. With an amide sugar at the reducing end, a small oligosaccharide contacts the surface in an orientation which leads to less partitioning into the aqueous layer than if the orientation were inverted. The two phenomena —orientation and extent of partition— are independent to some extent. It should be noted that trisaccharides where the middle residue can be either GlcNAc or a neutral hexose do not differ much in retention in HILIC, compared with the consequences of such substitution at the reducing end [15]. A substitution in the middle of the oligosaccharide probably does not have much effect on its orientation or the degree of partitioning.

3.2. HILIC of underivatized complex carbohydrates

Fig. 6 shows the resolution of the underivatized glycan library cleaved from native bovine fetuin via hydrazinolysis. This library reportedly contains glycans which were N- and O-linked [6]. The most abundant single species is an O-linked disialylated tetrasaccharide [6]. This is consistent with the retention times in Fig. 6. Reasonable retention was obtained even though the mobile phase did not contain an electrolyte; evidently it is not necessary with larger oligosaccharides. These generally contain amide sugars, which

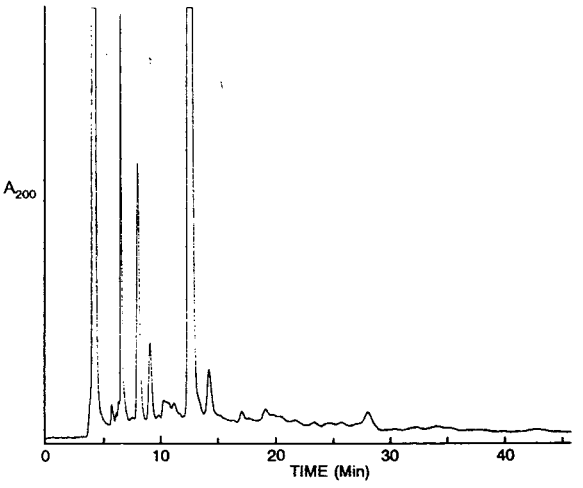

Fig. 6. HILIC of the complex carbohydrate library from native bovine fetuin. Sample: 6 μg (cf. Materials and methods section). Mobile phase: MeCN–water (80:20, v/v) (no TEAP). Other conditions as in Fig. 1.

would be good alternatives to sialic acids as contact regions. Since elution was isocratic, it was possible to detect the glycans at 200 nm. The lack of anomer separation probably reflects the presence of good contact regions in addition to the reducing end. The degree of anomer separation is in fact influenced by the composition of larger glycans [19].

3.3. HILIC of derivatized complex carbohydrates

This class was evaluated with biantennary N-linked oligosaccharides from apotransferrin. The PA derivatives were prepared as described in the Materials and methods section. Fig. 7 shows their isocratic separation by HILIC. N-Linked glycans are generally larger than the O-linked glycans prominent in Fig. 6, and less MeCN is necessary to obtain adequate retention. Retention and resolution are better with 65% MeCN (Fig. 7-II) than with 60% (Fig. 7-I). The last major peak (eluting at 18 min in Fig. 7-II) is the structure indicated. Mass spectral data (not shown) indicate that the peak eluting at 13 min in Fig. 7-II is the indicated glycan minus a terminal Gal residue. Davies et al. [7] have noted the presence of (Gal-minus) forms in commercial asialofetuin. The monosialyl form of this glycan was also examined. Judging from the data in Figs. 7-I and -II, such a sample could contain the following four components: (1) the monosialylated form with the structure indicated; (2) the monosialylated form minus a terminal Gal residue; (3 and 4) the asialo forms (± a Gal residue). Fig. 7-III indicates that all four of these forms are present, with the monosialyl forms (± a Gal) resolved at 60%. Clearly sialylation increased retention in comparison with the asialo forms. Separation of the monosialyl forms was worse at higher levels of MeCN (Fig. 7-IV), in contrast to the effect on the asialo forms (Fig. 7-II). Evidently the effectiveness of sialic acid as a contact region decreased relative to the other residues as the level of MeCN increased. This is consistent with the retention factors in Fig. 5.

Fig. 8 shows analysis of the same samples by

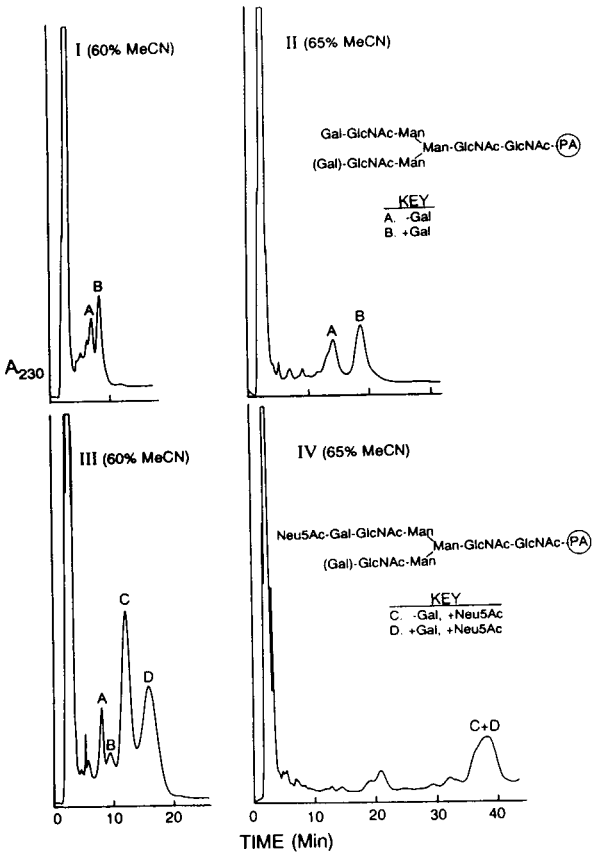

Fig. 7. HILIC of biantennary oligosaccharides from apotransferrin (PA derivatives). Column: PolyGLYCOPLEX, 200 × 2.1 mm (5 μm). Mobile phase (isocratic): MeCN–water (60:40, v/v) (I and III) or (65:35, v/v) (II and IV). Flow-rate: 0.25 ml/min.

HPAEC. The two major asialo forms are resolved to baseline, with sharp peaks. However, the two major monosialyl forms coincide under these conditions (Fig. 8, bottom). The presence of the sialyl group appears to dominate the interaction with the stationary phase in this mode; removal of the Gal does not affect retention.

3.4. HILIC of a GPI anchor glycan

Some proteins are attached to membranes through a glycan which is attached, via inositol, to a phospholipid. Such a "GPI anchor" glycan was obtained from the coat of a trypanosome as

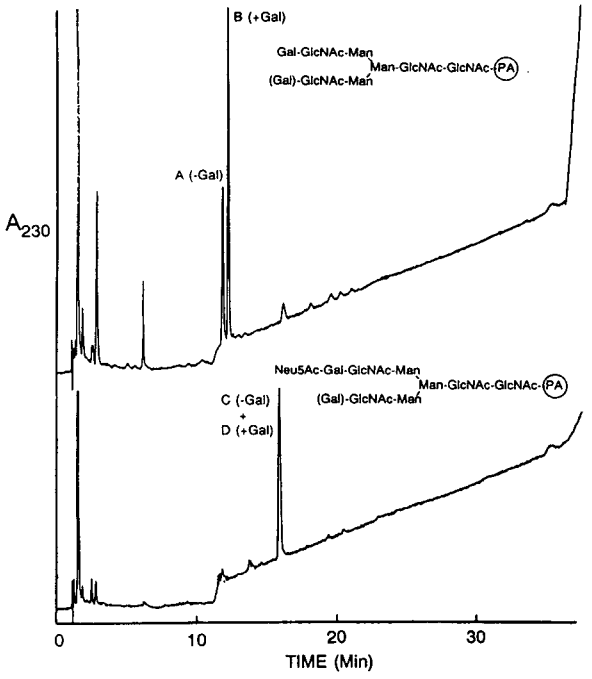

Fig. 8. HPAEC of biantennary oligosaccharides (same sample as Fig. 7). Column: CarboPac PA1. Flow-rate: 1.0 ml/min. Mobile phases: (eluent A) 100 m*M* NaOH; (eluent B) 100 m*M* NaOH + 500 m*M* sodium acetate. Gradient: 0–2 min, 1% B; 2–27 min, 1–50% B; 27–45 min, 50–100% B.

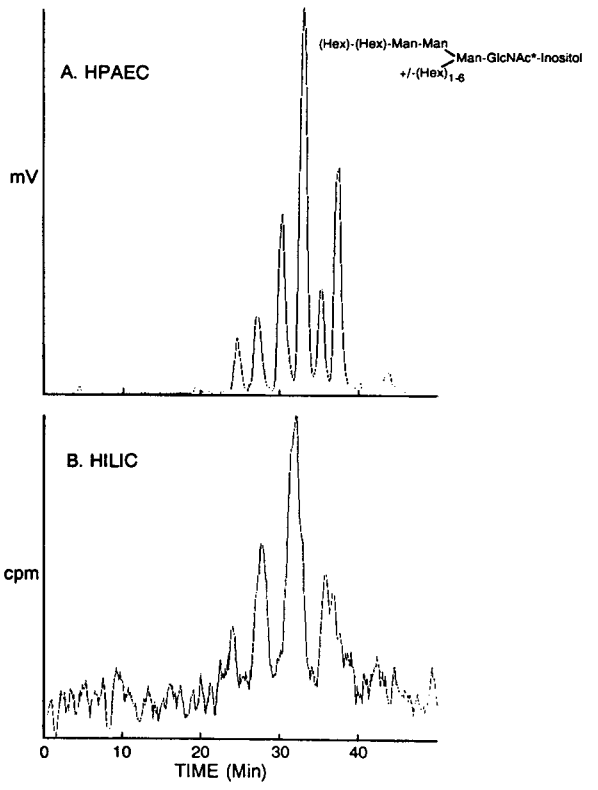

Fig. 9. GPI-anchor glycans (see Materials and methods section). The sample contained approx. 10 000 cpm, labelled at the GlcNAc residue as described in the Materials and methods section. (A) HPAEC; column: CarboPac PA1; mobile phases: (A) 150 m*M* NaOH, (B) 150 m*M* NaOH + 0.25 *M* sodium acetate; gradient: 5–20% B over 50 min; flow-rate: 0.6 ml/min; detection: PAD. (B) HILIC; column: PolyGLYCOPLEX, 200 × 4.6 mm (5 μm); mobile phase (isocratic): MeCN–water (65:35, v/v); flow-rate: 0.6 ml/min; detection: radioactivity detector (on-line).

described in the Materials and methods section. Fig. 9 shows the analysis of the product by HPAEC with detection by PAD (top) and HILIC with on-line radioactivity detection (bottom). The composition of the termini is quite variable, and is described elsewhere [32]. Both modes afford somewhat similar selectivity, although the efficiency of HPAEC is significantly better. The poor signal-to-noise ratio in the HILIC run reflects the small quantity of sample analyzed. Recovery of applied counts from this system is in excess of 95%.

3.5. Applications with MS

Fig. 10 shows a mixture of xyloglucans resolved by HILIC; the reducing termini have been derivatized with a *p*-nitrobenzene (PNB) derivative. The volatility of HILIC mobile phases permits convenient MS identification of eluted solutes. This was investigated with the xyloglucan mixture. The effluent was split between an absorbance detector and electrospray MS. Since the PNB-oligosaccharides were not reliably protonated upon elution (in contrast to results obtained with PA derivatives), a small amount of acetic acid was added post-column to insure that the derivatives were sufficiently charged for analysis by electrospray MS.

In Fig. 11 (left), it appears that resolution was significantly worse with a microbore column than with the regular analytical column used for Fig. 10. From comparison with the mass spectrum

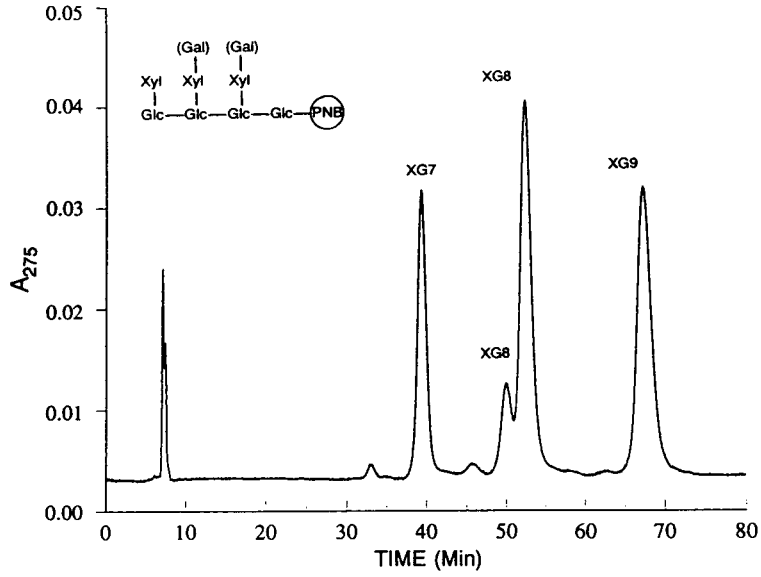

Fig. 10. HILIC of xyloglucans (PNB derivatives). XG7, XG8 and XG9 contain 0, 1 and 2 Gal residues, respectively. The two peaks labelled XG8 represent isomers with Gal in alternative positions [23]. Column: PolyGLYCOPLEX, 200 × 9.4 mm (5 μm). Mobile phase (isocratic): MeCN–water (70:30, v/v). Flow-rate: 1.0 ml/min.

(Fig. 11, right), it is evident that this loss of resolution reflects extracolumn bandspreading from connections and a UV detector not optimized for microbore work.

The mass spectrum in Fig. 11 was obtained using the total ion current (TIC) mode; the MS functioned as a general HPLC detector. The window of ion current can also be narrowed to

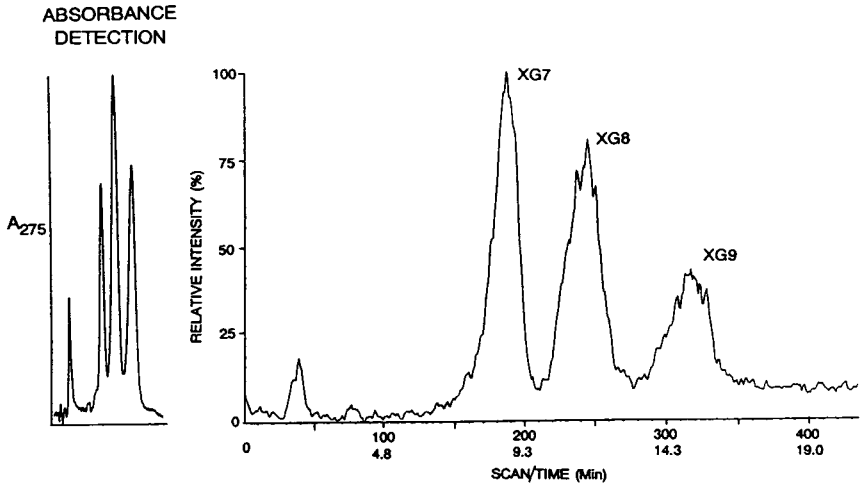

Fig. 11. Microbore HILIC–on-line MS of PNB-xyloglucans. Column: PolyGLYCOPLEX, 150 × 1.0 mm. Mobile phase as in Fig. 10. Flow-rate: 50 μl/min. Sample: 150 ng/1 μl (injected using a Rheodyne reverse-flow valve; see Materials and methods). Detection: (UV) A_{275} = 0.025 AUFS; MS, see Materials and methods. With these conditions, the positional isomers of PNB-XG8 were not resolved.

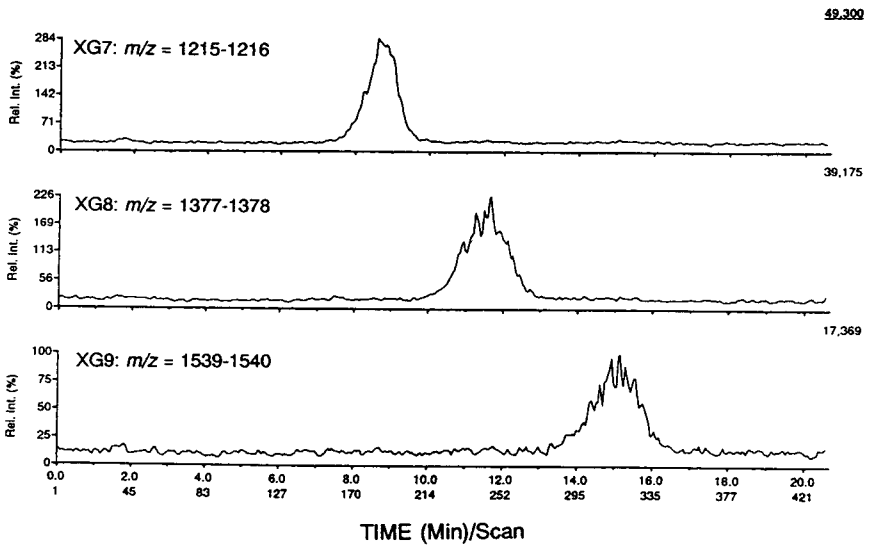

Fig. 12. Microbore HILIC-MS of PNB-xyloglucans: computer-generated selected ion chromatograms of Fig. 11.

the point that only a single species is detected, as shown in Fig. 12. This demonstrates the feasibility of determining the presence and molecular mass of a particular complex carbohydrate even if not completely resolved from others in the eluent. A similar study has been performed with PA derivatives on a RP-HPLC column [33].

The above data were obtained with approximately 50 pmol each of the PNB-xyloglucans. Optimization of the extracolumn equipment and the chromatographic conditions should permit analysis of carbohydrate derivatives in the low picomole range.

3.6. Selectivity of HILIC vs. RP-HPLC

RP-HPLC can be used with volatile mobile phases, which makes it convenient to use for direct MS of complex carbohydrate derivatives. Fig. 13 compares the performance of HILIC and RP-HPLC with PNB derivatives of complex carbohydrates from pea seedlings. The selectivity of the two modes is somewhat complementary, but overall the selectivity of HILIC is superior to that of RP-HPLC in this case. It should be noted that while Davies et al. [7] were able to resolve underivatized complex carbohydrates on a Hypercarb S column in the RP-HPLC mode, the column was unable to distinguish between (Gal-plus) and (Gal-minus) forms (cf. Fig. 7), and monosialyl forms were poorly resolved from asialo forms.

4. Discussion

4.1. HILIC with PolyGLYCOPLEX and other columns

HILIC with the PolyGLYCOPLEX column is promising with all of the categories of complex carbohydrates examined. Isocratic elution with 65 or 70% MeCN may suffice to resolve most complex carbohydrates in an acceptable time frame. Retention of smaller carbohydrates may require 80% MeCN. With particularly complex samples, it may be necessary to use a gradient from 80–65% MeCN. There may be solubility problems with larger underivatized glycans. However, PolyGLYCOPLEX seems to afford a given degree of retention at lower levels of MeCN than is necessary with other neutral HILIC materials. For example, if one corrects for differences in column volume, with the same glycan and mobile phase, retention time is about

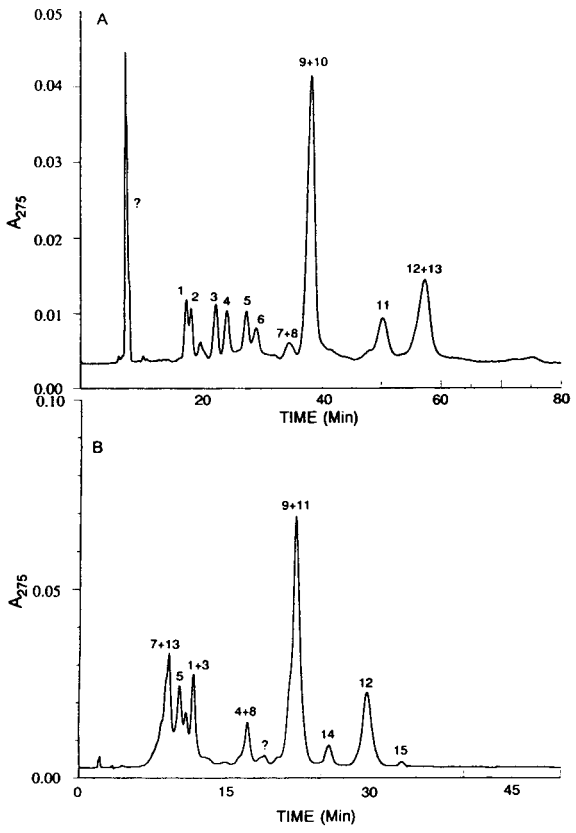

Fig. 13. HILIC and RP-HPLC of carbohydrates (PNB derivatives) from extract of pea root (*P. sativum*). (A) HILIC; column and conditions as in Fig. 10. (B) RP-HPLC; column: see Materials and methods; elution: 9–12% MeCN (aqueous) in a linear gradient over 50 min; flow-rate: 1.0 ml /min. Mobile phases were sparged with helium prior to use. Components were determined by off-line electrospray MS of collected fractions. Electrospray MS is unable to identify the specific pentose and hexose residues and their sequences, or to identify branched structures. Peaks (P = pentose; H = hexose; F = fucose): 1 = $(P)_4$; 2 = $(H)_3$; 3 = $(P)_5$; 4 = $(H)_3(P)_2$; 5 = $(H)_4$; 6 = $(P)_6$; 7 = $(H)_5$; 8 = $(H)_4(P)_2$; 9 = $(H)_4(P)_3$; 10 = $(P)_7$; 11 = $(H)_5(P)_3$; 12 = $(H)_5(P)_3F$; 13 = $(H)_6$; 14 = $(H)_6(P)_3F$; 15 = $(H)_6(P)_3(F)_2$.

four times longer on PolyGLYCOPLEX than on GlycoPAK N (e.g., Fig. 7 vs. Ref. [19], Fig. 2).

Sialic acids, amide sugars, and neutral hexoses all contribute significantly to retention when incorporated into an oligosaccharide which contains at least one good contact residue. The degree to which each residue affects retention depends on whether or not it is at the reducing end and on the level of organic solvent in the mobile phase. Relative to amide sugars, sialic acids and neutral hexoses contribute more to retention at lower levels of organic solvent than at higher levels. This permits selectivity to be manipulated. In order to generate detailed rules relating retention to composition, it will be necessary to examine the retention times of a large set of complex carbohydrates, using several sets of elution conditions (e.g., low vs. high organic; presence or absence of electrolytes).

Amino-silica and basic polymeric materials have two disadvantages relative to PolyGLYCOPLEX. First, they are inconvenient to use with sialylated oligosaccharides because of the extra electrostatic attraction; it necessitates increasing salt gradients. Second, some of the more common groups for derivatizing complex carbohydrates are positively charged at low pH. They are effectively run on amino-silica columns only at pH ranges high enough to uncharge the derivative (e.g., pH 7.3 with PA derivatives). Neutral HILIC columns do not have this disadvantage, although this is not apparent to all users; the pH 7.3 mobile phases have been uncritically carried over in some published work with such columns.

4.2. HILIC vs. other modes

HPAEC

Both methods have good selectivity for residue composition, number, and linkage position. HPAEC is decidedly more efficient. PAD is convenient with HPAEC. However, PAD can also be used with HILIC, through post-column addition of sodium or lithium hydroxide solution [34–36]. The non-volatile nature of HPAEC mobile phases is inconvenient for sample collection and MS analysis. The latter is possible through the use of in-line ion-suppressor membranes to remove cations post-column [37,38]; the procedure currently requires larger glycans to be run in the negative ion mode. HILIC seems to be more straightforward for direct MS analysis, since no post-column treatment is necessary.

RP-HPLC

In RP-HPLC, the only really good contact region is the chromophore or fluorophore at the reducing end. This may account for the lesser selectivity of RP-HPLC compared with HILIC.

The selectivity of the two modes is sufficiently complementary that it is reasonable to continue to use them in a two-dimensional sequence [3,18].

References

[1] A. Varki, *Glycobiology*, 2 (1992) 25.
[2] S. Schenkman and D. Eichinger, *Parasitol. Today*, 9 (1993) 218.
[3] M. Engstler and R. Schauer, *Parasitol. Today*, 9 (1993) 222.
[4] R.W. Veh, J.-C. Michalski, A.P. Corfield, M. Sander-Wewer, D. Gies and R. Schauer, *J. Chromatogr.*, 212 (1981) 313.
[5] N. Tomiya, J. Awaya, M. Kurona, S. Endo, Y. Arata and N. Takahashi, *Anal. Biochem.*, 171 (1988) 73.
[6] Y.C. Lee, B.I. Lee, N. Tomiya and N. Takahashi, *Anal. Biochem.*, 188 (1990) 259.
[7] M.J. Davies, K.D. Smith, R.A. Carruthers, W. Chai, A.M. Lawson and E.F. Hounsell, *J. Chromatogr.*, 646 (1993) 317.
[8] T. Patel, J. Bruce, A. Merry, C. Bigge, M. Wormald, A. Jaques and R. Parekh, *Biochemistry*, 32 (1993) 679.
[9] M.R. Hardy and R.R. Townsend, *Proc. Natl. Acad. Sci. U.S.A.*, 85 (1988) 3289.
[10] R.R. Townsend and M.R. Hardy, *Glycobiology*, 1 (1991) 139.
[11] A.J. Alpert, *J. Chromatogr.*, 499 (1990) 177.
[12] P. Orth and H. Engelhardt, *Chromatographia*, 15 (1982) 91.
[13] L.A.Th. Verhaar and B.F.M. Kuster, *J. Chromatogr.*, 234 (1982) 57.
[14] Z.L. Nikolov and P.J. Reilly, *J. Chromatogr.*, 325 (1985) 287.
[15] W.M. Blanken, M.L.E. Bergh, P.L. Koppen and D.H. van den Eijnden, *Anal. Biochem.*, 145 (1985) 322.
[16] S. Hase, S. Koyama, H. Daiyasu, H. Takemoto, S. Hara, Y. Kobayashi, Y. Kyogoku and T. Ikenaka, *J. Biochem.*, 100 (1986) 1.
[17] M.L.E. Bergh, P. Koppen and D.H. van den Eijnden, *Carbohydr. Res.*, 94 (1981) 225.
[18] N. Takahashi, Y. Wada, J. Awaya, M. Kurono and N. Tomiya, *Anal. Biochem.*, 208 (1993) 96.
[19] B. Bendiak, J. Orr, I. Brockhausen, G. Vella and C. Phoebe, *Anal. Biochem.*, 175 (1988) 96.
[20] S. Hase, K. Hatanaka, K. Ochiai and H. Shimizu, *Biosci. Biotech. Biochem.*, 56 (1992) 1676.
[21] M.A.J. Ferguson, P. Murray, H. Rutherford and M.J. McConville, *Biochem. J.*, 291 (1993) 51.
[22] M.A.J. Ferguson, in N.M. Hooper and A.J. Turner (Editors), *Lipid Modification of Proteins: A Practical Approach*, IRL Press, Oxford, 1992, pp. 191–230.
[23] W.S. York, L.K. Harvey, R. Guillen, P. Albersheim and A.G. Darvill, *Carbohydr. Res.*, 248 (1993) 285.
[24] R. Guillen, W.S. York, G. Impallomeni, P. Albersheim and A.G. Darvill, in preparation.
[25] W. Von Deyn, W.S. York, P. Albersheim and A.G. Darvill, *Carbohydr. Res.*, 201 (1990) 135.
[26] M. Pauly, W.S. York, R. Guillen, P. Albersheim and A.G. Darvill, in preparation.
[27] A.J. Alpert, *J. Chromatogr.*, 359 (1986) 85.
[28] S. Honda, *Anal. Biochem.*, 140 (1984) 1.
[29] C. Brons and C. Olieman, *J. Chromatogr.*, 259 (1983) 79.
[30] N.M.K. Ng Ying Kin and L.S. Wolfe, *Anal. Biochem.*, 102 (1980) 213.
[31] J. Fausnaugh-Pollitt, G. Thevenon, L. Janis and F.E. Regnier, *J. Chromatogr.*, 443 (1988) 221.
[32] M.A.J. Ferguson and A. Mehlert, in preparation.
[33] J. Suzuki-Sawada, Y. Umeda, A. Kondo and I. Kato, *Anal. Biochem.*, 207 (1992) 203.
[34] A.S. Feste and I. Khan, *J. Chromatogr.*, 607 (1992) 7.
[35] T. Soga, Y. Inoue and K. Yamaguchi, *J. Chromatogr.*, 625 (1992) 151.
[36] A.S. Feste and I. Khan, *J. Chromatogr.*, 630 (1993) 129.
[37] R.C. Simpson, C.C. Fenselau, M.R. Hardy, R.R. Townsend, Y.C. Lee and R.J. Cotter, *Anal. Chem.*, 62 (1990) 248.
[38] W.M.A. Niessen, R.A.M. van der Hoeven, J. van der Greef, H.A. Schols, A.G.J. Voragen and C. Bruggink, *J. Chromatogr.*, 647 (1993) 319.

ELSEVIER

Journal of Chromatography A, 676 (1994) 203–208

JOURNAL OF CHROMATOGRAPHY A

Organic modifiers in the anion-exchange chromatographic separation of sialic acids

Jianqiang Xia, Penny J. Gilmer*

Department of Chemistry, Florida State University, Tallahassee, FL 32306-3006, USA

Abstract

The combined effects of the organic modifiers and the ionic strength in the eluent on the separation of sialic acids were investigated on an anion-exchange Mono Q HR5/5 column. A log–log plot of capacity factors of sialic acids *vs.* eluent anion concentration demonstrates good linearity. The major retention mechanism is explained as anion exchange. Moreover, the plot of capacity factors of sialic acids *vs.* reciprocal of eluent anion concentration indicates that other retention mechanisms exist in addition to anion exchange. The organic modifiers (methanol and acetonitrile) in the mobile phase have significant influence on the retention time and resolution. The eluent anion concentration and the fraction of organic modifier produce a very flexible system that can be optimized for the separation of sialic acids. Five standard sialic acid derivatives have been separated by choosing a suitable eluent anion concentration and the fraction of organic modifier. The optimized conditions have been applied to separate sialic acids released from bovine submandibular mucin. 5,9-Diacetylneuraminic acid (Neu5,9Ac_2) can be separated from N-acetylneuraminic acid (Neu5Ac) and N-glycolylneuraminic acid (Neu5Gc) but is overlapped with other peaks. Neu5Ac and Neu5Gc are completely separated.

1. Introduction

Sialic acids are components of glycoproteins and glycolipids. They constitute a family of neuraminic acid (5-amino-3,5-dideoxy-D-nonulosonic acid) derivatives [1]. The most common sialic acids are N-acetylneuraminic acid (Neu5Ac) and N-glycolylneuraminic acid (Neu5Gc) (pK values about 2) [2]. Other naturally occurring forms are from O-substitution of one or more of the hydroxyl groups of Neu5Ac or Neu5Gc with acetyl, methyl, lactyl or sulphate groups. Unsaturated and dehydro forms of sialic acids have also been reported in nature [3]. These modifications show tissue specificities and are known to affect a wide spectrum of biological phenomena. In order to further explore the biological functions of sialic acids, it is necessary to release and separate these compounds from biological materials.

Because sialic acids from biological sources have a low concentration and a high diversity, the separation must be performed by the following multistep procedure: (1) separation from other water insoluble constituents; (2) separation from neutral sugars and other water soluble materials; (3) separation of individual sialic acid derivatives. The first two steps are not difficult and have been established. The present work is concerned with the separation of individual component sialic acids.

Sialic acids are not volatile enough to be

* Corresponding author.

0021-9673/94/$07.00
SSDI 0021-9673(94)00338-A

separated directly by gas chromatography. Liquid chromatography, especially ion-exchange chromatography, because it takes advantage of the ionic character of the carboxyl groups, can be a good choice for separation of sialic acids from neutral sugars. The reported cation [4] and anion [5–8] exchange chromatographies have not yet achieved complete separation of Neu5Ac, Neu5Gc and 5,9-diacetylneuraminic acid ($Neu5,9Ac_2$) (resolution < 1.5). In 1990, Manzi *et al.* [9] evaluated anion-exchange chromatography of sialic acids on Aminex A-28 and A-29 columns with sodium sulphate as the eluent without organic modifiers, and reported that the overlapping of peaks in complex mixtures is too high and elution times are very close. Moreover, it is easy to miss the presence of a minor component.

In order to further improve the separation of sialic acids, it is necessary to investigate the effect of organic modifier content of the mobile phase on the separation of sialic acids in anion-exchange liquid chromatography. However, until now, according to our knowledge, there is no report on using organic modifiers in this type of separation. In this paper, the effect of methanol and acetonitrile concentrations of the mobile phase on retention and selectivity of five sialic acid derivatives was studied. The optimized conditions can be applied to separate sialic acids released from bovine submandibular mucin (BSM).

$Neu5,9Ac_2$ can be separated from Neu5Ac and Neu5Gc but is overlapped with other peaks. Neu5Ac and Neu5Gc are completely separated. The organic modifiers may be used in other ionic chromatographic separation of charged species.

2. Experimental

2.1. Chemicals

BSM, Neu5Ac, Neu5Gc, cytidine 5′-monophospho-N-acetylneuraminic acid (CMP-Neu5Ac), 2,3-dehydro-2-deoxy-N-acetylneuraminic acid (Neu2en5Ac) and histamine were purchased from Sigma (St. Louis, MO, USA). $Neu5,9Ac_2$ was kindly provided by Dr. Chi-Huey Wong (Scripps Research Institute, La Jolla, CA, USA).

2.2. Hydrolysis of BSM [4]

BSM (3 mg) was dissolved in 5 ml 0.01 *M* hydrochloric acid in a sealed glass tube, the tube was heated for 1 h at 80°C in a water bath incubator with shaking. The reaction mixture was then cooled immediately to room temperature and centrifuged at 50 000 *g*, the supernatant was filtered through a PVDF syringe filter (0.45 μm), the sample solution was lyophilized and then dissolved in 0.5 ml water. The sample solution was injected onto the HPLC column.

2.3. HPLC

HPLC analysis was performed on a Beckman liquid chromatography apparatus, equipped with a liquid chromatography controller 421A, a programmable detector 166, and a 114M pump. Separations were achieved at room temperature on an analytical pre-packed Mono Q HR 5/5 column (50 × 5 mm) (Pharmacia). Mono Q was a strong anion exchanger based on a beaded hydrophilic resin consisting of monodispersed 10-μm particles with $-CH_2N^+(CH_3)_3$ charged groups. The ionic capacity was 0.27–0.37 mmol/column.

All the standard samples (0.8–2.0 mg) were dissolved in HPLC water. Samples were applied to the column with 20-μl sample loop. The eluent flow-rate was 0.5 ml/min and monitored by the UV detector at 205 nm. Histamine and tetraethylammonium bromide were monitored at 260 nm.

3. Results and discussion

Anion-exchange chromatography is a form of adsorption chromatography in which ionic solutes display reversible electrostatic interactions with a charged stationary phase. A basic equation (Eq. 1) has been published for ion exchange in terms of the capacity factor (k') and the concentration of the eluent anion [E]. It predicts

Table 1
The retention times (min) of histamine and tetraethylammonium bromide at different NaH_2PO_4 concentrations (pH was 4.50 at 7.50 m*M*)

	NaH_2PO_4 (m*M*)						
	4.97	7.50	9.94	20.0	40.0	60.0	80.0
$Et_4N^+Br^-$	1.77	1.76	1.77	1.76	1.82	1.73	1.87
Histamine	1.59	1.59	1.59	1.64	1.68	1.70	1.70

a linear dependence of log k' on the logarithm of eluent concentration if the resin capacity (C) is constant [10].

$$\log k' = -(a/b)\log[\mathrm{E}] + (a/b)\log C + \text{constant} \quad (1)$$

where a and b are the charges on the sample ion and the eluent ion, respectively.

According to Eq. 1, a plot of log k' *vs.* log [E] will yield a straight line with a negative slope of a/b. The slope varies only with the valence of the solute (a) or the valence of the counterion (b). The capacity factor k' was determined from the retention time of the component (t_r) and that of an unretained compound (t_0): $k' = (t_r - t_0)/t_0$. Histamine [11] and tetraethylammonium bromide were chosen as unretained tracers. The void time determined by histamine was less than that determined by tetraethylammonium bromide, as shown in Table 1. Moreover, histamine has a higher UV absorbance coefficient at 260 nm. Therefore, histamine was preferred for the determination of t_0. It should be noted, however, that the accurate determination of k' is still a main problem in liquid chromatography [12].

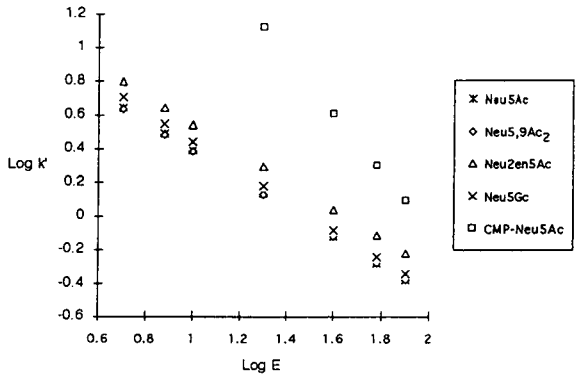

Fig. 1. The log–log plot of the capacity factors of sialic acids and NaH_2PO_4 concentration (m*M*).

The effect of the mobile counter anion on the anion exchanger was studied in more detail. The influence of the anion concentration was studied for NaH_2PO_4. The results are shown in Table 2.

It can be seen that CMP-Neu5Ac can be separated by changing the counter anion concentration. The counter anion concentration has significant influence on the retention time of the remaining sialic acid derivatives, but has less influence on the resolution. A plot of log k' *vs.* log of counter anion concentration shows good linear relationship (Fig. 1). The slope of each component is summarized in Table 3. If the resin capacity is constant, this plot should yield lines with a slope of -1 for the first four sialic acids and -2 for the last one in Table 3. The result is

Table 2
The retention times (min) of sialic acids at different NaH_2PO_4 concentrations (pH was 4.50 at 7.50 m*M*)

	NaH_2PO_4 (m*M*)						
	4.97	7.50	9.94	20.0	40.0	60.0	80.0
Neu5Ac	8.53	6.41	5.56	3.92	2.95	2.59	2.39
Neu5,9Ac_2	8.38	6.36	5.48	3.88	2.94	2.59	2.41
Neu5Gc	9.54	7.12	6.10	4.19	3.07	2.68	2.45
Neu2en5Ac	11.4	8.55	7.29	4.92	3.52	3.00	2.71
CMP-Neu5Ac	nd[a]	nd	nd	23.2	8.29	5.09	3.80

[a] nd = Not determined.

Table 3
Linear regression results of Eq. 1 for the analytes with NaH_2PO_4 eluent.

	a/b (calculated)	a/b (predicted)	R^2 [a]
Neu5Ac	−0.86	−1	0.999533
Neu5,9Ac$_2$	−0.85	−1	0.999709
Neu5Gc	−0.88	−1	0.999557
Neu2en5Ac	−0.85	−1	0.995870
CMP-Neu5Ac	−1.71	−2	0.999937

[a] R^2 is a statistical measurement of the validity of the model. It ranges up to 1, with 1 being optimal.

close to the predicted values from Eq. 1. Therefore, the primary mechanism for the chromatography is anion exchange.

In order to further explore the retention mechanism, we use the following model to describe anion-exchange chromatography:

$$R^+E^- + S^- \rightleftharpoons R^+S^- + E^-$$

The anion-exchange constant is:

$$K_e = [RS][E^-]/([RE][S^-]) \quad (2)$$

where $R^+ = -CH_2-N^+(CH_3)_3$; $E^- = H_2PO_4^-$; S^- = Neu5Ac or Neu5Gc anion ($R-COO^-$)

$$HS + H_2O \rightleftharpoons H_3O^+ + S^-$$

The acid ionization constant is:

$$K_a = [H_3O^+][S^-]/[HS] \quad (3)$$

the capacity factor:

$$k' = n_s/n_m = (C_s/C_m)V_s/V_m \quad (4)$$

where n_s and n_m are moles of solute in the stationary phase and mobile phase; C_s and C_m concentration of solute in stationary phase and mobile phase; and V_s and V_m volume of stationary phase and mobile phase, respectively.

The distribution coefficient is:

$$D = C_s/C_m = [RS]/([S^-] + [HS]) \quad (5)$$

$$k' = K_eV_s\{[RE]/[V_m(1 + [H_3O^+]/K_a)]\}(1/[E^-]) \quad (6)$$

where [RE] is determined by the ionic capacity of the resin.

According to Eq. 6, at infinite anion concentration, the plot of capacity factors of Neu5Ac and Neu5Gc *vs.* the reciprocal of NaH_2PO_4 concentration should be linear and pass through origin. However, in Fig. 2 the y-intercepts are not zero. This means that some other mechanisms exist in addition to anion exchange.

Generally, normal-phase or reversed-phase separation mechanism exists in anion-exchange chromatography. Both of these mechanisms could be affected by organic modifiers. We chose methanol and acetonitrile as the organic modifiers added into the 7.50 mM NaH_2PO_4 solution. The influences of the mobile phases on the separation capacity factors (k') was investigated by varying the amount of organic additives. The results are plotted in Figs. 3 and 4.

It is clear that without organic modifiers, the system has insufficient selectivity to separate the sialic acids. However, the selectivity increases considerably with increasing organic modifier concentration.

The capacity factors (k') of Neu5Ac and Neu5Gc increase with increasing organic fraction. We reason that the organic modifiers change the interaction between solute anion and stationary phase cation according to Coulomb's law:

$$F = q_1q_2/(r^2\epsilon)$$

where ϵ is the dielectric constant of the medium

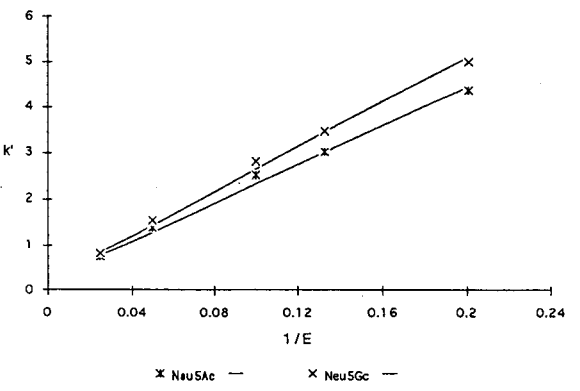

Fig. 2. Relationship between the capacity factors of sialic acids and the reciprocal of NaH_2PO_4 concentration (mM^{-1}).

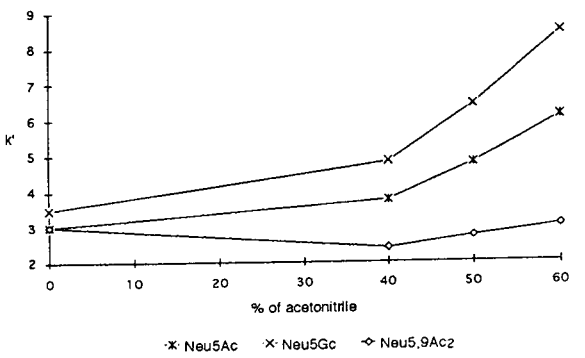

Fig. 3. Relationship between the capacity factors of sialic acids and the fraction of acetonitrile into 7.50 m*M* NaH_2PO_4 solution.

[13]. $\epsilon(H_2O) = 78.5$ (25°C); $\epsilon(CH_3OH) = 32.7$ (25°C) and $\epsilon(CH_3CN) = 37.5$ (20°C)

When the organic modifier is added, ϵ becomes smaller, the electrostatic attraction force (F) between solute anion and stationary phase cation becomes larger, and the capacity factor (k') becomes larger. The organic additives also affect all the ionic equilibria in the mobile phase.

Very interestingly, at the same organic fraction, the effects of methanol and acetonitrile on k' of Neu5Ac and Neu5Gc are different. At lower organic fractions, the organic solvent influences on the hydrophobic interaction between solute and stationary phase, the secondary mechanism behaves as reversed phase, with the k' value with acetonitrile being less than with methanol. The organic solvent affecting the hydrophobic interactions is even more obvious with $Neu5,9Ac_2$ in Fig. 3. However, at higher organic fractions, the k' value with methanol is smaller than with acetonitrile. Because methanol instead of acetonitrile can form hydrogen bonds with Neu5Ac or Neu5Gc hydoxyl groups, when more methanol is added in the eluent, it reduces the induced electrostatic interactions between the hydroxyl groups of sialic acids and the positively charged layer on the stationary phase. In this case, at the same fractions of methanol and acetonitrile, the solute has a smaller k' value in methanol than in acetonitrile. Therefore, the secondary mechanism of the anion chromatography involves both hydrophobic and induced electrostatic interactions.

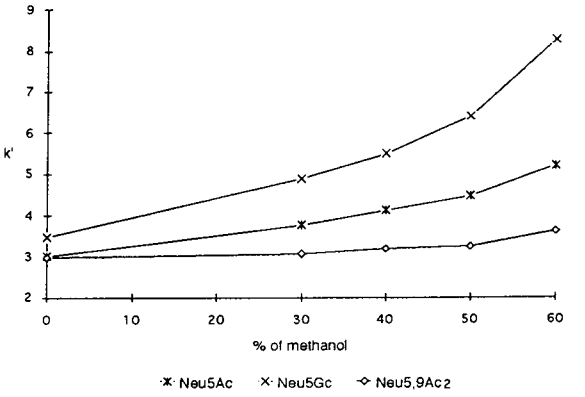

Fig. 4. Relationship between the capacity factor of sialic acids and the fraction of methanol into 7.50 m*M* NaH_2PO_4 solution.

Until now, the retention behavior of sialic acids can be explained at least qualitatively. The complex functions of organic modifiers provide wide flexibility in optimizing the separation of sialic acid derivatives. We found that methanol–7.50 m*M* NaH_2PO_4 (60:40, v/v) was the best eluent for separation of the sialic acid derivatives.

As a practical application of this study, we separated sialic acids released from BSM. Neu5Ac and Neu5Gc could be completely separated. The results are shown in Figs. 5 and 6.

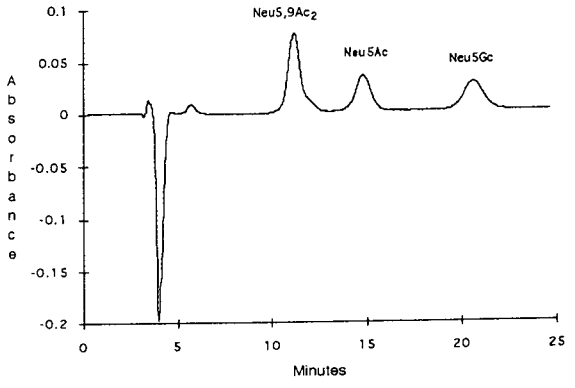

Fig. 5. Chromatogram of a mixture of $Neu5,9Ac_2$, Neu5Ac and Neu5Gc in aqueous solution. The separation was achieved on a Mono Q HR 5/5 column with a HRLC MA7Q anion-exchange column (BioRAD) (50 × 7.8 mm) as guard column. The eluent was methanol–7.50 m*M* NaH_2PO_4 (aq.) (60:40) solution. UV detector at 205 nm.

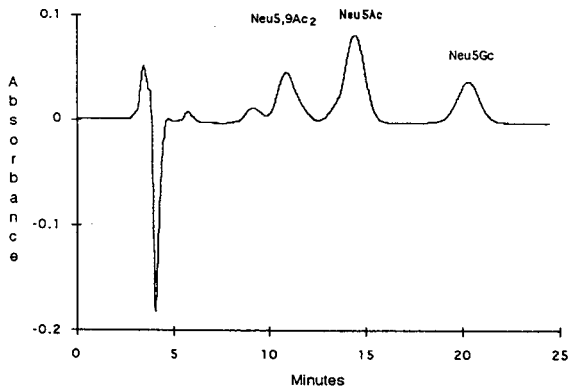

Fig. 6. Chromatogram of the hydrolysate of BSM. BSM (3 mg) was hydrolyzed in 5 ml of 0.01 *M* HCl for 1 h at 80°C (for sample preparation refer to experimental). The separation was achieved on a Mono Q HR 5/5 column with a HRLC MA7Q anion-exchange column (BioRAD) (50 × 7.8 mm) as guard column. The eluent was methanol–7.50 m*M* NaH_2PO_4 (aq.) (60:40) solution. UV detector at 205 nm.

The peak just prior to Neu5,9Ac_2 in Fig. 6 probably is Neu5,8,9Ac_3 or other derivatives with more than one OAc group.

Acknowledgements

The authors thank Research Corporation for financial support (grant No. R-105), and Hank Henricks and Umesh Goli in the BASS (Bioanalytical Synthesis Sequencing) Laboratory (Department of Chemistry, Florida State University, Tallahassee, FL, USA) for invaluable assistance.

References

[1] A.P. Corfield and R. Schauer, in R. Schauer (Editor), *Sialic Acids, Chemistry, Metabolism and Function*, Vol. 10, Springer, NY, 1982, p. 5.
[2] R. Schauer, *Trends Biochem. Sci.*, 10 (1985) 357.
[3] R. Schauer, *Adv. Carbohydr. Chem. Biochem.*, 40 (1982) 131.
[4] H. K. Ogawa, Y. Takeuchi, H. Uchibori, I. Matsumoto and N. Seno, *J. Chromatogr.*, 612 (1993) 145.
[5] A.K. Shukla and R. Schauer, *Anal. Biochem.*, 158 (1986) 158.
[6] A. K. Shukla, N. Scholz, E.H. Reimerdes and R. Schauer, *Anal. Biochem.*, 123 (1982) 78.
[7] G. Herrler, R. Rott, H.D. Klenk, H.P. Müller, A.K. Shukla and R. Schauer, *EMBO J.*, 4 (1985) 1503.
[8] R. Schauer, *Adv. Exp. Med. Biol.*, 174 (1984) 75.
[9] A. E. Manzi, S. Diaz and A. Varki, *Anal. Biochem.*, 188 (1990) 20.
[10] D.T. Gjerde and J.S. Fritz, *Ion Chromatography*, Hüthig, Heidelberg, 2nd ed., 1987, p. 73.
[11] Sj. van der Wal and J.F.K. Huber, *J. Chromatogr.*, 102 (1974) 353.
[12] N. Volpe, *Chromatographia*, 34 (1992) 216.
[13] T.H. Lowry, *Mechanism and Theory of Organic Chemistry*, 3rd ed., 1987, p. 177.

ELSEVIER

Journal of Chromatography A, 676 (1994) 209–217

JOURNAL OF CHROMATOGRAPHY A

High-performance capillary electrophoresis of proteins using sodium dodecyl sulfate–poly(ethylene oxide)

Kálmán Benedek*, Stephan Thiede

Amgen, Amgen Center, Thousand Oaks, CA 91360-1789, USA

Abstract

High-performance capillary electrophoresis using the replaceable poly(ethylene oxide) (PEO) polymer network in the presence of sodium dodecyl sulfate (SDS) is shown to be á viable alternative to SDS–polyacrylamide gel electrophoresis. The effects of the PEO molecular mass and polymer concentration on the separation of proteins were studied. The 100 000 PEO polymer provided good resolution of the protein standards and was selected for detailed studies. The preparation of this gel at various concentrations is relatively simple and makes it feasible for Ferguson analysis. Various recombinant proteins were analyzed using a universal calibration curve generated by the Ferguson analysis. The accuracy of the estimated molecular mass were very much protein dependent, in general it was about 10% off to their sequence based molecular mass.

1. Introduction

Capillary electrophoresis of proteins and peptides has become a successful and well documented analytical method [1]. The traditional method of choice for purity assessment of protein preparations is sodium dodecyl sulfate–polyacrylamide gel electrophoresis (SDS-PAGE). It is also often used for molecular mass estimation of proteins. The popular slab SDS-PAGE is time consuming and requires visualization of the separated protein bands by staining/destaining procedures. The capillary version of SDS-PAGE has been described and is currently undergoing development [2–4]. Presently, it is believed that 25 to 100 μm I.D. capillaries, filled with replaceable viscous polymer solutions offers more potential than crosslinked gels [5,6]. The capillaries are coated or uncoated depending on the nature of the sieving polymer network. In capillary electrophoresis, on-line detection is possible when the separation buffer, coating material or separation polymer network are transparent at the detection wavelength. It appears that replaceable high-molecular-mass dextrans [7], poly(ethylene oxides) [8], linear polyacrylamides [9], and other polymers are appropriate for detergent mediated protein separations [10].

The replaceable polymer network method also allows for easy preparation of separating polymers at a variety of concentrations, thus specific optimization can be tailored for various protein separations. Additionally, capillary electrophoresis offers the possibility of quantitative analysis [11].

Our study focused on the utilization of linear poly(ethylene oxide) (PEO) polymer solutions to evaluate the molecular mass of various recombinant proteins [12]. The separation buffers were UV transparent, thus allowing direct protein

* Corresponding author.

0021-9673/94/$07.00
SSDI 0021-9673(94)00229-3

detection at the low UV (214 nm) region. The most practical advantage of the PEO based solutions is that they do not require coated capillaries. The objective was to optimize protein separations and to study the effects polymer molecular mass and concentration in a defined separation buffer had on the separations. The systematic study was performed with commercially available standard proteins. The feasibility of the method is illustrated with the analysis of recombinant proteins, glycosylated and non-glycosylated, molecular mass ranging from 13 000 to 30 000 and covering a wide range of p*I* values (*ca.* 4.5–10.5).

2. Materials and methods

2.1. Instrumentation

A Beckman P/ACE System 2000 (Beckman Instruments, Fullerton, CA) automated capillary electrophoresis instrument, with System Gold instrument control and data evaluation software was used for analysis. The detection wavelength was 214 nm. The temperature of the analysis was set at 20°C unless it is stated otherwise.

2.2. Materials

The electrophoresis calibration kit for low-molecular-mass proteins was purchased from Pharmacia (Piscataway, NJ, USA) and contained the following proteins: phosphorylase *b* (94 000), bovine serum albumin (67 000), ovalbumin (43 000), carbonic anhydrase (30 000), soybean trypsin inhibitor (20 100) and α-lactalbumin (14 400). Crosslinked hemoglobin was from Sigma (St. Louis, MO, USA). The 10 000 polyethylene glycol (PEG), 100 000 and 1000 000 PEO polymers were obtained from Sigma and Aldrich (Milwaukee, WI, USA), respectively. Sodium dodecyl sulfate (SDS) stock solution was from Amres (Solon, OH, USA). Recombinant brain derived neurotrophic factor (BDNF), granulocyte stimulating factor (GCSF), erythropoetin (EPO) produced in *E. coli* or Chinese hamster ovary, platelet derived growth factor (PDGF-BB), consensus interferon (CON-IFN) are from Amgen.

2.3. Preparation of PEO or PEG polymer stock solutions

The PEO polymer stock solutions were prepared by dissolving the appropriate amount of polymer in 0.1% ethylene glycol containing distilled water. The aqueous polymer solutions were filtered through a 5.0-μm Acrodisc filter. The polymer content of the filtered solutions were determined by gravimetry.

2.4. Buffers

The separation buffers, which contained 100 m*M* Tris–2-(N-cyclohexylamino)ethanesulfonic acid (CHES) (pH 8.5), 0.1% SDS and PEO polymer at various concentrations were prepared by the combination of the 1.0 *M* Tris–CHES buffer (pH 8.5), 20% SDS and polymer stock solutions. All stock solutions were stored at 4°C when not in use.

2.5. Samples

The final sample buffer contained 0.06 *M* Tris–HCl, pH 6.6 with 5% 2-mercaptoethanol and 1% SDS. The samples were boiled for 5 min, then cooled on ice for 3 min, followed by centrifugation.

2.6. Capillaries

The separations were performed in 100 μm I.D. and 375 μm O.D. fused-silica capillaries from Polymicro Technologies (Phoenix, AZ, USA). Most of the work was done with capillaries of 20 cm effective and 27 cm total length. The capillaries were first washed with 1 *M* NaOH, HPLC-grade water, 1 *M* HCl and then conditioned with the separation buffer. Between runs the capillary was washed with 1 *M* HCl and water to remove surface adhered material.

2.7. Electrophoresis

For the evaluation of the separation characteristics of the PEO polymers the Pharmacia low-molecular-mass electrophoresis calibration kit proteins were used. The background buffer concentration, pH, as well as the SDS concentration were kept constant in all experiments, as described in the buffer and sample section above, no attempt was made to optimize the separations. The electrophoresis was performed in uncoated capillaries at 300 V/cm field strength. The samples were introduced by pressure injection and the duration of injection varied between 2 and 20 s according to the viscosity of the separation polymer network.

2.8. Calculations

The relative migration time (RMT) is calculated by dividing the migration time of the protein by the migration time of Orange G. The standard curve for molecular mass estimation is constructed by plotting the logarithm of the molecular mass as a function of 1/RMT. Linear regression provides the slope and intercept of the standard curve used for molecular mass estimation of unknown proteins. The Ferguson graphs are constructed by plotting the logarithm of 1/RMT of the individual proteins in different polymer solutions as a function of the polymer concentration. Linear regression provides the slope, which is the negative value of the retardation coefficient (K_r). The universal calibration curve is than drawn by plotting the logarithm of molecular mass as a function of the square root of K_r. Linear regression provides the slope and intercept for calculations used for the protein molecular mass estimation.

3. Results

3.1. Effect of polymer molecular mass on the separation of SDS–protein complexes

Solutions of high-molecular-mass PEO as a sieving network for capillary SDS electrophoresis has been used before in coated capillaries, but our preliminary experiments showed that they can be used in uncoated capillaries as well. Separation in uncoated capillaries is reproducible and the R.S.D. of migration times were less than 2% up to 15 to 20 consecutive runs. Separation in coated capillaries does not change the performance of the polymer network but increases the lifetime of the column. Consequently, for the following study PEO and PEG polymers were selected, which are commercially available in a wide range of molecular masses, have good UV characteristics and are soluble in the relevant buffers. The general formula for PEO and PEG is $-(O-CH_2-CH_2)_n-$. The difference is in the end groups and the length of the polymer, the shorter being PEG. For sake of simplicity, we choose to use the name PEO for both polymers.

The wide range of the available PEO polymers can be divided into three subgroups according to the polymer–protein molecular mass ratio using a median protein molecular mass (44 750). We selected one polymer from each group. In the first group the ratio was below one, for our 10 000 PEG it was 0.22. The ratio in the second group was 2.23 for the 100 000 PEO and in the third group the molecular mass ratio was 22.35 using the 1000 000 PEO.

Fig. 1A displays the electropherogram of standard proteins using a 3% (w/v) solution of the 10 000 PEG for their separation. The protein standards are poorly separated; both the resolution and efficiency are low. The two sharp peaks eluting prior to the proteins correspond to Orange G (larger) and its degradation product (smaller).

The second PEO (100 000) exhibited relatively good separation at the 1% concentration. The peaks are acceptable and distinguishable though the resolution is not satisfactory as shown in Fig. 1B.

The electropherogram using the 1000 000 PEO at 1% concentration is shown in Fig. 1C. All components of the standard mixture are baseline separated.

An improvement of the separation can be seen between the 100 000 and 1000 000 polymer network. The separation window, defined as the

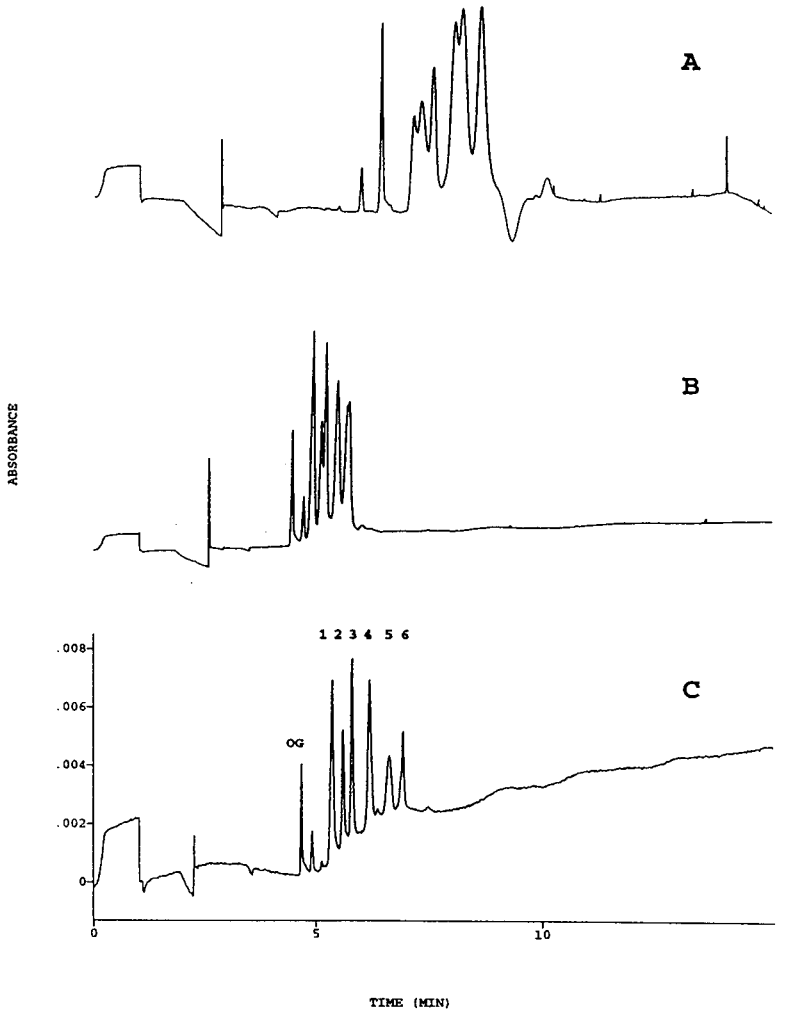

Fig. 1. SDS–PEO capillary polymer network electrophoresis of standard proteins using different molecular mass PEOs. (A) 10 000, (B) 100 000 and (C) 1000 000. The polymer concentration for A was 3% and 1% for B and C. The electrophoresis was performed in a 100-μm I.D. capillary. The effective and total length of the capillary was 20 and 27 cm, respectively. The proteins were separated at reversed polarity, at 300 V/cm field strength. The migration was followed at 214 nm. The sample was pressure injected. OG = Orange G; 1 = α-lactalbumin; 2 = soybean trypsin inhibitor; 3 = carbonic anhydrase; 4 = ovalbumin; 5 = bovine serum albumin; 6 = phosphorylase *b*.

difference between the migration time of the last and first protein peak, approximately doubles. Despite the good separation the increase in viscosity presents a practical filtration problem over 100 000 during the preparation of separation polymer networks. The 100 000 PEO polymer seems to be a reasonable compromise between performance and ease of preparation, thus we focused our further studies on its use for studying other parameters which might effect the separation.

3.2. Effect of polymer concentration on the separation

Fig. 2 displays the electropherograms of the protein standards using 2, 3, 4 and 5% solutions of 100 000 PEO. The most dramatic effect is the

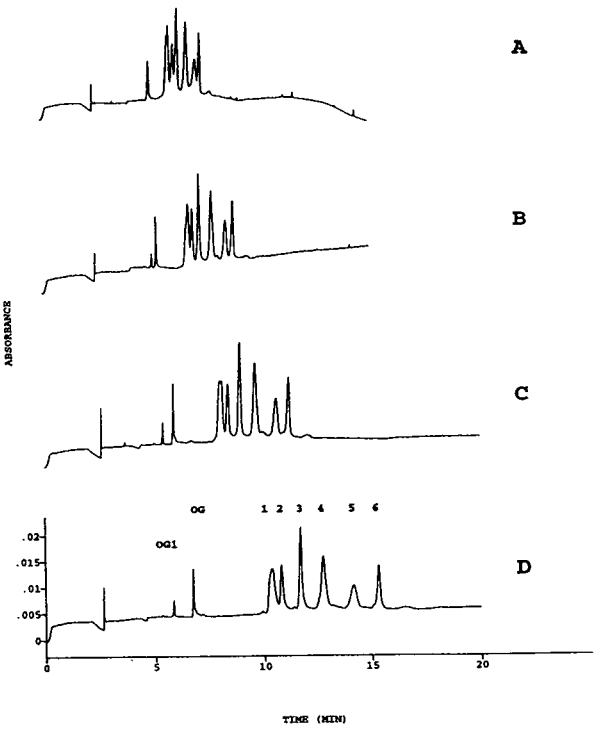

Fig. 2. The effect of polymer concentration on the SDS–PEO electrophoresis of proteins. The concentration of the 100 000 PEO polymer was (A) 2%, (B) 3%, (C) 4% and (D) 5%. For other conditions see Fig. 1.

apparent increase of the separation window and consequently the resolution of the samples. Below 1% the separation window was around 1.5 min (data not shown), which then increased to about 3 min at 3%. The separation window increases to about 6 min at 5% PEO concentration. It seems that the separation window increases exponentially with the concentration of the polymer network.

It should be mentioned that the peak efficiency for the protein peaks does not seems significantly change over the studied PEO concentration range. The efficiency is around 50 000 plates per meter, which is about one order of magnitude lower than expected, based on free solution data. In free zone electrophoresis the inclusion of polymers in the running buffer eliminates some of the diffusion related peak broadening. The lower efficiency is due to interactions between the PEO network [13,14], SDS [15,16] and the proteins. The SDS–protein–PEO system is complex with multiple equilibrium, the identification of all the factors involved in the peak broadening should be further investigated.

3.3. Protein molecular mass determinations

Theoretically, the free solution mobility of all SDS–protein complexes should be the same. Consequently, the migration of proteins in a sieving matrix should depend only on their hydrodynamic radius. The traditional method for molecular mass estimation is to use a standard curve constructed by plotting the migration times of standard proteins against their known molecular mass. Consequently, most errors in the molecular mass determination using the single standard curve method originate from discrepancies of the free solution mobility [17]. The usual source of error is the anomalous binding of SDS to the protein.

One way to avoid errors related to the single standard curve method is to measure the migration times at different polymer network concentrations, construct Ferguson plots and a universal calibration curve [18]. The use of relative migration times further improves the run-to-run reproducibility of the analysis. The Ferguson plot is the logarithm of the relative migrations plotted as a function of polymer concentration. The slope of the curve represents the retardation coefficient (K_r) while the intercept at zero polymer concentration corresponds to the free solution mobility of a protein. The logarithm of the molecular mass *vs.* the square root of the retardation coefficient of proteins provide a universal standard curve which then can be used for the estimation of the molecular mass of unknown proteins. The Ferguson analysis for traditional SDS-PAGE is extremely time consuming, especially because the analysis is recommended to be performed at at least six different gel concentrations [19]. Consequently this method of analysis is practically abandoned. The method, however, is in revival because the use of replaceable polymer networks makes the analysis more feasible again [20].

We prepared separation polymer networks

containing 2, 3, 4 and 5% PEO and analyzed the same protein mixture under otherwise identical conditions. Fig. 3A and B show the Ferguson plots for six proteins and the constructed universal standard curve. All regressions show acceptable linearity, the r^2 values are larger than 0.98. The intercepts are different and the intersection points located in the negative PEO concentration range. These anomalies could be the consequence of differences in free solution mobilities of the SDS–protein complexes (for example glycoproteins), sample preparation or any combination of the above. In an attempt to find the reason(s) behind this anomalous behavior, the following experiment was designed.

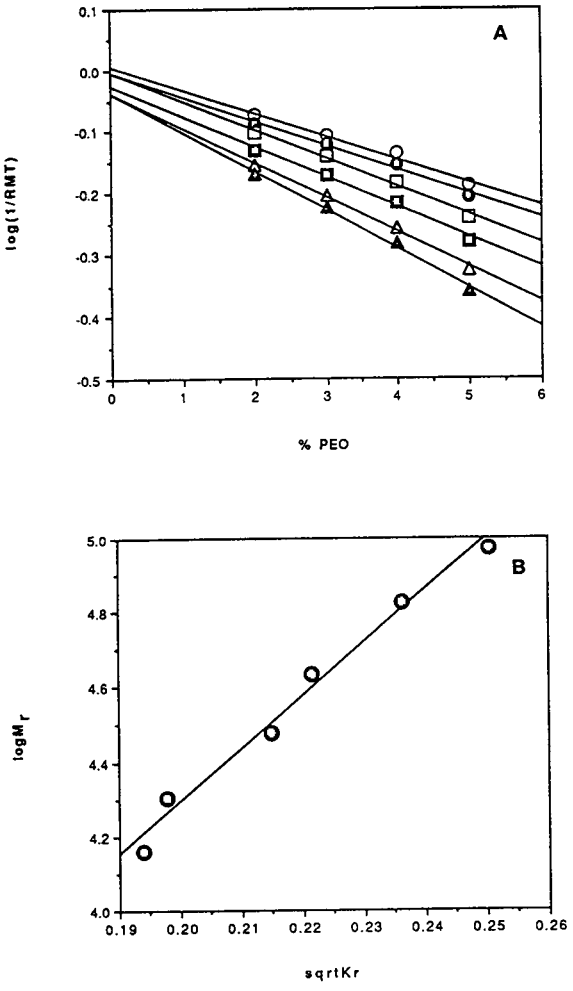

Fig. 3. (A) Ferguson plots of the standard proteins. ○ = α-lactalbumin; ● = soybean tripsin inhibitor; □ = carbonic anhydrase; ■ = ovalbumin; △ = bovine serum albumin; ▲ = phosphorylase *b*. (B) Universal calibration curve constructed based on the Ferguson plot.

It is assumed that polymeric protein samples containing the same subunits will behave similarly during sample preparation. The free solution mobility of these polymeric proteins should be the same or very similar. In order to check the performance of the SDS–PEO system, eliminating some of the sample related variances, cross-linked bovine hemoglobin's were selected. Such polymeric proteins are commercially available and contain monomers, dimers, trimers and tetramers. Fig. 4 displays their electropherograms at different PEO concentrations. The resolution again improves with increasing polymer network concentration. It is apparent that penta, hexa and heptamers are also present in the sample. The Ferguson plots of the hemoglobin "polymers" are displayed in Fig. 5. The linearity for each compound is excellent. The difference in the slopes proves that the separation is based on size differences between the molecular species. The intercepts at zero polymer network concentration are different, but the intersection points of the lines are in good agreement. Since we assumed that the model compounds have identical free solution mobility, the lines should intercept in close proximity to each other. Apparently SDS–PEO does not behave ideally, and the samples appear to interact with the PEO network. The electric field known to orient the molecules, can be a potential source for unusual migration behavior. Anomalous protein migration can be the source of major errors in the estimation of the molecular mass and the use of a universal calibration curve should eliminate some of these errors.

3.4. Molecular mass determination of recombinant proteins

The applicability of the SDS–PEO polymer network electrophoresis was further tested by estimating the molecular mass of recombinant proteins (BDNF, PDGF, CON-IFN, GCSF, EPO). Fig. 6 is the Ferguson plot constructed for

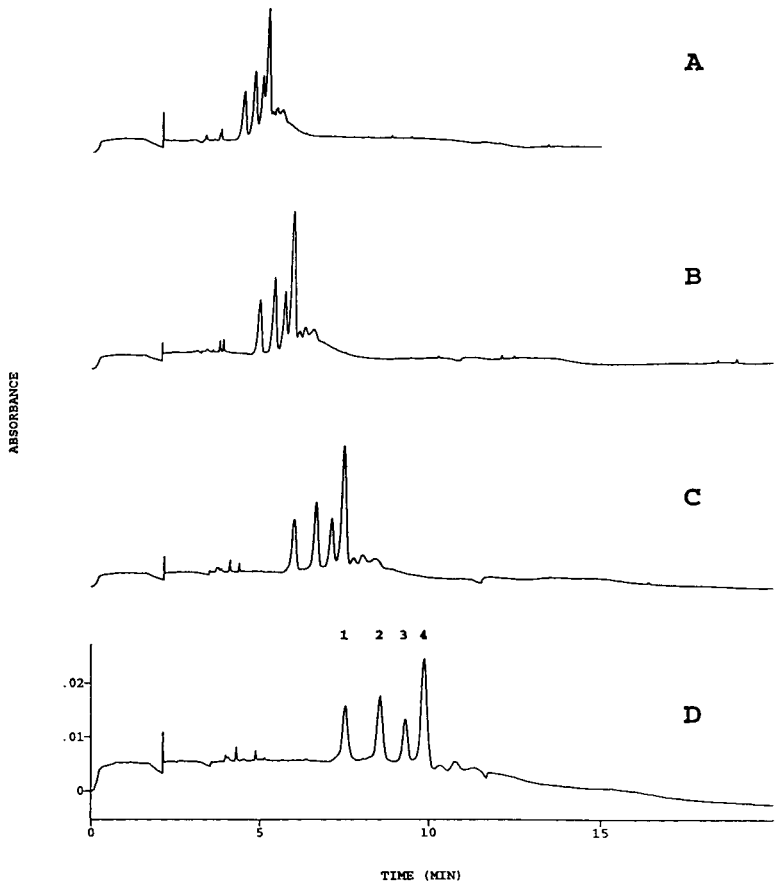

Fig. 4. Electropherograms of hemoglobin polymers using SDS–PEO electrophoresis. The concentration of the 100 000 PEO polymer was (A) 2%, (B) 3%, (C) 4% and (D) 5%. 1 = Monomer; 2 = dimer; 3 = trimer; and 4 = tetramer. All other conditions are as listed in Fig. 1.

some of the selected recombinant proteins. The mobility at zero polymer network concentration varies significantly, and the intersection points are also at different locations. Table 1 compiles the data about the samples with their calculated (literature) and estimated molecular mass using the Ferguson analysis. The single calibration curve method gave estimates with only a few percent difference as shown for the 3% polymer network in Table 1. With the exception of glycosylated EPO, PDGF and BDNF, the error of molecular mass estimation is reasonable.

The molecular mass of *E. coli* derived PDGF-BB is estimated as *ca.* 23 000, which is less than the dimeric molecular mass (26 780) of the native PDGF. PDGF contains two interchain disulfide bridges and it is possible that the general sample treatment used in this work is not appropriate to break the dimeric form of PDGF [21].

The glycosylated and non-glycosylated forms of r-Hu EPO gave two different molecular mass estimates. The *E. coli* derived EPO, which does not contain carbohydrate side moieties migrates as expected. The estimated molecular mass is around 20 000, which is higher than the calculated 18 000 molecular mass [22]. The glycosylated EPO, derived from CHO cells, has a molecular mass of about 30 000 and almost 40% of it is carbohydrate. Using the SDS–PEO

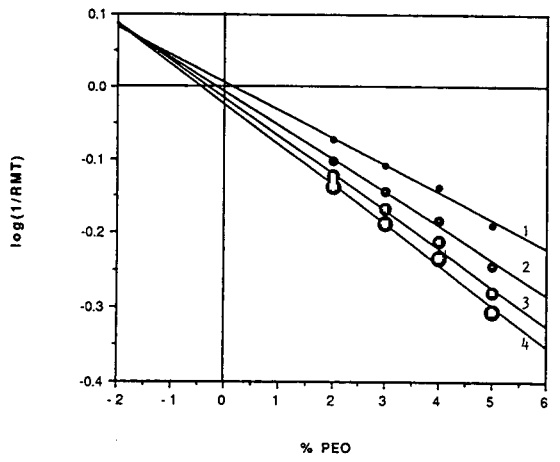

Fig. 5. Ferguson plots of hemoglobin polymers. 1 = Monomer; 2 = dimer; 3 = trimer; and 4 = tetramer.

polymer network electrophoresis system the molecular mass of EPO is estimated to be about 70 000. Glycosylated EPO migrates anomalously in size exclusion chromatography, giving an apparent molecular mass of 60 000 [23]. It was established that the anomalous migration is due to an unusually large viscosity radius caused by the glycosylation of EPO. However, in SDS-PAGE under reducing conditions, this anomaly was not observed. The phenomenon suggests that the mechanism of the migration in SDS–PEO polymer network electrophoresis is more similar to size exclusion chromatography than SDS-PAGE.

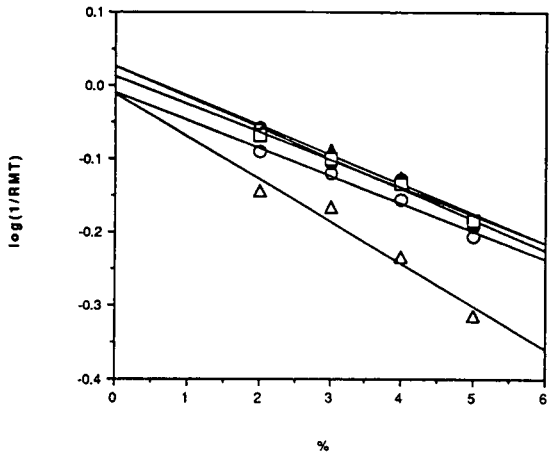

Fig. 6. Ferguson plots of recombinant proteins using SDS–PEO CE. ○ = BDNF; ● = PDGF; △ = EPO; ▲ = CON-IFN; □ = GCSF. The abbreviations can be found in the text. The analysis were performed using standard conditions, see Fig. 1.

4. Conclusions

Poly(ethylene oxides) based replaceable polymer networks are feasible alternatives for the SDS mediated separation of proteins. The separation in general improves with increasing PEO molecular mass and significant resolution improvement was observed with increasing polymer network concentrations. A 3% solution of a 100 000 PEO seems to be a reasonable compromise from a practical point of view. At higher concentrations and molecular mass the filtration of the polymer network stock solution is difficult and time consuming.

Protein molecular mass determination based on a single concentration determination, using log M_r *vs.* 1/relative migration time as a standard curve provides reasonable estimates in general. However the estimated molecular mass can sometimes be off by as much as 20–40%, depending upon the nature of the protein. For a better molecular mass estimation the Ferguson analysis is recommended. Due to the relatively easy preparation of the different concentration PEO solutions, this analysis is more feasible for replaceable polymer networks than for cross linked and immobilized sieving matrices.

Finally, the advantages of the SDS–PEO polymer network electrophoresis can be summarized as follows: uncoated fused-silica capillaries can be used; the polymers are UV transparent; the preparation of polymer stock solutions for SDS–PEO is relatively simple; the unbuffered polymer stock solutions are stable at 4°C for about a month. Separation parameters can be optimized rapidly since the pH, polymer concentration, buffer type, conductivity, viscosity are easy to vary. Optimized separations provide a fast method for molecular mass estimation. At this point the rapid detection of covalent dimers, trimers, etc. appears to be the most promising application

Table 1
Biochemical data and molecular mass estimation of recombinant proteins

	BDNF	PDGF	EPO[a]	EPO	CON-IFN	GCSF
M_r calculated	13 511	13 390	30 400	18 395	19 400	18 791
% Sugar	0	0	40	0	0	0
p*I*	~10.3	~10	4.2–4.6	~8.8	~5.5	~6.1
Native form	D[b]	D[c]	M[d]	M	M	M
M_r by Ferguson	16 978	23 105	75 457	23 934	20 671	17 225
M_r by 3% PEO	19 771	15 496	44 014	19 329	11 201	13 830

[a]Produced in Chinese hamster ovary.
[b]Non disulfide dimer.
[c]Disulfide dimer.
[d]Monomer.

for capillary electrophoresis using the SDS–PEO polymer network.

Acknowledgements

Special thanks are due to R. Rush for encouragement during the experiments and for his help in the preparation of the manuscript. Thanks are due to A. Guttman, W. Kenney and E. Watson for helpful suggestions and review of the manuscript.

References

[1] R.S. Rush, in J.W. Kelly and T.O. Baldwin (Editors), *Applications of Enzyme Biotechnology*, Plenum Press, New York, 1991, pp. 233–250.
[2] S. Hjerten, in H. Hirai (editor), *Electrophoresis'83*, Walter de Gruyter, New York, 1984, pp. 71–79.
[3] A.S. Cohen and B.L. Karger, *J. Chromatogr.*, 397 (1987) 409–417.
[4] K. Tsuji, *J. Chromatogr.*, 550 (1991) 823–830.
[5] A. Guttman, J.A. Nolan and N. Cooke, *J. Chromatogr.*, 632 (1993) 171–175.
[6] D.N. Heiger, A.S. Cohen and B.L. Karger, *J. Chromatogr.*, 516 (1990) 33–48.
[7] K. Ganzler, A.S. Cohen and B.L. Karger, presented at the *3rd International Conference on High-Performance Capillary Electrophoresis, San Diego, CA, 1991*, Poster No. 31.
[8] H.J. Bode, *FEBS Lett.*, 65 (1976) 56–58.
[9] A. Widhalm, C. Schwer, D. Blass and E. Kenndler, *J. Chromatogr.*, 546 (1991) 446–451.
[10] K. Ganzler, K.S. Greve, A.S. Cohen, B.L. Karger, A. Guttman and N.C. Cooke, *Anal. Chem.*, 64 (1992) 2665–2671.
[11] A. Guttman, J. Nolan, P. Shieh and N. Cooke, *Am. Biotech. Lab.*, 11 (1993) 36.
[12] A. Guttman, J. Horváth and N. Cooke, *Anal. Chem.*, 65 (1993) 199–203.
[13] A. Maconnachie, P. Vasudevan and G. Allen, *Polymers*, 19 (1978) 33–36.
[14] R.B. Bird, R.C. Armstrong, O. Hassager and C.F. Curtiss, *Dynamics of Polymeric Liquids*, Wiley, New York, 1977.
[15] J.A. Reynolds and C. Tanford, *Proc. Natl. Acad. Sci. U.S.A.*, 66 (1970) 1002–1007.
[16] J A. Reynolds and C. Tanford, *J. Biol. Chem.*, 245 (1970) 5161–5165.
[17] D. Rodbard and A. Crambach., *Proc. Natl. Acad Sci. U.S.A.*, 65 (1970) 970–977.
[18] K.A. Ferguson, *Metabolism*, 13 (1964) 985–1002.
[19] D. Rodbard and A. Crambach, *Anal. Biochem.*, 40 (1971) 95.
[20] W.E. Werner, D.M. Demorest and J.E. Wiktorowicz, *Electrophoresis*, 14 (1993) 759.
[21] S.J. Prestrelski, T. Arakawa, W.C. Kenney and D.M. Byler, *Arch. Biochem. Biophys.*, 285 (1991) 111.
[22] J.M. Davis, T. Arakawa, T.W. Strickland and D.A. Yphantis, *Biochemistry*, 26 (1987) 2633.
[23] L.O. Narhi, T. Arakawa, K.H. Aoki, R. Elmore, M.F. Rohde, T. Boone and T.W. Strickland, *J. Biol. Chem.*, 266 (1991) 23022.

ELSEVIER

Journal of Chromatography A, 676 (1994) 219–226

JOURNAL OF CHROMATOGRAPHY A

Capillary sodium dodecyl sulfate gel electrophoresis of proteins I. Reproducibility and stability

Paul C.H. Shieh*, Dao Hoang, Andras Guttman, Nelson Cooke

Beckman Instruments Inc., 2500 Harbor Blvd., Fullerton, CA 92634, USA

Abstract

This paper investigates the use of a non-cross-linked polymer gel as a separation matrix for sodium dodecyl sulfate (SDS) capillary gel electrophoresis of proteins. The method employs a polyacrylamide coated capillary filled with a polyethylene oxide–gel buffer solution. A standard seven-protein mixture was chosen for the evaluation of coating stability and reproducibility. It was found that the coating is stable for more than 400 runs with a 1 *M* HCl wash between each run. The hydrophilic nature of polyethylene oxide also allows high resolution and high efficiency for all protein peaks. The linear plot of log M_r vs. mobility demonstrates a pure sieving mechanism of polyethylene oxide matrices. The molecular masses of twenty-nine standard proteins determined by SDS capillary gel electrophoresis are in good agreement with those obtained from the SDS polyacrylamide gel electrophoresis (PAGE) slab gel method. The capability to replace the gel after each run allows improved run-to-run and batch-to-batch reproducibility. The relative standard deviation (R.S.D.) in migration time of 19 injections of the seven-protein standard mixture, with the 190 injections of crude fetal calf serum in between, falls in the range of 0.351 to 0.453%. The application of this technique for the separation of proteins in chicken egg white and bovine milk is demonstrated.

1. Introduction

Sodium dodecyl sulfate–polyacrylamide slab gel electrophoresis (SDS-PAGE) has been a well established analytical method for the separation and characterization of proteins [1,2]. The technique has proved useful for the estimation of protein molecular mass, purity assessment, and the structure of subunits. Although the method is widely used for these applications, it can be time consuming and difficult to quantitate and automate. Capillary gel electrophoresis (CGE) [3–6], a recently developed technique, offers an alternative approach to gel electrophoresis with the advantages of fast separation, quantitative analysis, on column detection, and automation.

Both cross-linked and non-cross-linked polyacrylamide gels have been used for the SDS-PAGE separation of proteins in slab gels [7,8]. These matrices can also be used in CGE. Hjerten was the first to show SDS-PAGE separation of membrane proteins by a polyacrylamide gel filled capillary [9]. Cohen and Karger provided a detailed description of SDS protein and peptide separations by cross-linked and non-cross-linked polyacrylamide gels [3]. Tsuji also reported the

* Corresponding author.

0021-9673/94/$07.00
SSDI 0021-9673(94)00468-O

separation and quantitation of recombinant proteins by a similar method [10]. These fixed polyacrylamide gel capillaries, however, have several limitations. One problem is poor detection at low UV wavelengths due to the strong absorption of the polyacrylamide polymer. Higher wavelengths can be used, but with a lower detection limit. A second limitation is that the gel in the capillary can be easily contaminated or damaged by sample matrix if it is not replaceable, limiting the number of useful runs.

Recently, Ganzler *et al.* reported SDS separation of proteins using a UV transparent, replaceable, non-cross-linked polymer as the sieving matrix [11]. Guttman *et al.* also reported the separation of proteins in the molecular mass range of 29–205 kDa using a replaceable linear polymer matrix [12,13]. The use of these polymer networks as a sieving matrix offers several advantages compared to fixed gel SDS-PAGE capillary electrophoresis. First, the replaceable gel offers longer life time of the gel capillary compared to SDS-PAGE capillary electrophoresis. Secondly, the polymers employed have no absorption in the low UV range, and hence provide the possibility to detect proteins at wavelengths which allow higher sensitivity than the standard 280 nm wavelength. Thirdly, the capability of replacing gel after each run prevents sample carry over from previous runs, allowing better quantitation.

This paper evaluates the use of polyethylene oxide and polyethylene glycol mixtures as the sieving matrix for protein separations by SDS capillary electrophoresis in the molecular mass range of 14–205 kDa. A hydrophilic coating was applied on the capillary wall to reduce non-specific adsorption on the capillary surface and to minimize electroosmotic flow. The polymer network has low viscosity and is UV transparent at 214 nm. Protein molecular mass determinations by this method are similar to the results obtained from SDS-PAGE slab gels. A standard seven-protein mixture was used to evaluate the performance of the capillary. Results are presented regarding capillary stability, reproducibility and protein molecular mass determinations. Finally, separations of proteins in chicken egg white and bovine milk are presented to demonstrate the general applicability of the method.

2. Experiment

2.1. Instrumentation

Capillary gel electrophoresis was performed on a P/ACE 2200 (Beckman Instruments, Fullerton, CA, USA) with cathode at the injection end and anode at the detector end. The eCAP SDS 14-200 kit with coated capillary (100 μm I.D., 27 cm total length, 20 cm to detector) and replaceable polymer–buffer (Beckman Instruments) were used for all SDS capillary electrophoresis studies. The temperature of gel filled capillary was controlled to $+/-0.1$°C by a liquid cooling cartridge system of the P/ACE instrument. The analysis was monitored at 214 nm and the data was analyzed by System Gold software (Beckman Instruments) with IBM personal computer.

2.2. Materials

The replaceable polymer, a mixture of polyethylene glycol and polyethylene oxide was obtained from the eCAP SDS 14-200 kit (Beckman Instruments). The molecular mass standard mixture, containing α-lactalbumin (bovine milk), carbonic anhydrase (bovine erythrocytes), ovalbumin (chicken egg white), albumin (bovine serum), phosphorylase *b* (rabbit muscle), β-galactosidase (*Escherichia coli*), and myosin (rabbit muscle), is also supplied with the kit. All other protein standards and 2-mercaptoethanol were purchased from Sigma (St Louis, MO, USA). Chicken egg and bovine milk were purchased from local grocery store.

2.3. Protein sample preparation

Protein standard mixture

One vial of protein standard mixture (3.4 mg/vial) was dissolved in 750 μl of sample buffer and 750 μl of doubly deionized (DDI) water. A volume of 200 μl of protein solution was transferred to a polypropylene vial. A volume of 5 μl

of 2-mercaptoethanol and 10 μl of 1% orange G were added to the vial and mixed for 10 s. The final mixture was boiled for 5 min and then cooled in an ice bath. The sample was stored in a freezer prior to the injection.

Proteins of interest

A volume of 2 ml of chicken egg white or bovine milk was diluted with DDI water in 1:1 ratio and filtered through a 0.4-μm filter. A volume of 100 μl of filtrate was transferred to a polypropylene vial and 85 μl of sample buffer, 5 μl of 2-mercaptoethanol and 10 μl of 1% orange G were added to the vial. The final mixture was boiled for 5 min and cooled in an ice bath before CGE analysis.

2.4. HPCE methods

CGE was performed under the following conditions. Prior to the run, the capillary was rinsed with 1 *M* HCl solution for 1 min followed by eCAP SDS 14-200 gel/buffer for 3 mins. The samples were injected by pressure [0.5 p.s.i. (3447.38 Pa) for 30 s] into the capillary. The separation was carried out at 300 V/cm (8.1 kV for 27 cm capillary) and 20°C. Since the protein SDS complexes were negatively charged, reversed polarity was used for all separations.

3. Results and discussion

3.1. Linearity study

In SDS capillary electrophoresis, the protein molecule is fully denatured by boiling in excess amount of SDS and thiol reducing agent such as 2-mercaptoethanol. After denaturation, the protein S–S bond was reduced and the three dimensional structure is extended to a rod shape. The SDS in the sample buffer binds to the proteins, regardless of protein size or shape, in a 1:1.4 ratio. The charge per unit mass of the protein–SDS complex can be assumed constant since all the charge on protein was masked by SDS. As the mobility of each complex in electrophoresis is practically identical, assuming no other interaction between proteins and the polymer network, the separation is based only on the sieving mechanism. Fig. 1 demonstrates the separation of the seven-standard protein mixture (M_r 14 200–205 000 daltons) by SDS capillary electrophoresis in less than 15 min. The separation was found to be similar to those on the cross-linked and non-cross-linked polyacrylamide gel. Fig. 2 shows the linear plot of logarithm of molecular weight and mobility in capillary gel electrophoresis. The mobility was found to be proportional to the logarithm of molecular mass of proteins. The high degree of linearity of the plot ($r = 0.99$) suggests a pure sieving mechanism of the polymer matrix. This fact was also supported by a Ferguson analysis study [14]. The calibration curve obtained in this way can be used for protein molecular mass estimation of unknown samples. Table 1 compares the molecular mass estimation of 32 standard proteins by SDS capillary and slab gel electrophoresis. From the results, both methods are in good agreement for most proteins.

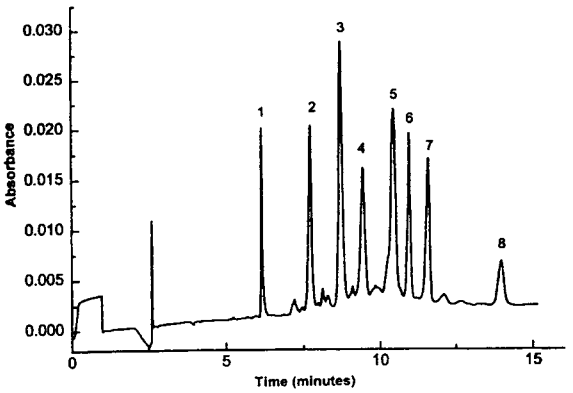

Fig. 1. Separation of seven SDS–protein complexes by the eCAP SDS 14-200 kit. Conditions: see Experimental section. Solutes: 1 = orange G, reference marker; 2 = α-lactalbumin; 3 = carbonic anhydrase; 4 = ovalbumin; 5 = bovine serum albumin; 6 = phosphorylase *b*; 7 = β-galactosidase; 8 = myosin.

3.2. Stability study

Most fixed, gel filled capillaries have a limited life time due to bubble formation or sample contamination inside the capillary. Since the

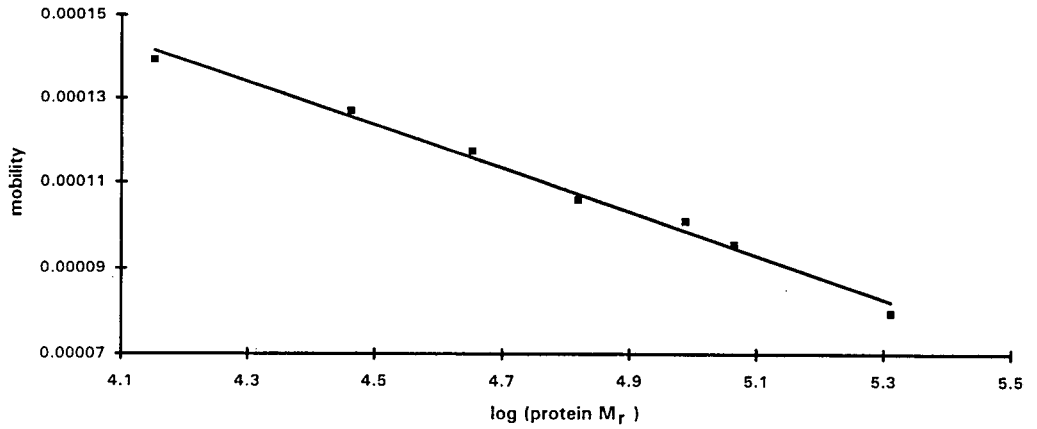

Fig. 2. Linearity plot of logarithm of protein molecular mass vs. mobility.

Table 1
Protein molecular mass estimation by slab gel SDS-PAGE and SDS capillary electrophoresis

Proteins	CGE	Slab gel SDS-PAGE
α-Lactalbumin	14 251	14 200
Lysozyme	14 313	14 300
Myoglobin	17 231	18 800
β-Lactoglobulin	18 464	18 000
Monoamine oxidase	65 121	60 000
Alcohol dehydrogenase	41 932	41 000
Glyceral phosphate dehydrogenase	36 135	35 700
Enolase	50 333	42 000
α-Amylase	58 866	50 000
Carbonic anhydrase	29 960	29 000
Ovalbumin	43 264	45 000
Bovine serum albumin	66 004	66 000
Fumarase	44 302	49 000
Luciferase	42 854	42 000
Hexokinase	51 786	51 000
Catalase	56 614	60 000
Soybean tripsin inhibitor	21 267	20 100
Cytochrome oxidase	191 925	200 000
Urease	92 420	83 000
Phosphorylase *b*	98 970	97 400
Puruvate carboxylase	134 902	130 000
L-Amino acid oxidase	70 019	70 000
β-Galactosidase	126 000	116 000
L-Lactic dehydrogenase	32 683	36 500
Asparagenase	40 460	37 000
Triosephosphate isomerse	27 306	26 600
α-Macroglobulin	188 853	180 000
Transkatolase	74 468	70 000
Heptoglobin	84 233	85 000

matrix can not be replaced, a new capillary is required when performance deteriorates. In this paper, a low viscosity polymer solution and a hydrophilic polymer coated capillary were used for SDS–protein separations. Since the polymer solution can be replaced after each run, a fresh matrix is used for every analysis. The hydrophilic polymer coating also prevents sample interaction with the capillary surface. If the capillary coating is not stable, a charge from the capillary wall or coating may be exposed, which can lead to band broadening due to sample adsorption or the generation of electroosmotic flow. Fig. 3 illustrates the separations of the seven-protein standards after the 1st, 200th and 400th injections, respectively. After 400 runs, good peak shape and constant migration time are still observed. These results demonstrate that the capillary can be used for more than 400 injections without any noticeable degradation. The capability of replacing gel after each run combined with the stable coating used in this study significantly increases overall capillary stability.

3.3. *Reproducibility study*

A critical consideration of capillary gel electrophoresis is the reproducibility of sample migration time. Several factors, such as temperature control, coating stability, and protein adsorption affect this performance. Using the P/ACE capillary electrophoresis system, the temperature of the gel filled capillary was controlled to +/− 0.1°C by the liquid cooling system. The neutral coating also reduces any interaction between proteins and capillary surface. In our experiments, we tested the reproducibility of the capillary with protein standard mixture, and with the injection of fetal calf serum sample between runs. The crude fetal calf serum contains large amounts of protein including albumins and immunoglobulins. The serum sample was diluted with DDI water (1:1 ratio) and pretreated with the standard denaturation procedure. Table 2 shows the R.S.D., range from 0.351 to 0.453%, of uncorrelated migration times for the first and last few runs of standard proteins. The highly reproducible results may be attributed to the

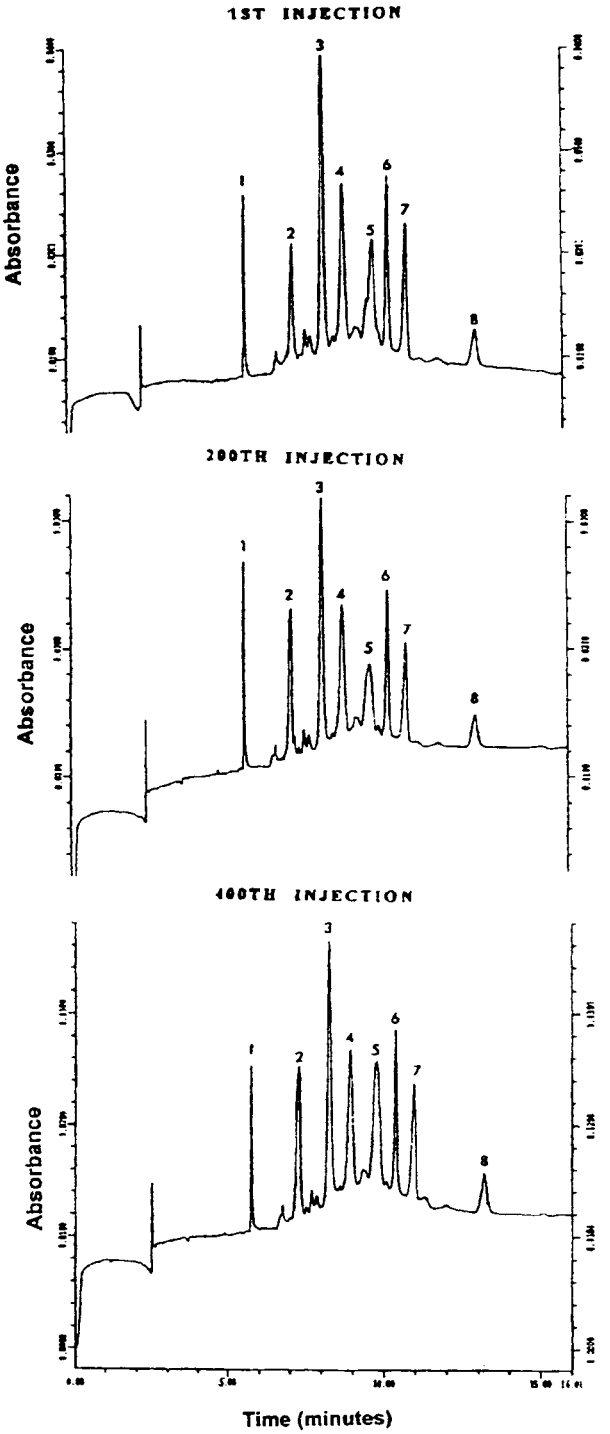

Fig. 3. Stability study of the eCAP SDS 14-200 kit. Conditions: see Experimental section. From top to bottom, 1st injection, 200th injection, and 400th injection, respectively.

Table 2
SDS 14-200 reproducibility study

Run[a]	OG	α-LAC	CA	OVA	BSA	PHOS	β-GAL	MYO
1st	5.94	7.50	8.44	9.15	10.12	10.60	11.19	13.40
2nd	5.94	7.50	8.43	9.14	10.12	10.59	11.18	13.40
3rd	5.93	7.49	8.42	9.13	10.10	10.58	11.17	13.38
4th	5.90	7.44	8.38	9.07	10.05	10.53	11.12	13.32
5th	5.90	7.45	8.39	9.08	10.04	10.53	11.12	13.31
6th	5.93	7.47	8.42	9.11	10.07	10.55	11.14	13.34
7th	5.94	7.50	8.45	9.16	10.14	10.61	11.21	13.43
8th	5.89	7.43	8.38	9.08	10.04	10.52	11.11	13.31
9th	5.88	7.42	8.36	9.06	10.01	10.50	11.09	13.29
191st	5.93	7.45	8.44	9.08	10.08	10.58	11.20	13.45
194th	5.90	7.44	8.42	9.07	10.06	10.57	11.18	13.43
195th	5.90	7.44	8.40	9.06	10.04	10.56	11.15	13.41
199th	5.88	7.45	8.40	9.08	10.05	10.56	11.16	13.42
200th	5.87	7.43	8.39	9.06	10.03	10.55	11.15	13.41
Av.	5.90	7.46	8.41	9.09	10.06	10.56	11.15	13.39
S.D.	0.024	0.030	0.030	0.041	0.042	0.038	0.043	0.061
R.S.D. (%)	0.400	0.398	0.351	0.448	0.413	0.358	0.388	0.453

[a] Injections 1–9: protein standard; Injections 10–190: fetal calf serum; Injections 191–200; protein standard.

good temperature control, stable coating, HCl wash and replaceable gel.

Another important issue of capillary gel electrophoresis is the batch-to-batch reproducibility of gel capillaries. For replaceable polymer solutions, the chain length of polymer and viscosity of solution can be significantly increased. Tables 3 and 4 show the reproducibility study of three different batches of gel buffers and capillaries. R.S.D. values range from 0.59 to 1.12%.

3.4. Applications

Fig. 4 shows the separation of commercial low fat milk by SDS capillary electrophoresis. Proteins can be identified by their molecular mass estimated from the migration of the standard proteins. High speed separation and good resolution were obtained from the analysis. Fig. 5 illustrates the SDS-protein separation of chicken egg white. Proteins such as lysozyme, ovalbumin, conalbumin are baseline separated in less than 15 min. In comparison to native protein separation with uncoated silica capillary, the SDS capillary electrophoresis offers much higher peak efficiency and resolution [15].

4. Conclusions

Fast separations of SDS–protein complexes have been demonstrated on a UV transparent polymer network matrix. The straight-line plot of log protein molecular mass vs. mobility demonstrates the pure sieving mechanism during the separation. The column can be used for more than 400 sample injections without loss in performance when employing a HCl wash in between runs. Migration time reproducibility in different runs and batches are in general less than 1% R.S.D. The method provides fast analysis of protein mixtures on the basis of the difference in protein molecular masses. Real samples without sample pre-treatment may be directly analyzed by this method. As a final note, evaluation of proteins higher than 205 000 daltons subjected to further investigation.

Table 3
SDS 14-200 gel buffer lot-to-lot reproducibility

Buffer	OG	α-LAC	CA	OVA	BSA	PHOS	β-GAL	MYO
Lot No. 1								
Inj. 1	6.45	8.08	9.11	9.83	10.89	11.42	12.07	14.48
Inj. 2	6.43	8.05	9.08	9.80	10.87	11.39	12.03	14.42
Inj. 3	6.43	8.06	9.08	9.80	10.88	11.40	12.03	14.45
Inj. 4	6.42	8.05	9.08	9.80	10.87	11.40	12.03	14.44
Inj. 5	6.42	8.04	9.07	9.80	10.86	11.39	12.02	14.42
Lot No. 2								
Inj. 1	6.32	8.25	9.22	9.98	11.92	11.56	12.17	14.46
Inj. 2	6.30	8.28	9.18	9.96	11.00	11.54	12.13	14.44
Inj. 3	6.29	8.26	9.19	9.96	11.02	11.54	12.14	14.45
Inj. 4	6.29	8.25	9.20	9.96	11.02	11.55	12.16	14.47
Inj. 5	6.30	8.25	9.21	9.96	11.00	11.56	12.17	14.47
Lot No. 3								
Inj. 1	6.43	8.24	9.28	9.98	11.03	11.57	12.20	14.55
Inj. 2	6.42	8.22	9.26	9.96	11.00	11.54	12.16	14.51
Inj. 3	6.42	8.22	9.25	9.96	10.99	11.53	12.14	14.50
Inj. 4	6.41	8.21	9.25	9.94	10.98	11.52	12.14	14.48
Inj. 5	6.41	8.21	9.24	9.94	10.97	11.52	12.14	14.49
R.S.D. (%)	0.96	1.12	0.82	0.77	0.59	0.62	0.51	0.24

Table 4
SDS 14-200 capillary lot-to-lot reproducibility

Buffer	OG	α-LAC	CA	OVA	BSA	PHOS	β-GAL	MYO
Lot No. 1								
Inj. 1	6.13	7.68	8.75	9.41	10.27	10.91	11.53	13.83
Inj. 2	6.13	7.67	8.72	9.40	10.28	10.91	11.52	13.82
Inj. 3	6.12	7.68	8.70	9.39	10.28	10.89	11.50	13.79
Inj. 4	6.12	7.68	8.70	9.38	10.28	10.87	11.47	13.76
Lot No. 2								
Inj. 1	6.23	7.82	8.87	9.54	10.57	11.09	11.73	14.06
Inj. 2	6.22	7.84	8.85	9.52	10.54	11.06	11.69	14.00
Inj. 3	6.22	7.84	8.84	9.51	10.53	11.05	11.67	13.99
Inj. 4	6.21	7.83	8.83	9.50	10.51	11.04	11.66	13.98
Lot No. 3								
Inj. 1	6.12	7.71	8.68	9.37	10.35	10.87	11.46	13.73
Inj. 2	6.09	7.69	8.65	9.36	10.35	10.88	11.48	13.81
Inj. 3	6.09	7.70	8.66	9.37	10.36	10.90	11.51	13.86
Inj. 4	6.10	7.71	8.68	9.38	10.37	10.92	11.53	13.88
R.S.D. (%)	0.89	0.92	0.93	0.73	1.10	0.77	0.83	0.77

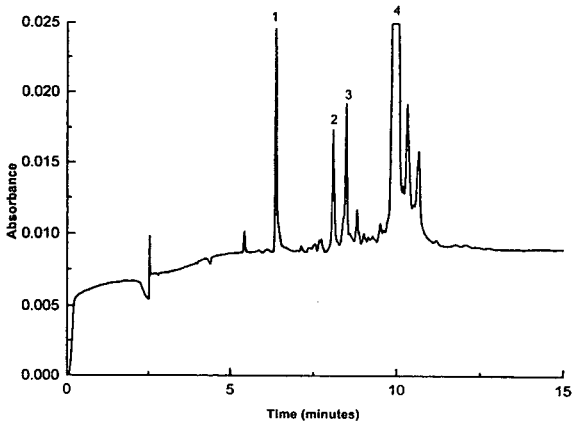

Fig. 4. SDS–protein separation of bovine milk. Conditions: see Experimental section. Solutes: 1 = orange G, reference marker; 2 = α-lactalbumin (M_r 14 200); 3 = β-lactoglobulin (M_r 18 000); 4 = casein.

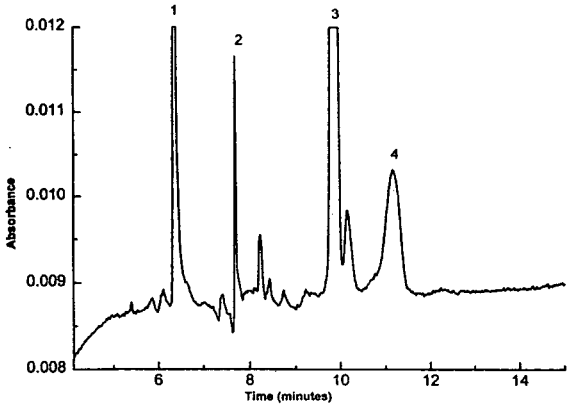

Fig. 5. SDS–protein separation of egg white. Conditions: see Experimental section. Solutes: 1 = orange G, reference marker; 2 = lysozyme (M_r 14 300); 3 = ovalbumin (M_r 45 000); 4 = conalbumin (M_r 77 000).

References

[1] K. Weber and M. Osborn, *J. Biol. Chem.*, 244 (1969) 4406.
[2] D.B. de Wald, L.D. Adams and J.D. Pearson, *Anal. Biochem.*, 154 (1986) 502.
[3] A.S. Cohen and B.L. Karger, *J. Chromatogr.*, 397 (1987) 409.
[4] A. Widhalm, C. Schwer, D. Blass and E. Kenndler, *J. Chromatogr.*, 546 (1991) 446.
[5] A. Guttman, A.S. Cohen, D.H. Heiger and B.L. Karger, *Anal. Chem.*, 62 (1990) 137.
[6] D. Wu and F.E. Regnieer, *J. Chromatogr.*, 608 (1992) 349.
[7] T.S. Work, *J. Mol. Biol.*, 10 (1964) 544.
[8] A.H. Gordon and L.N. Louis, *Anal. Biochem.*, 21 (1967) 190.
[9] S. Hjerten, in H. Hirai (Editor), *Electrophoresis' 83*, Walter de Gruyter, New York, 1984, pp. 71–79.
[10] K. Tsuji, *J. Chromatogr.*, 550 (1991) 823.
[11] K. Ganzler, K.S. Grene, A.S. Cohen, B.L. Karger, A. Guttman and N. Cooke, *Anal. Chem.*, 64 (1992) 2665.
[12] A. Guttman, J. Nolan and N. Cooke, *J. Chromatogr.*, 632 (1993) 171.
[13] A. Guttman, J. Horvath and N. Cooke, *Anal. Chem.*, 65 (1993) 199.
[14] A. Guttman, P. Shieh, J. Lindal and N. Cooke, *J. Chromatogr. A*, 676 (1994) 227.
[15] J.D. Mcculloch, *J. Liq. Chromatogr.*, 16 (1993), 2025.

ELSEVIER

Journal of Chromatography A, 676 (1994) 227–231

JOURNAL OF CHROMATOGRAPHY A

Capillary sodium dodecyl sulfate gel electrophoresis of proteins II. On the Ferguson method in polyethylene oxide gels

Andras Guttman*, Paul Shieh, John Lindahl, Nelson Cooke

Beckman Instruments, Inc., 2500 Harbor Boulevard, Fullerton, CA 92634, USA

Abstract

Capillary sodium dodecyl sulfate (SDS) gel electrophoresis is demonstrated to be a powerful new analytical method for the separation of protein molecules based on their molecular mass. Standard curves of logarithm molecular mass *versus* reciprocal relative migration time give the estimated molecular mass of sample proteins within the acceptable 10% error for most proteins. Larger errors are possible, however, when special groups such as carbohydrates (glycoproteins) or lipids (lipoproteins) are present due to a different ratio of binding SDS molecules. An automated Ferguson method is shown that corrects for this non-ideal behavior in capillary SDS–polyethylene oxide gel electrophoresis.

1. Introduction

Capillary gel electrophoresis (CGE) containing sodium dodecyl sulfate (SDS) as an ionic detergent is a newly established separation tool for the size separation and purity assessment of protein molecules using cross-linked [1] and linear polyacrylamide [2–6], dextran [4] and polyethylene oxide [7,8] gels. Classical SDS gel electrophoresis of proteins [9–11] is based on the phenomenon that most proteins bind SDS in a constant mass ratio of 1:1.4 [12,13], thus different size protein–SDS complexes having similar mass-to-charge ratios can be separated by means of a sieving matrix via electrophoresis. However, some types of proteins having specific side groups, such as carbohydrates (glycoproteins), lipids (lipoproteins) or other prostetic groups may bind SDS differently [14]. The irregular binding of SDS causes a different charge-to-mass ratio for these molecules resulting in inaccurate estimates in the apparent molecular mass [13,14]. The so called Ferguson method [15] can be used to help correct for this non-ideal behavior. Ferguson plots are constructed by plotting the logarithm of reciprocal migration time of the individual proteins as a function of different gel concentrations. Linear regression provides slopes which are the negative of the retardation coefficients (K_R). In this way a more universal calibration curve can be drawn by simply plotting the logarithms of molecular masses as a function of the retardation coefficients. In fact, K_R is proportional to the effective molecular surface area (or to the radius of a spherical molecule with the same surface area) and not directly upon on molecular mass [14]. Chrambach [13] showed that a linear relationship is obtained when $K_R^{1/2}$ is plotted against the molecular radius for spherical molecules in slab polyacrylamide

* Corresponding author.

0021-9673/94/$07.00
SSDI 0021-9673(94)00311-V

gel electrophoresis (PAGE). In capillary polyacrylamide gel electrophoresis, Werner *et al.* [16] attained a similar logarithm molecular mass *vs.* $K_R^{1/2}$ relationship.

Before the advent of SDS CGE the Ferguson method was extremely time consuming and labor intensive, due to the requirement of making different gel concentrations in slab format and the evaluation of the separated bands by regular staining/destaining procedures [7]. Here we describe a rapid automated Ferguson analysis method for protein molecular mass determination using a computer-controlled separation system.

Our data clearly show that the use of the automated Ferguson method in conjunction with capillary polyethylene oxide gel electrophoresis gives a more precise molecular mass estimate for those proteins with different SDS-binding levels.

2. Materials and methods

2.1. Apparatus

In the capillary electrophoresis studies, the P/ACE system 2100 capillary electrophoresis apparatus (Beckman Instruments, Fullerton, CA, USA) was used in reversed-polarity mode (cathode on the injection side). The separations were monitored on-column at 214 nm. The temperature of the gel-filled capillary columns was controlled at 20°C by the liquid cooling system of the P/ACE instrument. The electropherograms were acquired and stored on an Everex 386/33 computer. Molecular masses of the protein samples were estimated by using the molecular mass determination option of the System Gold software package (Beckman).

2.2. Procedures

In all the capillary electrophoresis experiments the eCAP SDS 14-200 (Beckman) capillary electrophoresis size separation kit for SDS proteins was used. The 27 cm long (20 cm to the detector) and 0.1 mm I.D. coated eCAP SDS 14-200 fused-silica capillary column (Beckman) was washed with 1 *M* HCl after each run. The appropriately pretreated samples were injected by pressure (typically: 30–60 s, 0.5 p.s.i.; 1 p.s.i. = 6894.76 Pa) into the replaceable polyethylene oxide gel-filled capillary column.

To perform the Ferguson experiments the test mix and the sample proteins were run on a 20 cm effective length eCAP SDS 14-200 capillary column using various concentrations of the eCAP SDS 14-200 gel buffer at a constant field strength of 300 V/cm. The gel buffer is used in concentration received as well as diluted to 75, 67 and 50% with a dilution buffer [17].

2.3. Chemicals

The SDS protein molecular mass test mixture (M_r 14 200–205 000) and all the other proteins were purchased from Sigma (St. Louis, MO, USA). Before injection, the samples were diluted to 0.2–2 mg/ml with the eCAP SDS 14-200 sample buffer (final concentration: 60 m*M* Tris–HCl, 1% SDS, pH 6.6) and were boiled in a water bath for 5 min after adding 2.5% β-mercaptoethanol as reducing agent and 0.005% orange-G as internal standard. The samples were stored at −20°C or freshly used. All buffer and gel solutions were filtered through a 1.2-μm pore size filter (Schleicher & Schuell, Keene, NH, USA) and carefully vacuum degassed at 100 mbar.

3. Results and discussion

In SDS CGE for protein molecular mass determination, the sieving matrix used was a low-viscosity gel formulation of polyethylene oxide which is not bound to the inside surface of a coated capillary. This permits replacement of the gel buffer system in the coated capillary column by means of the pressure rinse operation mode of the electrophoresis apparatus (*i.e.*, replaceable gel). It is important to note that a coated capillary column should be used in these experiments to eliminate the electroosmotic flow and minimize non-specific adsorption of protein on the inner surface of the capillary [18].

Fig. 1 shows the separation of the standard protein test mixture of α-lactalbumin, carbonic anhydrase, ovalbumin, bovine serum albumin, phosphorylase *b*, β-galactosidase and myosin as well as the tracking dye of orange-G by SDS CGE. The standard curve for molecular mass estimation was constructed by plotting the logarithms of the molecular masses as a function of the electrophoretic mobility (inset in Fig. 1). While these standards show a linear relationship, there are some proteins that behave differently and do not fall on the standard regression line. This unusual behavior can be attributed to special groups on the polypeptide chain such as carbohydrates side chains (glycosylations) or lipids (lipoproteins). These groups do not bind SDS in the usual manner resulting in a change in the charge-to-mass ratio of the SDS–protein complex. This in turn causes an increase or decrease in the migration time in CGE and therefore higher or lower estimated apparent molecular mass. In these instances the well established classical Ferguson method can be used to obtain data with higher precision. Fig. 2 shows separations of amylase and IgG light and heavy chains by SDS CGE. Simply using the calibration curve shown in Fig. 1 gives estimated molecular masses of the peaks of interest that are off by 21% for amylase and 87 and 25% for the light and heavy chains, respectively of IgG (Table 1). Therefore the Ferguson method should be used to achieve a more precise estimate of the molecular masses of these types of molecules.

In practice, the electrophoretic mobilities of standard proteins and the proteins of interest are be determined from a series of separations using several concentrations of sieving media. In our

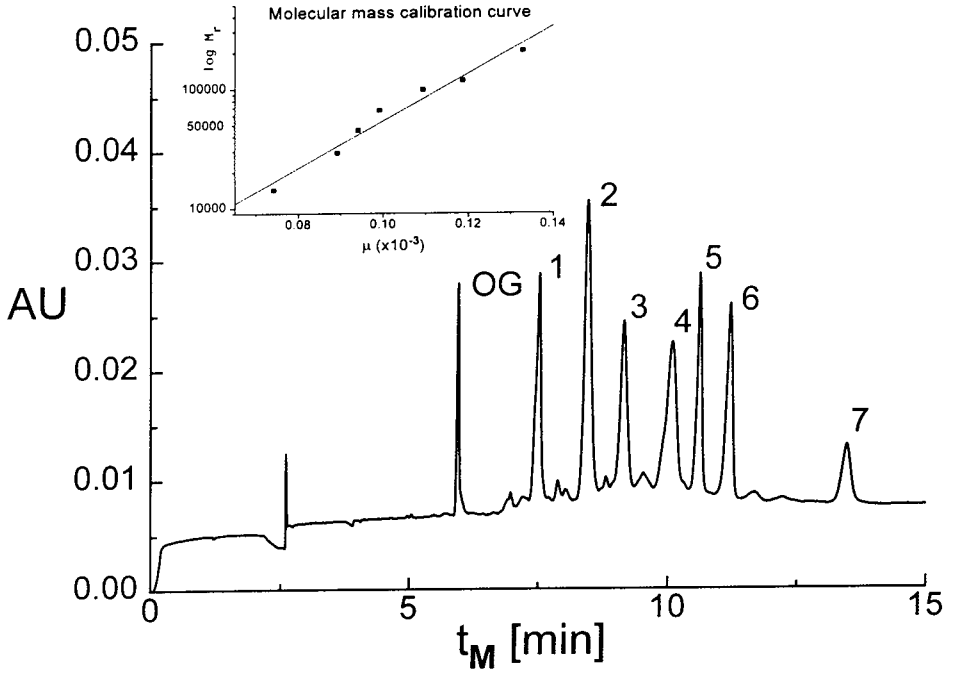

Fig. 1. SDS CGE pattern of the test mixture containing seven proteins on the eCAP SDS 14-200 gel. Peaks: 1 = α-lactalbumin (M_r 14 200); 2 = carbonic anhydrase (M_r 29 000); 3 = ovalbumin (M_r 45 000); 4 = bovine serum albumin (M_r 66 000); 5 = phosphorylase *b* (M_r 97 400); 6 = β-galactosidase (M_r 116 000); 7 = myosin (M_r 205 000). A tracking dye orange-G (OG) was added to the sample in the concentration of 0.005%. Conditions: injected amount: 0.1 μg protein; detection 214 nm; run temperature, 20°C; field strength, 300 V/cm; current, 25–30 μA. Inset: Calibration curve of mobility *vs.* logarithm molecular mass for protein molecular mass determination. t_M = Migration time.

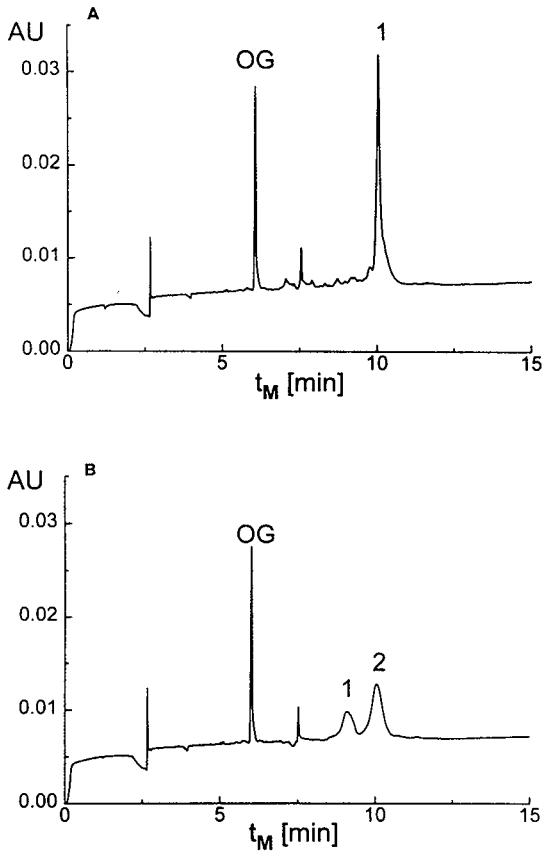

Fig. 2. SDS CGE of amylase (A) and the light and heavy chains of human IgG (B). Peaks: OG = orange-G tracking dye; (A) 1 = amylase; (B) 1 = IgG light chain; 2 = IgG heavy chain. Separation conditions as in Fig. 1.

Table 1
Comparison of estimated molecular mass data of amylase and light and heavy chain subunits of human IgG of Fig. 2, using regular standard curve method and the automated Ferguson method

Protein	Molecular mass		
	Lit. [19]	SDS 14-200	Ferguson
Amylase	56 500	68 200 (21%)	54 900 (3%)
IgG			
Light chain	23 000	4 280 (87%)	27 200 (17%)
Heavy chain	55 000	68 500 (25%)	49 300 (10%)

The values in parentheses after the SDS 14-200 and Ferguson methods show the difference between the measured and literature values.

case, CGE experiments were performed by the use of the original gel concentration in the eCAP SDS 14-200 kit and subsequent dilutions to 75, 67 and 50% of the original concentration. The logarithm of electrophoretic mobilities for each protein *versus* gel buffer concentration are then plotted to generate a series of curves forming the Ferguson plots [7,14]. The negative slopes associated with the proteins are converted to positive numbers which are equal to K_R (retardation coefficient) values for all proteins in the experiments. A plot of the logarithm of protein molecular mass *versus* $K_R^{1/2}$ can then be generated (Fig. 3) and used to determine the molecular masses of proteins, including those that do not bind with SDS in the regular 1 to 1.4 ratio. The exponent of K_R is 1/2 for spherical shaped molecules SDS-PAGE [13]. The same value was found for the polyethylene oxide-based eCAP SDS 14-200 gel buffer system using the suggested 300 V/cm field strength [17]. However, it is important to note that using extremely high field strengths, such as >1000 V/cm, the exponent of K_R can be different than 1/2. This phenomenon is probably due to the use of different sieving material (linear polyethylene oxide *versus* cross-linked polyacrylamide) and the higher field strength accompanied with CGE. This hypothesis is supported by our earlier results showing that high field strengths employed in CGE might cause orientation effects such as stretching of the

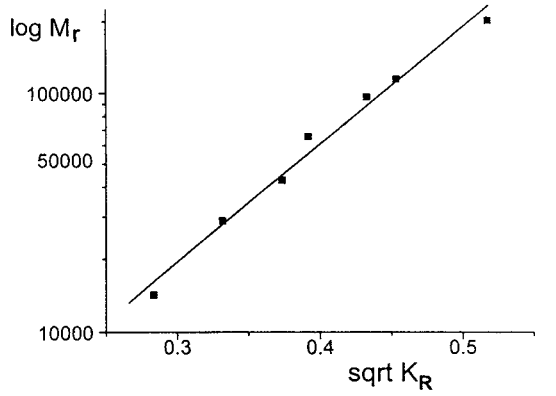

Fig. 3. Square root (sqrt) of retardation coefficient (K_R) *vs.* logarithm molecular mass plot of the standard proteins of Fig. 1.

random coil shaped SDS–protein complexes [20].

More detailed examination of these effects as well as other CGE parameters, *e.g.*, temperature, on the exponent of K_R is under further investigation.

Acknowledgement

The authors gratefully acknowledge Professor Barry L. Karger for his stimulating discussions.

References

[1] A.S. Cohen and B.L. Karger, *J. Chromatogr.*, 397 (1987) 409.
[2] K. Tsuji, *J. Chromatogr.*, 550 (1991) 823.
[3] A. Widhalm, C. Schwer, D. Blass and E. Kenndler, *J. Chromatogr.*, 546 (1991) 446.
[4] K. Ganzler, K.S. Greve, A.S. Cohen, B.L. Karger, A. Guttman and N. Cooke, *Anal. Chem.*, 64 (1992) 2665.
[5] W. Werner, D. Demorest, J. Stevens and J.E. Wictorowicz, *Anal. Biochem.*, 212 (1993) 253.
[6] A. Guttman, J. Nolan and N. Cooke, *J. Chromatogr.*, 632 (1993) 171.
[7] A. Guttman, J. Horvath and N. Cooke, *Anal. Chem.*, 65 (1993) 199.
[8] D. Wu and F. Regnier, *J. Chromatogr.*, 608 (1992) 349.
[9] K. Weber and M. Osborn, *J. Biol. Chem.*, 244 (1969) 4406.
[10] B.D. Hames and D. Rickwood (Editors), *Gel Electrophoresis of Proteins*, IRL, Washington, DC, 1983.
[11] U.K. Laemmli, *Nature*, 227 (1970) 680.
[12] J.A. Reynolds and C. Tanford, *Proc. Natl. Acad. Sci. U.S.A.*, 66 (1970) 1002.
[13] A. Chrambach, *The Practice of Quantitative Gel Electrophoresis*, VCH, Deerfield Beach, FL, 1985.
[14] A.T. Andrews, *Electrophoresis*, Claredon Press. Oxford, 2nd ed., 1986.
[15] K.A. Ferguson, *Metab. Clin. Exp.*, 13 (1964) 985.
[16] W. Werner, D. Demorest and J.E. Wictorowicz, *Electrophoresis*, 14 (1993) 759.
[17] *Beckman eCAP 14-200 kit, Instruction Manual 015-726434-A*, Beckman, Fullerton, CA, 1993.
[18] P. Shieh, D. Hoang, A. Guttman and N. Cooke, *J. Chromatogr. A*, 676 (1994) 219.
[19] *Atlas of Protein and Genomic Sequences*, CD-ROM produced by National Biomedical Research Foundation, June 30, 1992.
[20] A. Guttman, P. Shieh, D. Hoang, J. Horvath and N. Cooke, *Electrophoresis*, 15 (1994) 221.

ELSEVIER

Journal of Chromatography A, 676 (1994) 233–238

JOURNAL OF CHROMATOGRAPHY A

Two-dimensional electrophoresis as a complementary method of isolating peptide fragments of cleaved proteins for internal sequencing

Kiyoshi Nokihara*[a,b], Tomoko Kuriki[b], Naoki Morita[b]

[a]*Tokyo University of Agriculture and Technology, Koganei, Tokyo, Japan*

[b]*Biotechnology Instruments Department, Shimadzu Corp., Nishinokyo-Kuwabaracho 1, Nakagyo-ku, Kyoto 604, Japan*

Abstract

To determine the primary structure of proteins, usually proteolytic enzyme digests are separated by reversed-phase high-performance liquid chromatography (HPLC) and each fraction is collected and sequenced. The results obtained by different cleavages are combined to reveal the entire sequence. However, there are many N-terminal-blocked proteins and/or *intact* proteins or their particular fragments that are not eluted from HPLC columns. Internal fragments of such proteins were successfully isolated by the use of two-dimensional electrophoresis, after digestion. Electroblotted spots were easily sequenced to identify those difficult fragments which could not be obtained using HPLC.

1. Introduction

The complete amino acid sequence of proteins can usually be determined as follows. Initially, proteolytic enzyme digests of a protein are separated by reversed-phase high-performance liquid chromatography (HPLC), then each fraction is collected and sequenced. The partial sequences obtained by different cleavages are compared and overlapped to reveal the entire sequence. However, there are many N-terminal-blocked proteins that cannot undergo the Edman degradation. In addition, there are intact proteins, or their particular fragments, that cannot be separated or eluted from HPLC columns because of aggregation and adsorption. Sequence information cannot be obtained in these instances. This paper describes the isolation and identification of fragment peptides that allows the determination of their amino acid sequences, by the use of two-dimensional electrophoresis followed by electroblotting, as a complementary method to HPLC of protein digests.

2. Experimental

2.1. Materials

Trypsin, *Staphylococcus aureus* V8 protease and endoproteinase Lys-C were of sequence grade from Boehringer-Mannheim (Mannheim, Germany). Acrylamide and sodium dodecyl sul-

* Corresponding author. Address for correspondence: Biotechnology Instruments Department, Shimadzu Corp., Nishinokyo-Kuwabaracho 1, Nakagyo-ku, Kyoto 604, Japan.

0021-9673/94/$07.00
SSDI 0021-9673(94)00091-M

phate (SDS) were obtained from Bio-Rad Labs. (Richmond, CA, USA), N,N'-methylenebisacrylamide, N,N,N',N'-tetramethylethylenediamine (TEMED), ammonium peroxodisulphate (APS), Pharmalyte 3–10, Ampholine 3.5–10, Ampholine 5–8, low-molecular-mass marker and protein isoelectric point (p*I*) marker from Pharmacia–LKB Biotechnology (Uppsala, Sweden), glycine, glycerol, acetic acid, Coomassie Brilliant Blue R-250, Nonidet P-40, methanol, ethanol, 2-mercaptoethanol and phosphoric acid from Nacalai Tesque (Kyoto, Japan), 2-amino-2-(hydroxymethyl)-1,3-propanediol (Tris), 3-(cyclohexylamino)-1-propanesulphonic acid (CAPS) and human serum albumin (HSA) from Sigma (St. Louis, MO, USA), lysyl endopeptidase, *Achromobacter* protease I, hydrochloric acid, sodium hydroxide, bromophenol blue, formic acid, cyanogen bromide (CNBr) and phenylthiohydantoin (PTH-) amino acid standards from Wako (Osaka, Japan), urea from Fluka (Buchs, Switzerland) and a polyvinylidene difluoride (PVDF) membrane from Pall (New York, NY, USA). A protein from *Penicullium camembertii* (LPC) [1] was a generous gift from Dr. K. Isobe (GBF, Braunschweig, Germany).

2.2. Digestion

S-Carboxymethylated HSA was cleaved with CNBr according to ref. 2 and the digests were dissolved in the lysis buffer [3] at a concentration of 1.32 mg/ml. LPC was S-pyridylethylated, digested by trypsin and lyophilized. The resulting digests were dissolved in the lysis buffer at a concentration of 2 mg/ml and stored at −20°C until used.

2.3. HPLC separation and characterization of fragment peptides

Digests of LPC obtained using trypsin, endoproteinase Lys-C and *Staphylococcus aureus* V8 were lyophilized, separated as described in ref. 4 and characterized by sequencing and amino acid analysis.

2.4. Electrophoresis

Two-dimensional electrophoresis was performed using a TEP-2 instrument manufactured by Shimadzu (Kyoto, Japan). This apparatus [5] allows fully automated transfer from isoelectric focusing, the first-dimensional electrophoresis (1-DE) gel, to SDS polyacrylamide gel electrophoresis (PAGE), the second-dimensional electrophoresis (2-DE) gel. Running conditions and the transfer from 1-DE to 2-DE were performed automatically and precisely under the control of a microprocessor. The 1-DE gel was 1.5 mm in diameter and 140 mm long and the 2-DE gel was 160 mm long (separation gel 135 mm, stacking gel 25 mm), 160 mm wide and 1.5 mm thick. The temperature during electrophoresis can be accurately and directly regulated by the specially insulated metal plate and is independent of the ambient temperature. The composition of 1-DE gel was 9 *M* urea–6% Pharmalyte 3–10 (for HSA)–1.3% Ampholine 3.5–10–1.7% Ampholine 5–8 (for LPC)–5% T, 5% C–0.033% APS–0.067% TEMED. The cathode buffer for 1-DE was 0.02 *M* NaOH and the anode buffer was 0.085% H_3PO_4. Molecular mass and p*I* were calibrated prior to the sample analyses by the present apparatus. At 10°C, with a prerun at 200 V for 0.5 h, 1000 V for 4.8 h, followed by 1200 V for 1 h (for HSA), and a pre-run at 200 V for 1.0 h, followed by 1300 V for 7.0 h (for LPC), were performed in 1-DE, in which the gels were equilibrated in a solution of 62.5 m*M* Tris–5% 2-mercaptoethanol–2.3% SDS for 15 min (for HSA), 0.01 *M* H_3PO_4–5% 2-mercaptoethanol–2.5% SDS–8 *M* urea for 10 min (for LPC) *in situ*. With HSA, 2-DE was carried out according to Laemmli [6], and with LPC, 2-DE was carried out according to Swank and Munkres [7], which is suitable for peptide separations [8].

2.5. Electroblotting

Electroblotting onto the PVDF membrane was carried out at a constant 7 V/cm for 4.0 h at 4.0°C using Transphor TE42 (Hoeffer Scientific Instruments, San Francisco, CA, USA), with an electroblotting buffer consisting of 10 m*M* CAPS

(pH 11.0) containing 10% methanol and the pH was adjusted with 2 *M* NaOH. After blotting, the membrane was stained for 30 s in 0.2% Coomassie Brilliant Blue R-250 in 50% methanol–10% acetic acid and rapidly destained with 45% methanol–7% acetic acid.

2.6. Sequence analysis

Sequence analyses were performed using a PPSQ-10 gas-phase sequencer (Shimadzu), which allows highly sensitive isocratic elution for PTH-amino acid analysis [9]. The excised membrane was inserted directly in the reaction chamber of the sequencer. PTH-amino acid determination was performed by chromatogram subtraction in order to eliminate carry-over and background effects. The resulting PTH-amino acids were analysed by reversed-phase HPLC using a Wako-Pak WS-PTH column (250 mm × 4.6 mm I.D.) with 20 m*M* sodium acetate buffer (pH 4.7)–acetonitrile (60:40, v/v) containing 0.014% (w/w) of SDS at a flow-rate of 1.0 ml/min and detection at 269 nm.

3. Results and discussion

The present strategy allows the characterization of fragment peptides by sequence analysis, after isolation using two-dimensional electrophoresis followed by electroblotting. Chemically cleaved HSA was separated using TEP-2. The blotted PVDF membrane is shown in Fig. 1. Spot A (p*I* 6.2, relative molecular mass 27 000) was excised and sequenced to give an internal sequence of HSA from position 447, as indicated in Table 1. (Position 446 of HSA is a Met residue.) Forty residues were easily determined in a single run.

The digests of LPC, with different enzymes, were separated by reversed-phase HPLC and each peak was collected. All peaks were subsequently sequenced and analysed for their amino acid composition [4] and the entire sequence of LPC was thus determined. However, the results from mass spectrometry [10] and amino acid composition analysis of intact LPC were different from the above result. The fragments corresponding to positions 49–81 could not be found from digests separated by HPLC.

Table 1
Internal sequence obtained from spot A in Fig. 1 and amounts of PTH-amino acids (pmol)

1	2	3	4	5	6	7	8	9	10
Pro 55.2	(Cys)	Ala 67.7	Glu 80.1	Asp 51.5	Tyr 56.9	Leu 52.4	Ser 11.2	Val 42.1	Val 47.3
11	12	13	14	15	16	17	18	19	20
Leu 37.3	Asn 36.7	Gln 30.0	Leu 37.7	(Cys)	Val 32.6	Leu 31.4	Glu 17.4	His	Lys 25.0
21	22	23	24	25	26	27	28	29	30
Thr	Pro 15.1	Val 21.5	Ser	Asp 12.7	Arg	Val 14.2	Thr 6.9	Lys 14.8	(Cys)
31	32	33	34	35	36	37	38	39	40
(Cys)	Thr	Glu 14.3	Ser	Leu 9.7	Val 9.7	Asn 8.7	Arg	Arg	Pro

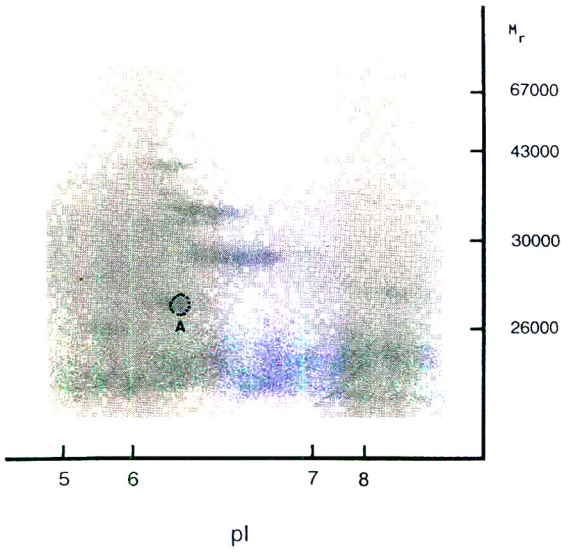

Fig. 1. Separated CNBr fragments of HSA on PVDF membrane. Spot A was excited and sequenced.

The tryptic digests of the S-pyridylethylated LPC were then separated by two-dimensional electrophoresis and electroblotted onto the PVDF membrane. Four spots were clearly observed (Fig. 2), excised and sequenced. Sequencing of spots A and B is summarized in Table 2. Several

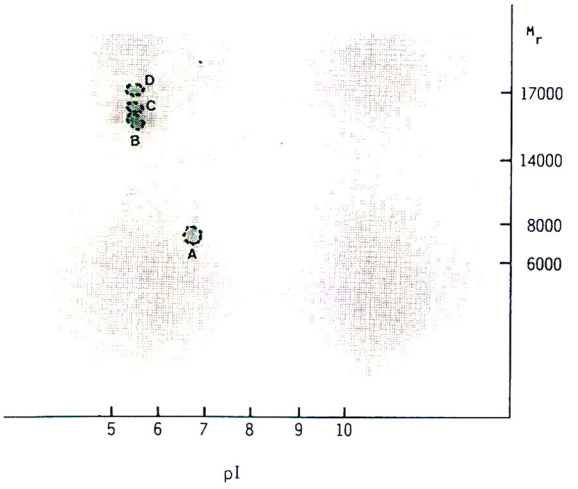

Fig. 2. Blotted membrane of tryptic digest of LPC after two-dimensional electrophoresis. Spots A, B, C and D were excised and sequenced.

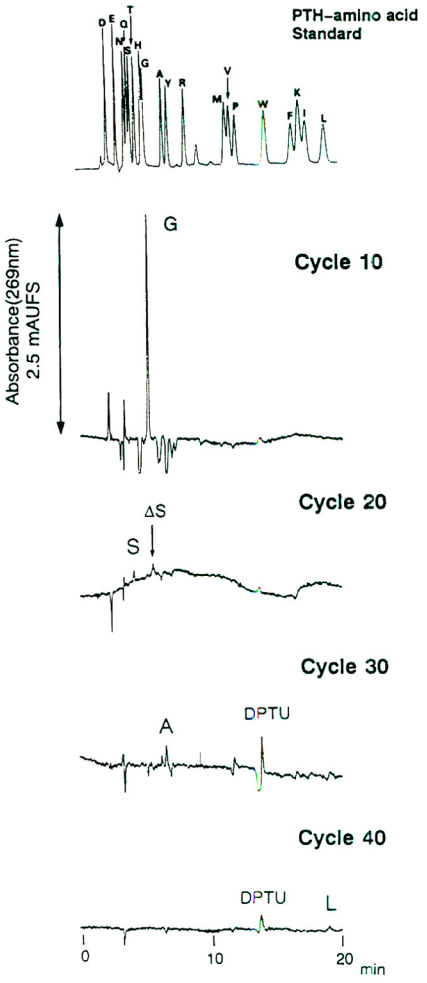

Fig. 3. Chromatograms of PTH-amino acid in the sequence analysis of spot B in Fig. 2.

chromatograms of the PTH-amino acids in the sequence analysis of spot B are shown in Fig. 3. Spots C and D gave the same sequence at the N-terminus as obtained from spot B, which was the sequence of positions 39–86 in the pyridylethylated LPC (Fig. 4). It seems that tryptic digestion of this region was only partially completed and the sequence of this region is resistant to trypsin, presumably owing to the conformation, and this leaves the fragments attached to the stationary phase of the column used for separation. The complete amino acid sequence of LPC has thus been determined.

Table 2
Internal sequence with amounts of PTH-amino acids (pmol) of LPC obtained from A, which gave positions 88–117, and B, which gave positions 39–86, in Fig. 4

Spot	1	2	3	4	5	6	7	8	9	10
A	Asn	Trp	Val	Ala	Asp	Ala	Thr	Phe	Val	His
	125	51	93	94	85	84	23	78	59	20
	11	12	13	14	15	16	17	18	19	20
	Thr	Asn	Pro	Gly	Leu	PEC	Asp	Gly	PEC	Leu
	16	50	38	31	39	24	31	22	17	22
	21	22	23	24	25	26	27	28	29	30
	Ala	Glu	Leu	Gly	Phe	Trp	Ser	Ser	Trp	Lys
	22	10	17	11	14	5	1	1		4
	1	2	3	4	5	6	7	8	9	10
B	Gly	Asn	PEC[a]	Pro	Glu	Val	Glu	Ala	Thr	Gly
	51	58		35	47	47	37	41	17	24
	11	12	13	14	15	16	17	18	19	20
	Ala	Thr	Val	Ser	Tyr	Asp	Phe	Ser	Asp	Ser
	33	14	27	6.4	17	21	17	4.3	15	6.1
	21	22	23	24	25	26	27	28	29	30
	Thr	Ile	Thr	Asp	Val	Ala	Gly	Tyr	Ile	Ala
	6.7	4.6	4.3	9.5	8.2	9.3	6.9	5.6		9.3
	31	32	33	34	35	36	37	38	39	40
	Val	Asp	His	Thr	Asn	Ser	Ala	Val	Val	Leu
	6.6	6.1	0.7		6.4			4.7	5.3	
	41	42	43	44	45	46	47	48	49	50
	Ala	Phe	Arg	Gly	Ser	Tyr	Ser	Val		

Spots C and D in Fig. 2 gave the same sequence as spot B, positions 39–64 of LPC [1].
[a] PEC = S-pyridylethylated cysteine.

4. Conclusions

Two-dimensional electrophoresis is a powerful complementary method for separating peptides and proteins, especially proteins which are difficult to separate by reversed-phase HPLC. The present strategy is useful for determining partial and internal sequences, especially of N-terminal-blocked proteins and for intact proteins or their particular fragments, which are not eluted from HPLC columns. Further, the excised spots on the PVDF membrane can also be used for amino acid analysis after direct hydrolysis [11]. These partial sequences can be used for DNA probes and allow the determination of the entire amino acid sequence of the proteins from the cDNA.

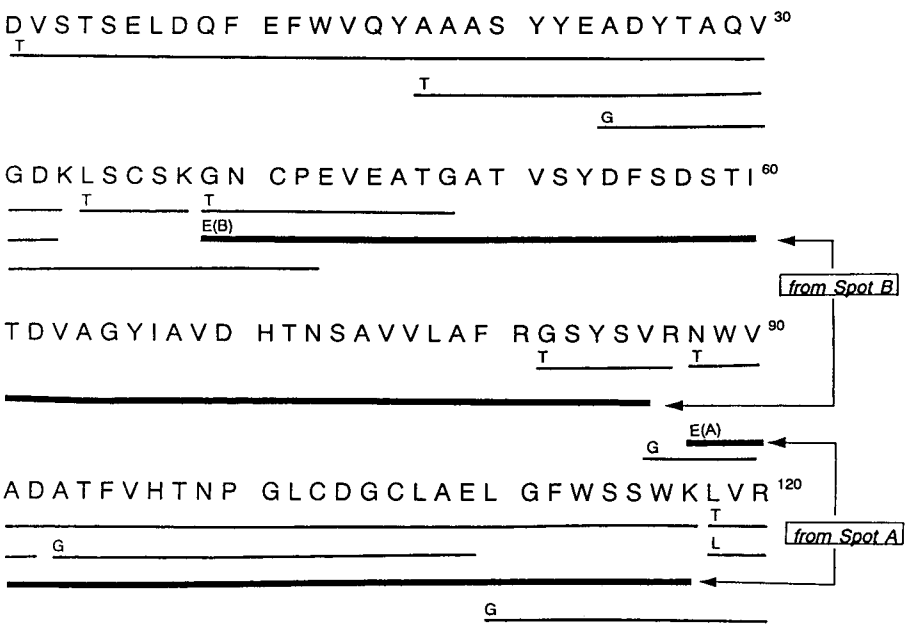

Fig. 4. Sequence of the present LPC determined by the present method. The prefixes T, L and G denote digests of trypsin, endoproteinase Lys-C and *S. aureus* V8 protease, respectively, determined by sequencing after fractionation by reversed-phase HPLC. E(A) and E(B) indicate sequences obtained by the present method from spots A and B, respectively, in Fig. 2.

5. References

[1] K. Isobe, K. Nokihara, S. Yamaguchi, T. Mase and R.D. Shimid, *Eur. J. Biochem.*, 203 (1992) 233–237.
[2] E. Gross, *Methods Enzymol.*, 11 (1967) 238–255.
[3] K. Nokihara, N. Morita and T. Kuriki, *Electrophoresis*, 13 (1992) 701–707.
[4] K. Isobe and K. Nokihara, *FEBS Lett.*, 320 (1993) 101–106.
[5] T. Nishine, S. Nakamura, M. Hazama and K. Nokihara, *Anal. Sci.*, 7 (1991) 285–288.
[6] U.K. Laemmli, *Nature*, 227 (1970) 680–685.
[7] R.T. Swank and K.D. Munkres, *Anal. Biochem.*, 39 (1971) 462–477.
[8] K. Nokihara, R. Beck and F. Herbst, *Anal. Lett.*, 21 (1988) 1371–1382.
[9] A. Harada, A. Ueda and N. Morita, *Shimadzu Rev.*, (1992) 81–85.
[10] H.C. Hedrich, K. Isobe, B. Stahl, K. Nokihara, M. Kordel, R.D. Schmid, M. Karas, F. Hillenkamp and F. Spener, *Anal. Biochem.*, 211 (1993) 288–292.
[11] K. Nokihara and F. Herbst, in N. Yanaihara (Editor), *Peptide Chemistry 1989*, Protein Research Foundation, Osaka, 1990, pp. 69–74.

ELSEVIER

Journal of Chromatography A, 676 (1994) 239–246

JOURNAL OF CHROMATOGRAPHY A

Simultaneous high-performance capillary electrophoretic determination of reduced and oxidized glutathione in red blood cells in the femtomole range

Giovanni Piccoli, Mara Fiorani, Beatrice Biagiarelli, Francesco Palma, Lucia Potenza, Antonella Amicucci, Vilberto Stocchi*

Istituto di Chimica Biologica "Giorgio Fornaini", Università di Urbino, Via Saffi, 2, 61029 Urbino, Italy

Abstract

This paper describes a high-performance capillary electrophoretic (HPCE) method which allows a quick, simultaneous and quantitative determination of reduced (GSH) and oxidized (GSSG) glutathione in mammalian red blood cells using a Supelco-bonded hydrophilic phase capillary CElect-P150. The extraction procedure of GSH and GSSG from erythrocytes using Microcon-10 membranes is very simple and allows a correct evaluation of these compounds present in the red blood cells. Furthermore, the HPCE method does not require removal of the excess N-ethylmaleimide used to block the glutathione in its reduced state, making the simultaneous evaluation of GSH and GSSG possible in a very short time (ca. 4 min), with a sensitivity at femtomole level.

1. Introduction

Glutathione (γ-L-glutamyl-L-cysteinyl-glycine; GSH), an essential tripeptide present in virtually all animal cells, is a component of a pathway that uses reduced nicotinamide–adenine dinucleotide phosphate (NADPH) to maintain the cellular redox state. It has an essential role in maintaining both proteins and other compounds such as ascorbate, α-tocopherol, etc. in their reduced states. Furthermore, it is involved in the reduction of ribonucleotides to deoxyribonucleotides (precursors of DNA) and is implicated in protecting the cell against oxidative damage, free radical damage and other types of toxicity [1]. Glutathione can be present in the cells in its oxidized (GSSG) and reduced states (GSH). Usually, most intracellular glutathione is in its reduced state, which in most tissues represents more than 99% of the total glutathione (GSH + GSSG) [2]. Commonly, GSH is present in the cell in 1–2 m*M* concentrations, while the concentration of GSSG is at the μ*M* level. However, the levels of oxidized and reduced glutathione can change significantly upon oxidative stress, and their evaluation provides useful information about the redox and detoxification status of cells and tissues [3–6]. Several procedures for the determination of GSH and GSSG from different biological sources have been reported in the literature: chemical [7] and enzymatic [8–10] methods, high-performance liq-

* Corresponding author.

0021-9673/94/$07.00
SSDI 0021-9673(94)00433-A

uid chromatography [2,11–19], flow cytometry [20–22] and, more recently, capillary electrophoresis (CE) [23,24]. GSH and GSSG can be detected using spectrophotometric [25,26], spectrofluorimetric [27–33] and electrochemical detectors [11,15,17,34–39] with different levels of sensitivity ranging from nmol [14,16] to pmol [12,13]. Correct measurement of glutathione disulfide is difficult both because of its low concentration and the ease with which GSH is oxidized to GSSG in biological extracts. One of the most common methods utilized for GSSG determination in red blood cells involves an enzymatic reaction using NADPH-dependent glutathione reductase which ensures high specificity and good sensitivity [40]. However, in order to prevent undesirable oxidation of GSH in the course of sample treatment, N-ethylmaleimide (NEM) must be added to block free thiol groups [10,40–42]. This reagent interferes with the subsequent enzymatic determination of GSSG by inhibiting the glutathione reductase. Furthermore, this method requires several extractions with diethyl ether to remove the excess NEM, followed by flushing with nitrogen to eliminate this diethyl ether. These numerous steps make this method laborious and time-consuming and, moreover, the additional manipulations required may lead to an inaccurate evaluation of glutathione. In this paper, we describe a procedure which allows a quick CE analysis of the GSH-NEM derivative and GSSG in the red blood cells in conjunction with a simple extraction procedure using a Microcon-10 membrane. This filtration procedure does not require the use of protein-precipitating agents (such as perchloric acid, metaphosphoric acid, trichloroacetic acid, etc.) commonly used to minimize the oxidative change of GSH to GSSG. This is an important point because Reed et al. [14] have shown that the use of these protein-precipitating agents is unsuitable for the correct determination of GSH and GSSG in whole blood samples. Furthermore, the CE method described here, using a Supelco-hydrophilic bonded phase capillary CElect-P150, allows the analysis of GSH and GSSG in red blood cells with a sensitivity at fmol level.

2. Experimental

2.1. Chemicals

GSH, GSSG and NEM were obtained from Sigma (St. Louis, MO, USA). Analytical reagent-grade potassium dihydrogenphosphate was purchased from Merck (Darmstadt, Germany). Microcon-10 microconcentrators were purchased from Amicon (Beverly, MA, USA). Filters (0.22 μm) were obtained from Millipore (Bedford, MA, USA). The water used for the experiments was doubly distilled. All buffers were filtered through a Millipore filter (0.22 μm) before HPCE analysis.

2.2. HPCE apparatus

CE analysis was performed using an automated P/ACE 2100 system (Beckman Instruments, CA, USA) interfaced with an IBM 55sx computer using System Gold software for control and data collection. The P/ACE 2100 system, equipped with UV detector, automatic injector and autosampler, was fitted with a 30 kV high-voltage power supply with a current limit of 250 μA.

2.3. Capillary

The capillary used throughout this work was a 27 cm Supelco bonded hydrophilic phase CElect-P150 (50 μm I.D. $\times$ 363 μm O.D.), with the detector cell at 20 cm (Supelco, Bellefonte, PA, USA). The capillary was assembled in a Beckman cartridge.

2.4. Preparation of samples

Whole blood was collected using heparin as anticoagulant. Rabbit red blood cells with a percentage of reticulocytes ranging from 40 to 60% were obtained from rabbits made anaemic by phenylhydrazine administrations [43]. The blood samples were centrifuged at 5000 g (3000 rpm) for 10 min, plasma and buffy coat were removed and the red cells were washed twice

with 0.9% (w/v) NaCl isotonic solution. In some experiments, the packed cells were resuspended 1:10 in the presence or absence of 0.1 m*M* Fe^{2+} and 10 m*M* ascorbate and then incubated for 90 min at 37°C, in a shaking water bath. In all experiments the red blood cells were lysed adding an equal volume of cold water in presence of (50 m*M*) NEM and leaving the solution in ice for 20 min. The stroma were removed by centrifugation at 14 000 rpm for 10 min. The supernatant was filtered using a Microcon-10 membrane (cut-off M_r 10 000) at 10 000 rpm for 5 min and the filtered solution was directly analyzed by HPCE.

2.5. CE analysis

The analysis was performed applying the sample under nitrogen pressure for 5 s using a sodium phosphate (35 m*M*, pH 2.1) buffer as electrolyte. The separating conditions of 15 kV were achieved in 1 min and held at a constant voltage for 9 min. The experiments were carried out at 25°C and detection was performed by UV absorption at 200 nm. After the analysis, preconditioning of the capillary using acid or basic treatments is not necessary, and new analyses can be performed by equilibrating the capillary using the electrolyte buffer for about 2 min.

2.6. Spectrophotometric determination of GSH and GSSG

The colorimetric method of GSH determination and the enzymatic assay for the GSSG evaluation were performed as described by Beutler [44].

3. Results and discussion

3.1. Separation of GSH and GSSG by HPCE

Fig. 1A shows the simultaneous separation of a 500 μM standard mixture of GSH and GSSG by CE using a Supelco CElect-P150 hydrophilic bonded phase capillary. As shown in the electropherogram, the analysis of the oxidized and reduced glutathione can be performed in a short time (less than 4 min) making this method significantly quicker than other high-performance liquid chromatographic, enzymatic or colorimetric procedures. The use of NEM to block the GSH in its reduced state has been suggested, however, in order to obtain a correct

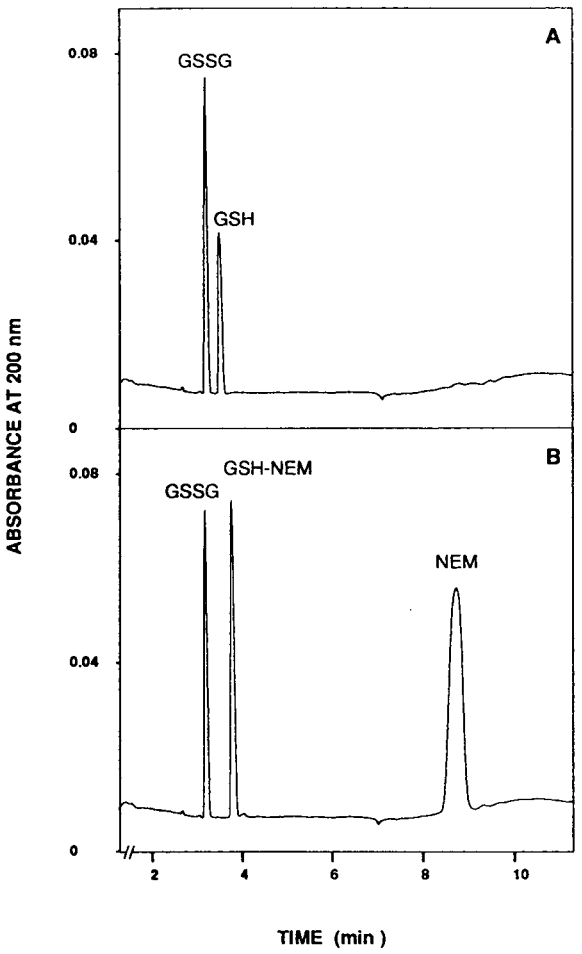

Fig. 1. Separation of standard mixture of GSH and GSSG by CE using the Supelco hydrophilic bonded phase capillary CElect-P150. (A) Separation of standard mixture of GSH and GSSG. (B) Separation of GSH and GSSG in presence of an excess of NEM. The analysis was performed applying the sample under nitrogen pressure for 5 s and using sodium phosphate (35 m*M*, pH 2.1) buffer as electrolyte. The experiment was carried out at 25°C and the detection was performed by UV absorption at 200 nm.

evaluation of GSH and GSSG in biological fluids, cells and tissues [10,40–42]. Fig. 1B shows the analysis of the GSH-NEM derivative and GSSG by CE under the same experimental conditions described in Fig. 1A. As shown in the electropherogram, the use of NEM does not interfere with the separation of these two compounds, allowing an even better separation. In fact, NEM reduces the electrophoretic mobility of the GSH-NEM derivative, increasing the separation time between GSSG and GSH-NEM by about 20 s. Under these conditions it is possible to correctly evaluate the two compounds even when one is present in great excess as compared to the other, as usually occurs in biological samples [2]. Furthermore, the GSH-NEM derivative detected at 200 nm shows a higher extinction coefficient, compared to the GSH absorption, showing the increased sensitivity of factor 2 (Fig. 1B). As reported in Fig. 1B, the excess of NEM does not interfere with the CE analyses of the GSH-NEM derivative and GSSG, since it is eluted from the capillary with a migration time of about 9 min. However, it is not necessary to wait for the end of the analysis (ca. 9 min) before injecting another sample, since it is possible to remove the excess NEM from the capillary by performing the equilibrating procedure with the phosphate electrolyte buffer. Under these conditions, analyses of the GSH-NEM derivative and GSSG can be performed every 5–6 min. This, together with the possibility of automating the analysis, makes this procedure of interest for routine analyses as in the case of clinical applications or in other biochemical studies.

3.2. GSH and GSSG calibration curves

Figs. 2 and 3 show the calibration curves for GSH and GSSG obtained by injecting a standard solution of reduced and oxidized glutathione ranging from 1 to 2000 μM. As shown in the figures, there is a very good correlation between the amount of GSH and GSSG injected and that detected by CE, even at low concentrations (1–100 μM). Furthermore, the reproducibility has been tested from analysis to analysis when a 50

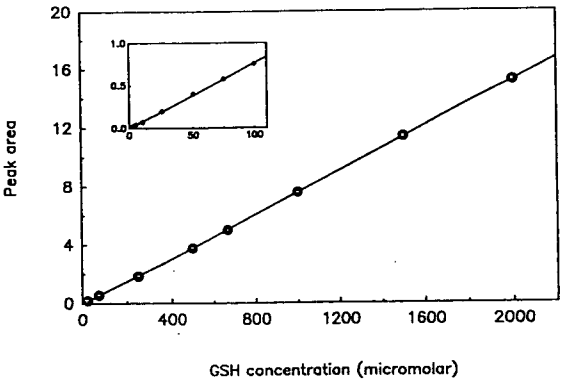

Fig. 2. Calibration curve of GSH-NEM. The experiment was performed injecting standard solutions of GSH-NEM ranging from 2 to 2000 μM. The inset shows the linearity of calibration curve at low standard concentrations (1–100 μM). Analysis conditions as in Fig. 1 ($R > 0.999$).

μM solution of GSH and GSSG is repeatedly injected. The relative standard deviations (R.S.D.s) determined on the basis of six different injections, 0.226% for GSH and 0.229% for GSSG, show that there is a very good correlation between the values of the standard solution of reduced and oxidized glutathione and that experimentally determined by HPCE. The same experiment was performed using a real sample obtained from red blood cells exposed to an oxidant system (Table 1). Also in this case the sample was injected six consecutive times and

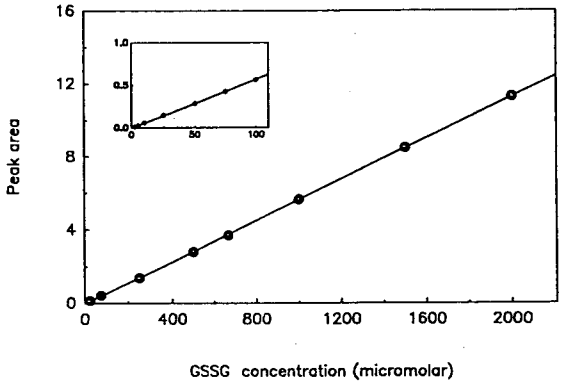

Fig. 3. Calibration curve of GSSG. The experiment was performed injecting standard solutions of GSSG ranging from 2 to 2000 μM. The inset shows the linearity of calibration curve at low standard concentrations (1–100 μM). Analysis conditions as in Fig. 1 ($R > 0.999$).

Table 1
Reproducibility of GSH and GSSG analysis in red blood cells by HPCE

Injection No.	GSH		GSSG	
	Migration time (min)	Concentration[a]	Migration time (min)	Concentration[a]
1	4.487	206.23	3.600	534.03
2	4.407	202.07	3.541	536.34
3	4.512	202.91	3.615	542.37
4	4.510	205.25	3.615	544.24
5	4.444	198.31	3.572	528.28
6	4.458	201.62	3.578	532.07
R.S.D. (%)	0.92	1.39	0.80	1.14

The sample used in the experiment was obtained from red blood cell suspension incubated for 30 min in the presence of an oxygen radical-generating system represented by Fe^{2+}/ascorbate. After the incubation the red blood cell suspension was processed as described in the Experimental section and the sample obtained was injected six consecutive times. The migration times and the concentrations of GSH and GSSG determined by HPCE analysis are reported.
[a] The data reported are expressed as nmol/ml hemolysate (1:1).

the data reported in Table 1 show the high reproducibility of the migration times of GSH and GSSG together with an experimental reproducible determination of their amounts. The detection limit, calculated from electropherograms obtained using the experimental conditions described above, indicates that it is possible to detect the GSH and GSSG present in samples at a concentration of 0.5–1 μM, corresponding to about 10–20 fmol. These results prove that the CE method developed is reliable and can be used for quantitative determinations of GSH and GSSG in biological samples.

3.3. Recovery of exogenous GSSG

The extraction procedure for the determination of glutathione in red blood cells was performed using a Microcon-10 membrane to filter the erythrocyte lysate.The reliability of this extraction procedure was checked by adding an exogenous GSSG solution to the hemolysate. The red blood cell lysate was diluted with an equal volume of 2 mM GSSG standard solution and the sample was then filtered for 5 min at 10 000 rpm using the Microcon-10 membrane. The filtered solution was then directly analyzed by CE. The complete recovery of the exogenous GSSG (1.007 μmol/ml of hemolysate 1:1), demonstrates the validity of the extraction procedure used. Furthermore, in order to assure the best analytical conditions, we performed various experiments either using low pressure of nitrogen or injecting the sample electrokinetically. The results obtained show that, for an accurate analysis of GSSG and GSH by CE using a CElect-P150 capillary (27 cm × 50 μm I.D.), it was necessary to inject the sample under pressure for 5 s. Injection times lower than 5 s can significantly influence the reproducibility of the amount of sample injected, while higher injection times can cause overloading.

3.4. Determination of GSH and GSSG in red blood cells

The procedures reported in the literature for evaluating the reduced and oxidized glutathione in red blood cells show some drawbacks, due to the extraction and analysis methods used [2,10,45]. In fact, the extraction must be performed using excess NEM to block the GSH in its reduced state, with a subsequent removal of the excess NEM from the sample requiring additional tedious and time-consuming steps. The CE method described in this paper together

with an appropriate extraction procedure, which does not require the use of protein precipitating agents, was shown to be suitable for the simultaneous analysis of GSH and GSSG in mammalian erythrocytes. We tested this procedure evaluating the levels of GSSG and GSH in human erythrocytes from adults and umbilical cord blood, rabbit reticulocytes and in the red blood cells exposed "in vitro" to an oxygen radical generating system. Fig. 4 shows the electropherograms of glutathione content in rabbit reticulocytes and human fetal erythrocytes. Fig. 5 shows how the levels of GSSG and GSH in human erythrocytes exposed to 0.1 mM Fe^{2+} and 10 mM ascorbate

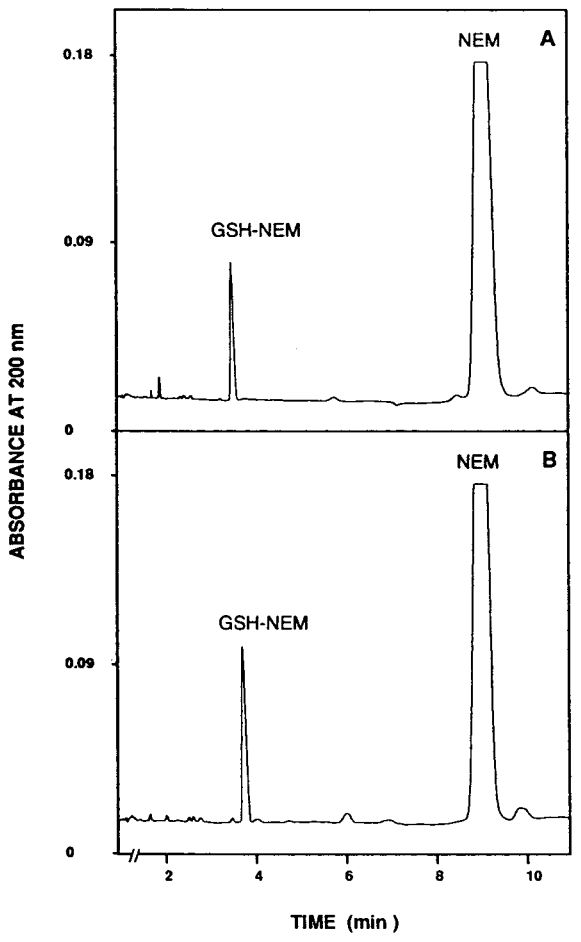

Fig. 4. CE analysis of GSH and GSSG levels in the human red blood cells from umbilical cord blood (A) and in rabbit reticulocytes (B). The red cells were lysed in presence of excess of NEM and deproteinized as described in the Experimental section. The levels of GSH were 1.17 and 1.68 μmol/ml of hemolysate (1:1) in umbilical cord blood and in rabbit reticulocytes, respectively. The GSSG concentrations were not detectable, being lower than 1 μM. Analysis conditions as in Fig. 1.

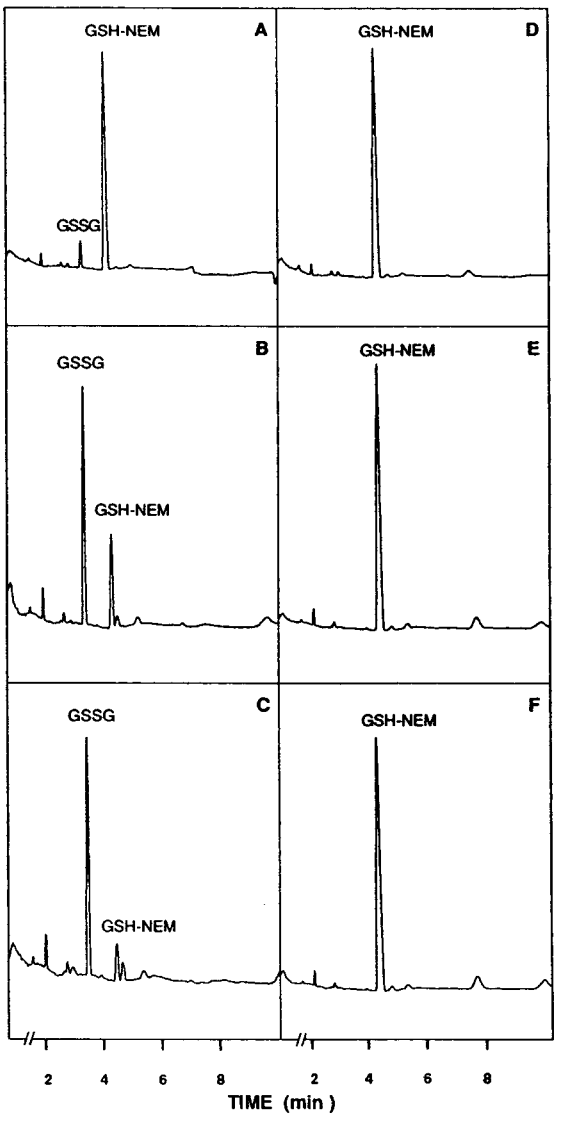

Fig. 5. GSH and GSSG levels in human red blood cells exposed to Fe^{2+}/ascorbate oxygen radicals generating system. (A) Red blood cells at starting point of exposure to the Fe^{2+}/ascorbate system; (B) red blood cells after 30 min of exposure; (C) red blood cells after 60 min of exposure; (D), (E) and (F) red blood cell controls incubated 0, 30 and 60 min, respectively, at 37°C. Analysis conditions as in Fig. 1.

changed. This oxidant radical generating system is able to produce free radicals which can provoke an intracellular metabolic impairment modifying the redox state of cells significantly [46]. As shown in Fig. 5A, B and C the level of GSH in the erythrocytes exposed to this oxidant system undergoes a dramatic drop, with a simultaneous increase in GSSG concentration from 0.020 μM to 0.40 mM. A fraction of GSSG thus formed in the erythrocytes incubated with iron/ascorbate flows-out of the cells, and can be detected in the external medium. Fig. 5D, E and F shows the electropherograms of GSH and GSSG in the human red blood cells not exposed to iron and ascorbate. As shown in the figure, incubation of intact red blood cells up to 60 min at 37°C, does not provoke any significant change of the GSH levels.

Furthermore, we have also compared the GSH and GSSG levels determined by spectrophotometric [44] and CE analyses in human red blood cells from normal adults and in the erythrocytes exposed to the iron/ascorbate system (Table 2). As shown in the table, there is a good relationship between the GSH values obtained spectrophotometrically and those determined by HPCE analysis. However, using the procedure described in this paper, the level of GSH in the human erythrocytes is about 10–12% higher compared to the values obtained using the method proposed by Beutler [44], while the levels of GSSG are not detectable. In fact, our data show that the concentration of GSSG in human red blood cells from whole blood samples collected and immediately used for the analysis is less than 1 μM. This result is in agreement with that obtained also by Eyer and co-workers [47,48]. Furthermore, the exposure of intact red blood cells "in vitro" to an oxidant system changes the intracellular GSH/GSSG ratio with a significant increase of oxidized glutathione that can be correctly evaluated (Table 2). The results reported in the table show that, at different incubation times, the GSH and GSSG levels reflect a correct evaluation of the total amount of glutathione equivalents in the red blood cells. In addition, it should be pointed out that using this procedure the amount of red blood cells required for a correct evaluation of GSH and GSSG is 100–200 μl, significantly lower than that used by other methods [44]. For example the evaluation of GSSG, according to Beutler [44] requires the use of 2.5 ml of packed erythrocytes.

In conclusion, the extraction of GSH and GSSG from red blood cells using Microcon-10 membrane, together with their simultaneous

Table 2
Levels of GSH and GSSG in human red blood cells using different procedures of extraction and analysis

Sample	Spectrophotometry[a]		HPCE	
	GSH	GSSG	GSH	GSSG
Control	5.14 ± 0.58	0.021 ± 0.0014	5.89 ± 0.36	N.D.
t_0	5.22	0.08	5.70	0.11
t_{30}	1.45	1.85	1.39	2.20
t_{60}	0.27	1.81	0.29	2.16
S_{60}	N.D.	0.013	N.D.	0.015

The data referred to the "control" were obtained collecting the blood samples from 10 healthy adult subjects and immediately used for the evaluation of GSH and GSSG levels after removal of plasma and buffy coat. A sample of intact red blood cells was also incubated up to 60 min, at 37°C, in the presence of Fe^{2+}/ascorbate system. At various incubation times (t_0,t_{30} and t_{60}) an aliquot of red blood cells was collected and analyzed for the GSH and GSSG levels. Under these experimental conditions, a certain amount of the intracellular GSSG flows-out from the cells and can be detected in the external medium (S_{60} corresponds to the supernatant after the incubation of intact erythrocytes for 60 min). All data are expressed as μmol/g hemoglobin except S_{60} that is expressed as μmol/ml external medium. N.D. = Not determined.

[a] The methods used were from Beutler [44].

evaluation by CE represent a reliable and simple method to evaluate the levels of these compounds in mammalian erythrocytes even when low amounts of blood are available.

Acknowledgements

This work was supported by P.F. Chimica Fine and Ingegneria Genetica.

References

[1] A. Meister, *Pharmac. Ther.*, 51 (1991) 55.
[2] M.E. Anderson, *Methods Enzymol.*, 113 (1985) 548.
[3] H. Sies, *Angew. Chem.*, 25 (1986) 1058.
[4] V.N. Reddy, *Exp. Eye Res.*, 50 (1990) 771.
[5] D.M. Ziegler, *Annu. Rev. Biochem.*, 54 (1985) 305.
[6] H. Hughes, H. Jaeschke and J.R. Mitchell, *Methods Enzymol.*, 186 (1991) 681.
[7] P.J. Hissin and R. Hilf, *Anal. Biochem.*, 74 (1976) 214.
[8] E. Raker, *J. Biol. Chem.*, 190 (1951) 685.
[9] J. Brehe and H.B. Burck, *Anal. Biochem.*, 74 (1976) 189.
[10] T.P.M. Akerboom and H. Sies, *Methods Enzymol.*, 77 (1981) 373.
[11] T. Kuninori and J. Nishiyama, *Anal. Biochem.*, 197 (1991) 19.
[12] B.A. Neuschwander-Tetri and F.J. Roll, *Anal. Biochem.*, 179 (1989) 236.
[13] A.M. Svardal, M.A. Mansoor and P.M. Ueland, *Anal. Biochem.*, 184 (1990) 338.
[14] D.J. Reed, J.R. Babson, P.W. Beatty, A.E. Brodie, W.W. Ellis and D.W. Potter, *Anal. Biochem.*, 106 (1980) 55.
[15] E. Morier-Teissier, N. Mestdagh, J.-L. Bernier and J.-P. Heńichart, *J. Liq. Chromatogr.*, 16 (1993) 573.
[16] J. Nischiyama and T. Kuninori, *Anal. Biochem.*, 138 (1984) 95.
[17] J.P. Richie, Jr. and C.A. Lang, *Anal. Biochem.*, 163 (1987) 9.
[18] S. Awasthi and F. Ahmad, *J. Chromatogr.*, 584 (1992) 167.
[19] J.C. Crawhalland and D. Kalant, *Anal. Biochem.*, 172 (1988) 479.
[20] J.A. Cook, H.I. Pass, A. Russo, S. Iype and J.B. Mitchell, *Int. J. Radial. Oncol. Biol. Phys.*, 16 (1989) 321.
[21] G.C. Rice, B.A. Bump, D.C. Shrieve, W. Lee and M. Kovacs, *Cancer Res.*, 46 (1986) 6105.
[22] G.A. Ublacker, J.A. Johnsonn, F.L. Siegel and R.T. Mulcahy, *Cancer Res.*, 51 (1991) 1783.
[23] M. Cappiello, A. Del Corso, M. Camici and U. Mura, *J. Biochem. Biophys. Methods*, 26 (1993) 335.
[24] P. Pascual, E. Martinezlara, J.A. Barcena, J. Lopezbarea and F. Toridio, *J. Chromatogr.*, 581 (1992) 49.
[25] D. Beales, R. Finck, A.E.M. McLean, M. Smith and I.D. Wilson, *J. Chromatogr.*, 226 (1981) 498.
[26] A.J. Alpert and H.F. Gilbert, *Anal. Biochem.*, 144 (1985) 553.
[27] H. Nakamura and Z. Tamura, *Anal. Chem.*, 53 (1981) 2190.
[28] H. Nakamura and Z. Tamura, *Bunseki Kagaku*, 37 (1988) 35.
[29] D.A. Keller and D.B. Menzel, *Anal. Biochem.*, 151 (1985) 418.
[30] G. Morineau, M. Azoulay and F. Frappier, *J. Chromatogr.*, 467 (1989) 209.
[31] A.I. Minchinton, *Int. J. Radiat. Oncol. Biol. Phys.*, 10 (1984) 1503.
[32] N.K. Burton and G.W. Aherne, *J. Chromatogr.*, 382 (1986) 253.
[33] S. Velury and S.B. Howell, *J. Chromatogr.*, 424 (1988) 141.
[34] T. Iwamoto, M. Yoshiura, K. Iriyama, N. Tomizawa, S. Kurihara, T. Lee and N. Suzuki, *Jikeikai Med. J.*, 32 (1985) 245.
[35] A.F. Stein, R.L. Dills and C.D. Klaassen, *J. Chromatogr.*, 381 (1986) 259.
[36] D. Dupuy and S. Szabo, *J. Liq. Chromatogr.*, 10 (1987) 107.
[37] W. Buchberger and K. Winsauer, *Anal. Chim. Acta*, 196 (1987) 251.
[38] K. Iriyama, T. Iwamoto and M. Yoshiura, *J. Liq. Chromatogr.*, 9 (1986) 955.
[39] G. Carro-Ciampi, P.G. Hunt, C.J. Turner and P.G. Wells, *J. Pharmacol. Methods*, 19 (1988) 75.
[40] F. Tietze, *Anal. Biochem.*, 27 (1969) 502.
[41] H. Güntherberg and S. Rapoport, *Acta Biol. Med. Ger.*, 20 (1978) 559.
[42] S.K. Srivastava and E. Beutler, *Anal. Biochem.*, 25 (1968) 70.
[43] V. Stocchi, M. Magnani, F. Canestrari, M. Dacha and G. Fornaini, *J. Biol. Chem.*, 256 (1981) 7856.
[44] E. Beutler, in *Red Cell Metabolism*, Grune and Stratton Inc., New York, 3rd ed., 1984, p. 131.
[45] J.C. Roberts and D.J. Francetic, *Anal. Biochem.*, 211 (1993) 183.
[46] V. Stocchi, B. Biagiarelli, M. Fiorani, F. Palma, G. Piccoli, L. Cucchiarini and M. Dacha; *Arch. Biochem. Biophys.*, 311 (1994) 160.
[47] D. Gallemann and P. Eyer, *Anal. Biochem.*, 191 (1990) 347.
[48] P. Eyer and D. Podhradsky, *Anal. Biochem.*, 153 (1986) 57.

END OF SYMPOSIUM PAPERS

Environmental Analysis

Techniques, Applications and Quality Assurance

Edited by **D. Barceló**

Techniques and Instrumentation in Analytical Chemistry Volume 13

Three aspects of environmental analysis are treated in this book:

- the use of various analytical techniques
- their applications to trace analysis of pollutants, mainly organic compounds
- quality assurance aspects, including the use of certified reference materials for quality control of the entire analytical process.

The book will serve as a general reference for post-graduate students as well as a practical reference for environmental chemists who need to use the analytical techniques for environmental studies. Analytical chemists needing information on the complexity of environmental sample matrices and interferences will also find this an invaluable reference.

Contents: Part 1. Field Sampling Techniques and Sample Preparation. 1. Sampling techniques for air pollutants (R. Niessner). 2. Sample handling strategies for the analysis of organic contaminants from environmental samples (M.-C. Hennion, P. Scribe). 3. Extraction, clean-up and recoveries of persistent trace organic contaminants from sediment and biota samples (D.E. Wells).
Part 2. Application Areas. 4. Current developments in the analysis of polychlorinated biphenyls (PCBs) including planar and other toxic metabolites in environmental matrices (D.E. Wells). 5. Official methods of analysis of priority pesticides in water using gas chromatographic techniques (D. Barceló). 6. Coupled-column reversed phase liquid chromatography as a versatile technique for the determination of polar pesticides (E.A. Hogendoorn, P. van Zoonen). 7. Liquid chromatographic determination of phenols and substituted derivatives in water samples (G. Marko-Varga). 8. HPLC methods for the determination of mycotoxins and phycotoxins (J.F. Lawrence, P.M. Scott). 9. Determination of radionuclides in environmental samples (V. Valkovic).
Part 3. Quality Assurance and Reference Materials. 10. Quality assurance in environmental analysis (W.P. Cofino). 11. Certified reference materials for the quality control of measurements in environmental monitoring (E.A. Maier). 12. Standard reference materials for the determination of trace organic constituents in environmental samples (S.A. Wise).
Part 4. Emerging Techniques. 13. Application of fluorescence spectroscopic techniques in the determination of PAHs and PAH metabolites (F. Ariese, C. Gooijer, N.H. Velthorst). 14. Characterization of surfactants in water by desorption ionization methods (F. Ventura). 15. Utilization of various LC-MS interfacing systems in environmental analysis; application to polar pesticides (M.H. Lamoree, R.T. Ghijsen, U.A.Th. Brinkman). 16. Hyphenated techniques applied to the speciation of organometallic compounds in the environment (O.F.X. Donard, R. Ritsema). 17. The potential of capillary electrophoresis in environmental analysis (M.W.F. Nielen).
Subject index.

© 1993 660 pages Hardbound
Price: Dfl. 465.00 (US $ 265.75)
ISBN 0-444-89648-1

ELSEVIER SCIENCE B.V.

ORDER INFORMATION

For USA and Canada
ELSEVIER SCIENCE INC.
P.O. Box 945
Madison Square Station
New York, NY 10160-0757
Fax: (212) 633 3880

In all other countries
ELSEVIER SCIENCE B.V.
P.O. Box 330
1000 AH Amsterdam
The Netherlands
Fax: (+31-20) 5862 845

US$ prices are valid only for the USA & Canada and are subject to exchange rate fluctuations; in all other countries the Dutch guilder price (Dfl.) is definitive. Customers in the European Community should add the appropriate VAT rate applicable in their country to the price(s). Books are sent postfree if prepaid.

Flow-Through (Bio)Chemical Sensors

By **M. Valcárcel** and **M.D. Luque de Castro**, Department of Analytical Chemistry, University of Córdoba, 14004 Córdoba, Spain

Techniques and Instrumentation in Analytical Chemistry Volume 16

Flow-through sensors are more suitable than classical probe-type sensors for addressing real (non-academic) problems. The external shape and operation of flow-through (bio)chemical sensors are of great practical significance as they facilitate sample transport and conditioning, as well as calibration and sensor preparation, maintenance and regeneration, all of which result in enhanced analytical features and a wider scope of application. This is a systematic presentation of flow-through chemical and biochemical sensors based on the permanent or transient immobilization of any of the ingredients of a (bio)chemical reaction (i.e. the analyte, reagent, catalyst or product) where detection is integrated with the analytical reaction, a separation process (dialysis, gas diffusion, sorption, etc.) or both.

The book deals critically with most types of flow-through sensors, discussing their possibilities and shortcomings to provide a realistic view of the state-of-the-art in the field. The large numbers of figures, the wealth of literature references and the extensive subject index complement the text.

© 1994 332 pages Hardbound
Price: Dfl. 355.00 (US$ 202.75)
ISBN 0-444-89866-2

ELSEVIER SCIENCE

ORDER INFORMATION
ELSEVIER SCIENCE B.V.
P.O. Box 330
1000 AH Amsterdam
The Netherlands
Fax: (+31-20) 5862 845
For USA and Canada
P.O. Box 945
Madison Square Station
New York, NY 10159-0945
Fax: (212) 633 3680
US$ prices are valid only for the USA & Canada and are subject to exchange rate fluctuations; in all other countries the Dutch guilder price (Dfl.) is definitive. Customers in the European Union should add the appropriate VAT rate applicable in their country to the price(s). Books are sent postfree if prepaid.

PUBLICATION SCHEDULE FOR THE 1994 SUBSCRIPTION

Journal of Chromatography A and *Journal of Chromatography B: Biomedical Applications*

MONTH	1993	J–M	J	J	A	
Journal of Chromatography A	652–657	658–669	670/1 + 2 671/1 + 2 672/1 + 2	673/1 673/2 674/1 + 2 675/1 + 2 676/1	676/2 677/1 677/2 678/1	The publication schedule for further issues will be published later.
Bibliography Section		681/1	681/2			
Journal of Chromatography B: Biomedical Applications		652–655	656/1 656/2	657/1 657/2	658/1 658/2	

INFORMATION FOR AUTHORS

(Detailed *Instructions to Authors* were published in *J. Chromatogr. A*, Vol. 657, pp. 463–469. A free reprint can be obtained by application to the publisher, Elsevier Science B.V., P.O. Box 330, 1000 AH Amsterdam, Netherlands.)

Types of Contributions. The following types of papers are published: Regular research papers (full-length papers), Review articles, Short Communications and Discussions. Short Communications are usually descriptions of short investigations, or they can report minor technical improvements of previously published procedures; they reflect the same quality of research as full-length papers, but should preferably not exceed five printed pages. Discussions (one or two pages) should explain, amplify, correct or otherwise comment substantively upon an article recently published in the journal. For Review articles, see inside front cover under Submission of Papers.

Submission. Every paper must be accompanied by a letter from the senior author, stating that he/she is submitting the paper for publication in the *Journal of Chromatography A* or *B*.

Manuscripts. Manuscripts should be typed in **double spacing** on consecutively numbered pages of uniform size. The manuscript should be preceded by a sheet of manuscript paper carrying the title of the paper and the name and full postal address of the person to whom the proofs are to be sent. As a rule, papers should be divided into sections, headed by a caption (*e.g.*, Abstract, Introduction, Experimental, Results, Discussion, etc.). All illustrations, photographs, tables, etc., should be on separate sheets.

Abstract. All articles should have an abstract of 50–100 words which clearly and briefly indicates what is new, different and significant. No references should be given.

Introduction. Every paper must have a concise introduction mentioning what has been done before on the topic described, and stating clearly what is new in the paper now submitted.

Experimental conditions should preferably be given on a *separate* sheet, headed "Conditions". These conditions will, if appropriate, be printed in a block, directly following the heading "Experimental".

Illustrations. The figures should be submitted in a form suitable for reproduction, drawn in Indian ink on drawing or tracing paper. Each illustration should have a caption, all the *captions* being typed (with double spacing) together on a *separate sheet*. If structures are given in the text, the original drawings should be provided. Coloured illustrations are reproduced at the author's expense, the cost being determined by the number of pages and by the number of colours needed. The written permission of the author and publisher must be obtained for the use of any figure already published. Its source must be indicated in the legend.

References. References should be numbered in the order in which they are cited in the text, and listed in numerical sequence on a separate sheet at the end of the article. Please check a recent issue for the layout of the reference list. Abbreviations for the titles of journals should follow the system used by *Chemical Abstracts*. Articles not yet published should be given as "in press" (journal should be specified), "submitted for publication" (journal should be specified), "in preparation" or "personal communication".

Vols. 1–651 of the *Journal of Chromatography*; *Journal of Chromatography, Biomedical Applications* and *Journal of Chromatography, Symposium Volumes* should be cited as *J. Chromatogr.* From Vol. 652 on, *Journal of Chromatography A* (incl. Symposium Volumes) should be cited as *J. Chromatogr. A* and *Journal of Chromatography B: Biomedical Applications* as *J. Chromatogr. B.*

Dispatch. Before sending the manuscript to the Editor please check that the envelope contains four copies of the paper complete with references, captions and figures. One of the sets of figures must be the originals suitable for direct reproduction. Please also ensure that permission to publish has been obtained from your institute.

Proofs. One set of proofs will be sent to the author to be carefully checked for printer's errors. Corrections must be restricted to instances in which the proof is at variance with the manuscript.

Reprints. Fifty reprints will be supplied free of charge. Additional reprints can be ordered by the authors. An order form containing price quotations will be sent to the authors together with the proofs of their article.

Ovomucoid Bonded Column for Direct Chiral Separation

ULTRON ES-OVM

Narrow-Bore Column (2.0 I.D. x 150 mm) for Trace Analyses
Analytical Column (4.6 I.D. , 6.0 I.D. x 150 mm) for Regular Analyses
Semi-Preparative Column (20.0 I.D. x 250 mm) for Preparative Separation

Analysis of Trace FLURBIPROFEN in Metabolite with NARROW-BORE COLUMN

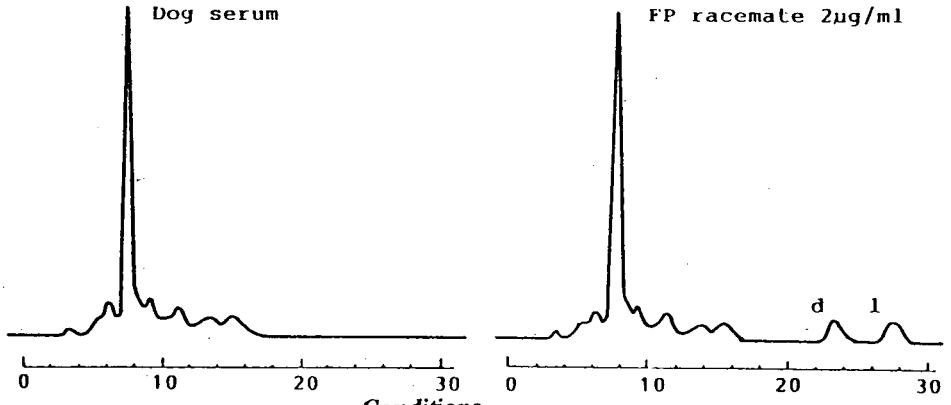

Conditions

Column: ULTRON ES-OVM(2.0I.D. x 150mm)
Mobile Phase: 20mMPhosphate Buffer(pH=3.0)/CH3CN =100/15
Flow Rate: 0.1ml/min
Temperature: 25°C
Injection: 5µl
Detection: UV- 247nm(0.05AUFS)

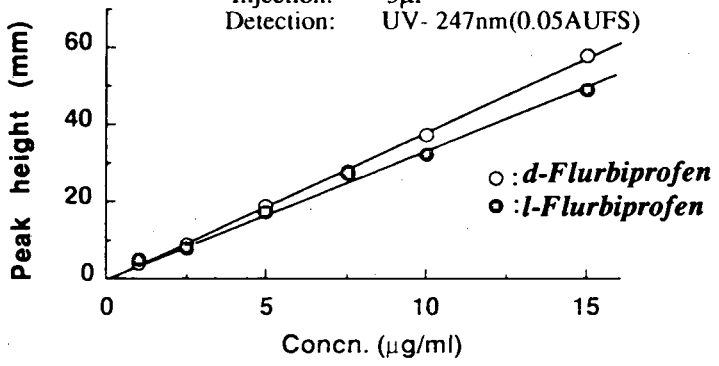

Calibration Curve for Each Enantiomer of Flurbiprofen

SHINWA CHEMICAL INDUSTRIES, LTD.

50 Kagekatsu-cho, Fushimi-ku, Kyoto 612, JAPAN
Phone:+81-75-621-2360 Fax:+81-75-602-2660

In the United States and Europe, please contact:

Rockland Technologies, Inc.

538 First State Boulevard, Newport, DE 19804, U.S.A.
Phone: 302-633-5880 Fax: 302-633-5893

This product is licenced by Eisai Co., Ltd.